JOURNAL AerospaceLab

ONERA
THE FRENCH AEROSPACE LAB

Issue 11
June 2016

DOI : 10.12762/2016.AL11

Challenges in Combustion for Aerospace Propulsion

Produced by
ONERA - BP 80100
Chemin de la Hunière
et des Joncherettes
91123 PALAISEAU CEDEX
France
www.onera.fr

ISSN: 2107-6596

Francis Dupoirieux
(ONERA)
Research Director,
Deputy Head of the Energetics Department, in charge of the academic research activity

DOI : 10.12762/2016.AL11-00

Research Activity to Tackle the Challenges in Combustion for Aerospace Propulsion

The use of combustion for aerospace propulsion is inescapable for the long term. The improvement of the energetic efficiency, safety and reliability, and the compliance with increasingly stringent environmental rules require the enhancement of existing technologies and/or a breakthrough in propulsion devices. A vigorous research activity must be pursued in the field of combustion to meet these goals. This issue of AerospaceLab gives the reader an overview of this intense activity, ranging from experimental to theoretical and numerical work.

Combustion is a process that is used to supply more than 80 % of the world primary energy. Since this process still mainly relies nowadays on fossil fuels, it creates about 70 % of the Green House Gases (GHG). Technological solutions are today available for industry, housing and ground transportation, to cease using carbonated fuel combustion, i. e., to progressively shift to low GHG emission processes. The situation is different in aeronautics and aerospace, where combustion remains the only process able to supply the specific power and energy required to propel aircraft, rockets and missiles. This means that the optimization of this process is mandatory, not only to ensure ever better operational safety and to decrease the operation costs, but also to meet environmental requirements concerning emissions and noise. Only research work aimed at improving existing combustion technologies as well as introducing technological breakthroughs in propulsion devices can allow us to achieve these objectives. This research work must be based on an experimental activity involving accurate non-intrusive measurements to give us a deep insight into turbulent reactive flows, and an activity in numerical simulation and modeling making possible a comprehensive analysis of these reactive flows. Experimental and numerical activities are complementary of each other: numerical tools need to be validated by experiments and, on the other hand, the interpretation and understanding of the experimental results is greatly enhanced by numerical simulations.

In the short term, the use of hydrogen for transport aircraft is not a viable solution because of storage difficulty and operation safety, and the best way to lower the CO_2 emissions of air transport, aside from improving the specific fuel consumption, is the use of biofuels recycling the atmospheric CO_2. The question of biofuel use is wide and goes far beyond the sole problem of combustion. Therefore, it will not be addressed here.

The objective of this AerospaceLab issue is to give an overview of the vigorous research activity in the field of combustion. We focus here on research work with a TRL (Technology Readiness Level) lower than or equal to 6, in other words, on research concepts that have not yet been tested on flying vehicles.

Concerning aircraft propulsion, this issue starts with a description of the main features of the major combustion facilities used at ONERA and CORIA Rouen for experimental research on aerospace propulsion [AL11-01 and AL11-02]. The physical phenomena involved in turbulent combustion and the corresponding models to be introduced into the numerical tools are then discussed, and the validation of these tools using experimental results is exemplified [AL11-05]. The way in which these complex numerical tools are applied to industrial combustors is presented in AL11-06. Various solutions are used to improve engine efficiencies and, consequently, decrease the specific fuel consumption, one of which is an increase in the combustion pressure. However, this leads to a higher combustion temperature and, consequently, to higher NOx emissions. In order to offset this effect, lean premixed combustion is preferred, but this is at the expense of the combustion stability. The instability issue for this type of reactive flow is addressed in AL11-09. Other topics of interest regarding reactive flows are combustion noise [AL11-10] and pollutant emissions [AL11-07, AL11-08, AL11-11]. Concerning the last topic, [AL11-07] deals with strategies to simulate the formation of pollutants, such as soot and NOx, and presents some experiments designed to validate these strategies. [AL11-08] describes experimental studies to accurately characterize the soot emissions of turbojet engines and [AL11-11] focuses on the experimental study of a low-emission combustor designed for mid-power industrial turbines. Finally, technological breakthroughs are exemplified by presenting concepts allowing increased combustion pressures, using either the detonation mode or a constant volume chamber [AL11-12].

The use of combustion is also required for rocket and missile propulsion. For such vehicles, the main issues are improving operation safety (by limiting the combustion instabilities, for instance) and optimizing the specific impulse and the operating cost. Despite the low number of flights, the emission of pollutant species, such as chlorinated species, can also be addressed if solid propellant is used. A close look at air breathing combustion in ramjets and scramjets respectively [AL11-03, AL11-04] is taken. For ramjets, the objective is to improve the combustion efficiency and to prevent instabilities;

for scramjets, the difficulty lies in mixing fuel and air, and in anchoring the flame without thermal choking and/or an exceedingly great pressure drop. The physicochemical phenomena involved in solid-fuel rocket propulsion are described in AL11-13, with special emphasis on the unsteady behavior of reactive flows inside rocket combustion chambers. This is followed by a paper that concentrates on hybrid propulsion, combining solid and gaseous propellants to obtain a more flexible engine thrust [AL11-14].

The last topic developed in the issue is liquid propulsion, a complex technology that requires the injection of propellants into a high-pressure chamber, either by means of sophisticated pumping devices or high-pressure tank storage. In addition, it often requires the storage of cryogenic propellants. Despite its complexity, liquid propulsion is commonly used because it yields a high specific impulse. Two papers describe research work in the field of cryotechnical propulsion, the first being dedicated to the experimental activity carried out with the ONERA MASCOTTE facility [AL11-15], and the second to the numerical simulation of H2-O2 combustion with injection of cryogenic oxygen [AL11-16].

This issue of the AerospaceLab Journal is far from being exhaustive, but it is aimed at convincing the reader that top level research combining experiments, physical modeling and numerical simulations remains mandatory to tackle the wide range of issues linked to combustion in propulsion systems for aeronautics and aerospace, which are issues that extend from operation safety to performance optimization and environmental impacts ■

A. Cochet, V. Bodoc
C. Brossard, O. Dessornes,
C. Guin, R. Lecourt
M. Orain, A. Vincent-Randonnier

(ONERA)

E-mail: alain.cochet@onera.fr

DOI : 10.12762/2016.AL11-01

ONERA test Facilities for Combustion in Aero Gas Turbine Engines, and Associated Optical Diagnostics

The aim of this paper is to provide an overview of the ONERA test facilities devoted to the study of combustion in gas turbine engines. The objectives of the experimental studies performed with these test rigs are very ambitious and extend from building databases for the validation of codes and models used in numerical simulation to applied research for evaluating the performance of advanced aero injection systems in mono-sector, multi-sector or full annular combustion chambers. For more than ten years, aside from standard measurements (i.e., pressure, temperature, mass flow rates, gas analysis sampling), optical diagnostics have been widely associated with the test campaigns carried out in these rigs. Many optical methods are now very commonly used to measure for instance flow velocity fields, size and velocity of droplets, and the location of combustion zones. Other methods that are more difficult to implement, or still under development, are being increasingly used or proposed for measuring physical or chemical parameters, such as temperature, size of soot particles or concentration of combustion products. Examples of the results obtained with the ONERA test facilities and optical diagnostics are given, in order to illustrate the studies presented in this paper.

Introduction

In the coming years, air transport will face societal and environmental challenges requiring cleaner and more efficient aero-engines to be designed. The development of advanced combustors is based on reliable numerical tools and high-class experiments involving a great amount of physical and chemical phenomena, such as combustion in a two-phase flow with complex chemistry, pollutant formation, or heat transfer and radiation. Experiments must thus be performed under thermodynamic conditions representative of those encountered in true engines. Test facilities capable of reproducing these specific operating conditions are available at ONERA and enable subsonic air-breathing reacting flows occurring within gas turbine based aero-engines to be studied.

These combustion test facilities are used to perform tests aimed at tuning the aero-engine injection system and combustor, building experimental databases to validate CFD codes and supporting the development of new diagnostics under harsh conditions.

Research on the injection system and combustor is being carried out in close cooperation with engines manufacturers, mainly within the framework of European projects. Reducing pollutant emissions and specific consumption, or evaluating alternative fuels for aeronautics, are some issues of interest in combustion testing with ONERA facilities.

For code validation, experimental databases must be obtained from experiments carried out in either basic configurations or very close to the true engine design and operation mode (i.e., multi-swirl injectors, multipoint fuel injection, pilot + main fuel injection).

For these experiments, various measurements are applied to characterize non-reacting and reacting flows inside aero-combustors. Aside from standard measurements using, for instance, pressure transducers, thermocouples, a gas sampling probe and an analyzer, optical diagnostics are increasingly being used. Their continuous development made it possible to achieve non-intrusive measurements of a very large set of physical and chemical quantities, such as gas velocities, soot

particle or fuel droplet sizes, gas concentrations, or temperatures. In order to apply these techniques, test models are equipped with optical accesses, the material of the windows being selected depending on the wavelength requirement of the applied diagnostics.

For a long time, many research centers and laboratories, in France and all over the world, have developed test facilities devoted to studies on combustion in gas turbine engines. For instance, many worldwide test facilities are listed in Reference [1] and the example of the French laboratory CORIA, located in Rouen, is detailed in Reference [2]. ONERA facilities are mostly devoted to applied research of interest for aero-engine manufacturers, although some of them are dedicated to fundamental research.

This article is aimed at providing an overview of the experimental test facilities of ONERA at its Palaiseau and Le Fauga-Mauzac centers. Each test facility will be briefly described and examples of fundamental and/or applied research carried out in these various facilities will be given, through the presentation of some past and recent results obtained. Optical measurements used to perform these studies will be also mentioned.

Test facility general features

Simulation of representative test conditions on test rigs

Aero-combustor testing requires facilities that are capable of simulating aero-thermodynamic conditions at the inlet of the combustion chamber; that is to say, downstream from the compressor. Chamber pressure, inlet temperature and injection system global equivalence ratios are the governing parameters to be respected for a representative simulation of the combustion chemical reactions inside the combustor. The air mass flow rate depends on the size of the combustor to be tested and is directly linked to the Reynolds number to be reproduced in the experiments. In addition, it is essential to obtain a convective Damkhöler number very close to those of real aero-engines.

BOX 1 – Combustor inlet air temperature versus compressor overall pressure ratio

The compressor overall pressure ratio P_2/P_1 and the temperature at the inlet of the combustion chamber are linked by Relation (1) at sea level

$$T_2 = T_1 \times \left[\frac{P_2}{P_1}\right]^{\left(\frac{1}{\eta_P}\right)\left(\frac{\gamma-1}{\gamma}\right)} \quad (1)$$

γ: heat capacity ratio
η_P: polytropic efficiency
T_2: total temperature at the compressor outlet and at the combustor inlet
T_1: total temperature at the compressor inlet (here, $T_1 = 288$ K)
P_2: total pressure at the compressor outlet and at the combustor inlet
P_1: total pressure at the compressor inlet

Figure B.1 shows the air temperature at the entrance of the combustion chamber vs. the overall pressure ratio under a sea level operating condition.

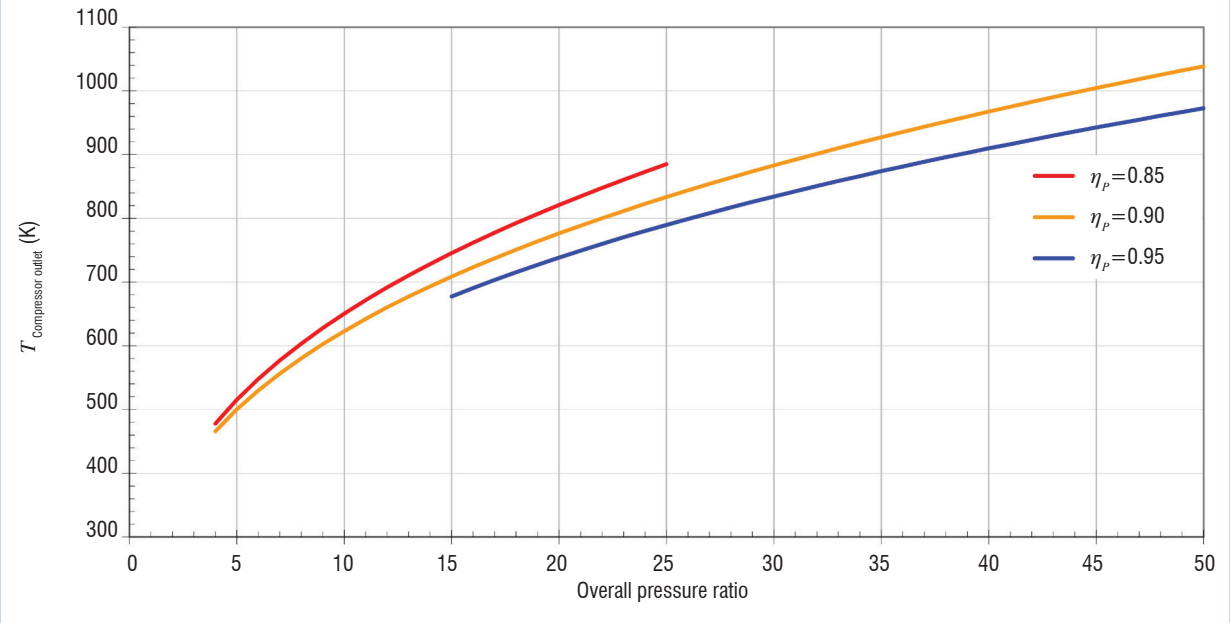

Figure B.1 - Air temperature at the compressor outlet vs. overall pressure ratio under a sea level operating condition for different values of polytropic efficiencies

In addition to the thermodynamic conditions attainable in each test rig, the nature of the phenomena under investigation can make the difference between the purposes of each test facility. For example, the ONERA/Le Fauga-Mauzac test facilities are focused on the characterization of the spray generated from advanced injection systems, whereas the ONERA/Palaiseau test facilities are more devoted to combustion studies with the same injection systems. Experimental data obtained with the facilities of each center are complementary and are both used for code and model validation.

Whatever the purpose of the studies taking place, the various test rigs are operated with connected pipes and in non-vitiated air, in order to investigate combustion in a fully representative chemical environment. One of the challenges to perform this kind of test is to provide the air mass flow rate at the right chamber pressure and inlet temperature (for instance, a pressure combustion chamber of 4.0 MPa corresponds roughly to an inlet temperature of 900 K). Regarding air heating, two technical options are mainly used. The first is a heat exchanger, in which the air mass flow rate is heated through a hot flux generated by air/hydrocarbon combustion inside a slave burner. The second is an electrical heater, in which the mass flow is heated using electric rods immersed in the air that supplies the test rig. In addition, gaseous or liquid fuel distribution lines are available, depending on the purposes of the studies. Some specific tanks can be implemented to operate the combustors with alternative fuels.

ONERA test facilities

As mentioned in the introduction, the test facilities described in this article are located at:

- ONERA/Le Fauga-Mauzac center: MERCATO and LACOM test rigs;
- ONERA/Palaiseau center: micro-combustion laboratory, EPICTETE test rig at LAERTE facility, M1 and MICADO (1 and 2) test rigs at the Aerothermodynamics Laboratories.

Test facilities are mainly characterized by the minimum and maximum chamber pressure, inlet temperature and air mass flow rate that they are capable of simulating. The maximum test duration depends on the test conditions (air mass flow and pressure) and air supply capabilities (continuous air flow up to 10 kg/s at 1.0-1.2 MPa and high pressure storage of 21 tons at 25 MPa). Table 1 summarizes the test facilities that are of interest in this paper with their operating condition ranges. They are listed according to increasing thermal power supplied to the test line.

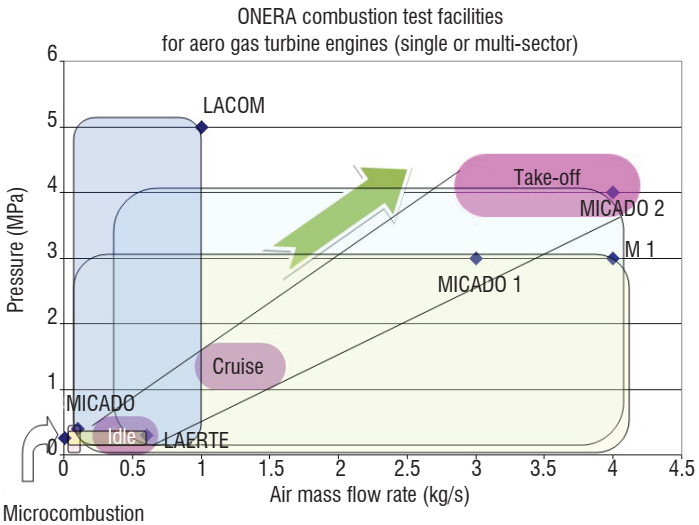

Figure 1 - ONERA test facility operating conditions shown in a pressure-air mass flow rate diagram

Additionally, Figure 1 shows the position of each test facility listed in Table 1 in a Pressure - Mass flow rate diagram. In this diagram, typical pressure domains, corresponding to the operating conditions of an actual aero-engine with mono-sector or multi-sector combustor, are shown. It can be seen that most test facilities are well suited to the high-pressure operating conditions typical of new combustors,

Test bench	Minimum air mass flow rate (kg/s)	Maximun air mass flow rate (kg/s)	Minimum pressure (MPa)	Maximum pressure (MPa)	Minimum air inlet temperature (K)	Maximum air inlet temperature (K)	Maximum air supply power (MW)
Microcombustion test bench*	0.0002	0.005	0.1	4	293	293	0
MERCATO	0.01	0.1	0.05	4	233	473	0.0246
EPICTETE test bench (LAERTE facility)	0.08	0.6	0.1	3	293	600	0.194
LACOM	0.1	1	0.1	50	293	900	0.68
MICADO 1 (ATD laboratories)	0.5	3	0.1	30	250	900	2.19
M1 (ATD laboratories)	0.1	4	0.05	30	250	900	2.91
MICADO 2 (ATD laboratories)	0.5	4	0.1	40	250	900	2.91

* No air preheating

Table 1 – Main Characteristics of ONERA test facilities

for either large engines in single sector studies or smaller engines in multi-sector studies. The LACOM test rig is more dedicated to studies in which the influence of very high pressure and temperature on physical phenomena is of interest, such as those of spray characteristics in two-phase flows.

Optical diagnostics applied to combustion studies

Full experimental investigation of the flow inside combustors requires visualizations and measurements of key physical quantities, such as gas velocity, gas temperature, and concentration of major and minor species, as well as droplet size, velocity and temperature in two-phase flows [3]. Due to the fact that they provide access to such quantities, optical diagnostics have become an indispensable tool. They allow a deeper understanding of the inner physical and chemical processes at play, which is required to validate and improve computer-based simulations and to assist applied research in practical combustors.

Over the past decades, optical diagnostics have been intensively used or developed at ONERA and applied to combustion test facilities. The techniques used and their proven applicability range at ONERA are summarized in Table 2.

Observation is often the first step: high-speed digital imaging of spontaneous radiation can be easily implemented on the test rigs and provides some insight into the flame structure and dynamics. In particular, by using an interference filter, OH* or CH* chemiluminescence emission signals can be isolated in order to trace reacting regions of the flow.

A whole range of laser-based techniques can then be used, depending on the quantities of interest and on optical access. Particle Image Velocimetry (PIV) has become one of the most widely used laser techniques in both research institutes and industry [4]. Its major asset is its capacity to deliver a quantitative and instantaneous measurement of the velocity, not only at one point like Laser Doppler Velocimetry (LDV) does, but over a whole plane simultaneously: both visualization and quantification of the 2D flow structure become available. Two or three components of the velocity can be obtained by using one or two cameras (stereoscopic PIV), respectively. Compared to non-reacting flows, the implementation of PIV in reacting flows requires additional technical constraints to be taken into account. The seeding of the flow must be performed with small (in the micron range) solid particles (usually metal oxides, such as MgO or TiO_2). For instance, dispersing systems used to generate such particles are prone to unsteady behavior, and precautions in the operating procedure must be taken in order to limit particle deposits on the windows. Another critical issue is window access: in combustion chambers, it is usually dictated by mechanical and thermal constraints. In particular, in stereoscopic PIV each camera has to view the laser sheet with an angle of approximately 45°: this results in limitations in the measurement plane locations that can be investigated using this technique.

Planar Laser-Induced Fluorescence (PLIF) imaging is species- and quantum state-specific, and is therefore sensitive to species composition, temperature, number density and velocity [5]. The OH radical is the most commonly used flame front indicator. Applied to this radical species, PLIF, like PIV, is able to provide instantaneous information over the whole plane of the flowfield, without the line-of-sight averaging inherent to OH* chemiluminescence imaging. Simultaneous information on fuel and flame spatial distributions can be obtained with two PLIF laser systems probing OH and kerosene vapor simultaneously [6]. Additionally, by seeding the flow with adequate fluorescing tracers or probing tracers naturally present in the flow, the mixture fraction distribution can also be obtained. Recently, PLIF applied to CO molecule has been developed and successfully applied to air-breathing engine flow investigation at ONERA [7].

Optical technique	High pressure applicability limit (as proven at ONERA)(MPa)
Chemiluminescence (OH*, CH*)	6.5
Backlight imaging	6.5
Shadowgraphy	6.5
Laser Doppler Velocimetry	1.0
Phase Doppler Anemometry	1.0
Particle Image Velocimetry	0.4 (0.2 under reacting flow conditions)
Mie Scattering planar imaging	0.2
Planar Laser-Induced Fluorescence	2.3 (OH, kerosene), 0.95 (CO) at a repetition rate of 10 Hz, 0.1 (OH) at a repetition rate of 10 kHz
Rayleigh scattering	0.5
Raman scattering	0.5
Coherent Anti-Stokes Raman Scattering	6.5 (N_2, H_2) at a repetition rate of 15 Hz, 0.1 (N_2) a repetition rate of 1 kHz
Tunable Diode Laser Absorption Spectroscopy	0.2

Table 2 – Optical techniques applied at ONERA on large-scale combustion rigs

Laser spectroscopy based on nonlinear processes is widely used, from the near IR to the near UV, in order to probe reactive media. Among others, Coherent Anti-Stokes Raman Scattering (CARS) was developed at ONERA and extensively used for temperature measurements in harsh reactive environments of interest in the aerospace field [8]. The basic principle of temperature measurements by CARS is to probe the relative population of the molecular levels, from which the thermodynamic temperature of the molecular system is drawn. Consequently, the concentration of the probed species can also be deduced [9].

When studying two-phase flows, preliminary visualization of the fuel spray structure is usually performed. Instantaneous spatially resolved Mie scattering planar imaging can be obtained by illuminating the spray with a pulsed laser sheet. When using high-speed lasers and cameras, this technique also provides valuable insight into the spray dynamics. It also enables the identification of regions of interest where further measurements should be conducted. Phase Doppler Anemometry (PDA) is a well-known technique that enables a local simultaneous measurement of the droplet size and velocity distribution. ONERA, in cooperation with CNRS, has developed new optical diagnostics in order to characterize the dispersed liquid phase in sprays in terms of droplet temperature, size and velocity. In particular, important work has been done on measuring the mean and local droplet temperature, by coupling Standard Rainbow Refractometry (SRR) and Laser Induced Fluorescence (LIF) for a monodisperse droplet stream [10]. Local characterizations of the discrete phase inside a polydisperse spray have also been carried out by the simultaneous use of the Global Rainbow Refractometry (GRR) method and the PDA technique.

Optical diagnostics have continued to evolve very fast thanks to permanent progress in laser technologies, electronic imaging systems and processing algorithms. In particular, the development of high frequency lasers and cameras have enabled the repetition rates of planar laser imaging techniques, such as PIV or PLIF, to be taken from the hertz to the kilohertz range in the last few years. Some developments are currently in progress at ONERA to increase the performance of laser diagnostics. A new femtosecond CARS system is being developed at the Physics and Instrumentation Department, in order to also increase the repetition rate of this technique from the hertz to the kilohertz range [11]. Through a tight cooperation between the Modeling and Information Processing Department and the Fundamental and Experimental Aerodynamics Department, considerable progress has been made in the development of fast and efficient algorithms for tomographic PIV, thus enabling velocity vectors to be measured simultaneously in an entire volume rather than only in a plane [12]. Even though reliable use of this technique in reacting flows remains challenging, these developments open up new capabilities and perspectives of spatial-temporal experimental measurements never reached so far. The combination of several optical diagnostics on the same test facility should also be examined in the future, in order not only to obtain different physical quantities simultaneously, but also to reduce the number and cost of experiments.

Finally, one of the main challenges will be to adapt or develop optical diagnostics capable of operating under higher temperature and pressure conditions more representative of real industrial combustors. The new MICADO test facility at ONERA will serve that purpose (see the MICADO section in this article). The maximum targeted chamber pressure is 4.0 MPa. At such pressure levels in reacting flows, significant light reabsorption or beam steering effects will exist. For PIV, for instance, so far tests under reacting flow conditions have been conducted at ONERA in studies with chamber pressure levels limited to 0.2 MPa [13-15]. One of the main challenges will be to adapt the PIV technique so that it can be used at chamber pressure levels as high as possible. In particular, beam steering is one of the issues that must be addressed. The beam steering effects, generated by optical index gradients in the combustion chamber, result in image blurring and could be very significant in highly turbulent flows at high chamber pressures.

Description of the test facilities

Micro-combustion test rig

This facility has been developed by ONERA in order to study an ultra-micro gas turbine engine that can deal with power between a few tens of watts up to some kilowatts with high specific energy and specific power. The latest portable devices or small drones use Lithium-ion (Li-ion) secondary batteries as power sources. These batteries can have relatively large power densities, but their energy densities hardly reach 200-250 Wh/kg, which limits the endurance. Charging time and very cold external temperatures may also be critical issues. Common hydrocarbon fuels have energy densities around 12 kWh/kg. A system able to convert only a small percentage of this energy density could reach higher energy densities than existing batteries. Therefore, over the past decade, and due to the increase in micro-power requirements, many efforts have been dedicated to building a micro heat engine capable of producing electricity. Micro power generators based on reciprocating engines, thermoelectric devices or thermo-photovoltaic devices, Wankel engines, Rankine cycle based engines, Stirling engines, fuel cells and micro-turbines are being or were investigated. In particular, a 400 W electric micro-turbine complete system was demonstrated by IHI. This system can be refueled with simple gas cartridges. The heat management and control of the exhaust gas temperature were also demonstrated by Isomura et al. [16]. Among those systems, fuel cells should have the best efficiency, whereas the micro gas turbine should achieve the highest power density.

This is the reason why ONERA decided to focus on ultra-micro gas turbines [17] and, in this context, designed and built a micro-turbine test rig on which a micro-combustor was firstly tested (Figure 2).

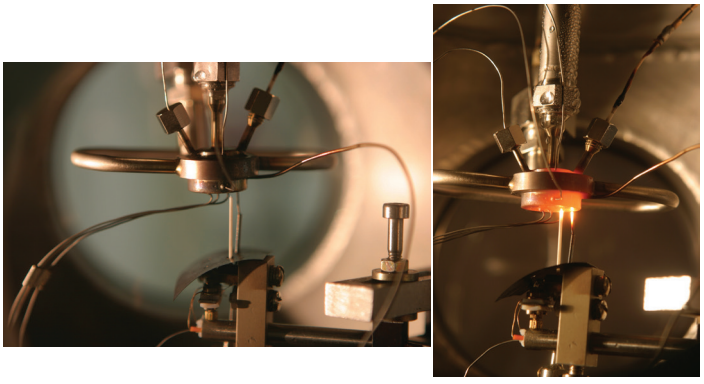

Figure 2 - Photographs of the micro-combustor

This test rig has the capacity of dealing with fuel flow rates of a few mg/s and air flow rates of up to 5 g/s. Fuels such as hydrogen, methane or propane can be used.

For the micro-combustor tests, a special vessel was designed to pressurize the flow at the nominal pressure corresponding to the pressure turbine inflow (Figure 3).

Figure 3 - ONERA micro-combustor in its vessel

Measurements such as outlet wall temperature, exhaust gas temperature and chamber pressure can be made. Special diagnostics such as infra-red thermography (Figure 4) can also be used, as well as spontaneous Raman and Rayleigh scattering (Figure 5), to obtain composition and temperature profiles at the exhaust, respectively.

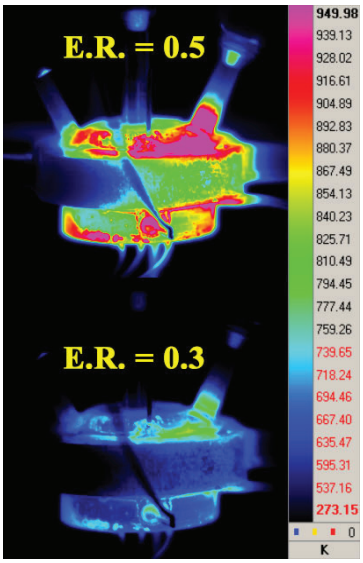

Figure 4 – Infrared thermography image example

A complete micro-turbine designed for around 50 W electric power was machined and tested (see Figure 6, the scale is given by the coin near the micro-turbine test rig) up to 170,000 rpm (2.8 kHz). At this time, its operability was demonstrated for a few watts of electric power output. In this case, in addition to the pressure and temperature measurements mentioned before, the rotation speed is also measured using Philtec optic-fiber devices connected to a high sampling rate oscilloscope. Rotation speeds up to 850,000 rpm can be measured.

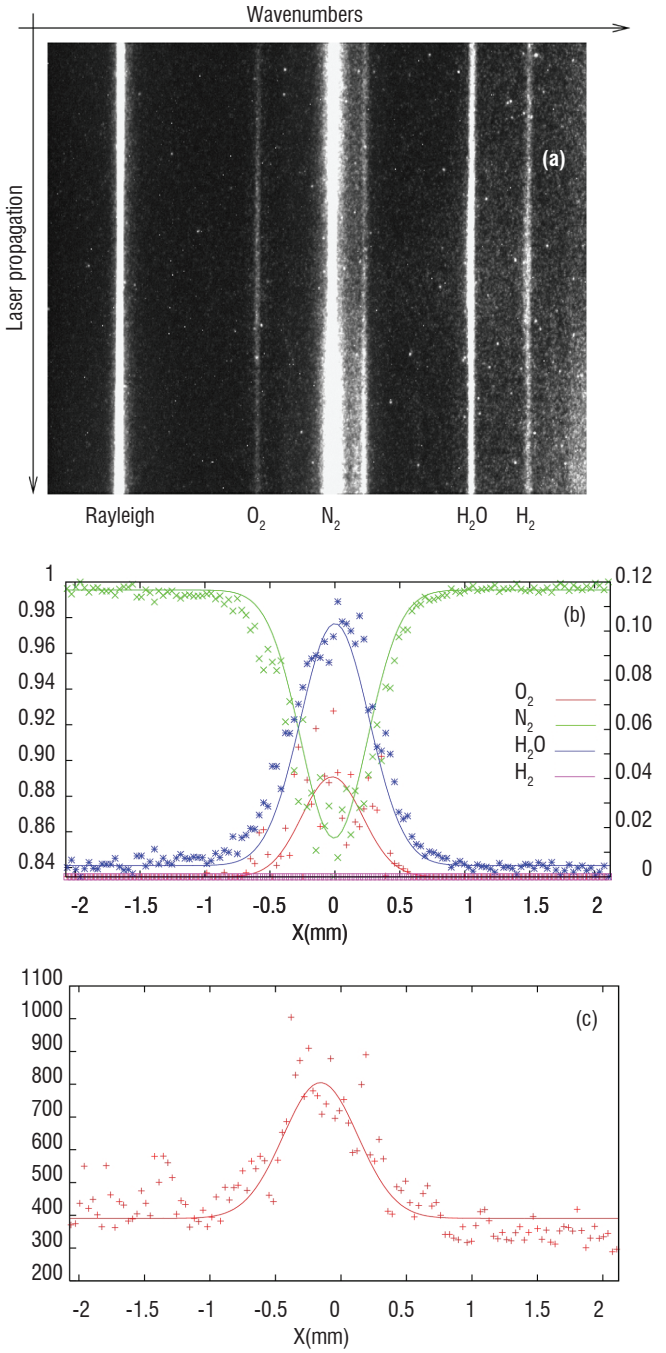

Figure 5 – Example of spontaneous Raman and Rayleigh scattering results: raw signal (a), molar fraction (b) and temperature (c)

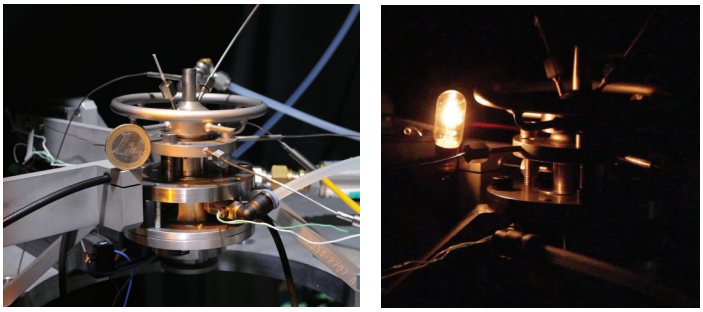

Figure 6 – Complete 50 W micro-turbine tested

MERCATO

The MERCATO (Experimental Means for Research in Air-breathing Combustion by Optical Techniques) test facility, located at ONERA/Le Fauga-Mauzac and shown in Figure 7, is a small air-breathing propulsion research facility. Air and fuel are supplied at low flow rates, up to 100 and 10 g/s respectively, but in a wide range of temperatures from 233 K to 473 K for air and from 233 K to ambient for fuel. Air is cooled through an Air/LN2 (liquid nitrogen) cooling tower and fuel is cooled through a cooling bath. The pressure in the test chamber can be varied from 0.05 MPa to around 0.4 MPa. This facility has been developed and extensively used to investigate the ignition phenomenon, especially under altitude conditions [18-20], and to build an experimental database of a two-phase flow under non-reacting and reacting conditions [21, 22].

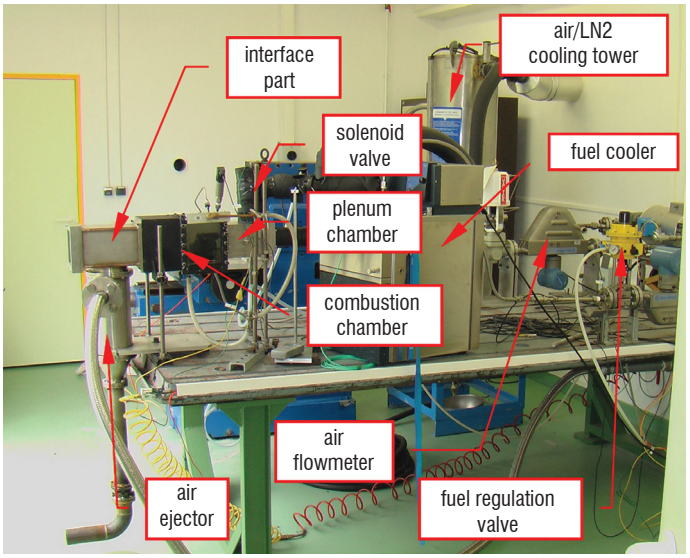

Figure 7 – MERCATO test rig

Concerning the ignition phenomenon in turbojet engines, a recent investigation [20] has been performed on the ignition performances of various alternative fuels according to their aromatic content, given in Table 3. The tests were performed inside the mono-sector combustion chamber shown in the photograph in Figure 7. The experiments were carried out under altitude conditions, at an air pressure of 0.06 MPa and an air temperature of 233 K (-40°C), which corresponds to a cold start at about 4000 m altitude.

The results are summarized in the graph in Figure 8, which shows the global equivalence ratio needed for ignition vs. the fuel blend, designated by its acronym on the horizontal axis. This graph shows how the ignition performance, i.e., the boundary limit (red dash), evolves according to the fuel composition.

FUEL	AROMATICS (%)	ACRONYM
Jet A-1	20.6	JETA
SPK	2.5	SPK
Jet A-1 + SPK	8	SPK08A
SPK + Aromatic cut	20.6	SPK20AC
SPK + Aromatic cut	8	SPK08AC
Aromatic cut	100	AC

Table 3 – Fuel compositions investigated in the ignition performance tests

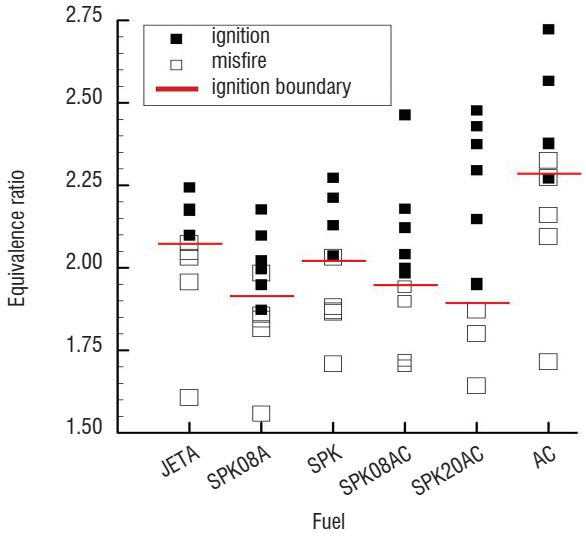

Figure 8 – Ignition performance test results

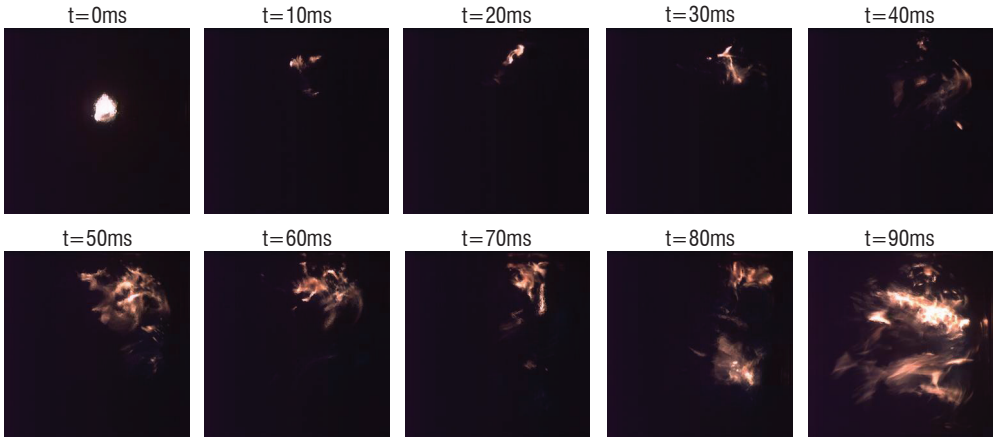

Figure 9 – Ignition sequence recorded with a high speed camera; 1 kHz frame rate, 130x130mm² image size

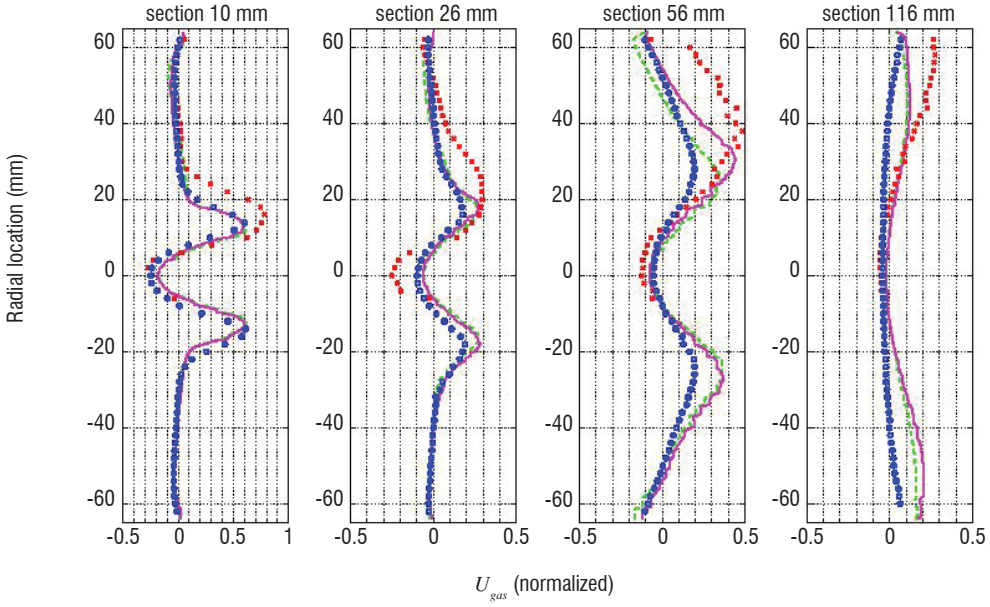

Figure 10 – Gaseous phase mean velocity profiles (axial component)
• experimental non-reacting • experimental reacting
– numerical reacting Arrhenius scheme – numerical reacting Cramer scheme

During this kind of experiment, a high-speed camera (1 kHz frame rate) is often used to visualize the ignition occurrence and flame propagation. The images, reported in Figure 9, are then processed in order to measure some characteristics of the ignition: burning kernel trajectory and size evolution.

The need for deeper knowledge on two-phase flow characteristics before, during and after ignition, has motivated the detailed characterization of these flows under non-reacting and reacting conditions, sometimes during short ignition experiments. These flow characterizations were performed by using LDA, PDA and PIV laser diagnostics. A comprehensive database [21,22] was built on the mono-sector configuration, which has been used extensively [23-25] for different section lengths. The comparison, shown in Figure 10, between experimental and numerical results for the gaseous axial velocity component of the stabilized reacting two-phase flow, shows that major improvements are still needed in spray combustion. For example, in 10 and 26-mm long sections (see Figure 10), the numerical results (RANS simulation, green marks and pink line) are closer to the non-reacting experimental results (blue marks) than to the reacting ones (red marks) [26] as they should be. It is planned to increase the database with vapor concentration measurements to be obtained by using LIF laser diagnostics and with drop size and velocity measurements under altitude conditions.

EPICTETE test rig (LAERTE facility)

The LAERTE facility was built in the early 1990s to develop and apply advanced optical diagnostics devoted to combustion studies of gaseous or liquid fuels (methane, Jet-A1) in high turbulence flows [27-29]. It is fed with a preheated air flow (80 g·s^{-1} ≤ $\dot{m}_{air}$ ≤ 600 g·s^{-1} ; 300 K ≤ T_{air} ≤ 600 K ; 0.10 MPa ≤ P_{ch} ≤ 0.20 MPa) based on a heat exchanger.

The 1.4 m long combustion chamber has a 100 mm × 100 mm square section. The air mass flow is measured upstream from the combustor inlet using a choked nozzle. The combustor walls are water cooled, thus allowing long duration tests. Large optical accesses (100 mm × 260 mm quartz windows) are used to perform optical diagnostics. A flush-mounted spark igniter is inserted through the lower combustor wall. An exit nozzle equipped with a throttling plug is connected downstream from the combustor to control the chamber pressure (moving this plug also modifies the acoustic impedance).

In the EPICTETE configuration of the rig, the combustor is equipped with a single-swirl injector (Turbomeca Makila DLN; roughly the same injector as for PRECCINSTA experiments [30]). Fuel can be injected via the pilot or main fuel supply (non-premixed or premixed conditions, respectively). Various diagnostics were implemented in EPICTETE experiments, most of them with $\dot{m}_{air}$ = 80 g·s^{-1}, T_{air} = 400–450 K and P_{ch} = 0.20 MPa. For these conditions, the reduced mass flow rate almost corresponds to the normal use of this industrial injector (7–8 kg·s^{-1}·K$^{0.5}$·MPa^{-1}).

For methane/air combustion, velocity measurements obtained for both the reacting and non-reacting cases by high-speed PIV (1–10 kHz) have been performed in the median longitudinal plane (3–5 mm thick laser plane; thickness imposed by the large azimuthal speed of the particles and the interframe delay of the camera). 1 kHz measurements were obtained over a 100 mm × 100 mm field. Selecting a reduced field (37.5 mm × 30 mm) located in the mixing layer region enabled 10 kHz measurements to be achieved to visualize time-resolved eddy convection, as can be seen in Figure 11. In the mixing region, the flow velocity can reach up to 100 m·s^{-1} (averaged velocity field based on 3072 samples at 1 kHz). The related fluctuating velocity is close to 50 m·s^{-1}.

OH* and CH* chemiluminescence images have also been obtained using a high-speed intensified camera (2 kHz).

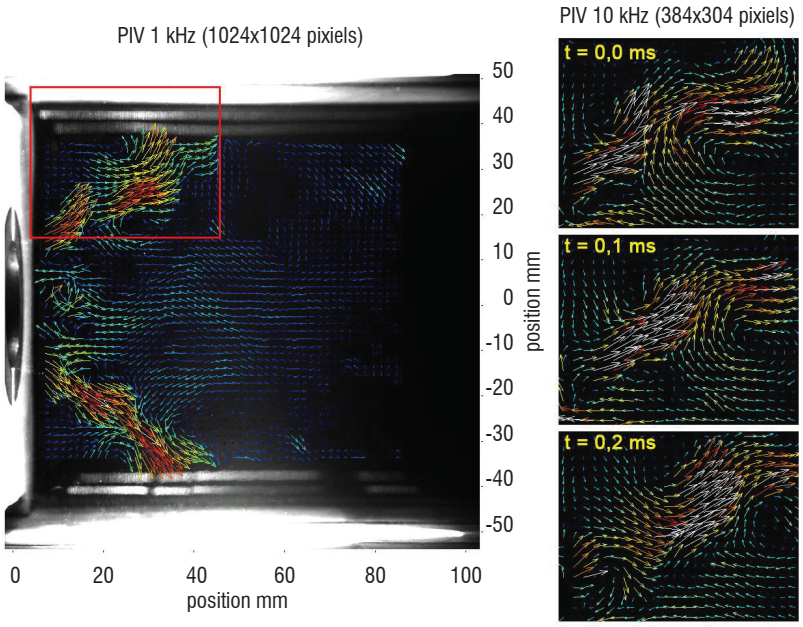

Figure 11 – Instantaneous velocity field measurements
obtained with the PIV technique for methane/air combustion
($\dot{m}_{air}$ = 80 g·s^{-1} ; T_{air} = 410–425 K ; P_{ch} = 0.20 MPa ; $E.R.$ = 0.75)

The combustion of Jet-A1 fuel was also investigated. Figure 12 shows an overview of the Jet-A/air flames for various pressure and global equivalence ratio conditions.

The kerosene spray was characterized by using high-speed Laser-Induced Mie Scattering (4 kHz) and Phase Doppler Interferometry, enabling the determination of the vortex core precession frequency (between 500 Hz and 1200 kHz depending on the test conditions).

For T_{air} ≥ 440–450 K ($\dot{m}_{air}$ = 80 g·s^{-1} ; P_{ch} = 0.20 MPa), occurrences of a combustion instability behavior have been observed: change of the kerosene spray and flame shapes, strong pressure fluctuation (±3%), sudden shift of the PVC frequency from 830 Hz to 1125 Hz.

Finally, a specific module including thin-layer based fluxmeters was developed at ONERA to estimate the heat flux density at the wall of the combustor (from 70 to 290 kW·m^{-2}, depending on measurement location and test conditions).

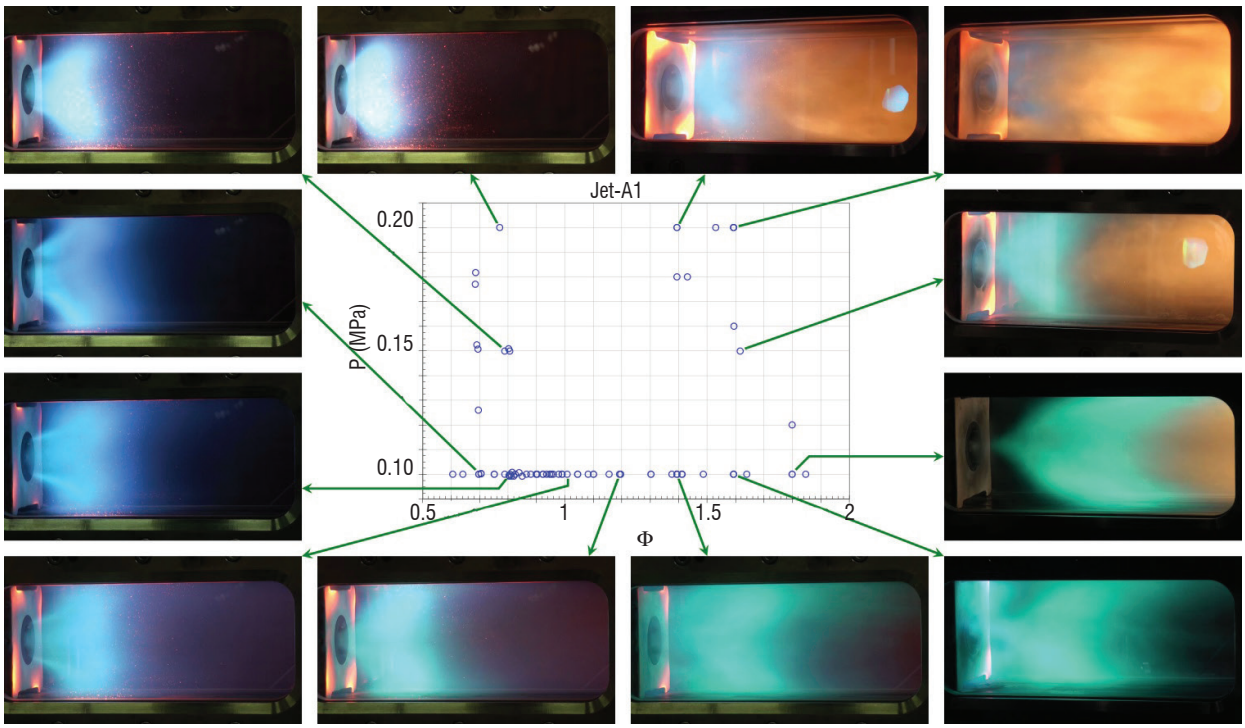

Figure 12 – Overview of the Jet-A/air flame for various pressure and global equivalence ratio conditions
(T_{air} = 400–450 K ; $\dot{m}_{air}$ = 80 g·s^{-1})

LACOM

Figure 13 – LACOM test facility

The Multiphase Combustion Laboratory (LACOM), shown in Figure 13, was initially designed to study the phenomena associated with the injection of liquid fuels into gas turbines under reacting and non-reacting conditions [31,32]. The test rig was designed to partially recreate the temperature and pressure conditions of a real combustor. On one hand, the experimental characterization of the liquid spray at the exit of a real scale injection system provides a reference database useful for the validation of the model implemented in numerical simulation codes. On the other hand, it finds an immediate application in the characterization of new design injectors under real conditions. The laboratory upgrades (addition of a second air feed line) enable the characterization of effusion cooling systems (i.e., based on multiperforated walls). The main characteristics of the laboratory are now detailed. The air feeding system can deliver a mass flow rate of 1 kg/s for each feed line, which can be heated through two electrical heaters of 1MW/250 kW up to 900 K/450 K, respectively.

The injection test rig consists mainly of a plenum and a test chamber. The plenum is designed to house the injection system. Thermocouples and pressure gauges are used to provide real-time values of the air and fuel temperatures and pressure. The test chamber is equipped with large windows, which allow the use of optical measurement techniques at various wavelengths without light distortion. The test chamber is water-cooled, which enables experiments to be run over long periods of time. A sonic throat, which is also water-cooled, is installed downstream from the test chamber, to allow tests at high pressure (up to 5.0 MPa). The line for the study of wall effusion cooling was designed to work at up to 3.0 MPa and to heat multiperforated material samples up to 1200 K. The cooling efficiency can be evaluated by thermocouple measurements or by infrared thermography.

Finally, the exhaust module limits the rig impact on the environment. Indeed, the air and water mixed with combustion/evaporation products are cleaned before ejection into the atmosphere. Moreover, in order to avoid noise pollution, the main part of the exhaust module is located underground.

Flow description relies on various measurement techniques, mostly based on non-intrusive optical techniques: Mie scattering, Phase Doppler Interferometry (PDI), Particle Image Velocimetry (PIV), Laser Induced Fluorescence (LIF) and Infrared Thermography.

Research project examples

KIAI/LOTAR (Knowledge for Ignition, Acoustics and Instabilities/ Liquid-fueled ONERA ThermoAcoustic Rig)

Combustion instabilities generally lead to large pressure or velocity fluctuations inside the combustor, which can generate significant heat transfer at the combustor walls or large amplitude vibrations of the combustor structure. This can result in combustor damage, or even in its destruction. The thermo-acoustic instabilities observed in liquid-fueled combustors involve the coupling of various complex phenomena, such as spray atomization, vaporization, combustion, turbulence, chemistry, flow instabilities and acoustics. Due to their interaction, it is very difficult to understand the isolated influence of each of these phenomena. It is thus necessary to perform detailed experimental studies of the phenomenon, in order to improve the knowledge of the underlying physics in combustion instabilities and subsequently improve its modeling.

The LOTAR test rig was developed to enable combustion instabilities to be properly investigated with well-controlled boundary conditions, thanks to detailed acoustic characterization and using laser-based measurements. The experiments, performed within the framework of the European project KIAI, included the characterization of the gas flowfield, spray properties (both liquid and vapor phases), combustor acoustics and flame dynamics (flame transfer function). An example of the time evolution of the kerosene spatial distribution (liquid and vapor phases) is given in Figure 14 (a). Large spatial and temporal variations along the cycle are noticed. Similar results were observed with OH radicals and the post-processing of the images enabled the local Rayleigh index presented in Figure 14 (b) [33] to be derived.

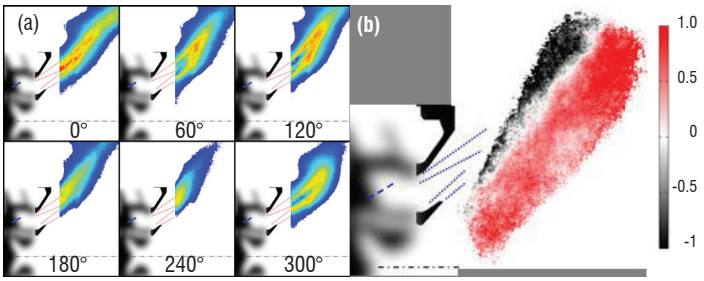

Figure 14 – Temporal evolution of the kerosene spatial distribution (liquid and vapor phases) along the limit cycle (a), Spatial distribution of the local Rayleigh index (b)

SAPHIR

Combustor walls of gas turbines are subjected to very high gas temperatures levels and must be cooled and protected by effusion cooling. The cooling air is injected through small holes, creating a protecting film along the wall. The objective of this project is to study the cooling efficiency of various perforation patterns.

The temperature distribution on the multiperforated material sample is measured by thermocouples and infrared thermography.

M1 (ATD laboratories)

M1 test rig is one of the ONERA test facilities for air-breathing propulsion studies named AeroThermoDynamics Laboratories (ATD labs). The M1 test rig with its three test lines is mainly devoted to aero-engine injection system and combustor testing. From injection system evaluation on a tubular combustor to sector or full annular combustion chamber for small engine characterization, the M1 test rig has a wide range of capabilities.

The maximum test conditions are the following:

- Air mass flow rate $0.1 \leq \dot{m}_{air} \leq 4$ kg/S
- Air temperature $250 \leq T_{air} \leq 900$ K
- Combustion chamber pressure 0.05 MPa$\leq P_{ch} \leq 3$ MPa
- Fuel mass flow rate (kerosene) ≤ 0.25 kg/s

Air preheating is achieved by using 4 heat exchangers operating in parallel connection, each with a capacity of 1 kg/s, 900 K and 3.0 MPa. The fuel supply (kerosene) is provided at a maximum pressure of 8.0 MPa with a separate supply for each test line. Ignition is achieved by a spark igniter or a hydrogen/air torch.

Conditions of altitude relight can be simulated using a supersonic ejector connected to the combustor exit and fed with air from heat exchangers. The combustor pressure can then be decreased down to 0.05 MPa with a cold airflow (down to 250K), directly generated by high pressure storage.

A large set of measurements can be used on this test rig to obtain various physical quantities: static pressure, temperature, mass flow rate, dynamic pressure, burnt gas concentrations by gas analysis (CO, CO_2, NO_x, HC), smoke measurements (Smoke Number, volume and mass concentrations, as well as number size distributions), and also, inside the combustor, the velocity flowfield using LDV or PIV laser diagnostics, as well as OH radical, kerosene vapor and CO concentration maps by using PLIF laser diagnostics along the axial and radial dimensions of the combustor. The CARS technique can also be used to map gas temperatures with its probability density distributions. Figure 15 shows a photograph of the test facility. This test rig was renovated between 1996 and 2000 and has been used very intensively since 2001.

Figure 15 – Photograph of the M1 test facility

It has been involved in numerous European projects on combustion in aeronautical combustors and particularly in the evaluation of advanced injection systems and new combustor concepts to reduce NOx emissions. For instance, many European projects, such as BRITE-EURAM, LOPOCOTEP and SIA-TEAM (soot formation) in FP5; INTELLECT-DM, TLC, NEWAC and TECC-AE in FP6; and currently LEMCOTEC and IMPACT-AE in FP7; sometimes completed by French programs such as TOSCA, have enabled LPP (Lean-Premixed-Prevaporized), RQL (Rich-Quench-Lean) and, more recently, MSFI (Multi-Stage-Fuel-Injection) technologies to be investigated and optimized for aeronautical gas turbines. Using its M1 test rig, ONERA has largely contributed to the development of these innovative combustors, some aspects of which are described below.

Research project examples

Self-ignition and flashback tests on LPP injectors [34]

LPP (Lean Premixed Prevaporized) combustors are very efficient for reducing NOx emissions, but the concept is penalized by problems of self-ignition and flashback, especially in engines with a high overall pressure ratio. Therefore, within the framework of the BRITE-EURAM program, ONERA developed a special experimental setup, equipped with a water-cooled tubular combustor, for characterizing these phenomena in a LPP injector under realistic operating conditions.

Several concepts developed by the Turbomeca, Volvo, Rolls-Royce and Snecma manufacturers were tested in the facility. The safe operating limits for each concept were determined. The limit on the air-fuel mixture residence time in the injection system to prevent self-ignition was established according to the pressure and air temperature for a global equivalence ratio of between 0.4 and 0.7.

Optical measurements on a single sector combustor equipped with a MSFI injector [35]

The MSFI concept enables two independent flames to be generated from the same injection system. Its configuration features a concentric arrangement of a main fuel stage embedded into a large swirling air stream carrying the largest part of the air mass flow, and a nested pilot injector located in the center. Both flames are swirl-stabilized. The pilot fuel is introduced by a spray nozzle in the injector axis, whereas the main fuel is injected from an annular cavity through multiple holes. The investigated injector versions mainly differed by their pilot zone.

The combustor used for these measurements was developed within the TLC research program. It is presented in Figure 16. This water-cooled visualization sector has a 105 mm × 105 mm square cross section and an 82 mm length. Its section converges upstream from the combustor exit. The volume is the same as the volume of one sector in the real Snecma annular combustor. It is equipped with three optical accesses for laser diagnostics. The thermal protection of optical windows is provided by strong air film cooling, representative of the real annular combustor.

A sonic throat, which can be partly obstructed by a water-cooled needle, enables the control of the pressure inside the combustor. Upstream from this nozzle, a sampling probe collects burnt gas and soot particles for emission measurements. These measurements were used to calibrate the Snecma and ONERA computation codes and some of them are presented in this paper [36].

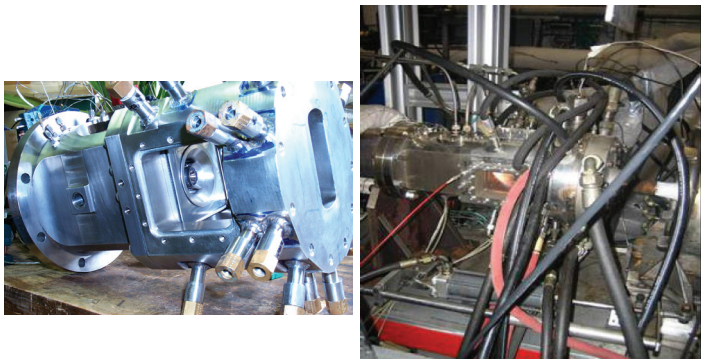

Figure 16 – Photographs of the TLC combustor

They also enabled the discovery of potential correlations between the flame structure, vapor fuel location and emission performances.

Simultaneous measurements of planar laser-induced fluorescence applied to OH and kerosene vapor, and then CARS temperature mapping were performed for various operating conditions up to a pressure of 2.2 MPa.

Optical measurements on the second and third generations of MSFI injector

Two other configurations of MSFI injector were studied within the framework of the TOSCA and TECC programs, and then the LEMCOTEC and IMPACT-AE programs (based on a different configuration named "D8"). Various fuel distributions between the pilot and main zones have been used over the ICAO certification points. Examples of PLIF-OH, PLIF-kerosene and PLIF-CO are presented in Figure 17 for idle conditions, when only the pilot injector is operated. The main difference between the D8 and TOSCA configuration relates to the location of the pilot fuel injection. With the D8 configuration, the fuel vapor is located in the continuation of the pilot bowl, with a hollow cone-like shape. Its flame front develops on both sides of the fuel cone. With the TOSCA configuration, fuel vapor remains located at the center of the pilot zone. Its flame front develops at the periphery of the fuel zone.

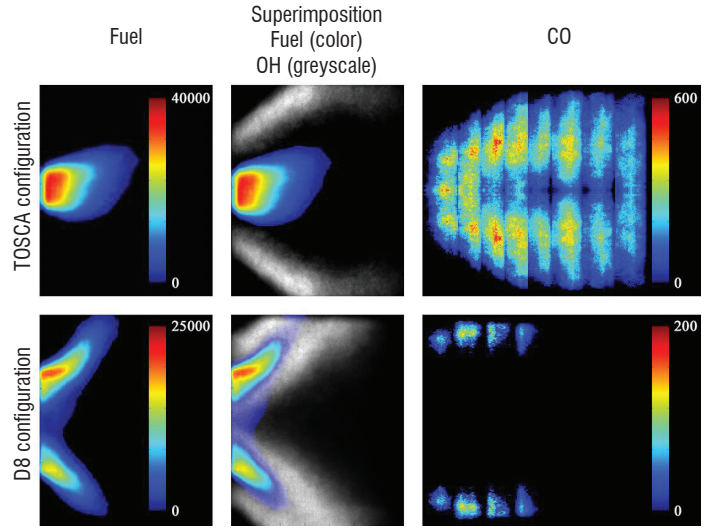

Figure 17 – PLIF mean images (400 laser shots) of OH – kerosene – CO, comparison between TOSCA and D8 configurations under idle conditions

For the D8 configuration, CO is located in the outer zone of the flame front, whereas for the TOSCA configuration it is located closer to the axis, at the interface between the flame front and the kerosene vapor. With these new injectors, the CO emissions are three times lower than those recorded with the first injector at low power, with identical level of NO_x at high power.

Testing of a multi-sector combustor equipped with 4 MSFI injectors

In order to optimize the fuel split of MSFI injectors and evaluate pollutant emissions in an environment representative of the real engine, a multi-sector combustor was studied by Snecma. This combustion chamber was designed based on the results of the single combustor tests. It included 4 MSFI injectors and represented a 4:18 subscale section of a SAM146 type full-annular combustor (Figure 18). The two side plates of the pressure vessel were fitted with large optical accesses. A gas sampling probe, attached to a metal plate, could be implemented as a dummy window. It consisted of a flat U tube with 6 separate sampling points. A computer-controlled multiplexing system scanned each sampling point and a hydraulic actuator could move the probe through the combustor exit plane.

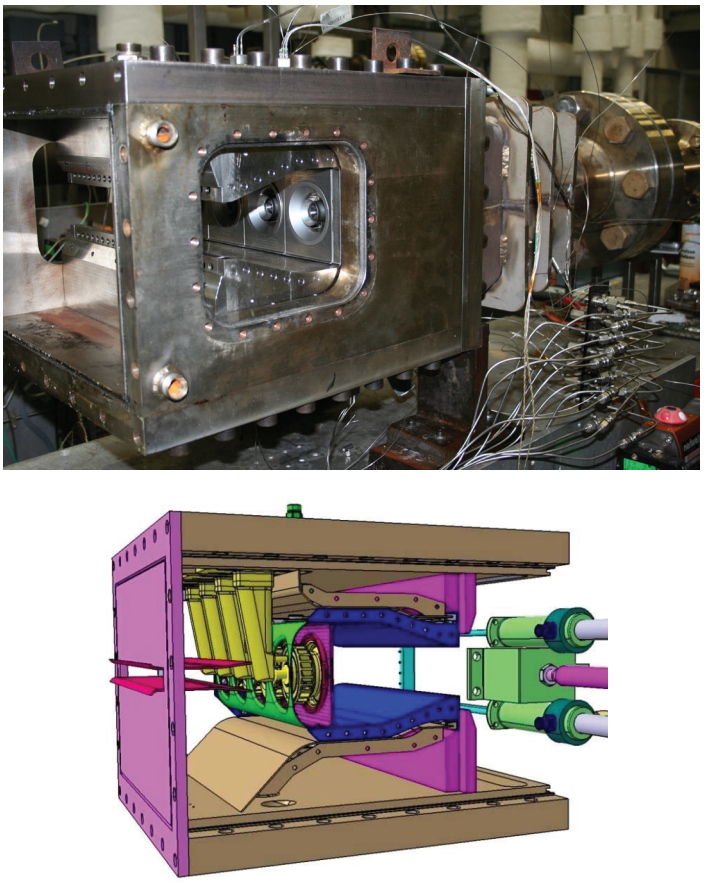

Figure 18 – Multi-sector combustor equipped with its 4 MSFI injectors

Tests on this multi-sector combustor have enabled the following:

- enhancement of the combustion chamber operability and the thermal management, in particular by the improvement of the igniter location and knowledge of the sub-atmospheric relight capability;
- evaluation of the pollutant emissions for various operability conditions and various fuel splits.

Examples of the results are presented in Figure 19 through spatial maps for NO_x indices and flame temperatures under lower take-off operating conditions.

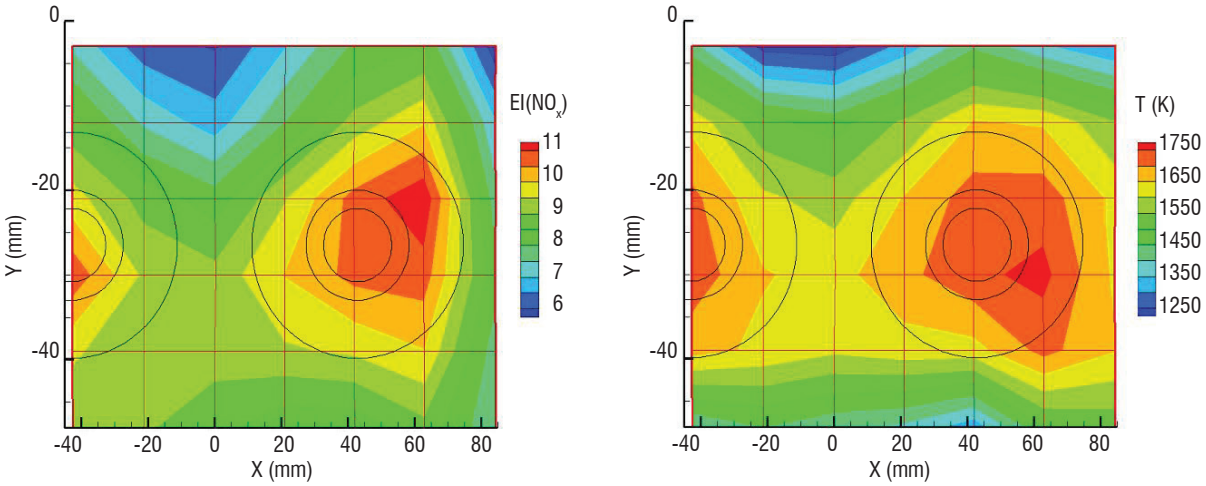

Figure 19 – Maps of local NO_x indices and flame temperatures under lower take off operating conditions

MICADO 1 and 2 (ATD laboratories)

The development of a new test rig, named MICADO, is in progress at the ONERA Palaiseau center (MICADO is a French acronym that stands for "Investigation Means for Air-breathing Combustion using Optical Diagnostics"). The current status can be visualized in Figure 20. This test rig will be dedicated to:

- the study of combustion with test conditions representative of single or multi-sector aeronautical engine combustors;
- the development of the associated advanced diagnostics (a laser control room will be built in 2016 in an adjacent room to host optical diagnostics teams).

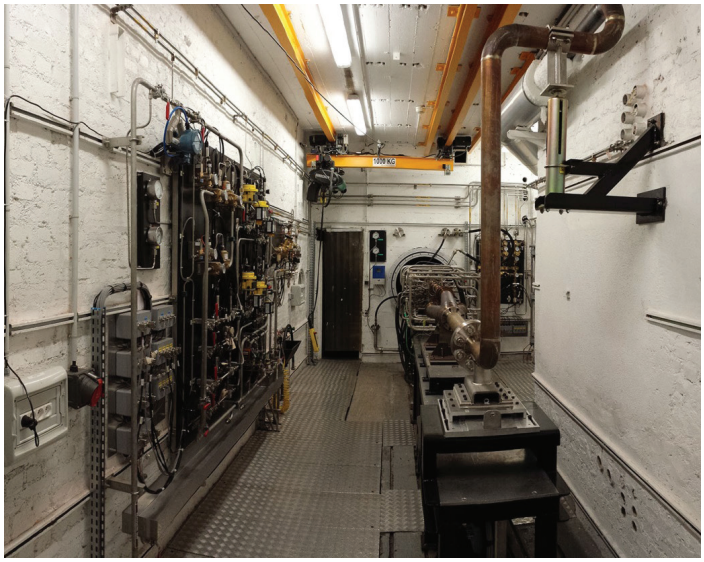

Figure 20 – The MICADO test rig under development

The combustor will be fed with a high-pressure and high-temperature (HP–HT) air flow. For the first phase of this project (so-called "MICADO 1"), the maximum air flow conditions will be $\dot{m}_{air} \leq 3.0$ kg·s^{-1}, $T_{air} \leq 900$ K ; $P_{ch} \leq 3.0$ MPa. Early validation tests of the HP–HT air flow delivery began at the end of 2015 with a ramjet combustor. Preliminary tests of the MICADO combustor are planned for the fall of 2016.

Further development of the HP–HT air flow delivery unit (so-called "MICADO 2") will upgrade testing conditions to $\dot{m}_{air} \leq 4.0$ kg·s^{-1}, $T_{air} \leq 900$–950 K , $P_{ch} \leq 4.0$ MPa. Figure 21 shows the test conditions targeted with the MICADO test rig, and covering the aero-engine (i.e., turbojet, turboprop or helicopter turbine) flight envelope.

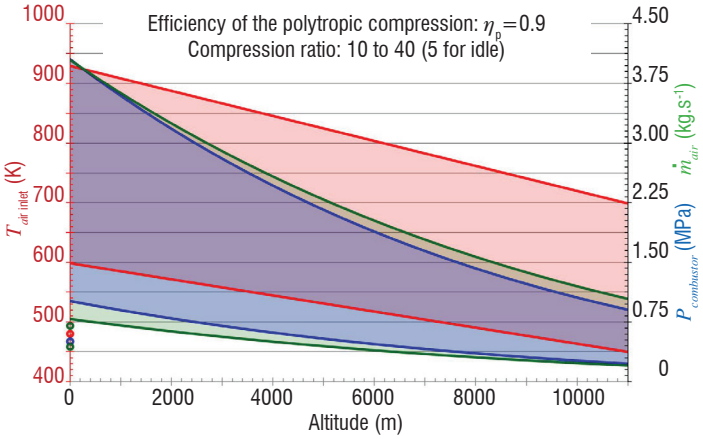

Figure 21 – Flight envelope conditions targeted with the MICADO test rig

The MICADO combustion chamber will have a 100 mm × 100 mm square section, which almost corresponds to large engine single-sector cross-sections. This will ensure realistic conditions for the Reynolds, Damkhöler and Karlowitz numbers in the combustor. The combustor will be water-cooled, thus enabling continuous running conditions. It will be fully equipped with wide optical accesses (89 mm × 88 mm on each wall). Air and fuel will enter the combustor through an axial single-swirl injector, fuel being injected through the main (premixed) and/or pilot (non-premixed) supplies. Fuel will either be gaseous or liquid (methane or kerosene) with $\dot{m}_{fuel} \leq 100$ g·s^{-1} for each injection line. The swirler will be removable, in order to adjust the swirl-number if needed.

A sampling probe will enable online gas and/or soot analysis (sampling location around 140 mm downstream from the combustor dome). The chamber pressure will be adjusted by means of an exit nozzle equipped with a throttling plug.

CONCLUSION

This article provides an overview of the ONERA test facilities, both operational and under development, such as the MICADO test rig. Pressure, temperature and mass flow rates can be varied over a wide range of values and many of the test rigs allow test conditions very close to the real parameters of the aero gas turbine engines investigated. With this set of test rigs, ONERA is capable of studying combustor scales from micro gas turbine engines (0.001 kg/s) up to full annular advanced combustors for helicopter engines (4 kg/s at 2.0 MPa). These test facilities are used to carry out studies not only for industrial purposes but also for more fundamental scientific research aimed at building experimental databases on basic configurations. This last point is crucial for the validation of codes and models used for the numerical simulation of 3D turbulent reacting flows inside aerospace combustors.

Experimental tests are increasingly associated with optical measurements, visualizations (high-speed video, OH* and CH* chemiluminescence) and laser-based optical techniques (LDV, PIV, PDA, PDI, PLIF/OH, PLIF/CO, CARS, etc.). Most of these measurement methods are now developed with a high repetition rate, in order to obtain not only the mean value of the measured quantity, but also some unsteady data that are of interest in unsteady phenomena or transient stages.

Advanced injection systems and combustors, capable of running on various kinds of gaseous or liquid fuels, can be studied in the ONERA test facilities. Pollutant reduction, decrease in specific consumption, improvement of global thermal behavior, mass reduction and unsteady operation are scientific and technical topics of interest at ONERA. French manufacturers in the aerospace propulsion field, Snecma and Turbomeca are the main partners, either in the national programs or through the European Research and Development Framework Programs in which ONERA is often involved ■

References

[1] C.D. SLABAUGH, A.C. PRATT, R.P. LUCHT, S.E. MEYER, M. BENJAMIN, K. LYLE, M. KELSEY - *The Development of an Optically Accessible, High Power Combustion Test Rig.* Review of scientific Instrument 85 (035105) 2014.

[2] F. GRISCH, A. BOUKHALFA, G. CABOT, B. RENOU, A. VANDEL - *CORIA Facilities for Aircraft Engine Type Combustion and Associated Optical Diagnostics*. AerospaceLab, Issue 11, 2016.

[3] F. DUPOIRIEUX - *Optical Diagnostics Used at ONERA to Characterize Turbulent Reactive Flows and to Validate Aero- and Rocket Engine Combustor Modeling*. AerospaceLab, Issue 1, December 2009.

[4] C. BROSSARD, J.-C. MONNIER, P. BARRICAU, F.-X. VANDERNOOT, Y. LE SANT, F. CHAMPAGNAT, G. LE BESNERAIS - *Principles and Applications of Particle Image Velocimetry.* AerospaceLab, Issue 1, December 2009.

[5] F. GRISCH, M. ORAIN - *Role of Planar Laser-Induced Fluorescence in Combustion Research.* AerospaceLab, Issue 1, December 2009.

[6] M. ORAIN, F. GRISCH, E. JOURDANNEAU, B. ROSSOW, C. GUIN, B. TRETOUT - *Simultaneous Equivalence Ratio and Flame Structure Measurements in Multipoint Injector Using PLIF*. Comptes Rendus Mécaniques, Vol. 337, p 373-384 (2009).

[7] M. ORAIN, C. GUIN, O. CARRIVAIN - *Measurements of Fuel, Hot Gases and Pollutant Spatial Distributions in Aeronautical Multipoint Injectors Using PLIF*. Journal of Propulsion and Power, In preparation (2016).

[8] B. ATTAL-TRÉTOUT, F. GRISCH, D. PACKAN, I. RIBET-MOHAMED, M. LEFEBVRE - *Laser Spectroscopy for in Situ Diagnostics*. AerospaceLab, Issue 1, December 2009.

[9] M. HABIBALLAH, M. ORAIN, F. GRISCH, L. VINGERT, P. GICQUEL - *Experimental Studies of High-Pressure Cryogenic Flames on the Mascotte Facility.* Combustion Science and Technology, Vol. 178, p 101-128 (2006).

[10] V. BODOC, C. LAURENT, Y. BISCOS, G. LAVERGNE - *Advanced Measurement Techniques for Spray Investigations*. AerospaceLab, Issue 1, December 2009.

[11] M. SCHERMAN, M. NAFA, T. SCHMID, A. GODARD, A. BRESSON, B. ATTAL-TRETOUT, P. JOUBERT - *Ro-vibrational Coherent anti-Stokes Raman Scattering Spectroscopy in Hybrid fs/ps Regime Using a Volume Bragg Grating for N2 Thermometry*. Optics Letters, In Press (2015).

[12] A. CHEMINET, B. LECLAIRE, F. CHAMPAGNAT, A. PLYER, R. YEGAVIAN, G. LE BESNERAIS - *Accuracy Assessment of a Lucas-Kanade Based Correlation Method for 3D PIV*. 17th International Symposium on Applications of Laser Techniques to Fluid Mechanics, Lisbon, Portugal, 7-10 July, 2014.

[13] V. SABEL'NIKOV, C. BROSSARD, M. ORAIN, F. GRISCH, M. BARAT, A. RISTORI, P. GICQUEL - *Thermo-Acoustic Instabilities in a Backward-Facing Step Stabilized Lean-Premixed Flame in High Turbulence Flow.* 14th International Symposium on Applications of Laser Techniques to Fluid Mechanics, 2008.

[14] A. RISTORI, G. HEID, C. BROSSARD, S. REICHSTADT - *Detailed Characterization of the Reacting One-phase and Two-phase Flow Inside a Research Ramjet Combustor.* XVIIth ISABE Symposium, Munich, Germany, 2005.

[15] A. RISTORI, C. BROSSARD, T. LE PICHON - *Caractérisation de l'écoulement instationnaire dans un statoréacteur de recherche par PIV et visualisations OH* à haute cadence simultanées.* 14ème Congrès Francophone de Techniques Laser (CFTL2014), Marseille, France, September, 2014.

[16] K. ISOMURA - *A Promising Technology for Powering Humanoid Robots? - Development of an Ultra-compact Gas Turbine Capable of Generating Large Amounts of Power Anywhere*. Japan Quality Review 13 (2012) 24-27.

[17] O. DESSORNES, S. LANDAIS, R. VALLE, A. FOURMAUX, S. BURGUBURU, C. ZWYSSIG, Z. KOZANECKI - *Advances in the Development of Microturbine Engine*. Journal of Engineering for Gas Turbines and Power, July 2014, vol.136, pages 1-9.

[18] R. LECOURT, F. BISMES, G. HEID - *Experimental Investigation of Ignition of an Air-Kerosene Spray in Altitude Conditions*. ISABE-2009-1235.

[19] A. LANG, R. LECOURT, F. GIULIANI - *Statistical Evaluation of Ignition Phenomena in Turbojet Engines*. GT2010-23229, ASME Turbo Expo 2010: Power for Land, Sea and Air, June 14-18, 2010, Glasgow, UK.

[20] R. LECOURT - *Ignition Performances of Alternative Fuels under Altitude Conditions according to their Aromatics Content*. ISSA-2015-046, International Symposium on Sustainable Aviation May 31- June 3, 2015 Istanbul, TURKEY.

[21] R. LECOURT, G. LINASSIER, G. LAVERGNE - *Detailed Characterisation of a Swirled Air/Kerosene Spray in Reactive and Non-Reactive Conditions Downstream from an Actual Turbojet Injection System*. GT2011-45173, Proceedings of ASME Turbo Expo 2011: Power for Land, Sea and Air , June 6-10, 2011, Vancouver, CANADA.

[22] R. LECOURT, L. ROSSONI, S. GOYER, G. LINASSIER - *Gas Phase Velocity Measurements in a Swirled Air/Kerosene Burning Spray downstream from an Actual Turbojet Injection System*. AIAA 2014-3659, Propulsion and Energy Forum, 50th AIAA/ASME/SAE/ASEE Joint Propulsion Conference, July 28-30, 2014, Cleveland, OH.

[23] N. GARCIA ROSA, G. LINASSIER, R. LECOURT, P. VILLEDIEU AND G. LAVERGNE - *Experimental and Numerical Study of High-Altitude Ignition of a Turbojet Combustor.* Heat Transfer Engineering, 32(11–12):949–956, 2011.

[24] W.P. JONES, C. LETTIERI, A.J. MARQUIS, S. NAVARRO-MARTINEZ - *Large Eddy Simulation of the two-phase flow in an experimental swirl-stabilized burner*. International Journal of Heat and Fluid Flow 38 (2012) 145–158.

[25] A. EYSSARTIER, B. CUENOT, L. Y. M. GICQUEL, T. POINSOT - *Using LES to Predict Ignition Sequences and Ignition Probability of Turbulent Two-Phase Flames*. Combustion and Flame 160 (2013) 1191–1207.

[26] G. LINASSIER - *Etude expérimentale et numérique de l'allumage des turboréacteurs en conditions de haute altitude*. PhD thesis (2012).

[27] P. GICQUEL, C. CLANET, P. MOREAU - *Présentation des travaux expérimentaux réalisés sur le banc A3C*. ONERA technical report RTS 56/7104 EY.

[28] V. SABELNIKOV, C. BROSSARD, M. ORAIN, F. GRISCH, M. BARAT, A. RISTORI, P. GICQUEL - *Thermo-Acoustic Instabilities in a Backward-Facing Step Stabilized Lean-Premixed Flame in High Turbulence Flow*. 2008, 13 th Int. Symp. on Flow Visualization, Nice (France).

[29] N. FDIDA, C. BROSSARD, A. VINCENT-RANDONNIER, D. GAFFIE - *Characterization of the Kerosene Spray in a Swirl-Stabilized Flame*. 2012, International Symposium on Applications of Laser Techniques to Fluid Mechanics, Lisbon (Portugal).

[30] W. MEIER, P. WEIGAND, X.R. DUAN, R. GIEZENDANNER-THOBEN - *Detailed Characterization of the Dynamics of Thermoacoustic Pulsations in a Lean Premixed Swirl Flame*. Combustion and Flame, 150 (2007) 2–26.

[31] V. GUTIERREZ FERNANDEZ, G. LAVERGNE, P. BERTHOUMIEU – *Dynamic Primary Atomization Characteristics in an Airblast Atomizer, High Pressure Conditions.* Atomization and Sprays, Vol.21 – 2011, pages 1-16.

[32] V. GUTIERREZ FERNANDEZ, G. LAVERGNE, P. BERTHOUMIEU – *Geometric Primary Atomization Characteristics in an Airblast Atomizer, High Pressure Conditions*. Atomization and Sprays, Vol.21 – 2011, pages 17-29.

[33] J.M. APELOIG, H.X. D'HERBIGNY, F. SIMON, P. GAJAN, M. ORAIN, S. ROUX (2015) - *Liquid-Fuel Behavior in an Aeronautical Injector Submitted to Thermoacoustic Instabilities.* Journal of Propulsion and Power, 31(1), 309-319.

[34] C. GUIN - *Characterization of Auto-Ignition and Flashback in Premixed Injection Systems*. AVT Symposium on Gas Turbine Engine Combustion, Emissions and Alternative Fuels; Lisbon, October 12-16, 1998.

[35] F. GRISCH, M. ORAIN, B. ROSSOW, E. JOURDANNEAU, C. GUIN - *Simultaneous Global Equivalence Ratio and Flame Structure Measurements in Multipoint Injector Using PLIF.* AIAA 2008-4868; July 2008, Hartford.

[36] F. DUPOIRIEUX, N. BERTIER, C. GUIN, K.P. GEIGLE, C. EBERLE, P. GERLINGER - *Methodology for the Numerical Prediction of Pollutant Formation in Gas Turbine Combustors and Associated Validation Experiments*. AerospaceLab, issue 11, 2016.

Acronyms

BRITE-EURAM	(Basic Research in Industrial Technologies for Europe - European Research on Advanced Materials)
CARS	(Coherent Anti-Stokes Raman Scattering)
CFD	(Computational Fluid Dynamics)
DEFA	(Fundamental and Applied Energetics Department)
DLN	(Dry Low NO_x)
DMAE	(Aerodynamics and Energetics Modeling Department)
EPICTETE	(Study Etude des Phénomènes en Combustion Turbulente Et Transferts Energétiques)
GRR	(Global Rainbow Refractometry)
ICAO	(International Civil Aviation Organization)
IHI	(Ishikawajima-Harima Heavy Industries)
IMPACT-AE	(Intelligent design Methodologies for low PollutAnt CombusTors for Aero-Engines)
INTELLECT-DM	(INTtegratEd Lean Low Emisson CombusTor - Design Methodology)
IR	(InfraRed)
KIAI	(Knowledge for Ignition, Acoustics and Instabilities)
LACOM	(Multiphase Combustion Laboratory)
LAERTE	(Laboratory for the study of reacting flows and their investigation techniques)
LDA	(Laser Doppler Anemometry)
LDV	(Laser Doppler Velocimetry)
LEMCOTEC	(Low EMission COre TEChnnologies)
LIF	(Laser Induced Fluorescence)
LOPOCOTEP	(LOw POllutant COmbustor TEchnology Program)
LOTAR	(Liquid-fueled ONERA ThermoAcoustic Rig)
LPP	(Lean Premixed Prevaporized)
MERCATO	(Experimental Means for Research in Air-breathing Combustion by Optical Techniques)
MICADO	(Investigation Means for Air-breathing Combustion using Optical Diagnostics)
MSFI	(Multi Stage Fuel Injection)
NEWAC	(NEW Aeroengine Core Concepts)
OPR	(Overall Pressure Ratio)
PDA	(Phase Doppler Anemometry)

PDI	(Phase Doppler Interferometry)
PIV	(Particle Imaging Velocimetry)
PRECCINSTA	(PREdiction and Control of Combustion INSTAbilities for industrial gas turbines
RANS	(Reynolds Averaged Navier Stokes)
RQL	(Rich Quench Lean)
SIA-TEAM	(Soot In Aeronautics)
SRR	(Standard Rainbow Refractometry)
TECC-AE	(Technology Enhancement for Clean Combustion in Aero-Engines)
TLC	(Towards Lean Combustion)
TOSCA	(Technologies for injection System Operability in Aeronautical Combustors)
UV	(UltraViolet)

AUTHORS

Alain Cochet graduated as an Engineer in 1977 from ENSAM ("Ecole Nationale Supérieure des Arts et métiers") and in 1978 from ESTA ("Ecole Spéciale des Techniques Aérospatiales"). He joined Onera in 1980 as a research engineer in the Energetics Department. His main activity was in experimental studies related to ducted rocket and ramjet propulsion. In 1990, he was named head of the "Ramjet and Aeronautical Combustor Division". Then later, in 1998, he was named head of the "Air-breathing Propulsion Research Unit" of the Fundamental and Applied Energetics Department, which is his current position.

Virginel Bodoc graduated from the Military Technical Academy of Bucharest in 2003. Over the following years he worked as a Research Engineer at the Military Equipment and Technology Research Agency of Bucharest. After receiving a Master Degree Diploma from the INP Toulouse in 2007, he joined ONERA as a Marie Curie doctoral fellow and defended his PhD in 2011. Since 2010, he has been involved in various research projects conducted at the LACOM combustion laboratory (Fauga-Mauzac center). Within the research team, his main field of activity is the development and application of optical measurement techniques (PIV, PDA/LDA, LIF, Rainbow Refractometry and Infrared Absorption) to characterize reacting and non-reacting gas/droplet flows. Since 2013, he has been in charge of the LACOM facility technical survey.

Christophe Brossard received his Engineering Degree in Energetics from the "Institut National des Sciences Appliquées" in Rouen, France, in 1991. He received his Doctorate Degree in Energetics from the University of Rouen in 1995. From 1996 to 2001, he worked at the Propulsion Engineering Research Center at Pennsylvania State University, USA. Since 2001, he has worked as a research scientist in the Fundamental an Applied Energetics Department at ONERA, focusing on flow field characterization, in different non-reacting and reacting environments, using optical laser-based diagnostic techniques (PIV, LDV, PDA, PLIF).

Olivier Dessornes graduated from the French engineering school ESTACA in 1990. He joined ONERA in 1990 where he is a research engineer working in the Fundamental and Applied Energetics Department (DEFA). He is mostly involved in experimental activities. His current fields of interest are scramjet propulsion, energy micro sources and hybrid propulsion.

Christian Guin graduated as Engineer in 1980 from CNAM (Conservatoire National des Arts et Métiers). He joined ONERA in 1974 as a technician and, since 1980, has worked as a research engineer in the Energetics Department. He has been involved in experimental combustion studies for ducted rockets and ramjets and then, since 1995, in new turbojet combustor concepts. He developed and has been in charge of the M1 high pressure test facility, devoted to the turbojet combustor studies at ONERA.

Renaud Lecourt graduated as Engineer from the "Ecole Centrale de Lyon" in 1978, and obtained a Masters Degree in Aerospace Sciences from the "Ecole Nationale Supérieure de l'Aéronautique et de l'Espace" in 1979. He has been a research engineer at ONERA for 35 years. He worked in liquid rocket propulsion, on injection and combustion, for 20 years and is now working on the same topics in air-breathing propulsion. He has a vast experience in optical diagnostics (PTV, PIV, LDA/PDA, laser sheet technique) under difficult conditions (high pressure and temperature conditions, burning sprays, vacuum, downstream from actual injectors).

Mikael ORAIN, MSc in Physics (1996), Diploma in Energetics and Fluid Mechanics from Coria (1997), PhD in Mechanical Engineering from the Imperial College London (2001). Research scientist at Onera in charge of developing laser-based techniques for the measurement of temperature and species concentration in reacting and non-reacting multiphase flows, with a specific emphasis on applications to large-scale facilities representative of aircraft or rocket engines. He has been involved in several National (ASTRA, BIOPTIC, EGISTHE, ECLAIR) and European research programs (TLC, NEWAC, KIAI, LEMCOTEC, IMPACT-AE, FACTOR).

Axel Vincent-Randonnier graduated from Université Pierre et Marie Curie where he obtained MSc and PhD degrees in Energetics and Process Engineering in 2002. He joined ONERA in 2004 for post-doctoral activities on plasma assisted combustion. Since 2006, he has been in charge of LAERTE subsonic and supersonic combustion facilities at ONERA – Palaiseau Center. Since 2012, he has been in charge of the MICADO project aimed at developing a new test rig dedicated to the study of high-pressure air-breathing combustion with optical diagnostics.

F. Grisch, A. Boukhalfa, G. Cabot, B. Renou, A. Vandel
(CORIA-UMR 6614- Normandie Université, CNRS-Université et INSA de Rouen)

E-mail : frederic.grisch@coria.fr

DOI : 10.12762/2016.AL11-02

CORIA Aeronautical Combustion Facilities and Associated Optical Diagnostics

The scientific activities presented in this article are within the field of the design of new concepts of combustion chambers and the exploration of their benefits to increase the combustion and environmental efficiencies of advanced air-breathing propulsion systems. These scientific activities are performed in the "*Complexe de Recherche Interprofessionnel en Aérothermochimie*" (CORIA) research laboratory, a joint research institute organized between the CNRS, the University of Rouen and the INSA-Rouen Engineering School. CORIA contributes through its recognized expertise in numerical simulation, optical diagnostic measurements and experiments in large-scale combustors to improving the understanding of multi-scale multi-physics physical mechanisms governing the lean combustion of future combustion chambers. In this context, the "*Centre de Combustion Avancée pour l'Aéronautique du Futur*" (C-CAAF) recently created at CORIA is aimed at providing:

- An instrumentation and optical diagnostic platform gathering various laser/optical diagnostic techniques (PIV, LDV for the characterization of the aerodynamic field, PDPA, GRT for the characterization of the distribution of fuel droplets, CARS for measuring the thermal field and main species concentration, OH-PLIF and Schlieren for analyzing the flame structure, LII, NO-PLIF, CO-PLIF for measuring pollutants in the flame, etc.). These laser/optical diagnostic techniques are used to provide unique laboratory tools to perform time-resolved, simultaneous, multidimensional measurements of scalar parameters governing turbulent and multi-phase combustion. Furthermore, these diagnostic tools can be combined to obtain detailed correlations on these scalar parameters.

- Multiple set-ups, from academic burners to complex combustors operating at high pressures. Through the perfect control of their operating conditions, academic burners are designed to assist in the development and validation of innovative optical diagnostic tools. They also provide a precise determination of the relevant chemical and physical parameters, enabling conclusions to be drawn about the underlying partly-coupled combustion processes. Technical combustion chambers are developed to provide a high-fidelity experimental database, in order to improve the innovative architectures of ultra-low NOx aeronautical injectors operating with real multi-component liquid fuels (kerosene, alternative fuels, biofuels, etc.), to identify the interaction mechanisms between several fuel injection systems and to validate the predictive capability of gas turbine combustion models.

Introduction

Future aero-engines need to be affordable, highly efficient and environmentally friendly. NOx strict regulations on emissions coming into effect in 2020 (ACARE regulations) will demand further NOx and fuel burn reductions. Combined with increased pressure ratios and turbine inlet temperatures for improving the efficiency of engine components, significant steps must be taken to push these modern combustion technologies to their limits with regard to their ability to reduce pollutant emissions and preserve engine operability (combustion efficiency, ignition and light around altitude restart and pull-away capability, combustion dynamics in terms of noise an combustion instabilities). In order to meet its operational requirements, lean combustion has been selected by aeronautical manufacturers as a promising ultra-Low NOx combustion concept for aero-engine combustors. However, the success of these innovative combustion techniques strongly depends on many parameters, such as the architecture of the combustor and the design of the fuel injection system, which affect many physical mechanisms (atomization, fuel evaporation, fuel/air mixing, flame stabilization, pollutant formation, etc.).

Consequently, it is mandatory to investigate with the greatest detail most of the various physical and chemical mechanisms that govern turbulent combustion in relation with the architecture of the injection device.

In this context, the C-CAAF (*Centre de Combustion Avancée pour l'Aéronautique du Futur*) Research center, which gathers the French CORIA Research Laboratory, the public engineering-funded school INSA-Rouen and the industrial partner SAFRAN-Tech, has been created to establish a center for technological innovations in the field of aeronautical combustion systems. This platform supports the experimental and computational study of fundamental combustion phenomena, in order to expand the scientific knowledge base, validate combustor-design codes, improve the combustion performances, reduce the pollutant emissions and enhance the affordability, maintainability and reliability of current and future generation propulsion systems for commercial aviation. This complex state-of-the-art provides unique laboratory tools for the experimental characterization of combustion through the development, demonstration and application of advanced laser-based/optical diagnostic techniques on various test benches allowing academic, as well as applied experiments. These capabilities are complemented by a series of specialized modeling and simulation methodologies for assessing and predicting the detailed chemistry and physics of combustion processes occurring in aero-engine combustors. Another objective of this center is also to be recognized as a center of expertise and experimental resources and unique scientific computing in Europe gathering European R&D centers in the field of aeronautical combustion.

With this purpose, the recent educational and research industrial chair "Powering the future with Clean and Efficient Aero-engines" (PERCEVAL) has been initiated by CORIA in close cooperation with the aeronautical manufacturer SAFRAN Tech, the French National Research Agency (ANR) and ONERA to assess the optimization of combustion efficiency and reduction of pollutant emissions of innovative stage lean combustors. The methodology adopted to support this research includes 1) the optimization of the architecture of innovative injection devices by CFD, 2) the development of innovative and reliable optical diagnostics to obtain spatial and temporal quantitative measurements of various scalar parameters (velocity, temperature, species concentration, etc.) in high-pressure environments, 3) a detailed experimental investigation of the underlying generating mechanisms with non-intrusive optical measurement techniques under operating conditions relevant to aero-engines and 4) high-performance computing of the experiments with high-resolution time-resolved LES solvers (AVBP and YALES 2). In this scientific experimental activity, the research topics investigated in detail are focused on the improved understanding of high-pressure turbulent two-phase flow combustion and include:

- Fuel injection,
- Fuel evaporation,
- Vapor fuel/air mixing,
- Aerodynamics,
- Turbulence,
- Ignition,
- Flame structure & flame dynamics,
- Combustion instabilities,
- Flame/wall interaction,
- Pollutant formation (CO, NOx and soot) and exhaust emissions.

These phenomena are understandable by using a variety of optical measurements based on various light/matter interactions. For this purpose, the CORIA features a large array of advanced laser technologies, including many one-of-a-kind optical sources and detectors. The laser sources provide a broad spectral coverage, from the ultraviolet through the visible part of the spectrum to the near infrared, for flow visualization and spectroscopic investigations of complex reacting and non-reacting flowfields. Continuous-wave and pulsed (nano-, pico-, and femtosecond) laser sources are used, in conjunction with various scientific-grade cameras and ultrafast imaging devices in order to provide tremendous spatial and temporal resolution and data acquisition bandwidth for critical applications. A host of linear and nonlinear laser based/optical techniques have been specially developed and applied, in order to perform non-intrusive instantaneous measurements in multi-phase reacting flows of time-resolved, simultaneous, multidimensional flowfield and scalar distributions. The scalars of interest include temperature, fluid velocity, spray characteristics, molecular fuel composition, key intermediate species and pollutants (CO, NO and soot). Optical diagnostics are suited for high-pressure (0.1 – 5.0 MPa) and high temperature (300 – 2500 K) operating conditions. The optical techniques include emission spectroscopy (temperature, species composition), planar laser-induced fluorescence (PLIF) (flame structure, temperature minor species and fuel concentration, NO and CO pollutants), laser-induced incandescence (LII) (2D soot distribution), planar Rayleigh scattering (PRS) (density and temperature fields), reactive Mie scattering (RMS) (spray pattern), laser Doppler velocimetry (LDV) (velocity, turbulence properties), particle-image velocimetry (PIV) (2D and 3D velocity distribution), spontaneous Raman scattering spectroscopy (temperature, main species concentration, mixture fraction), coherent anti-Stokes Raman scattering spectroscopy (CARS) (temperature, main species concentration), phase Doppler particle analysis (PDPA) (particle size distribution), femtosecond ballistic imaging (velocity and structure of dense spray), ultrafast pump-probe spectroscopy and femtosecond time-resolved laser-induced fluorescence (temperature, species concentration), the global rainbow scattering technique (size and temperature of droplets), advanced techniques for Schlieren reconstruction (flow visualization), high-speed imaging and data analysis at repetition rates of up to 10 kHz (emission, PLIF, PIV) and high-speed fs/ps CARS and fs/ps LIF (10 kHz).

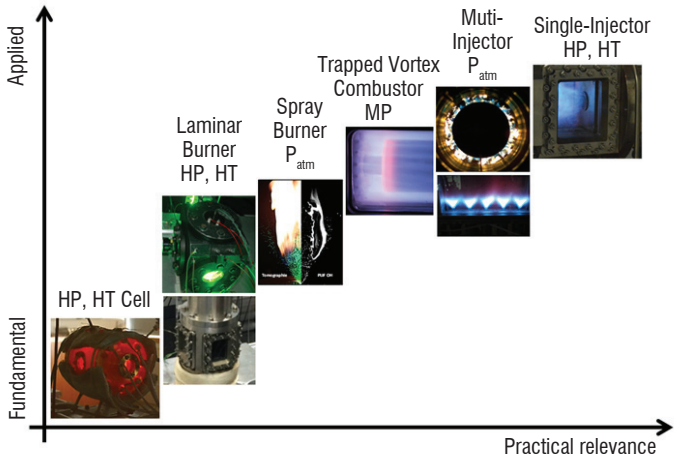

Figure 1 - Presentation of the experimental facilities with respect to the practical relevance

Test and validation cases of engine components must be performed in high-pressure high-temperature combustion facilities, with large optical accesses, in which detailed investigations of nonreactive and reactive flow fields are feasible with reliable measurement techniques. All of the experiments must also be carried out under operating conditions relevant to aero-engines, with well-controlled boundary conditions being required to accurately validate the numerical simulations. In order to do this, CORIA has adopted a stepped strategy in combustion devices and aeronautical research, which consists in systematically studying relevant combustion phenomena throughout well-balanced sets of test rigs. Figure 1 shows the experimental setups selected for this purpose, ranking the level of their practical relevance and experimental level of accessibility. In the following, these different set-ups are presented and some available results are also discussed.

High-pressure optical cell

In modern combustion chambers, evaporation and mixing effects of multi-component fuels are highly relevant. While multi-component fuel evaporation models are being developed to predict these physical phenomena, there is still a serious lack of experimental information providing guidance on the role of preferential evaporation of the fuel components during injection. Consequently, it is of great interest to conceive measurement strategies able to assess this effect on the resulting fuel/air mixture. This research is aimed at proposing innovative measurement strategies for investigating the role of multi-component fuel volatility in fuel/air preparation [1-3]. The technique is based on the identification of suitable fuel/fluorescent tracer mixtures for the study of the evaporation of multi-component fuels, including standard petroleum-derived fuels and biofuels. In a general manner, the methodology developed in the current study consists in mixing several fluorescent markers within the multi-component fuel, in order to track in real-time the evaporation of various fuel volatility classes. Fluorescent tracers were selected in order to ensure that their

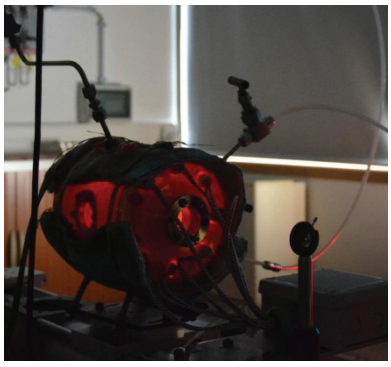

Figure 2 - High-Pressure Optical Cell
pressure range = 0.1 – 4.0 MPa, temperature range = 300 - 1000 K [4]

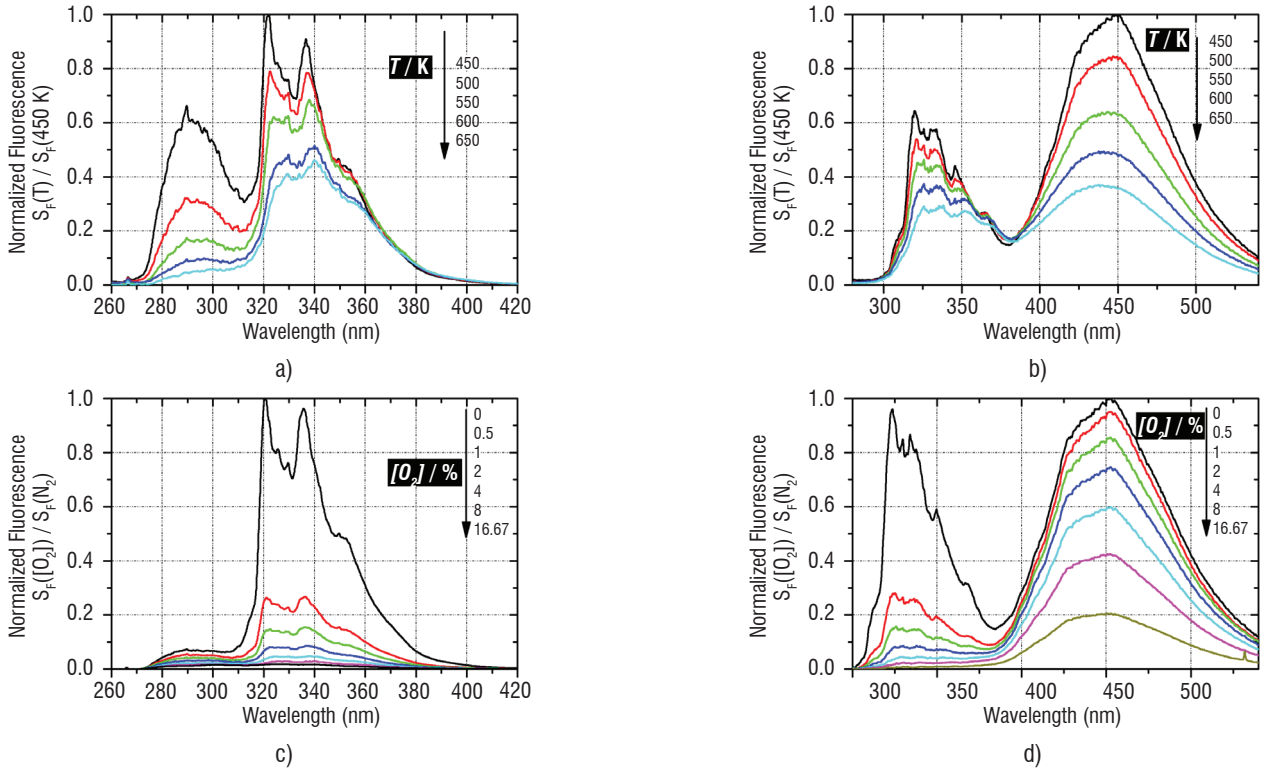

Figure 3 - Evolution as a function of temperature (a), (b) and oxygen concentration (c), (d) of the Fluorescence of 1,2,4-trimethylbenzene/acenapthtene and napthtalene/fluoranthene diluted in the BTL and diesel surrogate fuels respectively. The pressure is 0.1 MPa.

co-evaporative characteristics with the fuel volatility classes (i.e., boiling points) are respected and their fluorescence emission spectra are fully separated, while also providing high sensitivities with temperature and species composition. This selection is obtained from spectroscopic parameters (fluorescence, absorption, etc.) of various organic molecules recorded in a high-pressure high-temperature optical cell, in which the operating conditions of the experiments are well-controlled (Fig. 2).

In order to illustrate some of these experiments, fluorescence measurements on suitable tracer mixtures enabling the analysis of the evaporation of multi-component fuels including standard petroleum-derived diesel and Biomass-to-Fuel (BtL) fuels are presented [5]. Among the fluorescent organic molecules, the aromatic mixtures 1,2,4-trimethylbenzene/acenapthtene and napthtalene/fluoranthene were selected to separately track the co-evaporation of the lightest and heaviest products within BtL and diesel fuels respectively. In order to evaluate the effects of temperature and oxygen quenching on the photophysical properties of these tracers, the fluorescence spectra were recorded in the high-pressure optical cell under various conditions. Fig. 3 depicts results for both aromatic mixtures in cases in which a 266 nm excitation laser wavelength is used. As observed in Fig. 2, the resulting fluorescence spectra of both tracers appear in two distinct spectral domains, easily separated by the use of convenient optical filters. Furthermore, the intensity of the fluorescence emission displays different trends with temperature and oxygen concentration. Similar dependences with pressure then offer opportunities for imaging scalar parameters, such as the equivalence ratio and temperature during BtL and diesel spray evaporation via a dual-channel filtered detection of the resulting fluorescence tracers [5].

This optical cell is also used to evaluate the performances of various laser diagnostic techniques (CARS, PLIF, Spontaneous Raman scattering, etc.) and to assess their accuracy and their quality under various thermodynamic conditions [6]. As an illustration of these studies, the detection of nitric oxide by LIF was developed because NO is considered as one of the key combustion-generated pollutants. For this purpose, LIF experiments were conducted in the high-pressure optical cell, in order to record and quantify the behavior of NO fluorescence with scalar parameters like temperature, pressure and species composition. As an example, a portion of the NO (0,0) excitation fluorescence spectra is shown in Fig. 4 for various temperature and pressure conditions. Here, there are several features that remain fairly well isolated at high pressures, although their peaks are substantially reduced between 0.1 and 0.5 MPa. As identified in the figure, not all of these features are single lines; for instance, the feature at 225.63 nm is $Q_{21}(20.5) + P_{21} + R_{21}(10.5)$. Although not a single transition, this group of rotational transitions is still suitable for both validation experiments, as well as PLIF imaging, in which a simulation model is to be applied to render the images quantitative.

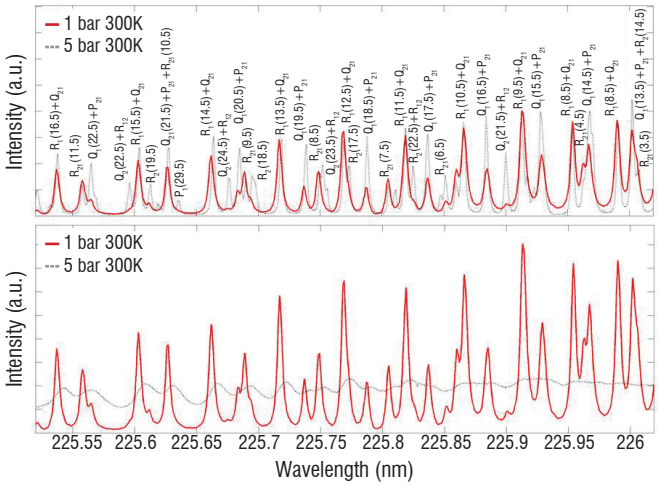

Figure 4 - Excitation fluorescence spectra of NO transitions near 226 nm at (top) T= 300 and 800 K, P=0.1 MPa, (bottom) 0.1 and 0.5 MPa, T=300 K.

The knowledge of the fluorescence emission spectra of NO in the 0.1 - 2.0 MPa pressure range (Fig. 5) has furthermore facilitated the development of a comprehensive experimental database so that the fluorescence signal simulation results with an in-house fluorescence software application can be compared under a wide range of thermodynamic conditions [6]. Furthermore, the knowledge of the evolution of the dependences of the fluorescence signal on both temperature and species composition (especially O_2 concentration) enables the implementation of new NO measurement strategies suitable for quantifying the NO fluorescence signals in terms of species concentration in combustion engine experiments.

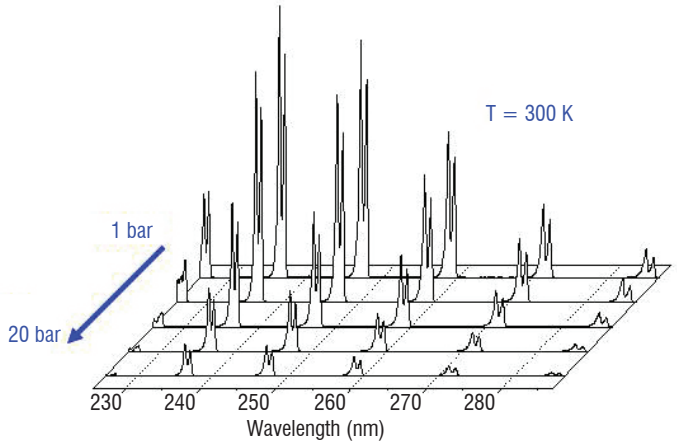

Figure 5 - Emission fluorescence spectra of NO as a function of pressure; T = 300K.

High-pressure laminar burners

The purpose of this scientific activity is to give experimental insight about the detailed analysis of the pollutant formation mechanisms and flame stability criteria during the combustion of multi-component fuels. In order to do this, a current approach used to reduce pollutant emissions is to burn the fuel/air mixture under lean conditions. This solution is not without consequences for the flame dynamics, which can produce combustion instabilities leading to flashback. One approach to quantify the flame stability is then to know the laminar burning velocity. This parameter is also useful for kinetic scheme validation and for qualifying turbulent flame structure and turbulent flame velocity. Another physical parameter to be considered is the chemical composition of multi-component fuels. Given that their chemical kinetic models are not yet optimized for real operating conditions, their effects on combustion instability production and pollutant formation are still imprecise. Two academic high-pressure setups have been developed to be used to develop criteria regarding flame stability and to validate the performances of the fuel kinetic model under those conditions (Fig. 6).

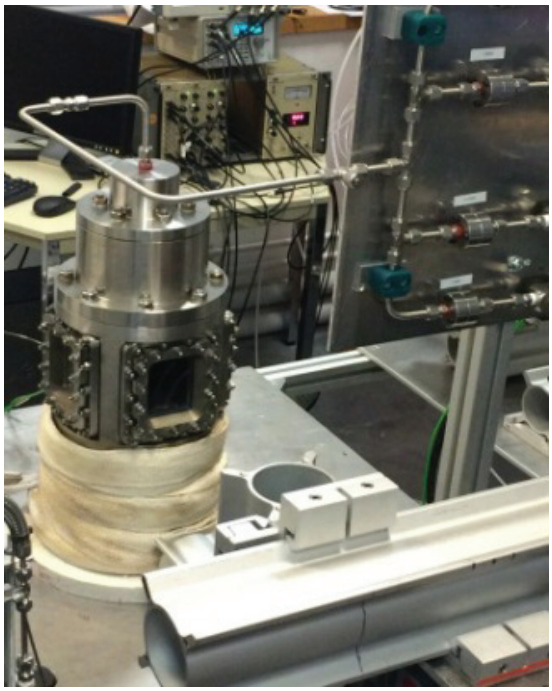

a)

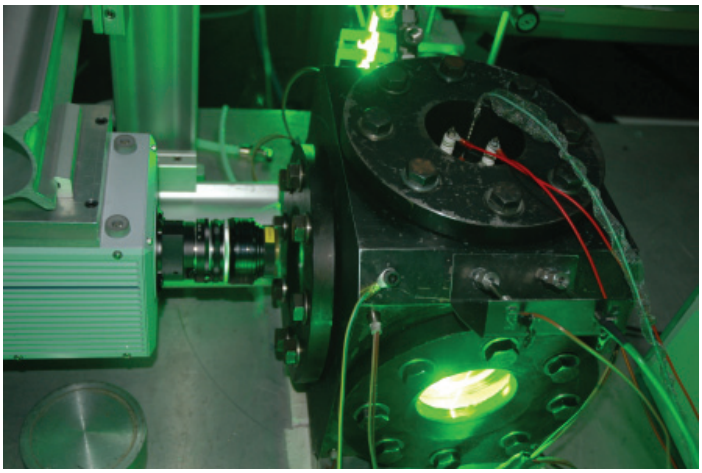

b)

Figure 6 - (a) Laminar high-pressure burner operating at pressures of up to 3.0 Mpa and an inlet temperature of 600K. (b) Spherical bomb operating at pressures of up to 2.0 Mpa and T=580K..

The first high-pressure burner is designed to measure the behavior of the laminar burning velocity with pressure (0.1-3.0 MPa), equivalence ratio (0.5 – 1.4) and inlet temperature (300 – 600 K). An axisymmetric premixed burner was designed to generate a steady conical laminar premixed flame, stabilized on the outlet of a contoured nozzle in a high pressure vessel [7]. The high-pressure vessel, constructed out of stainless steel, has an inner surface of 100 x 100 mm^2 and a length of 160 mm (Fig. 6a). It is equipped with four large UV quartz optical windows customized to probe the flame with optical imaging diagnostics. Preheating of the pressure vessel is performed using electrical wire heaters positioned around its external surface. The burner can operate with a large variety of gaseous fuels (CH_4, C_3H_8, etc.) or liquid fuels (kerosene, biofuel, diesel, gasoline, etc.). Liquid fuel was pressurized in a 1.0 liter tank connected to a liquid flow-meter associated with a Controlled Evaporator and Mixer (Bronkhorst), which heats and mixes fuel vapor with N_2 inert carrier gas at controlled mass flow rates and temperature. The CEM outlet is connected to a stainless steel mixing cell preheated at a temperature ranging between 373 and 600 K, and controlled with a type K thermocouple in order to prevent any condensation of the fuel vapor. Additional nitrogen and oxygen initially mixed and preheated by a heater before the mixing cell inlet are used to reproduce the synthetic species composition of air and to modify the equivalence ratio of the heated fuel vapor/air mixture. The non-invasive diagnostics used to perform these experiments are the Schlieren, OH* chemiluminescence and OH-PLIF diagnostics to measure the laminar flame velocity, NO- and CO-PLIF to probe the gaseous pollutants, Coherent anti-Stokes Raman scattering to measure the temperature in the exhaust gases and 2-λ Indium laser-induced fluorescence to measure the 2D temperature distribution in the fresh gases.

As an illustration of the performances of the high-pressure burner, the laminar burning velocities for two aviation multi-component fuels are presented in this section [8]. The multi-component fuels investigated are the Jet A-1 fuel, which represents the common aviation commercial fuel, and the LUCHE surrogate jet fuel consisting in a reduced mixture of n-decane ($C_{10}H_{22}$), aromatic (C_9H_{12}) and naphthenic (C_9H_{18}) molecules. Measurements of laminar burning velocities are performed using two optical imaging techniques, the OH* chemiluminescence and the OH planar laser induced fluorescence (OH-PLIF) diagnostic. For instance, images of the laminar flames produced in the high-pressure burner and recorded with OH-PLIF are shown in Fig. 7. From each image, the laminar burning velocity is then deduced from the flame surface area methodology.

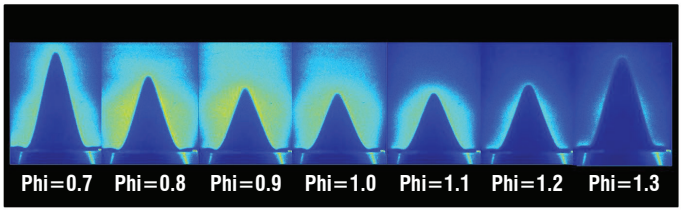

Figure 7 - Evolution of the structure of the laminar flame of a premixed kerosene/air combustion for various equivalence ratios. P=0.5 MPa, T_{air}= 400 K.

As shown in Fig. 8a, the comparison between the burning velocities of Jet A-1/air and LUCHE fuel/air mixtures, recorded at atmospheric pressure and a preheating temperature of 400 K, reveals that the laminar burning velocity of the surrogate fuel is slightly greater than the laminar flame speed for the Jet-A1 fuel in situations where the equivalence ratio ranges between 0.8 and 1.1. For the other equivalence ratios, both values are found to be equivalent. The same tendency is also observed for higher pressure conditions (Fig. 8b). For instance, the laminar flame speeds recorded in the 0.1- 0.8 MPa pressure range differ slightly when $\phi = 0.7$, whereas noticeable discrepancies can be observed for $\phi = 0.8$. These results enable us to draw conclusions regarding the performance of the chemical kinetic mechanism of the LUCHE surrogate jet fuel to simulate the combustion of Jet-A1 commercial fuel.

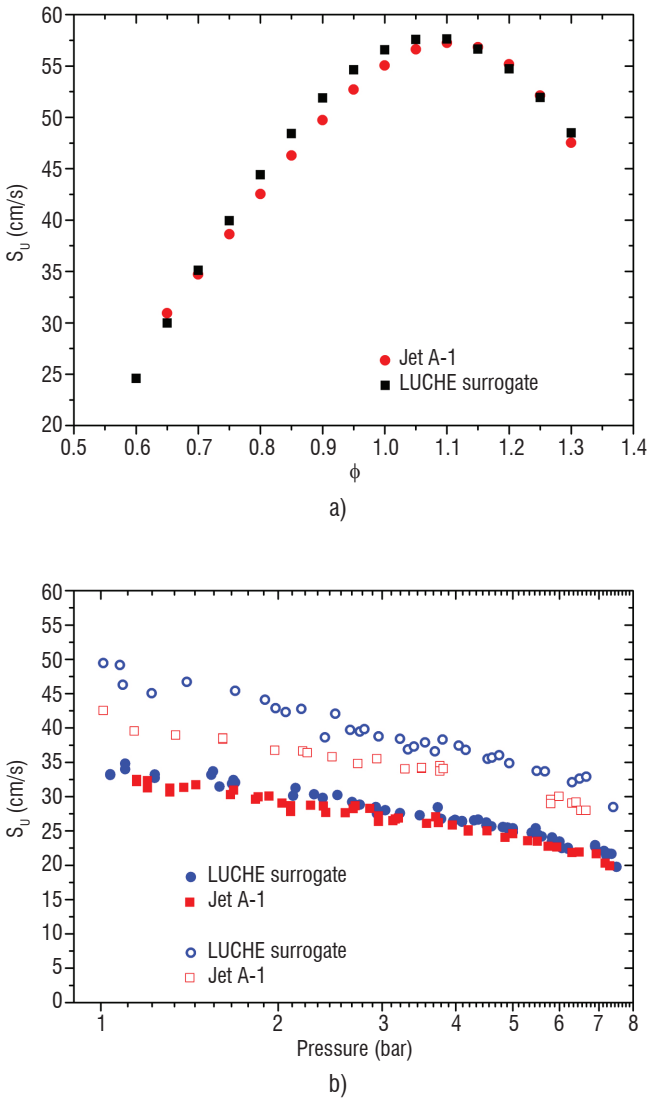

Figure 8 - (a) Evolution of the laminar flame speed as a function of the equivalence ratio for Jet A1 and LUCHE surrogate fuels, P=0.1 MPa (b) Behavior of the laminar flame speed of Jet A1 and LUCHE surrogate fuels as a function of pressure, T=400 K.

The second experimental facility is a spherical closed vessel that enables stretched laminar flame speeds and the associated Markstein lengths of a selection of hydrocarbon fuels (Fig. 6b) to be determined. Experiments can be performed under thermodynamic conditions close to those encountered in internal combustion engines (2.0 MPa and maximum temperature of 573 K). The radius of the inner chamber is 85 mm and the inner volume of the stainless steel combustion chamber is 2.6 l. Two types of fuels, gaseous or liquid, can be used. Fuels that are gaseous under ambient conditions are loaded directly from bottles through mass controllers. Liquid fuels are first vaporized in a heated chamber by using a controlled evaporator mixer and then loaded through heated lines into the vessel. In order to obtain a homogeneous mixture, all gases are premixed in a tank before injection into the combustion chamber and the equivalence ratio of the mixture is measured and regulated by Coriolis or thermal mass flow controllers. An electrical heating system regulates the temperature of the mixing tank and of the combustion chamber. The compressed fuel/air mixture is supplied continuously from the bottom of the combustion chamber. Ignition takes place 1 min later, in order to avoid any flow perturbation during the flame propagation. The combustible mixture is spark-ignited at the center of this chamber by two stainless steel electrodes linked to a capacitive discharge ignition system using minimum spark energies to avoid ignition disturbances. During the ignition process, the evolution of the chamber pressure is measured by a dynamic pressure transducer and both the time evolution of the flame radius and the spatial fresh gas velocity are obtained by high speed tomography [9, 10].

Based on a new tool for extracting the laminar burning velocity from the flame propagation speed and the local fresh gas velocity at the entrance of the flame front [10], this facility has been used, among other things, to evaluate the effects of the pressure, equivalence ratio and ethanol mole fraction on laminar burning velocity of isooctane/air flames. This approach gives additional information in terms of flame sensitivity to flame stretch represented by the Markstein length relative to the fresh gases and a direct measurement of the unstretched laminar burning velocity without any assumptions on regarding adiabaticity and regarding the fuel mixture properties. The overall accuracy of the measurements obtained from the repeatability of the experiments was less than ±1.5 cm/s at P = 0.1 MPa and increased with pressure to reach ±3 cm/s at P = 1 MPa. Fundamental burning velocities and associated Markstein lengths have been experimentally determined and compared with numerical results. A globally good agreement was obtained with the literature data for pure fuels [11]. A general correlation has been proposed to express the effect of the pressure, equivalence ratio and ethanol mole fraction in isooctane at a temperature of 373 K. The accuracy of this correlation and the ranges of validity are provided in Figure 9. Giving the potential of this facility, the matrix of experimental conditions could be completed to include the temperature effect, in order to achieve thermodynamical conditions similar to those encountered in SI engines.

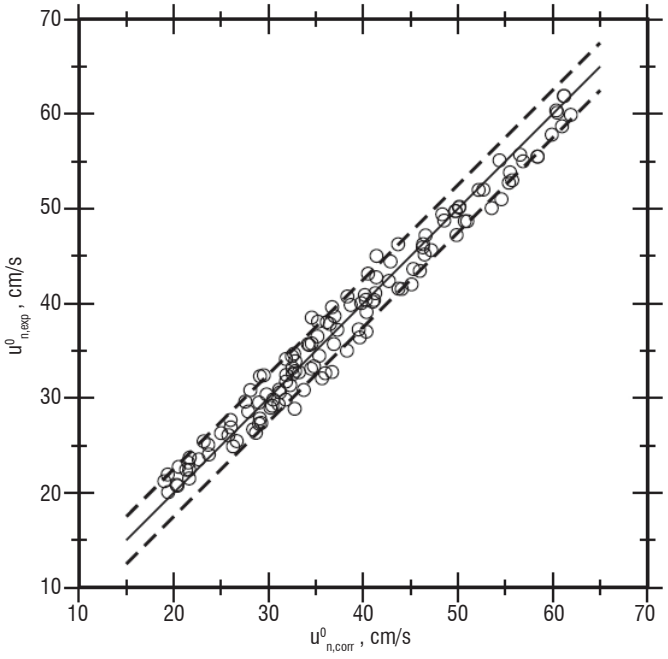

Figure 9 - Burning velocity obtained by correlation compared with the experimental data. The dashed lines indicate two-sigma uncertainties. The solid line indicates the equality between measured laminar burning velocity and the values predicted by the correlation. Reprinted from [11].

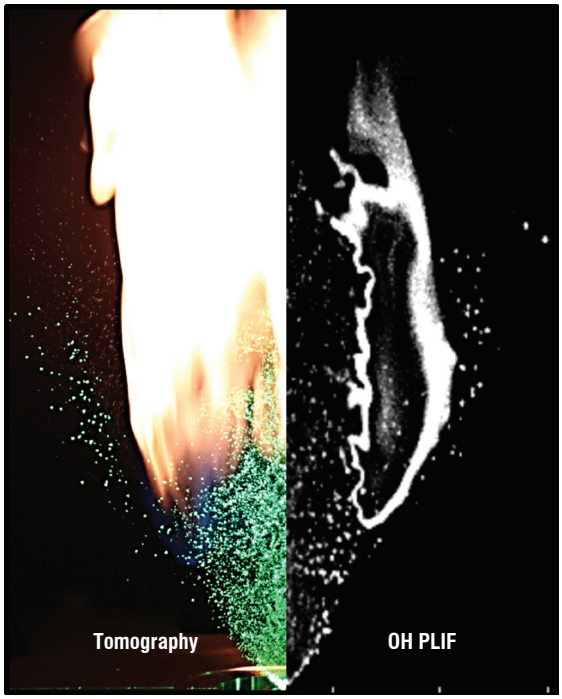

a)

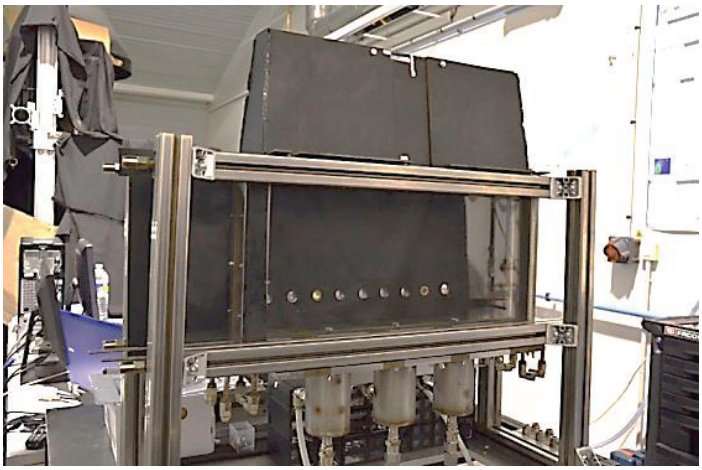

b)

Figure 10 - (a) Spray jet flame burner. (b) Multi-injector KIAI burner

Ignition and lightening around

In many combustion applications, such as during the relight of an aviation gas turbine during flight, the phenomenon of ignition from a localized spark is important. Understanding the mechanisms involved can provide tools to alter the design of gas turbine burners and combustion chambers for improved flight safety and fuel efficiency. In this context, two burners were dedicated to the experimental study of ignition phenomena in confined swirled flows, operating in gaseous or two-phase flows (Fig. 10). The operating conditions are relevant to aeronautical conditions and the various ignition steps (flame kernel ignition, ignition and flame stabilization at the exit of the first injector and light around) are studied accurately by means of spatially and temporally resolved optical diagnostics.

The first burner consists of one liquid fuel injector, with or without confinement (Fig. 10a), and ignition can be performed at various locations within the combustion chamber, in order to [12]:

- evaluate the optimal spark location to achieve an efficient burner ignition,
- understand the ignition mechanisms related to the effects of local conditions: turbulence, mixing, fuel evaporation, flame kernels trajectories and ignition scenario.
- achieve extended and accurate experimental databases for a relevant validation of CFD codes dedicated to the design of aeronautical combustion chambers.

The second burner is made of five injection systems (similar to the previous one) with a variable distance between two-successive injectors (Fig. 10b). This facility leads the impact of this distance (which is a key parameter for the design of the combustion chamber) on the mechanism of light around to be identified. These experimental studies are also carried out with the purpose of providing open databases to enable a joint analysis of these phenomena with LES numerical simulations (AVBP or YALES 2 numerical codes) [13]. In order to illustrate these purposes, experimental and numerical approaches (LES) have been conducted simultaneously to analyze the light around phenomena in the multiple-injector burner facility and to evaluate the influence of spacing between two consecutive fuel injectors [13, 14]. Increasing spacing between consecutive injectors directly impacts the flame propagation mode and thus the ignition delay. Two major propagation modes were identified both in LES and experiments. Small spacing (less than 150 mm) enables a purely spanwise, rapid and safe propagation (Fig. 11). A critical distance is identified (160 mm), above which propagation mechanisms begin to change. Above this limit, propagation occurs not only in the spanwise direction, but also in the axial direction. When this distance is further increased, flame propagation becomes mainly axial and full ignition is delayed or fails (seen only in the experiments).

A detailed analysis showed that the various propagation modes where basically driven by two key mechanisms:

- The flame is affected by the flow aerodynamics, which change with the injector spacing. Low spacing flow aerodynamics promote a rapid suction through the swirling motion leading to a spanwise flame propagation mode, while high spacing flow structure changes are favorable to an axial propagation mode. The spanwise propagation mode is associated with a short traveling time of the flame from one injector to the other and a low variability, while the axial propagation mode is characterized by longer propagation times and a much higher variability.
- A thrust effect due to the thermal expansion of the burnt gases has been revealed. It produces a continuous flame progress that modifies the surrounding cold gas flow. It may increase the spanwise velocity and is the major flame propagation mechanism in regions of weak mean flow, such as the LRZ (Lateral Recirculation Zone). These propagation modes result in different overall ignition times, which increase with the injector spacing.

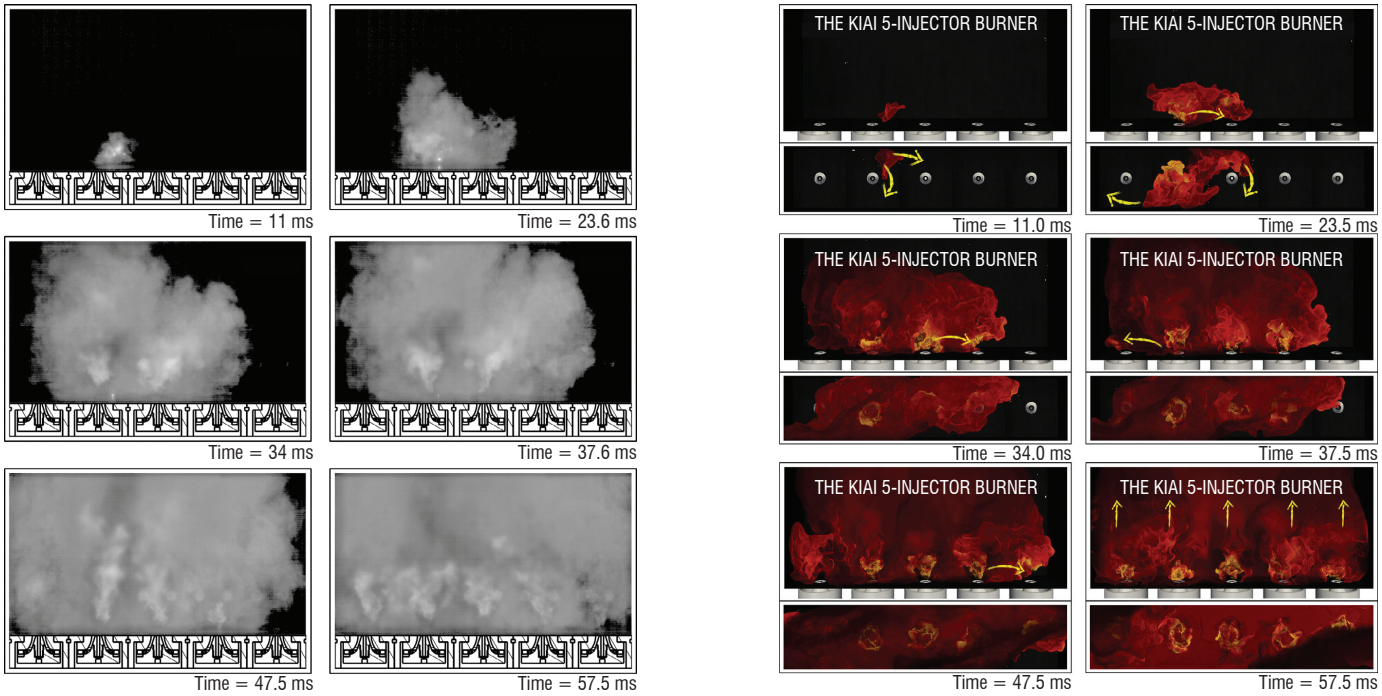

Figure 11 - (Left). High-speed flame emission visualization of the flame showing a spanwise propagation for a small spacing case, 90mm. (Right). Instantaneous snapshots of the same ignition sequence visualized by the volume rendering of heat release, front and top views. Reprinted from [13].

Comparisons between experiments and LES have shown the capability of LES to reproduce ignition sequences, as well as the added value of LES in this ignition process investigation, using the additional data available.

Trapped vortex combustor (TVC)

Flame stability is a key fundamental issue in the design of new aero-engine combustors. In conventional aero-engine combustors, flame stabilization is commonly achieved through the use of a swirler, under which a central recirculation zone is formed to transport hot combustion gases back toward the injection nozzle, thereby providing the heat required to maintain combustion. However, this technology can produce combustion instabilities, especially in lean combustion regimes. In order to overcome these limitations, an innovative burner based on the concept of a trapped vortex combustor (TVC) has been developed (Fig. 12).

The operating conditions of the test rig are controlled up to 500 K, 100 g/s for the air mass flow rate and 0.5 MPa [15 - 17]. This burner uses a cavity in which vortices are trapped to stabilize the flame. The effectiveness of this geometry lies in the presence of a shear layer at the flow separation and significant flow recirculation zones within the cavity. Both contribute to improving the mixing of the burned gases contained in the cavity and the incoming lean mixtures. The cavity-based combustor was experimentally investigated by laser metrology (PIV and CH*-chemiluminescence phases of the pressure signal), in order to analyze the effects of various parameters, such as the geometry of the cavity (height, width) and the fuel injection characteristics (wealth, location of the fuel channel). Recent developments in time-resolved measurement techniques (PIV, OH-PLIF) at 5 kHz repetition rates also provide additional insight into the importance of the shear layer behavior on the flame stability and flame-holding [17]. For example, the interaction of the reactive zone located in the shear layer within the flow dynamics of the three inlets of the TVC was clearly observed and studied in unstable cases (Fig. 13).

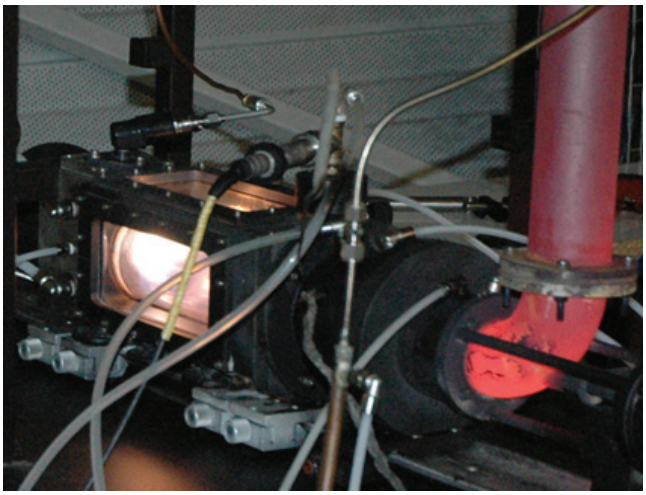

Figure 12 - Test Rig equipped with TVC combustor; Operating conditions: P_{max}=0.5 MPa, T_{inlet}=500 K, Air flowrate: 100 g/s

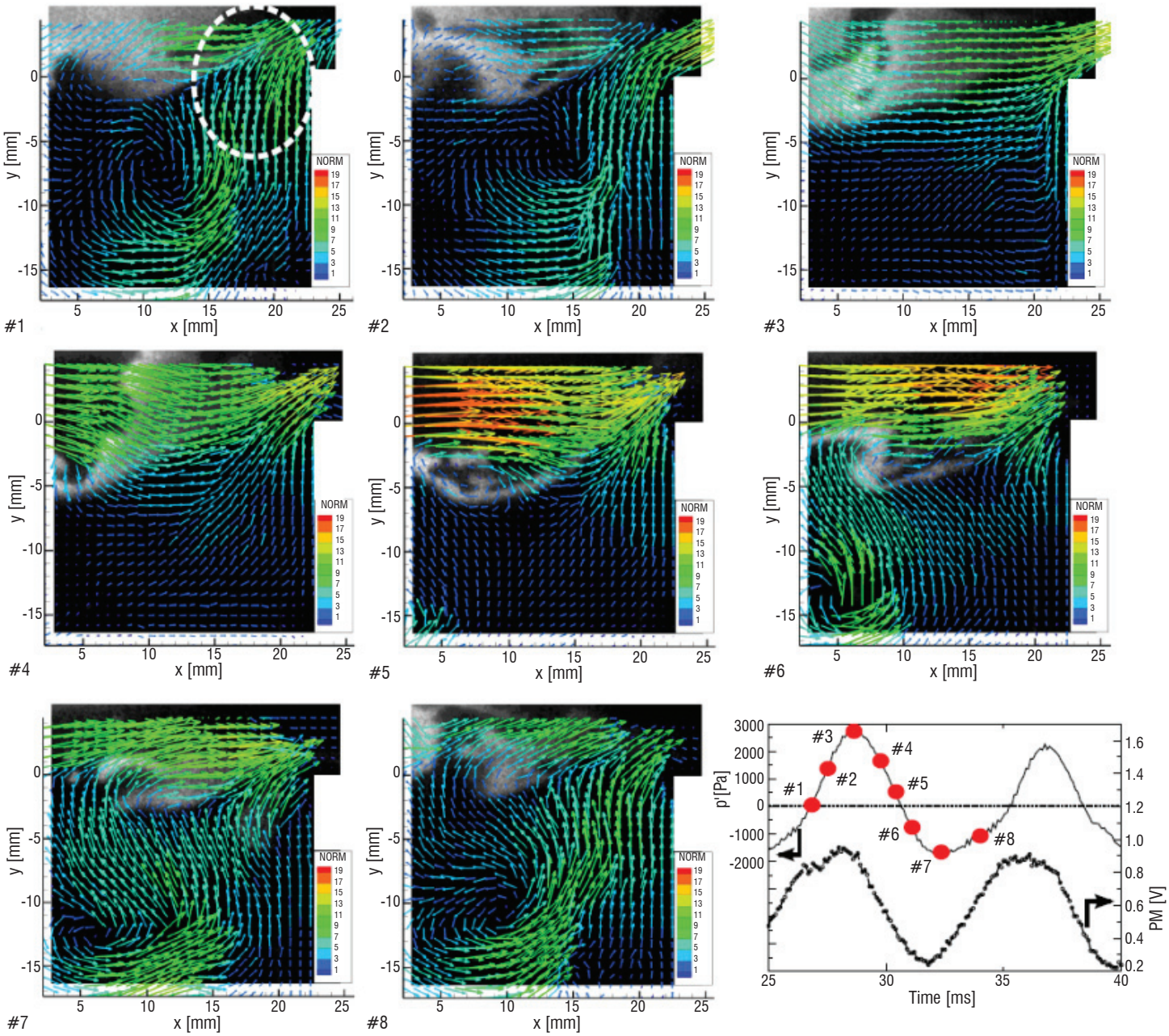

Figure 13 - Simultaneous and time-resolved PIV and OH-PLIF measurements during an unstable pressure cycle (5 kHz) and the corresponding chamber pressure and flame luminosity during the cycle. Reprinted from [17].

Annular combustion chamber (ALICE)

The purpose of the ALICE combustion facility is the development of an atmospheric test rig, in order to evaluate the performances of a real aeronautical combustion chamber (Fig. 14). The setup enables the operating conditions encountered in an Auxiliary Power Unit (APU) and observed during the ignition phase of a helicopter engine at ground level to be faithfully reproduced. Numerous sensors, such as piezo-resistive pressure and thermocouple transducers, enable the measurement of the pressure and temperature conditions inside and at the exit of the combustion chamber. The combustion chamber monitoring allows the following operating conditions: air mass flow rate between 0 and 300 g/s, air inlet temperature between 300 and 480 K and fuel flow rate between 0 and 5 g/s. A gas analyzer is also available for measuring the temperature profiles and/or the chemical composition of the exhaust gases (NO, CO, CO_2, HC, O_2).

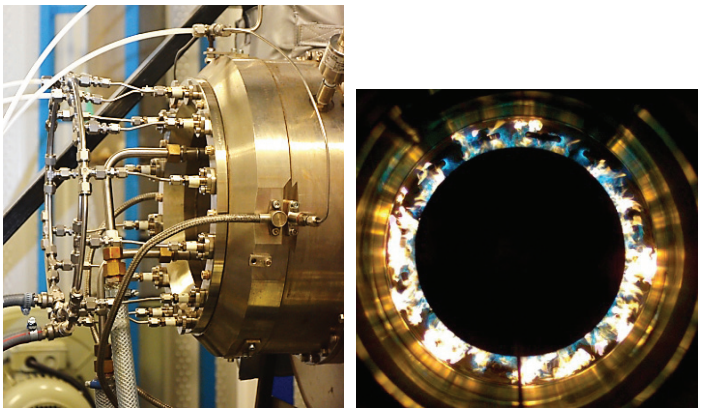

a) b)

Figure 14 - (a) ALICE facility; (b) view of the combustion chamber during lean extinction.

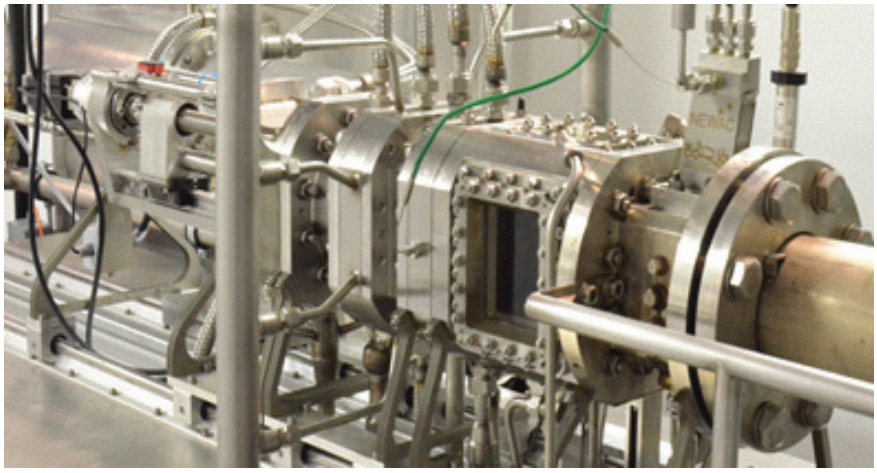

Figure 15 - High-pressure, high-temperature single injector test rig (HERON). Operating conditions: P_{max}=2.0 MPa, T_{inlet}=900K, Air flowrate=300g/s

The objectives of this test rig are mainly to:

- study the various steps of the ignition process (energy deposition, lightening around and flame stabilization) using a high speed flame imaging technique,
- define the combustion chamber stability diagram,
- determine the relevant physical and chemical parameters leading to flame blow off,
- study the effect of the combustion chamber architecture on the combustion efficiency.

HIGH pressure facility for aero-engine combustion (HERON)

Lean-burn involves inherent challenges with respect to weak extinction stability due to fuel air premixing prior to combustion and drives the development of practical solutions with respect to operability, altitude relight and combustion efficiency at fuel staging points. Lean-burn combustors require fuel staging to obtain full combustor operability and to enable typical aero-engine turn-down ratios while burning lean at high power conditions. In order to derive detailed design rules for producing low pollutant emissions, the application of non-intrusive measurement techniques is also a very key challenge within the development process. Conventional tests giving information at the combustor exhaust provide insight into whether a design is successful or not, but they do not tell why. The effort of building optically accessible combustors and probing the flame with optical techniques is thus a promising approach to contribute to the development and optimization of these injection systems [18 - 19]. In order to study such combustion concepts, the new optically accessible test rig HERON (High prEssuRe facility for aerO-eNgine combustion) was designed to operate under the severe pressure and temperature conditions encountered in ground and aeronautical gas turbines. The combustion chamber modules offer a well-adapted infrastructure to the study of industrial fuel injection systems. The combustion chamber performances are optimized to study advanced low-NOx injection systems for helicopters up to their nominal operating ranges and aero-engines injection systems up to 2/3 of their nominal ranges. A fuel preparation skid enables the injection module to be controlled and fed with liquid multi-component fuels (kerosene, biofuel, etc.) or a gaseous fuel mixture (CH_4, CO_2, CO and H_2) with well-controlled chemical composition. The pressure chamber is regulated by an adaptive nozzle up to 2.0 MPa. The mass flow and air temperature are controlled up to 300 g/s and 900 K. HERON is an optically accessible test rig enabling the investigation of a single sector of a combustion chamber. Large optical accesses (100 mm x 80 mm) have been designed, in order to apply all of the optical diagnostics developed in the CORIA Laboratory (Fig. 15).

Among the various studies performed with the HERON test rig, the characterization of innovative low-NOx injection systems (Lean Premixed Prevaporized, Lean Premixed and multi-point injection systems) was investigated. In most cases, the flames are aero-dynamically stabilized by swirl, leading to compact flames over a wide tuning range. Swirl-induced breakdown induces burned gas recirculation to the flame root and the mixing of hot gas and radicals with fresh gas leads to continuous ignition and flame stabilization. The dynamic processes of the flowfield/flame interaction governing such behavior are complex and not well understood today. However, this process can be subject to instabilities in the form of thermoacoustic pulsations, unsteady stabilization or even flame extinction. Until recently, the measurement strategies used to study such processes were commonly focused on laser-based point-wise as well as planar measurements of scalar parameters (velocity, temperature and species concentration) enabling the determination of mean and statistical variations of thermo-dynamic and thermo-chemical properties. However, several questions still remain, which cannot be answered by such temporally non-correlated single-shot information. This concerns, for instance, the origin of the local flame extinction or the evolution of coherent flow field structures and their interplay on the flame front. It is then advantageous to complement these “conventional” measurements by additional information recorded at high repetition rates allowing the tracking of specific flowfield/flame interactions. In order to promote this methodology, particle image velocimetry (PIV) and planar laser-induced fluorescence of the hydroxyl radical (OH-PLIF) were applied simultaneously at 5 kHz in the HERON test rig to study the dynamics of a lean partially-premixed turbulent swirl-stabilized kerosene/air flame from an LP injection system developed by TURBOMECA [20]. For instance, Fig. 16 shows a sequence of four consecutive images from simultaneous PIV and OH-PLIF measurements. The field of view is 60 mm x 50 mm and lies above the nozzle, as indicated in Fig. 16. The images in gray represent the OH-PLIF distributions. The vectors represent the in-plane component of velocity and the colors indicate the out-of-plane motion of the flow field. The simultaneous PIV and OH-PLIF measurements revealed that the reaction zone is

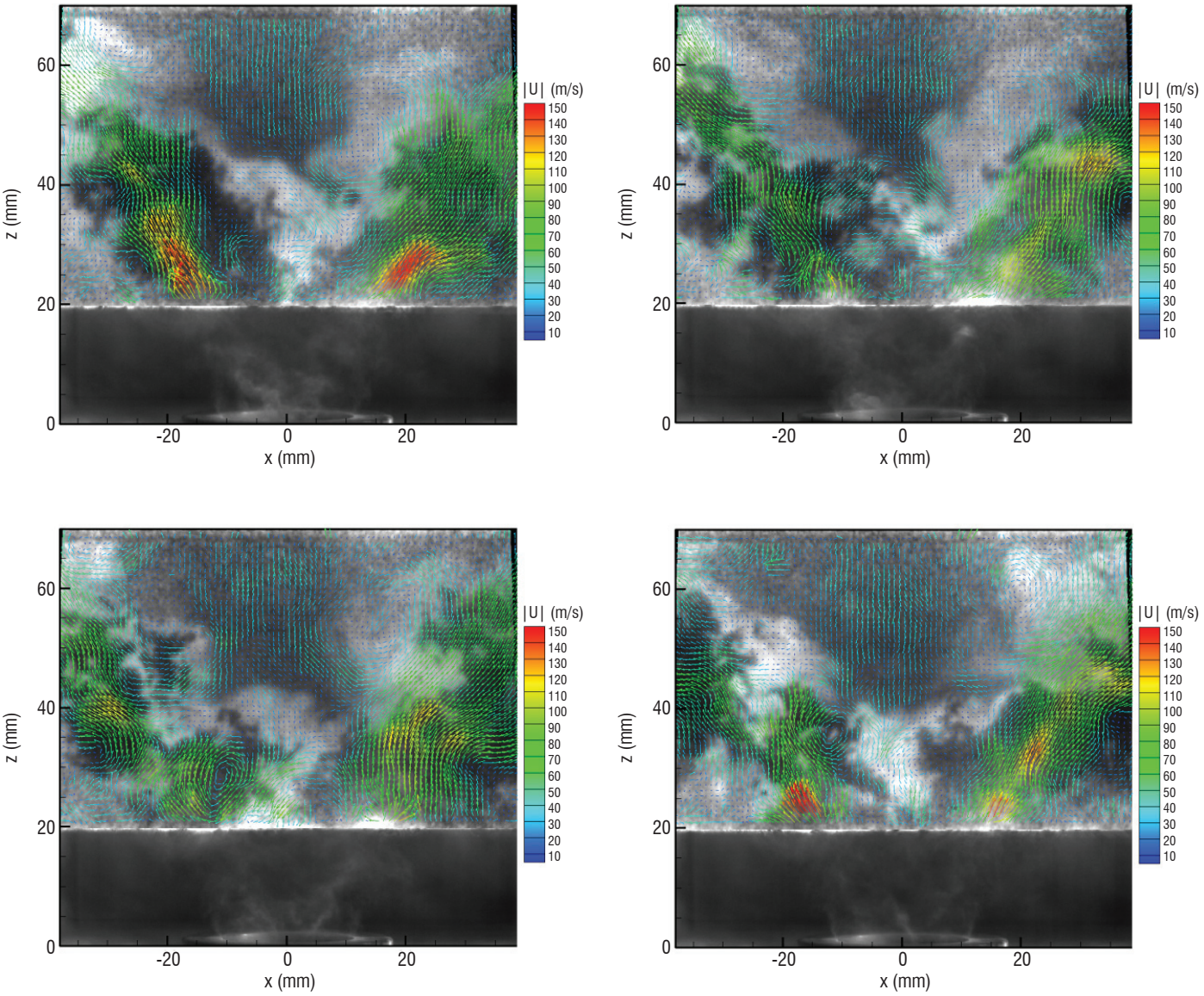

Figure 16 - Image sequence from simultaneous OH-PLIF/PIV measurements in a Lean Premixed burner at a 5 kHz frame rate. The field of view is 60mm x 50 mm. The position and shape of the nozzle are shown below the distributions. Operating conditions: P=0.1 MPa, $Qm_{air}=30g/s$, $T_{air}=473K$.

mainly located between the hot product recirculating flow within the central part of the flow and the incoming flow of fresh gas, resembling a stagnation flow flame. Furthermore, large-scale vortical structures that appear to dominate parts of the flow field and to strongly contort the reaction zone are observed.

In the near future, another laser diagnostic technique (CARS, PDA, NO-and CO-PLIF, kerosene-PLIF, etc.) will be used to provide an exhaustive evaluation and understanding of the complex underlying turbulence-chemistry interaction in the combustion chamber. Furthermore, given that the wall of the combustion chamber being is optically accessible, the wall/flame interaction will be also investigated for various boundary conditions (perforated walls, etc.), in order to quantify its impact on combustion and pollutant formation. On this basis, new innovative technological solutions will be proposed to the industrial partner, in order to improve the architecture of future fuel injection systems. Experiments will be also performed with special attention to the definition of the boundary conditions, which is of paramount importance when the data will be used to validate the combustion models and the LES simulation codes ■

Acknowledgements

This work was supported by the Upper Normandy Region of France and the European Regional Development Fund (FEDER), which are gratefully acknowledged.

References

[1] M. Orain, P. Baranger, B. Rossow, F. Grisch - *Fluorescence Spectroscopy of 1,2,4-Trimethylbenzene at High Temperatures and Pressures: Application to Temperature Measurements*. Applied Physics B, 100, Issue 4, 945-952, 2010

[2] M. Orain, P. Baranger, B. Rossow, F. Grisch - *Fluorescence Spectroscopy of Naphthalene at High Temperatures and Pressures: Implications for Fuel-Concentration Measurements*. Applied Physics B, 102, Issue 1, 163-172, 2010

[3] M. Orain, P. Baranger, C. Ledier, J. Apeloig, F. Grisch - *Fluorescence Spectroscopy of Kerosene Vapour at High Temperatures and Pressures: Potential for Gas Turbines Measurements*. Applied Phyics B, 116, Issue 3, 729-745, 2015

[4] B. Rossow, F. Grisch - *Étude de l'évaporation différentielle carburants multi-composant par fluorescence induite par laser de traceurs aromatiques*. 14ème Congrès Francophone de Techniques Laser (CFTL) - Marseille (France) 2014

[5] C. Ledier, M. Orain, F. Grisch - *Measurement of Biofuel Vapor Concentration in Sprays Using New Planar Laser-Induced Fluorescence*. 4th European Conference for Aero-Space Science (EUCASS) - Saint-Petersburg (Russia) 2011

[6] P. Gautier, B. Barviau, G. Godard, J. Apeloig, S. Hochgreb, F. Grisch - *Détection des émissions des polluants NO et CO dans les flammes par fluorescence induite par laser (LIF)*. 14ème Congrès Francophone de Techniques Laser (CFTL) - Marseille (France) 2014

[7] Yi. Wu, V. Modica, F. Grisch - *Elevated Pressure and Temperature Effect to Laminar Flame Speed of Acetone/Air Mixture*. Proceeding of the 25th International Colloquium on the Dynamics of Explosions and Reactive Systems (ICDERS) – Leeds (UK) 2015

[8] Yi. Wu, V. Modica, F. Grisch - *Laminar Flame Speed Measurements of Multi-Component Jet A1 and LUCHE Kerosene Surrogate Fuels in Elevated Pressure and Temperature Conditions*. 7th European Combustion Meeting – Budapest (Hungary) 2015

[9] J. Jayachadran, A. Lefebvre, R. Zhao, F. Halter, E. Varea, B. Renou and F. N. Egolfopoulos - *A Study of Propagation of Spherically Expanding and Counterflow Laminar Flames Using Direct Measurements and Numerical Simulations*. Proceedings of the Combustion Institute, 35, pp. 695-702, 2015

[10] E. Varea, V. Modica, A. Vandel, B. Renou - *Measurement of Laminar Burning Velocity and Markstein Length Relative to Fresh Gases Using a New Post-processing Procedure: Application to Laminar Spherical Flames for Methane, Ethanol and Isooctane/Air Mixtures*. Combustion and Flame, 159(2): pp. 577-590, 2012

[11] E. Varea, V. Modica, B. Renou, M.A. Boukhalfa - *Pressure Effects on Laminar Burning Velocities and Markstein Lengths for Isooctane–Ethanol–Air Mixtures*. Proceedings of the Combustion Institute, 34(1): pp. 735-744, 2013

[12] M. Cordier, A. Vandel, G. Cabot, B. Renou, M.A. Boukhalfa - *Laser-Induced Spark Ignition of Premixed Confined Swirled Flames*. Combustion Science and Technology, 185, pp 379-407, 2013.

[13] D. Barré, L. Esclapez, M. Cordier, E. Riber, B. Cuenot, G. Staffelbach, B. Renou, A. Vandel, L.Y.M. Gicquel, G. Cabot - *Flame Propagation in Aeronautical Swirled Multi-Burners : Experimental and Numerical Investigation*. Combustion and Flame, 161, pp. 2387-2405, 2014

[14] M. Cordier, A. Vandel, B. Renou, L.Y.M. Gicquel - *Experimental and Numerical Analysis of an Ignition Sequence in a Multiple-Injectors Burner*. ASME Turbo Expo. 2013 GT 2013 – 94681 - 2013

[15] P. Xavier, A. Vandel, G. Godard, B. Renou, F. Grisch, G. Cabot, M.A. Boukhalfa, M. Cazalens - *Analysis of the Flame Structure in a Trapped Vortex Combustor Using Low and High Speed OH-PLIF*. ASME Turbo Expo2014, GT2014-25207, 2014

[16] P. Xavier, M. Pires, A. Vandel, B. Renou, G. Cabot, M.A. Boukhalfa, M. Cazalens - *Determination of Criteria for Flame Stability in an Annular Trapped Vortex Combustor.* ASME Turbo Expo2015, GT2015-43214, 2015

[17] P. Xavier, A. Vandel, G. Godard, B. Renou, F. Grisch, G. Cabot, M.A. Boukhalfa, M.L Cazalens - *Investigation of Combustion Dynamics in a Cavity-Based Combustor with High-Speed Laser Diagnostics*. Exp. Fluids, 57:50, 2016

[18] J. Burguburu, G. Cabot, B. Renou, M.A. Boukhalfa, M. Cazalens - *Comparisons of the Impact of Reformer Gas And Hydrogen Enrichment on Flame Stability and Pollutant Emissions for a Kerosene/Air Swirled Flame with an Aeronautical Fuel Injector*. International Journal of Hydrogen Energy, 36:6925-2936, 2011

[19] J. Burguburu, G. Cabot, B. Renou, M.A. Boukhalfa, M. Cazalens - *Effects of H_2 Enrichment on Flame Stability and Pollutant Emissions for a Kerosene/Air Swirled Flame with an Aeronautical Fuel Injector*. Proceeding of the Combustion Institute, 33, pp. 2027-2935, 2011

[20] E. Salaün, P. Malbois, A. Vandel, G. Godard, F. Grisch, B. Renou, G. Cabot, A.M. Boukhalfa - *Experimental Investigation of a Spray Swirled Flame in a Gas Turbine Model Combustor*. 18th International Symposia on Applications of Laser Techniques to Fluid Mechanics, Lisbon (Portugal) 2016

AUTHOR

Frédéric Grisch has completed his PhD in 1988 (University of Rouen, France). He then worked in the Physics, Instrumentation and Sensing Department of Onera (France) as senior researcher. He is now Professor at the department of Energy and Propulsion of INSA-Rouen since 2011. He is also affiliated with Onera as scientific consultant since 2012. His research activities lie in the area of Combustion Science, with current emphasis on Laser Diagnostics, Gas Turbine Combustion, Fluid Mechanics and Heat Transfer. He is presently in charge of the Industrial Chair PERCEVAL supported by SAFRAN Tech and the French National Research Agency.

Mourad Boukhalfa has obtained his PhD in 1988 (University of Orleans, France). Professor at the department of Energy and Propulsion of INSA-Rouen, he spent the past 22 years on the development of optical diagnostics for the study of Combustion science, Fluid Mechanics and Heat Transfer. He has developed a strong expertise in the analysis of flame structure and instability on swirl premixed and partially premixed, in high temperature and pressure conditions. He is presently Head of the CORIA Research Laboratory.

Gilles Cabot has obtained his PhD in 1992 (University of Rouen, France). He is Professor of combustion and thermal engineering at the University of Rouen. He is Head of the thermal engineering department of the Technology Institute of the University of Rouen. His research activity lies in area of high-pressure turbulent combustion. He is also in charge of the management of the experimental facilities for aero-engine combustion studies at the CORIA research laboratory.

Bruno Renou has obtained his PhD in 1999 (INSA-Rouen, France) in combustion sciences. He is Professor and Head of the department of Energy and Propulsion of INSA-Rouen from 2013. He has strong experience in laminar and turbulent combustion. He is also involved in the development of optical diagnostics to characterize the flame structure, flame ignition, flame instabilities and pollutant emissions. Effort is also made to develop physical analysis of these phenomena, in link with numerical simulations.

Alexis Vandel is a research engineer at CORIA laboratory since 2008. He is active as a high-level technical support for aero-engines facilities. He participates in the implementation of experimental test benches, test campaigns and contracting activities. He also implements laser diagnostics and ensures data acquisition. He has a strong experience in low- and high-repetition rate combined laser diagnostics.

T. Le Pichon, A. Laverdant

E-mail: Thomas.Le_Pichon@onera.fr

DOI: 10.12762/2016.AL11-03

Numerical Simulation of Reactive Flows in Ramjet Type Combustors and Associated Validation Experiments

Twenty years ago, a review listed the main challenges to overcome to accurately predict the reactive flow fields in ramjet combustion chambers. These issues were grouped into five topics: flow organization, combustion phenomena, stability and performance, unsteady combustion and heat transfer. The aim of this paper is to give a brief overview of the numerical and experimental studies that have been carried out since this inventory in the specific program named "Research Ramjet" to improve CFD codes. First, the experimental setup designed to obtain a better understanding and to build-up an experimental database in order to validate numerical simulations is described. Then, the progress made with regard to these technical issues is presented. Significant improvements came from the implementation of Large Eddy Simulations. However, some challenges still remain, including the prediction of the overall performance parameters and the combustion instabilities.

Introduction

The ramjet is an air-breathing propulsion system very suitable for supersonic speeds, between Mach 2 and Mach 5. Sometimes referred to as an aerothermodynamical nozzle, or even a flying stovepipe, its basic concept is quite simple (Figure 1). The thermodynamic cycle, similar to that of gas turbines', is based on the Brayton cycle. Its main originality lies in the compression stage, which is accomplished thanks to the ramming effect of the incoming air flow: no rotating component is necessary. As always, there is a price to pay for this nice feature: ramjets develop no static thrust. An auxiliary engine is required for low-speed propulsion.

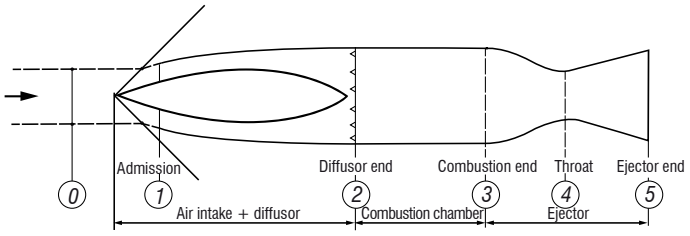

Figure 1 - Basic sketch of a ramjet combustor and characteristic sections [26]

Between the Thirties and the Sixties, ramjet was believed to be appropriate for aircraft propulsion. Several flying prototypes were built by the French engineer R. Leduc and Nord Aviation to demonstrate the feasibility of this engine [24][33]. However, gas turbine improvements during the same period put a curb on these developments. Meanwhile, the interest for ramjet-propelled missiles was skyrocketing. Several experimental missiles were launched (e.g., ONERA's Stataltex, which reached Mach 5 in 1965) [27][28][29], and military applications were developed [15][29][55]. All of the first configurations were accelerated using an auxiliary jettisonable booster. A new concept arose in the Seventies, leading to a more compact missile: the Integral Rocket Ramjet (IRR) [33]. The basic idea is to use a common combustion chamber for the boosted and the sustained phases of flight. As a result, the solid booster is housed in the combustion chamber and the flameholders are removed. The dump-type configuration generates recirculation zones, which stabilize combustion (Figure 2). Two IRR were intensively studied in France: the Liquid-Fueled Ramjet (LFRJ) and the Solid Ducted Rocket (SDR). In the latter case, a fuel-rich solid propellant is used to generate a gaseous fuel supply.

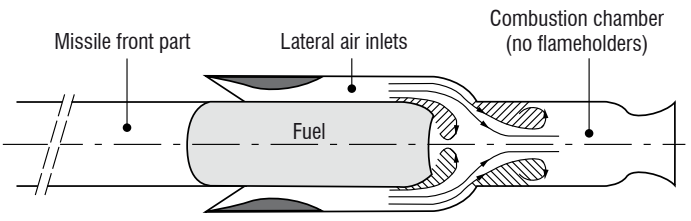

Figure 2 - Sketch of an Integral Rocket Ramjet (IRR) [4]

As for any engine, several phases are necessary to develop a new ramjet. Up to now, those steps were mainly based on a process of trial and error. Experimental research demanded a great deal of costly and time-expensive tests: design tests on components, connected-pipe tests, semi-free (or possibly free) jet tests, and finally, after several years, flight tests. Numerical simulations have been identified for

several years as one of the most promising tools to drastically reduce cost and time for the development of new engines. This could be accomplished provided that a CFD code, able to predict the performance parameters and the unsteady phenomena in any ramjet combustion chamber, is identified. Unfortunately, one can fairly admit that no CFD code has been able to demonstrate such abilities and many challenges are still to be faced.

Published material on reactive gaseous or two-phase flows in ramjet combustion chambers, which can be used to improve and validate numerical simulations, is very limited. The Lateral Injection Combustor (LIC) is a lab-scale two-inlet side-dump combustor, which has been extensively investigated in the EM2C laboratory [30][50]. Numerous experimental techniques have been used to study the non-reacting and reacting flows during stable or unstable operating conditions, and a significant database has been built. Nevertheless, significant features of the reactive flows in industrial SDR or LFRJ are missing: the internal flow is 2-D (the 3-D vortex motions resulting from the air stream impingement are not represented), boundary conditions (and especially inlet and outlets) are not representative of industrial combustors, and only gaseous fuel has been used. Experiments on industrial-type LFRJ side-dump combustors have been published, in the Eighties. These studies were aimed at understanding the impact of geometry on pressure oscillations [52][9] or on overall performance parameters [52][57]. Unfortunately, the internal combustor geometries are not exhaustively described, and the salient features of the internal reactive flows are not investigated.

In order to overcome this problem, a study named “Research Ramjet Program” was initiated some years ago at ONERA [39]. Within this framework, a specific side-dump combustion chamber has been designed in order to provide the experimental data necessary to validate CFD codes. This engine, quite unique in the world, is described in the first part of this paper.

About twenty years ago, a review article listed the main challenges to be overcome to improve the numerical simulations of ramjet combustors [22]. These technical issues were gathered into five topics: flow organization, combustion phenomena, performance and stability, unsteady combustion, and heat transfer. An in-depth analysis of each of these issues is beyond the scope of this paper. It is rather an attempt to highlight experimental and numerical studies that have been carried out at ONERA, within the framework of the Research Ramjet program, to tackle these problems.

Experimental apparatus

A combustion chamber has been designed, in order to examine and understand the basic physical phenomena that govern the flows in ramjet type combustors, and build an experimental database to assess, improve and validate computations.

As a result, a modular experimental setup, equipped with large windows, has been assembled (Figure 3). The configuration is a two-inlet side-dump ramjet combustor, which can be operated as a SDR or as a LFRJ. In the first case, gaseous propane is injected into the head-end through two circular tubes (Figure 4a). In the second one, liquid fuel injectors are installed in the two inlets (Figure 4b) and/or in the head-end.

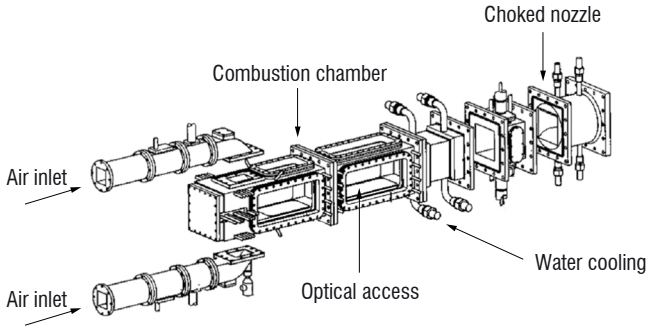

Figure 3 - Sketch of the modular Research Ramjet setup

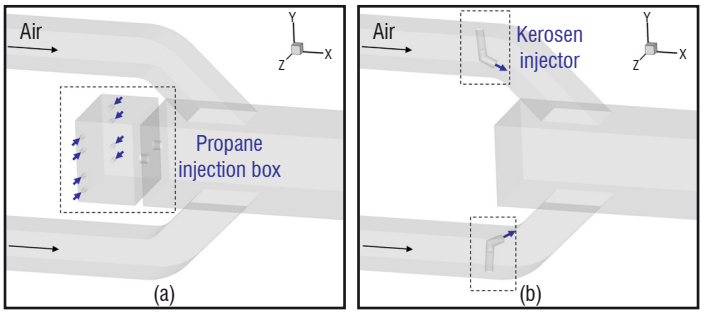

Figure 4 - Two potential configurations for the fuel injection: (a) gaseous propane in the head-end part of the combustor (SDR), (b) liquid kerosene in the air inlets (LFRJ)

The key dimensions (Figure 5) have been defined to be representative of real engines. The combustion chamber has a square cross-section (100 mm x 100 mm) and is fed by two lateral air inlets (50 mm x 50 mm). The square cross-section has been chosen to facilitate the integration of optical accesses, allowing direct views of flames and flow probing with laser sheets. There is an axisymmetric convergent - divergent nozzle at the end of the combustor. Note that, due to the modularity of the experimental setup, many geometric parameters can be varied.

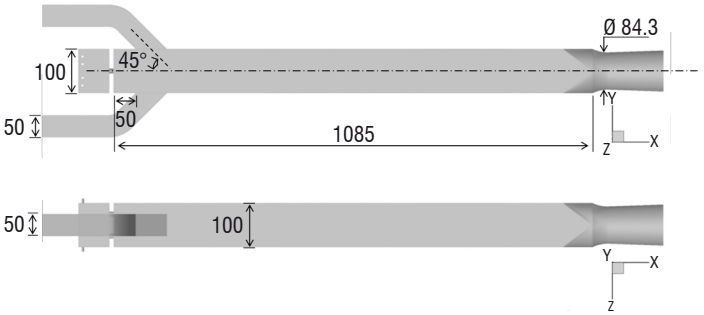

Figure 5 - Main dimensions (in mm) of the SDR configuration of the Research Ramjet combustion chamber

The setup is dedicated to connected-pipe tests, conducted in the ONERA air-breathing test facilities. An image of the ignited Research Ramjet combustor on a test-rig is given in Figure 6. Operating conditions, *i.e.*, incoming air mass flow rates ($\dot{m}_2$) and total temperatures (T_{i2}), are representative of real flight conditions (see Table 1). For each of these regimes, ranges of stagnation pressure in the aft part of the combustion chamber (P_{i4}), which depend mainly on overall equivalence ratios, are given in Table 1. Note that the incoming air flow is not vitiated: a heat exchanger is used to increase its temperature.

Moreover, the air mass flow rate in each inlet is monitored with a sonic throat and the walls of the combustor are water-cooled to allow long-duration tests.

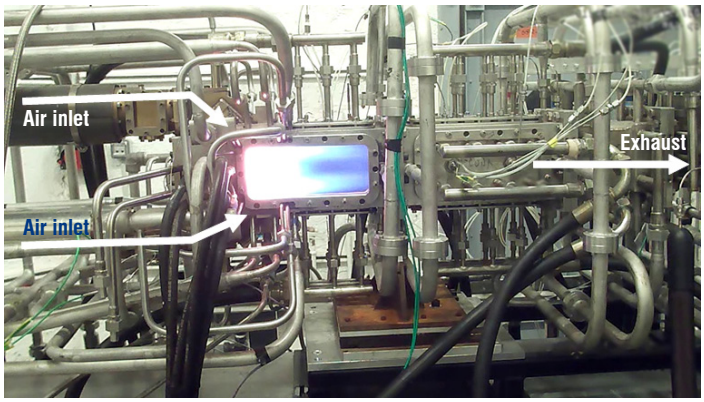

Figure 6 - The research ramjet combustion chamber on the test-rig in the ONERA facilities

In order to enable a more detailed characterization of the aerodynamics and fuel-to-air mixing process, a specific fully-transparent setup has been designed (Figure 7) [38][39]. In this case, only cold and non-reacting flows can be used for experimentations.

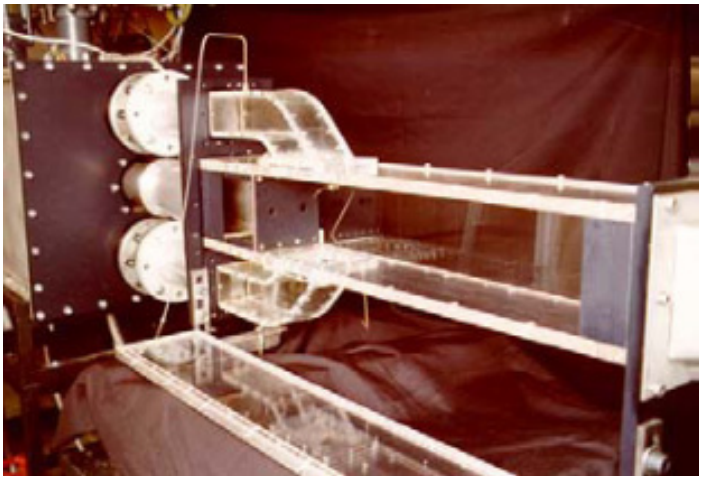

Figure 7. The transparent experimental setup

	$\dot{m}_2$ [kg.s^{-1}]	T_{i2} [K]	P_{i4} [bar]
High Altitude (HA)	0.9	750	1.5 – 2.5
Middle Altitude (MA)	1.9	600	3 – 5
Low Altitude (LA)	2.9	520	5 – 7

Table 1 - Operating conditions (air mass flow rate $\dot{m}_2$ and total temperature T_{i2}) and approximate ranges of pressure in the combustion chamber (P_{i4})

Flow topology

As mentioned in [22], flow patterns inside side-dump ramjet combustors are fully three-dimensional, composed of vortex motions and axial recirculating flows. These complex features are mostly driven by the sudden expansion and the impingement of the air streams in the first part of the chamber.

Non-reacting flow topology on the Research Ramjet configuration was first examined by conducting water-tunnel experiments on the transparent setup [20][40][41]. During those tests, water was made to flow through the two side inlets, while a dye (liquid fluorescein) was injected into the head-end. A laser sheet generator was used to light internal planes and highlight recirculation zones inside the chamber. The flow organization in the vertical symmetry plane and in three transverse sections as obtained with this technique is shown in Figure 8. The main recirculation (also named “dome”) is located near the head-end of the chamber, upstream from the jet-on-jet impingement zone. Two other significant recirculating regions (sometimes named “lateral zones”) are located downstream from the air inlets, on the top and bottom walls of the chamber. The dome and lateral zones are linked by the four corner vortices shown on the transverse sections in Figure 8.

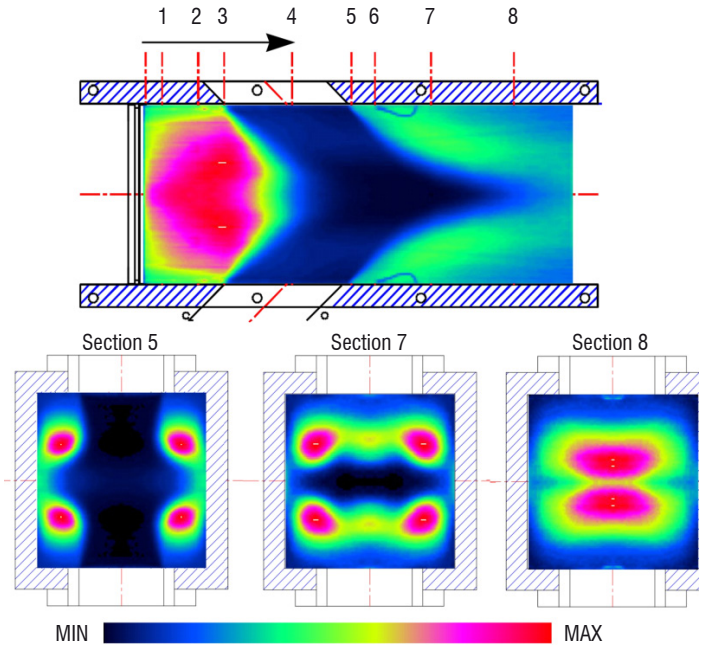

Figure 8 - Visualization of fuel-to-air mixing using the local colorimetry method on the transparent Research Ramjet configuration

An in-depth analysis of the fuel-to-air mixing in the non-reactive Research Ramjet configuration has been performed using the Particle Image Velocimetry (PIV) technique and gas sampling measurements [19][37][38][41][43]. This time, the side inlets of the transparent setup were fed with air, and gaseous carbon dioxide was injected into the head-end to simulate the fuel injection.

The reactive flow fields in the side-dump Research Ramjet configuration exhibit the same features as the non-reactive ones. This was demonstrated using Laser Doppler Velocimetry (LDV) and PIV measurements [5][37][42][43][44] applied to the Research Ramjet combustion chamber.

All of these data, mostly quantitative, obtained from non-reactive and reactive configurations, have been gathered in the experimental database and used to assess the capacity of numerical simulations to predict the flow patterns inside ramjet combustors.

Reynolds Averaged Navier-Stokes (RANS) computations, and later Large Eddy Simulations (LES), have been applied to predict the internal flow fields in the Research Ramjet configurations and compared to available measurements. Whenever only the overall topology is

sought, the mean flow given by RANS computations may be sufficient. Figure 9 illustrates the major features of the reactive flow field as evidenced with a RANS computation for the reactive High Altitude SDR case. As can be seen, the presence of the main recirculation zones is predicted by the steady calculation.

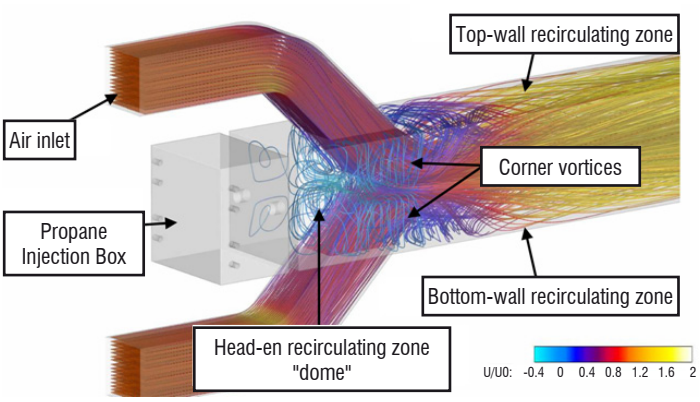

Figure 9 - Visualization of streamtraces colored by mean adimensionalized axial velocity for the SDR case provided by a RANS computation[1]

However, as shown in [37], when it comes to the mean velocity and fuel concentration profiles in the recirculation zones, or to the size and length of these large structures, only LES can yield satisfactory results. This is due to the fact that the large scale turbulent motions of the flow, which control the flow patterns, are resolved by LES.

As a result, significant improvements have been achieved concerning the prediction of the fuel concentration and velocities in the non-reactive transparent setup compared to RANS calculations [36][37][43]. Concerning the reactive SDR configuration, axial and transverse adimensionalized velocity profiles as obtained with LES[2] and RANS[1] computations for the High Altitude flight regime at the equivalence ratio $\Phi = 0.75$ are given in Figure 11. The location of these profiles is given in Figure 10. As can be seen, the conclusion for the SDR reactive case is the same as for the non-reactive one: velocity profiles are better predicted using the LES approach.

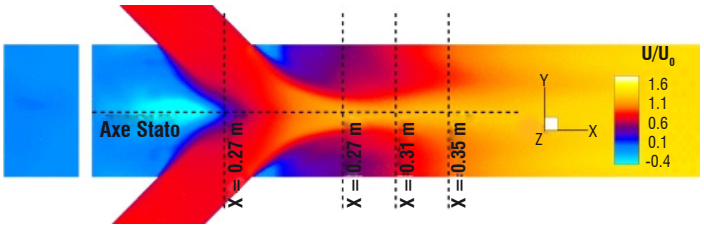

Figure 10 - Location of the velocity profiles

Significant improvements have been made over the past two decades with regard to the prediction of the flow organization, especially with the implementation of LES [37]. Even if the large scale structures, which are important features of the ramjet combustors, are present in the results of the RANS computations, LES is up to now the most predictive tool.

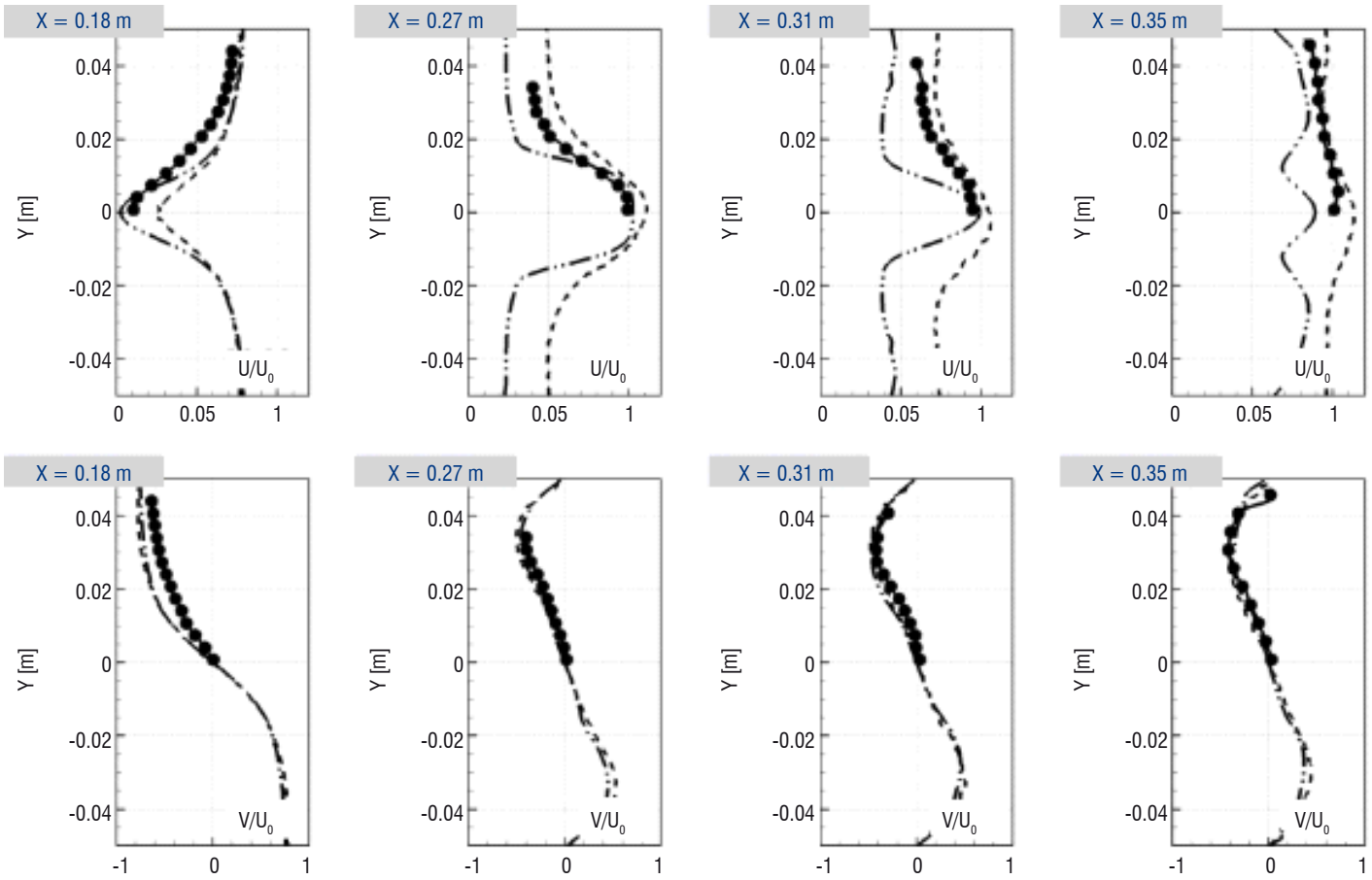

Figure 11 - Adimensionalized velocity profiles in the Research Ramjet combustor, for a High Altitude flight condition, at an overall equivalence ratio of 0.75. U refers to the axial velocity, V to the transverse velocity, and U0 to the reference velocity. Comparison between experimental data (–●–), RANS (— ·· —) and LES (— —)

1 Main parameters are given in [23] and in Box 1 §1.
2 Unpublished work. Main parameters are given in Box 1 §2.

Combustion phenomena

Whichever configuration (SDR or LFRJ) or operating condition is used, combustion is likely to occur in three characteristic parts of the flow: (i) the top and bottom recirculating zone, (ii) the helicoid flows linking the head-end to the aft-part of the chamber and (iii) the head-end part of the chamber. Experimental observations have shown that flame anchoring is not spatially fixed. Without altering the operating conditions, combustion can be seen shifting periodically or intermittently from the top and bottom recirculating zone to the head-end part of the chamber [41][42].

The flame front location in the various configurations has been first exposed by direct visualizations of the OH* emission [40][41]. Furthermore, the OH-Planar Laser-Induced Fluorescence (OH-PLIF) technique has also been implemented to describe the spatial structure of the reaction zones [40][41]. Those visualizations have helped to develop a better understanding of the combustion regime of ramjet engines.

Time-averaged images provided with direct OH* visualizations showed that the flame position is strongly dependent on various parameters. Among them, the location of the fuel injection, or even the fuel itself, is a parameter that has a significant impact. The three visualizations of the OH* emission shown in Figure 12 were taken for a High Altitude flight regime at an overall equivalence ratio of 0.50. The difference between Figure 12a and Figure 12b is the fuel injected (respectively gaseous propane and liquid kerosene), and the difference between Figure 12b and Figure 12c is the position of the injectors (respectively in the head-end and in the air inlets).

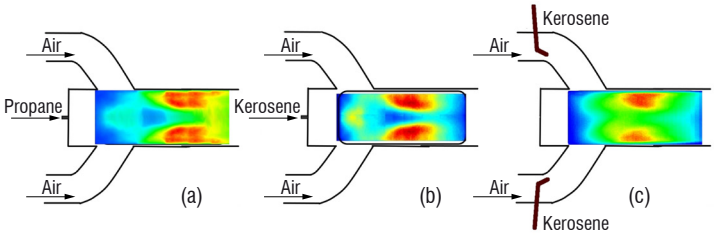

Figure 12 - Impact of fuel injection on mean flame front position revealed by OH* chemiluminescence for a High Altitude flight regime with an overall equivalence ratio of 0.50: (a) gaseous propane injected into the head-end, (b) liquid kerosene injected into the head-end, (c) liquid kerosene injected into the air inlets (arbitrary levels)

The overall equivalence ratio also has a significant impact on the flame front position. Figure 13 illustrates the fact that, for the SDR configuration, when the overall equivalence ratio is decreased, the mean flame front location moves upstream, from the lateral recirculation zone to the dome.

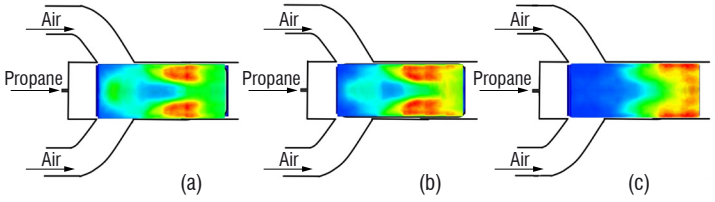

Figure 13 - Impact of the overall equivalence ratio on the mean flame front position revealed by OH* chemiluminescence for a High Altitude flight regime on the SDR configuration: (a) $\Phi = 0.35$, (b) $\Phi = 0.50$ and (c) $\Phi = 0.75$

The RANS approach was first applied to predict the influence of the equivalence ratio on the flame location. Unfortunately, one must admit that prediction of such influence with this steady approach is difficult. Figure 14 shows the temperature contours computed in the vertical symmetry plane for the two equivalence ratios 0.35 (Figure 14a, to be compared with Figure 13a) and 0.75 (Figure 14b, to be compared with Figure 13c): the mean flame position for the $\Phi=0.75$ case is quite well-predicted, but not the flame shift towards the head-end at $\Phi=0.35$. Nonetheless, one should specify that high speed camera visualizations have shown that combustion is intermittent in the head-end region, whatever the equivalence ratio [41]. Flames are anchored in the two lateral recirculation regions downstream from the air inlet and travel intermittently toward the head-end part of the combustor, along the four corner vortices. The lower the equivalence ratio, the deeper the travel upstream from the corner vortices in the dome region. Thus, given that only the mean flow field is computed with the RANS approach, this unsteady feature is not predicted, and flames stay only in the lateral zones.

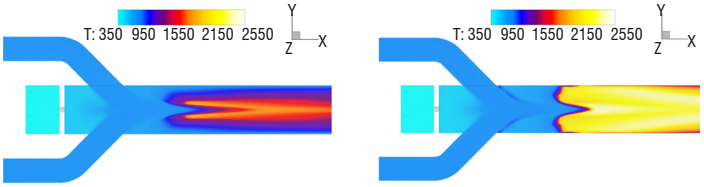

Figure 14 - Mean temperature in the vertical symmetry plane of the SDR Research Ramjet configuration computed with a RANS approach[3] in the High Altitude flight regime: (a) $\Phi = 0.35$ and (b) $\Phi = 0.75$

Once more, improvements have been achieved with the implementation of the LES technique. The mean flame front displacement upstream as the equivalence ratio was decreased has been successfully predicted for the SDR Research Ramjet configuration [17][46]. The chemical kinetic scheme for the air-propane reaction, although very simple and reduced to a single global reaction, is a key for this success. In fact, the pre-exponential constant of Arrhenius' law has been adjusted to yield a correct laminar flame speed over an extended range of equivalence ratios, and especially in the rich zones. As a consequence, the prediction of the flame position was much more satisfactory than that obtained with other approaches that did not use such a correction (see for example [45]). In addition, this correction enables the two main low-frequency longitudinal modes of the combustor (at approximately 100 and 400 Hz) evidenced during the experiments for these operating conditions [46][47] to be recovered.

Nevertheless, this success in predicting the correct flame position for the SDR configuration does not mean that the modeling of the turbulent combustion inside ramjet combustors is no longer an issue. First of all, no information has been given about the combustion efficiency prediction with this approach (note that the performance parameters are discussed in the next paragraph). The number of species involved in the global scheme may be too small to accurately predict the temperature in the combustor, which affects the prediction of the performance parameter. Improvements could be achieved with the use of a more detailed scheme. Moreover, other flight conditions should be studied, as well as the two-phase reactive flows in the LFRJ configuration, which may add some difficulties in the combustion phenomena [22]. Finally, conditions near the stability limits of the combustor, as well as unstable conditions, should also be assessed.

3 Main parameters are given in [23] and in Box 1 §1

Performance and stability

Overall efficiencies

Two quantities are of prime interest when developing a new ramjet combustor: the combustion efficiency η_c and the pressure loss coefficient η_{24}. The combustion efficiency is defined as the ratio between the burnt equivalence ratio, determined at the end of the combustion chamber, and the injected equivalence ratio. The pressure loss coefficient is the ratio between the stagnation pressures at the end of the combustion chamber and at the end of the diffuser in the air inlets.

Pressure and temperature probes have been installed in reference sections of the Research Ramjet combustion chamber to evaluate, following a recommended procedure [1], these two performance parameters. Those quantities have been collected for each configuration, under various operating conditions.

One should admit that the accurate prediction of these two quantities is no easier today than it was twenty years ago [22]. Despite progress in numerical tools and modeling, no approach has demonstrated its capacity to predict these quantities, whatever the configuration or operating regime. Table 2 gathers some results obtained with different numerical approaches for the SDR configuration in the High Altitude flight regime at two equivalence ratios. The pressure loss coefficient is rather well predicted by all of the methods, with a gap ranging between 1 and 3 points. The comparison of the combustion efficiencies, however, brings to light wider discrepancies (between 2 and 14 points). Among the approaches selected here, none seems really adequate yet to predict this parameter.

The improvement of the models used in the numerical simulations to predict the performance parameters will be one of the main goals of future work. This issue is closely related to the others, as these two efficiencies are overall parameters that include a large number of physical phenomena (turbulence, combustion, wall friction, heat losses, etc.).

Overall equivalence ratio	Approach	Reference / main parameters	Pressure loss η_{24}	Combustion efficiency η_c
0.75	Experimental	-	0.88	0.81
	RANS	[23] + see Box 1 §1 for main parameters.	0.89	0.83
	LES	[37] + see Box 1 §2 for main parameters.	0.90	0.95
	LES	[46]	0.86	Not calculated
0.35	Experimental	-	0.87	0.80
	RANS	[23] + see Box 1 §1 for main parameters.	0.86	0.70
	LES	[46]	0.84	Not calculated

Table 2 - Prediction of overall efficiencies for two equivalence ratios in the High Altitude flight regime

Box 1 - Main parameters of the RANS and LES simulations performed with the CEDRE software and referred to in this paper

1 - RANS [SDR configuration]

Computational domain

3-D ; 1/4th of the geometry

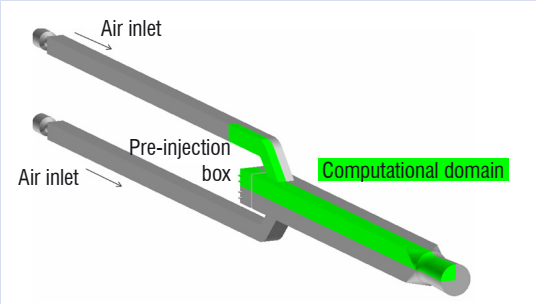

Mesh

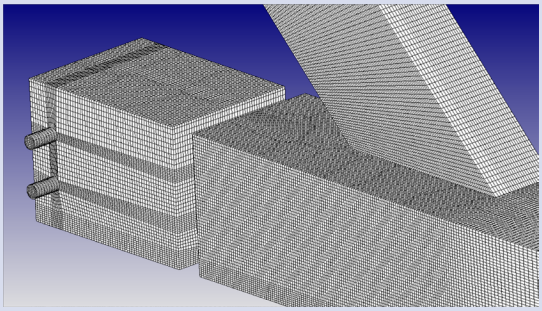

Cell type: hexahedra
No. of cells: 1.5×10^6 cells
Average size: $\Delta x \approx 1$ mm in the dome region
Near-wall size: $Y+ \approx 100$

Numerical schemes

Spatial scheme: 2nd order
Temporal integration: Implicit 1st order

Physical models

Turbulence: Two-equation k-ℓ model
Combustion: RANS-PaSR [2],[31] + 4 steps reduced scheme for air-propane reaction [21]

2 - LES [SDR configuration]

Computational domain

3-D ; from the sonic throats in the air inlets to the exhaust nozzle

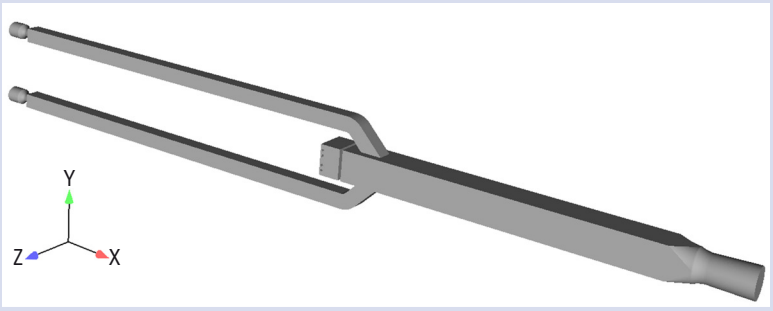

Mesh

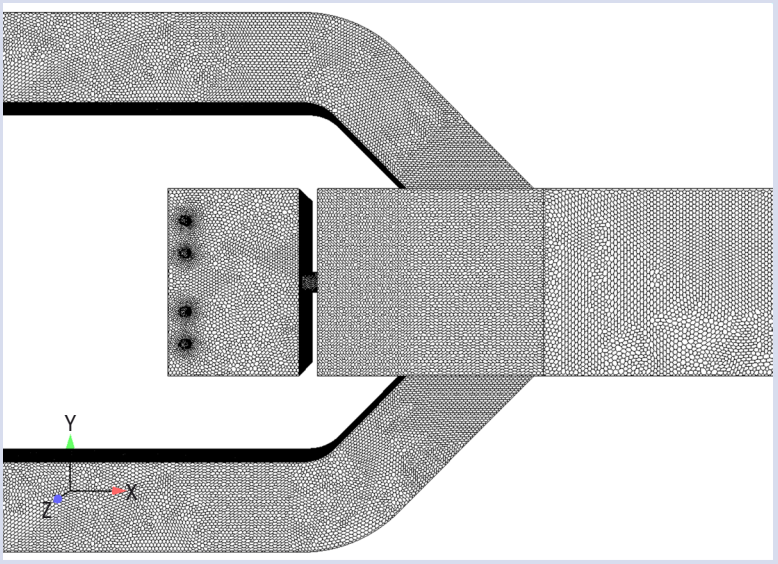

Cell type:	polyhedra
No. of cells:	2×10^6 cells
Average size:	$\Delta x \approx 1$ mm in the dome region
Near-wall size:	$Y+ \approx 100$

Numerical schemes

Spatial scheme: 2nd order

Temporal integration: Implicit 2nd order

Physical models

Turbulence: Smagorinsky closure [53]

Combustion: Arrhenius + 1 step adjusted reduced scheme for air-propane reaction [45]

Prediction of stability limits

At any flight regime, two limiting fuel/air ratios can be encountered: one involves excess fuel (rich) and the other involves excess air (lean) leading to the blow-off of the combustor. Of most practical interest is blow-off at fuel lean conditions, referred to as Lean Blow-Out (LBO). A study [23] has been carried out to improve the understanding of the physical processes involved in ramjet LBO and the calculations that could be done to predict this limit. In order to build an experimental database on this phenomenon, tests have been performed with the Research Ramjet: from a nominal operating condition, the overall equivalence ratio was progressively reduced until the flame blow-out. Combustion modeling related to the RANS approach is the first to have been considered to address the problem of predicting the flame blow-out. In particular, a Partially Stirred Reactor (PaSR) combustion model has been used to predict the LBO of the Research Ramjet operated as a SDR combustor in the High Altitude flight regime.

The PaSR combustion model is based on the Eddy Dissipation Concept model introduced by Magnussen [25]. The fluid is divided into two zones: the fine-scale structure regions, which are spatially intermittent, and which occupy a volume that is only a small part of the domain of fluid, and the “surrounding fluid”. Reactants are supposed to be homogeneously mixed inside the fine-scale structures of the flow. Therefore, the fine-scale structures are supposed to behave like well-stirred reactors, with uniform internal composition and temperature, and potentially high reaction rates due to favorable mixing condi-

tions. The PaSR model provides a system of equations that defines the volume of the fine-scale structures, describes the chemical reaction process inside the fine-scale structure regions, and then relates the fine-scale structure parameters to the surrounding fluid characteristics. Further details about this model can be found in [2] and [31]. This model is well-suited for numerical simulations of combustion in ramjet engines, as it meets two major criteria: chemistry is not supposed to be infinitely fast, and premixed and non-premixed flames can be handled (no assumption is made on the combustion regime). A criterion for the extinction of the fine-scale structure regions has been added to the PaSR model. The basic idea is as follows [6]: when the residence time in the fine-scale structures becomes smaller than a typical chemical time scale, extinction occurs. This critical time scale can be viewed as the blow-off residence time of the perfectly stirred reactor (PSR) corresponding to the fine-scale structure.

Significant results have been obtained [23]. In particular, using the PaSR combustion model and the local extinction criterion, the LBO limit is predicted at $\Phi = 0.30$, which is fully satisfactory compared to the measured limits, which lie between 0.28 and 0.30. This study has partly demonstrated the ability of this approach to predict the LBO limit of a practical ramjet combustion chamber. Nevertheless, further calculations are necessary to assess and validate the ability of numerical simulations to predict the LBO limits of any gaseous or liquid-fueled ramjet combustor.

Combustion instabilities

Understanding and predicting self-induced combustion instabilities in ramjet combustion chambers – and in any combustion chamber in general – is still a challenge. Combustion instabilities in ramjet combustors can have dramatic consequences: unstarting of the inlets, destruction of the thermal insulator, deterioration of the equipment attached to the engine structure, and even destruction of the burner.

Many driving mechanisms have been proposed to explain the transfer of energy to the unsteady motions in ramjet combustors. For liquid-fueled ramjets, a coupling between acoustics and the transient phenomena related to fuel injection, such as primary and secondary break-up, heating and vaporization, or with the fuel supply system itself, has been suggested [11]. Nevertheless, there is still a lack of experimental evidence to demonstrate that such couplings are responsible of combustion instabilities in ramjets. More attention has been paid to four other mechanisms: the unsteady behavior of the shock waves in the air inlets [10], the vortex shedding at the dump planes [51], the oscillations induced by the jet-on-jet impingement [32], and the coupling between the convective waves of entropy or vorticity and the acoustic waves [11]. All of those phenomena are prone to trigger instabilities, but, once again, being able to choose among them and point out, for any ramjet combustor, the root cause of the instability is still very difficult.

Concerning the experimental information available in the published material about unsteady motion in practical ramjet combustion chambers, only pressure measurements are available (e.g., [9] and [52]). One must recognize that it is insufficient to identify which mechanism is responsible for the unsteady behavior of the combustor. In this context, the Research Ramjet combustion chamber may be a very useful tool. First, pressure measurements have been performed to study the pressure oscillations encountered under various operating conditions, with piezoelectric transducers at a sampling frequency of up to 40 kHz [41][42][44]. Then, high speed cameras have been implemented to study the flame front oscillations at a sampling frequency of 2 kHz [41][42][44]. The spectra obtained with the analysis of the visualizations for the SDR configuration in the High Altitude flight regime at $\Phi=0.35$ are displayed in Figure 15: the two main low-frequency modes of the burner at approximately 100 and 400 Hz, also evidenced by pressure transducers [41][42], are obtained by the study of the flame dynamics.

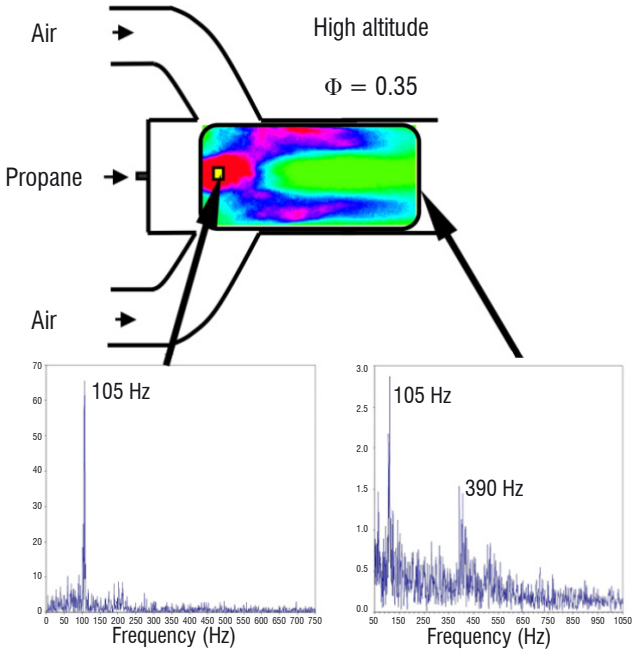

Figure 15 - FFT analysis of the flame visualizations obtained with a 2 kHz camera for the High Altitude $\Phi=0.35$ flight regime of the SDR configuration

In order to enable an in-depth analysis of the coupling mechanisms in a ramjet combustor that may be responsible for self-sustained unsteady motions, the coupling of unsteady experimental measurements is being applied within the framework of the Research Ramjet program. Thanks to this approach, very useful and quite unique data could be gathered. Recently, simultaneous visualizations of velocity fields, acquired with the PIV technique, and OH* emission at a sampling rate of 2 kHz, combined and synchronized with high-frequency pressure probe measurements, have been performed [44]. In this first attempt on the Research Ramjet combustor, it was applied to a stable operating case. In the future, the coupling of these two techniques could be applied to study hydrodynamic instabilities and, especially, the interactions between the vortex shedding at the dump plane (through velocity measurements) and the heat release (through radical OH visualization), which is one of the most likely mechanisms for combustion instability in ramjet engines. Such measurements would be, anyway, very useful to validate unsteady numerical simulations.

LES appears as the main tool to predict the occurrence of combustion instabilities in ramjet combustors. However, as mentioned in [22], the simulation of combustion instabilities is more complicated than the other issues mentioned above. Among the technical difficulties to be addressed, one can mention:

- The necessity for accurately predicting the instantaneous heat release, as it is the main provider of the energy transferred to the acoustics. In this respect, special care must be taken when modeling the kinetics, the interaction of combustion and turbulence, etc. Combustion modeling within the framework of LES

is still an open issue, which is beyond the scope of this paper (for additional information see, for example, the reviews in [7], [34] or [35]);

- The requirement for having a good description of the boundary conditions. Of prime interest are the upstream (oscillatory shocks in the inlet diffusers) and downstream (chocked nozzle) boundaries. Ramjet combustion chambers are usually compact enough to include air inlets and an exhaust nozzle in the computational domain at an affordable cost, making additional models like NSCBC unnecessary;
- The requirement for predicting the behavior of the disperse phase in the liquid-fueled ramjet combustors, and all of the phenomena related to it (secondary break-up, droplet heating and evaporation, droplet interaction with walls, etc.). Although it is not discussed in this paper, studies are being performed within the framework of the program to improve the simulation of the disperse phase in ramjet combustors;
- And, of course, the requirement for using a CFD code with numerical schemes as robust and accurate as possible, able to predict the propagation of the convective and acoustic waves without too much dissipation and dispersion, on unstructured meshes, with both supersonic and subsonic zones.

Results of LES aimed at predicting combustion instabilities in ramjet combustion chambers have not been published yet. However, increasing success of the LES approach to predict occurrence of combustion instabilities in other types of burners can be found in the literature (e.g., [13] [14] [16] [18] [54]). Consequently, there is no doubt that this technique may bring satisfactory results in the near future for ramjet combustors.

Conclusion and perspectives

A brief overview of the numerical and experimental studies conducted at ONERA to improve numerical simulations of ramjet combustors has been presented. Since the writing of a review article twenty years ago listing the main issues, many studies have been carried out to progress, especially within the framework of a specific program named “Research Ramjet”. A specific combustion chamber has been designed and optical measurement techniques have been applied in order to build-up a detailed database on internal reactive and non-reactive flows. Improvements have been achieved in the understanding of the physical phenomena and in the predictability of the numerical prediction. However, further studies are still required to accurately predict any operating condition in the entire flight range. Intermediate results of numerical simulations have been presented. The Lean Blow-Out of the SDR combustor has been successfully predicted with a RANS-PaSR model. Nevertheless, further calculations are necessary to assess and validate the ability of this approach to predict the LBO limits of any gaseous or liquid-fueled ramjet combustor. Auspicious results have been provided by LES, concerning the internal gaseous reactive and stable flow of ramjet engines. Nevertheless, none of the simulations performed has demonstrated its ability to accurately predict the overall performance parameters of the combustion chamber, namely the combustion efficiency and the pressure loss. One of the most encouraging prospects is the improvement of the near-wall physical phenomena simulation, such as friction and convective heat transfer, which affect the overall efficiencies. This could be effectively achieved by Detached Eddy Simulation. Note that this technique has already been successfully implemented with CEDRE [48][49]. Future experimental and numerical work should also focus on the self-sustained unsteady motions in ramjet combustors, with the aim of understanding the coupling mechanisms and developing the capacity of LES to predict combustion instabilities. ■

Acknowledgements

The authors thank the French *Délégation Générale de l’Armement* (DGA) for its financial support in the Research Ramjet program and its permission to publish these results. The authors also wish to thank their colleagues at ONERA for their contributions to this work.

References

[1] *Experimental and Analytical Methods for the Determination of Connected-Pipe Ramjet and Ducted Rocket Internal Performance.* AGARD Advisory Report 323, 1994.

[2] M. BERGLUND, E. FEDINA, C. FUREBY, J. TEGNER, V. SABEL'NIKOV – *Finite Rate Chemistry Large-Eddy Simulation of Self-Ignition in a Supersonic Combustion Ramjet.* AIAA Journal, Vol. 48, No. 3, pp. 540–550, 2010.

[3] N. BERTIER, L.-H. DOREY – *Mécanisme réactionnel avec PEA pour la combustion du kerosene dans l'air.* Rapport Technique RT 3/17454 DEFA, Onera, 2010.

[4] P. BERTON, R. MARGUET, B. PETIT – *Le Statoréacteur à l'Onera. Histoire et Perspectives.* Colloquium AAAF "Le Statoréacteur en France : Histoire et Avenir", 1991.

[5] C. BROSSARD, P. GICQUEL, M. BARAT, A. RISTORI – *Experimental Study of a High Speed Flow Inside a Dual Research Ducted Rocket Combustor Using Laser Doppler.* 11th International Symposium on Applications of Laser Techniques to Fluid Mechanics, 2002

[6] S. BYGGSTOYL – *A Model for Flame Extinction in Turbulent Flow.* 4th Symposium on Turbulent Shear Flows, 1983.

[7] S. CANDEL – *Combustion Dynamics and Control: Progress and Challenges*. Proceedings of the Combustion Institute, Vol. 29, Issue 1, pp 1-28, 2002.

[8] P. CAZIN – *Les Statoréacteurs à Combustible Liquide.* AGARD/PEP Lecture Series No.136 on "Ramjet and Ramrocket Propulsion Systems for Missiles", 1984.

[9] W. H. CLARK – *An Experimental Investigation of Pressure Oscillations in a Side Dump Ramjet Combustor.* AIAA/SAE/ASME 16th Joint Propulsion Conference, 1980.

[10] F.E.C. CULICK, T. ROGERS – *The Response of Normal Shocks in Diffusers.* AIAA Journal, Vol. 21, No.10, pp. 1382-1390, 1983.

[11] F.E.C. CULICK – *Combustion Instabilities in Liquid-Fueled Propulsion Systems – An overview.* AGARD Conference Proceedings, 450, 1988.

[12] F.E.C. CULICK – *Unsteady Motions in Combustion Chambers for Propulsion systems.* RTO AGARDograph AG- AVT- 039, 2006.

[13] C. DUWIG, C. FUREBY – *Large Eddy Simulation of Unsteady Lean Stratified Premixed Combustion.* Combustion and Flame, Vol. 151, pp. 85-103, 2007.

[14] B. FRANZELLI, E. RIBER, L.Y.M. GICQUEL, T. POINSOT – *Large Eddy Simulation of Combustion Instabilities in a Lean Partially Premixed Swirled Flame.* Combustion and Flame, Volume 159, Issue 2, pp. 621-637, 2012.

[15] R. S. FRY – *A Century of Ramjet Propulsion Technology Evolution.* Journal of Propulsion and Power, Vol. 20, No.1, 2004.

[16] A. GHANI, T. POINSOT, L. GICQUEL, G. STAFFELBACH – *LES of Longitudinal and Transverse Self-excited Combustion Instabilities in a Bluff-body Stabilized Turbulent Premixed Flame.* Combustion and Flame, Vol. 162, Issue 11, pp. 4075-4083, 2015.

[17] L. Y. M. GICQUEL, A. ROUX – *LES to Ease Understanding of Complex Unsteady Combustion Features of Ramjet Burners.* Flow Turbulence Combust., Vol. 87, pp. 449-472, 2011.

[18] X. HAN, J. LI, A.S. MORGANS – *Prediction of Combustion Instability Limit Cycle Oscillations by Combining Flame Describing Function Simulations with a Thermoacoustic Network Model.* Combustion and Flame, Vol. 162, Issue 10, pp. 3632-3647, 2015.

[19] G. HEID, A. RISTORI – *An Optical Method for Local Equivalence Ratio Measurements Applied to Hydraulic Simulation of a Ramjet Combustion Chamber.* Proceedings of PSFVIP-4, 2003.

[20] G. HEID, A. RISTORI – *Local Fuel Concentration Measurements in a Research Ramjet Combustion Chamber by Gas Sampling Analysis with Carbon Dioxide Injection at the Head End of the Combustor.* 17th International Symposium on Air Breathing Engines (ISABE), 2005.

[21] W. P. JONES, R. P. LINDSTEDT – *Global Reaction Schemes for Hydrocarbon Combustion.* Combustion and flame, Vol. 73, pp. 233-249, 1988.

[22] A. LAVERDANT – *Basic Research on Liquid Fuel Ramjets, Bibliographical Review and Critical Analysis.* La Recherche Aérospatiale, Vol. 5, pp. 311-323, 1995

[23] T. LE PICHON, V. SABEL'NIKOV, Y. MOULE, A. COCHET – *Assessment of a Partially Stirred Reactor Combustion Model to Predict the Lean Blow-Out limit of a Ramjet Combustor.* 18th AIAA International Space Planes and Hypersonic Systems and Technology Conference, 2012.

[24] R. LEDUC – *Early Work and Latest Realizations with Ram-Jet Engines.* American Rocket Society Semi-Annual Meeting, Cleveland, Ohio, June 1956.

[25] B. C. MAGNUSSEN – *The Eddy Dissipation Concept: a Bridge Between Science and Technology.* ECCOMAS Thematic Conference on Computational Combustion, Lisbon, Portugal, 2005.

[26] R. MARGUET, M. BARRERE, R. CERESUELA – *Propulsion des véhicules hypersoniques.* Note technique ONERA No.169, 1970.

[27] R. MARGUET – *Ramjet Research and Applications in France.* 9th International Symposium on Air Breathing Engines (ISABE), 1989.

[28] R. MARGUET, P. BERTON, F. HIRSINGER – *L'étude du statoréacteur supersonique et hypersonique en France de 1950 à 1974 (Application aux moteurs combines aérobies).* 75th AGARD/PEP on Hypersonic Combined Cycle Propulsion, 1995.

[29] R. MARGUET, P. CAZIN, F. FALEMPIN, B. PETIT – *Review and Comments on Ramjet Research in France.* 13th International symposium on Airbreathing engines (ISABE), 1997.

[30] X. MONTAZEL – *Étude expérimentale et modélisation de la combustion turbulente dans les foyers de statoréacteurs.* PhD thesis, Ecole Centrale Paris, 1994.

[31] Y. MOULE, V. SABEL'NIKOV, A. MURA – *Modeling of Self-Ignition Processes in Supersonic Non Premixed Coflowing Jets Based on a PaSR Approach.* 17th AIAA International Space Planes and Hypersonic Systems and Technologies Conference, 2011.

[32] N. S. NOSSEIR, U. PELED – *The Pressure Field Generated by Jet-Jet Impingement.* 10th Aeroacoustics Conference, 1986.

[33] B. PETIT – *Ramjets and Scramjets.* Encyclopedia of Physical Science and Technology, Third Edition, pp. 867-884, 2002.

[34] H. PITSCH – *Large-Eddy Simulation of Turbulent Combustion.* Annu. Rev. Fluid Mech., no 38, pp 453-482, 2006.

[35] T. POINSOT, D. VEYNANTE - *Theoretical and Numerical Combustion.* Second Edition, 2005.

[36] S. REICHSTADT, N. BERTIER, A. RISTORI, P. BRUEL – *Towards LES of Mixing Processes Inside a Research Ramjet Combustor.* 18th International Symposium on Air Breathing Engines (ISABE), 2007.

[37] S. REICHSTADT – *Etude du mélange et de la combustion monophasique dans un statoréacteur de recherche.* PhD thesis, Université de Pau et des Pays de l'Adour, 2007.

[38] A. RISTORI, G. HEID, A. COCHET, G. LAVERGNE – *Experimental and Numerical Study of the Turbulent Flow inside a Dual Inlet Research Ducted Rocket Combustor.* 14th International Symposium on Air Breathing Engines (ISABE), 1999.

[39] A. RISTORI, A. COCHET – *Research Ramjet Program: an Initiative to Improve Knowledge on Ramjet Reactive Flowfields.* 4th Onera/DLR Aerospace Symposium, 2002.

[40] A. RISTORI, G. HEID, C. BROSSARD, A. BRESSON – *Characterization of the Racting Two-Phase Flow Inside a Research Ramjet combustor.* International Conference on Liquid Atomization and Spray Systems (ICLASS), 2003.

[41] A. RISTORI, G. HEID, C. BROSSARD, S. REICHSTADT – *Detailed Characterization of the Reacting One-Phase and Two-Phase Flow Inside a Research Ramjet Combustor.* 17th International Symposium on Air Breathing Engines (ISABE), 2005.

[42] A. RISTORI, C. BROSSARD, P. GICQUEL, M. BARAT, F. SOULIGNAC – *Caractérisation détaillée de l'écoulement par PIV et des instabilités de combustion par caméra vidéo rapide intensifiée dans la région du dôme du Statoréacteur de Recherche.* Congrès francophone de Techniques Laser (CFTL), 2006.

[43] A. RISTORI, S. REICHSTADT, C. BROSSARD, G. HEID – *PIV and Gas Sampling Analysis Measurements for Fuel-to-Air Mixing Study Inside a Research Ramjet Combustor.* 13th International Symposium on Flow Visualization / 12th French Congress on Visualization in Fluid Mechanics, 2008.

[44] A. RISTORI, C. BROSSARD, T. LE PICHON – *Caractérisation de l'écoulement instationnaire dans un Statoréacteur de Recherche par PIV et visualisations OH* à hautes cadences simultanées.* 14ème Congrès Francophone de Techniques Laser (CFTL), 2014.

[45] A. ROUX, S. REICHSTADT, N. BERTIER, L. Y. M. GICQUEL, F. VUILLOT, T. POINSOT – *Comparison of Numerical Methods and Combustion Models for LES of a Ramjet.* C. R. Mecanique, Vol. 337, No.6, p. 352-361, 2009.

[46] A. ROUX – *Simulation aux Grandes Echelles d'un statoréacteur.* PhD thesis, Institut National Polytechnique de Toulouse, 2009.

[47] A. ROUX, L. Y. M. GICQUEL, S. REICHSTADT, N. BERTIER, G. STAFFELBACH, F. VUILLOT, T. J. POINSOT – *Analysis of Unsteady Reacting Flows and Impact of Chemistry Description in Large Eddy Simulations of Side-Dump Ramjet Combustors.* Combustion and Flame, Vol. 157, No.1, pp. 176-191, 2010.

[48] B. SAINTE-ROSE, N. BERTIER, S. DECK, F. DUPOIRIEUX – *A DES Method Applied to a Backward Facing Step Reactive Flow.* C. R. Mécanique, Vol. 337, Issues 6–7, pp. 340-351, 2009.

[49] B. SAINTE-ROSE, N. BERTIER, S. DECK, F. DUPOIRIEUX – *Numerical Simulations and Physical Analysis of an Overexpanded Reactive Gas Flow in a Planar Nozzle.* Combustion and Flame, Vol. 159, Issue 9, pp. 2856-2871, 2012.

[50] J-M. SAMANIEGO – *Etude des instabilités de combustion dans les statoréacteurs.* PhD thesis, Ecole Centrale Paris, 1992.

[51] K. C. SCHADOW, E. GUTMARK – *Combustion Instability Related to Vortex Shedding in Dump Combustors and their Passive Control.* Prog. Energy Combust. Sci., Vol. 18, pp. 117-132, 1992.

[52] B. SJÖBLOM – *Full-Scale Liquid Fuel Ramjet Combustor Tests.* 9th International Symposium on Air Breathing Engines, Vol. 1, pp 273-281, 1989.

[53] J. SMAGORINSKY – *General Circulation Experiments with the Primitive Equations. I. The Basic Experiment.* Monthly Weather Review, Vol. 91, No.3, 1963.

[54] G. STAFFELBACH, L.Y.M. GICQUEL, G. BOUDIER, T. POINSOT – *Large Eddy Simulation of Self Excited Azimuthal Modes in Annular Combustors.* Proceedings of the Combustion Institute, Volume 32, Issue 2, pp. 2909-2916, 2009.

[55] Y. M. TIMNAT – *Recent Developments in Ramjets, Ducted Rockets and Scramjets.* Prog. Aerospace Sci., Vol. 27, pp. 201-235, 1990.

[56] C. WESTBROOK, F. DRYER – *Simplified Reaction Mechanisms for the Oxidation of Hydrocarbon Fuels in Flame.* Comb. Science and Technology, Vol. 27, pp. 31-43, 1981.

[57] K-A. ZETTERSTRÖM, B. SJÖBLOM, A. JARNMO – *Solid Ducted Rocket Engine Combustor Tests.* 6th International Symposium on Air Breathing Engines, pp 9-16, 1983.

Acronyms

CEDRE	(*Calculs d'Ecoulements Diphasiques Réactifs pour l'Energétique)*
CFD	(Computational Fluid Dynamics)
CFL	(Courant Friedrichs Lewy)
DES	(Detached Eddy Simulation)
EDC	(Eddy Dissipation Concept)
EM2C	(*Energétique Moléculaire et Macroscopique, Combustion)*
HA	(High Altitude)
IRR	(Integral Rocket Ramjet)
LBO	(Lean Blow-Out)
LDV	(Laser Doppler Velocimetry)
LES	(Large Eddy Simulation)
LIC	(Lateral Injection Combustor)
LFRJ	(Liquid-Fueled Ramjet)
PaSR	(Partially-Stirred Reactor)
PIV	(Particle Image Velocimetry)
PSR	(Perfectly Stirred Reactor)
RANS	(Reynolds Averaged Navier-Stokes)
RRP	(Research Ramjet Program)
SDR	(Solid Ducted Rocket)

AUTHORS

Thomas Le Pichon graduated from ENSMA and joined ONERA in 2009 as a research engineer. His activities are mainly focused on ramjet propulsion, including experimental and numerical studies. He has been responsible for the Research Ramjet Program since 2009.

Alain Laverdant graduated in 1976 from ESTACA, obtained his Masters Degree in Energetics and Fluid Mechanics in 1978, and his PhD in 1981. He received his *Thèse d'Etat* in combustion in 1991. He has been a Research Engineer in the Energetics Department of ONERA since 1981, and his activities are focused on acoustic combustion instabilities and reactive numerical simulations. He received the Estrade-Delcros, Houllevigue, Saintour, Jules Mahyer Prize from the French Science Academy in 1991.

D. Scherrer, O. Dessornes, M. Ferrier, A. Vincent-Randonnier, V. Sabel'nikov
(ONERA)
Y. Moule
(MBDA France)

E-mail: dominique.scherrer@onera.fr

DOI : 10.12762/2016.AL11-04

Research on Supersonic Combustion and Scramjet Combustors at ONERA

An overview of selected ONERA research activities on supersonic combustion and scramjet propulsion for civilian applications since 1992 is presented. The main part is devoted to basic research on supersonic combustion, including experimental database acquisition and combustion modeling. More applied studies on injection and flame stabilization in research scramjet combustors are then described and the article ends with a presentation of activities dedicated to real scramjet combustor design and characterization. This research was carried out either within the framework of three majors programs, PREPHA (1992-1997), JAPHAR (1997-2001), and LAPCAT II (2008-2013), or with internal funding.

Introduction

Supersonic combustion has been a research topic at ONERA since the 1960s. Supersonic combustion tests in simple configurations were performed between 1962 and 1967 at the Palaiseau research center [1]: this research demonstrated the possibility of achieving stable combustion with liquid kerosene and gaseous hydrogen in a Mach=2.5-3 air flow. At the same time, system studies concluded to the possibility of operating a fixed geometry dual mode ramjet for a flight range between Mach 3 and Mach 7 [2]. An important program, ESOPE, was then initiated in 1966 to assess the propulsive balance of an axisymmetric dual mode ramjet by means of ground tests and to compare it to the theory [3]. This activity was sustained by basic research on mixing and ignition in a supersonic air flow [4][5]. The ESOPE engine was tested under Mach 6 conditions in the ONERA Modane S4 hypersonic wind tunnel. Only transonic combustion was obtained under these flight conditions: the flow was choked somewhere in the combustor so combustion started in the subsonic regime and continued in the supersonic regime after the thermal throat. Tests under Mach 7 conditions, where supersonic combustion was expected, were finally not performed due to the cancellation of the program in 1972: it was then considered that hypersonic airbreathing propulsion was plagued with too many uncertainties, in particular in assessing the propulsive balance, and priority was given to rocket engines for high-speed propulsion.

The renewal of supersonic combustion studies at ONERA dates from 1992 with the PREPHA program (1992-1997), which involved ONERA and all of the French aerospace industry, under the aegis of the CNES, the DGA and the Research Ministry [6]. The main goal of the program was to study and ground-test the components (air intake, combustor, nozzle) of a scramjet concept for a space launcher application. In addition to the development of know-how for the design of scramjet components, this program provided the opportunity to develop high-enthalpy propulsion facilities at ONERA Palaiseau (Laerte for basic research on supersonic combustion and ATD5 for small scale scramjet combustors) and AEROSPATIALE Le Subdray for larger scramjet combustors. The large scale scramjet CHAMOIS was tested under Mach 6 conditions at AEROSPATIALE Le Subdray and the small scale scramjet MONOMAT was tested under conditions between Mach 4 and Mach 7.5 in the ATD5 facility at ONERA. In parallel, an important activity was dedicated to combustion modeling and validation, including the acquisition of an experimental database on supersonic combustion and the development of suitable optical diagnoses.

At the end of the PREPHA program, the DLR and ONERA decided to engage in a common research activity on airbreathing hypersonic propulsion: the JAPHAR program (1997-2001) [7][8]. The studies were anchored on a 10 m long experimental vehicle in the Mach 4 to 8 flight range. The experimental and numerical studies concerned all of the vehicle components, but the largest part of the activities was dedicated to the fixed-geometry dual-mode ramjet combustor. Tests of this combustor in the ATD5 facility demonstrated the capacity to operate the combustor in the various expected combustion regimes depending on the flight Mach number. In parallel, the experimental database initiated in the PREPHA program was completed with new measurements.

After the JAPHAR program, scramjet research at ONERA was reoriented mainly towards military applications, but a significant activity was maintained on civilian applications. In 2003, common experimental research on strut injectors for scramjet combustors was undertaken between ONERA and JAXA [9]. Between 2008 and 2013, ONERA participated in the LAPCAT II European program, aiming to develop technologies for a hypersonic passenger transport aircraft [10][11]. In parallel, a continuous combustion modeling and CFD code development activity was maintained with internal funding.

This paper gives an overview of the most significant research activities at ONERA since 1992 in the field of scramjets for civilian applications. They are presented from the most fundamental to the most applied. Following this introduction, the second part of the article is dedicated to the acquisition of an experimental database on supersonic combustion within the framework of PREPHA and JAPHAR programs. The third part deals with supersonic combustion modeling. In the fourth part, we present some studies on injection (ONERA-JAXA cooperation) and flame stabilization (LAPCAT II) in research scramjet combustors. Finally, the fifth part is dedicated to the design and study of scramjet combustors within the framework of JAPHAR and LAPCAT II programs.

Experimental database on supersonic combustion with axial and wall injection

Within the framework of PREPHA (1992-1997) and JAPHAR program (1997-2001), a quite complete experimental database on supersonic combustion has been set up at Onera on the Laerte combustor for the sake of code validation (Figure 1). This small size combustor (45×45 mm² in entrance) has a constant section for a 370 mm length, followed by a slightly diverging part (1.15° half angle) for a 500 mm length. It is fed with air at Mach 2. The test rig is equipped with a heat exchanger, that brings the air flow temperature up to 800 K, and with a hydrogen burner with oxygen replenishment that finally provides a maximum stagnation temperature of 1850 K for a total pressure of 7 bar. This provides a static temperature of 1100 K at the combustor entrance, which ensures self ignition of the fuel (gaseous hydrogen). For fuel injection, two configurations are available. The first one is an axial injection at Mach 2 of a cylindrical 6 mm diameter jet, located 33 mm downstream of the combustor entrance, in the center of the air flow. The second one is a Mach 2 wall injection (not represented), at a 45° angle with the air flow, located on the upper wall, 86 mm downstream of the combustor entrance. The fuel is gaseous hydrogen, which can be heated to a maximum temperature of 500 K by a heat exchanger.

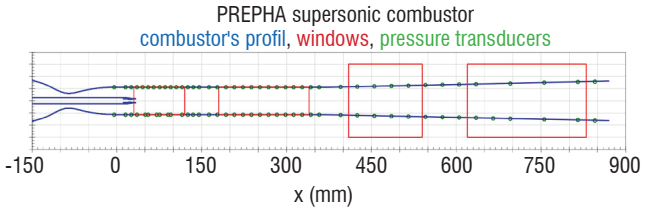

Figure 1- sketch of the Laerte combustor

For the axial injection, quite a complete database has been acquired on this configuration. It includes:

- wall pressure measurements;
- OH radical visualizations by spontaneous emission and PLIF [12], which also provides OH concentration (the calibration of the PLIF signal enables the mass fractions to be determined with an uncertainty of about 20%);
- H_2 jet visualizations by PLIF with acetone seeding [12];
- temperature measurements by CARS on N_2 and H_2 molecules [12][13];
- velocity measurements by laser interferometric velocimetry [14];
- velocity measurements by Particles Imaging Velocimetry (performed by a DLR Lampoldshausen team) [15];
- stagnation temperature measurements at the exit of the test channel.

For wall injection, the database includes:

- wall pressure measurements;
- OH radical visualizations by OH spontaneous emission and PLIF;
- H_2 jet visualizations by PLIF with acetone seeding;
- temperature measurements by CARS on H_2 molecules.

Figure 2 and Figure 3 show, for the axial injection at $x/D=30$ (D is the hydrogen jet diameter), the difference between OH visualization by spontaneous emission and by PLIF. For spontaneous emission, the signal is integrated over the entire width of the combustor and the exposure time is 1 ms, which averages the picture. Conversely, PLIF provides a view in the laser plane with a very short exposure time (12 ns), which allows the details of the reactive zone to be seen: it appears that combustion takes place at the periphery of the jet, in intermittent pockets.

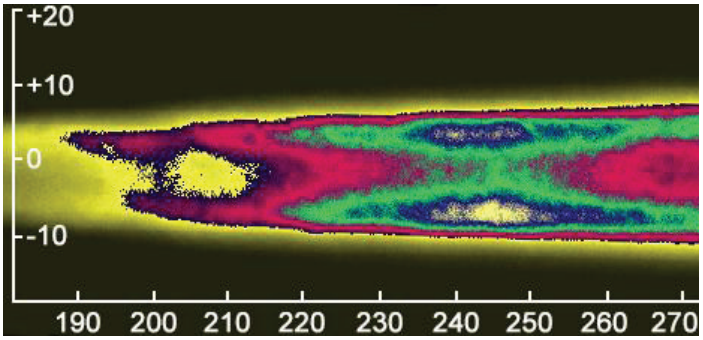

Figure 2 - Axial injection - OH spontaneous emission

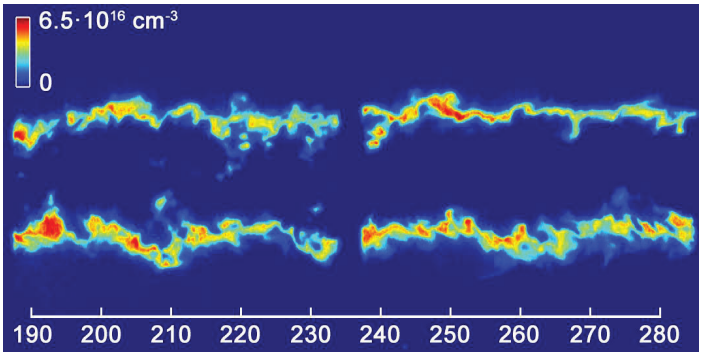

Figure 3 - Axial injection - OH visualization by PLIF

The collected data can be used for code validation. Figure 4 shows a comparison between the RANS computation and the experiment for the transverse contour of the OH mass fraction at $x/D=35$. Since the visualizations do not provide accurate absolute values, the experimental contour deduced from the PLIF visualization has been scaled, in order to fit the maximum value with the computed one.

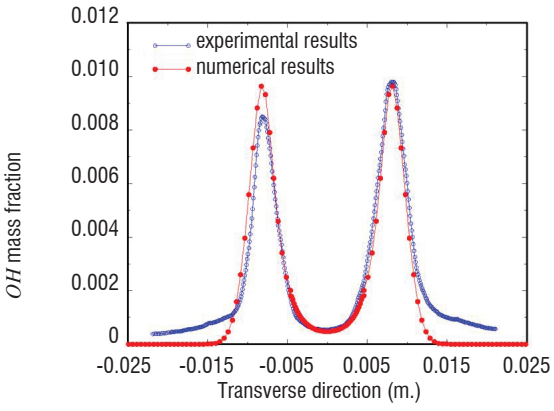

Figure 4 - Axial injection - OH mass fraction transverse contour

One can see that the position of the maxima is well respected by the computation, as well as the level inside the jet. A small discrepancy exists outside the jet, where the computed values vanish more quickly than the experimental ones.

Particle Image Velocimetry measurements were performed on the Laerte combustor for axial injection by a DLR Lampoldshausen team [15]. The application of PIV to high speed flows with large velocity gradients requires the use of submicron tracer particles, in order to minimize the particle slip velocity. In this case, the air flow was fed with Aerosil R812 particles (surface treated silica, hydrophobic, primary diameter 12 nm). Figure 5 provides an example of PIV measurement, slightly downstream from the injection, before ignition occurs. The measured velocity fields allow the instantaneous vortices to be visualized: they clearly show the structure of the flow and can be used, for example, to determine the size of the vortices and the shear layer expansion rate.

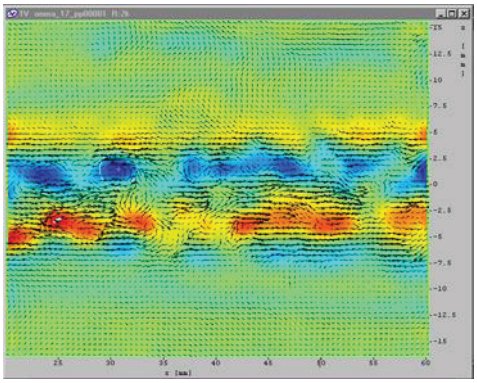

Figure 5 - Axial injection - PIV- Instantaneous velocity fluctuations (difference with mean values) and vortex strength

Instantaneous temperature measurements were obtained by Coherent Anti-Stokes Raman Scattering (CARS) on H_2 (inside the hydrogen jet) and N_2 (outside the jet) molecules. CARS thermometry is well suited for time-resolved measurements in turbulent flows. Figure 6 shows the transverse time-averaged temperature contour downstream from the injection, before ignition. The 160 K measured temperature in the jet core and the 1200 K temperature in the air flow are in agreement with the expected values.

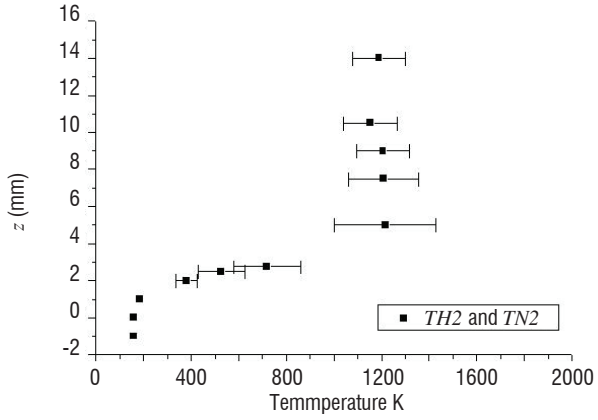

Figure 6 - Axial injection - CARS temperature measurement at x=43 mm (10 mm downstream from the injection)

Visualization of the hydrogen jet can be achieved by seeding the jet with acetone and performing PLIF on this molecule. This was done for wall injection in combination with PLIF on OH. These visualizations are illustrated in Figure 7. The exit from the wall injector (left) and a zone further downstream (right) were visualized. Pictures (a) and (c) correspond to PLIF on acetone and allow the hydrogen jet to be visualized. One observes that the jet remains adhered to the wall. Pictures (b) and (d) correspond to PLIF on OH. The residual OH due to the heater is visible, but one can see that no ignition exists in the vicinity of the injection: high OH signals are visible only in the second zone, firstly at the jet periphery, then quickly inside the jet, which indicates the presence of large-scale oscillations of the jet.

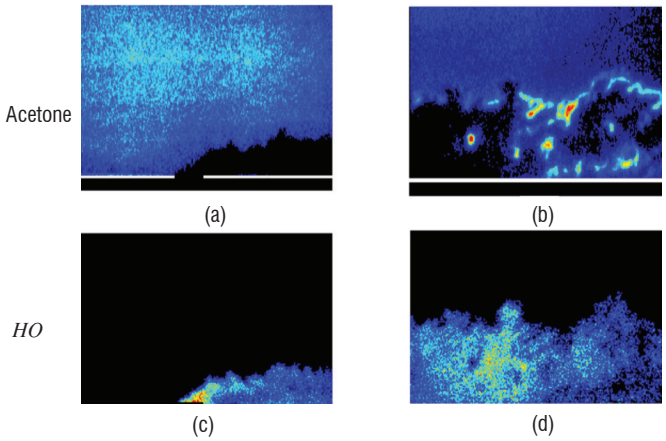

Figure 7 - Wall injection - Acetone and OH PLIF visualizations

Turbulent combustion modeling in supersonic flows

Due to the difficulty in reproducing true flight conditions in ground tests, computational fluid dynamics (CFD) offers an attractive tool for the study of high-speed turbulent reactive flows. However, the most standard closures for combustion modeling, which are based on the fast chemistry approximation, are not appropriate for such type of conditions, where combustion is largely governed by finite-rate chemistry effects and self-ignition phenomena.

Under these conditions, chemical reaction timescales indeed tend to have the same order of magnitude as turbulent timescales, with resulting Damköhler number values close to unity. In such combustion regimes, the application of fast chemistry assumptions associated with either equilibrium approximation or flamelet closures, where the flow field modeling is decoupled from chemistry, therefore becomes less appropriate, and finite-rate chemistry-based closures seem more appealing to describe supersonic combustion.

The focus of this study is thus on the development and validation of a finite-rate chemistry-based closure suitable for the description of supersonic combustion: the unsteady partially stirred reactor (U-PaSR) closure. The model is described in § "Turbulence-chemistry interaction (TCI) model: U-PaSR" and validation computations are presented in § "Validation of the model on the supersonic lifted jet flame of Cheng". Rather than the Laerte experiment, which has been extensively used in the past [16][17][18][19], the supersonic lifted jet flame of Cheng was retained for these validation computations, because this configuration presents the advantage of having been simulated by different teams, allowing fruitful comparisons.

Turbulence-chemistry interaction (TCI) model: U-PaSR

The high non-linearity of the instantaneous reaction rate $\dot{\omega}_k(T, Y_k)$ (Arrhenius Law) makes its filtered or averaged counterpart very difficult to model. When dealing with high-speed (supersonic)

combustion applications, a first-order simplification is often retained as a preliminary step, within the framework of the quasi-laminar (QL) combustion assumption, or homogeneous reactor (HR) approximation, which ignores the influence of the composition and temperature fluctuations: the subgrid scale (SGS) chemical rate of any k species is approximated by $\dot{\omega}_k\left(\tilde{T},\tilde{Y}_k\right)$, where $\tilde{\phi}$ designates the Favre average of a quantity ϕ. However, the composition and temperature fluctuations may play a crucial role in the thermal runaway processes that take place in the mixing layer until ignition occurs.

The unsteady partially stirred reactor (U-PaSR) model thus offers an interesting basis to incorporate the effects associated with these heterogeneities, within either a Reynolds-averaged Navier–Stokes (RANS) or a large eddy simulation (LES) framework. This model is an evolution of the Eddy Dissipation Concept (EDC) model introduced in the early works of Vulis [20], and Magnussen, see [21], [22], [23] .

Like the EDC model, the U-PaSR model relies on the highly intermittent character of turbulence and implies that chemical reactions are concentrated in fine-scale structures, where most of the viscous dissipation and molecular mixing processes take place. Turbulent mixing actually operates in the vicinity of very fine scale elongated structures, i.e., filament-like vortex structures or worms, the transverse dimension of which are of the order of the Kolmogorov length scale η_K (between 6 and 10 η_K). The structures that concentrate dissipation (mixing) processes coexist with non-homogeneous but weak vorticity zones, where scalar mixing is simply considered as inefficient for combustion. Following this physical representation of the flow, the U-PaSR model makes the assumption that each elementary volume of fluid is divided into fine-scale structure regions (denoted by *), featuring high scalar dissipation rate levels and surroundings (denoted by 0). The fine-scale structure regions (*) are supposed to behave like a perfectly stirred reactor (PSR), with potentially high reaction rates due to favorable mixing conditions. They are surrounded by other regions (0) featuring a vanishingly small reaction rate. From a mathematical point of view, the mean reaction rate $\bar{\dot{\omega}}_k$ can be expressed as:

$$\bar{\dot{\omega}}_k = \int_\Psi P(\psi)\dot{\omega}_k(\psi)d\psi$$

where P denotes the joint scalar PDF (Probability Density Function), $\psi=\left[T,Y_k\right]^T$ is the sample composition vector and Ψ is the associated domain of definition of the PDF. Considering the important levels of the mixing rate in zone (*), it is supposed to behave as a homogeneous medium and is thus represented in the PDF by a Dirac delta peak located at $\psi=\psi^*$. Strictly speaking, the zone (0) may be far from being homogeneous, since it is characterized by inefficient mixing levels but, for the sake of simplicity, the corresponding state (0) is also assimilated in the model to a single Dirac delta peak located at $\psi=\psi^0$: this approximation has no effect on $\bar{\dot{\omega}}_k$, since the reaction rates are vanishingly small in the zone (0). Thus, the resulting PDF is assumed to be bimodal:

$P(\psi)=\gamma^*\delta\left(\psi-\psi^*\right)+\left(1-\gamma^*\right)\delta\left(\psi-\psi^0\right)$, where γ^* denotes the volume fraction of the zone (*).

The mean chemical rate can then be expressed as:

$$\bar{\dot{\omega}}_k=\gamma^*\dot{\omega}_k\left(\psi^*\right)+\left(1-\gamma^*\right)\dot{\omega}_k\left(\psi^0\right)$$

Following the above discussion, the second contribution in this equation is considered to be zero. The mean chemical source term can therefore be rewritten as:

$$\bar{\dot{\omega}}_k=\gamma^*\dot{\omega}_k\left(\psi^*\right)$$

T^* and the Y_k^* are determined by the resolution of the following evolution equations:

$$\frac{\partial\bar{\rho}Y_k^*}{\partial t}+\bar{\rho}\frac{Y_k^*-Y_k^0}{\tau_m}=\dot{\omega}_k\left(T^*,Y_k^*\right)$$

$$\frac{\partial\bar{\rho}h^*}{\partial t}+\bar{\rho}\sum_{k=1}^{n}\frac{Y_k^*h_k^*-Y_k^0h_k^0}{\tau_m}=\sum_{k=1}^{n}h_{k_f}\dot{\omega}_k\left(T^*,Y_k^*\right)$$

These equations can be viewed as the mass and energy balance equations for the zone (*), where the convective terms have been neglected.

The state ψ^0 does not need evolution equations, since it can be determined by the relation $\tilde{\psi}=\gamma^*\psi^*+\left(1-\gamma^*\right)\psi^0$ where $\tilde{\psi}$ is provided by the gas solver. In practice, the only additional equations to be solved are the equations for h^* and Y_k^*, which can be rewritten as:

$$\frac{\partial\bar{\rho}Y_k^*}{\partial t}+\bar{\rho}\frac{Y_k^*-\tilde{Y}_k}{\tau_m\left(1-\gamma^*\right)}=\dot{\omega}_k\left(T^*,Y_k^*\right)$$

$$\frac{\partial\bar{\rho}h^*}{\partial t}+\bar{\rho}\sum_{k=1}^{n}\frac{Y_k^*h_k^*-\tilde{Y}_k\tilde{h}_k}{\tau_m\left(1-\gamma^*\right)}=\sum_{k=1}^{n}h_{k_f}\dot{\omega}_k\left(T^*,Y_k^*\right)$$

Finally, γ^* is modeled by the expression $\gamma^*=\tau_{ch}/\left(\tau_{ch}+\tau_m\right)$, where τ_{ch} is the chemical time scale and τ_m is the mixing time scale.

In this equation, τ_m is estimated as the harmonic mean value of the Kolmogorov time scale τ_k and the subgrid time scale τ_Δ, i.e., $\tau_m=\sqrt{\tau_K\tau_\Delta}$, where $\tau_\Delta=\Delta/\nu'$ and $\nu'=\sqrt{2k/3}$ (see [24], for instance). The Kolmogorov time scale is deduced from $\tau_K=\sqrt{\nu/\varepsilon}$, where $\varepsilon=k^{3/2}/\Delta$ and $k=\left(\frac{\nu_t}{0.069}\Delta\right)^2$.

There are different possible ways to estimate the chemical time scale τ_{ch} . Here, following a recent computational investigation performed with the same closure [25], it is evaluated by using the transit time obtained from a one-dimensional laminar premixed flame calculation performed at stoichiometry. The transit time is defined as the ratio of the premixed flame thickness δ_L to its propagation velocity S_L. The choice of this time to estimate the chemical time scale is retained only for the sake of simplicity. However, it seems worth noting here that, following the early analyses by Liñan, the characteristic chemical time scale that can be obtained from a diffusion flame at the limit of extinction is itself similar to the present estimate [26]. The choice of this peculiar time scale may therefore be relevant for both diffusion and premixed flames.

Validation of the model on the supersonic lifted jet flame of Cheng

Experimental setup and associated data

The NASA Langley Research Center (LaRC) has been deeply involved in the study of supersonic combustion over the years. Test campaigns were carried out on various experimental setups. Among these, a Mach 2 supersonic burner described by Jarret et al [27] was developed

and studied in detail by Cheng et al [28][29]. The purpose of such an experimental setup, schematically depicted in Figure 8, is to analyze the elementary physical processes involved in the auto-ignition of hydrogen-air mixtures and the stabilization of non-premixed combustion under supersonic conditions. From that perspective, sonic hydrogen is injected into a coflowing supersonic jet of hot vitiated air. The apparatus is axisymmetric and includes a cylindrical central fuel injector (2.36 mm in diameter) and an annular nozzle (17.78 mm in diameter). The vitiated air stream is accelerated through a convergent-divergent nozzle and reaches Mach 2 at a static temperature of 1250 K (see Table 1). Such a high value of the temperature favors the early development of the chemical processes within the mixing layer, leading to self-ignition and diffusion flame stabilization.

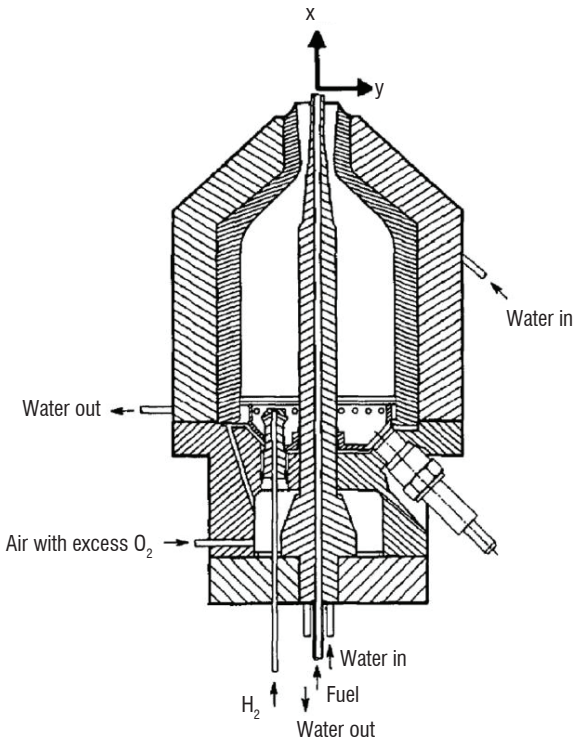

Figure 8 - Schematic diagram of the supersonic burner, from reference [29]

A primary combustion chamber provides the required stagnation conditions through hydrogen combustion in oxygen–enriched air. The combustion chamber and the fuel injector are water-cooled. However, even if the cooling water temperature is measured, its value is not reported in available references. The wall temperature profile in the combustion chamber therefore remains completely unknown. In addition to this, the internal geometry of the primary combustion chamber is not detailed. The nominal operating conditions studied by Cheng et al[29] are reported in Table 1.

Since both streams are slightly above ambient pressure at the nozzle exit, they give birth to a system of successive low amplitude compression and expansion waves. Multiple measurements were conducted in this geometry. Simultaneous measurements of temperature and species concentrations (main species and OH radical) were obtained by resorting to ultraviolet spontaneous vibrational Raman scattering and laser-induced predissociative fluorescence techniques. For instance, Jarett et al [27] reported mean temperature and chemical species (N_2 and O_2) concentration profiles resulting from coherent anti-Stokes Raman scattering measurements (CARS), as well as mean velocity profiles obtained by Laser Doppler Anemometry (LDA). The publications by Cheng et al [28] [29] gather mean and root mean square (RMS) profiles for temperature and mole fractions of major species O_2 , H_2 , H_2O , N_2 and OH at seven cross-sections located at axial distances $X/D = \{0.85; 10.8; 21.5; 32.3; 43.1; 64.7; 86.1\}$. Scatter plots of temperature and main species mole fractions are also available at six different locations $(X/D; Y/D) = \{(0.85, -0.65); (10.8, -0.65); (32.3, -1.1); (32.3, 1.1); (43.1, 0); (86.1, 0)\}$. The experimental database thus provides detailed data on the fluid mechanical scales and on the flow composition at $X/D = 0.85$, a very short distance from the nozzle exit compared to the experimental flame stabilization lift-off height ($X/D \approx 25$). Finally, Dancey [30] reported radial profiles of mean and RMS axial velocity measured with LDA. Experimental profiles of average data and associated RMS values have been gathered at seven distinct downstream locations for the major chemical species, namely, N_2 , O_2 , H_2 and H_2O, as well as for the OH radical and temperature. They have been evaluated from 500 to 2000 independent laser shots. The obtained RMS values reported by Cheng et al[29] confirm that temperature and species fluctuation levels can reach up to 20% and 40%, respectively. Given that the flame involves self-ignition, and combustion between non-premixed or partially premixed reactants under strongly fluctuating flow conditions, it offers a challenging test case for numerical simulation of high-speed turbulent combustion.

Geometrical parameters	
Nozzle exit i.d. (mm)	17.78
Fuel injector i.d. (D) (mm)	2.36
Fuel injector o.d. (mm)	3.81
Vitiated air conditions - Stagnation conditions	
Total pressure (Pa)	778,000 (±4%)
Total temperature (K)	1750
Vitiated air mass flow rate (kg/s)	0.09633 (±2.2%)
Exit conditions	
Pressure (Pa)	107,000
Temperature (K)	1250
Mach	2
Velocity (m/s)	1420
O_2 mode fraction (-)	0.201
N_2 mode fraction (-)	0.544
H_2O mode fraction (-)	0.255
Fuel conditions - Stagnation conditions	
H_2 ma&ss flow rate (kg/s)	0.000362(±3%)
Exit conditions	
Pressure (Pa)	112,000
Temperature (K)	545
Mach	1.0
Velocity (m/s)	1780
H_2 mode fraction (-)	1.0

Table 1- Supersonic burner nominal operation conditions

Large eddy simulation of the supersonic lifted jet flame

Numerical aspects

All computations were performed with the ONERA in-house code CEDRE, which is the reference tool at ONERA for energetics and multiphysics applications [32][33].

Computational domain and mesh

In order to properly specify the boundary conditions at the entrances, the internal geometry of the nozzle is included in the computational field. An important effort has been devoted to the representation of the nozzle exit and the description of the associated compressible shear layers. The computational field is supplemented by a large buffer region, to handle the far field boundary conditions without any numerical stability problems.

The mesh is composed of hexahedrons inside the flow field and prism layers alongside the walls. The characteristic cell size at the exit of the nozzle, inside the jet, is 0.2 mm. The prism layer alongside the walls of the primary combustion chamber is composed of five layers spread over a 0.1 mm thickness. Details of the mesh in the vicinity of the nozzle are represented in Figure 9. The number of cell elements of the final mesh is approximately 31,000,000. The whole mesh is divided into 480 domains handled by 480 bi-processor 3.07 GHz Westmere cores.

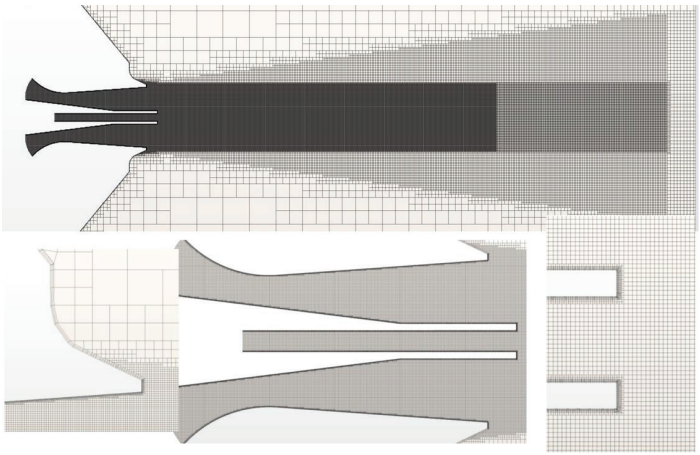

Figure 9 - Cheng lifted flame - Details of the mesh

Subgrid scale models

The subgrid scale turbulent viscosity μ_{SGS} is modeled through a standard Smagorinsky model, where the constant C_S has been set to 0.1. The U-PaSR closure is used to integrate the TCI effects. The chemical composition is described using nine species (H_2, H_2O, N_2, O_2, OH, H, O, HO_2 and H_2O_2) and the finite rate chemical reactions are described with the nineteen-step chemical scheme proposed by Jachimowski [31].

Numerical schemes

For this application, inviscid fluxes are computed using the HLLC (Harten-Lax-van Leer Contact) approximate Riemann solver proposed by Toro et al[34] and second-order accuracy is achieved via variable extrapolation, also often referred to as the Monotonic Upwind Scheme for Conservation Laws (MUSCL). It is applied in conjunction with Van Leer flux limiters to ensure the monotonicity of the numerical scheme. Temporal integration is processed with a second order explicit Runge–Kutta numerical scheme.

Boundary conditions

The boundary conditions at the entrances are set in terms of total quantities. A similar strategy has been retained in the RANS investigations conducted by Gerlinger [35] and Karl [36]. In practice, the stagnation temperature level of the vitiated air at the entrance has been set at 2050 K. This value, larger than that provided by Cheng in [29], enables the level of temperature to be recovered at the exit plane of the nozzle, which was measured by CARS and reported by Cheng [29]. Gerlinger [35] previously discussed the necessity of proceeding with such adjustments in his detailed investigation of the influence of inflow conditions on the numerical simulation of this lifted supersonic lifted flame. The experiments were carried out in a long-duration facility and therefore hot walls are considered to be isothermal at a temperature $T_w = 500$ K. No turbulence is injected at the entrances, mainly due to a lack of experimental data, especially for the turbulence spectrum, in the nozzle exit section.

Results and discussion

Flame structure

An instantaneous representation of the flame structure is depicted in Figure 10. In the top picture, a snapshot of the instantaneous temperature field superimposed with a H_2 mass fraction iso-surface (white) is provided. In the bottom picture, Q-criterion and OH mass fraction iso-surfaces are presented, both colored by temperature. Four regions can be outlined from the flame structure. The induction zone ($0 < X/D < 10$), the auto-ignition zone ($10 < X/D < 18$), the stabilization region ($18 < X/D < 26$), where the flame anchors at the beginning of a shock diamond and, finally, the end of the combustion zone ($30 < X/D < 34$).

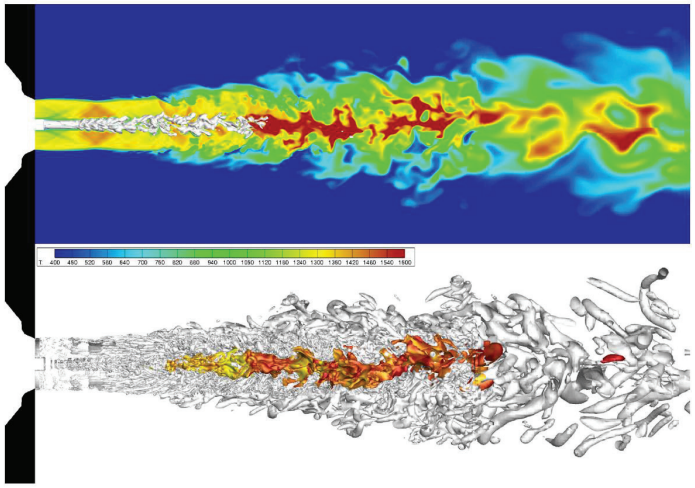

Figure 10 - Flame structure – Instantaneous field of temperature and H_2 mass fraction iso-surface [0.05] (top) - Iso-surfaces of Q-criterion [1x10^9 (s^2)] and OH mass fraction [0.01] colored by temperature (bottom)

The external mixing layer, between the ambient and vitiated air streams, develops quite differently from the internal mixing layer between the vitiated air and hydrogen coflowing jets. The value of the convective Mach number associated with the external mixing layer is so large that compressibility effects may play a quite important role.

This may restrict the mixing of ambient air with the vitiated air stream, since the growth and entrainment rates of compressible shear layers are known to be much smaller than those of incompressible flows at the same velocity and density ratios. This may also favor the birth of shocklet structures. Figure 10 shows that the transition from a two-dimensional destabilization mode to a fully developed three-dimensional mixing layer takes place rapidly. In comparison with the external mixing layer, the internal mixing layer that develops between the hydrogen jet and the vitiated air coflowing jet is characterized by a much smaller value of the convective Mach number, and therefore the two dimensional instability is the most rapidly amplified disturbance. From this figure, it can be noticed that the non-premixed jet flame is detached from the nozzle and it is found to stabilize at around twenty diameters from the injector exit plane, which is in satisfactory agreement with experimental results.

A typical instantaneous field of the heat release rate is reported in Figure 11. In practice, intensive heat release is located in regions that are micromixed at the present level of computational resolution, i.e., characteristic mesh size. At these locations, the fine-scale structure volume fraction γ^* is around unity, which confirms that these regions are chemically-controlled, see Figure 11. The auto-ignition region is characterized by an upstream peak in HO_2 radical formation in the middle of the jet. A detailed inspection of the flame stabilization region shows that it is significantly affected by a shock diamond structure positioned at $X/D \sim 20$, and this structure is itself significantly influenced by pressure waves issued from the external mixing layer. The compressible coflowing jet shock pattern indeed clearly contributes to the ignition of the hydrogen/air mixture inside the jet through shock-induced temperature rises.

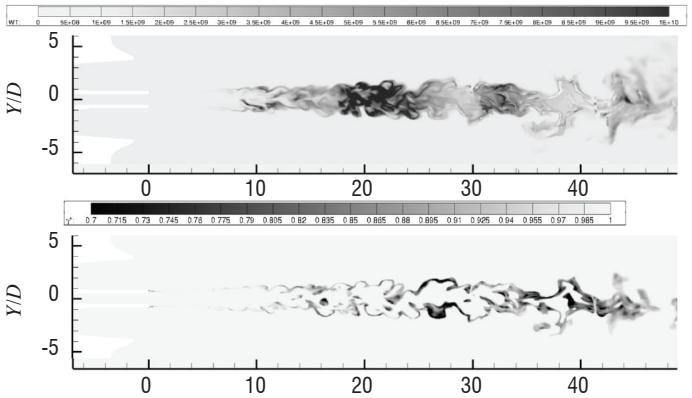

Figure 11 - Field of the instantaneous heat release (W m^{-3}) (top) - Instantaneous field of the volume fraction of fine-scale structures γ^* (bottom)

Temperature and composition profiles

We proceed here with a quantitative evaluation of our computational results. The mean and RMS profiles of the temperature and mole fractions of the main species are compared with experimental results on the symmetry axis, see Figure 12. It is noteworthy that the calculated RMS values are based on resolved temporal fluctuations only, i.e., without any consideration of the residual SGS fluctuations. The temperature rise along the flame axis calculated from the numerical simulation matches the experimental one quite closely. The mean lift-off height is predicted with a good level of accuracy; however, the flame temperature at the far end of the jet seems to be underestimated. The mean mole fraction profiles of hydrogen and water also seem to be quite well predicted. The mean oxygen mole fraction profile is the only one that displays some discrepancies with regard to the experimental results, especially in the far field. As observed in other numerical simulation results, see for instance [37], the oxygen mean concentration profile indeed exhibits a non-monotonic behavior, contrary to what is observed in the experiments. The first peak of the oxygen mole fraction (located at $X/D = 15$) is mainly due to mixing between the coflowing jets. The decrease afterwards is attributed to combustion in the stabilization region. Finally, the last increase of the oxygen mole fraction (starting from $X/D = 35$) is the outcome of an overestimated level of dilution with the external ambient air. The poor description of the external mixing layer development is the most probable reason that explains this incorrect representation of external air entrainment. The RMS profiles from the numerical simulation globally follow the experimental trend, except for hydrogen, for which the resolved fluctuations seem to be overestimated.

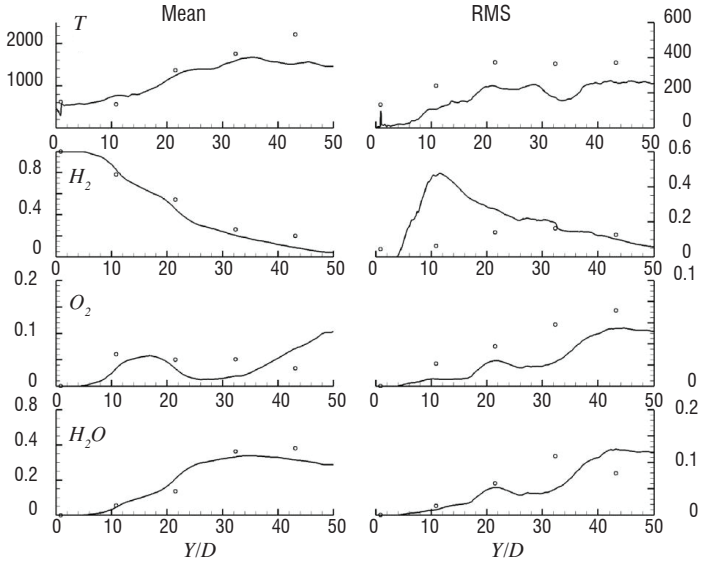

Figure 12 - Mean and RMS of the composition (temperature and mole fractions) on the symmetry axis - Comparison between numerical results and experimental data

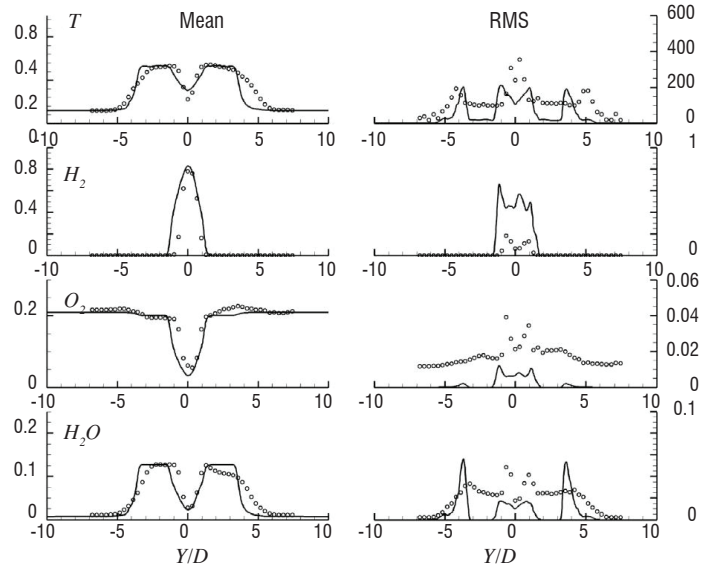

Figure 13 - Mean and RMS profiles of the temperature and main species mole fractions at $X/D = 10.8$

The mean and RMS profiles of the temperature and mole fractions of the main species are also compared with experimental results at four transverse sections (Figure 13 to Figure 16). The results from the numerical simulation of the mean quantities obtained in the first section ($X/D = 10.8$, Figure 13) compare well with the experimental results.

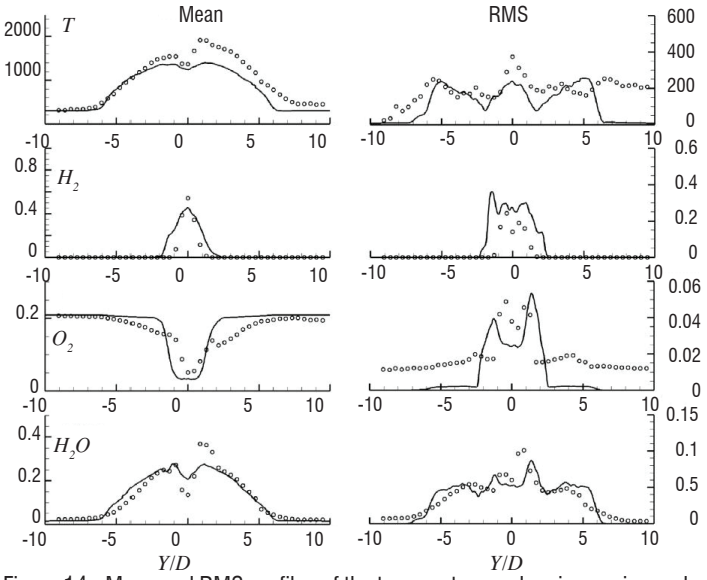

Figure 14 - Mean and RMS profiles of the temperature and main species mole fractions at $X/D = 21.5$

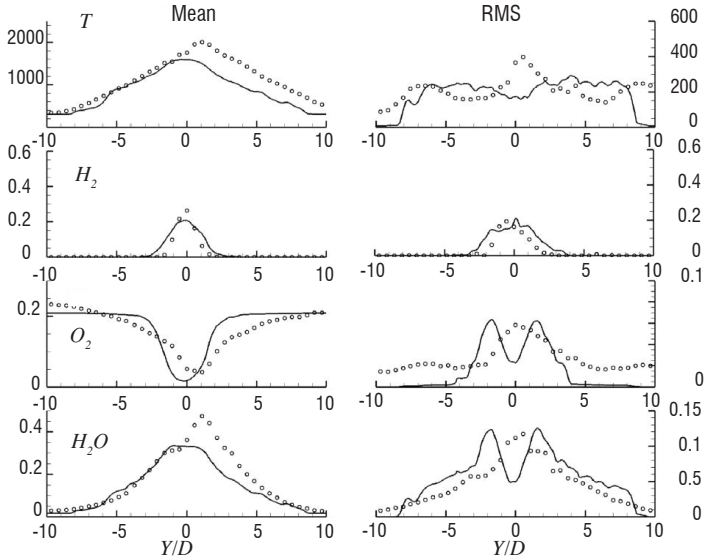

Figure 15 - Mean and RMS profiles of the temperature and main species mole fractions at $X/D = 32.3$

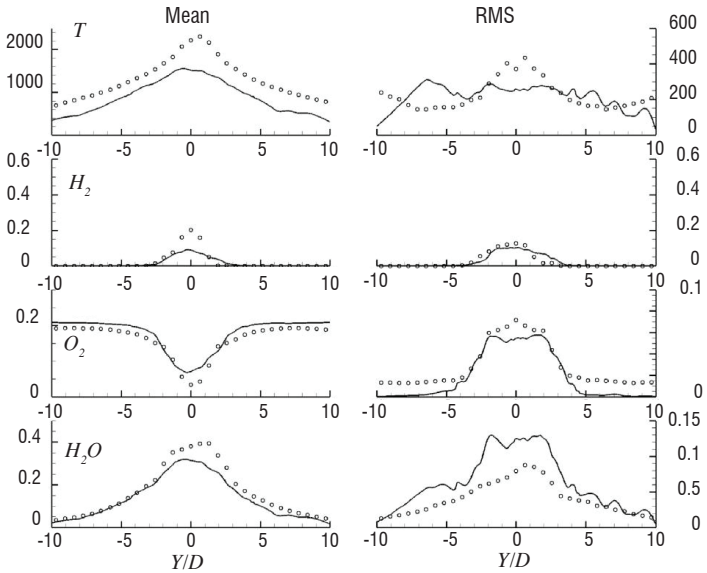

Figure 16 - Mean and RMS profiles of the temperature and main species mole fractions at X/D = 43.1

No particular asymmetry is observed. The outcoming flow seems to be well resolved, due to the combined use of a highly refined mesh at the exit of the nozzle and relevant boundary conditions settled in terms of total quantities. RMS trends and order of magnitude are correctly predicted, but the computed levels do not perfectly match the experimental measurements. The impact of standard steady boundary conditions is here clearly visible, especially on the RMS profiles of temperature fluctuations, the levels of which are significantly underestimated in the vitiated air stream. For these conditions, the description of the successive shock reflections (and expansions) off the boundary of the jet, and the resulting standing shock wave pattern in the jet (diamond structure or Mach structure) seems to be central to the quality of the numerical prediction, and temperature fluctuations appear to be of second-order importance to correctly predict the stabilization zone and lift-off height.

Except for the asymmetrical aspect, the numerical results again show a satisfactory agreement with the experimental data in the second section ($X/D = 21.5$, Figure 14). Hydrogen and oxygen profiles are especially well predicted. In this section, the prediction of composition fluctuations is also improved. The possible influence of unsteady boundary conditions seems to be unimportant at this location and the fluctuating quantities are much more impacted by the development of the two mixing layers, which seems to be well-captured. The RMS of temperature fluctuations is in satisfactory agreement with experimental measurements, except inside the hydrogen jet. However, it is worth noting that the mesh is not refined enough to satisfactorily describe the unsteady behavior of the external mixing layer and the associated ambient air entrainment. The levels of the oxygen concentration fluctuations are therefore greatly underestimated for $Y/D > 5$ or $Y/D < -5$.

In the following section ($X/D = 32.3$, Figure 15), the asymmetry of the experimental data still remains very marked. Mean profiles resulting from the numerical simulation match the lower branch of these asymmetrical data rather satisfactorily. The RMS profiles are in good general agreement with the results. The levels are relatively well predicted, except for the RMS of the temperature, as well as the RMS of the oxygen and water vapor concentrations inside the jet.

Finally, in the last section ($X/D = 43.1$, Figure 16), the whole mean temperature profile is underestimated by the numerical simulation, especially in the flame. However, RMS levels resulting from the numerical simulation are in good agreement with the experimental results for hydrogen and oxygen and, except inside the jet, they are also correctly represented for the temperature and water vapor concentration.

More detailed information on the U-PaSR model and associated validation computations can be found in [38] and [39].

Studies on injection and flame stabilization

Combustion of a transverse hydrogen wall jet in a supersonic air flow at very high flight Mach number

Designing a scramjet injection system is particularly challenging, since this device has to promote ignition, mixing and combustion while limiting total pressure losses. Sonic injection of fuel normal to the combustor wall is an interesting option for small size combustors. High temperatures are met in front of the jet because total temperature is recovered at this location, and pressure losses are moderate, since there is no injection strut. For these reasons, this flow configuration has been widely studied, mostly for non-reacting flows or for moderate supersonic Mach numbers [40][41][42][43].

run	P_{tot} (bar)	H_{tot} (MJ/kg)	M_∞	P_∞ (Pa)	T_∞ (K)	M^e	P^e (Pa)	T^e (K)	AoA (°)	PR
R1294	473	9.45	9.59	322	470	4.64	4545	1770	20	396
R1312	175	2.6	8.70	684	156	2.80	23391	990	30	214

Table 2 - Flow conditions

In this study, a Mach 1 hydrogen jet normal to a flat plate at angle of attack in a supersonic flow has been tested in the ONERA F4 hyper-enthalpy arc-heated wind-tunnel (see Figure 17).

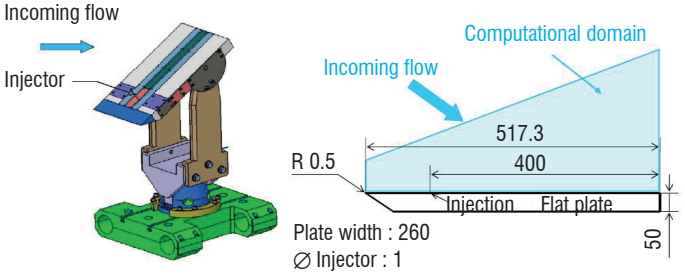

Figure 17 - CAD view of the plate - Sketch of the plate with computational domain

Two runs are considered here: R1294 and R1312. Table 2 gathers the flow conditions for these two runs: air total conditions (P_{tot}, H_{tot}), test section conditions (M_∞, P_∞, T_∞) and static conditions downstream from the leading edge shock, outside of the boundary layer (M^e, P^e, T^e). PR is the injection total pressure to static pressure ratio $PR = P_{tot,inj} / P^e$. The PR values are much greater than one, which indicates a highly under-expanded jet.

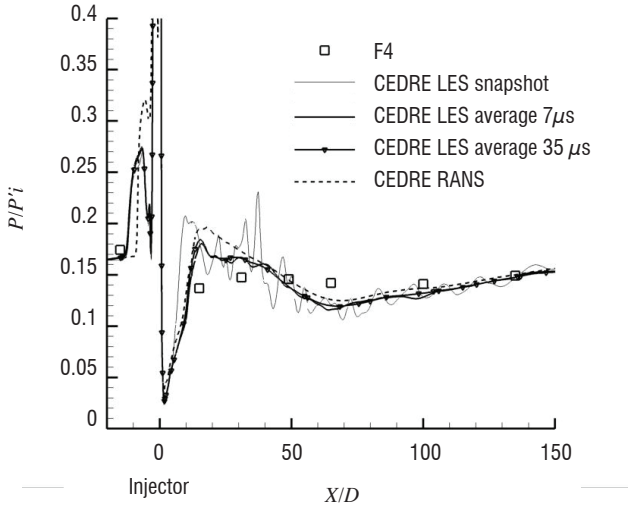

Figure 18 - R1294. Comparison between the experimental (F4) and computational (RANS and LES) pressure profiles on the symmetry plane.

LES (for R1294) and RANS (for R1312) simulations of this configuration have been performed using the ONERA code CEDRE. For R1294, experimental and numerical results are compared in Figure 18, in terms of pressure profiles in the symmetry plane. LES results are presented for a snapshot, a time integration over 7 μs, and over 35 μs. The comparison between the two integrated curves shows that a good time convergence has been reached (at least in terms of pressure distributions). A reasonable agreement is found between CFD and experiment, despite extreme flow conditions: high Mach numbers (9.59 in the far-field flow) and a large temperature range between the inside and near-field flow of the jet (see Figure 19).

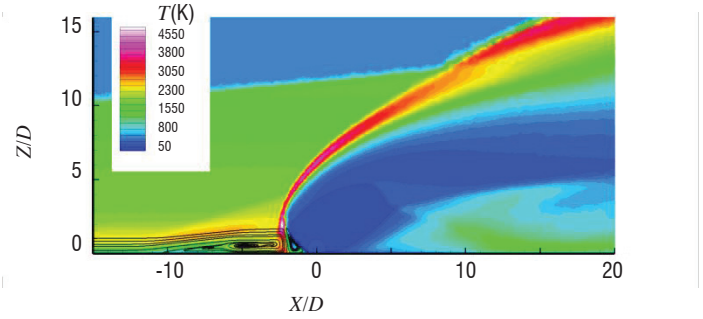

Figure 19 - R1294 (mean flow). Temperatures in the vicinity of the injection. Streamlines in the upstream boundary layer.

The dynamics of the flow are shown in the following animation (Figure 20), which presents the Mach number, a passive scalar and the OH mass fraction in the symmetry plane of the flow. The jet expands in the supersonic flow and then is recompressed by a barrel shock (see top view). This barrel shock generates an obstruction to the main flow, which reacts with a bow shock. Between these two shocks, a strong shear layer develops and creates large eddies that are responsible for turbulent mixing, as can be seen in the passive scalar plot. As soon as hydrogen is mixed with air in the shear layer, it immediately burns because of the high temperatures in this region. One can also notice high levels of OH mass fraction upstream from the injection, near the wall. This is due to the combustion of hydrogen that is trapped in the recirculation bubble, which forms because of the adverse pressure gradient encountered by the boundary layer flow as it approaches the bow shock foot (see also Figure 19).

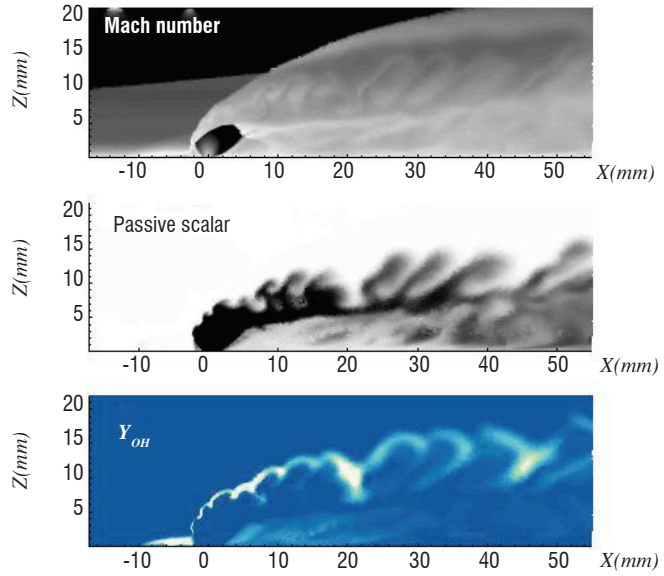

Figure 20 - Mach number animation (top), passive scalar (middle) and OH mass fraction (bottom) in the symmetry plane

Concerning Run R1312, the experimental OH^* visualization is compared, in Figure 21, to the calculated OH mass fractions (RANS) integrated over the width of the plate. For clarity reasons, the top view represents only the experimental results. A good agreement is observed between the experimental and numerical approaches.

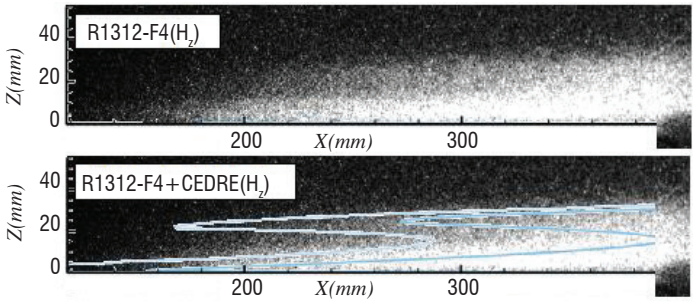

Figure 21 - R1312 - Experimental OH^* emission (top) and its comparison with computed mass fraction isolines (bottom)

Experimental characterization of strut injectors

Two major difficulties in supersonic combustion are the fuel-air mixing efficiency and flame stabilization. To overcome this, a variety of fuel injection schemes have been proposed and investigated extensively [44][45][46]. Strut injection is one of the candidates to enhance supersonic mixing, because it can introduce both fuel and vortices directly into the supersonic core flow. The technical difficulties in the application of strut injectors are the generation of vortices, ignition and flame stabilization. Streamwise vortices have been investigated extensively by trying various ways of generation and use [47][48][49][50]. The results revealed that, depending on how the streamwise vortices are generated and used, they can provide a significant mixing enhancement. The counterpart is an increase in the combustion pressure gradients, which can lead to separated regions and engine unstart. At ONERA and JAXA, strut injectors have been implemented in scramjet combustors and extensively tested. ONERA developed a multi-staged fuel injection strut, specifically designed to enhance ignition and flameholding near the strut base [45]. On the other hand, JAXA studied the use of streamwise vortices generated by "Alternating-Wedge struts" to enhance supersonic mixing and combustion [51][52][53]. In order to better understand the mixing and combustion mechanisms involved in both strategies, a joint program was set up in 2002 between ONERA and JAXA. The goal was to test different strut injector concepts in the same combustor and the same facility and to compare their performances in terms of mixing, ignition and combustion.

Test facility and combustor

Experiments were conducted in the supersonic combustion test facility implemented at ONERA/Laerte. The combustor was designed and manufactured by JAXA. It is connected to the test rig by a Mach 2.5 contoured nozzle (Figure 22). The combustor is fed with vitiated air, heated to 1620 K by two successive hydrogen burners. Oxygen is injected upstream from the auxiliary burners, in order to maintain the mole fraction of oxygen in the vitiated air flow at 21%. The facility air pressure storage is 25 MPa. Fuel is gaseous hydrogen.

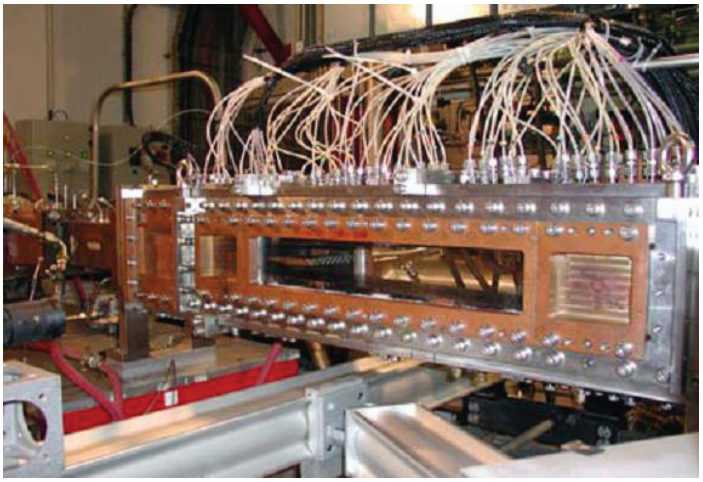

Figure 22 - View of the JAXA supersonic combustor connected to the Mach 2.5 nozzle

The combustor is basically two dimensional and has a 355 mm long constant area first part (50 mm × 100 mm cross section), followed by a 600 mm long diverging second part (expansion half-angle of 1.72° applied to top and bottom walls). The combustor has a constant 100 mm width. The whole combustor is made of copper. The tested strut injector is installed at the transition between the constant area section and the diverging section (Figure 23).

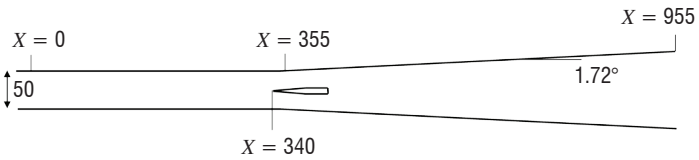

Figure 23 - Sketch of the JAXA supersonic combustor

The strut leading edge is located at x= 340 mm. Here, x is the longitudinal distance from the combustor entrance (i.e., the exit of the Mach 2.5 nozzle). For all of the struts, the fuel injection orifice is located at x = 433 mm.

Figure 24 - View of a strut injector in the combustor

Strut injector concepts tested

Five strut injector concepts were tested. They are shown in Figure 25 (ONERA concept, without streamwise vortices) and in Figure 26

(JAXA concepts, with streamwise vortices). The ONERA strut is made of a leading wedge followed by a constant section part. Fuel is injected at two levels: the first one at the walls of the strut (four jets on each side, directed at an angle of 45° with the walls), at the beginning of the constant section part, and the second one at the base of the strut (three jets parallel to the air flow). It will be named the "staged injection strut" in the following. The JAXA struts have a unique injection level, parallel to the air flow, and are characterized by alternating upward and downward expansion ramps arranged at the base of the strut in order to generate either counter-rotating or co-rotating streamwise vortices in the air flow: these vortices are at the origin of the mixing enhancement. Hydrogen is injected through 6 holes, each one directly on the axis of a streamwise vortex. The JAXA struts will be named "alternating wedge struts". A more detailed description of all of these injectors can be found in [54].

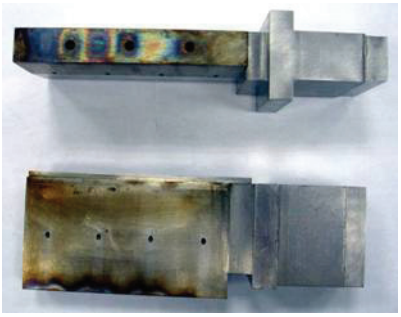

Figure 25 - ONERA strut injector concept (without streamwise vortices)

Figure 26 - JAXA strut injector concepts (with streamwise vortices)

Main results

The various injector concepts tested were compared through wall pressure measurements, spontaneous emission visualizations and OH-PLIF visualizations. We present here some results obtained with the staged injection strut named ONH10 in [54] and with the alternating wedge strut named CNR11-R36 in [54].

Spontaneous emission visualizations are presented in Figure 27. With the staged injection strut, stable ignition clearly takes place at the strut base, which acts as a flameholder. One observes that the lateral jets do not ignite spontaneously and seem to be ignited downstream, by the flame issued from the base jets: at this stage, the flame height increases suddenly and continues to grow more slowly downstream. The consequence is that combustion presents two regions: a first one, very stable but rather thin, which concerns only the base jets, and a second one, much larger, when the combustion has propagated to the lateral jets. On the other hand, ignition seems somewhat less stable with the alternating wedge strut, but it apparently occurs for all jets at a short distance from the strut base. Then, the flame height increases rapidly due to the effect of the streamwise vortices.

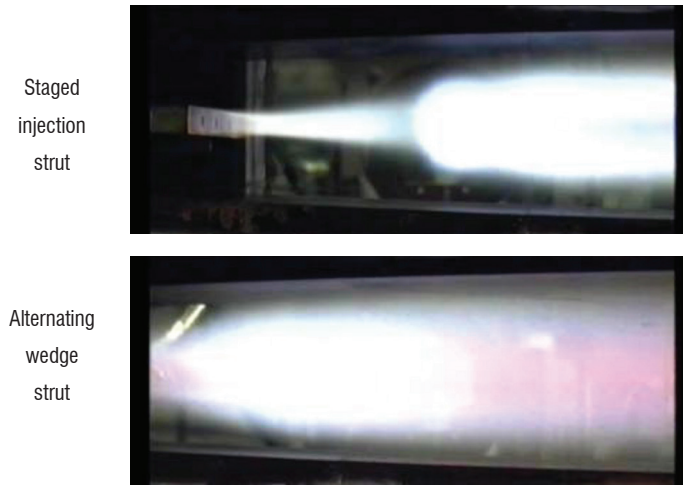

Figure 27 - Spontaneous emission visualization for the staged injection strut (top) and the alternating wedge strut (bottom)

The instantaneous OH-PLIF images in two transverse planes (x=40 mm and x=100 mm from the strut base) confirm this tendency (Figure 28). It is clearly visible that the alternating wedge strut actually generates larger scale motion in the combustor cross-section compared to the staged injection strut. However, the ignition is less stable and does not concern the central jets in a first step; this was not visible from the spontaneous emission images, which integrate the emission over the whole width.

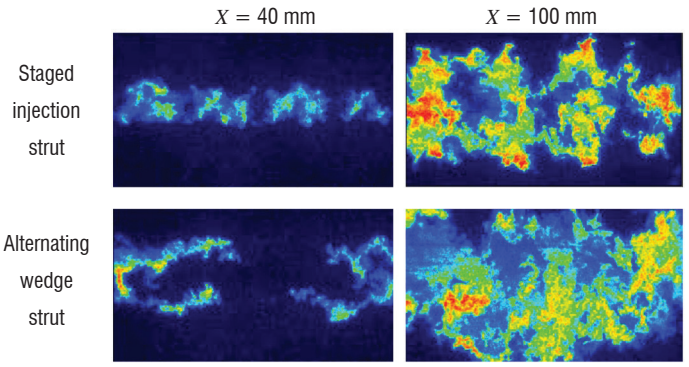

Figure 28 - Instantaneous OH-PLIF images at x=40 mm (left) and x=100 mm (right) for the staged injection strut (top) and the alternating wedge strut (bottom)

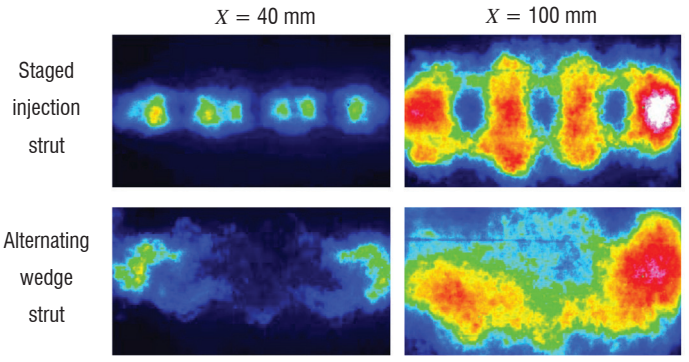

Figure 29 - Time-averaged OH-PLIF images at x=40 mm (left) and x=100 mm (right) for the staged injection strut (top) and the alternating wedge strut (bottom)

The better efficiency of the alternating wedge strut seems a little less obvious when one looks at time-averaged OH-PLIF images (Figure 29): combustion is actually more spread out with the alternating wedge strut, but not necessarily much more efficient.

These tendencies are confirmed by the wall pressure rise (not represented here), higher all along the combustor for the alternating wedge strut, except at the end, where the pressure is similar for all struts (see [54]) indicating that the global combustion efficiency may be not so different. More detailed information on these results can be found in [54].

It should be added that, more recently, numerical simulations of this combustor were performed by C. Fureby [55]. The computational results provide precious help in understanding the experimental results.

Experimental study of self-ignition and combustion in a research scramjet

Since 2010, the Laerte facility at ONERA – Palaiseau has been equipped with a new dual-mode ramjet combustor (Figure 30), which was developed, manufactured and used within the LAPCAT II project (EU 7th Framework Program, 2008-2013 [56][10][11][57]). The goal of the study was to investigate the self-ignition conditions in the combustor, in order to evaluate the effect of air vitiation on ignition. The internal geometry of the combustor was identical to that initially developed by ITLR, which was in charge of pure air tests.

The combustor (Figure 31) comprises four parts: the first (55 mm < x_1 < 280 mm) has a constant cross-section, the following sections (280 mm < x_2 < 598 mm < x_3 < 952 mm < x_4 < 1257 mm) have, respectively, diverging half-angles of 1°, 3° and 1° to prevent/stunt thermal choking. Large fused silica windows can be placed at different locations, allowing optical access. The combustor is fed with hot vitiated-air (heating by H_2/air combustion and O_2 replenishment to maintain the O_2 molar fraction at 0.21). The total temperature and pressure can reach up to 1800-1900 K and 1.0-1.2 Mpa, respectively. The supersonic flow is generated by a De Laval nozzle (Mach = 2.0 in this case, Mach = 2.5 being also available). The facility is operated in the blow-down mode, with the mock-up walls working as a heat-sink. The combustion chamber is made of a copper alloy and the inner walls include a 0.3 mm thick YSZ (Yttria-Stabilized Zirconia) thermal barrier coating. The combustor outlet is connected to a 400 mm diameter exhaust pipe, where the pressure is around 0.1 MPa. A computer controls the reproducibility and stability of the operating conditions.

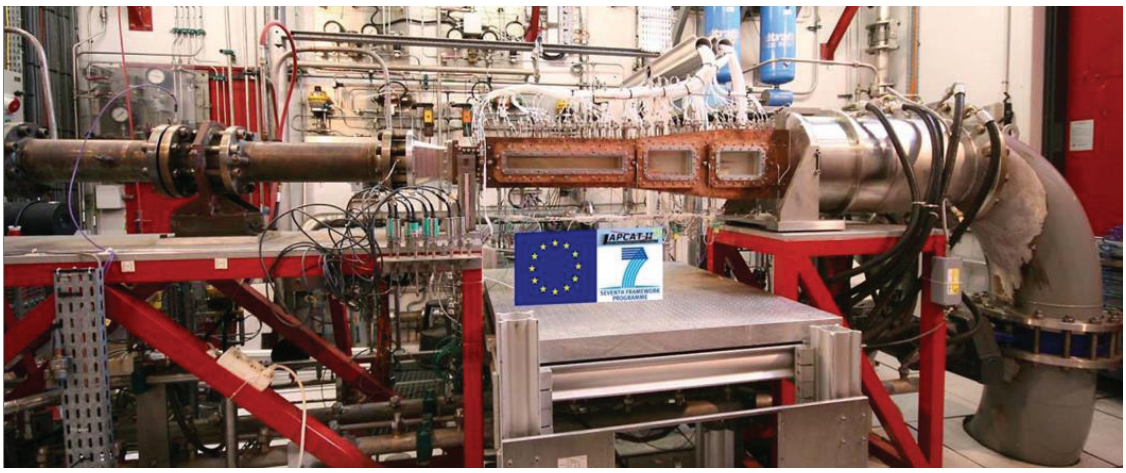

Figure 30 - Lapcat2 combustor installed in the Laerte facility

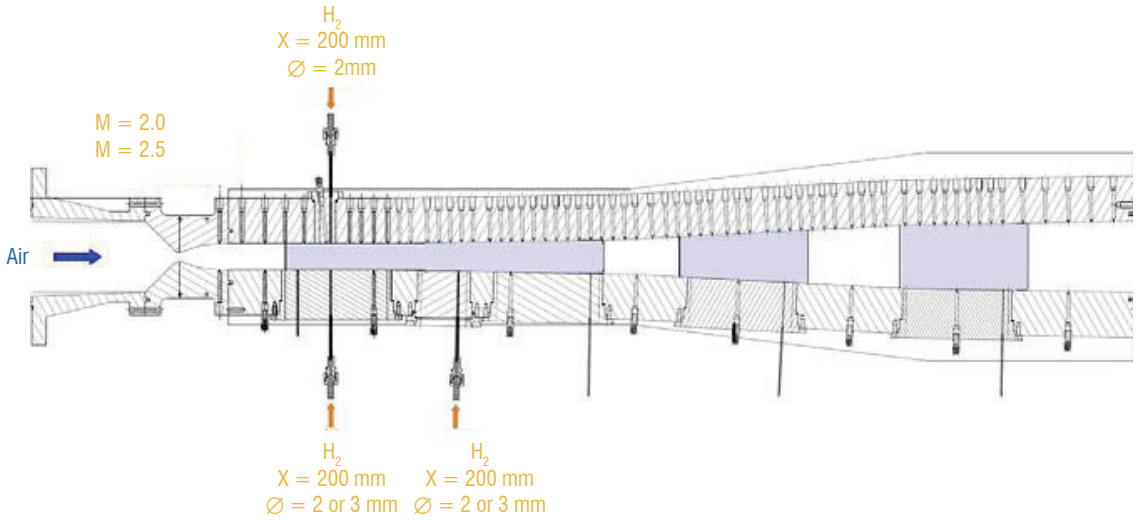

Figure 31 - Side view of the combustor equipped with wall hydrogen injectors

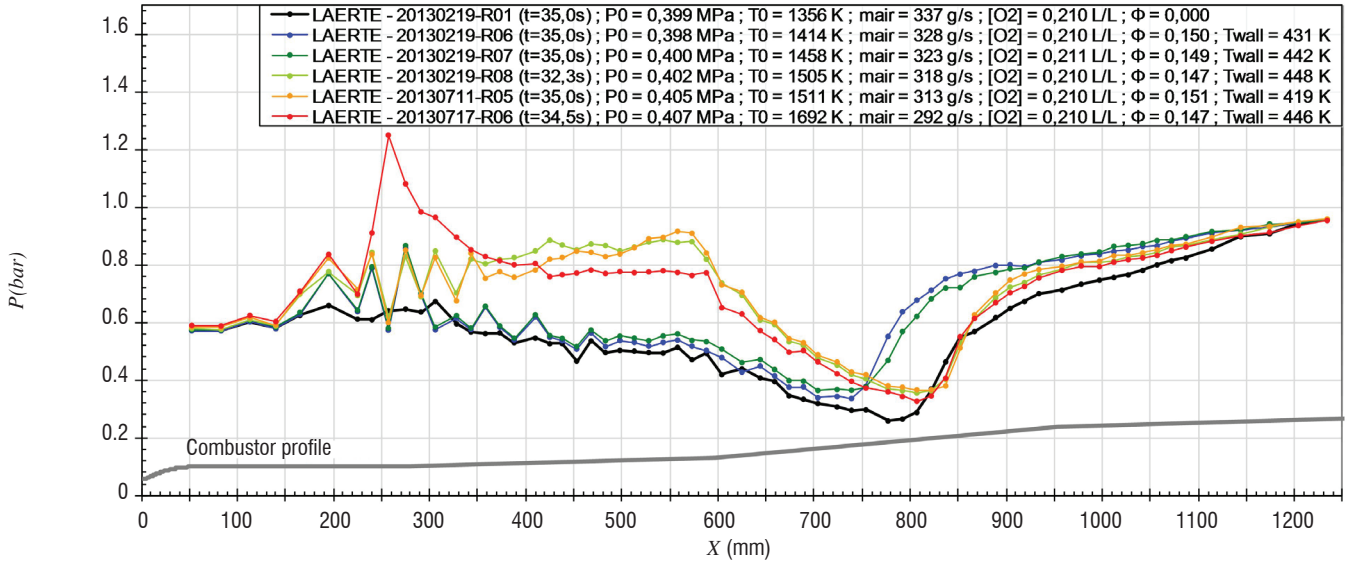

Figure 32 - Pressure profiles for increasing T_0 (P_0 = 0.40 MPa and $E.R.$ = 0.15)

The fuel used was pure gaseous hydrogen. Injection can be achieved from single sonic injectors located in the upper and lower walls, at x = 200 mm (upper wall, lower wall, or both) or at x = 368 mm (lower wall only). For the tests presented here, we used the two ϕ=2 mm injectors at x = 200 mm.

Given that the combustor is not water cooled, the overall duration of a test run is limited to around 1 minute, but the useful duration, i.e., at the required temperature, lasts between 5 s and 15 s, depending on the test conditions.

The ignition limit for the supersonic combustion of wall injected hydrogen in a hot air cross-flow has been explored with tests at various total temperatures, for the same equivalence ratio ($E.R.$ = 0.15). The wall pressure profiles are presented in Figure 32. Without injection, the pressure profile indicates a supersonic expansion in the diverging parts of the combustor, up to the separation of the flow at $x\approx$ 800 mm due to overexpansion. With injection, three regimes can be identified from the pressure profiles, depending on the total temperature.

For T_0 = 1414 K and T_0 = 1458 K, no significant supersonic combustion can be observed: combustion occurs only downstream from the separation shock. The injection shock and its successive reflections are visible from x = 200 mm.

For T_0 = 1505 K and T_0 = 1511 K, the static temperature is sufficient to allow self-ignition of hydrogen at $x \approx$ 310 mm, just after the beginning of the first diverging section. Ignition is followed downstream by a weak supersonic combustion. The pressure profiles for these two temperatures are nearly identical.

For T_0 = 1692 K, ignition occurs closer to the injection, at $x \approx$ 240 mm, and is at the origin of a flow separation, which results in a high pressure peak.

These results are confirmed by the flow visualizations presented in Figure 33 for three values of T_0. For T_0 = 1414 K (Test Run 20130219-R06), combustion is visible only in the second window: around 659 mm ≤ x ≤ 828 mm). For T_0 = 1458 K (Run 20130219-R07), combustion mostly occurs in the same region, but a faint emission seems to be visible along the last third of the first window and a small pressure increase is noticed in the pressure profile (Figure 32). This could perhaps correspond to a cool flame. For T_0 = 1505 K (Run 20130219-R08), supersonic combustion is clearly visible through the first window, with ignition at $x \approx$ 310 mm.

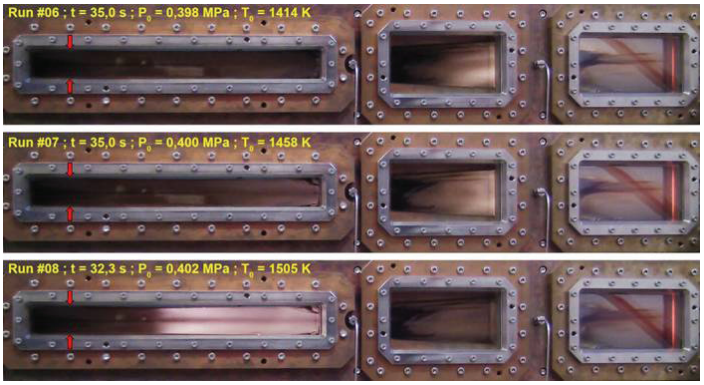

Figure 33 - Images of the combustion for increasing T_0 (P_0=0.40 MPa and $E.R.$=0.15) ; red arrows indicate the position of the fuel injection

Schlieren imaging technique (Figure 34) gives complementary information on the fuel injection, mixing and ignition processes (P_0 = 0.41 MPa, T_0 = 1697 K, $E.R.$ = 0.15). An injection pattern consisting in a bow-shock and barrel shock is clearly visible (around x = 195–205 mm), as described in the literature [58]. Downstream from the fuel injection point, the mixing region is evidenced. 50 mm to 80 mm downstream from the injection point, a kind of λ-shock system oscillates, in the wake of which combustion starts. The pressure peaks caused by the injection shocks and the λ-shock appear on the pressure profile at x = 200 mm and x = 240–260 mm, respectively (see also Figure 32 – 20130717-R06).

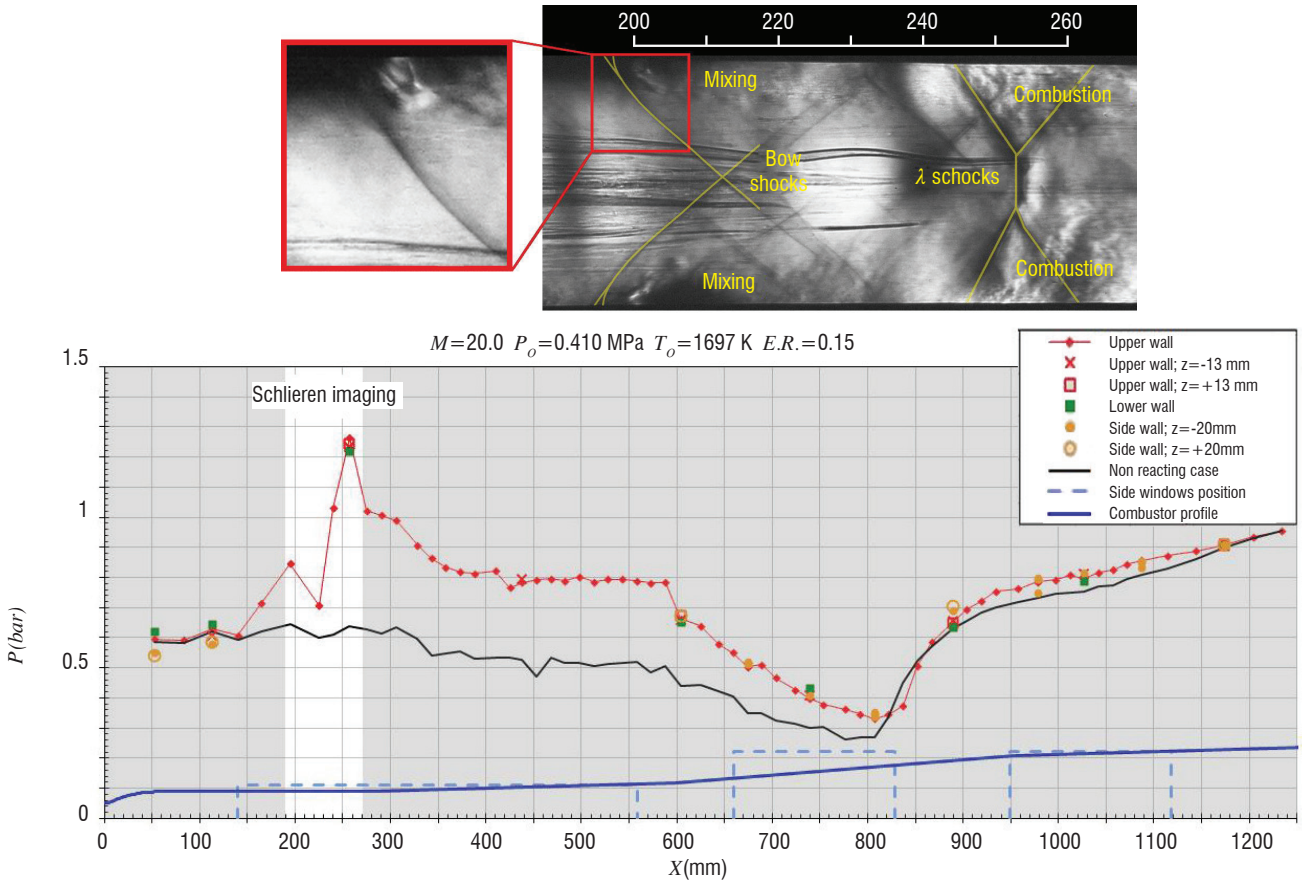

Figure 34 - Fuel injection and ignition (P_0 = 0.410 MPa, T_0 = 1697 K, $E.R.$ = 0.15)
Upper right: annotated Schlieren view (1280×504 pixels; 12 kHz)
Upper left: zoom on the injection region (128×128 pixels; 210 kHz)
Bottom: related pressure profile

This experimental study has been supplemented with a RANS numerical simulation of the supersonic combustion, revealing the prime effect of the wall conditions (temperature and roughness) on the ignition distance. Moreover, the ignition distance has been demonstrated to be significantly shorter in vitiated air than in pure air. More detailed information on both experimental and numerical aspects can be found in [56].

Design and study of scramjet combustors

Design, test and simulation of the JAPHAR dual-mode ramjet

In 1997, ONERA and the DLR decided to join their efforts on hypersonic air-breathing vehicles within the framework of the JAPHAR program. For this purpose, a vehicle demonstrator in the flight range Mach = 4 to 8 was chosen as a guideline for the studies, and a dual-mode ramjet engine was designed for this vehicle. In order to work as a dual-mode ramjet, the hydrogen fueled combustion chamber has two parts and two injection stages. The first part is slightly diverging and is mainly dedicated to supersonic combustion at a high flight Mach number, whereas the second one allows subsonic combustion at a lower flight Mach number, with a thermal throat located near the chamber end (Figure 35). The vehicle engine was defined to be completely supersonic at Mach 8 when all of the hydrogen is injected from the first injection stage. The length is roughly 2.4 meters.

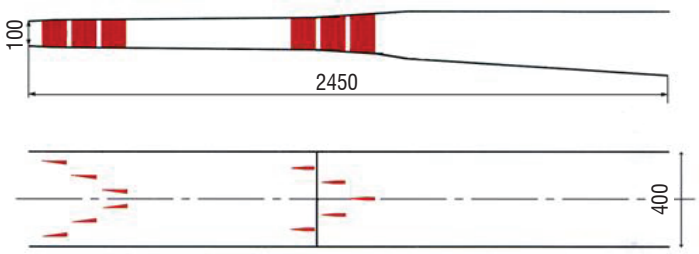

Figure 35 - Sketch of the Japhar vehicle dual-mode ramjet

The fuel injection distribution between the two injection stages enables the combustion regions to be controlled, as well as the position of the normal shock and of the thermal throat for the subsonic combustion regime.

Taking into account the capacities of the ONERA test facility, an experimental engine with smaller dimensions was extrapolated from the vehicle engine studied during the JAPHAR project (Figure 36). The chamber entrance cross-section is 100×100 mm² (100×400 mm² for one vehicle engine module). The chamber height and length are kept identical, but the injection system is modified to be suited to a smaller width. As a result, the first injection stage has only one strut and wall injections, whereas the vehicle chamber has several struts. The wall injectors of the experimental chamber enable a mixing representative of that achieved in the real chamber. The second injection stage is constituted by two struts.

In addition, to facilitate the strut assembly and to be able to modify the chamber geometry easily, the struts are oriented at 90° compared to the vehicle initial position (Figure 36 compared to Figure 35).

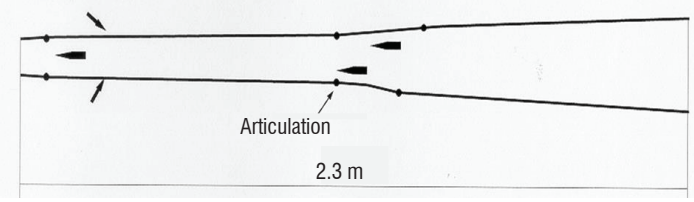

Figure 36 - Sketch of the JAPHAR experimental dual-mode ramjet

Figure 37 - View of the test setup in the ATD 5 test cell

Prior to the tests, the chamber was studied numerically using the ONERA in-house 3D reactive code CEDRE.

The computations predicted that this engine should allow three different combustion regimes to be obtained - subsonic, transonic and supersonic - depending on the flight Mach number, which is illustrated in Figure 38 where subsonic zones (blue regions) are shown and Figure 39, which represents the pressure fields for 3 different flight Mach numbers. In order to obtain these combustion regimes, the fuel injection distribution between the first and the second stage was 25% - 75% for Mach 5.3 and 6.6, 80% - 20% for Mach 7.5 .

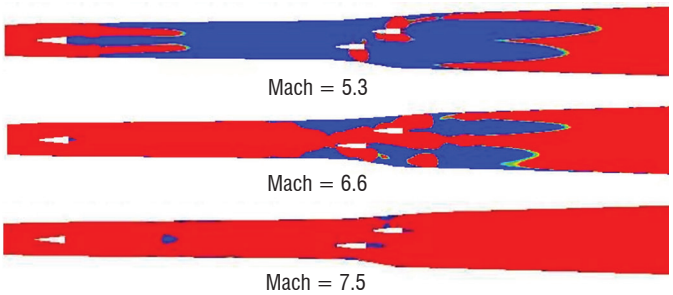

Figure 38 - Predictive computations - Sub/supersonic regions

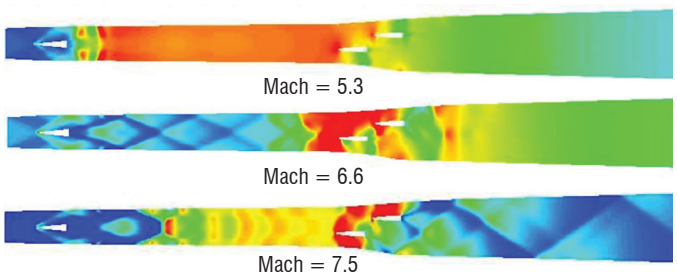

Figure 39 - Predictive computations - Pressure field

Tests campaigns were performed later for simulated flight Mach numbers of 4.9, 5.8 and 7.6. These values differ slightly from those retained for predictive computations, due to subsequent changes in the shape of the vehicle forebody. The actual test conditions are given in Table 3. New computations were performed after the tests with these conditions for test/computation comparisons.

M_∞	M_1	Pi_1 (bar)	Ti_1 (K)	P_1 (Pa)	T_1 (K)
7.6	3.11	29.0	2470	51450	1135
5.8	2.58	12.7	1500	59750	740
4.9	1.987	6.45	1171	81400	710

Table 3 - Test conditions

The air that was pre-heated through H_2 combustion and reoxygenation has the following mass fraction compositions (Table 4):

M_∞	O_2	N_2	H_2O
7.6	0.280	0.414	0.306
5.8	0.249	0.598	0.153
4.9	0.251	0.647	0.102

Table 4 - Inflow gas composition (mass fraction)

In addition to ER (Equivalence Ratio) exploration, several injection distributions were investigated throughout the tests (see Table 5).

Test case	1st level of injection	2nd level of injection
IR1	0%	100%
IR2	20%	80%
IR3	40%	60%
IR4	100%	0%

Table 5 - Tested injection distribution

For Mach 4.9 conditions, tests were performed with the IR1 and IR2 injection distributions. Figure 40 shows the fairly good agreement between test and computation at $ER=1$, with Injection Distribution IR2. The combustion regime is fully subsonic, with the normal shock located at the first injection strut and the thermal throat located just downstream from the second injection stage.

For Mach 5.8 conditions, the IR1, IR2 and IR3 injection distributions were experimented. The computed and experimental pressure distribution at $ER=1$ with Injection Distribution IR3 are shown in Figure 41. The combustion regime is partly subsonic and partly supersonic. The shock is located downstream from the first injection stage and the thermal throat is located at the second injection stage so that the fuel injected at this stage burns in a supersonic flow. The agreement between test and computation is again very good.

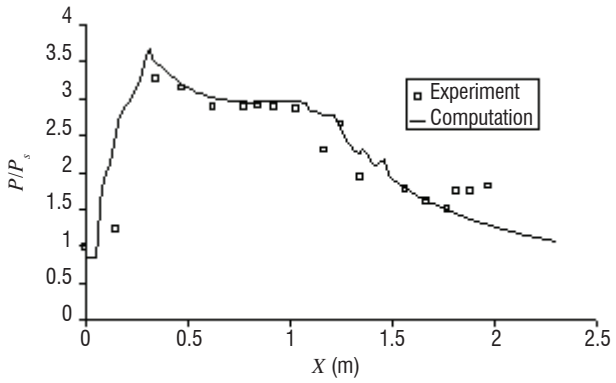

Figure 40 - Mach 4.9 - ER=1 - IR2 - Computed and experimental pressure distributions

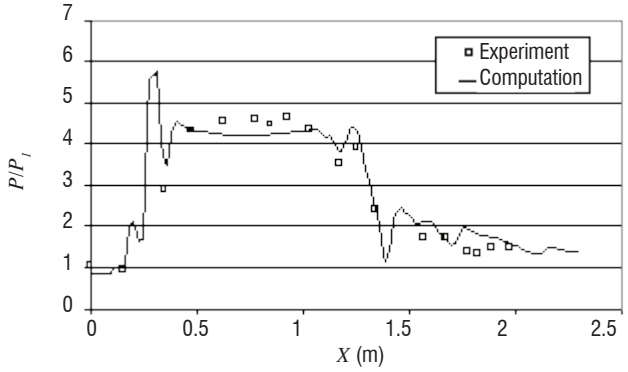

Figure 41 - Mach 5.8 - ER=1 - IR3 - Computed and experimental pressure distribution

For Mach 7.6 conditions, only Injection Distribution IR4 was experimented. With the initial combustor geometry, a significant discrepancy was observed between tests and computations. This was due to a deformation of the combustor during the tests, due to the great thermal stresses endured by the mock-up under these conditions. A consequence of this deformation was, in particular, a reduction of the cross-section at the end of the first part of the combustor. Taking into account the deformation of the combustor in the computations led to a better agreement with the experimental results, as seen in Figure 42 for ER=1. Due to the deformation, combustion is not fully supersonic: the flow is choked at the end of the first part of the combustor. Fully supersonic combustion was obtained only for ER<0.8.

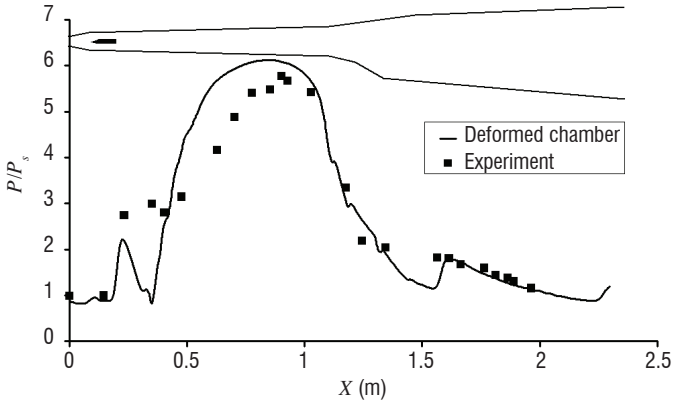

Figure 42 - Mach 7.6 - ER=1 - IR4 - Computed and experimental pressure distribution

The JAPHAR test campaign and the associated 3D computations demonstrated the possibility of operating a fixed geometry dual-mode ramjet at high equivalence ratio from Mach 4 to 8. The various combustion regimes that were predicted – subsonic, transonic and supersonic – were experimentally observed. Furthermore, it was shown that the shock and thermal throat positions could be controlled by adjusting the injection distribution. A very good agreement between computation and experimental results was obtained. More detailed information can be found in [59], [60], [61].

Test and Nose-to-Tail simulation of the SSFE scramjet

As the flight Mach number increases to supersonic and hypersonic values, it becomes necessary to carefully integrate the propulsion system on the airframe, in order to maximize inlet performance while limiting engine mass and drag. A typical hypersonic vehicle layout can be seen in Figure 43: much of the compression of the engine incoming air flow is produced by the vehicle fore-body; conversely, the after-body is used for the expansion process.

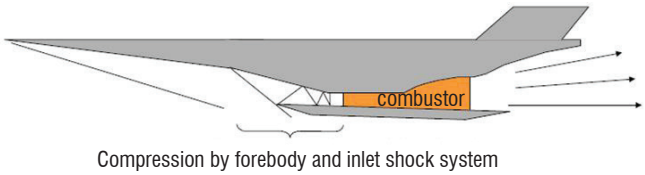

Figure 43 - Typical scramjet powered hypersonic vehicle layout

Therefore, in order to assess engine performance, it appears crucial to test it along with the entire vehicle, or at least with its entire flow path (i.e., the bottom of the fore and after-body). From an experimental point of view, free-jet facilities are thus required. These facilities must provide high total pressure and total enthalpy to simulate hypersonic flight Mach numbers.

From a numerical point of view, simulations must be conducted on the entire vehicle, including the combustion process in the engine. Various approaches can be considered for these 'Nose-to-Tail' (NtT) computations. It is possible to take advantage of the hyperbolic nature of the steady supersonic Navier-Stokes equations [62]. Then, computation can be performed 'by blocks', with each block being fed by the upstream block and feeding the downstream one. In addition, Parabolized Navier-Stokes can be used for the airframe. In the combustor, where large zones of subsonic flow can occur, various approaches can be used, from the zero-dimensional study to the tree-dimensional unsteady Navier-Stokes computations (RANS or LES). However, with increasing computational capabilities, 'integrated' NtT simulations (only one block for the whole computation) can now be considered.

We compare here free-jet tests of a hypersonic vehicle small-scale model in the ONERA F4 hyper-enthalpy arc-heated wind-tunnel, with NtT simulations performed with the ONERA code CEDRE.

The model tested here is a small-scale wave-rider (see Figure 44) designed by ESTEC [63][64][65] and manufactured by the DLR within the framework of the LAPCAT II European program (Long-term Advanced Propulsion Concepts and Technologies, funded by the European Commission as part of the 7th Framework Program and involving 16 European research labs and industries). This model has also been tested in the DLR high enthalpy shock tunnel [66] (HEG). The original vehicle is 94m long, 41m wide and weighs 400 tons at take-off. The 1.44 m long small-scale version, designed for the wind tunnel experiments, is also known as the SSFE (Small Scale Flight Experiment) model. Figure 45 shows the SSFE model installed

in the F4 test section. For obstruction reasons, and because only the internal flow path is being analyzed, the wings have not been machined. Adequate air/fuel mixing is obtained using three injection struts. Two struts are placed close to the combustor inlet at x=450 mm and another is placed farther downstream in the symmetry plane, at x=600 mm. The model is equipped with 40 Kulite pressure sensors.

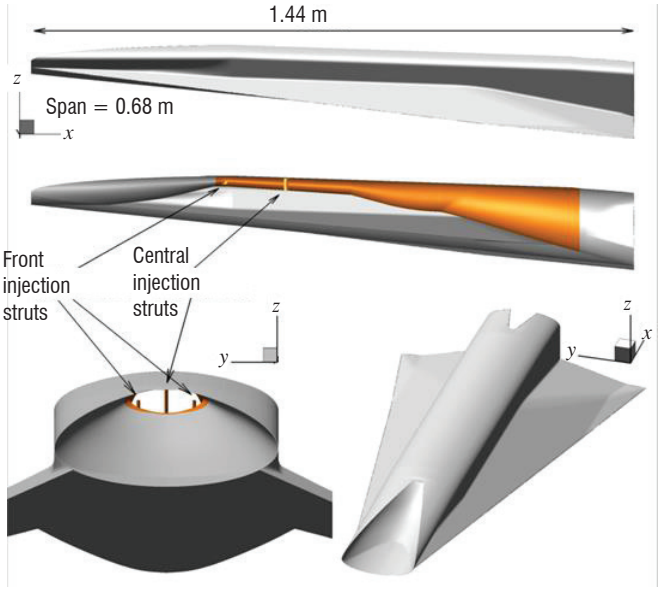

Figure 44 - CAD views of the ESTEC wave-rider model

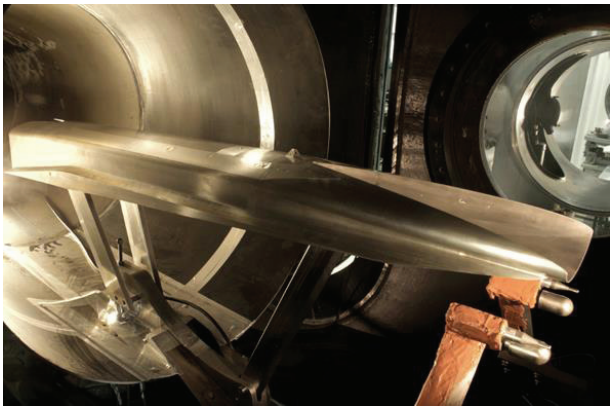

Figure 45 - View of the SSFE model installed in the F4 test section

Combustor pressure profiles for two runs (R1334 & R1343) at Mach 8 are presented in Figure 46 and Figure 47. Run R1334 is fuel-off, whereas Run R1343 is fuel-on with an equivalence ratio equal to 1. Pitot pressures in the test section and total enthalpy are given in the figures. CFD simulations are conducted considering:

1. a fully turbulent boundary-layer (Menter's SST turbulence model).
2. a fully laminar boundary-layer.
3. a transitional boundary-layer (the transition location is set 'artificially' at combustor inlet).

Fuel-off simulations (Figure 46) show that taking into account the transition on the fore-body of the vehicle is of prime importance when computing the flow in the engine. This highlights the strong dependence of the engine flow on the fore-body flow for hypersonic vehicles and the interest of free-jet testing and NtT simulation.

Fuel-on results are shown in Figure 47 for the transitional case. A good agreement is obtained in the first part of the combustor (x<700 mm), then the simulation under-predicts pressure levels. Several reasons can be considered to explain this discrepancy, but the most acceptable one is the air vitiation due to the electric arc that is used to generate hyper-enthalpy conditions in the arc chamber of the wind-tunnel.

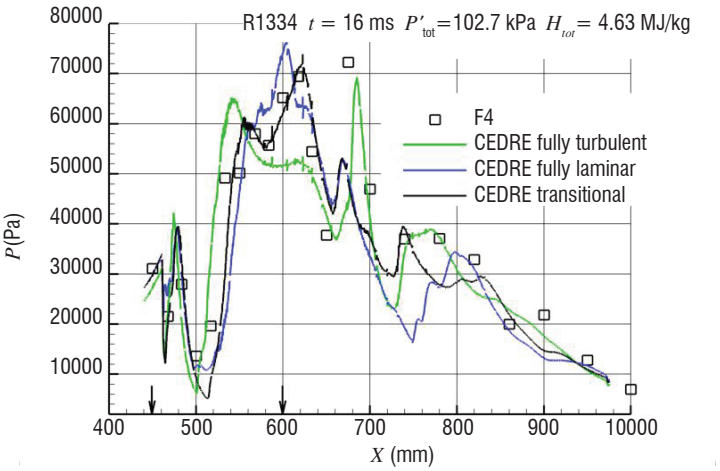

Figure 46 - R1334. Test / CFD comparison of pressure profiles for the three boundary layer transition modeling (the arrows show the injection locations)

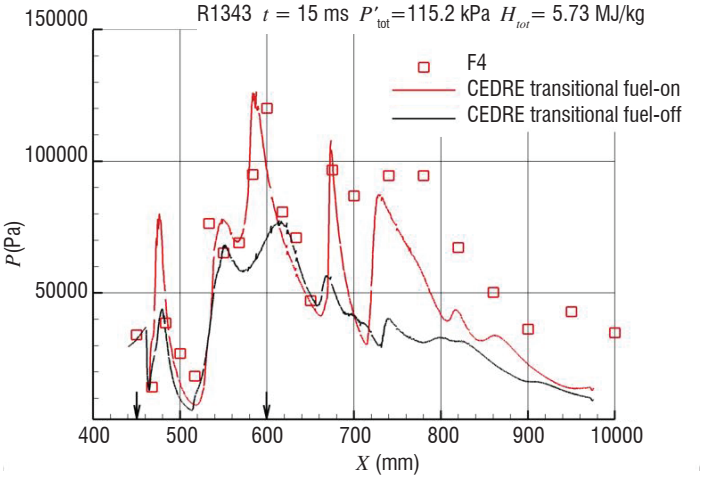

Figure 47 - R1343. Test / CFD comparison of pressure profiles (the arrows show the injection locations)

Conclusion

After a ten year period between 1962 and 1972, studies on supersonic combustion ramjets were stopped at ONERA for twenty years, mainly due to the difficulty in assessing the propulsive balance of an airbreathing hypersonic vehicle with sufficient accuracy. For this reason, the decision was made to concentrate efforts on rocket engines for high-speed propulsion. Since the renewal of scramjet activities in 1992, successive important programs have allowed a significant research activity to be maintained at ONERA and MBDA, its industrial partner, on this topic. The physics of supersonic combustion is now well understood, in particular the various and complex interactions between aerodynamics and heat release. Thanks to the development of both codes and supercomputers, CFD predictions are today reasonably reliable, so the design process of an airbreathing hypersonic vehicle has been mastered. However, the capacity to accurately predict the propulsive balance of such a vehicle from computations and ground tests is still perfectible, due to the great sensitivity of the propulsive balance to any small error in the outcoming impulse: progress on this aspect remains a key issue for the development of airbreathing hypersonic vehicles in the future ■

Acknowledgements

ONERA wishes to thank all of its partners in research programs on supersonic combustion, in particular MBDA, DLR, JAXA, ESA and ITLR. Special thanks to A. Mura (ENSMA) for fruitful discussions and for his contribution to the modeling activities.

References

[1] A. MESTRE, L. VIAUD - *Combustion supersonique dans un canal cylindrique.* Supersonic flow chemical processes and radiative transfer, D.B. Olfe, V. Zakkay, Pergamon Press, 1964

[2] R. MARGUET, C. HUET - *Recherche d'une solution optimale de statoréacteur à géométrie fixe, de Mach 3 à 7, avec combustion subsonique puis supersonique.* T.P. ONERA n°656, 1968

[3] F. HIRSINGER - *Optimisation des performances d'un statoréacteur supersonique - Etude théorique et expérimentale.* ISABE, Marseille, 1972, T.P. ONERA n° 1106

[4] O. LEUCHTER - *Etude des évolutions chimiques dans une couche de mélange hydrogène-air.* T.P. ONERA n° 981 , 1971

[5] O. LEUCHTER - *Problèmes de mélange et de combustion supersonique d'hydrogène dans un statoréacteur hypersonique.* T.P. ONERA n° 973, 1971

[6] F. FALEMPIN, D. SCHERRER, G. LARUELLE, P. ROSTAND, G. FRATACCI, J.L. SCHULTZ - *French Hypersonic Propulsion Program PREPHA - Results, Lessons and Perspectives.* 8th International Space Planes and Hypersonic Systems and Technologies Conference, AIAA-98-1565, April 27-30, 1998, Norfolk

[7] P. NOVELLI, W. KOSCHEL - *JAPHAR – A Joint ONERA-DLR Research Project on High Speed Airbreathing Propulsion.* ISABE paper 99-7091, 14th Symposium ISABE, Florence (Italy), September 05-10, 1999

[8] P. NOVELLI, W. KOSCHEL - *Progress of the JAPHAR Cooperation Between ONERA and DLR on Hypersonic Airbreathing Propulsion.* 10th International Space Planes and Hypersonic Systems and Technologies Conference, Kyoto (Japan), AIAA 2001-1870, April 24-27, 2001

[9] T. SUNAMI, P. MAGRE, A. BRESSON, F. GRISCH, M. ORAIN, M. KODERA - *Experimental Study of Strut Injectors in a Supersonic Combustor Using OH-*PLIF. 13th International Space Planes and Hypersonic Systems and Technologies Conference, May 16-20, 2005, Capua, Italy

[10] J. STEELANT - *Sustained Hypersonic Flight in Europe: First Technology Achievements within LAPCAT II.* 17th AIAA International Space Planes and Hypersonic Systems and Technologies Conference, San Francisco (CA), 2011, AIAA 2011–2243

[11] J. STEELANT, R. VARVILL, S. DEFOORT, K. HANNEMANN, M. MARINI - *Achievements Obtained for Sustained Hypersonic Flight within the LAPCAT II Project,* 20th International Space Planes and Hypersonic Systems and Technologies Conference, AIAA-2015-3677, Glasgow, UK, 5-8 July 2015

[12] A. BRESSON - *OH/Acetone* PLIF *and CARS Thermometry in a Supersonic Reactive Layer.* 10th International Space Planes and Hypersonic Systems and Technologies Conference, Kyoto (Japan), April 24-27, 2001

[13] P. MAGRE, P. BOUCHARDY - *Nitrogen and Hydrogen Coherent Anti-Stokes Raman Scattering Thermometry in a Supersonic Reactive Mixing Layer.* Proceedings of the Combustion Institute, Volume 28, Issue 1, 2000, pp. 697-703

[14] D. FOURNET, P. MAGRE, G. COLLIN - *Mesure de Profils de Vitesse par Vélocimétrie Laser dans un Ecoulement Supersonique en Combustion.* 6é Congrès Francophone de Vélocimétrie Laser, Saint-Louis, France, 22-25 September 1998

[15] H. WEISGERBER, R. MARTUNOZZI, U. BRUMMUND, P. MAGRE - *PIV Measurements in a Mach 2 Hydrogen-Air Supersonic Combustion.* AIAA-2001-1757. 10th International Space Planes and Hypersonic Systems and Technologies Conference, Kyoto (Japan), April 24-27, 2001

[16] E. GEORGE, P. MAGRE, V. SABEL'NIKOV - *Self-Ignition of Hydrogen-Hydrocarbons Mixtures in a Hot Supersonic Confined Coflow of Air.* 13th AIAA International Space Planes and Hypersonic Systems and Technologies Conference, 2005

[17] D. GAFFIÉ, U. WEPLER, P. MAGRE, W. KOSCHEL, P. NOVELLI - *Numerical Investigation of Supersonic Reacting Hydrogen Jets in a Hot Air Coflow.* 10th AIAA International Space Planes and Hypersonic Systems and Technologies Conference, 2001

[18] D. DAVIDENKO, I. GÖKALP, E. DUFOUR, D. GAFFIÉ - *Kinetic Mechanism Validation and Numerical Simulation of Supersonic Combustion of Methane-hydrogen Fuel.* 11th AIAA International Space Planes and Hypersonic Systems and Technologies Conference, 2002

[19] V. QUINTILLA, P. MAGRE, D. SCHERRER, P. DESTORS, E. DUFOUR - *Experimental and Numerical Investigation of Supersonic Reacting Hydrogen/Methane Jets in hot Air Coflows.* 13th AIAA International Space Planes and Hypersonic Systems and Technologies Conference, May 16-20, 2005, Capua, Italy

[20] L. VULIS - *Thermal Regimes of Combustion*, McGraw-Hill, New York, 1961

[21] B. MAGNUSSEN - *On the Structure of Turbulence and a Generalised Eddy Dissipation Concept for Chemical Reactions in Turbulent Flow,* 19th AIAA Aerospace Sciences Meeting, 1981

[22] B. MAGNUSSEN - *The Eddy Dissipation Concept.* ECCOMAS Thematic Conference on Computational Combustion, 2005

[23] I. ERTESVAG, B. MAGNUSSEN - *The Eddy Dissipation Turbulent Energy Cascade Model.* Combust. Sci. Technol. 159 (1) (2000) 213–235

[24] M. BERGLUND, E. FEDINA, C. FUREBY, J. TEGNER, V.A. SABEL'NIKOV - *Finite Rate Chemistry Large Eddy Simulation of Self-Ignition in Supersonic Combustion Ramjet.* AIAA Journal, Vol. 48, No 3, March 2010 , pp. 540–550

[25] Y. MOULE, V.A. SABEL'NIKOV, M. SMART, A. MURA - *Computational Fluid Dynamics Investigation of a Mach 12 Scramjet Engine.* J. Propul. Power 30, 2014, pp. 461–473

[26] A. LINÁN - ACTA ASTRON. 1, 1974, pp. 1007–1039

[27] O. JARRETT, A. CUTLER, R. ANTCLIFF, T. CHITSOMBOON, C. DANCEY, J. WANG - *Measurements of Temperature, Density, and Velocity in Supersonic Reacting Flow for CFD Code Validation.* 25th JANNAF Combustion Meeting, vol. 1, 1988, pp. 357–374

[28] T. CHENG, J. WEHRMEYER, R. PITZ, O. JARRETT, G. NORTHAM - *Finite-Rate Chemistry Effects in a Mach 2 Reacting Flow.* 27th AIAA Joint Propulsion Conference, 1991

[29] T. CHENG, J. WEHRMEYER, R. PITZ, O. JARRETT, G. NORTHAM - *Raman Measurement of Mixing and Finite-Rate Chemistry in a Supersonic Hydrogen-Air Diffusion Flame.* Combustion and Flame, Vol 99, Issue 1, 1994, pp. 157-173

[30] C. DANCEY - *The Turbulent Flow Field Downstream of an Axisymmetric Mach 2 Supersonic Burner: LDA Measurements.* 32nd AIAA Joint Propulsion Conference, 1996

[31] C. JACHIMOWSKI - *An Analysis of Combustion Studies in Shock Expansion Tunnels and Reflected Shock Tunnels.* Tech. Rep., NASA, 1992

[32] A. REFLOCH, B. COURBET, A. MURRONE, P. VILLEDIEU, C. LAURENT, P. GILBANK, J. TROYES,L. TESSÉ, G. CHAINERAY, J. DARGAUD, E. QUÉMERAIS, F. VUILLOT - *CEDRE Software*. Aerospace Lab Journal 2, 2011

[33] D. SCHERRER, F. CHEDEVERGNE, P. GRENARD, J. TROYES, A. MURRONE, E. MONTREUIL, A. CHAZOTTES, F. VUILLOT, N. LUPOGLAZOFF, M. HUET, B. SAINTE-ROSE, P. THORIGNY, N.BERTIER, J.-M. LAMET, T. LE PICHON, E. RADENAC, A. NICOLE, L. MATUSZEWSKI, M.ERRERA - *Recent CEDRE Applications.* Aerospace Lab Journal 2, 2011

[34] E. TORO, M. SPRUCE, W. SPEARES - *Restoration of the Contact Surface in the HLL-Riemann Solver*. Shock Waves 4 , 1994, pp. 25-34

[35] P. GERLINGER, K. NOLD, M. AIGNER - *Influence of Reaction Mechanisms, Grid-Spacing, and Inflow Conditions on the Numerical Simulation of Lifted Supersonic Flames*. Int. J. Numer. Methods Fluids 62 , Issue 12, 2010, pp. 1357-1380

[36] S. KARL - *Numerical Investigation of a Generic Scramjet Configuration*. Ph.D. thesis, The University of Dresden, 2011

[37] P. BOIVIN, A. DAUPTAIN, C. JIMÉNEZ, B. CUENOT - *Simulation of a Supersonic Hydrogen-Air Auto-Ignition Stabilized Flame Using Reduced Chemistry*. Combustion and Flame, Vol 159, Issue 4, 2012, pp. 1779–1790

[38] Y. MOULE, V. SABEL'NIKOV, A. MURA - *Highly Resolved Numerical Simulation of Combustion in Supersonic Hydrogen-Air Coflowing Jets.* Combustion and Flame 161 (2014), pp. 2647-2668

[39] Y. MOULE - *Modélisation et simulation de la combustion dans les écoulements rapides*. Applications aux Superstatoréacteurs, ENSMA PhD Thesis, 2013

[40] A. BEN-YAKAR, M. MUNGAL, R. HANSON - *Time Evolution and Mixing Characteristics of Hydrogen and Ethylene Transverse Jets in Supersonic Crossbows*. Physics of Fluids 18, 026101 (2006)

[41] V. VITI, R. NEEL, J. SCHETZ - *Detailed Flow Physics of the Supersonic Jet Interaction Flow Field*. Physics of Fluids 21 (2009)

[42] S. KAWAI, S. LELE - *Large-Eddy Simulation of Jet Mixing in Supersonic Crossflows*. AIAA Journal 48, 2063-2083 (2010)

[43] M. GAMBA, V. MILLER, M. GODFREY MUNGAL - *The Reacting Transverse Jet in Supersonic Crossow: Physics and Properties.* AIAA paper 2014-3107, AIAA Aviation / 19th AIAA International Space Planes and Hypersonic Systems and Technologies Conference (Atlanta, Georgia, 16-20 June, 2014)

[44] D. SCHERRER - *Optimisation de l'injection d'hydrogène dans un écoulement d'air supersonique*. 1er Colloque du Programme de Recherches Concertées Combustion dans les Superstatoréacteurs, CNRS, Paris, 21-22 October 1991

[45] D. SCHERRER, O. DESSORNES, N. MONTMAYEUR, O. FERRANDON - *Injection Studies in the French Hypersonic Technology Program*. AIAA-95-6096, 6th International Space Planes and Hypersonic Systems and Technologies Conference, April 3-7, 1995, Chattanooga

[46] O. DESSORNES, C. JOURDREN - *Mixing Enhancement Techniques in a Scramjet*. AIAA-98-1517. 8th International Space Planes and Hypersonic Systems and Technologies Conference, April 27-30, 1998, Norfolk

[47] J. SWITHENBANK, N.A. CHIGIER - *Vortex Mixing for Supersonic Combustion*. Proceedings of the 12th Symposium (International) on Combustion, 1968, pp. 1153-1162

[48] L.A. POVINELLI, F.P. POVINELLI, M. HERSCH - *A study of Helium Penetration and Spreading in a Mach 2 Airstream Using a Delta Wing Injector*. NASA TN D-5322, 1969

[49] G.B. NORTHAM, I. GREENBERG, C.S. BYINGTON - *Evaluation of Parallel Injector Configurations for Supersonic Combustion*. AIAA-89-2525, 1989

[50] E.J. GUTMARK, K.C. SCHADOW,, K.H. YU - *Mixing Enhancement in Supersonic Free Shear Flows*. Annual Review of Fluid Mechanics, Vol. 27, 1995, pp. 375-417

[51] M. NISHIOKA, T. SUNAMI - *Some Thoughts and Experiments on the Supersonic Mixing Enhancement*. Journal of fluid Mechanics of Japan, Vol. 14, pp. 377-389, 1995 (in Japanese)

[52] T. SUNAMI, M.N. WENDT, M. NISHIOKA - *Supersonic Mixing and Combustion Control Using Streamwise Vortices.* AIAA-98-3271, 1998

[53] T. SUNAMI, A. MURAKAMI, K. KUDO, M. KODERA, M. NISHIOKA - *Mixing and Combustion Control Strategies for Efficient Scramjet Operation in Wide Range of Flight Mach Numbers*. AIAA-2002-5116, 11th International Space Planes and Hypersonic Systems and Technologies Conference, 1992, Orléans

[54] T. SUNAMI, P. MAGRE, A. BRESSON, F. GRISCH, M. ORAIN, M. KODERA - *Experimental Study of Strut Injectors in a Supersonic Combustor Using OH*-PLIF. 13th International Space Planes and Hypersonic Systems and Technologies Conference, May 16-20, 2005, Capua, Italy

[55] C. FUREBY, K. NORDIN-BATES, K. PETTERSON, A. BRESSON, V. SABELNIKOV - *A Computational Study of Supersonic Combustion in Strut Injector and Hypermixer Flow Fields*. Proceedings of the Combustion Institute 35 (2), 2015, pp. 2127-2135

[56] A. VINCENT-RANDONNIER, Y. MOULE, M. FERRIER - *Combustion of Hydrogen in Hot Air Flows within LAPCAT–II Dual Mode Ramjet Combustor at Onera-LAERTE Facility – Experimental and Numerical Investigation*. 19th AIAA International Space Planes and Hypersonic Systems and Technologies Conference, Atlanta (GA), 2014, AIAA 2014–2932

[57] S. DEFOORT, M. FERRIER, L. SERRE, D. SCHERRER, C. PARIDAENS, P. HENDRICK, A. INGENITO, C. BRUNO - L*APCAT-II: Conceptual Design of a Mach 8 TBCC Civil Aircraft, Enforced by Full Navier-Stokes 3D Nose-to-Tail Computation.* 17th AIAA International Space Planes and Hypersonic Systems and Technologies Conference, San Francisco (CA), 2011, AIAA 2011–2317

[58] A. BEN-YAKAR, R. HANSON - *Experimental Investigation of Flame-Holding Capability of Hydrogen Transverse Jet in Supersonic Cross-Flow.* 36th Int. Symp. on Combustion, 27 (2), 1998, 2173-2180

[59] O. DESSORNES, D. SCHERRER, P. NOVELLI - *Testing and Weighing of the Japhar Dual Mode Ramjet Engine*. ISABE paper 2001-1135, Bengalore (India)

[60] O. DESSORNES, D. SCHERRER - *Weighing of the JAPHAR Dual Mode Ramjet Engine*. AIAA paper 2002-5187, Orléans (France), 2002

[61] O. DESSORNES, D. SCHERRER - *Tests of the JAPHAR Dual Mode Ramjet Engine*. Aerospace Science and Technology, 2005, volume 9, issue 3, pages 211-221

[62] C.E.JR. COCKRELL, W.C. ENGELUND, R.D. BITTNER, T.N. JENTINK, A.D. DILLEY, A. FRENDI - I*ntegrated Aeropropulsive Computational Fluid Dynamics Methodology for the Hyper-X Flight Experiment.* Journal of Spacecraft and Rockets 38-6 (2001)

[63] T. LANGENER, J. STEELANT, S. KARL, K. HANNEMANN - *Design and Optimization of a Small Scale Mach=8 Scramjet Propulsion System*. Space Propulsion 2012. SP2012-2394071, May 2012, Bordeaux, France

[64] T. LANGENER, J. STEELANT, S. KARL, K. HANNEMANN - *Layout and Design Verification of a Small Scale Scramjet Combustion Chamber.* 21st International Symposium on Air breathing Engine. ISABE-2013-1655, September 9-13 2013, Busan, Korea

[65] T. LANGENER, J. STEELANT, S. KARL, K. HANNEMANN - *Numerical Validation of a Free-Flying Scramjet Powered Vehicle at Realistic Wind Tunnel Conditions.* Space Propulsion 2014. SP2014-2971766, May 19-22 2014, Cologne, Germany

[66] K. HANNEMANN, J. SCHRAMM, S. LAURENCE, S. KARL - *Experimental and Numerical Analysis of the small Scale LAPCAT II Scramjet Flow Path in High Enthalpy Shock Tunnel Conditions.* Space Propulsion 2014. SP2014-2969350, May 19-22 2014, Cologne, Germany

AUTHORS

Dominique Scherrer graduated from « Ecole Centrale de Paris » in 1979. He joined ONERA in the Energetics Direction in 1981. His main research topics concerned droplet combustion modeling, combined cycle propulsion, scramjet design and CFD. He has been the CEDRE project manager between 1996 and 2002. He is deputy director of the Fundamental and Applied Energetics Department since 1997.

Olivier Dessornes graduated from the French engineering school ESTACA in 1990. He joined ONERA in 1990 where he is a research engineer working in the Fundamental and Applied Energetics Department (DEFA). He is mostly involved in experimental activities. His current fields of interest are scramjet propulsion, energy micro sources and hybrid propulsion.

Marc Ferrier graduated from HEI (Lille) in 2002 and received his Ph.D. Degree in Fluid Dynamics in 2008 for his work on boundary layer transition in supersonic flow. He is now a research engineer at ONERA, where he works on supersonic combustion.

Axel Vincent-Randonnier graduated from Université Pierre et Marie Curie where he obtained MSc and PhD degrees in Energetics and Process Engineering in 2002. He joined ONERA in 2004 for post-doctoral activities on plasma assisted combustion. Since 2006, he has been in charge of LAERTE subsonic and supersonic combustion facilities at ONERA – Palaiseau Center. Since 2012, he has been in charge of the MICADO project aimed at developing a new test rig dedicated to the study of high-pressure air-breathing combustion with optical diagnostics.

Yann Moule graduated from ENSMA (Poitiers) in 2007 and received his Ph.D. Degree in Energetics in 2012. His research work at Onera focused on combustion in supersonic flows and scramjet engines. He joined MBDA France in 2014, where he is working as a propulsion engineer.

Vladimir Sabelnikov gratuated (1971) from Moscow Institute of Physics and Technology (MIPT), Dolgoprudny, Russia, Ph.D. (1974), and Doctor of Science (1984) degrees from MIPT also. In 1974, he joined the Central Aerohydrodynamics Institute (TsAGI, Moscow, Russia), where he was Leading Scientist until 2000. Since 2000, he is a Leading Scientist in Energetic department of ONERA. His current research interests include the study of combustion instabilities in gas turbines, supersonic combustion in ducts, scramjets, combustion in microcombustors, the plasma control of combustion, the development of Eulerian Monte Carlo method to solve the transported PDF equation in turbulent combustion, and the development of new PaSR and EPaSR models of turbulent combustion.

Modeling Challenges in Computing Aeronautical Combustion Chambers

B. Fiorina, A. Vié, B. Franzelli, N. Darabiha
(Laboratoire EM2C, CNRS, Centrale-Supélec, Université Paris-Saclay)
M. Massot
(Laboratoire EM2C, CNRS, Centrale-Supélec, Université Paris-Saclay, ONERA)
G. Dayma, P. Dagaut
(ICARE, CNRS, Université d'Orléans)
V. Moureau, L. Vervisch, A. Berlemont
(CORIA-UMR 6614-Normandie Université, CNRS-Université, INSA de Rouen)
V. Sabelnikov
(ONERA)
E. Riber, B. Cuenot
(CERFACS)

E-mail:
benoit.fiorina@centralesupelec.fr

DOI : 10.12762/2016.AL11-05

This article reviews the modeling challenges for performing Large Eddy Simulations of aero-nautical combustion chambers. Since the kerosene is injected in a liquid phase into the combustion chamber, the description of the atomization is of primary importance. The article first discusses the numerous numerical challenges encountered during this process, which leads to the formation of small droplets that constitute a spray. The existing numerical and modeling methods to describe a spray of kerosene droplets are then presented. The article then focuses on the description of the complex combustion kinetics. Hundreds of species and thousands of reactions have to be considered to predict ignition, flame stabilization and pollutant emissions. Due to lengthy computational times, detailed chemical schemes are too large to be directly used in CFD. This article then presents the major existing chemical reduction strategies. Significant interactions of the reactions layers with the flow vortices occur at the subgrid scale. The question of turbulent combustion modeling is therefore discussed in an LES context. Finally, the prediction of soot and NOx formation is presented. The review is illustrated by several examples representative of practical situations encountered in aeronautical combustors.

Introduction

The numerical simulation of aeronautical combustion chambers involves very complex physical phenomena. First of all, due to the high velocity of the airflow through the combustor, the reacting flow is highly turbulent. It can be numerically simulated using three levels of accuracy [1]: Reynolds Average Navier Stokes (RANS) simulations, predicting only mean flow characteristics; Large Eddy Simulations (LES), where turbulent large scales are explicitly calculated whereas the effects of smallest ones are modeled; Direct Numerical Simulations (DNS), where the full instantaneous Navier-Stokes equations are solved without any model for turbulent transfer. DNS is extremely expensive in terms of computational resources and therefore in practice is limited to simplified geometries with reduced chemical kinetics (Richardson, 2010). LES offers significant advantages when compared to RANS techniques, because unsteady large-scale motions, important for flame propagation, stabilization, flow mixing, and consequently chemical species predictions, are resolved. Also, by giving access to local and instantaneous data, it enables a better understanding and description of some complex unsteady phenomena, such as flame/turbulence interactions and pollutant formation, which are not well captured by statistical quantities. Thanks to the development of massively parallel computers, LES of practical industrial combustors, exhibiting complex geometry features, is now achievable [2].

LES of turbulent flames in an aeronautical combustor is a challenging multi-physics problem. The kerosene is first injected in a liquid phase into the combustion chamber. Due to the velocity difference between the fuel jet and the coflowing air, the liquid jet undergoes complex atomization processes, which ultimately lead to the formation of small droplets. It then constitutes a spray that feeds the flame front with evaporated fuel. The droplet size and their spatial distribution directly impact the flame position. The combustion process is also very challenging from a chemical point of view. Hundreds of species and thousands of reactions have to be considered in order to predict subtle phenomena, such as ignition or re-ignition, flame stabilization and

pollutant emissions. For computational time limitations, detailed chemical schemes are too large and chemical reductions strategies are needed to introduce reliable chemistry ingredients in LES. In practical combustion chambers the grid size is of the order of 1 mm. However, many physical phenomena occur at a smaller scale (i.e., at the so-called “sub-grid” scale) and have to be modeled. This is especially the case of chemically reactive zones, whose thickness is of the order of 0.1 mm, and the case of interactions between the flame and the turbulence. The challenges are even greater in the case of pollutant predictions because of their considerably smaller concentrations and the many pathways leading to their formation or destruction. Pollutant mole fractions amount to a few tenths to a few hundreds ppms.

The objectives here are to give an overview of the modeling challenges encountered when performing LES of aeronautical combustion chambers. The state-of-the art of liquid atomization, spray description and combustion modeling is presented. For that purpose, this article is organized as follows: Issues relative to primary atomization are first presented. The description of the liquid spray is then discussed. Chemical kinetics of kereosene/air combustion is presented in § " Kerosen chemistry modeling ", whereas § " Turbulent combustion models " summarizes the challenge of introducing detailed chemistry phenomena in turbulent flow solvers. Finally, the question of pollutant formation is developed: the prediction of soot and NOx formation are presented.

Primary atomization modeling

Atomization is a highly non-linear phenomenon that occurs when liquid fuel is injected into the combustor [3]. Primary break-up is the early phase of the atomization process when the continuous liquid core is transformed into ligaments and large droplets. The typical size of these features ranges between a few to a hundred microns. Resolving these features is presently out of reach in spray combustion simulations, which have to take into account the combustor geometry and the flame dynamics occurring at larger scales. Consequently, the impact of primary atomization on the spray formation needs to be modeled in aeronautical burner simulations.

Beyond this scale resolution issue, the simulation of primary atomization faces numerous numerical challenges: at the liquid/gas interface, the density, the pressure and the viscosity are discontinuous. Dedicated algorithms have been developed over the last decades to accurately include these jump conditions in high-fidelity 3-D unsteady simulations. The Ghost-Fluid Method proposed by Fedkiw et al [4] has been widely adopted to take into account the pressure jump at the interface without any numerical smearing. This method requires the precise location of the gas/liquid interface during the simulation. Many algorithms have been developed to track the interface and to ensure a sufficiently accurate calculation of the interface curvature and a correct mass conservation [5, 6, 7, 8]. Most of these methods have been derived within the framework of finite-differences and their application has been limited to simple geometries.

Within the framework of the European project FIRST, the feasibility of primary atomization simulation in realistic geometries has been investigated. The Accurate Conservative Level Set method [8] has been implemented in an unstructured finite-volume solver named YALES2, which is dedicated to the simulation of turbulent combustion in aeronautical burners. This methodology has been applied to several complex injectors. Two examples are shown in Figs. 1 and 2. The first configuration consists in the so-called triple disk injector [9], whose particular injector geometry creates a liquid sheet that atomizes rapidly. For this configuration, three different Large-Eddy Simulations were performed with various mesh resolutions. The finest mesh resolution, with 1.6 billion tetrahedra, enables the large-scale dynamics to be recovered as the ligament formation, but it is still not enough to capture all of the flow features from the experiment at the secondary atomization scale. The second configuration is a realistic injector provided by Turbomeca, SAFRAN Group. In this configuration, the prefilming inside an airblast swirl injector was investigated. Large-Eddy Simulations with 1.6 billion tetrahedra for 1/8th of the full geometry were conducted. Figure 2 shows the location of the interface and the velocity magnitude at the interface. While the cell count is high, the mesh resolution at the interface is not fine enough and only large-scale dynamics of the liquid sheet are captured. In this particular case, where the gas Weber number is large and the liquid sheet has large displacements, primary atomization modeling would benefit from Adaptive Mesh Refinement (AMR) methods [10] to concentrate the degrees of freedom at the interface.

Spray description

The fuel droplets generated during the atomization process are convected by the air flow and constitute a spray phase which has a great impact on the full simulation. This phase will indeed prepare the flammable mixture for the combustion process. Many questions have to be asked beforehand, such as the simulation strategy, the choices of the physical models or the boundary conditions to be used, as well as the means of validation.

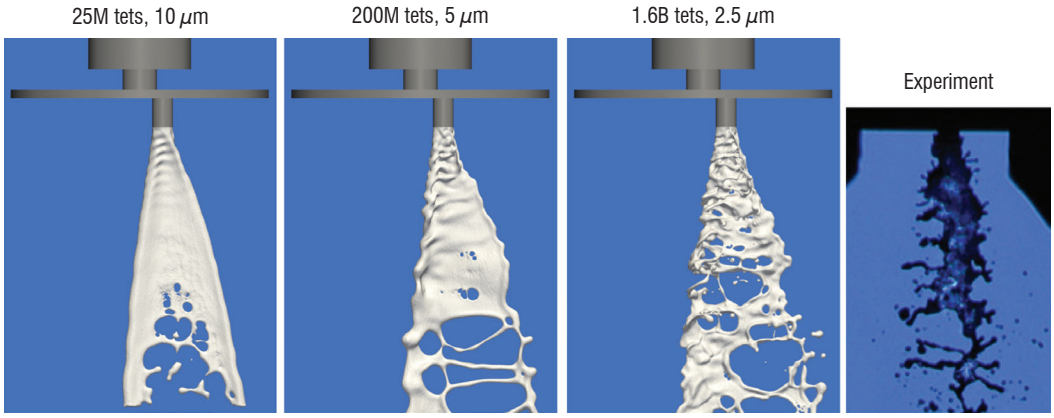

Figure 1 - Mesh refinement study of primary atomization at the exit of the triple disk injector.

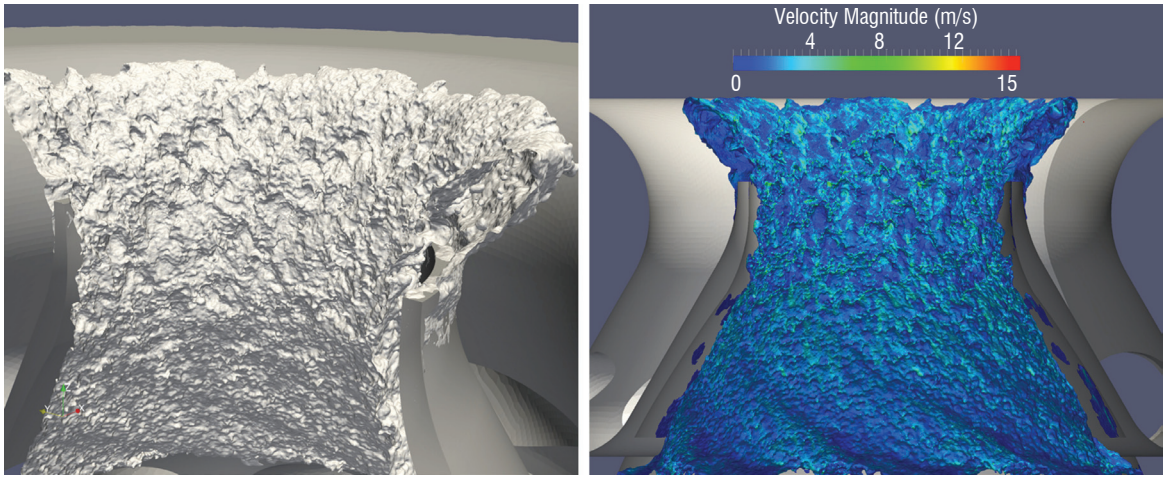

Figure 2 - Investigation of primary atomization in a realistic airblast swirl injector.

Simulation strategy

In order to describe the spray, the most commonly-used strategy is to consider a point-particle assumption, i.e., the droplet is smaller than any scale of the flow, and to use a Lagrangian Droplet Tracking method (LDT), for which individual droplets or parcels of droplets are transported by means of ODE systems on droplet state variables (position, velocity, size, etc.). To a lower extent, Eulerian methods that resolve statistical information, such as droplet concentration, are sometimes preferred for their intrinsic ability in parallel computing.

Lagrangian approaches

Lagrangian approaches are widely used because they are viewed as a reference and they also seem more intuitive than Eulerian strategies. They are based on an ODE system that solves the time evolution of the droplet state. Depending on the point of view adopted, this description may be deterministic or probabilistic. In the deterministic framework, each numerical particle corresponds to a physical droplet, and the resulting set of droplets corresponds to an individual realization of the spray. From the probabilistic point of view, the ODE system is aimed at solving a Williams-Boltzmann equation [11] on the Number Density Function (NDF). The resulting set of droplets is thus a particular discretization of a set of realizations of the spray phase, similar to Monte-Carlo simulations [12, 13], and a stochastic description must be provided for droplet evolution [14, 15].

In LES of combustors, a stochastic point of view may be required [16], in which the parcels will represent sets of physical droplets. At this point, the choice of the best statistical representation in terms of parcels [13] is not straightforward and not necessarily unique, adding a degree of freedom to Lagrangian computations. Paulhiac [17] highlights this issue and proposes strategies for the statistical distribution of parcels. However, the most effective solutions in the literature are case-dependent and a statistical convergence verification is still required for Lagrangian simulations. Aside from that, efforts on the parallel efficiency of Lagrangian simulations are certainly of interest, for example using task-oriented paradigms or dual-constraint decomposition [18].

With regard to the numerical resolution, one important source of error is the projection strategy used to exchange droplet source terms with the gas phase. Actually, the classical point-particle approach cannot ensure mesh convergence. Strategies have been proposed in the literature [19, 20] to overcome this, using for instance Gaussian projection with a mesh-independent width. This kind of approach needs to be adapted to unstructured grid simulation, like in [17], and a more careful analysis and justification of the projection kernel, linked to the resolved scales for instance, needs to be carried out.

Finally, an interesting issue is the modeling of sub-grid scale effects on two-way coupling between carrier phase and disperse phase. In the literature, models have been devised to take into account the impact of sub-grid scales on the droplet motion [21, 16, 22], and have been applied to combustors simulations [23, 24]. However, no model has yet been developed to account for the effect of the disperse phase on the carrier phase sub-grid scale, either in the dynamics or in terms of temperature and composition. Such a development may be of great interest due to its link to the mixture formation and, consequently, the combustion process.

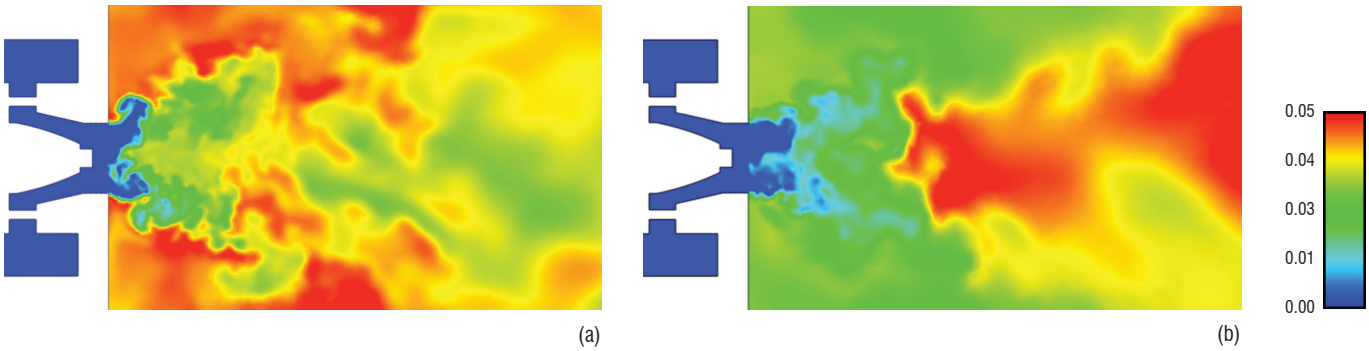

Figure 3 - Simulation of the MERCATO test rig of ONERA [34]. Vapor fuel mass fraction obtained with (a) mono disperse and (b) multifluid models for non-reactive conditions.

Eulerian Moment methods

Compared to Lagrangian methods, Eulerian approaches have the advantage of solving a fluid description similar to the gas phase, which enables the use of the same type of parallelism algorithm. Moreover, statistical convergence is intrinsically achieved, sine Eulerian methods directly solve the moments of the NDF. However, they come with two drawbacks compared to Lagrangian methods. First, moment methods need closures for the moment system, since for any moment set higher order moments are required to close the fluxes. The closure must be dictated by the physics of the problem and will induce a modeling error that does not exist for Lagrangian methods. Second, moment methods lead to a system of partial differential equations for which specific numerical methods have to be used in order to reduce numerical dissipation. For the simulation of aeronautical combustors, the two most important issues are the description of the size polydispersion of the droplets and the robust and accurate numerical resolution of the moment system on unstructured grids and complex geometries.

Concerning the size polydispersion, injection strategies can lead to polydisperse sprays with droplet sizes ranging from one micron to 200μm, and this polydispersion persists inside the combustion chamber. Simulations [25, 26] have exhibited the impact of size polydispersion on the spray and, for instance, experiments from [27] have identified the polydispersion as a potential origin for flame stabilization or flame bifurcation because of size-conditioned dynamics. In the literature, many polydisperse Eulerian strategies are available, ranging from Multifluid methods that discretize the size space into sections, to high order moment methods, see [28, 29, 30, 31, 32] and references therein. However, even though high order moment methods have been used for automotive engines [33], the only method that has been used to describe the cold flow of an aeronautical configuration is the first order Multifluid method [26], see Fig. 3, which is still expensive since 10 sections are required. The second order Multifluid method of Laurent et al [32.1, 32.2, 32.3] used for solid propulsion in the CEDRE code is for now the most attractive strategy, which reduces the required number of sections.

Concerning the numerical resolution of the moment equations, several works have evidenced the difficulty to accurately and robustly solve moment equations in complex configurations and unstructured grids using conventional methods (see [35] and references therein). In fact, due to the droplet phase inhomogeneity induced by the injection and the turbulence, the disperse phase exhibits strong gradients and vacuum zones. This requires the use of stabilization techniques, such as artificial viscosity or flux limiters, which still need an iterative process to adjust numerical parameters in order to obtain the best solution. A major challenge is thus to design numerics that are intrinsically stable and robust. In the literature, the only works that deal with the numerics of Eulerian methods on unstructured grids have been performed in the AVBP code of CERFACS and the CEDRE code of ONERA. The former is based on a Taylor-Galerkin scheme [36] initially developed for the gas phase. For Eulerian simulations, specific attention has been given to artificial diffusion operators, in order to stabilize the simulations [37, 38, 39]. The latter uses a realizable multislope MUSCL method [40] adapted to two-phase flows, which is limited to second order accuracy. In order to achieve sufficient accuracy while ensuring robustness, a method of great potential is the Discontinuous Galerkin (DG) approach. For example, in [41], it has been shown that it is possible to design DG schemes [42] for moment equations that satisfy all stability requirements as well as strongly increasing accuracy compared to the MUSCL strategy, even at second order.

Apart from these two issues, velocity and temperature polydispersions, especially in the context of LES, will have to be properly modeled. For these two issues, two types of strategy exist. The Algebraic-Closure-Based Moment Methods (ACBMM) [43, 44] model the unclosed terms using information on moments and have already been used to simulate complex configurations using the AVBP code [45, 46, 26]. The Kinetic-Based Moment Methods [47] use assumptions regarding the underlying kinetic distribution. A comparison has been made in [48], showing that both methods have a close level of accuracy, with ACBMM having an advantage in terms of number of equations (5 against 10 in 3D) and KBMM having an advantage in terms of numerics (hyperbolic structure of the equations [49]). The extension of such models to two-way coupling has yet to be proposed, since it is essential for combustion problems, and should be inspired by previous work in the RANS context [50, 51].

Physical models

In order to describe the spray evolution, the physical processes that affect the spray must be defined. The spray regime encountered in combustors restricts the most important processes to the drag force and the heat and mass transfers, since these are the most likely to drive the spray trajectory, as well as its exchanges with the gas phase. The most widely used model to express the drag force is the Schiller-Naumann correlation [52], which acts as a Reynolds-based correction of the classical Stokes law [53] and has been shown to be valid in the diluted regime. At this point, the most prominent question for drag force is whether or not to evaluate one of its parameters: the unperturbed gas velocity. In [54], the authors point out this issue by demonstrating that, even in the point-particle limit, the model should not directly take the gas velocity at the droplet location as an unperturbed velocity. Such a modification should be more deeply tested and evaluated in real applications, in order to see its impact. Concerning heat and mass transfers, a wide range of models can be found in the literature, with different sets of assumptions and different validation cases. A comprehensive review is available in [55]. Many recent models have been focused on the evaluation of the gas phase properties at the droplet surface, by considering for instance complex transport in the case of reduced chemistry [56] or corrected Stefan fluxes [57]. Shashank et al [58] have also investigated the sensitivity of models to the 2/3-1/3 approximation [59] for gas phase reference quantities, and have shown the great impact of this choice. In the end, the most difficult issue is the validation of the evaporation model with regard to reference experiments. First, designing an experiment to evaluate vaporization is not straightforward. For instance, Chauveau et al [60] have demonstrated the impact of the support fiber to be non-negligible. Second, most droplet evaporation experiments are performed on pure hydrocarbons, and more data are required for kerosene under various conditions. Third, the impact of droplet motion as well as droplet combustion on the vaporization correlations must be properly validated for kerosene under realistic conditions. For example, a model for taking into account isolated droplet combustion has been proposed in [17].

Physical processes besides evaporation and drag force should also be taken into account. For instance, droplet secondary break-up modeling can have an impact on simulations [61] and would need further

investigations regarding the numerous available break-up models, see for instance [62] and references therein, for the sensitivity to the chosen model. Models for droplet/wall interactions, as well as film formation and break-up, would also be of interest, since many injection devices could lead to the impact of the jet in the swirler region or at the combustion chamber walls. Such a physics is not straightforward to handle, since it would require the film formation from droplet impacts to be modeled, as well as the film breakup into droplets. In the work of Chaussonnet et al [63, 64], the authors proposed a first model to account for such a transition by describing the film formation from Lagrangian droplets and modeling the droplet generation from the film break-up.

Injection modeling

Although it is not possible at this time to simulate the primary atomization process from the injection location to the combustion chamber, two-phase combustion chambers have been simulated over the past decade by using boundary conditions for the disperse phase: instead of injecting a coherent liquid jet, boundary conditions are moved downstream into the disperse phase region, and a distribution of droplets is injected [21, 65, 66, 24]. In order to choose the appropriate profiles at the boundary condition, models have been devised based on phenomenological models and appropriate volume balances. However, these models still rely on experimental data to adjust parameters such as droplet diameters, in general taken at the closest measurement location. Such a solution is helpful to run computations, but is not a long-term solution since experiments will always be needed to adjust the injection model. In order to avoid these constraints, the most evident solution is the use of high-fidelity injection simulations that accurately reproduce all of the features of the primary atomization process, in order to provide more insightful descriptions of the injection system, for instance by giving the droplet size distribution from the injection exit. In addition to the development of boundary conditions, methods are also under development to ensure the transition between the separated and disperse phases, and will be a building block for future complete simulations, see [67, 68, 69.1, 69.2, 69.3, 69.4] for instance.

Validation

Finally, an important point concerning disperse phase simulations relates to the validation strategy. Actually, due to the complexity of the physics and the difficulties in accessing information in a reactive configuration, particular attention must be paid to this specific issue. Actually, two ANR projects were initiated this year, which will give a specific focus on this issue. First, the project named NEXTFLAME (EM2C/CERFACS) will investigate two-phase combustion in a counterflow burner, for which a detailed characterization of inflow conditions and spray flame characteristics will be available. Second, the TIMBER project (EM2C/CERFACS/CORIA/SAFRAN) will investigate two-phase ignition in annular chambers, and for this purpose will use simple benchmark cases. Both projects will give the community reference test cases that will possibly be used for in-depth validation of simulation strategies.

Kerosene chemistry modeling

From a chemical kinetic point of view, the combustion of aviation fuels is a challenging problem. Jet fuels, such as Jet A-1 and JP-8, are complex mixtures of over one thousand hydrocarbons containing from 8 to 16 atoms of carbon. Moreover, the chemical composition of a given jet fuel can vary and different fuels are used world-wide with compositions that differ significantly from one location to another. Finally, jet fuels also contain additives (such as antioxidants, corrosion inhibitors or metal deactivators), which are determined by the specific use of the fuel. Both the physical properties of the jet fuel and its global reactivity, as well as its propensity to produce different pollutants such as soot, depend on this composition. Due to the complexity of these mixtures, the detailed composition cannot be used as an input for combustion modeling purposes. Until the last decade, aviation fuel combustion was modeled using a single component. After reduction, the chemical kinetic mechanism fits CFD requirements well, especially in terms of number of species. With the continuing increase of computer power and the interest in alternative aviation fuels whose chemical composition again differs from that of conventional jet fuels, new strategies were developed to better predict heat release and pollutant formation during the combustion in gas turbine engines. These strategies rely on the idea that all of the individual hydrocarbons present in a jet fuel (conventional or alternative) can be classified into four different families: n- and iso-paraffins, naphthenes and aromatics, with relative abundances depending on the fuel. All of these families have specific chemical reactions and different reactivities. A so-called surrogate can be formulated as a mixture of well-chosen hydrocarbons representative of their own family. A first approach was developed by Guéret et al [70] with a mixture of three hydrocarbons (79% n-undecane, 10% n-propylcyclohexane, 11% 1,2,4-trimethylbenzene) to model the oxidation of a Jet A-1 in a jet-stirred flow reactor at atmospheric pressure. It was found that the identified reaction products formed during the oxidation of the ternary mixture and the kerosene were very similar in terms of concentration. Furthermore, a quasi- global chemical kinetic reaction mechanism was developed to reproduce the experimental data. The authors concluded that a kinetic model involving an equivalent mixture of a small number of pure hydrocarbons can represent the oxidation of kerosene.

Then, Dagaut et al [71] formulated four chemical surrogate model fuels of increasing complexity from pure n-decane (100%mol.), n-decane/n-propylbenzene (74%/26%mol.), n-decane/n-propylcyclohexane (74%/26%mol.) and n-decane/n-propylbenzene/n-propylcyclohexane (74%/15%/11%mol.). The oxidation of these four mixtures was studied in a jet-stirred reactor at atmospheric pressure, over a temperature range from 900 to 1300 K and variable equivalence ratios, and compared to the oxidation of Jet A-1 obtained under the same conditions. It was found that the 3-component fuel model was the most appropriate to simulate the jet stirred reactor experiments, as well as a fuel-rich premixed kerosene-oxygen-nitrogen flame. In 2006, Dagaut and Cathonnet [72] published a review of kerosene combustion in which they reported recent advances on the formulation of kerosene surrogate fuels, as well as experimental kinetic studies on kerosene and surrogate ignition, oxidation and combustion and the latest kinetic modeling efforts. The relevance of the approach using chemical families was demonstrated through numerous simulations of Jet A-1 and JP-8 surrogate combustion, but the authors highlighted the lack of experimental data under flame conditions. A similar initial idea by Colket et al [73] was to design a simplified surrogate composed of n-decane (50%vol.), n-butylcyclohexane (25%vol.) and n-butylbenzene (25%vol.) to better match the hydrogen/carbon ratio (1.91 for JP-8) and set the aromatic content at the limit of the aviation fuel regulations. Ignition temperature, extinction strain rates and CO mole fractions were

measured and this group concluded that this surrogate was more reactive and more difficult to extinguish than typical jet fuels. Finally, a roadmap was proposed for the development of jet fuel surrogates. The targets identified by Colket et al [73] were pushed further by Dooley et al[74]. They decided to focus the design of comprehensive surrogates not only on the H/C ratio but also on the derived cetane number (DCN), the threshold sooting index (TSI) and the molecular mass. They started with fourteen different mixtures of n-decane, iso-octane and toluene. DCNs were measured using an ignition quality tester and TSIs were determined from a linear relationship taking into account the TSI of pure components and mixture fractions. Finally, their surrogate was composed of n-decane (42.67%mol.), iso-octane (33.02%mol.), and toluene (24.31%mol.). They measured mole fraction profiles in a flow reactor and ignition delays in a shock tube and a rapid compression machine at high pressures, and strained extinction limit of diffusion flames for both their surrogate and a Jet A fuel. It was found that such a surrogate was able to closely emulate the global combustion parameters of the Jet A fuel chosen in the study (POSF 4658), as well as the chemical kinetic related behavior, even though they admitted that the present surrogate did not exactly match all of their goals. More recent works have addressed the combustion of alternative jet fuels, for instance through Alfa-Bird (Alternative Fuels and Biofuels for Aircraft Development), a European Union funded research project testing biofuels and alternative fuels as a means of ensuring the long-term viability of the international air transportation industry. Mzé-Ahmed et al [75] studied the oxidation of a coal-to-liquid Fischer-Tropsch synthetic jet fuel and compared it to a quaternary mixture made of n-decane (47.2%mol.), iso-octane (15.5%mol.), n-propylcyclohexane (42.2%mol.) and n-propylbenzene (12.2%mol.). They concluded that the surrogate represented the oxidation of the synthetic jet fuel reasonably well, but that it required more realistic alkanes and naphthenes to be involved. This conclusion was emphasized by Dagaut et al [76] studying the oxidation of gas-to-liquid Fischer-Tropsch synthetic jet fuel. As compared to the GtL, the surrogate (65.2%mol. n-decane, 37.5%mol. iso-octane and 10.3%mol. n-propylcyclohexane) was shown to have a similar reactivity but some species (iso-butene) were largely over-estimated, indicating that iso-octane might not be a good representative compound of the iso-alkane family. In the most recent works [77], a fraction of iso-octane has been replaced by a mixture of 2-methylheptane and 3-methylheptane, in order to better match the combustion behavior of the iso-alkane family. Also, decalin and tetralin have been introduced into the composition of the surrogate in addition to n-propylcyclohexane and n-propylbenzene, in order to achieve a more realistic representation of the naphthene and aromatic families. This flexible detailed kinetic mechanism was able to successfully reproduce the oxidation of a GtL and a CtL under high pressure and from fuel-lean to fuel-rich conditions. The interest of such a flex-fuel kinetic mechanism is that it can be reduced on purpose (for one typical fuel, under few thermodynamic conditions) to match CFD requirements.

Turbulent combustion models

Chemistry reduction

An accurate prediction of the temperature evolution and the species formation across a flame requires a reliable description of chemical mechanisms. Detailed schemes correspond to an exhaustive list of all possible elementary reactions between a given fuel and an oxidizer. However, as explained in Section 4, detailed kerosene/air reaction schemes involve hundreds of species and thousands of elementary reactions. Despite the continuous increase in computational power, detailed chemistry flame computations remain prohibitive for practical aeronautical combustors. In practice, detailed chemistry computations are mainly applied to 1-D laminar kerosene-air flames [78] and 3-D DNS of turbulent flame, but limited to small domain size and Reynolds number, and to light hydrocarbons [79].

Identification of a skeletal mechanism

For this purpose, methods have been developed to reduce the chemistry. The first reduction step is the identification of a skeletal mechanism where, for a given range of parameters, unimportant reactions and species are suppressed. Methods for the systematic reduction of mechanisms to a skeletal level have been proposed in [80, 81, 82, 83]. The resulting skeletal mechanisms are still in general too large to be included in 3-D reactive flow simulations. A second reduction step is therefore needed for practical simulations.

Popular procedures to systematically reduce mechanism are the Quasi Steady-State approximation (QSSA) and/or the Partial Equilibrium approximation (PEA). QSSA assumes that the rates of production and destruction of a selection of species are much greater than their net rate of formation. This yields algebraic relations for production rates of these species among the elementary rates. The PEA assumes that the rates of some reactions are so high that partial equilibrium is established, also giving rise to algebraic relations between the elementary reaction rates. An extensive description of these methods, together with the mathematical framework and illustrations with practical examples, is given in the review article [84].

One of the first attempts to reduce detailed schemes within the context of kerosene chemistry was performed by Luche et al [85]. From a detailed mechanism comprising 225 species and 3493 irreversible reactions proposed previously, the authors first obtained a skeletal mechanism including 134 species and 2132 reactions by using atomic flux analysis. This skeletal mechanism was further reduced to 1220 reactions by removing redundant reactions with the principal component analysis method. A last step was applied using the quasi-steady-state approximation for species with a short lifetime, and two reduced schemes including 33 and 40 species were finally obtained. These reduced mechanisms offered a good compromise between predictive qualities and computation time. Another example of a reduced mechanism is given in [86]. The skeletal JetSurF 1.0-l1 mechanism [87][1], including 123 species and 977 reactions has been systematically reduced using a directed relation graph (DRG), DRG-aided sensitivity analysis, and linearized quasi steady state (QSS) approximations, leading to an analytical 24-species mechanism for n-dodecane.

Empirically-reduced mechanisms

An alternative to describe combustion chemistry is the use of empirically reduced mechanisms. These ad hoc models composed of one to four steps are built to reproduce global flame properties, such as the laminar flame speed, the burnt gas composition or the auto-ignition

[1]JetSurF 1.0-l1 is already a simplified version of JetSurf 1.0 [88]

times. Reaction rates are determined by tuning, guessing and trial and error. Pioneering work is due to Westbrook and Dryer [89], who proposed one and two-step global reactions with Arrhenius kinetics by tuning the pre-exponential factor, the activation energy and the reaction order. More recently, the applicability of one-step irreversible Arrhenius kinetics with unity reaction order to the description of partially-premixed methane-air combustion has been investigated in [90]. For more complex hydrocarbons, a simple technique has been proposed [91, 92] to derive one-step and two-step schemes for kerosene-air flames. In order to fit the laminar burning velocity over a wide range of operating conditions, the pre-exponential constants of the two reactions are tabulated as a function of the local equivalence ratio. The fuel and oxidizer exponents are adjusted to reproduce the dependence of premixed laminar burning velocity on mean pressure. However, the optimization of these mechanisms remains limited by the thermochemical properties of the species involved, which remain unchanged. A solution to overcome this issue is to develop virtual schemes involving virtual species and reactions [93]. The use of virtual species, whose thermodynamic properties are optimized, improves the domain of validity of global step mechanisms.

Tabulated chemistry methods

An alternative to address fluid/chemistry interactions at a reduced computational cost consists in tabulating the chemistry. A chemical look-up table is generated prior to a CFD simulation, in which main thermo-chemical ingredients are stored as a function of a reduced set of variables. Some techniques to construct the chemical look-up table, such as the Intrinsic Low Dimensional Manifold (ILDM) developed by Maas and Pope [94], are based on a mathematical reduction of the chemical system dynamics. However, a large number of coordinates, around four or five, are required when hydrocarbons fuels are considered. Alternatives to ILDM that require less dimensions are Flame Prolongation of ILDM (FPI) [95, 96] or Flamelet Generated Manifold (FGM) [97]. Both techniques assume that the chemical flame structure can be described by a reduced phase subspace from elementary combustion configurations. For instance, the chemical subspace covered by partially-premixed flames can be approximated from a collection of 1-D laminar flames [98].

The suitability of tabulated chemistry for kerosene combustion has been recently investigated by simulating 1-D laminar spray counterflow flames [99]. Figure 4 shows a comparison between detailed and tabulated chemistry simulations. Both methodologies use the same skeletal mechanism developed by Luche [85], so only assumptions relative to chemistry tabulation are challenged. The temperature profile is well reproduced by the tabulated chemistry method, but small discrepancies are observed in the CO prediction. These errors are due to the fact that a single flame archetype (premixed flamelets) is used to build the chemical look-up table, whereas the structure of the spray counterflow flame is more complex. This assumption, valid to capture the temperature, is too crude to capture complex chemical phenomena, such as the pollutant formation.

This result illustrates the limitation of tabulated chemistry methods, which assume that a turbulent flame is composed of a set of laminar flame elements. The identification of the combustion elements representative of the overall turbulent chemical flame structure is not always obvious. The use of a single flamelet archetype is efficient to capture the chemical structure of well-identified flames (such as purely premixed flames or diffusion flames), but introduces bias in the prediction of the chemical structure of more complex situations such as stratified flames [98]. In order to capture the complex flame structures that develop in the reactive flow, more coordinates have to be added to the look-up table. In order to track multiple flamelet regimes within a single look-up table, Bykov and Maas [100] and Nguyen et al [101] proposed to solve the projection of the full set of species balance equations in a restricted subset of the composition space. Another solution, suggested recently by Franzelli et al [78], is to combine partially-premixed flamelets to generate a chemical look-up table.

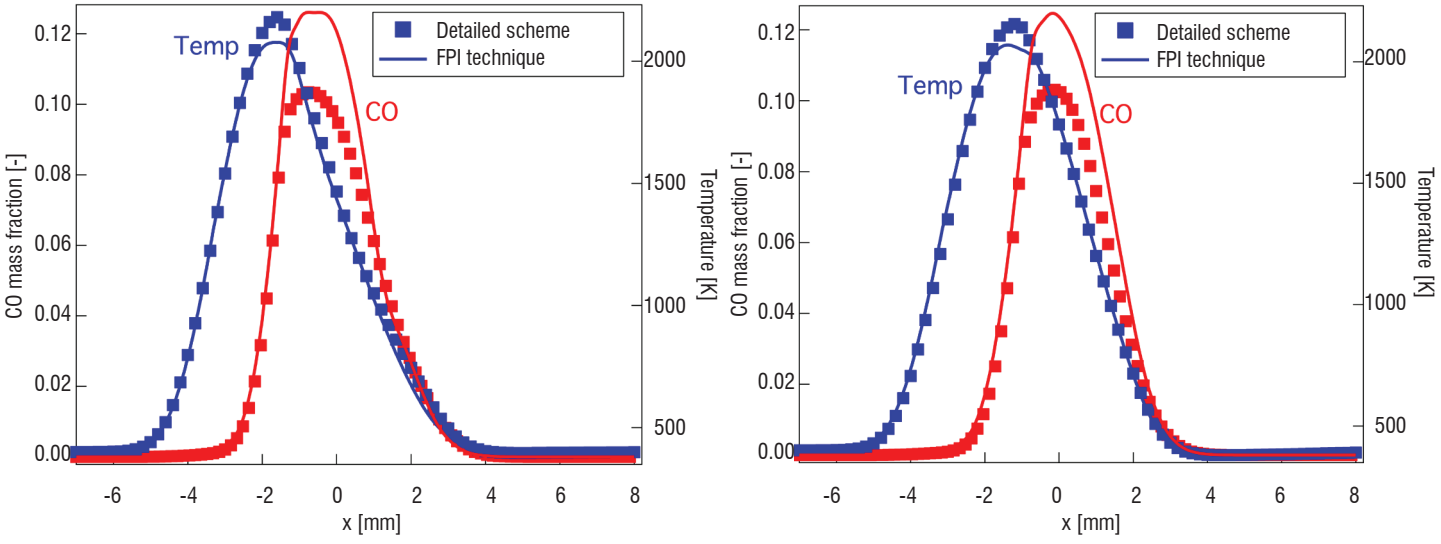

(a) 40 μm droplet diameter

(b) 100 μm droplet diameter

Figure 4 - Chemical flame structure of a 1-D laminar spray counterflow flame using a detailed chemistry (solid) and a FPI tabulated chemistry approach (symbols).

LES of turbulent combustion

Two major issues must be overcome to perform LES of turbulent combustion:

- The flame thickness is typically thinner than the grid size. Indeed, the flame reactive layer is usually about 10-100 micrometer wide, while the filter size remains above 1 millimeter [102].

- Part of the flame wrinkling induced by the turbulence is not resolved by the LES. Therefore dedicated models for flame/turbulence interactions are needed [1].

Regarding the first point, an efficient solution to solve flame propagation on a coarse grid is to artificially thicken the flame front by modifying the diffusion coefficient and the Arrhenius pre-exponential constant [103, 104]. This methodology, which is straightforward to implement in a LES solver, has been successfully applied on gas turbine combustion chambers, both within the context of global-step chemistry [105] and that of tabulated chemistry [106]. Another solution is to introduce a filter larger than the mesh size, in order to resolve the filtered flame structure. This method has been followed by Boger et al [107] and Duwig et al [108] with a single-step description of the chemistry. This strategy has been followed within the context of tabulated chemistry with the development of the F-TACLES (Filtered TAbulated Chemistry for Large Eddy Simulation) model, which was first formulated for premixed [109], then stratified adiabatic [110] and non-adiabatic combustion [?]. This modeling strategy has been applied by [111] to understand the formation of the hot regions observed at the wall surface of a helicopter combustion chamber. Another approach is to solve a scalar field, where an iso-surface is defined to represent the instantaneous flame front position. This method called "G-equation" was first applied to LES in [112]. The mathematical formalism of the G-equation has been updated for LES in the corrugated flamelet regime [113] and in the thin reaction zones regime [114]. The G-equation model has been coupled to tabulated chemistry in [115].

The second issue concerns the sub-grid flame/turbulence interaction modeling. Indeed, the turbulence of the flow generates vortices (or eddies), which wrinkle the flame front over a wide range of length scale. In practical LES computation grids, a significant part of the flame wrinkling occurs at the sub-grid scale and requires modeling [1]. Significant progress has been recently achieved with the development of dynamic sub-grid scale models [116], which have been successfully coupled with the flame filtering concept [117, 118]. They demonstrate that this combination is very efficient to predict the flame stabilization process and the temperature distribution in the combustion chamber.

Some above mentioned methods have been recently challenged in a collaborative study in which five research institutions have been involved to simulate a turbulent stratified flame (TSF) measured at the Technische Universitt Darmstadt (TUD) [119]. The groups involved in the simulations are TUD, the Institute for Combustion Technology (ITV, Aachen), Lund University (LUND), the EM2C laboratory at Ecole Centrale Paris (EM2C) and Duisburg-Essen University (UDE). All groups performed Large Eddy Simulations using Low Mach Number solvers. EM2C employed the Filtered Tabulated Chemistry for LES (F-TACLES) model [109], extended to capture the propagation of non-adiabatic flames [120]. TUD applied a premixed flamelet tabulation with local flame thickening [119]. ITV used a flamelet progress variable approach also based on premixed flamelet tabulation, but coupled with a level set approach [115]. LUND described the combustion chemistry through a 4-step mechanism combined with Implicit LES [121]. UDE used an artificially-thickened flamelet generated manifolds technique on many low cost cells.

These computational strategies differ by many aspects of numerics, turbulent combustion models and meshing. However, all modeling strategies were designed to produce the correct laminar flame speed under non-adiabatic conditions. Most simulations agree on the mean flame brush position, but it is clear that sub-grid turbulence must be considered to achieve the correct turbulent flame speed. Instantaneous snapshots of the flame, shown in Fig.5, illustrate the ability of the methods to capture the flame lift-off height. Discrepancies in the flame wrinkling resolution are caused by the different grids and numerical methods, as well as by the various LES combustion models used.

An alternative, adapted to the simulation of high Reynolds moderate Damkohler number turbulent flames [122, 123], is to use LES-EPaSR (extended Partially Stirred Reactor) and RANS-EPaSR models, which incorporate the influence of finite rate kinetics. It is assumed (similarly to the EDC model of Magnussen) that chemical reactions take place only in the fine vortex structures, characterized by high intensity

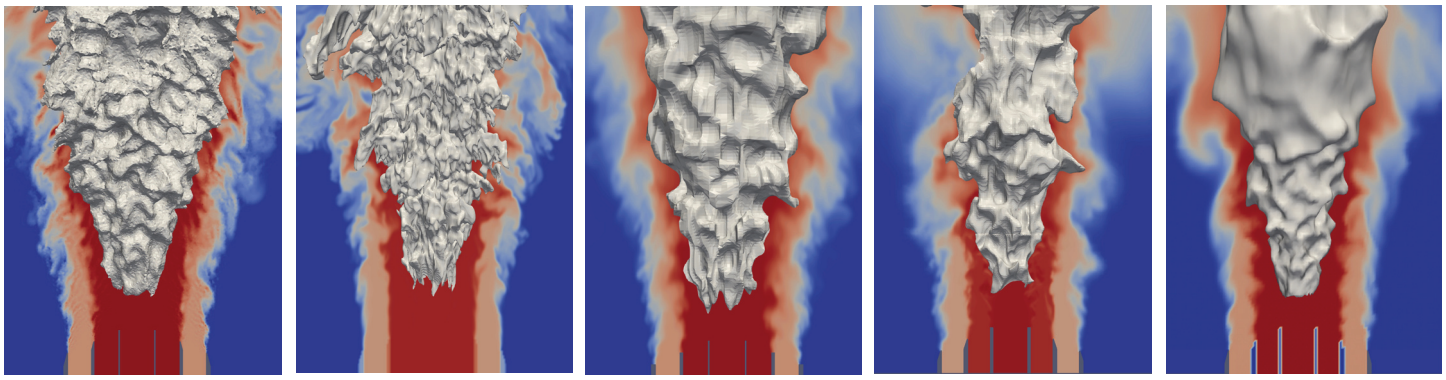

(a) EM2C (b) UDE (c) ITV (d) LUND (e) TUD

Figure 5 - Instantaneous snapshots from non-adiabatic simulations of the TSFA flame: 3-D views of 1850 K temperature iso-surface conditioned on the flame surface. 2-D field showing the mixture fraction iso-contours.

velocity gradients, molecular mixing and dissipation. Using the similarities with the mathematical treatment of multiphase flows, equations are derived for the fine-structure composition and volume fraction, which are solved together with the LES or RANS equations for the resolved scales. If convection and unsteady effects can be neglected, the EPaSR model is reduced to the PaSR model. The EPaSR model was validated against experimental data, e.g., lean premixed bluff-body stabilized flame, supersonic combustors and many other cases [122] [123] [124] [125].

Pollutant formation

Soot

Soot particles are solid fractal aggregates of small size caused by an incomplete combustion of hydrocarbons. Not only do they have a negative impact on health and the environment, but they can also cause a significant loss of efficiency of aeronautical combustors due to soot radiation, deposits and wall deterioration. Soot production is the result of complex processes of both formation and destruction, including the generation of first nuclei from gaseous precursors (the polycyclic aromatic hydrocarbons - PAHs), gas-solid and solid-solid collisional processes (condensation and coagulation, respectively) and chemical reactions at the soot particle surface (surface growth and oxidation) [126]. Therefore, soot production depends on the fuel used, the mixture quality, the operating point and the combustion mode. It is generally characterized by the soot volume fraction and the particle number density, giving access to a mean soot particle diameter. However, the particle size distribution (PSD) provides a better description of soot emission, although it requires more sophisticated experimental diagnostics and detailed numerical models to be analyzed and/or predicted.

Today, using numerical simulations to predict soot production in aeronautical combustors is extremely challenging for different reasons:

- Complexity of the physical process: due to the complex nature of soot production, detailed models are required to describe both the gaseous and the solid phases [127, 128, 129]. Such detailed models are prohibitive in real systems and simplified descriptions are required. However, the simplification procedure is not straightforward and may lead to strong inaccuracies on soot prediction.

- Multi-physics coupling: soot production strongly depends on the flame structure, the concentration of soot precursors and radicals, as well as the temperature. Acceptable discrepancies with regard to gaseous predictions lead to large errors on soot production. As an example, overestimating the precursor concentration by twice the amount leads to an overestimation by one order of magnitude of the soot volume fraction [130]. Therefore, high fidelity models are necessary for the gas phase chemistry and flame-turbulence interactions. Moreover, the presence of soot in the flame is a major source of radiative heat transfer. The non-linear coupling between soot particles and radiation must be correctly reproduced to accurately predict soot production [131], requiring the use of multi-physics coupling strategies.

- Lack of experimental databases for soot production in real combustors: this is mainly due to the difficulties in achieving measurements for both the gaseous and solid phases [132]. In academic turbulent flame configurations, Laser Induced Incandescence (LII) is the main technique used to non-intrusively measure the time-resolved soot particle volume fraction [133, 134, 135]. Combined diagnostics are increasingly being used to investigate the relation between soot, on the one hand, and flow dynamics, soot precursors and the front flame on the other hand [136, 137, 138]. High speed measurements also enable the soot-turbulence interaction [138, 139] to be characterized. Applying such diagnostics to realistic geometries is still very complex. It has recently been done for the first time at DLR by Geigle et al [140, 141, 142] in a swirled turbulent ethylene-air non-premixed flame at moderate pressure (3 and 5 atm). By combining LII, soot luminosity, OH fluorescence (PLIF) and luminosity, Particle Image Velocimetry (PIV) and Coherent Anti-Stokes Raman Spectroscopy (CARS), the DLR database offers a detailed characterization of the flow, the flame structure and the soot production for soot modeling validation.

Despite these difficulties, soot production in an aeronautical burner has been investigated using both Reynolds Averaged Navier Stokes (RANS) and Large Eddy Simulation (LES).

First attempts to predict soot production in real gas turbine combustors were based on RANS [143, 144, 145, 146, 147, 148], whose accuracy was quite limited. This approach is however not suitable for soot formation prediction because this complex phenomenon is controlled by local and history-dependent processes that cannot be modeled by RANS [135].

Since LES captures the temporal and spatial evolution of the local flow structures, it is a valid alternative. The first LES of soot production in turbulent laboratory-scale flames have proven the potential of this approach at a reasonable computational cost [149, 150, 151]. Aimed at real combustors, LES was recently performed in the DLR aero-engine model combustor [130, 152] (Fig. 6), using a semi-empirical two-equation soot model [153]. As for the gas ethylene-air chemistry, both a fully tabulated method and a hybrid method (two-step reduced

Figure 6 - LES of the DLR swirled turbulent flame [130].
Isocontour of temperature colored by the axial velocity (red-to-yellow) and soot ligaments colored by their number density (black-to-white).

chemistry for the flame-tabulated chemistry for the soot precursors) [154] were evaluated. Comparisons with experiments showed correct agreement in terms of soot position, but large differences in terms of soot levels in the combustion chamber. The sensitivity of the soot volume fraction to the gas chemical description was analyzed [130, 152].

As for real aeronautical burners, the first LES computation was proposed by Mueller and Pitsch [155], based on a tabulated chemical description for the gaseous phase and on a method of moments for the solid phase characterization. Radiation was accounted for via a simple optically thin approach. Lecocq et al [154] proposed the first LES of soot production in a real helicopter combustion chamber coupled with a thermal radiation solver. This simulation, based on an hybrid model for the gas and on a semi-empirical two-equation soot description, enabled the effect of soot radiation on the prediction of the soot volume fraction and the soot number density to be studied. Due to the unavailability of experimental results, it is not possible to make any statement regarding the accuracy of these calculations.

Despite the feasibility of LES for soot production modeling, the models both for the gas and the solid phases must be largely improved and their validation must be extended to measurements in real aero-engines. Some of the most relevant improvement pathways are suggested in the following. The list is however not exhaustive, due to the multi-physics complexity of the problem:

- Gaseous phase description and its coupling with soot: a correct description of the gaseous phase, i.e., temperature, PAH and intermediate species such as OH, is essential to predict the chemical soot production processes. Detailed chemistries are not affordable in LES of complex burners, requiring reduction procedures to account for large PAHs, strain rate effects on soot precursors and soot feedback on the gaseous phase. Tabulated methods and hybrid techniques are promising ways to be explored [154, 156, 157, 158, 159].

- Descriptions of soot PSD: with regard to spray flames, both Eulerian approaches (sectional models, method of moments and hybrid methods) and Lagrangian models should be preferred to semi-empirical models to describe soot particle population (see § " Spray description "). Among them, the method of moments, which offers a good comprise between computational cost and accuracy, is the only PSD model that has already been applied in a LES of a aero-engine combustor. This strategy has been widely developed for soot prediction [160, 161], enabling a possible extension to a bi-variate volume-surface description that can account for the fractal nature of soot. The capability of the other techniques to reproduce PSD evolution in real applications is still to be shown.

- Soot-turbulence interaction: soot production in turbulent flames is characterized by the presence of small pockets or ligaments [138, 162]. Such structures cannot be resolved on the grid accessible today in numerical simulations of realistic applications. Suitable sub-grid models accounting for turbulence effects on soot [163] are required in order to correctly reproduce the spatial evolution of soot, as well as its intermittency.

- Accounting for detailed soot radiative properties: soot radiation may contribute greatly to the total heat flux of a combustor chamber, consequently affecting the flow temperature field and soot production causing a non-linear feedback. A detailed description of soot radiative properties, based for example on particle morphology or composition [164], should be accounted for and coupled with the flow solver.

- Extension to realistic conditions: most of the modeling developments, as well as the experimental measurements, are focused on simple fuels, such as ethylene or methane, or are for simpler operating conditions (low pressure for example). The DLR experimental database, for example, concerns ethylene flames up to 5 atm. Research activities under realistic conditions for a kerosene surrogate is an active on-going topic, which should provide a better insight of soot production and lead to more accurate models.

Due to the complex nature of soot, new models must be expressly developed to reproduce the solid phase characteristics. Such developments are expected to notably improve the numerical prediction of soot production in real aero-combustors.

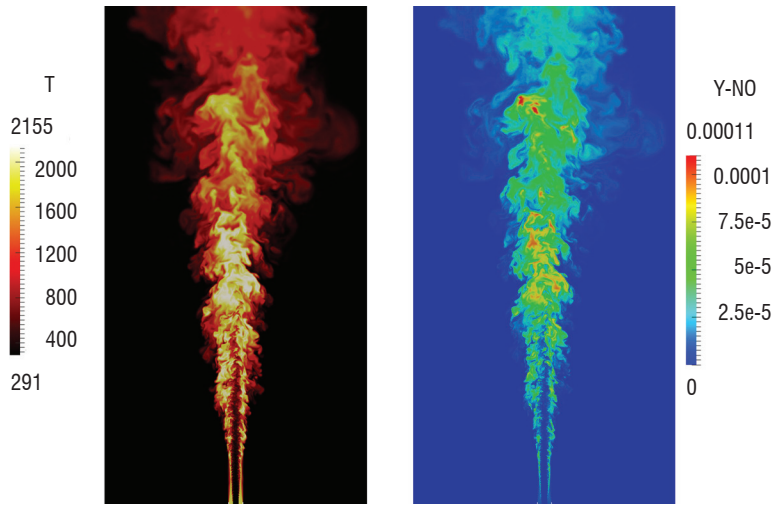

Figure 7 - Instantaneous temperature field (left) and instantaneous field of YN O (right), computed on a grid of 347 million mesh cells with a minimal resolution of 41 μm at the burner lip.

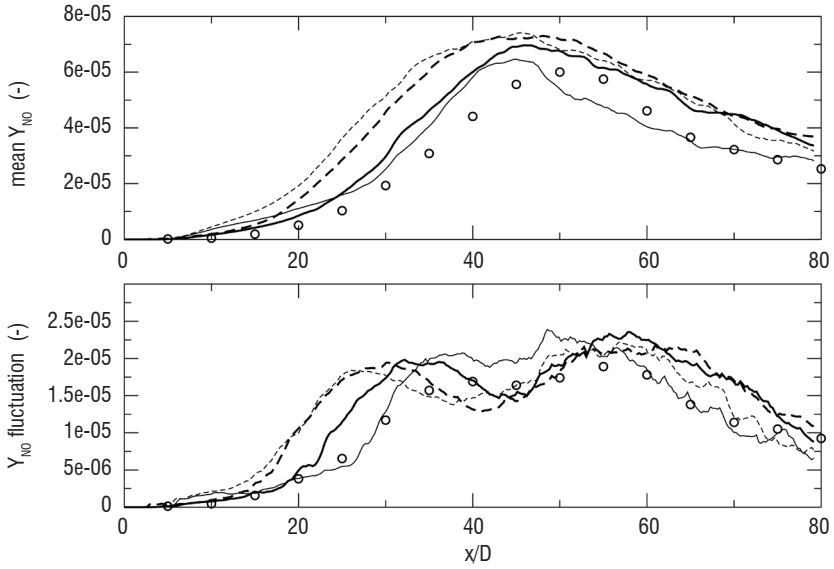

Figure 8 - Axial mean and rms NO mass fraction at the jet-fame centerline.
Symbols: experiment, Dashed lines: variable Lewis number modeling. Continuous lines: unity Lewis number modeling.
Resolution at the burner lip: 41 μm (Bold); 82 μm (Thin).

NOx

The heating of air in combustion systems produces nitric-oxides. This primary thermal source of NO features large characteristic time scales, at least much larger than the typical flow residence times of aero-engine combustion chambers [165, 166, 167]. NO levels are therefore always far from their chemical equilibrium reference state and predicting them is not an easy task. In addition, NO is also produced within the fuel oxidation thin layers, through a prompt nitric-oxide mechanism [168]. Even in a first approximation, this second mechanism cannot be neglected in accurate modeling, specifically in the fuel-rich zone of non- premixed flames in gas turbines [169, 170]. The numerical simulation of NO concentrations in this context has been the subject of multiple studies in both RANS and LES [171].

One of the major challenges in NO prediction is thus the large range of time scales that must be accounted for in the modeling, from fast fuel-oxidation, controlling the prompt mechanism, up to the slow thermal NO mechanism. Recently, an innovative approach called NOMANI (Nitrogen Oxide emission model with one-dimensional MANIfold) was dis- cussed [172], which includes the slow and fast chemical processes and which is well adapted to aeronautical engines, in which air is added downstream from the main combustion zone, in order to dilute the combustion products. In order ensure a precise estimation of the NO concentration in the flame front, as well as in the burnt gases, two progress variables are introduced in NOMANI. The first progress variable is derived from major carbon species, to monitor fuel oxidation. The second progress variable is based on the NO mass fraction and through variations in equivalence ratio, the NOMANI formalism provides a framework to account for secondary air-dilution. NOMANI is based on an a priori tabulation of the NO chemical sources and the effects of fluctuations unresolved by the mesh are accounted for using the PCM-FPI approach [173, 174].

NOMANI has been implemented in the flow solver YALES2 [175] and the SANDIA flame-D [176] was simulated to validate the NO prediction (see Figures 7 and 8). Since its preliminary validation on laboratory jet flames, NOMANI has been adopted by SAFRAN for NO prediction in the design loop of combustion chambers.

Conclusions

This article presented the modeling challenges encountered when performing LES of aeronautical combustion chambers. Issues relative to primary atomization, spray description, kerosene chemistry, combustion modeling and pollutant formation have been described. For each topic, we have given the current state-of-the-art within the context of Large Eddy Simulation. Several illustrative examples, representative of practical situations encountered in gas turbines, have been proposed. Future challenges are the fully coupled simulation, covering the interactions between all phenomena and all time and length scales involved, from the primary atomization at the fuel nozzle to the pollutant emitted at the exit of the combustion chamber ■

References

[1] T. POINSOT and D. VEYNANTE - *Theoretical and Numerical Combustion*. Third Edition. T. Poinsot, 2011.

[2] M. BOILEAU, G. STAFFELBACH, B. CUENOT, T. POINSOT, C. BERAT - *LES of an Ignition Sequence in a Gas Turbine Engine.* Combust. Flame, 154(1-2):2 – 22, 2008.

[3] A. H. LEFEBVRE - *Atomization and Sprays.* Combustion : An International Series. Taylor & Francis, Bristol, 1989.

[4] R. P. FEDKIW, T. ASLAM, B. MERRIMAN, and S. OSHER - *A Non-oscillatory Eulerian Approach to Interfaces in Multimaterial Flows (the Ghost Fluid Method).* J. Comput. Phys., 152(2):457–492, 1999.

[5] S. OSHER and J. A. SETHIAN - *Fronts Propagating with Curvature-Dependent Speed: Algorithms Based on Hamilton*-Jacobi formulations. J. Comput. Phys., 79(1):12–49, November 1988.

[6] C.W. HIRT and B.D. NICHOLS - *Volume of Fluid (vof) Method for the Dynamics of Free Boundaries.* Journal of Computational Physics, 39(1):201 – 225, 1981.

[7] T. MENARD, S. TANGUY, and A. BERLEMONT - *Coupling Level Set/Vof/Ghost Fluid Methods: Validation and Application to 3D Simulation of the Primary Break-up of a Liquid Jet.* International Journal of Multiphase Flow, 33(5):510 – 524, 2007.

[8] O. DESJARDINS, V. MOUREAU, and H. PITSCH - *An Accurate Conservative Level Set/Ghost Fluid Method for Simulating Turbulent Atomization.* J. Comp. Physics, 227(18):8395–8416, 2008.

[9] S. GROUT, C. DUMOUCHEL, J. COUSIN, and H. NUGLISCH - *Fractal Analysis of Atomizing Liquid Flows.* International Journal of Multiphase Flow, 33(9):1023 – 1044, 2007.

[10] M. J. BERGER and P. COLELLA - *Local Adaptive Mesh Refinement for Shock Hydrodynamics.* Journal of Computational Physics, 1989.

[11] F. A. WILLIAMS - *Spray Combustion and Atomization.* Phys. Fluids, 1:541–545, 1958.

[12] G. A. BIRD - *Molecular Gas Dynamics and the Direct Simulation of Gas Flows*. Oxford Science Publications, 42, 1994.

[13] J.K. DUKOWICZ - *A Particle-Fluid Numerical Model for Liquid Sprays.* Journal of Computational Physics, 35:229–253, 1980.

[14] J.P. MINIER - *On the Lagrangian Stochastic Methods for Turbulent Polydisperse two-Phase Reactive Flows.* Progress in Energy and Combustion Science, 50:1–62, 2015.

[15] J.P. MINIER and C. PROFETA - *Kinetic and Dynamic Probability-Density-Function Descriptions of Disperse Turbulent two-Phase Flows.* Physical Review E, 92(053020), 2015.

[16] M. BINI and W.P. JONES - *Large-Eddy Simulation of Particle-Laden Turbulent Flows.* Journal of Fluid Mechanics, 614:207–252, 2008.

[17] D. PAULHIAC - *Modélisation de la combustion d'un spray dans un brûleur aéronautique.* PhD thesis, INP Toulouse, 2015.

[18] L. GUEDOT - *Développement de méthodes numériques pour la caractérisation des grandes structures tourbillonaires dans les brûleurs aéronautiques.* Application aux systèmes d'injection multi-points. PhD thesis, INSA Rouen, 2015.

[19] J. CAPECELATRO and O. DESJARDINS - *An Euler–Lagrange Strategy for Simulating Particle-Laden Flows.* Journal of Computational Physics, 238:1 – 31, 2013.

[20] R. ZAMANSKY, F. COLETTI, M. MASSOT, and A. MANI - Radiation Induces Turbulence in Particle-Laden Fluids. Physics of Fluids, 26(7):1–7, 2014.

[21] S. V. APTE, K. MAHESH, P. MOIN, and J. C. OEFELEIN - *Large-Eddy Simulation of Swirling Particle-Laden Flows in a Coaxial-Jet Combustor.* Int. J. Multiphase Flow, 29:1311–1331, 2003.

[22] M. GOROKHOVSKI and R. ZAMANSKY - *Lagrangian Simulation of Large and Small Inertial Particles in a High Reynolds Number Flow: Stochastic Simulation of Sub-Grid Turbulence/Particle Interactions.* Center of Turbulence Research - Proceedings of the summer program, pages 37–46, 2014.

[23] W.P. JONES, S. LYRA, and S. NAVARRO-MARTINEZ - *Numerical Investigation of Swirling Kerosene Spray Flames Using Large Eddy Simulation.* Combustion and Flame, 159(4):1539 – 1561, 2012.

[24] W.P. JONES, A.J. MARQUIS, and K. VOGIATZAKI - *Large-Eddy Simulation of Spray Combustion in a Gas Turbine Combustor.* Combustion and Flame, 161(1):222 – 239, 2014.

[25] G. HANNEBIQUE - *Etude de la structure des flammes diphasiques dans les brûleurs aéronautiques.* PhD thesis, Université de Toulouse, 2013.

[26] A. VIÉ, S. JAY, B. CUENOT, and M. MASSOT - *Accounting for Polydispersion in the Eulerian Large Eddy Simulation of an Aeronautical-type Configuration*. Flow Turbulence and Combustion, 90(3):545–581, 2013.

[27] A. RENAUD - *Etude de la stabilisation des flammes et des comportements transitoires dans un brûleur étagé à combustible liquide à l'aide de diagnostics rapides*. PhD thesis, CentraleSupelec, 2015.

[28] F. LAURENT and M. MASSOT - *Multi-Fluid Modeling of Laminar Poly-Dispersed Spray Flames: Origin, Assumptions and Comparison of the Sectional and Sampling Methods.* Combust. Combustion Theory and Modelling, 5:537–572, 2001.

[29] D. L. MARCHISIO and R. O. FOX - *Solution of Population Balance Equations Using the Direct Quadrature Method of Moments.* Journal of Aerosol Science, 36:43–73, 2005.

[30] A. VIÉ, F. LAURENT, and M. MASSOT - *Size-Velocity Correlations in Hybrid High Order Moment/Multi-Fluid Methods for Polydisperse Evaporating Sprays: Modeling and Numerical Issues.* Journal of Computational Physics, 237:177–210, 2013.

[31] C YUAN, F. LAURENT, and R. O. FOX - *An Extended Quadrature Method of Moments for Population Balance Equations.* J. Comp. Phys., 51:1–23, 2012.

[32.1] F. DOISNEAU, F. LAURENT, A. MURRONE, J. DUPAYS, M. MASSOT - *Eulerian Multi-Fluid Models for the Simulation of Dynamics and Coalescence of Particles in Solid Propellant Combustion*. Journal of Computational Physics, 234 (2013) 230-262.

[32.2] A. SIBRA, J. DUPAYS, A. MURRONE, F. LAURENT, M. MASSOT - *Simulation of Reactive Polydisperse Sprays Strongly Coupled to Unsteady Flows in Solid Rocket Motors: Efficient Strategy Using Eulerian Multi-Fluid Methods*. submitted to Journal of Computational Physics (2015) 1-41
https://hal.archives-ouvertes.fr/hal-01063816

[32.3] F. LAURENT, A. SIBRA, and F. DOISNEAU - *Two-Size Moment Multi-Fluid Model: a Robust and High-Fidelity Description of Polydisperse Moderately Dense Evaporating Sprays*. Communications in Computational Physics, to appear, p. 1-41, 2016 - https://hal.archives-ouvertes.fr/hal-01169730

[33] D. KAH, O. EMRE, Q.H. TRAN, S. de CHAISEMARTIN, S. JAY, F. LAURENT, and M. MASSOT - *High Order Moment Method for Polydisperse Evaporating Sprays with Mesh Movement: Application to Internal Combustion Engines.* International Journal of Multiphase Flow, 71:38 – 65, 2015.

[34] N. GARCIA-ROSA - *Phénomènes d'allumage d'un foyer de turbomachine en conditions de haute altitude.* PhD thesis, Université Toulouse III, 2008.

[35] J. DOMBARD - *Direct Numerical Simulation of Non-Isothermal Dilute Sprays Using the Mesoscopic Eulerian Formalism*. PhD thesis, Institut National Polytechnique de Toulouse, 2011.

[36] O. COLIN and M. RUDGYARD - *Development of High-Order Taylor–Galerkin Schemes for LES*. J. Comp.Physics, 162:338–371, 2000.

[37] N. LAMARQUE - *Schémas numériques et conditions limites pour la simulation aux grandes échelles de la combustion diphasique dans les foyers d'hélicoptère*. PhD thesis, Institut National Polytechnique de Toulouse, 2007.

[38] L. MARTINEZ - *Simulation aux grandes échelles de l'injection de carburant liquide dans les moteurs à combustion interne*. PhD thesis, Institut National Polytechnique de Toulouse, 2010.

[39] J. DOMBARD - *Direct Numerical Simulation of Non-Isothermal Dilute Sprays Using the Mesoscopic Eulerian Formalism*. PhD thesis, INP Toulouse, 2011.

[40] C. LE TOUZE, A. MURRONE, and H. GUILLARD - *Multislope MUSCL Method for General Unstructured Meshes*. Journal of Computational Physics, 284:389–418, 2015.

[41] M. SABAT, A. LARAT, A. VIÉ, and M. MASSOT - *On the Development of High Order Realizable Schemes for the Eulerian Simulation of Disperse Phase Flows: a Convex-State Preserving Discontinuous Galerkin Method*. Journal of Computational Multiphase Flows, 6(3):247–270, 2014.

[42] X. ZHANG and C.-W. SHU - *Positivity-Preserving High Order Discontinuous Galerkin Schemes for Compressible Euler Equations with Source Terms*. J. Comput. Phys., 230(4):1238–1248, February 2011.

[43] E. MASI, O. SIMONIN, E. RIBER, P. SIERRA, and L.Y.M. GICQUEL - *Development of an Algebraic-Closure- Based Moment Method for Unsteady Eulerian Simulations of Particle-Laden Turbulent Flows in very Dilute Regime*. International Journal of Multiphase Flow, 58:257–278, 2014.

[44] E. MASI and O. SIMONIN - *Algebraic-Closure-Based Moment Method for Unsteady Eulerian Simulations of Non-Isothermal Particle-Laden Turbulent Flows at Moderate Stokes Numbers in Dilute Regime*. Flow Turbulence and Combustion, 92(1-2):121–145, 2014.

[45] E. RIBER, V. MOUREAU, M. GARCIÀ, T. POINSOT, and O. SIMONIN - *Evaluation of Numerical Strategies for Large Eddy Simulation of Particulate Two-Phase Recirculating Flows*. Journal of Computational Physics, 228(2):539–564, 2009.

[46] M. SANJOSÉ, J.-M. SENONER, F. JAEGLE, B. CUENOT, S. MOREAU, and T. POINSOT - *Fuel Injection Model for Euler-Euler and Euler-Lagrange Large-Eddy Simulations of an Evaporating Spray Inside an Aeronautical Combustor*. International Journal of Multiphase Flow, 37(5):514 – 529, 2011.

[47] F. LAURENT, A. VIÉ, C. CHALONS, R. O. FOX, and M. MASSOT - *A Hierarchy of Eulerian Models for Trajectory Crossing in Particle-Laden Turbulent Flows Over a Wide Range of Stokes Numbers*. Annual Research Briefs of the CTR 2012, Center for Turbulence Research, Stanford University, pages 193–204, 2012.

[48] A. VIÉ, E. MASI, O. SIMONIN, and M. MASSOT - *On the Direct Numerical Simulation of Moderate- Stokes-Number Turbulent Particulate Flows Using Algebraic-Closure-Based and Kinetic-Based Moment Methods*. In Proceedings of the Summer Program 2012, Center for Turbulence Research, Stanford University, pages 355–364, 2012.

[49] A. VIÉ, F. DOISNEAU, and M. MASSOT - *On the Anisotropic Gaussian Closure for the Prediction of Inertial-Particle Laden Flows*. Communications in Computational Physics, 17(1):1–46, 2015.

[50] R.O. FOX - *On Multiphase Turbulence Models for Collisional Fluid-Particle Flows*. Journal of Fluid Mechanics, 742:356–424, 2014.

[51] O. EMRE, R. O. FOX, M. MASSOT, S. DE CHAISEMARTIN, S. JAY, and F. LAURENT - *Eulerian Modeling of a Polydisperse Evaporating Spray under Realistic Internal-Combustion-Engine Conditions*. Flow Turbulence and Combustion, 93(4):689–722, 2014.

[52] L. SCHILLER and A. NAUMANN - *A Drag Coefficient Correlation*. V.D.I Zeitung, 77:318–320, 1935.

[53] G.G. STOKES - *On the Effect of the Inertial Friction of Fluids on the Motions of Pendulums*. Trans.Cambridge Phil. Soc., 9, 1851.

[54] J. HORWITZ and A. MANI - *Accurate Calculation of Stokes Drag for Point-Particle Tracking in Two-Way Coupled Flows*. Submitted to Journal of Computational Physics, 2015. http://arxiv.org/abs/1509.07542.

[55] S.S. SAZHIN - *Advanced Models of Fuel Droplet Heating and Evaporation*. Progress in Energy and Combustion Sciences, 32:162–214, 2006.

[56] P. SIERRA - *Modeling the Dispersion and Evaporation of Sprays in Aeronautical Combustion Chambers*. PhD thesis, INP Toulouse, 2012.

[57] V. EBRAHIMIAN and C. HABCHI - *Towards Predictive Evaporation Model for Multi-Component Hydrocarbon Droplets at all Pressure Conditions*. Int. J. Heat Mass Transfer, 54:3552–3565, 2011.

[58] E. K. SHASHANK, E. KNUDSEN, and H. PITSCH - *Spray Evaporation Model Sensitivities*. Annual Research Briefs of the CTR 2011, Center for Turbulence Research, Stanford University, pages 213–224, 2011.

[59] G. L. HUBBARD, V. E. DENNY, and A. F. MILLS - *Droplet Evaporation: Effects of Transients and Variable Properties*. Int. J. Heat Mass Transfer, 18:1003–1008, 1975.

[60] C. CHAUVEAU, F. HALTER, A. LALONDE, and I. GOKALP - *An experimental Study on the Droplet Vaporization: Effects of Heat Conduction through the Support Fiber*. In ILASS, Como Lake, Italy, 2008.

[61] J.M. SENONER - *Simulation aux Grandes Échelles de l'écoulement diphasique dans un brûleur aéronautique par une approche Euler-Lagrange*. PhD thesis, Université de Toulouse, 2010.

[62] C. CHRYSSAKIS and D.N. ASSANIS - *Development and Validation of a Comprehensive CFD Model of Diesel Spray Atomization Accounting for High Weber Numbers*. SAE PAPER 2006-01-1546, pages 1–15, 2006.

[63] G. CHAUSSONET - *Modeling of Liquid Film and Breakup Phenomena in Large-Eddy Simulations of Aero- Engines Fueled by Airblast Atomizers*. PhD thesis, INP Toulouse, 2014.

[64] G. CHAUSSONET, O. VERMOREL, E. RIBER, and B. CUENOT - *A New Phenomenological Model to Predict Drop Size Distribution in Large-Eddy Simulations of Airblast Atomizers*. International Journal of Multiphase Flow (accepted), 80:29–42, 2015.

[65] L. MARTINEZ, A. BENKENIDA, and B. CUENOT - *A Model for the Injection Boundary Conditions in the Context of 3D Simulation of Diesel Spray: Methodology and Validation*. Fuel, 89(1):219–228, 2010.

[66] M. SANJOSÉ, J.M. SENONER, F. JAEGLE, B. CUENOT, S. MOREAU, and T. POINSOT - *Fuel Injection Model for Euler-Euler and Euler-Lagrange Large-eddy Simulations of an Evaporating Spray Inside an Aeronautical Combustor*. International Journal of Multiphase Flow, 37(5):514 – 529, 2011.

[67] J. REVEILLON, J. CHESNEL, B. DURET, and F. X. DEMOULIN - *Towards Fully Coupled Modeling of Liquid Atomization and Dispersed Spray Combustion*. In 1st ERCOFTAC Conference on Simulation of multiphase flows in gasification and combustion, 2013.

[68] D. ZUZIO, J.-L. ESTIVALEZES, P. VILLEDIEU, and G. BLANCHARD - *Numerical Simulation of Primary and Secondary Atomization*. Comptes Rendus Mécanique, 341(1–2):15 – 25, 2013.

[69.1] Y. LING, S. ZALESKI, and R. SCARDOVELLI - *Multiscale Simulation of Atomization with Small Droplets Represented by a Lagrangian Point-Particle Model*. International Journal of Multiphase Flow, 76:122 – 143, 2015.

[69.2] F. DRUI, A. FIKL, P. KESTENER, S. KOKH, A. LARAT, V. LE CHENADEC, M. MASSOT - *Experimenting with the p4est Library for AMR Simulatons of Two-Phase Flows*. ESAIM Proc., M. Campos Pinto and F. Charles Eds. Vol 53 (2016) 232-247

[69.3] M. ESSADKI, S. de CHAISEMARTIN, M. MASSOT, F. LAURENT, A. LARAT, S. JAY - *Adaptive Mesh Refinement and High Order Geometrical Moment Method for the Simulation of Polydisperse Evaporating Sprays*. accepted for publication in Oil & Gas Science and Technology (2016) 1-24

[69.4] M. ESSADKI, S. de CHAISEMARTIN, M. MASSOT, F. LAURENT, A. LARAT, S. Jay, *A New High Order Moment Method for Polydisperse Evaporating Sprays Dedicated to the Coupling with Separated Two-Phase Flows*. Automotive Engine, Proceedings of the 9th International Conference on Multiphase Flow (ICMF 2016) (2016) 1-8

[70] C. GUÉRET, M. CATHONNET, J. C. BOETTNER, and F. GAILLARD - *Experimental Study and Modeling of Kerosene Oxidation in a Jet-Stirred Flow Reactor*. Symposium (International) on Combustion, 23(1):211–216, 1991.

[71] P. DAGAUT, A. EL BAKALI, and A. RISTORI - *The Combustion of Kerosene: Experimental Results and Kinetic Modeling using 1- to 3-Component Surrogate Model Fuels*. Fuel, 85(7-8):944–956, 2006.

[72] P. DAGAUT and M. CATHONNET - *The Ignition, Oxidation, and Combustion of Kerosene: a Review of Experimental and Kinetic Modeling*. Progress in Energy and Combustion Science, 32(1):48–92, 2006.

[73] M. COLKET, T. EDWARDS, S. WILLIAMS, N. P. CERNANSKY, D. L. MILLER, F. EGOLFOPOULOS, P. LINDSTEDT, K. SESHADRI, F. L. DRYER, C. K. LAW, D. FRIEND, D. B. LENHERT, H. PITSCH, A. SAROFIM, M. SMOOKE, and W. TSANG - *Development of an Experimental Database and Kinetic Models for Surrogate Jet Fuels*. 45th AIAA Aerospace Sciences Meeting and Exhibit, 2007(724):1–21, 2007.

[74] S. DOOLEY, S. H. WON, M. CHAOS, J. HEYNE, Y. JU, F. L. DRYER, K. KUMAR, C. J. SUNG, H. WANG, M. A. OEHLSCHLAEGER, R. J. SANTORO, and T. A. LITZINGER - *A Jet Fuel Surrogate Formulated by Real Fuel Properties*. Combustion and Flame, 157(12):2333–2339, 2010.

[75] A. MZÉ-AHMED, P. DAGAUT, K. HADJ-ALI, G. DAYMA, T. KICK, J. HERBST, T. KATHROTIA, M. BRAUN-UNKHOFF, J. HERZLER, C. NAUMANN, and U. RIEDEL - *Oxidation of a Coal-to-Liquid Synthetic Jet Fuel: Experimental and Chemical Kinetic Modeling Study*. Energy & Fuels, 26(10):6070–6079, Oct 2012.

[76] P. DAGAUT, F. KARSENTY, G. DAYMA, P. DIÉVART, K. HADJ-ALI, A. MZÉ- AHMED, M. BRAUN-UNKHOFF, J. HERZLER, T. KATHROTIA, T. KICK, C. NAUMANN, U. RIEDEL, and L. THOMAS - *Experimental and Detailed Kinetic Model for the Oxidation of a Gas to Liquid (GtL) Jet Fuel*. Combustion and Flame, 161(3):835–847, mar 2014.

[77] P. DAGAUT, G. DAYMA, F. KARSENTY, and Z. SERINYEL - *The Combustion of Synthetic Jet Fuels (Gas to Liquid and Coal to Liquid) and Multi-Component Surrogates: Experimental and Modeling Study*. In ASME Turbo Expo, Montreal, 2015.

[78] B. FRANZELLI, B. FIORINA, and N. DARABIHA - *A Tabulated Chemistry Method for Spray Combustion*. Proc. Combust. Inst., 34:1659–1666, 2013.

[79] J. H. CHEN - *Petascale Direct Numerical Simulation of Turbulent Combustion-Fundamental Insights Towards Predictive Models*. Proceedings of the Combustion Institute, 33(1):99 – 123, 2011.

[80] B. BHATTACHARJEE, D. A. SCHWER, P. I. BARTON, and W. H. GREEN - *Optimally-Reduced Kinetic Models: Reaction Elimination in Large-Scale Kinetic Mechanisms*. Combustion and Flame, 135(3):191 – 208, 2003.

[81] T. LU and C. K. LAW - *A Directed Relation Graph Method for Mechanism Reduction*. Proc. Combust. Inst., 30:1333–1341, 2005.

[82] P. PEPIOT-DESJARDINS and H. PITSCH - *An Efficient Error-Propagation-Based Reduction Method for Large Chemical Kinetic Mechanisms*. Combustion Flame, 154(67–81), 2008.

[83] M. VALORANI, F. CRETA, F. DONATO, H. N. NAJM, and D. A. GOUSSIS - *Skeletal Mechanism Generation and Analysis for N-heptane with csp*. Proc. Combust. Inst., 31:483–490, 2007.

[84] D. A. GOUSSIS and U. MAAS - *Model Reduction for Combustion Chemistry*. In Tarek Echekki and Epaminondas Mastorakos, editors, Turbulent Combustion Modeling, volume 2011 of Fluid Mechanics and Its Applications, pages 193–220. Springer Netherlands, 2011.

[85] J. LUCHE, M. REUILLON, J.-C. BOETTNER, and M. CATHONNET - *Reduction of Large Detailed Kinetic Mechanisms: Application to Kerosene/Air Combustion*. Combustion Science and Technology, 176(11):1935– 1963, Nov. 2004.

[86] A. VIÉ, B. FRANZELLI, Y. GAO, T. LU, H. WANG, and M. IHME - *Analysis of Segregation and Bifurcation in Turbulent Spray Flames: a 3D Counterflow Configuration*. Proceedings of the Combustion Institute, 35(2):1675 – 1683, 2015.

[87] B. SIRJEAN, E. DAMES, D.A. SHEEN, and H. WANG - *Simplified Chemical Kinetic Models for High-Temperature Oxidation of C1 to C12 N-Alkanes*. 6th US National Combustion Meeting 2009, Ann, Arbor, Michigan., volume Paper 23F1, 2009.

[88] B. SIRJEAN, E. DAMES, D. A. SHEEN, X.-Q. YOU, C. SUNG, A. T. HOLLEY, F. N. EGOLFOPOULOS, H. WANG, S. S. VASU, D. F. DAVIDSON, R. K. HANSON, H. PITSCH, C. T. BOWMAN, A. KELLEY, C. K. LAW, W. TSANG, N. P. CERNANSKY, D. L. MILLER, A. VIOLI, and R. P. LINDSTEDT. *A High-Temperature Chemical Kinetic Model of n-Alkane Oxidation*.

[89] C. WESTBROOK and F. DRYER - *Simplified Reaction Mechanisms for the Oxidation of Hydrocarbon Fuels in Flames*. Combust. Sci. Technol., 27:31–43, 1981.

[90] E. FERNANDEZ-TARRAZO, A. L. SANCHEZ, A. LINAN, and F. A. WILLIAMS - *A Simple One-Step Chemistry Model for Partially Premixed Hydrocarbon Combustion*. Combust. Flame, 147(1- 2):32–38, 2006.

[91] G. BOUDIER, L.Y.M. GICQUEL, T. POINSOT, D. BISSIERES, and C. BÉRAT - *Effects of Mesh Resolution on Large Eddy Simulation of Reacting Flows in Complex Geometry Combustors*. Combustion and Flame, 155:196–214, 2008.

[92] B. FRANZELLI, E. RIBER, M. SANJOSÉ, and T. POINSOT - *A Two-Step Chemical Scheme for Kerosene–Air Premixed Flames*. Combustion and Flame, 157(7):1364 – 1373, 2010.

[93] M. CAILLER, N. DARABIHA, D. VEYNANTE, and B. FIORINA - *Building-Up Virtual Optimized Mechanism for Flame Modeling*. Submitted, 2016.

[94] U. MAAS and S. POPE - *Simplifying Chemical Kinetics: Intrinsic Low-Dimensional Manifolds in Composition Space*. Combust. Flame, 88:239–264, 1992.

[95] O. GICQUEL, D. ThÉVENIN, M. HILKA, and N. DARABIHA - *Direct Numerical Simulation of Turbulent Premixed Flames Using Intrinsic Low-Dimensional Manifolds*. Combust. Theory Modelling, 3:479–502, 1999.

[96] B. FIORINA, R. BARON, O. GICQUEL, D. ThÉVENIN, S. CARPENTIER, and N. DARABIHA - *Modelling Non- Adiabatic Partially-Premixed Flames Using Flame Prolongation of ILDM*. Combust. Theory Modelling, 7:449– 470, 2003.

[97] J. A. VAN OIJEN, F. A. LAMMERS, and L. P. H. DE GOEY - *Modelling of Complex Premixed Burner Systems by Using Flamelet-Generated Manifolds*. Combustion and Flame, 127(3):2124–2134, 2001.

[98] B. FIORINA, O. GICQUEL, L. VERVISCH, S. CARPENTIER, and N. DARABIHA - *Approximating the Chemical Structure of Partially-Premixed and Diffusion Counterflow Flames Using fpi Flamelet Tabulation*. Combustion and Flame, 140(3):147–160, 2005.

[99] B. FRANZELLI, A. VIÉ, M. BOILEAU, B. FIORINA, and N. DARABIHA - *Large Eddy Simulation of Swirled Spray Flame Using Detailed and Tabulated Chemistries*. Submitted, 2016.

[100] V. BYKOV and U. MAAS - *Combustion Theory and Modelling*, 11(6):839–862, DEC 2007.

[101] P.D. NGUYEN, L. VERVISCH, V. SUBRAMANIAN, and P. DOMINGO - *Multidimensional Flamelet-Generated Manifolds for Partially Premixed Combustion*. Combustion and Flame, 157(1):43–61, 2010.

[102] L.Y.M. GICQUEL, G. STAFFELBACH, and T. POINSOT - *Large Eddy Simulations of Gaseous Flames in Gas Turbine Combustion Chambers*. Progress in Energy and Combustion Science, 38(6):782 – 817, 2012.

[103] T.D. BUTLER and P.J. O'ROURKE - *A Numerical Method for Two-Dimensional Unsteady Reacting Flows*. Proc of the Comb. Institute, 16:1503 – 1515, 1977.

[104] O. COLIN, F. DUCROS, D. VEYNANTE, and T. POINSOT - *A Thickened Flame Model for Large Eddy Simulations of Turbulent Premixed Combustion*. Phys. Fluids A, 12(7):1843 – 1863, 2000.

[105] B. FRANZELLI, E. RIBER, L. Y.M. GICQUEL, and T. POINSOT - *Large Eddy Simulation of Combustion Instabilities in a Lean Partially Premixed Swirled Flame*. Combustion and Flame, 159(2):621 – 637, 2012.

[106] B. FRANZELLI, A. VIÉ, B. FIORINA, and N. DARABIHA - *Large Eddy Simulation of Swirling Kerosene/Air Spray Flame Using Tabulated Chemistry*. Proceedings of the Asme Turbo Expo: Turbine Technical Conference and Exposition, 2013, VOL 1A. Int Gas Turbine Inst, 2013. ASME Turbo Expo: Turbine Technical Conference and Exposition, San Antonio, TX, JUN 03-07, 2013.

[107] M. BOGER, D. VEYNANTE, H. BOUGHANEM, and A. TROUVÉ - *Direct Numerical Simulation Analysis of Flame Surface Density Concept for Large Eddy Simulation of Turbulent Premixed Combustion*. Twenty- Seventh Symposium (Int.) on Combustion. The Combustion Institute: Pittsburgh, Penn., pages 917 – 925, 1998.

[108] C. DUWIG - *Study of a Filtered Flamelet Formulation for Large Eddy Simulation of Premixed Turbulent Flames*. Flow, Turbulence and Combustion, 79(4):433–454, 2007.

[109] B. FIORINA, R. VICQUELIN, P. AUZILLON, N. DARABIHA, O. GICQUEL, and D. VEYNANTE - *A Filtered Tabulated Chemistry Model for LES of Premixed Combustion*. Combust. Flame, 157:465–475, 2010.

[110] P. AUZILLON, O. GICQUEL, N. DARABIHA, D. VEYNANTE, and B. FIORINA - *A Filtered Tabulated Chemistry Model for LES of Stratified Flames*. Combustion and Flame, 159(8):2704–2717, 8 2012.

[111] P. AUZILLON, E. RIBER, L. Y.M. GICQUEL, O. GICQUEL, N. DARABIHA, D. VEYNANTE, and B. FIORINA - *Numerical Investigation of a Helicopter Combustion Chamber Using LES and Tabulated Chemistry*. Comptes Rendus Mécanique, 341(1–2):257 – 265, 2013. Combustion, spray and flow dynamics for aerospace propulsion.

[112] S. MENON and W.H. JOU - *Large Eddy Simulations of Combustion Instability in an Axisymmetric Ramjet Combustor*. Combust. Sci. Technol., 75:53–72, 1991.

[113] H. PITSCH - *A Consistent Level Set Formulation for Large-Eddy Simulation of Premixed Turbulent Combustion*. Combust. Flame, 143(4):587–598, 2005.

[114] V. MOUREAU, B. FIORINA, and H. PITSCH - *A Level Set Formulation for Premixed Combustion Les Considering the Turbulent Flame Structure*. Combustion and Flame, 156(4):801–812, 2009.

[115] P. TRISJONO, K. KLEINHEINZ, H. PITSCH, and S. KANG - *Large Eddy Simulation of Stratified and Sheared Flames of a Premixed Turbulent Stratified Flame Burner Using a Flamelet Model with Heat Loss*. Flow, Turbulence and Combustion, 92(1-2):201–235, 2014.

[116] G. WANG, M. BOILEAU, and D. VEYNANTE - *Implementation of a Dynamic Thickened Flame Model for Large Eddy Simulations of Turbulent Premixed Combustion*. Combustion and Flame, 158(11):2199–2213, 2011.

[117] T. SCHMITT, A. SADIKI, B. FIORINA, and D. VEYNANTE - *Impact of Dynamic Wrinkling Model on the Prediction Accuracy Using the F-TACLES Combustion Model in Swirling Premixed Turbulent Flames*. Proc. Comb. Inst., 34(1):1261–1268, 2013.

[118] R. MERCIER, T. SCHMITT, D. VEYNANTE, and B. FIORINA - *The Influence of Combustion SGS Submodels on the Resolved Flame Propagation. Application to the LES of the Cambridge Stratified Flames*. Proceedings of the Combustion Institute, 35(2):1359–1366, 2015.

[119] G. KUENNE, F. SEFFRIN, F. FUEST, T. STAHLER, A. KETELHEUN, D. GEYER, J. JANICKA, and A. DREIZLER - *Experimental and Numerical Analysis of a Lean Premixed Stratified Burner Using 1D Raman/Rayleigh Scattering and Large Eddy Simulation*. Combust. Flame, 159(2669-2689), 2012.

[120] R. MERCIER, P. AUZILLON, V. MOUREAU, N. DARABIHA, O. GICQUEL, D. VEYNANTE, and B. FIORINA - *LES Modeling of the Impact of Heat Losses and Differential Diffusion on a Turbulent Stratified Flame*. Flow Turb. and Comb., 93(2):349–381, 2014.

[121] C. DUWIG, K.J. NOGENMYR, C. CHAN, and M.J. DUNN - *Large Eddy Simulations of a Piloted Lean Premix Jet Flame Using Finite-Rate Chemistry*. Combustion Theory and Modelling, 15(4):537–568, 2011.

[122] V. SABELNIKOV and C. FUREBY - *Extended LES-PASR Model for Simulation of Turbulent Combustion*. Haidn O. Frolov S. DeLuca L., Bonnal C., editor, Progress in Propulsion Physics, volume 4, chapter 5.3, pages 539–568. TORUS PRESS, Moscow, 2013.

[123] V. SABELNIKOV and C. FUREBY - *LES Combustion Modeling for high re Flames Using a Multi-Phase Analogy*. Combustion and Flame, 160:83–96, 2013.

[124] Y. MOULE, V. SABELNIKOV, and A. MURA - *Highly Resolved Numerical Simulation of Combustion in Super- Sonic Hydrogen-Air Coflowing Jets*. Combustion and Flame, 161:2647–2668, 2014.

[125] K. PETTERSON, A. BRESSON, C. FUREBY, K. NORDIN-BATES, and V. SABELNIKOV - *A Computational Study of Supersonic Combustion in Strut Injector and Hypermixer Flow Fields*. Proceedings of the Combustion Institute, 35:2127–2135, 2015.

[126] M. FRENKLACH, D. W. CLARY, W. C. GARDINER, and S. E. STEIN - *Detailed Kinetic Modeling of Soot Formation in Shock-Tube Pyrolysis of Acetylene*. Proc. Combust. Inst., 20(1):887–901, 1985.

[127] J. APPEL, H. BOCKHORN, and M. FRENKLACH - *Kinetic Modeling of Soot Formation with Detailed Chemistry and Physics: Laminar Premixed Flames of Hydrocarbons*. Combustion and Flame, 121(12):122 – 136, 2000.

[128] M BALTHASAR and M KRAFT - *A Stochastic Approach to Calculate the Particle Size Distribution Function of Soot Particles in Laminar Premixed Flames*. Combustion and Flame, 133(3):289 – 298, 2003.

[129] C. SAGGESE, S. FERRARIO, J. CAMACHO, A. CUOCI, A. FRASSOLDATI, E. RANZI, H. WANG, and T. FARAVELLI - *Kinetic Modeling of Particle Size Distribution of Soot in a Premixed Burner-Stabilized Stagnation Ethylene Flame*. Combustion and Flame, 162(9):3356 – 3369, 2015.

[130] B. FRANZELLI, E. RIBER, B. CUENOT, and M. IHME - *Numerical Modeling of Soot Production in Aero- Engine Combustors Using Large Eddy Simulation*. In Proceedings of GT2015, ASME Turbo Expo 2015, Montreal, Canada, pages GT2015–43630, 2015.

[131] F. LIU, H. GUO, G J SMALLWOOD, and O. L. GULDER - *Effects of Gas and Soot Radiation on Soot Formation in a Coflow Laminar Ethylene Diffusion Flame.* J Quant. Spectrosc. Radiat. Transfer, 73(25):409 – 421, 2002.

[132] P. DESGROUX, X. MERCIER, and K. A. THOMSON - *Study of the Formation of Soot and its Precursors in Flames Using Optical Diagnostics*. Proc. Combust. Inst., 34(1):1713 – 1738, 2013.

[133] G.J. NATHAN, P.A.M. KALT, Z.T. ALWAHABI, B.B. DALLY, P.R. MEDWELL, and Q.N. CHAN - *Recent Advances in the Measurement of Strongly Radiating, Turbulent Reacting Flows*. Prog. Energy Comb. Sci. , 38(1):41– 61, 2012.

[134] S.-Y. LEE, S. R. TURNS, and R. J. SANTORO - *Measurements of Soot, OH, and PAH Concentrations in Turbulent Ethylene/Air Jet Flames*. Combustion and Flame, 156(12):2264 – 2275, 2009.

[135] M. KÖHLER, K. P. GEIGLE, T. BLACHA, P. GERLINGER, and W. MEIER - *Experimental Characterization and Numerical Simulation of a Sooting Lifted Turbulent Jet Diffusion Flame*. Combustion and Flame, 159(8):2620–2635, 2012.

[136] T. L. HENRIKSEN, G. J. NATHAN, Z. T. ALWAHABI, N. QAMAR, T. A. RING, and E. G. EDDINGS - *Planar Measurements of Soot Volume Fraction and OH in a JP-8 Pool Fire*. Combustion and Flame, 156(7):1480 – 1492, 2009.

[137] V. NARAYANASWAMY and N.T. CLEMENS - *Simultaneous LII and PIV Measurements in the Soot Formation Region of Turbulent Non-Premixed Jet Flames*. Proc. Combust. Inst., 34(1):1455 – 1463, 2013.

[138] B. FRANZELLI, P. SCOUFLAIRE, and S. CANDEL - *Time-Resolved Spatial Patterns and Interactions of Soot, PAH and OH in a Turbulent Diffusion Flame*. Proc. Combust. Inst., 35(2):1921–1929, 2015.

[139] J.B. MICHAEL, P. VENKATESWARAN, C.R. SHADDIX, and T.R. MEYER - *Effects of Repetitive Pulsing on Multi- KHZ Planar Laser-Induced Incandescence Imaging in Laminar and Turbulent Flames*. 54(11):3331–3344, 2015.

[140] O. LAMMEL, K.-P. GEIGLE, R. LÜCKERATH, W. MEIER, and M. AIGNER - *Investigation of Soot Formation and Oxidation in a High-Pressure Gas Turbine Model Combustor by Laser Techniques*. Proceedings of GT2007, ASME Turbo Expo 2007: Power of Land, Sea and Air, May 14-17, 2007, Montreal, Canada, pages GT2007–27902, 2007.

[141] K.-P. GEIGLE, R. HADEF, and W. MEIER - *Soot Formation and Flame Characterization of an Aero-Engine Model Combustor Burning Ethylene at Elevated Pressure*. ASME Turbo Expo paper GT2013-95316, San Antonio, Texas, 2013.

[142] K.-P. GEIGLE, M. KÖHLER, W. O'LOUGHLIN, and W. MEIER - *Investigation of Soot Formation in Pressurized Swirl Flames by Laser Measurements of Temperature, Flame Structures and Soot Concentrations*. 35(3):3373–3380, 2014.

[143] H. T. BROCKLEHURST, C.H. PRIDDIN, and J.B. MOSS - *Soot Predictions with an Aero Gas Turbine Combustion Chamber*. Proceedings of the International Gas Turbine and Aeroengine Congress and Exposition, 1997.

[144] A. K. TOLPADI, A. M. DANIS, H. C. MONGIA, and R. P. LINDSTEDT - *Soot Modeling in Gas Turbine Combustors*. Proceedings of the International Gas Turbine and Aeroengine Congress and Exposition, 1997.

[145] H. BARTHS, N. PETERS, N. BREHM, A. MACK, M. PFITZNER, and V. SMILJANOVSKI - *Simulation of Pollutant Formation in a Gas-Turbine Combustor Using Unsteady Flamelets*. Proceedings of the Combustion Institute, 27:1841–1847, 1998.

[146] M. BALTHASAR, F. MAUSS, M. PFITZNER, and A. MACK - *Implementation and Validation of a New Soot Model and Application to Aeroengine Combustors*. J. Eng. Gas Turb. and Power, 124:66–74, 2002.

[147] E. RIESMEIER, S. HONNET, and N. Peters - *Flamelet Modeling of Pollutant Formation in a Gas Turbine Combustion Chamber Using Detailed Chemistry for a Kerosene Model Fuel*. J. Eng. Gas Turb. and Power, 126:889–905, 2004.

[148] C. EBERLE, P. GERLINGER, K.P. GEIGLE, and M. AIGNER - *Soot Predictions in an Aero-Engine Model Combustor at Elevated Pressure Using Urans and Finite-Rate Chemistry*. AIAA Joint Propulsion Conference, AIAA 2014-3472, 28.-30.07.2014, Cleveland, USA, 2014.

[149] H. EL-ASRAG, T. LU, C.K. LAW, and S. MENON - *Simulation of Soot Formation in Turbulent Premixed Flames*. Combustion and Flame, 150(1-2):108 – 126, 2007.

[150] P. DONDE, V. RAMAN, M. E. MUELLER, and H. PITSCH - *LES/PDF Based Modeling of Soot-Turbulence Interactions in Turbulent Flames*. Proc. Combust. Inst., 34(1):1183–1192, 2013.

[151] M. E. MUELLER, Q. N. CHAN, N. H. QAMAR, B. B. DALLY, H. PITSCH, Z. T. ALWAHABI, and G. J. NATHAN - *Experimental and Computational Study of Soot Evolution in a Turbulent Nonpremixed Bluff Body Ethylene Flame*. Combustion and Flame, 160(7):1298–1309, 2013.

[152] B. CUENOT, E. RIBER, and B. FRANZELLI - *Towards the Prediction of Soot in Aero-Engine Combustors with Large Eddy Simulation*. Summer Program Briefs, Center for Turbulence Research, Stanford, 2014.

[153] K. M. LEUNG and R. P. LINDSTEDT - *A Simplified Reaction Mechanism for Soot Formation in Nonpremixed Flames*. Combustion and Flame, 87:289–305, 1991.

[154] G. LECOCQ, D. POITOU, I. HERNANDEZ, F. DUCHAINE, E. RIBER, and B. CUENOT - *LES Model for Sooting Turbulent Nonpremixed Flames*. Flow, Turb. and Combustion, 92:947–970, 2014.

[155] M.E. MUELLER and H. PITSCH -*Large Eddy Simulation of Soot Evolution in an Aircraft Combustor*. Physics of Fluids, 25:110812, 2013.

[156] L-H. DOREY, N. BERTIER, L. TESS, and F. DUPOIRIEUX - *Soot and Radiation Modeling in Laminar Ethylene Flames with Tabulated Detailed Chemistry*. C. R. Acad. Sci., 339:759–769, 2012.

[157] M. E. MUELLER and H. PITSCH - *LES Model for Sooting Turbulent Nonpremixed Flames*. Combustion and Flame, 159(6):2166 – 2180, 2012.

[158] Y. XUAN and G. BLANQUART - *Effects of Aromatic Chemistry-Turbulence Interactions on soot Formation in a Turbulent Non-Premixed Flame*. Proc. Combust. Inst., 35(2):1911–1919, 2015.

[159] B. SHAHRIARI, M. THOMSON, and S. DWORKIN - *Development and Validation of a Partially Coupled Soot Model for Turbulent Kerosene Combustion in view of Application to Gas Turbines*. Proceedings of GT2015, ASME Turbo Expo 2015, Montreal, Canada, pages GT2015–43063, 2015.

[160] M.E. MUELLER, G. BLANQUART, and H. PITSCH - *Hybrid Method of Moments for Modeling Soot Formation and Growth*. Combustion and Flame, 156(6):1143 – 1155, 2009.

[161] S. SALENBAUCH, A. CUOCI, A. FRASSOLDATI, C. SAGGESE, T. FARAVELLI, and C. HASSE - *Modeling Soot Formation in Premixed Flames Using an Extended Conditional Quadrature Method of Moments*. Combust. Flame, 162(6):2529 – 2543, 2015.

[162] Y. XIN and J. P. GORE - *Two-Dimensional Soot Distributions in Buoyant Turbulent Fires*. Proc. Combust. Inst., 30(1):719 – 726, 2005.

[163] M.E. MUELLER and H. PITSCH - *Large Eddy Simulation Sub Filter Modeling of Soot-Turbulence Interactions*. Physics of Fluids, 23:115104, 2013.

[164] L. LIU, M. I. MISHCHENKO, and W. P. ARNOTT - *A Study of Radiative Properties of Fractal Soot Aggregates Using the Superposition T-Matrix Method*. Journal Quant. Spectr. Rad. Transfer, 109(15):2656 – 2663, 2008.

[165] Y. ZELDOVICH - *Acta Physicochim*. USSR, 21:577–628, 1946.

[166] G.G. DE SOETE - *Overall Reaction Rates of NO and N_2 Formation from Fuel Nitrogen*. Symposium (International) on Combustion, 15(1):1093–1102, 1975.

[167] A.H. LEFEBVRE - *Gas Turbine Combustion*. CRC, 1999.

[168] C.P. FENIMORE and H.A. FRAENKEL - *Proceedings of the Combustion Institute*, 18:143–149, 1981.

[169] W. BARTOK, VS ENGLEMAN, R. GOLDSTEIN, and E. DEL VALLE - *Basic Kinetic Studies and Modeling of Nitrogen Oxide Formation in Combustion Processes*. AIChE Symposium Series, 68(126):30–38, 1972. [170] P. Glarborg, J.A. Miller, and R.J. Kee. Kinetic modeling and sensitivity analysis of nitrogen oxide formation in well-stirred reactors. Combustion and Flame, 65(2):177–202, 1986.

[171] S.M. CORREA - *A Review of NOx Formation Under Gas-Turbine Combustion Conditions*. Combustion science and technology, 87(1-6):329–362, 1993.

[172] F. PECQUERY, V. MOUREAU, G. LARTIGUE, L. VERVISCH, and A. ROUX - *Modelling Nitrogen Oxide Emissions in Turbulent Flames with Air Dilution: Application to LES of a Non-Premixed Jet-Flame*. Combustion and Flame, 161(2):496–509, 2014.

[173] L. VERVISCH, R. HAUGUEL, P. DOMINGO, and M. RULLAUD - *Three Facets of Turbulent Combustion Modeling: DNS of Premixed V-Flame, LES of Lifted Nonpremixed Flame and RANS of Jet-Flame*. J. of Turbulence, 5(4):1–36, 2004.

[174] P. DOMINGO, L. VERVISCH, and D. VEYNANTE - *Large-Eddy Simulation of a Lifted Methane-Air Jet Flame in a Vitiated Coflow*. Combustion and Flame, 152(3):415–432, 2008.

[175] V. MOUREAU, P. DOMINGO, and L. VERVISCH - *From Large-Eddy Simulation to Direct Numerical Simulation of a Lean Premixed Swirl Flame: Filtered Laminar Flame-PDF Modeling*. Combustion and Flame, 158(7):1340– 1357, 2011.

[176] J.H. FRANK and R.S. BARLOW - *Simultaneous Rayleigh, Raman, and LIF Measurements in Turbulent Premixed Methane-Air Flames*. Symposium (International) on Combustion, 27(1):759 – 766, 1998. Twenty-Seventh Sysposium (International) on Combustion Volume One.

Acronyms

RANS	(Reynolds Average Navier Stokes)
LES	(Large Eddy Simulations)
DNS	(Direct Numerical Simulations)
AMR	(Adaptive Mesh Refinement)
LDT	(Lagrangian Droplet Tracking)
DG	(Discontinuous Galerkin)
ACBMM	(Algebraic-Closure-Based Moment Methods)
QSSA	(Quasi Steady-State Approximation
PEA	(Partial Equilibrium Approximation)
DRG	(Directed Relation Graph)
QSS	(Quasi Steady State)
ILDM	(Intrinsic Low Dimensional Manifold)
F-TACLES	(Filtered TAbulated Chemistry for Large Eddy Simulation)
TSF	(Turbulent Stratified Flame)
LII	(Laser Induced Incandescence)
PIV	(Particle Image Velocimetry)
CARS	(Coherent Anti-Stokes Raman Spectroscopy)
NOMANI	(Nitrogen Oxide emission model with one-dimensional MANIfold)

Benoît Fiorina, professor at CentraleSupélec, is conducting his research activities on combustion at the EM2C laboratory. After defending his PhD at CentraleSupélec in 2004, he spent two years at Stanford as a post-doctoral fellow. He joined CentraleSupélec in 2006 as assistant professor and is now professor since 2014. His domain of research is related to the modeling and the simulation of turbulent reactive flows, including detailed chemistry effects. He is also focusing on the simulation of plasma-assisted combustion. He defended his Habilitation diploma to conduct research in 2012. Since 2015, he is president of the French section of the Combustion Institute.

Aymeric Vié is Assistant Professor at CentraleSupelec in the EM2C laboratory (CNRS-UPR288). His research focuses on the mathematical modelling and numerical simulation of turbulent disperse phase flows. He graduated from Université Paul Sabatier (2007) and received his PhD from Institut National Polytechnique de Toulouse (IFPEN, 2010). He worked as a postdoctoral fellow at EM2C laboratory (2011-2013) and at the Center for Turbulence Research at Stanford University (2013-2014).

Benedetta Franzelli is Researcher of the French National Center for Scientific Research (CNRS) at the EM2C Laboratory (UPR288) at CentraleSupélec. Her research interests are in theoretical, experimental and numerical characterization of multi-phase turbulent reactive flows. At EM2C, she is in charge of leading the investigations of soot production in turbulent flames, mainly thorough high-speed optical diagnostics and large eddy simulations. She graduated at Politecnico di Milano (2007) and received her PhD from Institut National Polytechnique de Toulouse (CERFACS, 2011). As a Postdoctoral Fellow, she worked at the EM2C Laboratory (2012, 2013) and at the Center for Turbulence Research at Stanford University (2014). In the past, she worked on modeling and numerical simulation of complex chemical-related phenomena in reactive flows (spray flames, pollutant emissions, thermo-acoustic instabilities).

Nasser Darabiha is Professor Exceptional Category at CentraleSupélec Engineering School, Paris-Saclay University. He got his PhD from Ecole Centrale Paris (ECP) in 1984 and his Habilitation Diploma from Institut Polytechnique de Toulouse in 1994. He was the Director of the EM2C Laboratory at Ecole Centrale Paris from 2002 through 2010, Head of the Department of Energy of ECP from 2005 through 2007, and the Dean of The PhD School of ECP from 2011 to 2012. He has been promoted to Chevalier (2005) and then Officier (2012) of «Ordre des Palmes Académiques». He is a member of Concil of the « Fondation de Recherche pour l'Aéronautique et l'Espace». He is a member the Board of the International Flame Research Foundation. His research activities concern theoretical and numerical studies of combustion of gases, solids and sprays including detail chemistry and transport for the prediction of pollutants such as soot and NOx.

Marc Massot, PhD in Applied Mathematics from Ecole Polytechnique, is Full Professor at CentraleSupélec and is conducting his research at EM2C Laboratory,where he has installed an applied mathematics team since 2005, as well as scientific adviser at ONERA-DEFA. He was Visiting Professor at the Center for Turbulence Research, Stanford University, in 2011-2012 and intiated and chairs the Fédération de Mathématiques de l'Ecole Centrale Paris since 2013. He participated in the creation of the "Mésocentre" computing center at CentraleSupélec, for which he is the deputy director. His main fields of research are mathematical modeling and numerical analysis, analysis of PDEs and dynamical systems for multi-scale systems, with applications in combustion, two-phase flows, plasma physics and biomedical engineering. He has especially contributed to the development of Eulerian models and numerical method for polydisperse sprays in laminar and turbulent two-phase flows, with contributions to codes such as CEDRE, IFPC3D and AVBP.

Guillaume Dayma is professor at the University of Orléans since 2012. He obtained his PhD from the Institut National Polytechnique de Lorraine (Nancy) in 2003. He was a post-doc fellow at the Institute for Aerospace Studies from the University of Toronto. He was assistant professor at Paris VI University from 2006 to 2009 before moving to Orléans. His research activities aim at understanding the chemical phenomena during combustion. He develops detailed chemical kinetics mechanisms for hydrocarbons and oxygenated fuels. He is also teaching Physical Chemistry, Thermochemistry and Kinetics Mechanisms development at the University of Orléans. He is the author of 51 publications in peer-reviewed scientific journals.

Philippe Dagaut, Ph.D. from the University P. & M. Curie, Paris, 1986. He is Directeur de Recherche at CNRS-INSIS Orléans, group leader, and Editor-in-Chief of the journal Combustion and Flame. His research field is combustion chemistry (experimental and modelling).

Vincent Moureau is a CNRS researcher at CORIA in the combustion modeling group. He got his Master of Science from Ecole Centrale Paris in 2001 and obtained his PhD from Institut Français du Pétrole and Ecole Centrale Paris in 2004. After a two-year postdoctoral fellowship at Stanford University in the Center for Turbulence Research, he joined Turbomeca, SAFRAN group, as a combustion engineer from 2006 to 2008. Since 2009, his research is focused on turbulent combustion and spray modeling, and on the development of the YALES2 solver for Large-Eddy Simulation and Direct Numerical Simulation of turbulent flows in complex geometries using massively parallel computers. He received the Yves Chauvin award for his PhD thesis in 2005, the 3rd prize of the Bull Joseph Fourier award for the promotion of numerical simulation in 2010 and an IBM faculty award in 2011. He is the coordinator of the Scientific Group SUCCESS devoted to the promotion of super-computing for the CFD of complex flows in realistic geometries.

Luc Vervisch activities are in numerical simulation of reactive flows. Fuel efficiency and environmental issues are the major topics addressed. He uses Direct Numerical Simulation (DNS) to understand laminar and turbulent flames. He also contributes to the development of sug-grid scale closures for Large Eddy Simulation (LES). Luc Vervisch is currently Professor at the National Institute of Applied Science (INSA) Normandy University in Rouen and researcher at the CNRS laboratory CORIA. He was awarded in 2014 a Senior Professor position at Institut Universitaire de France (IUF) for his work on turbulent combustion modelling.

Alain Berlemont is Directeur de Recherche in CNRS. His research activities are developed in CNRS-CORIA, where more than 150 people are involved in different topics, such as combustion, two phase flows, plasmas, turbulence, sprays, dynamical systems and instabilities, measurement techniques. Previous research was on Lagrangian modeling of dispersed turbulent two phase flows, and since the last fifteen years Alain Berlemont and co-workers are developing level set method for interface tracking for atomization of liquid layers and liquid jets. A 3D computer code with Level Set / Ghost Fluid / VOF coupling under MPI parallelization has proved to be one of the most efficient code in the international scientific community, as they were the first to publish realistic simulations of 3D simulation of the primary break-up of a liquid jet.

Vladimir Sabelnikov gratuated (1971) from Moscow Institute of Physics and Technology (MIPT), Dolgoprudny, Russia, Ph.D. (1974), and Doctor of Science (1984) degrees from MIPT also. In 1974, he joined the Central Aerohydrodynamics Institute (TsAGI, Moscow, Russia), where he was Leading Scientist until 2000. Since 2000, he is a Leading Scientist in Energetic department of ONERA. His current research interests include the study of combustion instabilities in gas turbines, supersonic combustion in ducts, scramjets, combustion in microcombustors, the plasma control of combustion, the development of Eulerian Monte Carlo method to solve the transported PDF equation in turbulent combustion, and the development of new PaSR and EPaSR models of turbulent combustion.

Eleonore Riber graduated from ENSEEIHT engineering school in 2003 and then worked at IMFT in the field of two-phase flow modelling to obtain her PhD from Institut National Polytechnique de Toulouse in 2007. After one year as a researcher at IFPEN, she joined CERFACS in 2008. Her research work is mainly oriented towards modelling and Large Eddy Simulation of reacting turbulent flows in complex geometries on massively parallel machines. She has developed expertise in turbulent flows, spray combustion and pollutant modelling as well as chemistry reduction techniques.

Bénédicte Cuenot is the leader of the combustion research group at CERFACS, developing advanced softwares for the numerical simulation of turbulent combustion (code AVBP) and heat transfer (code PRISSMA for thermal radiation) in both academic and industrial systems. Dr. Cuenot teaches combustion in various universities and has authored about 70 peer-reviewed journal papers. She is also much experienced in coordinating international projects, mainly financed by the European Commission where she also acts as an expert evaluator.

Advanced Simulation of Aeronautical Combustors

B. Cuenot
(CERFACS)
R. Vicquelin
(CNRS, UPR 288, EM2C, Centrale-Supélec, U. Paris-Saclay)
E. Riber
(CERFACS)
V. Moureau, G. Lartigue
(CORIA, CNRS UMR6614, Normandie Université, Université et INSA de Rouen)
A. Figuer, Y. Mery
(SAFRAN AIRCRAFT ENGINES)
J. Lamouroux, S. Richard
(SAFRAN HELICOPTER ENGINES)
L.Gicquel
(CERFACS)
T. Schmitt, S. Candel
(CNRS, UPR 288, EM2C, Centrale-Supélec, U. Paris-Saclay)

E-mail: cuenot@cerfacs.fr

DOI : 10.12762/2016.AL11-06

The development of new aeronautical combustor concepts relies on the best possible knowledge of combustion phenomena, such as ignition and extinction, flame structure, combustion instabilities or pollutant emissions. Numerical simulation, and in particular the Large Eddy Simulation approach, is a powerful tool to understand, predict and control the coupled physics involved in turbulent combustion in both academic and applied configurations. Thanks to reliable physical models, accurate numerical methods and high efficiency on massively parallel computers, numerical simulation is now able to produce robust and reliable solutions in complex geometries, taking into account all technological and physical effects. Today, it is a research tool that contributes to improving our knowledge of turbulent reacting flows and in particular the interaction between turbulence and combustion chemistry. It is also an efficient tool for the design of aeronautical combustors, guiding test benches and possibly reducing their number.

Introduction

In recent years, numerical simulation has gained considerable importance in the understanding and prediction of combustion phenomena in both academic and applied configurations. It is a challenging domain that requires suitable descriptions of the turbulent flow and the chemistry, as well as their strong interaction and other coupled physics such as spray injection, heat transfer and acoustic resonances with the system modes, etc. The numerical simulation of turbulent reacting flows relies on the accurate modeling of the underlying physics, which has been developed by a large community in the past 50 years and is still the focus of intense research [1]. Its capabilities to address large, transient and multi-physics problems have been promoted by the development of High Performance Computing (HPC), that has considerably improved the fidelity of the results and opened new fields of research [2]. HPC also plays a key role in the implementation of numerical simulation in the industrial context, making it an efficient design tool capable of taking into account complex geometries with an increasing number of technological details.

Models and numerics for advanced simulation of aeronautical combustors

In the field of turbulent - inert or reacting - flows, numerical simulation techniques can be classified depending on their level of accuracy. Direct Numerical Simulation (DNS) consists in solving the turbulent flow equations without any modeling, which implies that the full range of turbulent scales must be resolved. This requires the number of discretization points N to increase as $Re^{3/4}$ in each direction, so that the total number of nodes in the grid increases as $Re^{9/4}$, where $Re = U\,L/\nu$ is the Reynolds number. In reacting flows, the very thin reaction zone requires even smaller grid cells. In contrast, the Reynolds-Averaged Navier Stokes (RANS) relies on the statistical moments (mean and rms) of the flow, solving ensemble-averaged flow equations with various closures for the turbulent Reynolds stresses and fluxes, and dropping out the description of the various scales of the turbulent flow. Due to their computational cost, DNS calculations are exclusively dedicated to academic, simple-geometry, small-scale configurations with a moderate Reynolds number, with the aim of

accurately describing the complex structure of turbulence and its interaction with a flame front. On the other hand, the fast RANS approaches are most suitable for industrial application, although their fidelity and capacity to represent complex non-linear physics are limited. It is known, for example, that RANS methods do not provide an adequate representation of rotating flows of the type induced by swirl injectors. In recent years, the Large Eddy Simulation (LES) technique has emerged as a good compromise between DNS and RANS, keeping high accuracy and fidelity at a reasonable CPU cost. This is achieved by applying a low-pass spatial filter to the flow equations, eliminating the smaller scales that are easily modeled. LES therefore still solves for physical variables, keeping their time and space scales down to the filter cut-off scale. Contrary to DNS, where high-order numerical schemes impose simple geometries, LES may rely on 3rd or even 2nd order non-dissipative schemes, which are still useable at a reasonable CPU cost in complex geometries. Lower order schemes, which are commonly used in RANS, are however not appropriate for LES where the subgrid scale turbulent viscosity is much smaller than in RANS.

Combustion chemistry must also be described, since it drives all flame characteristics and behaviors of interest within the framework of burner design: ignition and extinction, flame structure, burnt gas state, pollutant emissions, etc., are all strongly dependent on chemistry and of primary importance for the burner performances. For standard kerosene or jet fuels, combustion chemistry involves hundreds of chemical species and thousands of reactions, which strongly raise the CPU cost if directly computed. Many approaches exist to account for complex fuel chemistry and its interaction with the turbulent flow in the thin flame regime, which corresponds to the situation prevailing in engines [3, 4, 5, 6, 7]. One strategy is then to pretabulate the detailed chemistry flame structure as a function of one or two parameters (typically the progress variable and the mixture fraction), later introduced into the simulation via the Probability Density Function (PDF) of the tabulation parameters, or via the Flame Surface Density concept. Another strategy is to reduce the chemical scheme to a limited number of species and reactions, still guaranteeing the correct flame characteristics and behaviors. The flame structure can then be computed directly, modeling its interaction with turbulence through an additional model, such as the Thickened Flame model in the LES context (TFLES). Global chemical schemes, reduced down to 1 to 4 steps, are usually built with a fitting procedure, and are valid only under the fitting range conditions. More sophisticated methods are used to analytically derive reduced schemes [8], involving 10 to 25 species depending on the fuel, which reflect the main chemical paths and reproduce the correct system behavior under a wide range of conditions.

Ignition and extinction

From one sector to full burner ignition

Ignition constitutes a critical phase in aerospace propulsion. It must be completed in a safe and reliable way, i.e., always leading to a stabilized flame, while producing a minimum pressure peak, even under unfavorable conditions at high altitude, where rapid relight in case of accidental extinction of the combustor is required for engine certification. New combustion technologies currently developed to reduce pollutant emissions, make the ignition process even more critical.

The experimental characterization of ignition has been extensively studied on single burner ignition problems. One of the key issues is to predict the survival of the generated flame kernel in the turbulent flow field. Indeed, depending on the local flow conditions that are encountered by the kernel, it can either develop towards a turbulent flame or extinguish, leading to a measurable probability of ignition. Computing a full probability map numerically demands important computational resources, since many ignition events must be simulated. This has been achieved in recent work [9], where a good agreement between the numerical and experimental probability maps has quantitatively validated the predictability of LES. Such simulations also enabled a better physical understanding of the stochasticity of the ignition process to be achieved and a low-order predictive model that can be used repeatedly at the industrial design stage [10, 11] could be provided.

Applying LES to the full ignition process has been the next important challenge. Following the pioneering work of Boileau et al [6], Barré et al [12] performed a joint analysis of experiments and numerical simulation of ignition in a gaseous non-premixed multi-injectors burner, in order to study the effects of spacing between injectors on the ignition process and the mechanisms driving the flame propagation from burner to burner. More recently, a novel experimental device named MICCA [13] has been simulated [14, 15] with the AVBP solver, a code jointly developed by CERFACS and IFPEN [16]. This system comprises 16 swirling injectors in an annular geometry allowing full optical access to the flame. It is fed with a lean mixture of air and propane while a single spark igniter initiates the flame. In the simulation, the turbulent combustion is described with either the Filtered Tabulated Chemistry LES model F-TACLES [7] or the TFLES model [17]. With a mesh of 310 million tetrahedra, the simulation required 1.5 million CPU hours on TGCC-Curie thin nodes and was efficiently run on 6144 CPU cores. For both F-TACLES and TFLES models, numerical results closely match experimental data, as illustrated in Fig. 1. The flame brush at the largest scales is similar to that observed experimentally; the instantaneous flame configurations resemble those recorded by the camera. Transit times from one injector to the next match the measured ones, and the duration of the light-round of the order of 50 ms is also correctly predicted.

Extinction limits

The design of gas turbine burners requires the characterization of their operability, and in particular their lean blow-off limits (LBO) in terms of Fuel-Air Ratio (FAR). Flame extinction is however a complex transient process, driven by the two-phase flow, flame structure and their response to varying operating conditions. Experimentally, LBO is usually characterized by reducing the FAR gradually until extinction.

The same methodology has been applied to predict the LBO limit with LES for a variety of SAFRAN combustors and operating conditions (pressure and temperature). Simulations were performed with the AVBP solver, using the TFLES model [17] combined with a two-step kinetic mechanism for the kerosene chemistry [18]. For confidentiality reasons, extinction limits presented in Fig. 2 are normalized by the FAR at take-off power. A very good agreement between numerical and experimental results is obtained for the FAR extinction limit of real burners. In such a diagram, overall absolute errors are lower than ± 2 thousandths. The various configurations and operating conditions are also correctly ranked, validating the use of LES for LBO operability issues.

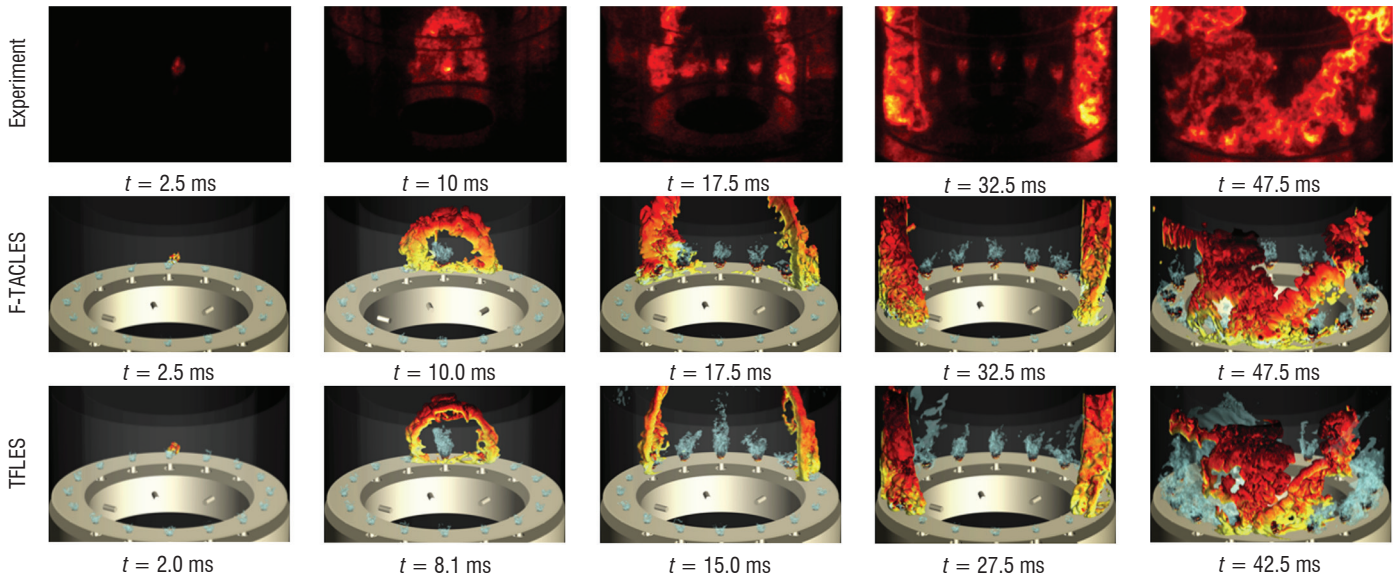

Figure 1 - Five instants in an ignition sequence of the MICCA chamber. Top row: Experimental views showing light intensity emitted by the fame during the light-round process, and represented in false colors to improve visualization. Middle and bottom rows: Respectively F-TACLES and TFLES simulations. Flame fronts are represented by an isosurface of progress variable c=0.9 for F-TACLES, corresponding to an isosurface of temperature T= 1781 K for TFLES. Both are colored by axial velocity levels (light yellow: -30ms-1; black: +15ms^{-1}). Blue isosurfaces correspond to the velocity field U = 25ms^{-1} (from [15]).

Combustor performances

Temperature distribution at the combustor exit

One of the uses of LES within the framework of combustion chamber design concerns the prediction of the temperature level and its spatial distribution at the combustor exit which is an input for high pressure turbine designers. Figure 3 shows a typical example of a straight-through combustion chamber geometry from SAFRAN along with the associated exit plane position.

For analysis and exchange of information with the turbine designers, a dimensionless temperature 1D profile (azimuthal average) is usually extracted from the LES field, leading to the so-called RTDF profile. Several LES calculations were carried out on about ten combustors, using exactly the same simulation set-up in terms of models and numerics. In Fig. 4, results are compared to measurements at various radii across the vane. They are normalized for confidentiality reasons by the maximum of the RTDF profile. There is a relatively good agreement between numerical results and measurements in the hot part of the vane, since the error lies within the ± 2 point tolerance zone (not shown).

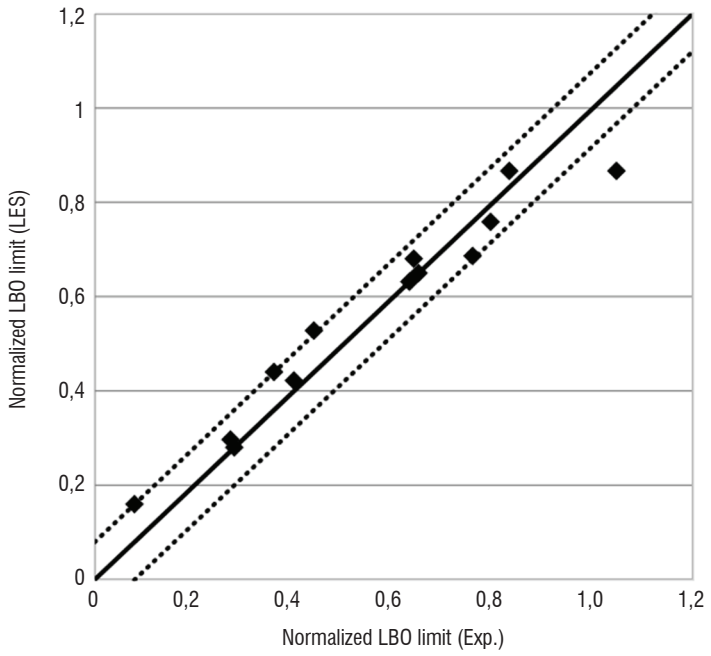

Figure 2 - LBO limit prediction (LES) vs. experimental data for a set of SAFRAN combustors under various operating conditions. Values are normalized by the fuel-air ratio at take-off power. Dotted lines correspond to the absolute error zone of ± 2 thousandths.

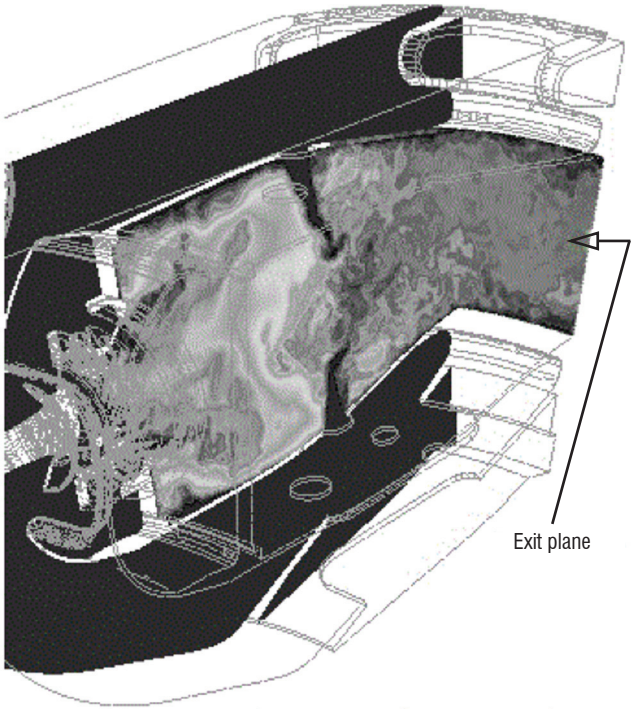

Figure 3 - Example of a straight-through combustion chamber and its exit plane location.

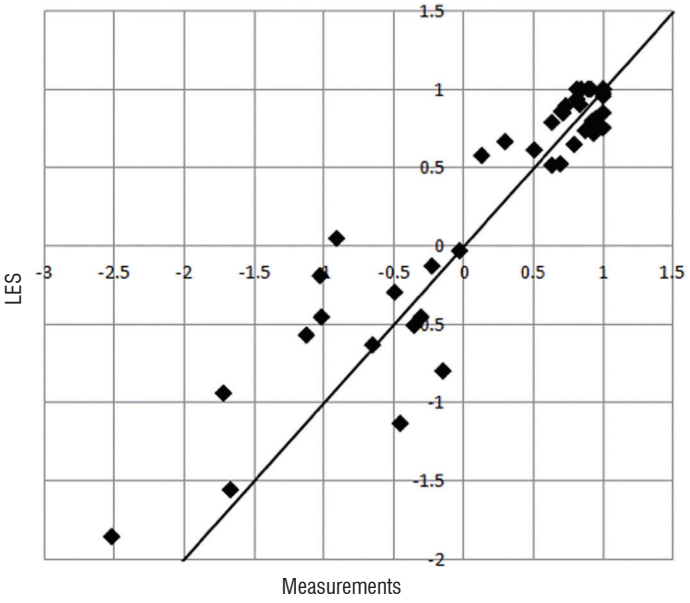

Figure 4 - Dimensionless temperature (RTDF) at various radii for a set of SAFRAN combustors. RTFD values are normalized by the maximum of the 1D profile.

A monotonic trend is also observed confirming that the hottest zones are well positioned. The largest differences are found near the walls, where temperature levels are not well captured. At this point, it should be noticed that effusion cooling at the combustor walls was described with a homogeneous approach [19], which is suspected to underestimate mixing in the liner vicinity. Improvement of the near wall behavior is expected with heterogeneous descriptions such as the one recently developed by CERFACS and SAFRAN TURBOMECA [20].

Combustion instabilities

Combustion instabilities are a major concern in the design process of industrial combustion chambers. They are characterized by strong pressure and heat release oscillations in the flame tube and can alter the integrity of the system. Compressible LES is an appropriate tool to study combustion instabilities, because it takes into account the main processes involved: flame dynamics, acoustics, turbulence and various dissipation mechanisms. LES of three industrial configurations from SAFRAN have been carried out for operating points featuring a strong acoustic response characterized by pressure oscillations at a particular frequency and amplitude. The acoustic mode appears naturally in the simulation after a transient phase, growing until it reaches a limit cycle. Comparisons between experimental and numerical frequencies are shown in Fig. 5 for the three combustion chambers. Two of them feature longitudinal acoustic modes that were obtained on a single sector of the combustion chamber [21, 22]. The third one features an azimuthal mode and can only be obtained by considering the full annular combustor [23].

The frequencies obtained in the simulations are quite close to those observed experimentally, showing that the acoustics and the combustion response are sufficiently well resolved. Some differences are observed for the amplitude, though the order of magnitude is correct. Current investigations rely on the complementary development of acoustic tools and reduced models to incorporate the action of the flame on the acoustic stability of an engine. In parallel, the question of the flame response to acoustic solicitations is naturally raised and the subject of dedicated LES-based studies [24].

Pollutants and soot

Prediction of NOx in aero-engines

Environmental constraints, and in particular Nitrogen oxides (NOx) and CO emissions, are also an important part of aeronautical burner design. NOx are mainly produced in a thermal pathway where both hot temperature and oxygen are present [25], complemented by a prompt pathway in the fuel oxidation layer of the flame front [26]. The time scale of the thermal NOx chemical pathway being far longer than that of kerosene oxidation in the flame front [27, 28], it requires dedicated modeling. Within the framework of tabulated chemistry models [29, 30], Pecquery et al recently proposed the NOMANI model (Nitrogen Oxide emission model with one-dimensional MANIfold) [31], which relies on two different progress variables to take into account both the thermal and prompt NOx pathways, as well as the dilution of the burnt gases by effusion holes after the primary zone of the combustor. In order to generate the 1D premixed laminar flames of the table for the

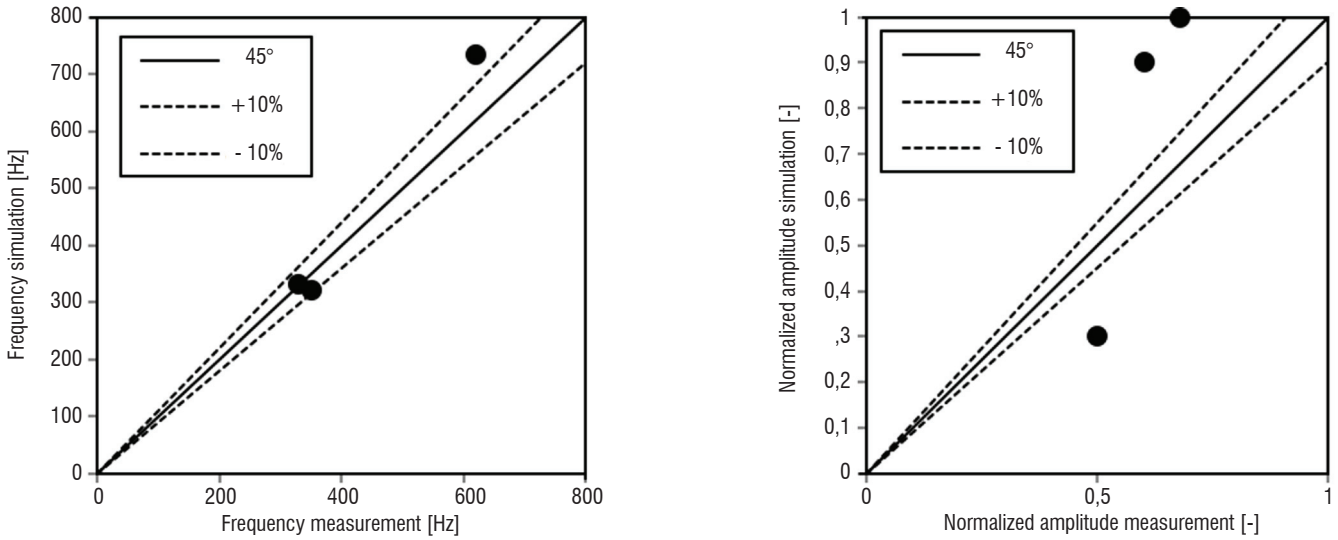

Figure 5 - Unstable modes for three different real scale combustors.
Comparaison between LES and experiments in terms of frequency (left) and normalized amplitude (right).

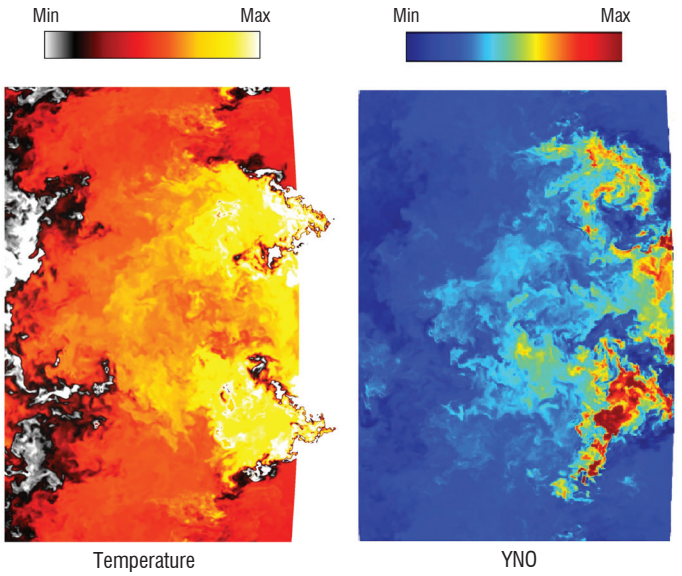

Figure 6 - Instantaneous fields of temperature and NO mass fraction at the center of the burner. Injection is on the right side.

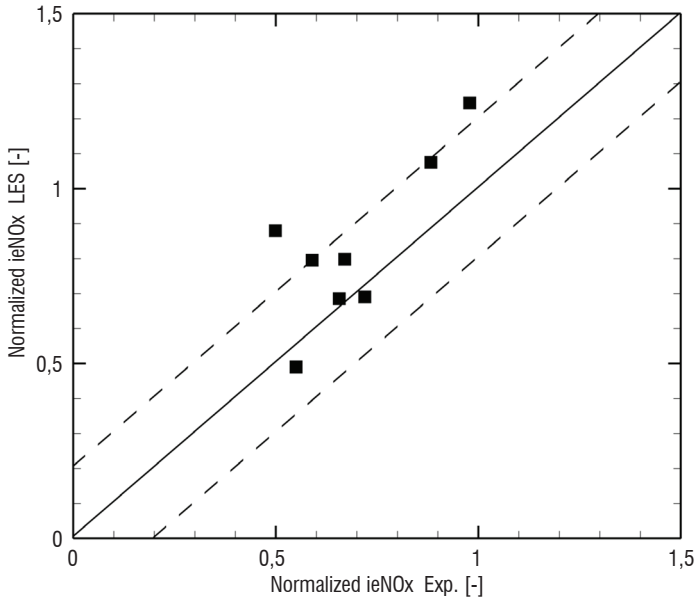

Figure 7 - LES normalized NOx emission index as a function of the experimental ones for various operating conditions and combustion chamber technologies.The dashed lines outline the experimental strong confidence zone.

full range of operating conditions of aeronautical burners in terms of pressure, inlet temperature and equivalence ratio, a parallel table generator based on the Cantera software [32] has been designed. The tool called MUTAGEN (MUlticore TAble GENerator) relies on pre-existing flame repositories, used as initial conditions to converge new flames, and allows look-up tables to be obtained, in the worst case within 2 to 3 hours on 16 cores for the reduced Luche mechanism [33, 34], which contains 92 species and 694 reactions.

The NOMANI model was implemented in the YALES2 solver developed at CORIA [35, 36]. The YALES2 code is dedicated to the LES of turbulent reactive flows on unstructured grids at low-Mach number. YALES2 has been specifically tailored for exploiting massively parallel computers and the handling of meshes with billions of cells [37]. The YALES2 code and the NOMANI model were recently applied at SAFRAN TURBOMECA to a low-NOx burner. These simulations count 380 million tetrahedra for a sector of two injectors and run on 2048 cores of the Airain machine at the TGCC center of the CEA. Instantaneous temperature and NO mass fraction fields at the center of the burner are represented in Fig. 6, illustrating the strong correlation between the two fields. In the primary zone, hot temperatures and high NO mass fractions appear in the same regions: in the central recirculation zone of each injection system and also to a less extent in the recirculation zones between the injection systems. The same methodology was applied to various operating conditions, combustion chambers and injector technologies at Safran. A reduced set of results is illustrated in Fig.7, where the numerical, normalized NOx emission indices are compared with experimental values. The results are consistent with the experimental data, and mostly within experimental uncertainties. These calculations pave the way for a better understanding of NO emissions in gas turbine combustors and the ability to optimize the air split in the burner for reduced NO production.

Soot

Soot participates in the energy balance in the production chamber, modifying the burnt gas temperature. It can cause a significant loss of efficiency of aeronautical combustors, due to soot deposits and wall deterioration. In addition, when emitted to the atmosphere, soot aggregates have a negative impact on health and the environment.

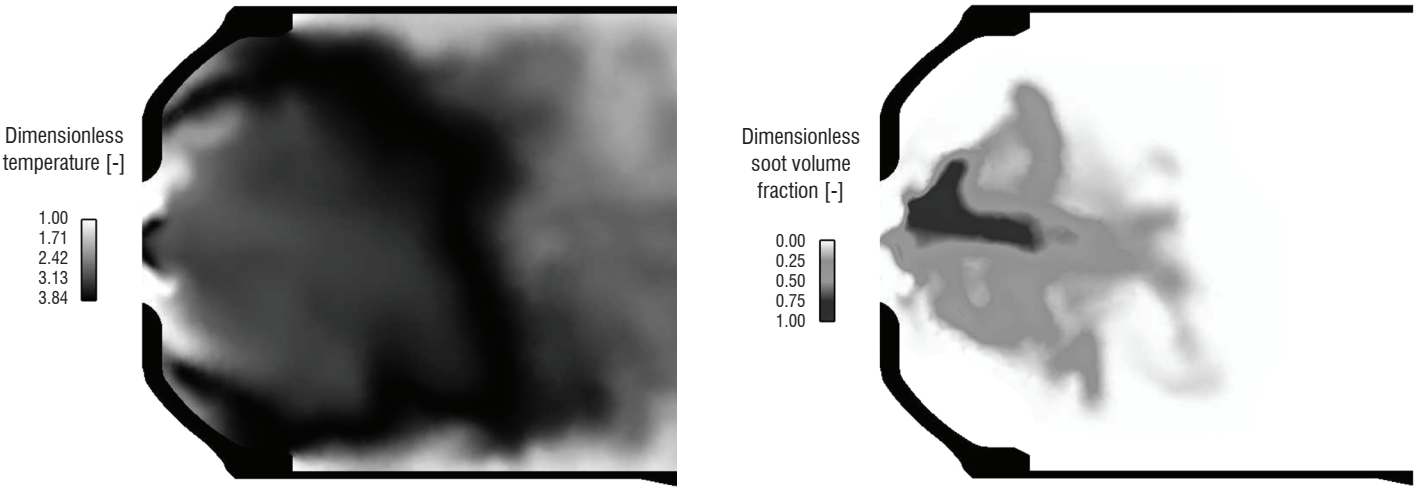

Figure 8 - Instantaneous dimensionless temperature and soot volume fraction fields in a SAFRAN TURBOMECA helicopter model combustor.

Soot production is the result of a complex heterogeneous chemical process, where gaseous precursors trigger the formation of solid particles that may aggregate and react on their surface. Like combustion, this chemical phenomenon is quite sensitive to turbulent transport and mixing, which makes soot highly intermittent and strongly dependent on the temporal and spatial evolution of the flow. Therefore, LES is the most adequate numerical method to investigate soot production in aircraft engines. To do so simplified soot models are used, and coupled to temperature and species fields, as well as thermal radiation.

Coupled LES-radiation simulations have been recently presented in [38, 39] to evaluate soot particles in a helicopter engine. The solid phase has been described by a phenomenological two-equation model [40], where acetylene is the only soot precursor and soot oxidation is due to OH and O2. A hybrid chemical description has been proposed by [38], combining a two-step global chemistry for the gas phase combustion [18] and a tabulated chemistry for the minor species involved in soot production but not present in the reduced chemistry. Finally, a Discrete Ordinates Method approach with optimized spectral models has been used to compute radiation [41]. It was shown that soot is produced and grows in the rich zones of the primary premixed flame, and is then consumed in a secondary diffusion flame (Fig. 8). Very few soot particles are found at the burner exit.

Comparing an adiabatic uncoupled and a non-adiabatic LES-radiation simulation, the radiation effect appeared to be rather weak in the gas phase (a difference of a few percent in the mean temperature field), but much larger in the soot volume fraction (around 35%), due to slower kinetics for the reactions responsible for the soot particle evolution.

Conclusions

The accuracy and reliability of numerical simulation, and in particular of the LES approach, have been demonstrated by considering some difficult combustion phenomena, such as ignition, combustion instabilities or pollutant emissions, in either well-controlled academic experiments or realistic, complex-geometry applications. The complementarity with experiments is clearly established and numerical simulation has now become an essential tool for research, as well as industrial design. Current and future challenges are to include even more physics, in a parallel coupled solver strategy and to extend computational domains to all elements of aeronautical gas turbines, from the compressor down to the turbine. Such objectives will be achieved with the next generation of massively parallel computers and will require important efforts on the solvers to keep them at the highest HPC standards ■

Acknowledgements

PRACE/GENCI are gratefully acknowledged for granting access to the resource Curie-TN based in France at TGCC. The PhD fellowship provided to M. Philip by the Initiative d'Excellence (IDEX) Paris-Saclay is also acknowledged.

References

[1] D. VEYNANTE, L. VERVISCH - *Turbulent Combustion Modeling*. Prog. Energy Combust. Sci. 28 (2002) 193–266.

[2] N. GOURDAIN, L. GICQUEL, G. STAFFELBACH, O. VERMOREL, F. DUCHAINE, J. F. BOUSSUGE, T. POINSOT - *High Performance Parallel Computing of Flows in Complex Geometries: II*. Applications, Comp. Sci. & Discovery 2 (2009) 015004.

[3] A. TRIANTAFYLLIDIS, E. MASTORAKOS, R. L. G. M. EGGELS - *LES–CMC Simulations of a Lifted Methane Flame*. Combust. Flame 156 (12) (2009) 2328–2345.

[4] S. MARTIN, J. KRAMLICH, G. KOSÁLY, J. RILEY - *The Premixed Conditional Moment Closure Method Applied to Idealized Lean Premixed Gas Turbine Combustors*. A. S. of Mechanical Engineers (Ed.), ASME Turbo Expo 2002: Power for Land, Sea, and Air, 573–580, 2002.

[5] F. DI MARE, W. P. JONES, K. R. MENZIES - *Large Eddy Simulation of a Model Gas Turbine Combustor*. Combust. Flame 137 (3) (2004) 278–294.

[6] M. BOILEAU, G. STAFFELBACH, B. CUENOT, T. POINSOT, C. Bérat - *LES of an Ignition Sequence in a Gas Turbine Engine*. Combustion and Flame 154 (1-2) (2008) 2–22.

[7] B. FIORINA, R. VICQUELIN, P. AUZILLON, N. DARABIHA, O. GICQUEL, D. VEYNANTE - *A Filtered Tabulated Chemistry Model for LES of Premixed Combustion*. Combust. Flame 157 (2010) 465–475.

[8] T. LU, C. LAW - *A Criterion Based on Computational Singular Perturbation for the Identification of Quasi Steady State Species: A Reduced Mechanism for Methane Oxidation with NO Chemistry*. Combust. Flame 154 (2008) 761–774.

[9] L. ESCLAPEZ, E. RIBER, B. CUENOT - *Ignition Probability of a Partially Premixed Burner Using LES*. Proc. Combust. Inst. 35 (3) (2015) 3133–3141.

[10] A. EYSSARTIER, B. CUENOT, L. Y. M. GICQUEL, T. POINSOT - *Using LES to Predict Ignition Sequences and Ignition Probability of Turbulent Two-Phase Flames*. Combust. Flame 160 (7) (2013) 1191–1207.

[11] L. ESCLAPEZ - *Numerical Study of Ignition and Inter-Sector Flame Propagation in Gas Turbine*. Ph.D. thesis, INP Toulouse, 2015.

[12] D. BARRÉ, L. ESCLAPEZ, M. CORDIER, E. RIBER, B. CUENOT, G. STAFFELBACH, B. RENOU, A. VANDEL, L. Y. M. GICQUEL, G. CABOT - *Flame Propagation in Aeronautical Swirled Multi-Burners: Experimental and Numerical Investigation*. Combust. Flame 161 (9) (2014) 2387–2405.

[13] J. F. BOURGOUIN, D. DUROX, T. SCHULLER, J. BEAUNIER, S. CANDEL - *Ignition Dynamics of an Annular Combustor Equipped with Multiple Swirling Injectors*. Combust. Flame 160 (8) (2013) 1398 – 1413.

[14] M. PHILIP, M. BOILEAU, R. VICQUELIN, T. SCHMITT, D. DUROX, J.-F. BOURGOUIN, S. CANDEL - *Simulation of the Ignition Process in an Annular Multiple-Injector Combustor and Comparison with Experiments*. J. Eng. Gas Turb. Power 137 (3) (2014) 031501–031501.

[15] M. PHILIP, M. BOILEAU, R. VICQUELIN, E. RIBER, T. SCHMITT, B. CUENOT, D. DUROX, S. CANDEL - *Large Eddy Simulations of the Ignition Sequence of an Annular Multiple-Injector Combustor*. Proc. Combust. Inst. 35 (3) (2015) 3159–3166.

[16] V. MOUREAU, G. LARTIGUE, Y. SOMMERER, C. ANGELBERGER, O. COLIN, T. POINSOT - *Numerical Methods for Unsteady Compressible Multi-Component Reacting Flows on Fixed and Moving Grids*. J. Comput. Phys. 202 (2) (2005) 710–736.

[17] O. COLIN, F. DUCROS, D. VEYNANTE, T. POINSOT - *A Thickened Flame Model for Large Eddy Simulations of Turbulent Premixed Combustion*. Phys. Fluids 12 (7) (2000) 1843–1863.

[18] B. FRANZELLI, E. RIBER, M. SANJOSE, T. POINSOT - *A Two-Step Chemical Scheme for Large-Eddy Simulation of Kerosene-Air Flames*. Combust. Flame 157 (7) (2010) 1364–1373.

[19] S. MENDEZ, F. NICOUD - *Large-Eddy Simulation of a Bi-Periodic Turbulent Flow with Effusion*. J. Fluid Mech. 598 (2008) 27—65.

[20] D. LAHBIB - *Modélisation aérodynamique et thermique des multiperforations en LES*. Ph.D. thesis, Université Montpellier II, 2015.

[21] E. MOTHEAU, Y. MERY, F. NICOUD, T. POINSOT - *Analysis and Modeling of Entropy Modes in a Realistic Aeronautical Gas Turbine*. J. Eng. Gas Turb. Power 135 (9) (2013) 092602.

[22] E. MOTHEAU, F. NICOUD, T. POINSOT - *Mixed Acoustic-Entropy Combustion Instabilities in Gas Turbines*. J. Fluid Mech. 749 (2014) 542–576.

[23] P. WOLF, G. STAFFELBACH, L. Y. GICQUEL, J.-D. MÜLLER, T. POINSOT - *Acoustic and Large Eddy Simulation Studies of Azimuthal Modes in Annular Combustion Chambers*. Combust. Flame 159 (11) (2012) 3398– 3413.

[24] M. BAUERHEIM, M. CAZALENS, T. POINSOT - *A Theoretical Study of Mean Azimuthal Flow and Asymmetry Effects on Thermo-Acoustic Modes in Annular Combustors*. Proc. Combust. Inst. 35 (2015) 3219–3227.

[25] A. LEFEBVRE - *Gas Turbine Combustion*. CRC, 1999.

[26] C. FENIMORE, H. FRAENKEL - *Formation and Interconversion of Fixed-Nitrogen Species in Laminar Diffusion Flames*. Proc. Combust. Inst. 18 (1981) 143–149.

[27] Y. ZELDOVICH - *The Oxidation of Nitrogen in Combustion and Explosions*. Acta Physicochim. USSR 21 (1946) 577–628.

[28] G. DE SOETE - *Overall Reaction Rates of NO and N2 Formation from Fuel Nitrogen*. Symposium (International) on Combustion 15 (1) (1975) 1093–1102.

[29] P. DOMINGO, L. VERVISCH, D. VEYNANTE - *Large-Eddy Simulation of a Lifted Methane-Air Jet Flame in a Vitiated Coflow*. Combust. Flame 152 (3) (2008) 415–432.

[30] A. BOUCHER, N. BERTIER, F. DUPOIRIEUX - *A Method to Extend Flamelet Manifolds for Prediction of NOx and Long Time Scale Species with Tabulated Chemistry*. Int. J. Sustainable Aviation 1 (2) (2014) 181–202.

[31] F. PECQUERY, V. MOUREAU, G. LARTIGUE, L. VERVISCH, A. ROUX - *Modelling Nitrogen Oxide Emissions in Turbulent Flames with Air Dilution: Application to LES of a Non-Premixed Jet-Flame*. Combust. Flame 161 (2) (2014) 496–509.

[32] D. GOODWIN - *An Open-Source, Extensible Software Suite for CVD Process Simulation*. Chemical Vapor Deposition XVI and EUROCVD 14 (2003) 2003–08.

[33] J. LUCHE - *Elaboration of Reduced Kinetic Models of Combustion. Application to a kerosene mechanism.* Ph.D. thesis, LCSR Orleans, 2003.

[34] J. LUCHE, M. REUILLON, J.-C. BOETTNER, M. CATHONNET - *Reduction of Large Detailed Kinetic Mechanisms: Application to Kerosene / Air Combustion*. Comb. Sci. Tech. 176 (2004) 1935–1963.

[35] V. MOUREAU, P. DOMINGO, L. VERVISCH - *From Large-Eddy Simulation to Direct Numerical Simulation of a Lean Premixed Swirl Flame: Filtered Laminar Flame-PDF Modeling*. Combust. Flame 158 (7) (2011) 1340–1357.

[36] V. MOUREAU, G. LARTIGUE - *YALES2 www.coria-cfd.fr*. URL www.coria-cfd.fr, 2015.

[37] M. MALANDAIN, N. MAHEU, V. MOUREAU - *Optimization of the Deflated Conjugate Gradient Algorithm for the Solving of Elliptic Equations on Massively Parallel Machines*. J. Comput. Phys. 238 (2013) 32–47.

[38] G. LECOCQ, D. POITOU, I. HERNANDEZ, F. DUCHAINE, E. RIBER, B. CUENOT - *LES Model for Sooting Turbulent Nonpremixed Flames*. Flow Turb. Combust. 92 (2014) 947–970.

[39] L. H. DOREY, N. BERTIER, L. TESSÉ, F. DUPOIRIEUX - *Soot and Radiation Modeling in Laminar Ethylene Flames with Tabulated Detailed Chemistry*. Comptes Rendus Mécanique 339 (12) (2011) 756–769.

[40] K. M. LEUNG, R. P. LINDSTEDT - *A Simplified Reaction Mechanism for Soot Formation in Nonpremixed Flames*. Combust. Flame 87 (1991) 289–305.

[41] D. POITOU, J. AMAYA, M. E. HAFI, B. CUENOT - *Analysis of the Interaction Between Turbulent Combustion and thermal Radiation Using Unsteady Coupled LES/DOM Simulations*. Combust. Flame 159 (2012) 1605–1618.

Acronyms

HPC	(High Performance Computing)
DNS	(Direct Numerical Simulations)
RANS	(Reynolds Average Navier Stokes)
LES	(Large Eddy Simulations)
PDF	(Probability Density Function)
TFLES	(Thickened Flame model in the LES context)
F-TACLES	(Filtered TAbulated Chemistry for Large Eddy Simulation)
LBO	(Lean Blow-Off limits)
FAR	(Fuel-Air Ratio)
NOMANI	(Nitrogen Oxide emission model with one-dimensional MANIfold)
NOx	(Nitrogen Oxides)

AUTHORS

Bénédicte Cuenot is the leader of the combustion research group at CERFACS, developing advanced softwares for the numerical simulation of turbulent combustion (code AVBP) and heat transfer (code PRISSMA for thermal radiation) in both academic and industrial systems. Dr. Cuenot teaches combustion in various universities and has authored about 70 peer-reviewed journal papers. She is also much experienced in coordinating international projects, mainly financed by the European Commission where she also acts as an expert evaluator.

Ronan Vicquelin is Associate Professor at Centrale Supélec. He is an expert in the fields of high performance computing, turbulent combustion and heat transfer. He is the leader of a HPC ANR project that focuses on flame ignition of a full-scale combustor.

Eleonore Riber senior researcher in the CFD group at CERFACS, obtained her PhD from Institut National Polytechnique Toulouse in 2007. After one year as a researcher at Institut Français du Pétrole - Energies nouvelles (IFPEN), she joined CERFACS in 2008. She contributes to the development of massively parallel two-phase reactive LES applied to energy, process and aerospace propulsion. She has developed expertise in DNS, LES, two-phase flows, chemistry and pollutant emissions modelling. She received two PRACE awards in 2012 (together with EM2C) and 2015 to study ignition mechanisms in a multiple-injectors annular combustor and pressure oscillations in solid rocket motors respectively.

Vincent Moureau is a CNRS researcher at CORIA in the combustion modeling group. He got his Master of Science from Ecole Centrale Paris in 2001 and obtained his PhD from Institut Français du Pétrole and Ecole Centrale Paris in 2004. After a two-year postdoctoral fellowship at Stanford University in the Center for Turbulence Research, he joined Turbomeca, SAFRAN group, as a combustion engineer from 2006 to 2008. Since 2009, his research is focused on turbulent combustion and spray modeling, and on the development of the YALES2 solver for Large-Eddy Simulation and Direct Numerical Simulation of turbulent flows in complex geometries using massively parallel computers. He received the Yves Chauvin award for his PhD thesis in 2005, the 3rd prize of the Bull Joseph Fourier award for the promotion of numerical simulation in 2010 and an IBM faculty award in 2011. He is the coordinator of the Scientific Group SUCCESS devoted to the promotion of super-computing for the CFD of complex flows in realistic geometries.

Ghislain Lartigue obtained is Ph.D at CERFACS in 2005. He then worked as an engineer for 5 years at the Research Division of GDF-Suez, the national gas company, where he developed combustion models and performed numerical simulations for key account customers. He then joined the CORIA lab where he is now co-developer of the YALES2 CFD code. His major fields of expertise are Large Eddy Simulation, combustion, numerical schemes and HPC.

Alexandre Figuer, combustion engineer, has been working at the Methods and Tools Development Department of Safran Snecma Villaroche since 2013. First working on combustion and aerothermal issues with RANS approach, he is now in charge of LES codes industrialization and calibration for combustion chambers design. In that context, he is working in close co-operation with CERFACS and CORIA labs.

Yoann Mery, PhD and research engineer, has been working at the combustor design team at Safran Snecma since 2010. First, as a research engineer with particular focus on pollutant prediction, advanced simulation (LES) and combustion instabilities (2010-2013). Then, in charge of the operability performances of combustors. Now he is a combustion expert (pollution and operability), and responsible for the upcoming emissions and smoke certification of the Silvercrest engine.

Jean Lamouroux, combustion engineer, received his PhD from EM2C in 2013. He joined TURBOMECA as a combustion methodology and tools engineer. His fields of expertise cover the LES modelling of turbulent combustion and pollutant formation.

Stéphane Richard, combustion engineer, received his PhD from EM2C and IFPEN laboratories in 2005. After 8 years working at IFPEN , he joined TURBOMECA as a combustion engineer, head of advanced computation methods for SAFRAN. His fields of expertise cover the LES modelling of turbulent combustion, two-phase flows and pollutant emissions, as well as chemistry kinetics, reduced order modelling for Automotive and Aeronautic engines.

Laurent Gicquel, senior Researcher at CERFACS/CFD, obtained his PhD in Mechanical Engineering from State University of New York (SUNY) at Buffalo in 2001 and his HdR from Institut National Polytechnique de Toulouse in 2007. He contributes to the development of massively parallel LES and acoustic solvers for industrial applications. His areas of expertise cover: turbulent reacting flows, Large-Eddy Simulations, Direct Numerical Simulations, two-phase flows, pollutant emissions, stochastic processes, combustion instabilities, turbomachinery flows. He is scientific expert for EU, ANR, DOE, NRC…

Thomas Schmitt is research scientist at EM2C, CNRS, CentraleSupelec. He defends his PhD at Cerfacs in 2009. He is now expert in the field of numerical simulation of turbulent combustion, applied to liquid rocket engine, gas turbine and combustion instabilities.

Sébastien Candel earned a PhD from the California Institute of Technology in 1972 and a Docteur ès Sciences degree from the University of Paris 6 in 1977. He is a University professor emeritus at Ecole Centrale Paris (now CentraleSupélec) and honorary professor at Institut Universitaire de France. His research contributions reported in more than 200 articles have mainly concerned combustion and aeroacoustics with applications in energy and aerospace propulsion. Among many distinctions, Sébastien Candel has been the recipient of the the Marcel Dassault Grand Prize of the French Academy of sciences, the Silver medal and Zeldovich Gold medal both from the Combustion Institute. Sébastien Candel is a member of the French Academy of sciences (its Vice-President for 2015 and 2016), the French Academy of technologies, the Air and Space Academy and he is a foreign member of the National Academy of Engineering of the United States.

F. Dupoirieux, N. Bertier, C. Guin, L.-H. Dorey
(ONERA)
K.P. Geigle, C. Eberle, P. Gerlinger
(DLR)

E-mail: francis.dupoirieux@onera.fr

DOI : 10.12762/2016.AL11-07

Methodology for the Numerical Prediction of Pollutant Formation in Gas Turbine Combustors and Associated Validation Experiments

For aircraft engine manufacturers the formation of pollutants such as NOx or soot particles is an important issue because the regulations on pollutant emissions are becoming increasingly stringent. In order to comply with these regulations, new concepts of gas turbine combustors must be developed with the help of simulation tools. In this paper we present two different strategies, proposed by ONERA and DLR respectively, to simulate soot or NOx formation in combustors. The first one is based on simple chemistry models allowing significant effort to be spent on the LES description of the flow, while the second one is based on more accurate, but also more expensive, models for soot chemistry and physics. Combustion experiments dedicated to the validation of these strategies are described next: The first one, performed at DLR, was operated at a semi-technical scale and aimed at very accurate and comprehensive information on soot formation and oxidation under well-defined experimental conditions; the second one, characterized at ONERA, was aimed at reproducing the severe conditions encountered in realistic gas turbine combustors. In the third part of the paper the results of combustion simulations are compared to those of the validation experiments. It is shown that a fine description of the physics and chemistry involved in the pollutant formation is necessary but not sufficient to obtain quantitative predictions of pollutant formation. An accurate calculation of the turbulent reactive flow interacting with pollutant formation and influencing dilution, oxidation and transport is also required: when the temperature field is correctly reproduced, as is the case of the ONERA simulation of the DLR combustor, the prediction of soot formation is quite satisfactory while difficulty in reproducing the temperature field in the TLC combustor leads to overestimations of NOx and soot concentrations.

Introduction

The combustion inside gas turbine burners generates emissions of the greenhouse gas CO_2, as well as pollutants such as NOx, CO, soot particles and UHC (Unburned HydroCarbons). Increasingly stringent regulations are being introduced to require lower emissions in newly manufactured aircraft engines. A decrease in CO_2 emissions is achieved through various paths, among these the increase in the OPR (Operating Pressure Ratio) of the gas turbine. The increase in the pressure inside the GT (Gas Turbine) combustor leads to a better thermodynamic efficiency of the engine and also tends to minimize the effect of incomplete combustion and therefore to limit CO and UHC emissions. On the other hand, this pressure increase leads to a higher combustor inlet temperature, which results in turn in a higher temperature inside the combustor and thus greatly favors NOx formation. The incorporation of more stringent regulations for NOx emissions is therefore a very challenging task, which requires the development of new combustor concepts. Figure 1, extracted from Ralph and Baker [1], shows the evolution of the regulations as well as the mid-term and long-term goals for NOx emissions. In figure 1, past and present regulations have a positive slope of tolerated emissions with increasing OPR in order to not impede the development of engines with a high OPR. However, in future this slope will be smaller: this makes the compliance with future NOx regulations much more difficult for high OPR engines.

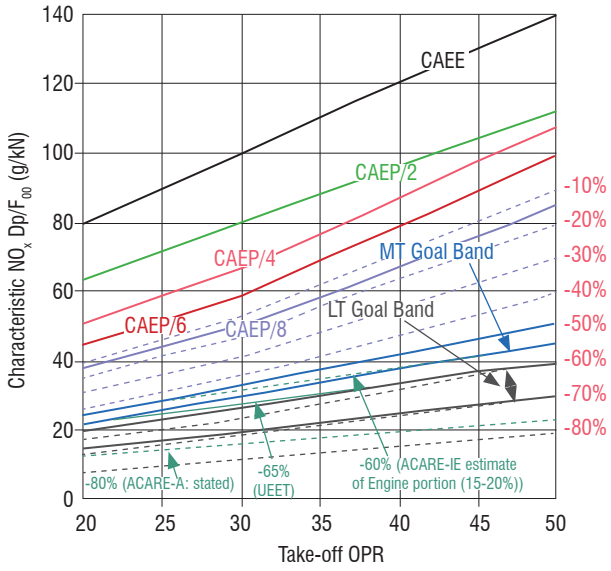

Figure 1 – Regulations and mid-term/long-term (MT/LT) goals concerning the NOx emissions per unit engine thrust as a function of the OPR at take off

Until now, the regulation for aircraft emissions of particulate matter, including soot, was based on the evaluation of the Smoke Number (SN) [2], which is quite rough considering that parameters such as particle size, particle number density or surface reactivity of particles are not accessible by the SN, but are essential to define the harmfulness of these emitted particles. In recent engine developments, the size of emitted particles decreased and the particle number simultaneously increased, while the filters used for measuring SN are significantly less sensitive to small particles. For that reason, significant efforts are spent to define measurement procedures for engine certification, which will be routinely used at the industrial level and replace the SN evaluation to yield more detailed information on the emitted particulate matter (Delhay *et al.* [3], Black *et al.* [4] and Petzold *et al.* [5]). This expected change in the regulations for particulate matter emissions is another point that must be tackled by engine manufacturers, without compromising achievements in NOx emission minimization.

In order to design new engines complying with these future regulations, aircraft manufacturers need support from numerical tools that are able to predict pollutant formation, especially NOx at high pressure and soot particles, which largely contribute to the harmful particles emitted by the combustion chamber. The design and development of low NOx combustors based on lean premixed combustion is particularly troublesome because they are prone to instabilities (see for example Cohen *et al.* [6], Lieuwen [7]). RQL (Rich Quick quench Lean) combustors (Feitelberg *et al.* [8], Jermakian *et al.* [9]) are less sensitive to thermoacoustics because the fuel rich section ensures combustion stability but, unfortunately, the potential for NOx reduction is limited. The more recently developed TAPS devices (Stickles and Barrett [10]) include pilot injection to stabilize the combustion and a main multi-hole injector to prompt the fuel-air mixing. The determination of the best geometry and optimal distribution between pilot and main injection at different flight regimes is very challenging.

Many attempts to predict NOx formation in gas turbine combustors can be found in the literature. Some are based on steady-state methods (Riesmeier *et al.* [11], for example) and contain an accurate description of the chemistry, but are not designed to capture combustion instabilities. Others are based on LES (Large Eddy Simulation) and can provide insight into instability mechanisms, but contain relatively simple chemistry (Schmitt *et al.* [12], for example). One possible approach to combine LES with a complex chemistry, including NOx formation, is tabulated chemistry (Godel *et al.* [13], for example). The validation of the methodology for these NOx simulations is not an easy task, because generally NO or NOx measurements are only achieved by gas sampling at the exit of the combustors (Ibas *et al.* [14], Landman *et al.* [15], for example). Sometimes, the sampling probe is moved inside the flame to obtain information at different locations, but in most examples the flame configuration is far from that encountered in gas turbine combustors (Li and Williams [16], Sze *et al.* [17], for example), moreover, the flow field governing the global flame behavior is significantly affected by such intrusive measurement techniques. Spatially resolved, non-intrusive NO measurements by LIF (Laser Induced Fluorescence) have also been carried out in flames (Meier *et al.* [18], Sick *et al.* [19], Meier *et al.* [20], Bessler *et al.* [21], van Essen *et al.* [22], for example), but again the configuration (pure diffusion or pure premixed flames) and the experimental conditions (laminar or low pressure flames, fuel reduced to pure CH_4 or H_2) are far from those of gas turbine combustors.

Some difficulties also appear in the development of numerical tools for soot predictions. The physics of soot formation is known to be very complex because it involves complex chemical mechanisms occurring both in the gaseous phase and at the interface between the small solid soot particles and the surrounding gaseous phase, see for example Bockhorn [23]. Developing reliable numerical tools for soot prediction requires the physical submodels to be adequately selected, in order to obtain the best compromise between accuracy and computation cost. Considering the high complexity of the phenomena that must be reproduced by the soot models, the numerical tool must be carefully validated by comparison with experiments. In the past, soot formation was first studied experimentally in laminar flames, in order to facilitate the measurements and to discard the additional complexity of turbulence; see for example Santoro *et al.* [24], Vandsburger *et al.* [25], Quay *et al.* [26], McEnally and Pfefferle [27]. Experimental studies in laminar flames are still being achieved, mainly to scrutinize the influence of pressure and/or mixture ratio on soot formation (Arana *et al.* [28], McCrain and Roberts [29], Thomson *et al.* [30], Desgroux *et al.* [31], Joo and Gülder [32]). These experiments serve to validate, without difficulties induced by the fluid flow complexity, physical models for soot formation intended to be introduced in CFD codes (Leung *et al.* [33], Blacha *et al.* [34]). Soot formation has also been experimentally studied in unsteady and turbulent flames, which provide conditions more resembling technical burners (Shaddix and Smyth [35], Qamar *et al.* [36], Lemaire *et al.* [37], Henriksen *et al.* [38], Köhler *et al.* [39], Mueller *et al.* [40], Geigle *et al.* [41-43]). In parallel, some attempts to simulate the soot formation in unsteady or turbulent flames have been made (Said *et al.* [44], Pitsch *et al.* [45], Zamuner and Dupoirieux [46], Yoo and Im [47], Lignell *et al.* [48], Narayanan and Trouvé [49], Köhler *et al.* [39], Bisetti *et al.* [50], Mueller and Pitsch [51], Attili *et al.* [52]). Nowadays, unsteady simulations of the DNS or LES type yield satisfactory results concerning the description of the turbulent flow, but are not yet able to reliably predict soot distributions, mainly because it is very difficult to correctly predict the concentration of soot precursors, which are made up of minor species such as acetylene (C_2H_2), benzene (C_6H_6), and polycyclic aromatic hydrocarbons (PAH). The prediction of the size distribution of the soot particles is particularly challenging. It can be obtained by resolution of transport equations, one for each size section, as obtained by Köhler *et al.* [39], or for moments of the soot particle size distribution as done by Mueller and Pitsch [51], or by a Lagrangian approach as was done by Zamuner and Dupoirieux [46], or Dupoirieux *et al.* [53]. Whatever

	DLR experiment	ONERA-SNECMA experiment
Main flow features	• C_2H_4/air non-premixed swirled injection • Optional air dilution in the downstream part of the combustor • Pressure from 1 to 5 bar	• Two-swirl air injection including pilot and multi-holes injectors for liquid kerosene • Pressure from 4 to 20 bar
Optical or sampling measurements and visualizations	• PIV velocity measurements (non-reactive and hot conditions) • CARS temperature measurements with complete local statistics • OH and PAH PLIF visualizations • LII soot measurements	• CARS temperature measurements with complete local statistics • OH and PAH PLIF visualizations • LII soot measurements • NO and NOx emission index by gas sampling and analysis

Table 1 – Main features of the validation experiments

the method, the computational effort is significant with a large number of transport equations to solve in the first case and a large number of fluid particles to track in the second case. According to the available computational power, different strategies can be used to apply numerical soot prediction to the practical situation of GT combustors: soot simulation in post-processing as used by Barths *et al.* [54], flamelet approach as used by Riesmeier *et al.* [11], or LES as used by Mueller and Pitsch [55]. In this paper we propose two strategies for soot prediction in GT combustors, which can be considered as a good compromise between accuracy and computational effort.

The next section presents two possible numerical methodologies, proposed by ONERA and DLR respectively, for the simulation of soot and NOx formation. Section "*Experiments for the validation of the numerical strategies of pollutant prediction*" describes experiments for the validation of these methodologies: the first one, performed at DLR (Geigle *et al.* [42]), can be considered as a semi-technical scale experiment and focuses on soot; the second one, carried out at ONERA, reproduces the real conditions encountered in a GT combustor. Section "*Calculation of the DLR burner for validation purposes*" displays validations resulting from the comparison of the simulations with the experiment of Geigle *et al.* [42,43], and Section "*ONERA Calculation of the TLC combustor*" presents the numerical results corresponding to the ONERA experiment. To clarify the presentation tables 1 and 2 hereafter summarize the validation experiments and calculations described in this paper.

Physical models and associated numerical methodology

ONERA methodology

The numerical methodology proposed for the prediction of soot formation in GT combustors is based on LES simulations carried out by the CEDRE software (Refloch *et al.* [56]). The resolution of the compressible Navier-Stokes equations for the gaseous phase is achieved by the solver CHARME and the evaporating fuel droplets are tracked using the Lagrangian solver SPARTE. These two solvers of CEDRE operate in a two way coupling mode: On the one hand, CHARME provides SPARTE with all of the information necessary to calculate the instantaneous drag force acting on droplets and the heat flux leading to heating and vaporization of the liquid phase; on the other hand, SPARTE provides CHARME with the mass flux, momentum, energy and turbulent kinetic energy delivered to the gaseous phase from the liquid droplets. The SPARTE module is used only in the second calculation presented in this paper, since the first burner studied (DLR combustor) is operated with gaseous fuel, i. e., ethylene.

In our LES calculations the usual Smagorinsky viscosity is used to take into account the effect of turbulent structures smaller than the mesh size and a law of the wall adapted to the turbulence subgrid model yields the stress tensor on the walls. The interaction between chemistry and turbulence is tackled with the help of the Artificially Thickened Flame model (ATF) for LES (Selle *et al.* [57]). In this approach the thickening factor F and the efficiency function E are introduced into the transport equations of the reactive species, to modify the diffusion and chemical term. The transport equation of the k^{th} species is then written as:

Simulation \ Experiment	DLR experiment		ONERA-SNECMA experiment	
DLR	• 3D URANS • Detailed finite rate chemistry for soot precursors • Sectional PAH model • Two-equation soot model	Comparison with: • OH visualizations • LII soot visualizations		
ONERA	• 3D LES • Thickened flame model and tabulated chemistry • Soot model of Leung	Comparison with: • CARS temperature measurements • LII soot measurements	• 3D LES • Thickened flame model and tabulated chemistry with β PDF • Soot model of Leung • Definition of a specific progress variable for thermal NO prediction	Comparison with: • CARS temperature measurements • LII soot measurements • NO and NOx emission index

Table 2 – Validation calculations

$$\frac{\partial \bar{\rho}\tilde{Y}_k}{\partial t}+\frac{\partial\left(\bar{\rho}\tilde{u}_i\tilde{Y}_k\right)}{\partial x_i}=\frac{\partial}{\partial x_i}\left\{\bar{\rho}\left[FED_k+\left(1-\alpha\right)D_k^t\right]\frac{\partial \tilde{Y}_k}{\partial x_i}\right\}+\frac{E}{F}\dot{\omega}_k$$

with $F=1+\alpha\left(F^{\max}-1\right)$ (1)

In this equation, α is a sensor function varying from 0 far from the flame (low values of $|\dot{\omega}_k|$) to 1 inside the flame (high values of $|\dot{\omega}_k|$). $F^{\max}$ is the parameter that determines the artificial thickening of the simulated flame and E is a function that takes values equal to 1 far from the flame and greater than 1 inside the flame. This function is aimed at recovering the effect of the flame folding lost by the artificial thickening and in our calculations its formulation is that described by Colin *et al.* [58]. In the numerical model, the diffusion coefficient inside the flame is equal to FED_k, where D_k is the physical laminar diffusion coefficient and FE is a factor much greater than 1, and far from the flame it is equal to D_k^t, the small scale turbulent diffusion coefficient given by the Smagorinsky formulation. As indicated in [57], a value of 25 for $F^{\max}$ seems reasonable to correctly resolve the flame front in the usual LES computation grids.

The source term $\dot{\omega}_k$ is usually governed by the chemical kinetics, which can be simplified if only the main steps of the fuel oxidation are taken into account. However, when soot formation has to be calculated, the situation is more complicated because the concentration of minor species, such as C_2H_2 or C_6H_6, which are soot precursors, or OH, which is a soot oxidizer, must be known. That means that a detailed chemistry including a large number of chemical species must be considered in the calculation. In order to avoid the resolution of a large number of transport equations for the chemical species, a tabulated chemistry approach is used in conjunction with the ATF model. Tabulated chemistry has been extensively used to simulate turbulent combustion in the last decades, see for example Maas and Pope [59], Gicquel *et al.* [60], Van Oijen *et al.* [61], Fiorina *et al.* [62] and Kuenne *et al.* [63]. From the theoretical point of view, the tabulated chemistry is well adapted to the opposite cases of combustion, i. e., premixed flames and diffusion flames, for which two different types of flamelet manifolds can be created, but not to intermediate situations of partially premixed flames that can be encountered in GT combustors. However, it can be shown (Vreman *et al.* [64]) that determining the features of a partially premixed flame from a set of laminar premixed flamelets covering a large domain of mixture ratios leads in practice to satisfactory results. Therefore our approach of tabulated chemistry is based on a premixed flamelet manifold indexed by two parameters: the progress variable C and the mixture fraction Z. Before normalization, the progress variable is defined as

$$C=\frac{Y_{CO}}{M_{CO}}+\frac{Y_{CO_2}}{M_{CO_2}}+\frac{Y_{H_2O}}{M_{H_2O}} \quad (2)$$

For a given value of the mixture fraction Z the progress variable C monotonically evolves from 0 in the fresh gases to a maximum value $C^{\max}(Z)$. This maximum value is commonly referred to as $C|_{eq}$ considering that species included in the definition of C have reached chemical equilibrium. The normalized progress variable c with values within the interval [0,1] is finally defined as

$$c=\frac{C}{C|_{eq}} \quad (3)$$

Note that for the simulation of NOx formation the definition of C must be adapted to take into account the large characteristic time scales associated with the thermal NO mechanism. In that case, an additional term with the mass fraction of NO is introduced in Eq. (2), as indicated in section "*Calculation of NOx emissions*".

The mixture fraction Z is defined as

$$Z=Y_C+Y_H \quad (4)$$

Y_C (respectively Y_H) is the mass fraction of carbon (respectively hydrogen) atoms, whatever their molecular combination. Z is obviously varying between 0, in points where no fuel and no species resulting from the fuel combustion are present (oxidizer side), to 1, where only unburnt fuel or non-oxidized species resulting from the fuel cracking are present (fuel side).

Transport equations for the main species, i. e., fuel, O_2, CO, CO_2, H_2O and N_2, are solved with a reaction source term calculated as

$$\dot{\omega}_k=\dot{\omega}_k^{TAB}\left(c,Z\right)+\frac{Y_k^{TAB}\left(c,Z\right)-\tilde{Y}_k}{\tau} \quad (5)$$

where the superscript TAB corresponds to values picked in the flamelet manifold and τ is a characteristic time linked to the chemistry (see Boucher *et al.* [65]). The last term of this equation is introduced to prevent departures of the concentrations calculated with the transport equations from the values given by the table for the same indexing parameters c and Z. In practice this correction term, introduced only for numerical reasons, is small in absolute value compared to the reaction source term picked from the table. The concentrations of all minor species such as NOx, soot precursors or soot oxidizers, i. e., NO, NO_2, C_2H_2, C_6H_6, OH, are directly picked from the chemical table. The resolution of transport equations for the main species rather than picking their concentrations in the chemical table is necessary to account for diffusion properties not linked directly to those of c and Z. The progress variable C is obtained through Eq. 2 from the concentration of the main species. Considering that a non-negligible part of the C and H atoms can be contained in non-transported species, Z is obtained by resolution of a transport equation with accurate inlet conditions deduced from the fuel composition. This equation describes the mixing between fuel and oxidizer and implicitly contains the assumption that all species have the same diffusion coefficient.

For soot predictions, simple models inducing a low CPU time have been considered: the model of Magnussen *et al.* [66], and the model of Leung *et al.* [33]. These models require two additional transport equations. For the Magnussen model, these equations concern the soot mass fraction Y_S and the number of inception nuclei per volume unit. In the Leung model two transport equations are solved to calculate the soot mass fraction Y_S and the number N of soot particles per mixture mass unit. Acetylene (C_2H_2) is the precursor of soot in the Leung model while fuel is the precursor in the Magnussen model. Soot oxidation is achieved by O_2 in both models, but in addition oxidation by OH is considered in the Leung model. After various tests on 1D flames, the Leung model has been selected at the expense of the Magnussen model, which turned out to be too rough. The Leung model takes into account the steps of nucleation, surface growth, oxidation and agglomeration:

	Reaction rate (kmol·m^{-3}·s^{-1})	Preexponential factor A (SI unit)	Temperature exponent β	Activation temperature T_a (K)
Nucleation	$K_n(T)[C_2H_2]$	0.1×10^5	0	21100
Surface growth	$K_g(T)[C_2H_2]$	1.4×10^4	0	12100
O_2 oxidation	$K_{Oxid.O2}(T)\cdot S\cdot[O_2]$	0.1×10^5	0.5	19680
OH oxidation	$K_{Oxid.OH}(T)\cdot S\cdot[OH]$	106	-0.5	0

Table 3 – Soot reaction kinetics

Nucleation: $C_{ü}H \rightarrow 2C_S + H$

Surface growth: $C_2H_2 + C_S \rightarrow 3C_S + H_2$

Oxidation: $C_S + \frac{1}{2}O_2 \rightarrow CO\,,\ C_S + OH \rightarrow CO + H$

Agglomeration: $nC_S \rightarrow (C_S)_n$

The notation C_s refers to carbon atoms included in soot particles. As it is written, the nucleation step means that one mole of acetylene can lead to two moles of carbon included in nascent soot particles. The source terms of the balance equations induced by these different steps can be found in the work by Leung *et al.* [33] and Lecocq *et al.* [67]. Kinetic details of nucleation, surface growth and oxidation reactions are listed in table 3.

In this table, S, which appears in the oxidation rates, refers to the total surface of soot particles per volume unit and the quantities $K_i(T)$ $(i=n, g, Oxid.O_2, Oxid.OH)$ depend on T according to

$$K_i(T) = AT^{\beta}e^{-\frac{Ta}{T}}$$

The agglomeration rate is given by

$$\vec{I} = \left\langle \left(1+\frac{u_0^2}{c_{ü}^2}\right) p\vec{u} + \vec{u}_0\left(\rho_0 u^2 + \frac{p^2}{\rho\, c^2}\right)\right\rangle \qquad (6)$$

where C_A is equal to 9, M_C is the molar mass of the carbon atom ($12\cdot10^{-3}$ kg), ρ_{soot} is the soot density (1800 kg/m^3), κ is the Boltzmann constant and ρ is the mixture density.

To sum up the numerical methodology, transport equations with chemical source terms deduced from the tabulated chemistry and adapted to LES are solved for the main species, and the soot parameters, i. e., the soot volume fraction and the number of particles per mixture mass unit, are obtained from transport equations with source terms given by the Leung model. In these source terms the concentration of minor species, such as C_2H_2 or OH, is directly taken from the chemical tables. A similar methodology is used by other teams, see Cuenot *et al.* [68].

DLR methodology

Soot and PAH sub-models are implemented in the DLR code THETA. THETA is an unstructured finite-volume solver, which has been optimized for low Mach number combustion problems. Combustion is modeled by finite-rate chemistry, where a separate transport equation is solved for each species. Chemical reactions involving soot and PAHs are formulated in Arrhenius form and solved by the finite-rate chemistry model, in the same way as the chemistry of gas phase species, thereby allowing full coupling of soot, PAHs and the thermo-chemical state of the gas phase. The soot and PAH sub-models conserve both mass and atoms.

Chemical and physical processes of soot evolution and the corresponding modeling strategies followed by DLR are summarized in figure 2. The kinetics of gas phase species, including combustion and pyrolysis of small hydrocarbons such as ethylene and the formation of small aromatics, e.g., benzene and toluene, is described by a detailed chemical mechanism including 43 species and 304 elementary reactions, which is derived from the mechanism of Slavinskaya and Haidn [69]. Sub-mechanisms for kerosene combustion (16 species / 68 reactions) and formation of nitrogen oxides (17 species / 103 reactions) can optionally be added to the chemical model.

Only a brief description of the PAH and soot models is given here; more details are given in the works of Di Domenico *et al.* [70], and Blacha *et al.* [34]. Polycyclic aromatics hydrocarbons (PAHs) are discretized by three mass classes (bins) and described by a sectional approach. PAH chemistry is divided into four processes: PAH formation by interaction of the first PAH bin and gas phase, acetylene condensation, collisions between different PAH classes and PAH oxidation by hydroxyl (OH) and molecular oxygen (O_2).

Two modeling strategies for the evolution of the soot aerosol are followed. In the sectional soot approach developed by Blacha *et al.* [34], the size distribution of soot particles is discretized by 25 bins covering particle diameters from 1.3 nm to 329 nm. Since the computational cost of the sectional soot model is high (a separate transport equation must be solved for each bin), a two equation soot model developed by Di Domenico *et al.* [70], is frequently applied for simulations of complex combustion configurations, such as the model combustor addressed in this work. In two equation models, spherical soot particles and mono-disperse particle size distributions are assumed and soot is described by two independent variables, i.e., soot mass fraction and particle number density. Soot nucleation is modeled by PAH growth reactions involving the last PAH bin and soot surface growth is modeled by condensation of acetylene and PAHs onto the soot surface. Soot oxidation by OH and O_2 is taken into account. Coagulation is considered, using a collision frequency formulation, which is applicable to any Knudsen number regime. In order to demonstrate predictive capability, the soot model was validated for different laminar flames (Blacha *et al.* [34]) and a turbulent sooting jet flame (Köhler *et al.* [39]), where a good overall agreement was found using the same set of model constants for all test cases.

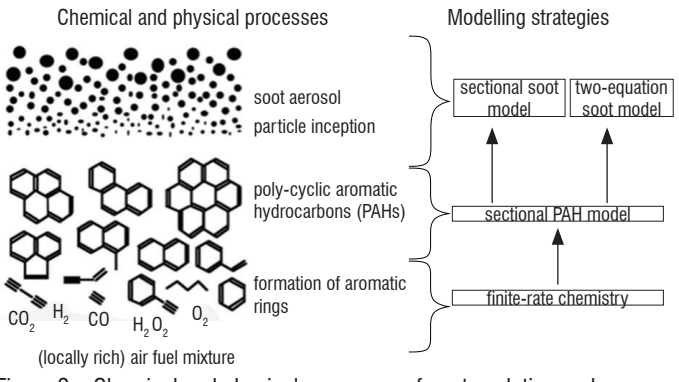

Figure 2 – Chemical and physical processes of soot evolution and corresponding modeling strategies followed by DLR

Experiments for the validation of the numerical strategies of pollutant prediction

The experimental validation of the numerical simulation of pollutant formation is a difficult task, because various issues must be considered: The accuracy of the pollutant prediction depends, on the one hand, on the detailed description of the physico-chemical phenomena triggering the pollutant formation and consumption and, on the other hand, on our ability to reproduce the main features of the turbulent flow. Another point is that we have to deal with different types of pollutants such as NOx, soot, CO, UHC (Unburnt HydroCarbons), which have their own physics and/or chemistry. As the prediction of soot formation is generally considered to be more challenging than that of NOx or CO, we focus here on the description of two experiments dedicated to the validation of numerical strategies to predict the soot formation in GT combustors. The first one has been performed by DLR and the second one by ONERA with the support of a DLR team for the soot measurements by laser-induced incandescence (LII).

DLR experiment

Burner setup

The objective of the DLR experiment is to reproduce some of the conditions encountered in gas turbine combustors (turbulence, swirl, increased pressure, secondary air injection), but to exclude the difficulties linked to the behavior of the liquid fuel phase. The burner described in more detail by Geigle *et al.* [41,42] is equipped with a dual swirl injector for a central and an annular air flow, which can be controlled separately, and a ring of tiny fuel nozzles injecting ethylene between both swirled air flows. At the exit of this injector, the flow is over stoichiometric on average, thus prompting soot formation in fuel-rich pockets. The combustor has a square cross section measuring 68 × 68 mm^2 with beveled edges and a length of 120 mm. Large combustion chamber windows measuring 127×59 mm^2 and thick pressure windows, both made of quartz, allow for good optical access; the former serve to maintain the high flame temperatures, the latter the pressure, which was increased up to 5 bar. Although the pressure can be much higher in GT combustors, already moderately increased pressure allows its effect on soot formation to be studied. 80 mm downstream from the main injector exit secondary air can be introduced through four pipes measuring 5 mm in diameter, fed through the four posts holding the combustion chamber windows. This secondary air injection is useful to study the oxidation of the soot particles formed in the upstream part of the burner. The exact geometry of the combustion chamber is shown in figure 3 and described by Geigle *et al.* [41-42].

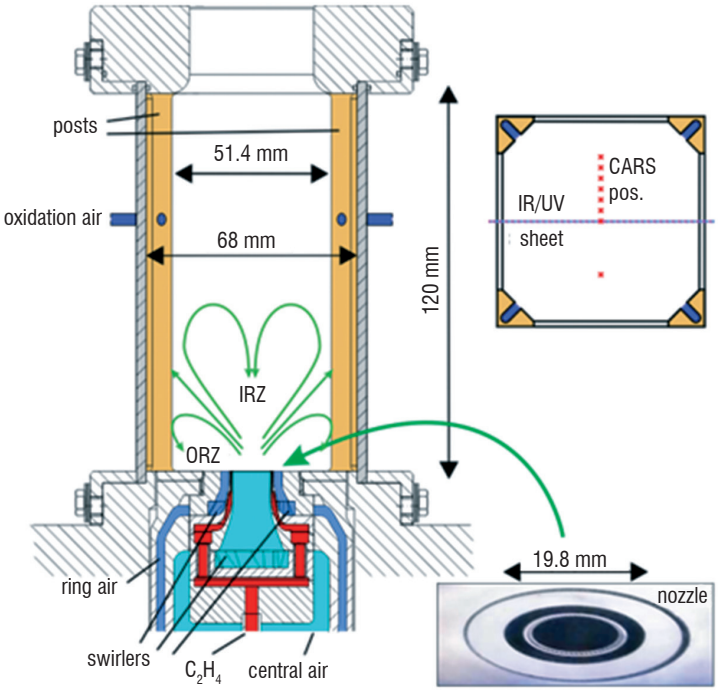

Figure 3 – Cross section of the DLR swirl burner operated with ethylene. The upper insert shows a horizontal cross-section at the height of the oxidation air inlets, as well as the locations of laser excitation for the diagnostics used

Laser-based diagnostics

A total of 16 operating points has been characterized by various laser diagnostic techniques, as presented in [41]. The suite of measurement techniques used consists of laser-induced incandescence (LII) for soot volume fraction distributions, laser-induced fluorescence (LIF) to determine OH and PAH distributions, shifted vibrational coherent anti-Stokes Raman scattering (SV-CARS) for temperature statistics and particle image velocimetry (PIV) (Geigle *et al.* [41-43], [71]). The challenging and/or time-consuming CARS and PIV techniques were only applied to a down-selection of operating conditions, while all flames are characterized by LII and LIF. The most comprehensive data set exists for the so-called reference flame at 3 bar and a primary equivalence ratio Φ of 1.2, which drops to 0.86 globally by addition of 40% oxidation air.

P [bar]	Φ	$P_{primary}$ [kW]	$Q_{air,c}$ [slpm]	$Q_{air,r}$ [slpm]	Q_{fuel} [slpm]	Q_{oxi} [slpm]	$Q_{air,c}/Q_{air}$	Q_{oxi}/Q_{air}	Φ_{global}	P_{global} [kW]
3	1.2	32.2	140.8	328.5	39.3	187.4	0.3	0.4	0.86	38.6

Table 4 – Flame conditions of the reference flame used as a validation case within this publication: Pressure, p, mass flows for air through the burner (central and ring), $Q_{air,c}$, and $Q_{air,r}$, fuel, Q_{fuel}, oxidation air through secondary air inlets, Q_{oxi}, equivalence ratios, Φ, Φ_{global}, thermal powers, P, P_{global}, and fractions $Q_{air,c}/Q_{air}$ and Q_{oxi}/Q_{air} with $Q_{air}=Q_{air,c}+Q_{air,r}$. Flow rates are referenced to 1.013 bar and 273 K.

A detailed description of the diagnostic application is contained in the work by Geigle *et al.* [41-43], [71]. Therefore, only a short overview is provided here. For the quantitative soot volume fraction measurements obtained by Geigle *et al.* [41], a well-characterized laminar laboratory flame (Trottier *et al.* [72]) was inserted into the optical setup instead of the pressurized swirl flame, to serve as reference for the calibration of the LII signal to soot concentration. A homogeneous laser sheet with a height of 30 mm was used for the 1064 nm excitation of the LII signal recorded at 450 nm perpendicular to the excitation plane. For spatial correlation with OH and PAH LIF distributions, the LII laser sheet was expanded to 47 mm and an additional 90 mm high UV light sheet was introduced by a suitable dichroic mirror. For OH excitation, the UV laser was tuned to the $Q_1(8)$ line of the $A^2\Sigma$-$X^2\Pi$ (1,0) transition at λ=283.55 nm, PAH were excited slightly off-resonant of the OH transition, requiring higher pulse energies. The ultraviolet species emission was separated from the path of the LII signal by a suitable UV mirror and detected through a band pass filter centered around 315 nm (OH) or 300-400 nm (PAH); a temporal delay of both laser pulses with a duration of 400 ns was applied to temporally separate both effects. For PAH, the combination of excitation and detection wavelengths allows the monitoring of mainly small aromatic molecules consisting of two to four aromatic rings. Exemplary ensemble-averaged distributions are shown in figure 4. Figure 4a shows the OH distribution generated by the primary flame fed by combustion air and fuel; here, the additional oxidation air was switched off. Figs. 4b-4d display the reference flame conditions with oxidation air switched on. The OH distribution shows significantly increased OH levels in the center of the combustor, which is generated by the additional oxidation air when coming into contact with unburnt hydrocarbons surviving the primary reaction zone. The PAH distribution appears a bit higher in the flame, delayed by few millimeters. Further delayed relative to PAH, soot is visible in a V-shaped distribution. The central combustor remains soot-free due to the oxidative influence of the oxidation air, which is partly transported upstream into the inner recirculation zone, as visible by the significant OH signal levels. Instantaneous distributions show that small soot filaments fill the gaps left in the OH distributions between primary combustion and the OH generated by the oxidation air [42]. Simultaneous PAH/soot maps allow the identification of isolated PAH clouds, PAH transforming into soot and isolated, transported soot filaments [43].

The upstream influence of the oxidation air is also visible in the stereo PIV images in figure 5. These images were recorded upon dual-pulse excitation with 100 mm tall laser sheets at 532 nm. For acquisition, two cameras were mounted as close as possible to the pressure flange of the combustor to yield a stereoscopic viewing angle of approx. 37°. The non-reactive case (3 bar, Φ=1.2, with oxidation air) is displayed in figure 5 left, clearly showing that the oxidation air is entrained upstream into the inner recirculation zone. For the reference operating point at Φ=1.2 under reactive conditions ensemble averaged velocities could be measured as a sum-of-correlation only due to the strong flame luminosity; replacing the initially used 10 nm bandwidth filter by a 2 nm filter provided a better suppression of soot luminosity, but resulted in a relatively small field of view due to its low transmission at non-perpendicular incident angles. A less sooting yet representative flame at Φ=0.9 is shown as ensemble average of 1000 instantaneous images in figure 5 right.

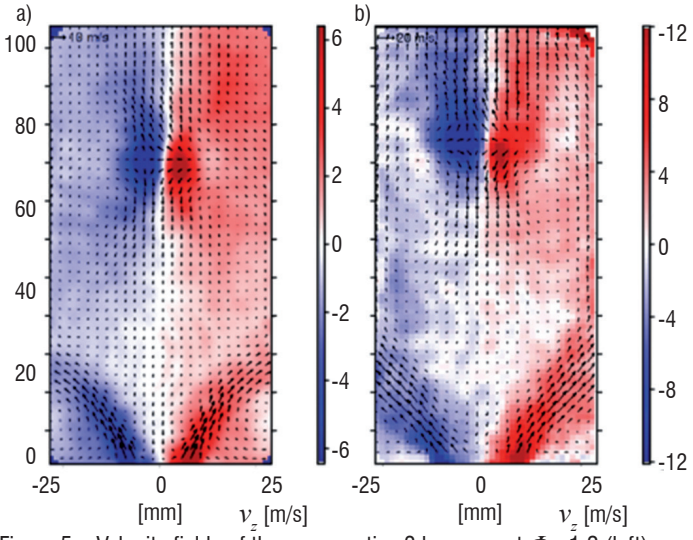

Figure 5 – Velocity fields of the non-reactive 3 bar case at Φ=1.2 (left) and a leaner yet sooting and representative reactive case at Φ=0.9 (right). Arrows show the in-plane velocity components, color represents the out-of-plane velocity

The application of CARS to the sooting swirl flames follows the approach presented by Tsurikov *et al.* [73]. Broadband N_2 vibrational CARS was applied in a folded BOXCARS configuration with excitation of the CARS signal by focusing and overlapping two narrowband laser beams at λ=582 nm and one broadband laser beam at $\lambda\approx$685 nm. The measurement volume was determined to be 1.6 mm long and 300 μm wide without flame. Figure 4d shows the measurement locations in the reference flame, figure 6 shows exemplary temperature statistics in the position on the axis where the oxidation air jets meet (a) and low in the inner recirculation zone (b). This type of temperature statistics, acquired at multiple locations in the flame, is highly valuable for model validation, as soot formation and oxidation strongly depend on local temperature.

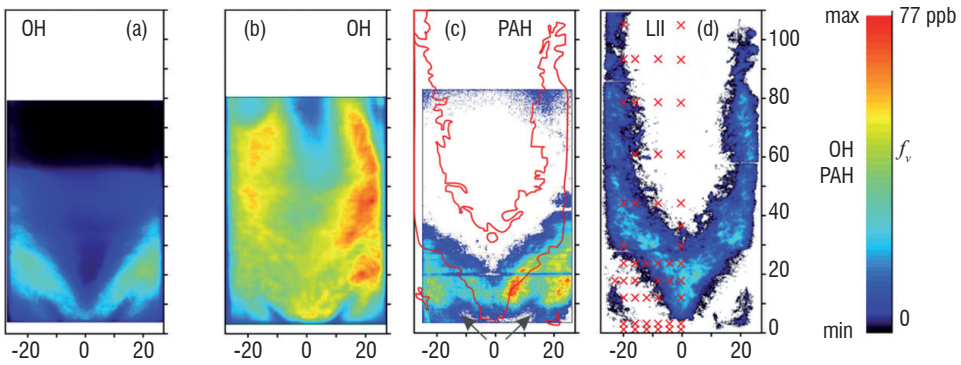

Figure 4 – Species distributions in reference flame (b) OH, (c) PAH, (d) soot. Without oxidation air injection (a) the OH distribution remains located at the bottom of the combustor; (c) also contains a contour of the soot distribution from (d), (d) shows labels where temperature statistics were measured by CARS

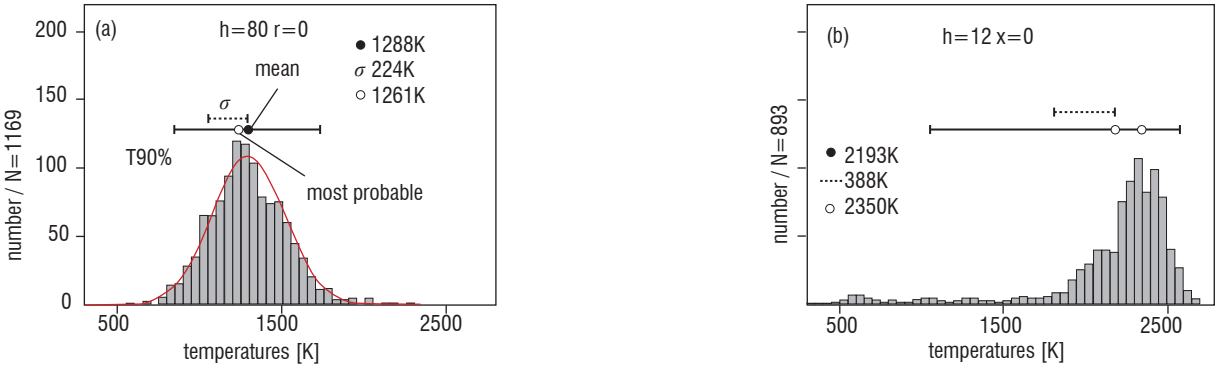

Figure 6 – Temperature statistics in the reference flame (a) at the stagnation point where the oxidation air jets meet and (b) low in the inner recirculation zone. The plots show mean and most probable temperatures and the width of the distribution, either as a range covering 90% of the instantaneous temperatures or as a width of a Gauss distribution where suited (dotted)

ONERA-SNECMA TLC experiment

The TLC experiment has been performed in the M1 facility of ONERA (see Cochet *et al.* [74]) within the framework of the TLC FP6 project [75] coordinated by Snecma Moteurs, known today as Safran Snecma. This experiment is aimed at providing a deep insight into a reactive flow subjected to conditions very close to those of a real aircraft gas turbine. It involves a single low NOx air-fuel injector feeding a combustor with a 105 × 105 mm² cross-section equipped with lateral visualization windows. The liquid fuel is introduced on the one hand through a pilot injector and on the other hand through a multi-hole device in proportions that vary according to the flight regime: at low power most of the fuel is introduced through the pilot in order to obtain stable combustion, whereas at high power multi-hole injection is used in order to minimize NOx emissions. At the end of the combustion chamber, a nozzle with adjustable cross-section serves to vary the pressure between 4 and 20 bar. 4 sets of experimental conditions corresponding to the taxi, approach, climb and cruise regimes respectively, have been considered. Each set has its own pressure, inlet air temperature, pilot/multi-hole distribution and FAR (Fuel Air Ratio). Figure 7 displays the configuration of the TLC experiment. Note on the right part of the figure the arm crossing the flow upstream of the exit nozzle: This arm is used for gas sampling followed by exhaust gas analysis.

All of the air used for combustion goes through a swirler in the air-fuel injector in order to give a strong swirl to the reactive flow. Figure 8 shows the configuration of the injector.

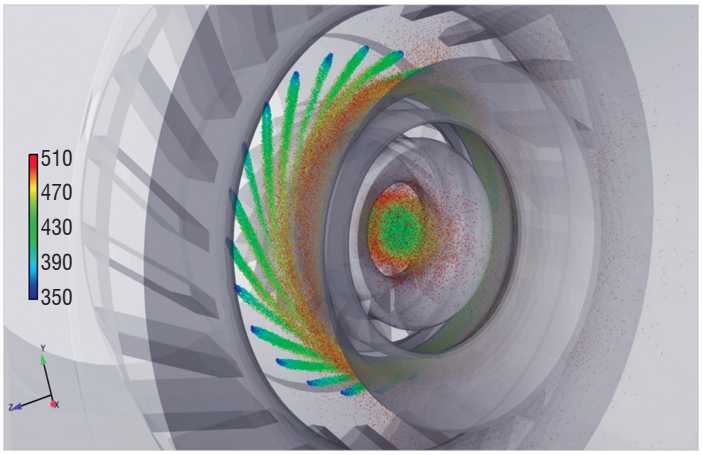

Figure 8 – Low NOx injector configuration; the colored part corresponds to simulated fuel droplets injected through the pilot (on the axis) and multi-hole devices (periphery); the color denotes the droplet surface temperature (scale in K)

In order to characterize the liquid phase PDA (Particle Doppler Anemometry), measurements have been carried out. They provide the early size and velocity distributions of the fuel droplets. These measurements are very useful to set the inlet conditions of the liquid phase in the calculation, because the simulation of the primary atomization is still out of reach in such semi-industrial cases. In order to locate the area where fuel evaporation and combustion take place LIF (Laser Induced Fluorescence)

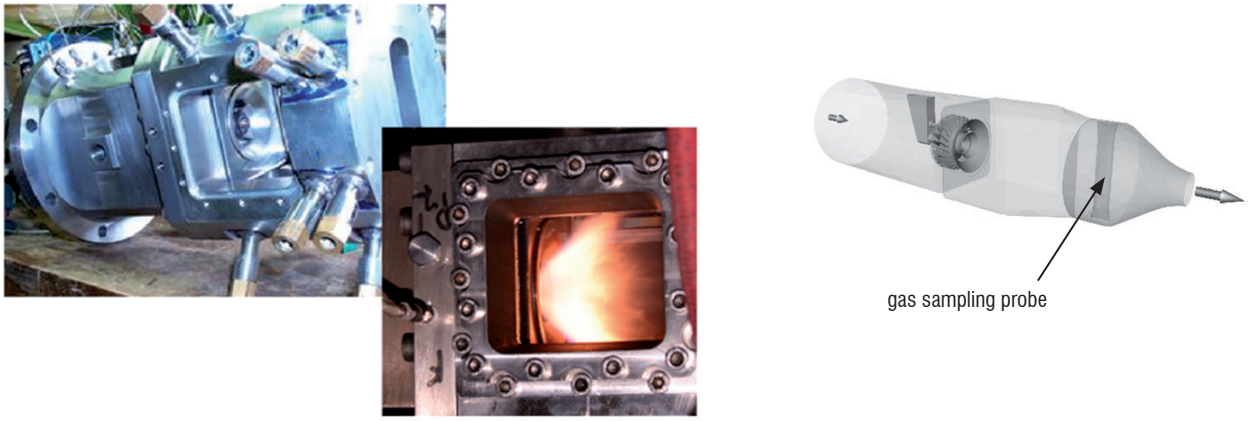

Figure 7 – Lateral view of the TLC combustor without and with combustion (left), schematic view of the TLC set-up with its downstream part including gas sampling probe and exit nozzle (right)

visualizations based on species resulting from fuel vaporization (mainly aromatics) and on the OH radical have been performed. Figure 9, extracted from the work of Orain *et al.* [76], shows that fuel evaporation takes place in a conical, v-shaped region located just downstream from the injector and that combustion, characterized by the presence of the OH radical (right), appears immediately downstream from the fuel evaporation in the shape of a very open cone, the upstream edge of which is attached to the injector.

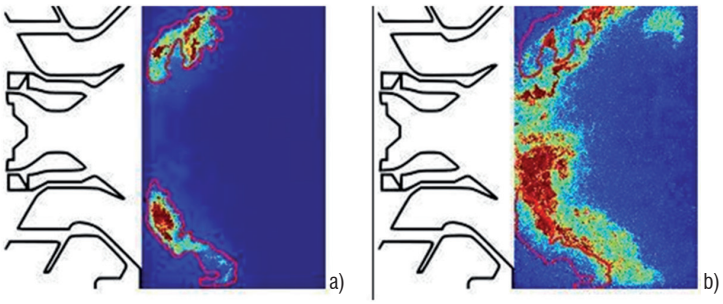

Figure 9 – Instantaneous LIF visualization of the fuel vapor (left, A), and of the OH radical (right, B); the same purple contour lines enclose the fuel vapor area on the left and right parts of the figure

Temperature is a crucial parameter because it greatly influences the features of the average flow, as well as the rate of pollutant formation. Temperature measurements by CARS have been achieved along 4 vertical lines crossing the combustor axis and situated respectively 20 mm, 29 mm, 51 mm and 65 mm downstream from the injector exit. Figure 10 shows the temperature profiles obtained for operating pressures of 4 and 19.5 bar in the last measurement cross-section.

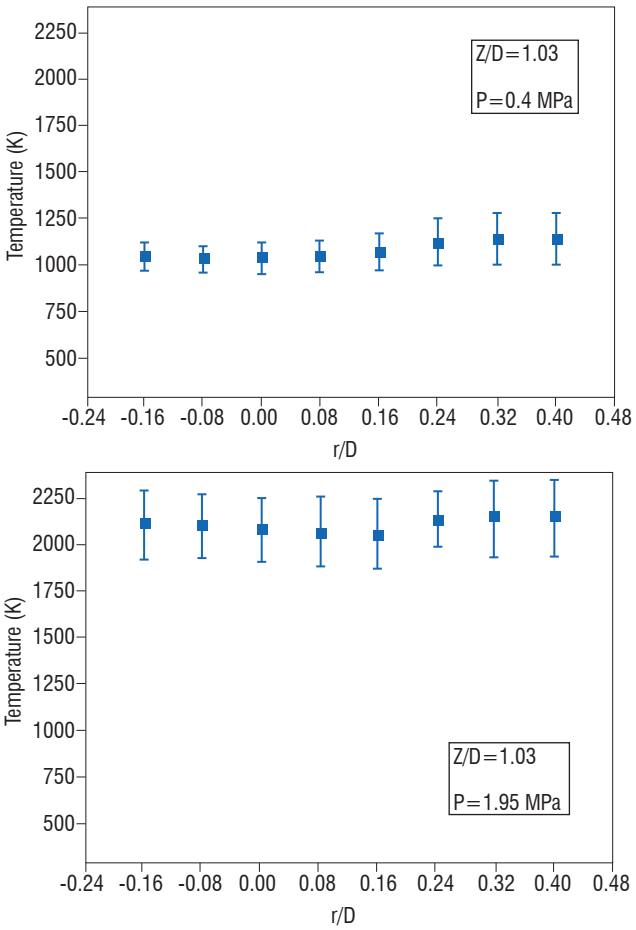

Figure 10 – Temperature profiles 65 mm downstream from the injector exit at 4 bar (left) and 19.5 bar (right) (abscissa: cross-coordinate r divided by D = 64 mm)

It can be noticed that these profiles are quite flat. This indicates a good quality of mixing in the central recirculation induced by the swirled injection. The temperature is much higher at high pressure because the FAR is larger at 19 bar (2.7 %) than at 4 bar (1.35 %).

A DLR team achieved LII measurements of soot in the TLC burner in the ONERA M1 facility for the 4 sets of experimental conditions [77]. Figure 11 shows the soot volume fraction field obtained for approach flight conditions (pressure of 9.5 bar), which are the most favorable to soot formation, knowing that take-off conditions are not inducing the highest rate of soot formation when a multi-hole injector is used.

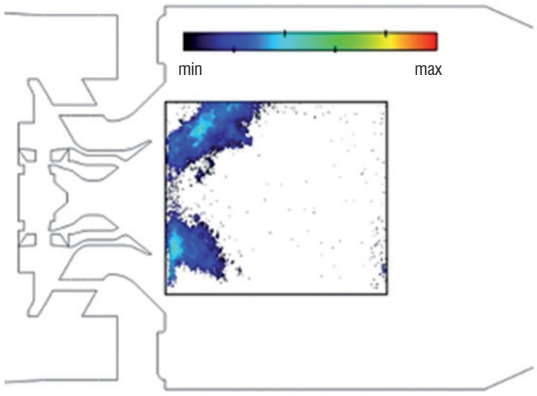

Figure 11 – Soot volume fraction field obtained by LII under approach flight conditions (arbitrary scale)

The emissions of other pollutants, such as NOx, CO, UHC were measured by various gas analyzers after sampling at the outlet of the combustor. These analyzers gave us the emission index of each pollutant, i. e., the quantity of pollutant created for a given quantity of fuel injected in the combustor. For example, the NOx emission index is 2.3 g of NOx per kg of fuel for approach flight conditions.

All of these measurements and visualizations make up a set of data that are very valuable for the validation of numerical simulations. This experiment is complementary to that performed at DLR: After the validation step based on the DLR experiment in the case of gaseous fuel, the TLC experiment enables us to check that the model describing the fuel vaporization is adequately coupled with the combustion and pollutant formation models. Note that the set of data will be considered as complete only after achievement of the PIV (Particle Imaging Velocimetry) campaigns that are planned for the TLC experiments: The knowledge of the velocity field is of great importance for the validation of the simulations.

Calculation of the DLR burner for validation purposes

ONERA simulation

The DLR experiment described in section "*DLR experiment*" has been selected to test our numerical strategy for soot prediction. Figure 12 shows a schematic view of the DLR burner and the associated upstream plenum in which injection of primary air and ethylene is prepared. The square and round sections correspond to the burner and plenum respectively. The swirled injection is located between the plenum and the burner. The four pipes connected to the second half of the burner correspond to secondary air injection aimed at oxidizing soot.

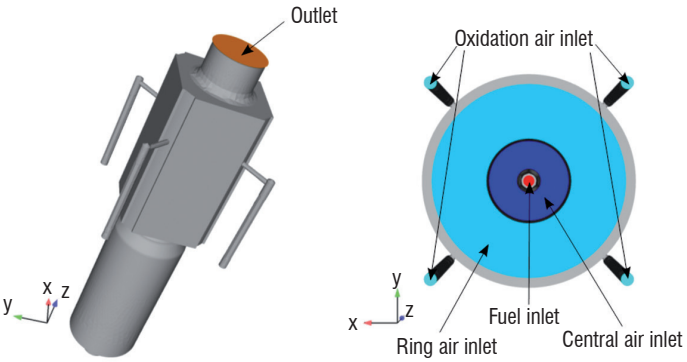

Figure 12 – The DLR burner: left, overall view of the burner and the plenum that supplies the injector; right, fluid supplies inside and beside the plenum upstream of the swirlers

The computational domain, shown in figure 13, includes a small part of the plenum, the swirled injection, the burner with the four injection sections for secondary air and a large open volume downstream from the combustor introduced to damp acoustic waves. The overall calculation grid is made up of 12.8 M tetrahedral cells. In order to take advantage of parallel processing the calculation grid has been divided into 256 parts distributed over the same number of processor cores. For the spatial discretization a MUSCL scheme of order 2 with a Roe type flux decomposition and a Van Leer type limiter is used. The time integration is implicit, which enables a relatively large time step of 10^{-6} s.

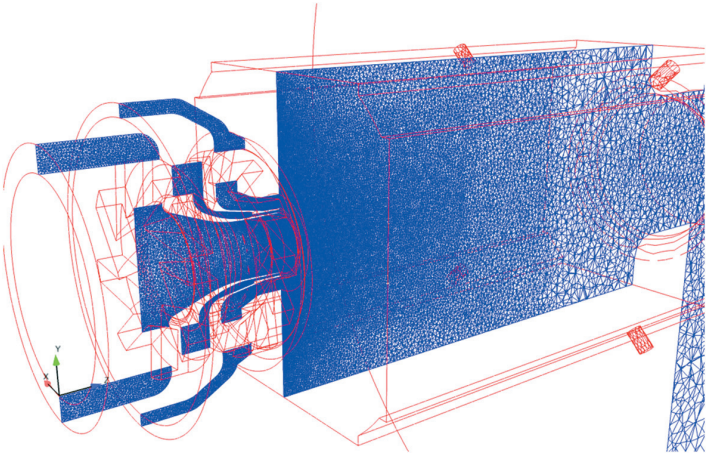

Figure 13 – Axial cut of the calculation grid

For the calculation, the case at 3 bar with secondary air injection has been selected among the 16 operating conditions studied [41]. As indicated in table 4, the global power of the burner is 38.6 kW and the equivalence ratio is 1.2 before dilution by secondary air and 0.86 after dilution. The injected volume flow rates from table 4 are translated in mass flow in table 5.

Boundary	Value
Central air inlet	*3.020 g/s*
Ring air inlet	*7.047 g/s*
Oxidation air inlet	*4.020 g/s*
Fuel inlet	*0.818 g/s*

Table 5 – Injection flow rates

On the burner walls, the following temperatures are imposed. The temperature is equal to 700 K on the lateral walls and 500 K on the wall orthogonal to the axis in the injection section.

Figure 14 shows instantaneous and time-averaged temperature fields obtained by the calculation. Hot gases are recirculated back to the injector by the central recirculation induced by the swirl and can be found inside the injector. A possible explanation of this phenomenon is that the internal injector surfaces have been considered as adiabatic, so the decrease in the gas temperature inside the injector can be underestimated. The zone of lower temperature around the axis in the second half of the burner is a result of secondary air injection.

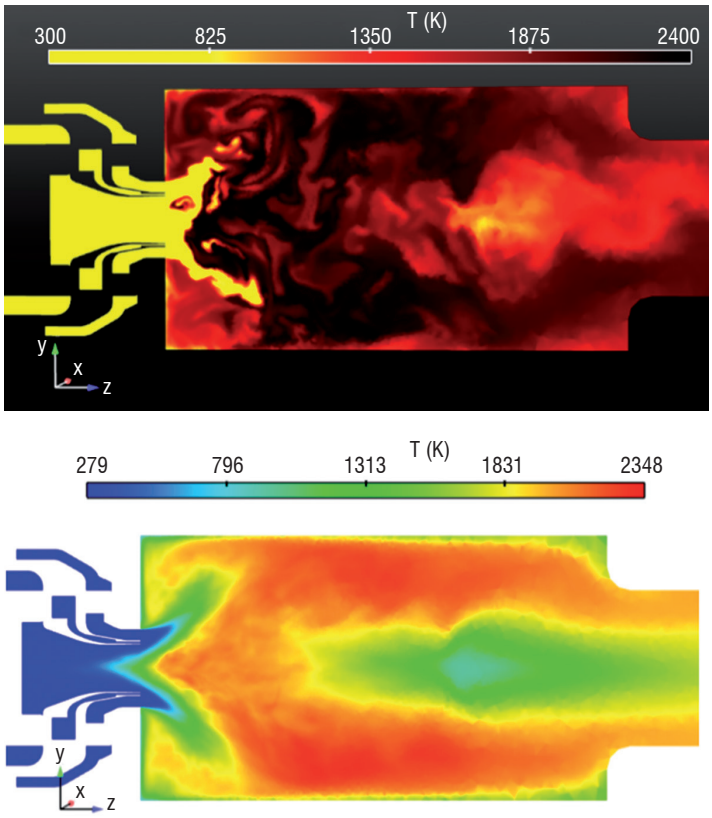

Figure 14 – Calculated instantaneous temperature field (top); averaged temperature field (bottom)

Temperatures obtained by averaging the LES calculation and those obtained experimentally by CARS are compared in figure 15. In the three profiles located near the inlet of the chamber (within the first three millimeters) we note that CARS measurements do not determine hot gases in the center of the injector, unlike the simulation, which gives a temperature of about 1000 K on the axis in the section x=3 mm. As mentioned previously, the presence of hot gases may be induced by non-adequate thermal boundary conditions inside the injector. However, since soot precursors such as acetylene are produced much further downstream, the discrepancy in the injection section has no influence on the soot formation. Despite an overestimation of the temperature for x between 12 and 24 mm, the agreement between measurements and simulation in cross-sections where the soot formation and oxidation are present is quite satisfactory. The simulation of soot formation can therefore be carried out with relative confidence concerning the temperature dependence of the source terms given by the Leung model.

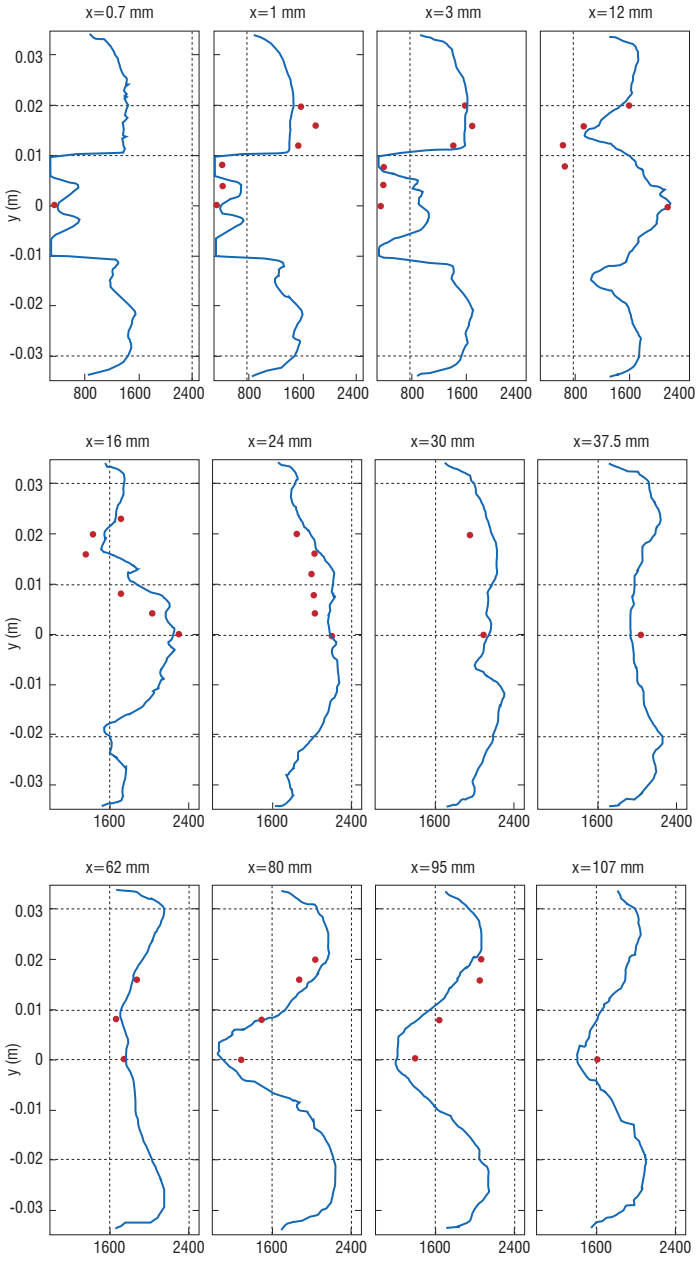

Figure 15 – Continuous lines: temperature profiles obtained by LES averaging; discrete points: CARS temperature measurements. All temperatures are plotted in K, x is the distance from the inlet section

Figure 16 shows, for a lengthwise cross-section, the map of the soot volume fraction obtained by the averaging of the LES calculation and the map resulting from time-averaging of the LII measurements. In this figure, the burner axis is vertical and the injection occurs at the bottom. The domain shown in the right part of the figure corresponds to the optically accessible regions of the combustor.

It appears that the calculation quite correctly reproduces the shape of the soot volume fraction distribution with soot formation in a conical region located downstream from the injector and the presence of soot near the walls further downstream. However, in the simulation, unlike in the experiment, the presence of soot does not extend as far as the end of the combustor. This indicates that the soot oxidation is too fast in the simulation and must be investigated further in future work. It can be noted that in both the calculation and the experiment soot is not present on the axis in the last two thirds of the burner: The secondary air penetrating deeply towards the combustor axis and partly recirculating upstream induces the complete oxidation of soot particles, or even prevents their formation in a large area around the burner axis. Another point to be noticed is that the absolute level of the soot volume fraction, of the order of a few hundredths of a ppm, is correctly reproduced by the calculation.

In view of these satisfactory results, our methodology has been applied to the TLC burner quite representative of the conditions encountered in GT combustors.

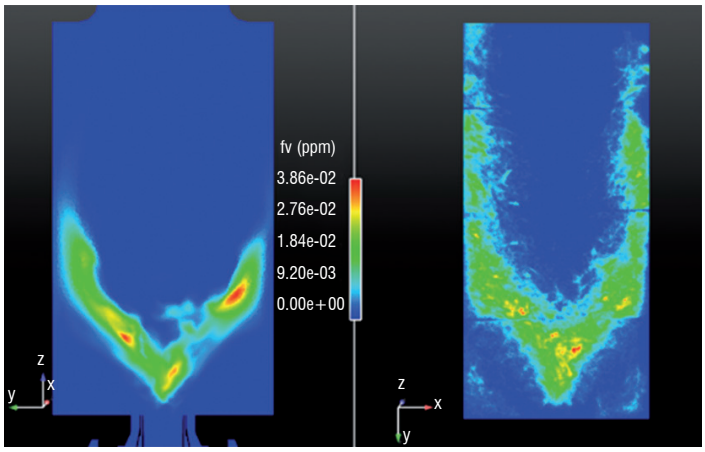

Figure 16 – Soot volume fraction in a lengthwise cross-section of the burner; left, averaged LES; right, LII time-averaged measurements

DLR simulation

Simulation Details

URANS simulations were performed on a 3D fully tetrahedral grid with 6.6 million points corresponding to 36.5 million tetrahedra. Inflow boundaries are placed well upstream of the swirlers. In order to take heat losses into account, isothermal walls are assumed. The estimated wall temperatures based on thermocouple measurements are 350 K for the swirlers, 600 K to 700 K for the combustion chamber and 900 K for the windows. Convective fluxes are discretized by a second-order upwind scheme, while a second-order central scheme is applied for diffusive fluxes. Time integration is carried out by a second-order backward differencing scheme. In order to ensure convergence, a time step width of 0.5 μs was applied.

Pressure-velocity coupling is performed by a projection method (Chorin [78]). Turbulence is treated by a two equation shear stress transport (SST) model (Menter [79]). A multivariate assumed probability density function (APDF) approach is used to close the chemistry turbulence interaction (Gerlinger [80]). The APDF approach is computationally efficient, since only two additional transport equations for the second order moments σ_T (temperature variance) and σ_Y (sum of species variances) are required. Heat radiation by soot is modeled by an optically thin approach (Di Domenico *et al.* [70]). In total, 57 transport equations are solved (five equations for momentum, pressure correction and specific enthalpy; two equations for turbulence modeling; 43 equations for gas phase species; five equations for PAHs and soot; and two equations for the second-order moments σ_T and σ_Y, respectively). Statistics were sampled over a physical time of 60 ms, which corresponds to approximately six flow-through times. The simulation took about 55 days on 256 cores (338000 CPU hours on Intel Xeon X5570 quad-core processors with a clock rate of 2.93 GHz).

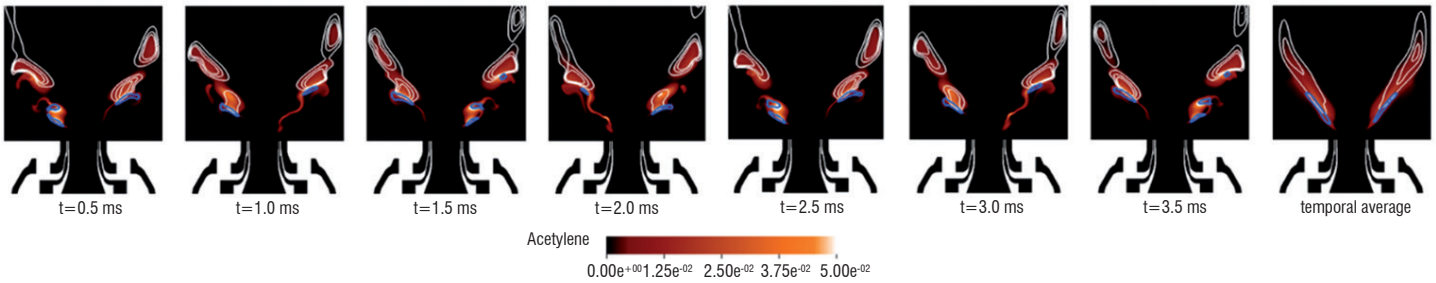

Figure 17 – Series of instantaneous and resulting time-averaged (right) distributions of calculated acetylene mass fractions as well as soot volume fraction isolines (white) and a PAH isoline (blue)

Motivation

The scope of this work is to investigate an efficient method (URANS, finite-rate chemistry with multivariate APDF source term closure and a two-equation soot model) for soot predictions under technically relevant conditions. It was shown in previous work (Eberle *et al.* [81]) that the time-averaged flame structure in terms of velocity field and temperature distribution is accurately predicted by this method, while some disagreement between the measured and predicted soot volume fraction f_v, in particular regarding the shape of the soot distribution, was observed. In contrast to URANS predictions, high soot concentrations were measured on the centerline of the flame. In this work, a time-resolved analysis is presented, providing detailed insight into soot evolution processes and showing the limitations of URANS for soot predictions under technically relevant conditions.

Soot inception and soot surface growth

In order to analyze soot nucleation and growth processes, distributions of acetylene are shown in figure 17 along with isolines of soot and PAH. PAH formation occurs in regions with high acetylene concentrations, since acetylene is a key species in the formation of the first aromatic ring, and small aromatics such as benzene and toluene are required for PAH formation. Conditions favorable for PAH formation are, for example, found at $t = 0.5$ ms in the left hand side flame wing in the vicinity of the injector, while, in contrast, not enough acetylene for PAH formation is present in the right hand side flame wing at $t = 1.0$ ms (the PAH structure observed further downstream was formed earlier).

Soot inception is modeled by PAH growth reactions, which involve the last PAH bin as reactant. Therefore, soot inception occurs only in regions where PAHs are present, for instance at 0.5 ms $< t <$ 1.0 ms in the l.h.s flame wing or at 1.5 ms $< t <$ 2.0 ms in the r.h.s flame wing. By tracking the respective PAH structures, it can be seen that PAHs contribute to further soot growth. Two pathways are possible: Soot inception or surface growth by condensation of PAHs on the soot surface. While regions with high PAH concentrations are small and spatially separated, large regions with high acetylene concentrations are observed. The maximum acetylene mass fraction is approximately five orders of magnitude higher than the maximum PAH mass fraction. By tracking the bottommost soot structure at $t = 0.5$ ms in the r.h.s flame wing, it can be seen that after the corresponding PAH structure is consumed at 1.5 ms $< t <$ 2.0 ms, acetylene continues to contribute to soot surface growth, until all acetylene in the vicinity of this soot structure is consumed at $t = 3.5$ ms. From $t = 3.5$ ms onwards, this soot structure is isolated from PAH and acetylene. In contrast to the measurements, no soot is predicted on the burner axis in the vicinity of the fuel injection. This discrepancy is attributed to the limitations of URANS as discussed below.

Unsteadiness and soot oxidation

In order to shed light on dominant unsteady motions and soot oxidation processes, distributions of the soot oxidants oxygen O_2 (left hand side) and OH (right hand side) are shown in figure 18 along with isolines of the soot volume fraction f_v. The narrow fuel jets are enveloped by the central and annular air jets. A periodic behavior with a frequency $f \approx 500$ Hz resembling a precessing vortex core is observed by tracking the O_2 mass fraction. At $t = 0.5$ ms a low penetration depth of the central air jet is observed, favoring rich combustion conditions and acetylene formation (see figure 17). The penetration depth of the central air then increases until the maximum is reached at $t = 1.5$ ms. At this time, the acetylene concentration is not sufficiently high for PAH production and consequently no new soot structures are formed. From $t = 1.5$ ms on, the penetration depth decreases until the minimum is reached again at $t = 2.5$ ms. At this time, high acetylene concentrations are found and PAHs are formed. Inception of new soot structures occurs between $t = 2.5$ ms and 3.0 ms.

At $t = 0.5$ ms, high O_2 concentrations might prevent soot from penetrating the outer recirculation zone. No significant interactions between oxygen and soot are observed further downstream, however. Soot oxidation by O_2 is thus not dominant in this test case. Soot oxidation by OH is discussed by tracking the soot structures present at $t = 0.5$ ms on the right hand side. The downstream soot structure (located above in the figure) is isolated from acetylene and PAHs at $t = 1.5$ ms and then, due to the subsequent absence of growth processes, oxidized by hydroxyl. At a given instance in space and time, soot and hydroxyl do not coexist due to the high oxidation rates. Unsteady simulations are thus required to properly resolve the correlation between hydroxyl and soot.

Geigle *et al.* [43] performed simultaneous measurements of OH and soot and found zones with low OH concentrations in the inner recirculation zone. These zones were filled with soot filaments. This is in contrast to URANS, which persistently predicts high OH concentrations in the cited region, thereby preventing the existence of soot due to the high oxidative potential of OH. The authors attribute the persistent prediction of hydroxyl to the limitations of URANS, which relies on statistically averaged equations and thus only resolves deterministic unsteady motions. Consequently the reproduction of concentration filaments seems difficult with URANS but Large-Eddy Simulations are expected to resolve the instantaneous hydroxyl distribution more accurately and to subsequently predict soot in this region with better agreement against measurements.

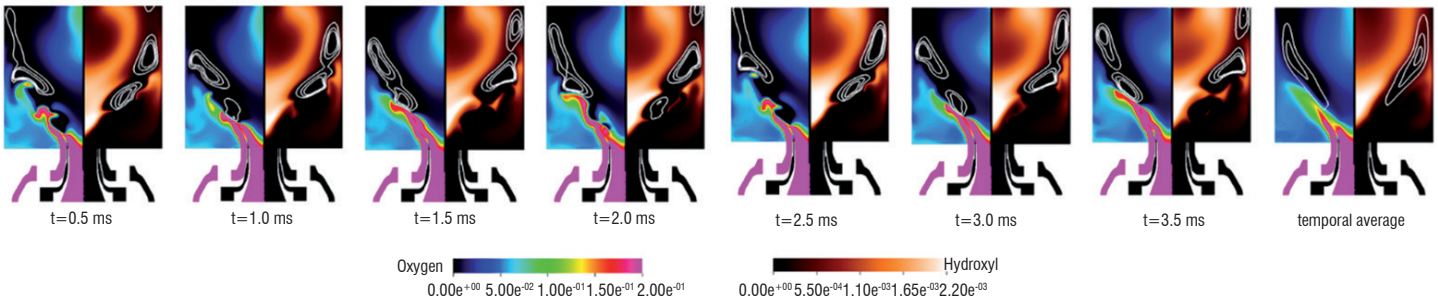

Figure 18 – Series of instantaneous and resulting time-averaged (right) distributions of calculated molecular oxygen (left hand side of the respective plot) and hydroxyl mass fractions (right hand side of the respective plot), as well as soot volume fraction isolines

Conclusions and outlook

URANS simulations of an aero-engine model combustor using finite-rate chemistry with a multi-variate assumed PDF source term closure and a two-equation soot model were successfully performed. A time-resolved analysis of soot evolution revealed that soot nucleation is influenced by a periodic unsteady motion at f ≈ 500 Hz. In contrast to the measurements, URANS does persistently predict high hydroxyl concentrations on the central axis of the burner, which prevents soot presence in this region. Large-eddy simulations will be performed next, in order to better predict the instantaneous hydroxyl distribution and to subsequently obtain better agreement between the calculated and measured soot volume fraction. In the planned simulations, a sectional soot model will be used to obtain information regarding the particle size distributions.

ONERA calculation of the TLC combustor

Main features of the simulated turbulent reactive flow

This section presents the conditions and the main features of the ONERA simulation of the TLC combustor. The liquid kerosene is introduced for one part close to the combustor axis through a pilot injector creating a liquid hollow cone along the burner axis (pilot stage), and for another part into an annular flow of swirled combustion air through a set of small holes equally distributed over a ring normal to the burner axis (main stage). Considering that the use of liquid fuel can induce stronger mixture fluctuations, an assumed PDF $P(Z)$ of the mixture fraction Z is introduced in the calculation of the reaction rate, so that Eq. (5) is replaced by

$$Ra(x,r) \propto \frac{1}{T}\int p'(x,r,t)\,q'(x,r,t)\,dt \qquad (7)$$

The computational domain, shown in figure 19, includes the plenum used to supply the injection, the TAPS injector, the combustor, the choked nozzle used to impose the required pressure in the combustor and a large open volume with large meshes to damp perturbations induced by acoustic waves traveling in the calculation domain when the low external pressure is recovered. Two calculation grids have been tested, one with 4 M tetrahedral cells, 2.1 M being assigned to the combustor, one with 10 M tetrahedral cells, 5 M being assigned to the combustor.

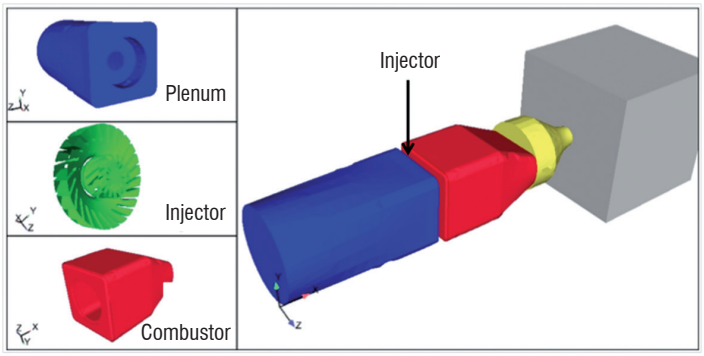

Figure 19 – Computation domain for the TLC calculation; plenum in blue, TAPS injector in green, combustor in red and choked nozzle in yellow

The operating conditions which are modeled are given in table 6. They correspond to an intermediate flight regime, which has been selected because the proportion of fuel injected through the pilot stage is relatively high (50 %). Thus, more soot is produced than at full power, for which a larger proportion of fuel is injected through the main stage. For combustion of the vaporized kerosene, the chemical kinetics of Luche *et al.* [82] is considered.

Condition	Value
Air inlet MFR through TAPS injector (Mass Flow Rate)	*0.485 kg/s*
Total MFR of cooling air along walls	*0.232 kg/s*
Kerosene MFR main stage	*6.434 g/s (50 % of the total fuel MFR)*
Droplet diameter (single value)	*25 µm*
Kerosene MFR pilot stage	*6.434 g/s (50 % of the total fuel MFR)*
Droplet diameter (single value)	*15 µm*
Air inlet temperature	*592 K*
Lateral wall temperature	*700 K*
Other walls	*Adiabatic conditions*
Chamber pressure	*9.5 bar*

Table 6 – Conditions of the TLC calculation

Before applying the above mentioned numerical strategy for soot prediction, a first calculation has been carried out with a simple combustion model (two step mechanism for kerosene oxidation) and a relatively coarse numerical grid made of 4 M cells. Some large discrepancies between the temperatures obtained by this calculation and the measured temperatures have been noted. Consequently, a more refined calculation grid including 10 M cells has been created and used for a new calculation achieved with the same simple combustion models. The refined grid greatly improved the numerical results, although the agreement on temperatures remained unsatisfactory. As the use of a larger grid was not possible for practical reasons, this grid of 10 M cells has been adopted to apply our numerical strategy for soot prediction. The use of a more sophisticated combustion model based on tabulated chemistry did not result in better agreement concerning the temperature.

Figure 20 shows the temperature field obtained numerically with tabulated chemistry and the grid of 10 M cells.

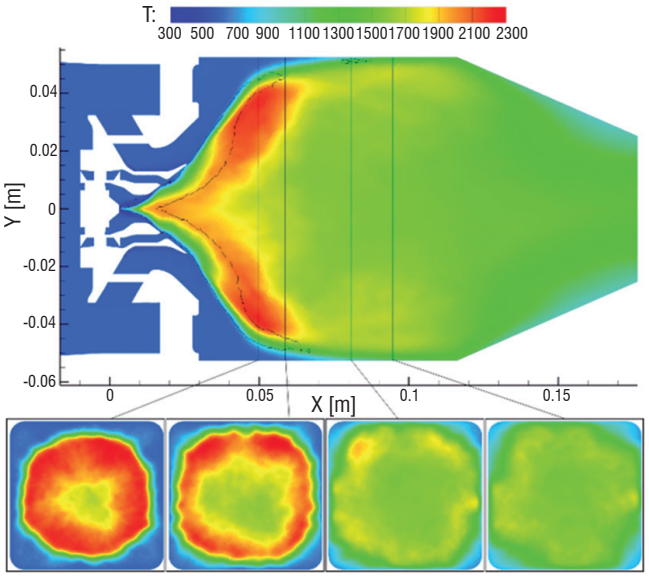

Figure 20 – Temperature field obtained numerically (temperatures in K); cross-section views are given for the four sections where CARS measurements have been performed

Figure 21 gives a comparison of the profiles of averaged temperature and temperature fluctuations obtained numerically and experimentally by CARS. BFER refers to the simple mechanism of kerosene oxidation, while FTC refers to the tabulated chemistry used to obtain the reaction terms of the main species and the concentration of the minor species involved in the soot formation or oxidation. The higher temperature obtained numerically in the recirculation induced by the injection swirl is difficult to explain: in Dorey [83], the CFD simulation was coupled with an accurate radiative transfer calculation using a Monte Carlo method, in order to take into account the radiative heat losses. Due to the low soot volume fraction and the important reabsorption of the emitted radiation by the media, the decrease in temperature induced by the radiative heat loss is hardly greater than 20 K: this heat loss does not explain the difference (relative) to the experiment. Surprisingly, the agreement between experiment and simulation is much better for the fluctuations than for the averaged values.

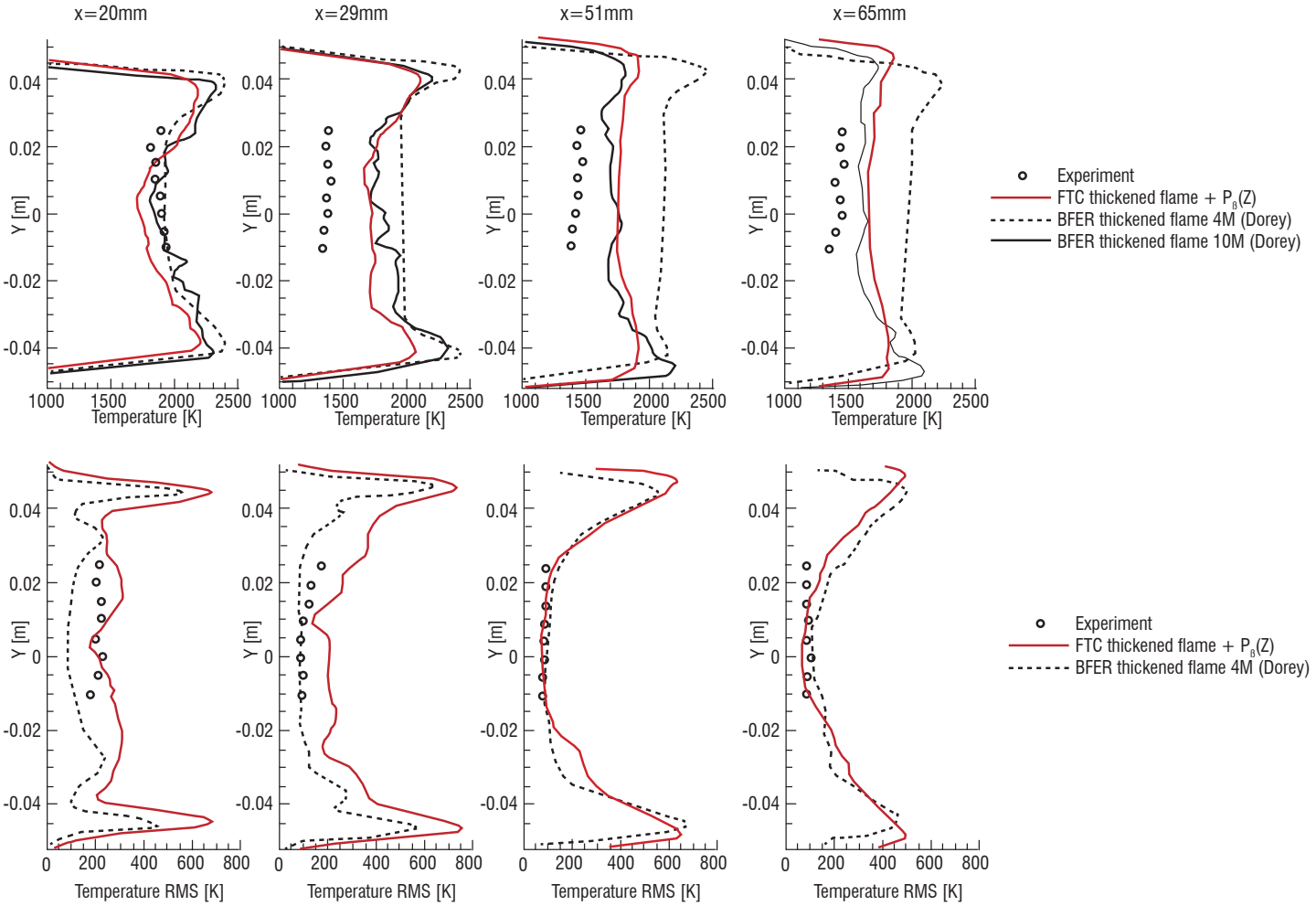

Figure 21 – Profiles of averaged temperature and temperature fluctuations obtained experimentally and numerically; temperature fluctuations have been evaluated only for the FTC calculation with 10 M cells and the BFER calculation with 4 M cells

Calculation of NOx emissions

Pollutants known as NOx are made up of the NO and NO_2 species, which are produced during combustion in small quantities compared to species resulting from the fuel oxidation. The tabulated chemistry described in section "*Physical Models and Associated Numerical Methodology*" gives access to minor species concentrations and therefore can be considered as an appropriate methodology to calculate NOx formation. However, implementation is far from trivial because NOx formation involves characteristic chemical times which are much larger than those of fuel oxidation. This means that the usual progress variable defined by Eq. (2) is not applicable to correctly discretize the NO mass fraction gradients in the chemical manifold, since a very small change in c can lead to a very large change in the NO mass fraction in the post-flame region. This problem can be addressed by including the NO mass fraction into the definition of the progress variable (Godel *et al.* [13], Boucher *et al.* [65]) or by transporting NO in the simulation instead of picking its concentration in the chemical table (Vreman *et al.* [64], van Oijen and de Goey [84]). As suggested by Van Oijen and De Goey [84], we have combined the two solutions: a transport equation is solved for the NO mass fraction and the variable progress is now defined, before normalization, as:

$$C = C_{init} + \kappa \frac{Y_{NO}}{M_{NO}} \qquad (8)$$

where C_{init} is the initial non-normalized progress variable, κ is a non-dimensional constant, M_{NO} is the molar mass of NO and Y_{NO} is the NO mass fraction. The value of κ has been taken equal to 100 as recommended by Boucher *et al.* [65]. Other authors (van Oijen and de Goey [84]) recommend a higher value, but such a high value is necessary only when the NO mass fraction remains very small and barely impacts the value of C. The introduction of the NO_2 mass fraction into the progress variable is not necessary: given that the conversion of NO into NO_2 is relatively slow in the considered combustors, Eq. (8) leads to a monotonic evolution of C with the oxidation process.

The tabulated chemistry based on the kinetics of Luche *et al.* [82] used in our simulations includes both mechanisms of prompt and thermal NO formation. The approach combining the new definition of the progress variable and the transport equation for NO leads to the NO mass fraction field shown in figure 22.

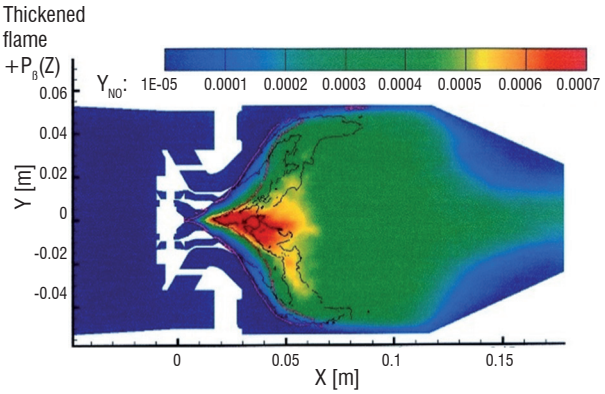

Figure 22 – NO mass fraction field in the lengthwise mid-plane

The high mass fraction observed in the conical part of the central recirculation results from high temperatures and a large residence time. Near the outlet section, the NO mass fraction is lower because most of the gas mixture reaching the combustor exit bypasses the central recirculation, thus avoiding a large residence time and high temperatures.

Strictly speaking, the tabulated chemistry approach used in these simulations is designed for premixed combustion and, even though the low NOx injector of the TLC combustor generates quite good mixing between fuel and air, not all of the combustion occurs in the regime of a perfectly premixed flame. However, it was checked by Boucher (see Figs. 11.23 and 11.24 of [85]) that the largest proportion of the combustion is of a premixed or partially premixed type and thus can be tackled by the tabulated chemistry approach. The emission indices for NO and NOx measured by gas sampling at the outlet of the combustor are 0.9 and 2.3 g/kg of fuel, respectively. The corresponding indices obtained by the simulation are 5.6 and 9.3 g/kg of fuel, respectively. This discrepancy between experiment and simulation is fully coherent with the results of section "*ONERA Simulation*" for the temperature: the effort made at this stage did not enable us to obtain a satisfactory agreement for temperatures in the core of the main recirculation zone. Considering the strong dependence of the NO reaction rate on temperature, it is not surprising that the simulation overestimates NO and NOx formation. Despite the significant deviations between simulation and experiment, we evaluate this result to be interesting because it perfectly illustrates that the prediction of pollutant formation requires not only a physical model accurately describing the evolution of pollutant species in a given thermo-chemical environment, but also a highly accurate reproduction of the main features of the reactive flow. The next step of work will be to improve the temperature prediction by paying an additional CPU effort into grid refinement. Planned velocity measurements will be also of great help to analyze the results, specifically potential sources for deviations of the temperatures, in greater detail.

Calculation of the soot mass fraction field

Despite the deficit of temperature prediction, the Leung model has been used with the FTC approach to calculate soot formation. The fields of the C_2H_2 (soot precursor) mass fraction and soot volume fraction are given in figure 23.

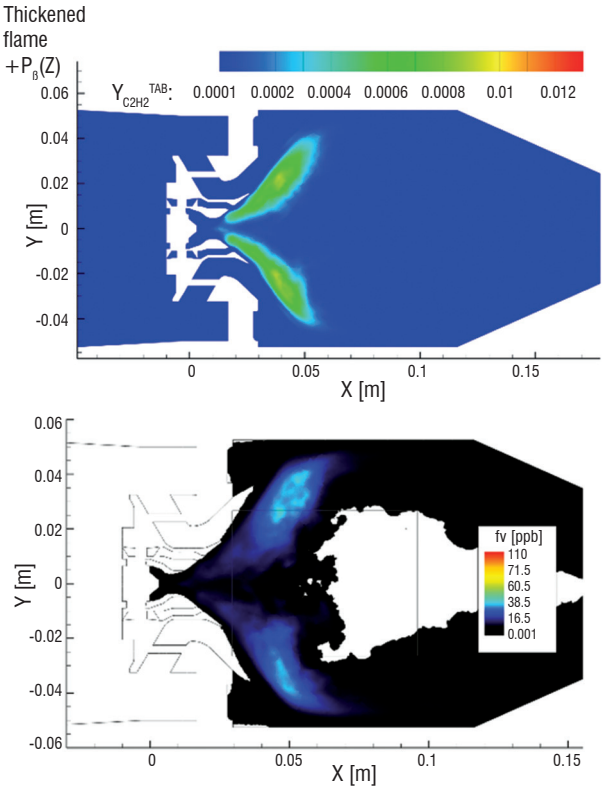

Figure 23 – Fields of the C_2H_2 mass fraction (top) and soot volume fraction (bottom) obtained numerically

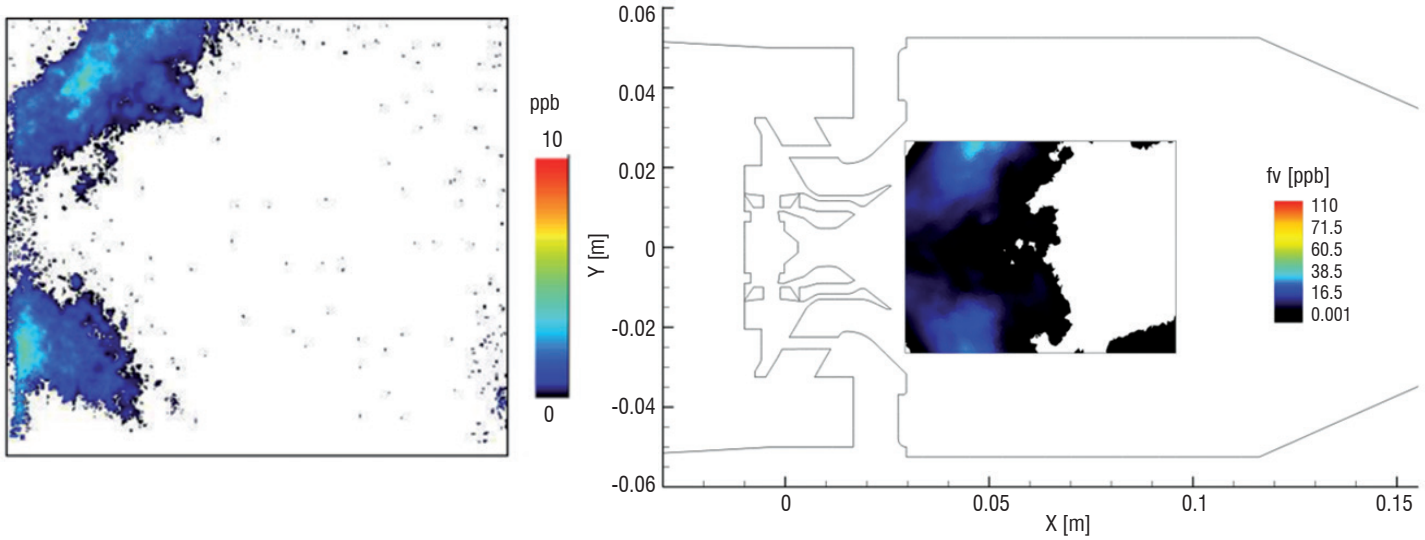

Figure 24 – Soot volume fraction obtained by LII (left) and by the calculation (right); the window shown in the calculated map corresponds to the measurement window displayed on the left

As for the DLR burner, soot is located in an open conical region, which does not extend very far downstream. However, unlike the DLR burner, soot is not present close to the wall because air cooling films are introduced along the lateral walls, i.e., combustor windows. The soot volume fraction map is slightly shifted downstream compared to the C_2H_2 mass fraction distribution. The numerical results concerning soot are compared to LII measurements in figure 24.

The shapes of the soot distributions obtained experimentally and numerically are similar, with a high soot volume fraction in the conical region located immediately downstream of the injection bowl and no soot on the axis of the combustor where the central recirculation of hot gases induced by the swirl takes place. The quantitative level of the soot volume fraction is however overestimated by an order of magnitude (factor 10) in the calculation. As for the NO and NOx indices, the overprediction of temperature is likely to be the reason for this discrepancy. Another point to emphasize is that all soot is oxidized before the outlet of the combustor, as shown in figure 9. This is in agreement with the sampling measurements made at the outlet of the combustor, which do not detect soot even at a level significantly below LII values. A calculation test made with the rough soot model of Magnussen gives quite good results in the region of the measurement window, but does not exhibit complete oxidation of the soot particles so a non-negligible amount of soot is found at the combustor outlet. This is not in agreement with the sampling measurements and validates our preference for the Leung model.

Conclusion

Examples of numerical strategies and associated validation experiments for the numerical prediction of pollutant formation in gas turbine combustors have been presented. The prediction of pollutant formation in complex turbulent reactive flows typical for GT combustors is a challenging task. To date, there is no solution to perfectly solve the problem at a moderate CPU cost. Therefore, a compromise must be found between the complexity of the physico-chemical model for pollutants and the description of the turbulent reactive flow fixing the parameters of the pollutant model. For soot prediction, two strategies have been proposed: the first one initiated by ONERA is based on the simple soot model of Leung *et al.* and emphasizes the unsteady description of the turbulent reactive flow; the other one initiated by DLR is based on a soot model with more physics, but investing less effort on the flow description. Both strategies lead to quite satisfactory results concerning the simulation of the semi-technical scale DLR experiment. The first one works with a soot model, which is less CPU consuming, but the second one can be applied to more general configurations without adjusting the soot model. A strategy was also proposed for the prediction of NOx. The discrepancy between simulation and experiment obtained when this strategy was applied to the TLC combustor confirms that the prediction of NOx essentially requires a correct prediction of the local temperature field.

The numerical strategies for pollutant prediction and the involved physical models must be carefully validated. Many laminar experiments can be found in literature to validate the basis of physical models, but experiments allowing for validation of the coupling between these physical models and the calculation of the turbulent reactive flow transporting the pollutants are less common. We have presented two different experiments, the first one at the semi-technical scale achieved by DLR, the second one at the technical scale achieved by ONERA with the participation of DLR for the soot measurements. The first one provides a deep insight into the process of soot formation, with valuable information on the influence of the dilution air injection on soot oxidation; the second one accurately reproduced the running conditions of a GT combustor, in particular the injection of liquid fuel through a low NOx injector. However, the second data set will have to be completed by gas velocity measurements ■

References

[1] M. RALPH and S. BAKER – *Aircraft Technology Improvements, Icao Technology Goals for Nox Second Independent Expert Review*. ICAO environmental report, Chapter 2, 2010.

[2] ICAO – E*nvironmental Protection*. Annex 16, Volume II, 2008.

[3] J. DELHAY, P. DESGROUX, E. THERSSEN, H. BLADH, P.-E. BENGTSSON, H. HÖNEN, J. D. BLACK and I. VALLET – *Soot Volume Fraction Measurements in Aero-Engine Exhausts Using Extinction-Calibrated Backward Laser-Induced Incandescence*. Appl. Phys. B, 95(2009):825-838, 2009.

[4] J. D. BLACK and M. P. JOHNSON – *In-Situ Laser-Induced Incandescence of Soot in an Aero-Engine Exhaust: Comparison with Certification Style Measurements*. Aerosp. Sci. Technol. 14 (2010):329-337, 2010.

[5] A. PETZOLD, R. MARSH, M. JOHNSON, M. MILLER, Y. SEVCENCO, D. DELHAYE, A. IBRAHIM, P. WILLIAMS, H. BAUER, A. CRAYFORD, W. D. BACHALO and D. RAPER – *Evaluation of Methods for Measuring Particulate Matter Emissions from Gas Turbines*. Environ. Sci. Technol., 45,8(2011):3562-3568, 2011.

[6] J. M. COHEN, N. M. REY, C. A. JACOBSON and T. J. ANDERSON – *Active Control of Combustion Instability in a Liquid-Fueled Low Nox Combustor*. Gas Turbine and Aeroengine Congress and Exhibition, Stockholm, Sweden, June 2-5, 1998.

[7] T. C. LIEUWEN – *Experimental Investigation of Limit-Cycle Oscillations in an Unstable Gas Turbine Combustor.* J. Prop. Power,18,1(2002):61-67, 2002.

[8] A. S. FEITELBERG and M. A. LACEY – *The GE Rich-Quench-Lean Gas Turbine Combustor*. J. Eng. Gas Turbines Power 120,3(1998):502-508, 1998.

[9] V. JERMAKIAN, V. G. MCDONELL and G. S. SAMUELSEN – *Experimental Study of the Effects of Elevated Pressure and Temperature on Jet Mixing and Emissions in an RQL Combustor for Stable, Efficient and Low Emissions Gas Turbine Applications*. Advanced Power and Energy Program, University of California, Irvine http://www.energy.ca.gov/2012publications/CEC-500-2012-001/CEC-500-2012-001.pdf, 2012.

[10] R. STICKLES and J. BARRETT – *TAPS II Technology, Final Report*. Technology Assessment, Open Report FAA, Continuous Lower Energy, Emissions and Noise, (CLEEN) Technologies Development, http://www.faa.gov/about/office_org/headquarters_offices/apl/research/aircraft_technology/cleen/reports/media/TAPS_II_Public_Final_Report.pdf, 2013.

[11] E. RIESMEIER, S. HONNET and N. PETERS – *Flamelet Modeling of Pollutant Formation in a Gas Turbine Combustion Chamber Using Detailed Chemistry for a Kerosene Model Fuel*. J. Eng. Gas Turbines Power, 126(2004):899-905, 2004.

[12] P. SCHMITT, T. POINSOT, B. SCHUERMANS and K. P. GEIGLE – *Large-Eddy Simulation and Experimental Study of Heat Transfer, Nitric Oxide Emissions and Combustion Instability in a Swirled Turbulent High-Pressure Burner*. J. Fluid Mech., 570(2007):17–46, 2007.

[13] G. GODEL, P. DOMINGO and L. VERVISCH – *Tabulation of Nox Chemistry for Large-Eddy Simulation of Non-Premixed Turbulent Flames*. Proc. Combust. Inst., 32(2009):1555-1561, 2009.

[14] M. ILBAS, I. YILMAZ and Y. KAPLAN – *Investigations of Hydrogen and Hydrogen–Hydrocarbon Composite Fuel Combustion And Nox Emission Characteristics in a Model Combustor*. Int. J. of Hydrogen Energy, 30:1139-1147, 2005.

[15] M. J. LANDMAN, M. A. F. DERKSEN and J. B. W. KOK – *Effect of Combustion Air Dilution by Water Vapor or Nitrogen on Nox Emission in a Premixed Turbulent Natural Gas Flame: an Experimental Study*. Combust. Sci. Tech., 178: 623–634, 2006.

[16] S. C. LI and F. A. WILLIAMS – *NOx Formation in Two-Stage Methane-Air Flames*. Combust. Flame, 118(1999):399-414, 1999.

[17] L. K. SZE, C. S. CHEUNG and C. W. LEUNG – *Appearance, Temperature, and NOx Emission of Two Inverse Diffusion Flames with Different Port Design*. Combust. Flame, 144(2006):237-248, 2006.

[18] W. MEIER, A. O. VYRODOV, V. BERGMANN and W. STRICKER – *Simultaneous Raman/Lif Measurements of Major Species and NO in Turbulent H_2/Air Diffusion Flames*. Appl. Phys. B, 63:79-90, 1996.

[19] V. SICK, F. HILDENBRAND and P. LINDSTEDT – *Quantitative Laser-Based Measurements and Detailed Chemical Kinetic Modeling of Nitric Oxide Concentrations in Methane-Air Counterflow Diffusion Flames*. Proc. Combust. Inst., 27(1998):1401–1409, 1998.

[20] W. MEIER, R. S. BARLOW, Y.-L. CHEN and J.-Y. CHEN – *Raman/Rayleigh/LIF Measurements in a Turbulent $CH_4/H_2/N_2$ Jet Diffusion Flame: Experimental Techniques and Turbulence-Chemistry Interaction*. Combust. Flame, 123(2000):326-343, 2000.

[21] W. G. BESSLER, C. SCHULZ, T. LEE, D.-I. SHIN, M. HOFMANN, J. B. JEFFRIES, J. WOLFRUM and R. K. HANSON – *Quantitative NO-LIF Imaging in High-Pressure Flames*. Appl. Phys. B, 75:97-102, 2002.

[22] V. M. VAN ESSEN, A.V. SEPMAN, A.V. MOKHOV and H.B. LEVINSKY – *The Effects of Burner Stabilization on Fenimore NO Formation in Low-Pressure, Fuel-Rich Premixed $CH_4/O_2/N_2$ Flames,* Proc. Combust. Inst., 31(2007):329-337, 2007.

[23] H. BOCKHORN – *Soot Formation in Combustion, Mechanisms and Models*. Springer Series in Chemical Physics 59, Springer-Verlag.

[24] R. J. SANTORO, H. G. SEMERJIAN and R. A. DOBBINS – *Soot Particle Measurements in Diffusion Flames*. Combust. Flame, 51(1983):203-218, 1983.

[25] U. VANDSBURGER, I. KENNEDY and I. GLASSMAN – *Sooting Counterflow Diffusion Flames with Varying Oxygen Index*. Comb. Sci. Tech., 39, (1984):263-285, 1984.

[26] B. QUAY, T.-W. LEE, T. NI and R. J. SANTORO – *Spatially Resolved Measurements of Soot Volume Fraction Using Laser-Induced Incandescence*. Combust. Flame, 97(1994):384-392, 1994.

[27] C. S. MCENALLY and L. D. PFEFFERLE – *Experimental Study of Nonfuel Hydrocarbons and Soot in Coflowing Partially Premixed Ethylene/Air Flames*. Combust. Flame, 121(2000):575-592, 2000.

[28] C. P. ARANA, M. PONTONI, S. SEN and I. K. PURI – *Field Measurements of Soot Volume Fractions in Laminar Partially Premixed Coflow Ethylene/Air Flames*. Combust. Flame, 138(2004):362-372, 2004.

[29] L. L. MCCRAIN and W. L. ROBERTS – *Measurements of the Soot Volume Field in Laminar Diffusion Flames at Elevated Pressures.* Combust. Flame, 140(2005):60-69, 2005.

[30] K. A. THOMSON, Ö. L. GÜLDER, E. J. WECKMAN, R. A. FRASER, G. SMALLWOOD and D. R. SNELLING – *Soot Concentration and Temperature Measurements in Co-Annular, Nonpremixed CH_4/Air Laminar Flames at Pressures up to 4 MPa*. Combust. Flame, 140(2005):222-232, 2005.

[31] P. DESGROUX, X. MERCIER, B. LEFORT, R. LEMAIRE, E. THERSSEN and J.F. PAUWELS – *Soot Volume Fraction Measurement in Low-Pressure Methane Flames by Combining Laser-Induced Incandescence and Cavity Ring-Down Spectroscopy: Effect of Pressure on Soot Formation*. Combust. Flame, 155(2008):289-301, 2008.

[32] H. I. JOO and Ö. L. GÜLDER – *Soot Formation and Temperature Field Structure in Co-Flow Laminar Methane–Air Diffusion Flames at Pressures from 10 to 60 Atm*. Combust. Flame, 32(2009):769-775, 2009.

[33] K. M. LEUNG, R. P. LINDSTEDT and W. P. JONES – *A Simplified Reaction Mechanism for Soot Formation in Nonpremixed Flames.* Combust. Flame, 87(1991):289-305, 1991.
[34] T. BLACHA, M. DI DOMENICO, P. GERLINGER and M. AIGNER – *Soot Predictions in Premixed And Non-Premixed Laminar Flames Using a Sectional Approach For PAHs And Soot*. Combust. Flame, 159(2012):181-193, 2012.
[35] C. R. SHADDIX and K. C. SMYTH – *Laser-Induced Incandescence Measurements of Soot Production in Steady and Flickering Methane, Propane, and Ethylene Diffusion Flames*. Combust. Flame, 107(1996):418-452, 1996.
[36] N.H. QAMAR, Z. T. ALWAHABI, Q. N. CHAN, G. J. NATHAN, D. ROEKAERTS and K. D. KING – *Soot Volume Fraction in a Piloted Turbulent Jet Non-Premixed Flame of Natural Gas*. Combust. Flame, 156(2009):1339-1347, 2009.
[37] R. LEMAIRE, A FACCINETTO, E. THERSSEN, M. ZISKIND, C. FOCSA and P. DESGROUX – *Experimental Comparison of Soot Formation in Turbulent Flames of Diesel and Surrogate Diesel Fuels*. Combust. Flame, 32(2009):737-744, 2009.
[38] T. L. HENRIKSEN, G. J. NATHAN, Z. T. ALWAHABI, N. QAMAR, T. A. RING and E. G. EDDINGS – *Planar Measurements of Soot Volume Fraction and OH in a JP-8 Pool Fire*. Combust. Flame, 156(2009):1480-1492, 2009.
[39] M. KÖHLER, K.P. GEIGLE, T. BLACHA, P. GERLINGER and W. MEIER – *Experimental Characterization and Numerical Simulation of a Sooting Lifted Turbulent Jet Diffusion Flame*. Combust. Flame, 159(2012):2620-2635, 2012.
[40] M. E. MUELLER, Q. N. CHAN, N. H. QAMAR, B. B. DALLY, H. PITSCH, Z. T. ALWAHABI and G. J. NATHAN – *Experimental and Computational Study of Soot Evolution in a Turbulent Nonpremixed Bluff Body Ethylene Flame*. Combust. Flame, 160(2013):1298-1309, 2013.
[41] K.P. GEIGLE, R. HADEF and W. MEIER – *Soot Formation and Flame Characterization of an Aero-Engine Model Combustor Burning Ethylene at Elevated Pressure*. J. Eng. Gas Turbines Power 136(2014), 021505, 2014.
[42] K.P. GEIGLE, M. KÖHLER, W. O'LOUGHLIN and W. MEIER – *Investigation of Soot Formation In Pressurized Swirl Flames by Laser Measurements of Temperature, Flame Structures and Soot Concentrations*. Proc. Combust. Inst., 35(2015):3373-3380, 2015.
[43] K.P. GEIGLE, W. O'LOUGHLIN, R. HADEF and W. MEIER – *Visualization of Soot Inception in Turbulent Pressurized Flames by Simultaneous Measurement of Laser-Induced Fluorescence of Polycyclic Aromatic Hydrocarbons and Laser-Induced Incandescence, and Correlation to OH Distributions*. Appl. Phys. B 119(2015):717-730, 2015.
[44] R. SAID, A. GARO and R. BORGHI – *Soot Formation Modeling for Turbulent Flames*. Combust. Flame, 108(1997):71-86, 1997.
[45] H. PITSCH, E. RIESMEIER and N. PETERS – *Unsteady Flamelet Modeling of Soot Formation in Turbulent Diffusion Flames.* Comb. Sci. and Tech., 158, Issue1(2000):389-406, 2000.
[46] B. ZAMUNER and F. DUPOIRIEUX – *Numerical Simulation of Soot Formation in a Turbulent Flame with a Monte-Carlo PDF Approach and Detailed Chemistry.* Comb. Sci. and Tech., 158, Issue 1(2000):407-438, 2000.
[47] C. S. YOO and H. G. IM – *Transient Soot Dynamics in Turbulent Nonpremixed Ethylene–Air Counterflow Flames*. Proc. Combust. Inst., 31(2007):701-708, 2007.
[48] D. O. LIGNELL, J. H. CHEN and P. J. SMITH – *Three-Dimensional Direct Numerical Simulation of Soot Formation and Transport in a Temporally Evolving Nonpremixed Ethylene Jet Flame*. Combust. Flame, 155(2008):316-333, 2008.
[49] P. NARAYANAN and A. TROUVÉ – *Radiation-Driven Flame Weakening Effects in Sooting Turbulent Diffusion Flames*. Combust. Flame, 32(2009):1481-1489, 2009.
[50] F. BISETTI, G. BLANQUART, M. E. MUELLER and H. PITSCH – *On the Formation and Early Evolution of Soot in Turbulent Nonpremixed Flames.* Combust. Flames, 159(2012):317-335, 2012.
[51] M. E. MUELLER and H. PITSCH – *LES Model for Sooting Turbulent Nonpremixed Flames.* Combust. Flame, 159(2012):2166-2180, 2012.
[52] A. ATTILI, F. BISETTI, M. E. MUELLER and H. PITSCH – *Damköhler Number Effects on Soot Formation and Growth in Turbulent Nonpremixed Flames*. Combust. Flame, 35(2015):1215-1223, 2015.
[53] F. DUPOIRIEUX, N. BERTIER, A. BOUCHER and P. GILBANK – *A Cost-Effective Backward Lagrangian Method for Simulation of Pollutant Formation in Gas Turbine Combustors by Post-Processing of Complex 3D Calculations*. Int. J. Sustainable Aviation, 1,(2014):160-180, 2014.
[54] H. BARTHS, N. PETERS, N. BREHM, A. MACK, M. PFITZNER and V. SMILJANOVSKI – *Simulation of Pollutant Formation in a Gas-Turbine Combustor Using Unsteady Flamelets*. Proc. Combust. Inst., 27(1998):1841-1847, 1998.
[55] M. E. MUELLER and H. PITSCH – *Large Eddy Simulation of Soot Evolution in an Aircraft Combustor.* Physics of Fluids, 25, 110812, 2013.
[56] A. REFLOCH, B. COURBET, A. MURRONE, P. VILLEDIEU, C. LAURENT, P. GILBANK, J. TROYES, L. TESSÉ, G. CHAINERAY, J.B. DARGAUD, E. QUÉMERAIS and F. VUILLOT – *CEDRE Software*. Aerospace Lab, Issue 2, 2011.
[57] L. SELLE, G. LARTIGUE, T. POINSOT, R. KOCH, K.-U. SCHILDMACHER, W. KREBS, B. PRADE, P. KAUFMANN and D. VEYNANTE – *Compressible Large Eddy Simulation of Turbulent Combustion in Complex Geometry on Unstructured Meshes*. Combust. Flame, 137(2004):489-505, 2004.
[58] O. COLIN, F. DUCROS, D. VEYNANTE and T. POINSOT – *A Thickened Flame Model for Large Eddy Simulations of Turbulent Premixed Combustion*. Physics of Fluids, Vol. 12, No. 7(2000):1843-1863, 2000.
[59] U. MAAS and S. B. POPE – *Simplifying Chemical Kinetics: Intrinsic Low-Dimensional Manifolds in Composition Space*. Combust. Flame, 88(1992):239-264, 1992.
[60] O. GICQUEL, N. DARABIHA and D. THÉVENIN – *Laminar Premixed Hydrogen/Air Counterflow Flame Simulations Using Flame Prolongation of ILDM with Differential Diffusion*. Proc. Combust. Inst., 28(2000):1901-1908, 2000.
[61] J. A. VAN OIJEN, F. A. LAMMERS and L. P. H. DE GOEY – *Modeling of Complex Premixed Burner Systems by Using Flamelet-Generated Manifolds*. Combust. Flame, 127(2001):2124-2134, 2001.
[62] B. FIORINA, O. GICQUEL, L. VERVISCH, S. CARPENTIER and N. DARABIHA – *Premixed Turbulent Combustion Modeling Using Tabulated Detailed Chemistry and PDF*. Combust. Flame, 30(2005)867-874, 2005.
[63] G. KUENNE, A. KETELHEUN and J. JANICKA – *LES Modeling of Premixed Combustion Using a Thickened Flame Approach Coupled with FGM Tabulated Chemistry*. Combust. Flame, 158(2011):1750-1767, 2011.
[64] A. W. VREMAN, B. A. ALBRECHT, J. A. VAN OIJEN, L. P. H. DE GOEY and R. J. M. BASTIAANS – *Premixed and Nonpremixed Generated Manifolds in Large-Eddy Simulation of Sandia Flame D and F*. Combust. Flame, 153(2008):394-416, 2008.
[65] A. BOUCHER, N. BERTIER and F. DUPOIRIEUX – *A Method to Extend Flamelet Manifolds for Prediction of NOx And Long Time Scale Species with Tabulated Chemistry*. Int. J. Sustainable Aviation, vol. 1, n° 2(2014):181-202, 2014.

[66] B. F. MAGNUSSEN and B. H. HJERTAGER – *On Mathematical Modeling on Turbulent Combustion with Special Emphasis on Soot Formation and Combustion*. Proc. Combust. Inst., 16(1977):719-729, 1977.
[67] G. LECOCQ, D. POITOU, I. HERNANDEZ, F. DUCHAINE, E. RIBER and B. CUENOT – *A Methodology for Soot Prediction Including Thermal Radiation in Complex Industrial Burners*. Flow Turbulence Combust., 92(2014):947-970, 2014.
[68] B. CUENOT, R. VICQUELIN, E. RIBER, V. MOUREAU, G. LARTIGUE, A. FIGUER, Y. MERY, J. LAMOUROUX, S. RICHARD, L.GICQUEL, T. SCHMITT and S. CANDEL – *Advanced Simulation of Combustion in Aeronautical Burners*. Aerospace Lab, Issue 11, 2016.
[69] N. A. SLAVINSKAYA and O. J. HAIDN – *Reduced Chemical Model for High Pressure Methane Combustion with Pah Formation*. Proc. 46th AIAA Aerospace Sciences Meeting, n° AIAA 2008-1012, 2008.
[70] M. DI DOMENICO, P. GERLINGER and M. AIGNER – *Development and Validation of a New Soot Formation Model for Gas Turbine Combustor Simulations*. Combust. Flame 157(2010): 246–258, 2010.
[71] K.P. GEIGLE, R. HADEF, M. STÖHR and W. MEIER – *Flow Field Characterization of Pressurized Sooting Swirl Flames and Correlation to Soot Distributions*. Proc. Combust. Inst., 2016.
[72] S. TROTTIER, H. GUO, G. J. SMALLWOOD and M. R. JOHNSON – *Measurement and Modeling of the Sooting Propensity of Binary Fuel Mixtures.* Proc. Combust. Inst. 31(2007):611-619, 2007.
[73] M. S. TSURIKOV, K.-P. GEIGLE, V. KRÜGER, Y. SCHNEIDER-KÜHNLE, W. STRICKER, R. LÜCKERATH, R. HADEF and M. AIGNER – *Laser-Based Investigation of Soot Formation in Laminar Premixed Flames at Atmospheric and Elevated Pressures*. Combust. Sci. Technol.,177(2005):1835-1862, 2005.
[74] A. COCHET, C. GUIN, A. VINCENT, O. DESSORNES, A. BRESSON, M. ORAIN and C. BROSSARD – *ONERA Test Facilities for Combustion in Aero Gas Turbine Engines and Associated Optical Diagnostics*. Aerospace Lab, issue 11, 2016.
[75] FP6-TLC, 2005-2010, http://ec.europa.eu/research/transport/projects/items/tlc_en.htm.
[76] M. ORAIN, F. GRISCH, E. JOURDANNEAU, B. ROSSOW, C. GUIN and B. TRÉTOUT – *Simultaneous Measurements of Equivalence Ratio and Flame Structure in Multipoint Injectors Using PLIF*. C. R. Mecanique, 337(2009):373-384, 2009.
[77] K. P. GEIGLE, J. ZERBS and C. GUIN – *Laser-Induced Incandescence for Soot Measurements in Technical Flames at Increased Pressure at the ONERA M1 Test Rig*. Proc. Deutscher Luft- und Raumfahrtkongress 2010, Paper 1235, 31.08.-02.09.2010, 2010.
[78] A. J. CHORIN – *Numerical Solution of the Navier-Stokes Equations.* Mathematics of Computation, 22,104(1968):745–762, 1968.
[79] F. R. MENTER – *Two-Equation Eddy-Viscosity Turbulence Models for Engineering Applications*. AIAA Journal, 32(1994):1598–1605, 1994.
[80] P. GERLINGER – *Investigation of an Assumed PDF Approach for Finite-Rate Chemistry.* Combust. Sci. Technol., 175(2003):841–872, 2003.
[81] C. EBERLE, P. GERLINGER, K. P. GEIGLE and M. AIGNER – *Numerical Investigation of Transient Soot Evolution Processes in an Aero-Engine Model Combustor.* Combust. Sci. Technol., 187(2015):1841–1866, 2015.
[82] J. LUCHE, M. REUILLON, J.-C. BOETTNER and M. CATHONNET – *Reduction of Large Detailed Kinetic Mechanisms: Application to Kerosene/Air Combustion*. Comb. Sci. and Tech., 176 (11)(2004):1935-1963, 2004.
[83] L.-H. DOREY – *Modélisation des phénomènes couplés combustion-formation des suies-transferts radiatifs dans les chambres de combustion de turbine à gaz*. Thèse de l'Ecole Centrale Paris, Energétique, 2012.
[84] J. VAN OIJEN and L. DE GOEY – *Predicting NO Formation with Flamelet Generated Manifolds*. Proc. European Combustion Meeting, 2009.
[85] A. BOUCHER – *Modélisation de la formation des polluants au sein des foyers aéronautiques par une méthode de chimie tabulée*. Thèse de l'Ecole Centrale Paris, Energétique, 2015.

Acknowledgement

This work has been funded by ONERA, the ANR (French National Research Agency) and the European Commission within the project Fuel Injector Research for Sustainable Transport (FIRST) under contract No. 265848. The authors gratefully acknowledge the computing time granted on the supercomputer JUROPA at Jülich Supercomputing Centre (JSC).

Acronyms

CARS (Coherent Anti-stokes Raman Spectroscopy)
FAR (Fuel Air Ratio)
GT combustor (Gas Turbine combustor)
LES (Large Eddy Simulation)
LII (Laser Induced Incandescence)
OPR (Operating Pressure Ratio)
PAH (Polycyclic Aromatic Hydrocarbon)
URANS (Unsteady Reynolds-Averaged Navier-Stokes resolution)

Nomenclature

c	progress variable	t	time, s	x_i	spatial coordinate, m
D_k	diffusion coefficient, m²/s	T	temperature, K	X	mass fraction
M_k	molar mass, kg	u_i	velocity component, m/s	Z	mixture fraction

Greek Letters

ρ	mixture density, kg/m³
ρ_{soot}	soot density, kg/m³
M_k	chemical reaction rate, kg m⁻³ s⁻¹
$\dot{\omega}_k$	temperature, K

Subscripts

i	i=1,2,3, spatial direction
k	chemical species

Superscripts

TAB	value picked from the chemical table

Francis Dupoirieux is deputy head of the Energetics department of ONERA, in charge of the scientific management of the activity. He created 3D CFD tools for the numerical simulation of turbulent reactive flows that have been widely used by research laboratories and industrial partners of ONERA. He also developed physical models of pollutant formation in flames. He is now involved in the development of the CEDRE code, dedicated to multiphysics problems in reactive flows. This task includes the definition of experiments for validating the models implemented in CEDRE and the global validation of this code. He is teaching thermodynamics and thermal transfer at the École Centrale Paris.

Nicolas Bertier, graduated from ENS Cachan and PhD from Paris VI University, is senior researcher in the Energetics department of ONERA. He is in charge of the numerical simulation of reactive flows in aeronautic combustors. He has developed and validated the numerical methods and combustion models required to carry out LES with the CEDRE code of ONERA. He is the leader of the CEDRE project. He is also teaching "energetics of aeronautic combustors" at Paris VI University and ISAE Toulouse.

Christian Guin graduated Engineer in 1980 from CNAM (Conservatoire National des Arts et Métiers). He joined ONERA in 1974 as technician and, since 1980, has been working as research engineer in the Energetic Department. He was involved in experimental combustion studies for ducted rocket and ramjet, and then, since 1995, on new combustor concepts for turbojet. He has developed the M1 high pressure test facility, devoted to the turbojet combustors studies at ONERA, and is in charge of the experiments carried out on this facility.

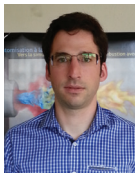

Luc-Henry Dorey is a research engineer at ONERA, working in the Fundamental and Applied Energetics Department (DEFA). He graduated from ISAE-ENSMA (Poitiers) in 2008 and received his PhD degree in energetics from Ecole Centrale Paris in 2012. His research field is mainly focused on combustion, acoustics, soot formation and two-phase flow modeling for CFD simulation of liquid-propellant rocket engines and gas turbines.

Klaus Peter Geigle received his PhD in Physical Chemistry, specifically on laser-based characterization of PAH, at the University of Cologne. Since 1999 he is focussing on experimental characterization of sooting atmospheric and pressurized flames at DLR as member of the department of combustion diagnostics. Main tool of those flame studies is laser-induced incandescence which he develops and applies in laboratory applications as well as at test rigs at other sites. The generated detailed and accurate data sets frequently serve for validation of numerical combustion models.

Christian Eberle graduated at the University of Stuttgart and since 2011 he is PhD student at the DLR institute of combustion technology. His PhD supervisor is Peter Gerlinger. The focus of Christian's research is the development and validation of predictive soot models for CFD applications.

Peter Gerlinger received his PhD 1994 in aeronautical engineering from the University of Stuttgart. He obtained in 2004 the habilitation in combustion technology and, since 2015, is apl. Professor at the University of Stuttgart. Main research topics are high order numerical simulation, turbulence chemistry interaction, convergence acceleration, and soot modeling.

I. K. Ortega, D. Delhaye
(ONERA)

F.-X. Ouf
(Institut de Radioprotection et de Sûreté Nucléaire)

D. Ferry
(Aix-Marseille Université, CNRS, CINaM UMR 7325)

C. Focsa, C. Irimiea, Y. Carpentier, B. Chazallon
(Laboratoire de Physique des Lasers, Atomes et Molécules UMR CNRS 8523, Université de Lille 1 Sciences et Technologies)

P. Parent, C. Laffon
(Aix-Marseille Université, CNRS, CINaM UMR 7325)

O. Penanhoat, N. Harivel
(SNECMA/SAFRAN Group)

D. Gaffié, X. Vancassel
(ONERA)

E-mail : ismael.ortega@onera.fr

DOI : 10.12762/2016.AL11-08

Measuring Non-Volatile Particle Properties in the Exhaust of an Aircraft Engine

The steady growth of air traffic and its foreseen expansion during future years have raised concerns about its potential impact on climate and ground-level air quality. So far, the smoke number has been used to evaluate the non-volatile particulate matter amount emitted by aircraft engines, but it is a poor proxy for modern engine emissions. Therefore, new sampling and measurement techniques have recently been tested on aircraft engine emissions, especially as a new ICAO particle emission standard is currently being developed. Number and mass of emitted particles are generally used, but are not sufficient to fully characterize soot emissions and further address atmospheric impact issues. Chemical composition is crucial to evaluate their atmospheric reactivity. This paper presents a complete set of techniques that have been used to characterize soot emissions from an aircraft engine in a comprehensive manner. It reports results from a campaign on a PowerJet SaM146 engine, performed within the framework of the MERMOSE (*Mesure et Etude de la Réactivité des émissions de MOteurS aEronautiques*) project. It emphasizes the influence of the engine regime, ranging from 30% to 100% of the takeoff thrust, on the various particle properties investigated, including the size, number, morphology and chemical composition.

Introduction

Emissions from aircraft engines include a large variety of gaseous and solid effluents (e.g. [15], [28], [16]). Although these emissions are small compared to other anthropogenic surface emissions (at the present time aviation CO_2 contributes to about 2% to 3% of all anthropogenic sources [21]), they are mostly released in the sensitive region of the upper troposphere and lower stratosphere. In fact, aviation represents a major source of anthropogenic pollution at high altitudes, where background concentrations of these trace substances are low and residence times are long. The unique location of aircraft emissions and the predicted growth of air traffic demand require that particular attention be given to the potential effects of these emissions. One of the key factors regarding aviation environmental impact assessments lies in our ability to accurately characterize aircraft engine emissions, especially soot particles. When emitted at ground level, they may significantly contribute to air quality issues. At typical cruising altitudes, they modify the composition of the atmosphere and hence the Earth's radiative budget, either directly or indirectly, since soot particles may influence contrail formation and subsequently the induced cirrus cloud properties.

Soot particles are sometimes referred to as black carbon (BC), considering their optical and radiative behavior. So far, non-volatile particulate matter (nvPM) emissions, defined as particles present in the engine exhaust at temperatures higher than 350 °C, have been addressed under the ICAO certification process, by using Smoke Number (SN) measurements. These are based on the collection of particles on a filter whose loss of reflectance is analyzed. However, this method has become obsolete and is currently being revised by the CAEP (Committee for Aviation Environmental Protection), for two main reasons. The first reason is that Smoke Number measurements have been developed for old generation engines, with higher levels of soot emissions. The filter collection method can no longer describe the whole size range of the emitted soot particles. In addition, no reliable relationship can be determined between the SN and particle mass or number emission index and it does not provide any information on the size distribution; the SN is therefore a poor proxy to describe nvPM emissions. The second reason is that harmonization is needed between the various transport sector emission measurements. The automobile industry has recently deployed a more suitable measurement protocol, which addresses nvPM properties more specifically, especially the number concentration and mass. As a result, the implementation of an improved and comparable methodology for aviation has become necessary and is described

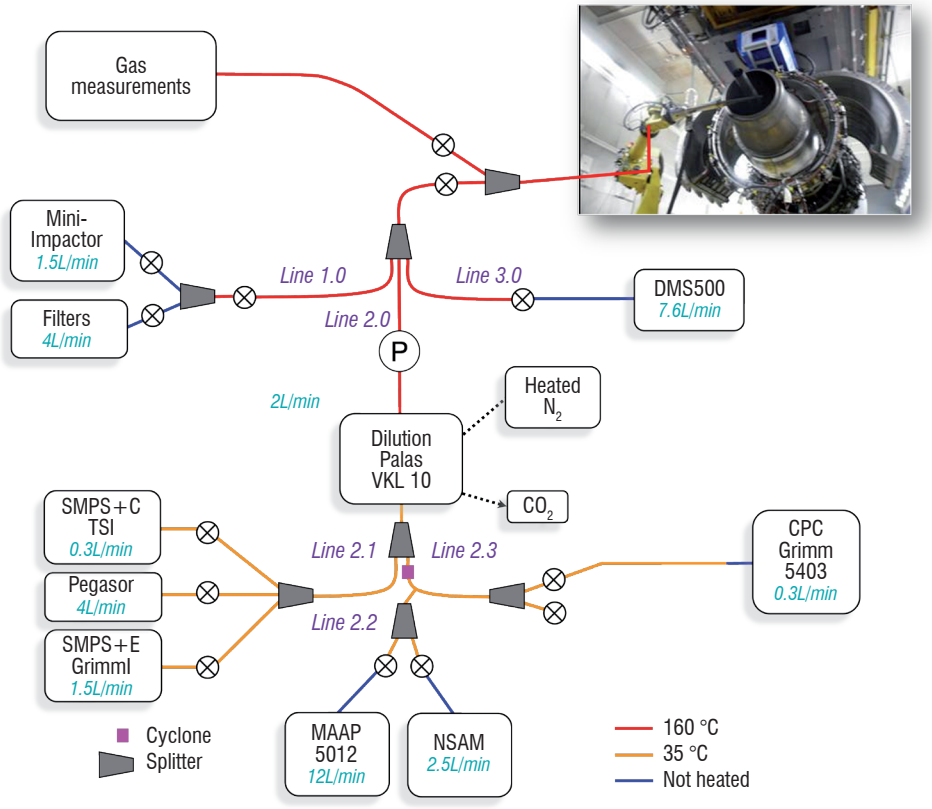

Figure 1 - Schematic diagram of the MERMOSE sampling line

in the AIR6241 (http://standards.sae.org/air6241). This protocol has set the basic methodology for characterizing aircraft engine emitted nvPM for certification purposes. However, such measurements are focused on the particle number and mass. Although these are key parameters to understand the potential environmental impact of aircraft engine emissions, the determination of the chemical composition, and especially the surface chemical composition of emitted particles, is essential to understand the atmospheric reactivity of soot and associated issues more comprehensively.

In this paper we describe a comprehensive experimental set-up to address the characterization of the properties of soot particles emitted by a turbojet engine. In a first section, we describe a typical aircraft exhaust sampling line, used during the MERMOSE project, in order to characterize the soot emitted by a SaM146 engine, its main technical requirements and the engine test plan. In a second part, we focus on the various measurement techniques used, regarding what physical and chemical parameters need to be retrieved and the instrument specific technology involved. Finally, in the last section, we present some results from the MERMOSE engine test campaign.

Experimental set-up

Sampling line

Measuring soot particle properties requires various techniques. For various reasons, the engine exhaust, comprising gaseous combustion products and particles, has to be sampled before being analyzed. The sampling system typically consists of various parts, which are precisely described when used for certification purposes. Generally, sampling is performed in three steps. The exhaust is first sampled by means of a single-hole probe or a rake. It is then transported through a stainless steel line and heated to avoid post-sampling reactions. Finally, the sample reaches the measurement instrument section, to be analyzed. The flow extracted from the probe, measured at atmospheric pressure, was 14 l/min for the gas analysis and 7 l/min for the particle analysis.

Figure 1 depicts the sampling system used to measure gaseous and particulate emissions from a SaM146 jet engine (see Figure 2) during the MERMOSE project.

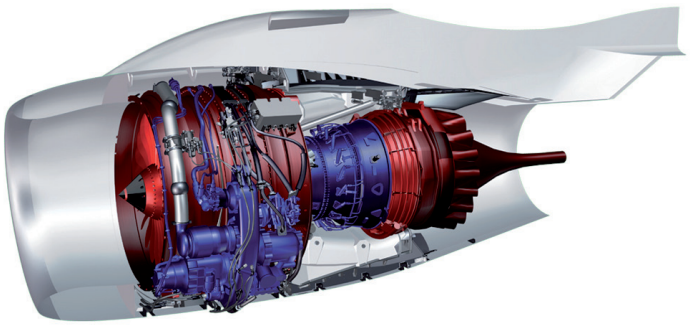

Figure 2 - Powerjet SaM 146 turbofan engine

This sampling line is not fully compliant with the AIR6241 protocol. The main aim of this essay was a complete physicochemical characterization of engine emissions and not certification. For this complete analysis, we used some specific instruments under certain working conditions that made it impossible to fulfill all of the requirements of the AIR6241 protocol. The exhaust was sampled by means of a robotic arm equipped with a single hole probe, located

5 cm away from the exit plane in the primary flow of the engine (tested in an unmixed flow configuration), and moved at various locations to ensure homogeneous sampling. A short section of the transport line after the probe was heated, on demand, in order to prevent vapors from condensing on existing primary particles (formed in the engine) or from nucleating and therefore forming new particles that would modify non-volatile particle measurements. This section was followed by two thermostated 3 m and 5 m lines maintained at 160°C. At the end of these lines, a flow splitter was used to alternately drive the sample to the measuring instruments for the analysis of gases or particles, since these two measurements could not be achieved simultaneously due to the flow rate limitations in the line.

The particle sampling line was divided into 3 thermostated sections:

- The first section was dedicated to particle collection for off-line measurements, (Line 1.0). We used two different collection techniques in parallel. Firstly, a mini impactor [23] to enable the deposition of particles on electron microscopy grids and on silicon windows to perform morphology, structure and chemical composition analyses. Secondly, we used filter samplers, where emitted particles were collected on very high efficiency quartz filters, mainly to measure the elemental to organic carbon ratio, but also to obtain additional data.
- A second separated line (Line 3.0) was equipped with a Fast Aerosol Mobility Size Spectrometer (DMS500) to determine in real time the particle number concentration and size distribution for a size ranging from 5 nm to 1000 nm.
- Finally, a third line (Line 2.0) was used, in which the sampled flow was diluted to decrease the particle concentration, enabling measurements to be made with various instruments and reducing post sampling reactions. It should be noted that the dilution factor obtained with this system was around 10. In addition, we did not use any catalytic stripper, therefore the analyzed PM include both volatile and non-volatile PM. The pressure was measured before the dilution stage using a capacitive absolute manometer thermostated at 200°C. The nitrogen used in the dilution stage was heated at 35°C, since this temperature is the maximum admitted at the instrument inlets. The dilution ratio was determined by measuring the carbon dioxide concentrations, upstream and downstream from the diluter. This ratio was used to correct the particle number measured. The line was split into three subsections to measure particle size distribution, number concentration, soot mass and surface area concentration. Two of the lines were equipped with a stainless steel cyclone (Lines 2.3 and 2.2), used to protect the instruments by cutting off particles larger than 1.69 μm.

Stainless steel lines tend to collect soot and a condensable or semi-volatile coating on their walls while combustion products are transported. No reliable measurement can be obtained during this transient phase, until the inner parts of the line are perfectly coated. The engine was therefore first run at full power for approximately 30 mn, following the AIR6241, and until the measurement instruments provided stable signals. After this line conditioning phase, the engine was operated at various settings, 7%, 30%, 70%, 85% and 100% of the take-off thrust respectively. These settings correspond to the LTO cycle certification regimes (idle, descent, climb-out and take-off) and to a representative regime for cruise conditions (70%). Finally, some post-sampling reactions have to be accounted for when retrieving engine emission indices or initial particle number density. We have done an analysis of the particle loss through the sampling line. We have used a sodium chloride aerosol to measure the penetration factors of the line. We found that these factors were independent of the size of particles. Therefore, they will not affect the shape of the measured size distribution (namely, the count median diameter (CMD) and geometric standard deviation (GSD)). As a consequence, we will consider in this work size distributions without any loss corrections. Without any further details on the influence of pressure and temperature conditions on particle losses, we will also report number, surface and mass concentrations without any correction.

On line measurement techniques

Particle number density

The standard instrument for measuring particle number concentration is the **Condensation Particle Counter** (CPC). In CPC counters, particles are detected and counted by laser scattering in a very similar way to a standard optical particle counter, but in a CPC particles are first grown by condensation to a size of 10-12 μm, enabling the detection of nanoparticles.

The CPC used in the campaigns uses the diffusional thermal cooling method to grow particles to detectable sizes (Figure 3). Using this principle, the CPC used during the campaign was able to measure particles above 5 nm.

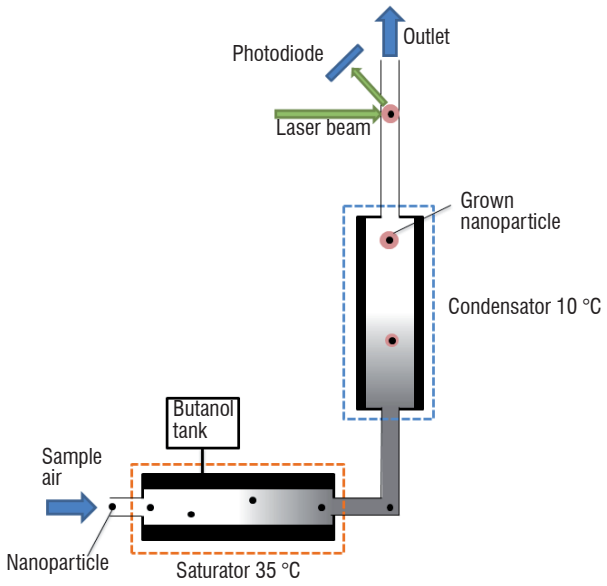

Figure 3 - CPC GRIMM 5.403 schematic diagram

A complementary instrument was used to measure particle number and mass on-line. The **Pegasor Particle Sensor M** (PPS-M) technology is based on the measurement of electrical charges carried by particles. PPS-M (Figure 4) comprises an ejector where the motive fluid flow is generated by pure, particle-free ionized gas. The motive fluid flow generates an under-pressure to the sample inlet and due to the negative pressure gradient, particle-containing gas flows into the sensor. Ionized air and sample flows are mixed, charging the particles in the sample flow very efficiently. Particle charging is linked to the particle size.

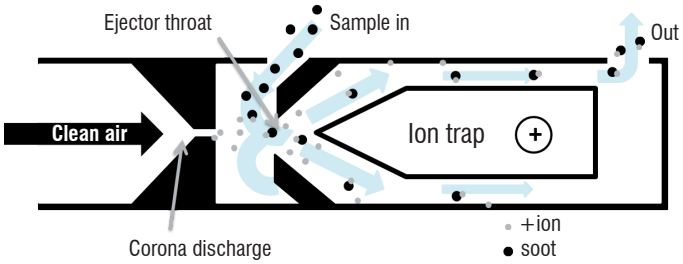

Figure 4 - Schematic representation of PPS-M

Ions that are not attached to the particles are removed from the gas flow by means of an ion trap. When the free ions are removed, the only mechanism carrying electrical current is the flow of charged particles. The electrical current escaping from the sensor with the charged particles can be measured giving a direct, fast, real-time measurement of the particle concentration. The measurement result can be expressed either as mass concentration or as number concentration, or both. With the setting used in the campaign, PPS-M was able to measure particles in the 0.02 – 2.5 μm range.

Particle size distribution measurements

Particle size distribution was measured by means of a **Scanning Mobility Particle Sizer and a Differential Mobility Sizer** DMS500.

- SMPS is based on the principle of the mobility of a charged particle in an electric field. Particles entering the system are neutralized such so that they have a Fuchs equilibrium charge distribution. Then, they enter a Differential Mobility Analyzer (DMA) where the aerosol is classified according to electrical mobility, with only particles of a narrow range of mobility exiting through the output slit. This monodisperse distribution then goes to a CPC, which determines the particle concentration at that size.

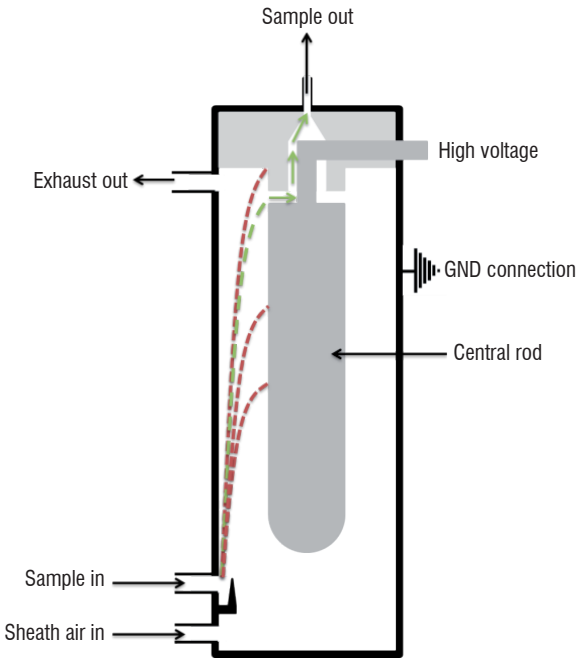

Figure 5 - Schematic representation of a DMA

The DMA (Figure 5) consists of a cylinder with a negatively charged rod at the center; the main flow through the DMA is a particle-free laminar 'sheath' air. The particle flow is injected at the external end of the DMA. Particles with a positive charge move across the sheath flow towards the central rod, at a rate determined by their electrical mobility. Particles of a given mobility exit through the sample slit at the top of the DMA, while all other particles exit with the exhaust flow. The size of the particles exiting through the slit is determined by the charge, the central rod voltage and the flow within the DMA. By exponentially scanning the voltage on the central rod, a full particle size distribution is constructed.

- The DMS500 uses a classifier column (Figure 6) operating at sub-atmospheric pressure. The DMS uses a cyclone that prevents particles larger than 1 μm from entering the instrument. The instrument operates at a fixed pressure of 0.25 bar. This low pressure reduces the residency time, avoiding particle agglomeration [33], helping to isolate the instrument from fluctuating sample pressure and allowing its wide size range (5-1000 nm). The sample gas passes through a corona charger into the classifier column.

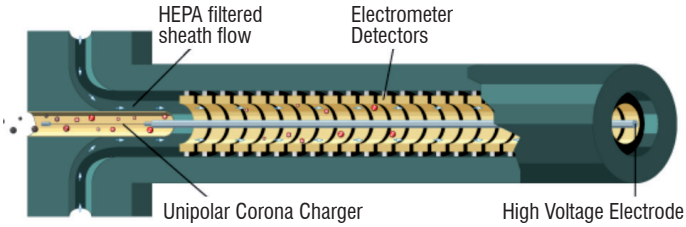

Figure 6 - DMS500 classifier column schematic diagram

The charged aerosol is then introduced into a strong radial electrical field inside a classifier column. This field causes particles to drift through a sheath flow to the electrometer detectors. Particles are detected at various distances down the column, depending on their electrical mobility. The outputs from the electrometers are then processed in real time to provide particle number and size data.

Off line measurement techniques

Black Carbon mass concentration

BC loads were measured using a Thermo Scientific™ 5012 MAAP. This instrument uses a multi-angle absorption photometer to analyze the modification of radiation fields in the forward and back hemisphere of a glass-fiber filter caused by deposited particles.

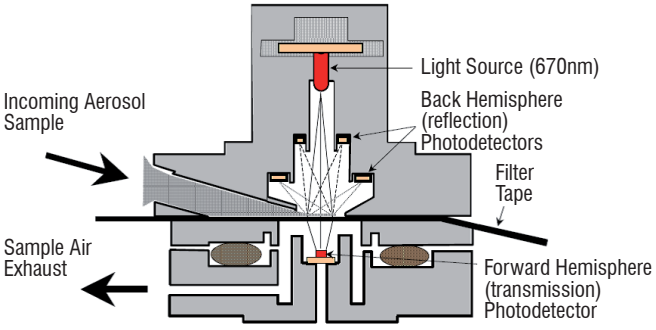

Figure 7 - MAAP detection chamber schematic diagram

The sample flows through the down-tube and is deposited on the glass fiber filter tape. The filter tape will accumulate an aerosol sample towards a threshold value, whereupon the filter tape will automatically advance prior to reaching saturation. Within the detection chamber (Figure 7), a 670 nm visible light source is aimed towards the deposited aerosol and filter tape matrix. The light transmitted into the forward hemisphere and reflected into the back hemisphere is measured by a series of photo-detectors. During sample accumulation, the light beam is attenuated from an initial reference reading from a clean filter spot. The reduction of light transmission, multiple reflection intensities and air sample volume are continuously integrated over the sample run period to provide a real-time data output of black carbon concentration measurements.

Surface area density

The **Nanoparticle Surface Area Monitor** (NSAM) measures the human lung-deposited surface area of particles (reported as $\mu m^2/cm^3$) corresponding to tracheobronchial (TB) and alveolar (A) regions of the lung. The way in which this instrument operates is based on the diffusion charging of sampled particles, followed by the detection of the charged aerosol using an electrometer. The aerosol sample is continuously drawn into the instrument (Figure 8). This flow is split into two flows. One passing through a HEPA filter to produce clean air, which is then ionized using a corona electrode, and the other introduced into the mixing chamber against the current of positive ions produced by corona discharge. The flows are reunited in a mixing chamber, where particles in the aerosol flow mix with the ions carried by the filtered clean air acquiring a positive charge. The separation of particles from direct interaction with the corona needle and/or the strong field near it reduces particle losses and makes the charging process more efficient and reproducible. The charged aerosol then passes through a trap to remove excess ions. The aerosol then moves on to an aerosol electrometer for charge measurement. In the electrometer, current is passed from the particles to a conductive filter and measured by a very sensitive amplifier. The intensity measured is converted in terms of deposited surface in two regions of the respiratory system: tracheobronchial and alveolar.

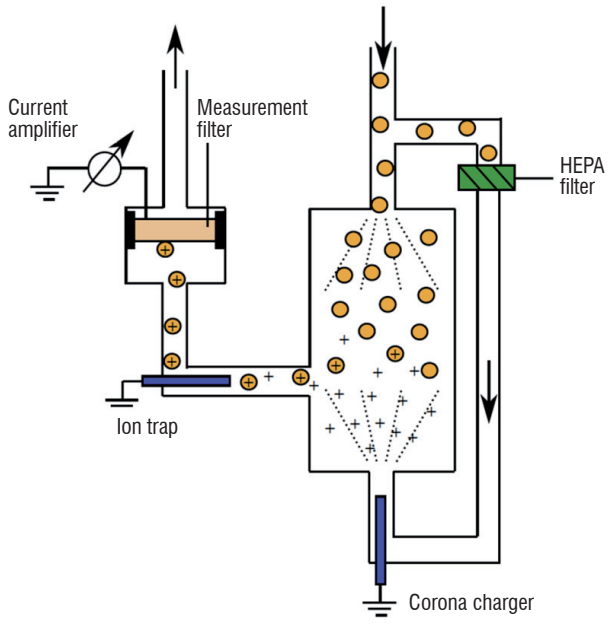

Figure 8 - NSAM 3550 [2] operating principle

The deposited surface area measured by NSAM can be used to determine an active surface equivalent diameter [2].

Morphology and structure characterization

The morphology and structure of the emitted particles were studied by **high-resolution transmission electron microscopy** (HR-TEM), **Raman spectroscopy, near-edge X-ray absorption fine structure spectroscopy** (NEXAFS) and **X-ray photoemission spectroscopy** (XPS).

- **HR-TEM** is an instrument for the high-magnification study of nanomaterials. TEM can simultaneously give information in real space (in the imaging mode) and reciprocal space (in the diffraction mode). The basic principle of TEM is quite similar to their optical counterparts, the optical microscope. The main difference is that TEM uses a focused beam of electrons instead of light to "image" and achieve information about the structure and composition of the sample. An electron gun produces a stream of electrons, which is accelerated towards the sample using a positive electrical potential. This stream is then focused using condenser lenses into a thin, focused, monochromatic beam. The beam strikes the sample and part of it is transmitted through it. This portion of the beam is again focused through objective lenses into an image.
  Samples were studied in both modes (image and diffraction) [25]. Images collected in the imaging mode provide morphological information, as well as the size of primary particles. Those obtained in the diffraction mode provide a more accurate measurement of the carbon layer spacing and enable the determination of the C-C bond lengths.

- **Raman spectroscopy** has been widely used to study various carbonaceous materials, including soot ([30], [31], [4] and references therein). It involves interactions of molecules with the electromagnetic field produced by a laser. The resulting scattered light (Raman scattering) is a radiation type that represents a measure of the vibrational frequency of molecules corresponding to vibrational and/or rotational transitions shifted from the incident laser beam frequency. Soot Raman spectra presents a first order band in the 1000-1700 cm^{-1} region; the complexity of this band varies for different samples and is related to their nature. The G band at 1580 cm^{-1} is solely observed in single crystal graphite. In more complex carbonaceous materials, the D1 and D2 bands appear as the number of defects increases. The D1 band at 1350 cm^{-1} corresponds to a breathing mode of carbon rings [9], which is Raman inactive in the case of perfect infinite graphitic planes. It becomes active and observable in Raman for finite graphene [13]. The D2 band at 1620 cm^{-1} is generally assigned to lattice vibrations analogous to that of the G band, but involving isolated graphene layers, i.e., not directly sandwiched between two other layers [12]. When the carbonaceous material is highly disordered, two further bands D3 and D4 appear. The D3 band at 1500 cm^{-1} is generally very broad and is often assigned to amorphous carbon ([8], [17], [10], [11]). In general, the D4 band is characteristic of highly disordered materials like soot or coal chars ([30], [22], [1], [36], [11]). Its origin is still under debate; some authors assign it to carbon sp^3-sp^2 at the periphery of the crystallites, or to C-C and C=C stretching vibrations in polyene-like structures ([22], [1], [10]).

- **NEXAFS** involves the excitation of electrons from a core level to partially filled and empty states. The decay of core-hole states results in the emission of Auger electrons from valence molecular orbitals (Figure 9), leading to the formation of cascades of secondary electrons in the material, generating a photocurrent proportional to the excitation probability. A NEXAFS spectrum in "total electron yield" mode consists in measuring this photocurrent as a function of the photon energy, in the vicinity of an absorption edge (carbon and oxygen K-edges are of main interest in soot). The peak positions and spectral lineshape in a NEXAFS spectrum are directly related to the nature of these unoccupied electronic states. Given that the photocurrent originates from 5 nanometers from the sample surface, in the case of soot, made up of primary particles of a few nanometers in diameter, this technique can be considered to probe their bulk. A variant of the NEXAFS technique consists in recording the spectra by measuring the Auger electron yield only ("partial electron yield" method),which arises from the 2-3 top-most layers because of their typical low mean free path in matter. Thus, this technique can be both surface and bulk sensitive and is capable of probing both the soot electronic structure and the surface functional groups simultaneously. In the context of carbon-based structures such as soot, NEXAFS measurements can detect specific bonds in molecules (e.g., C=C, C-C, and C-O bonds) [32].

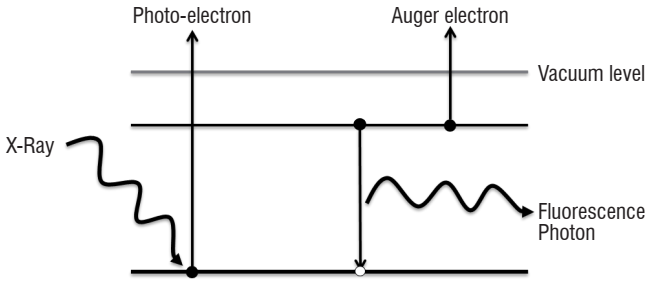

Figure 9 - Energy diagram of the photoabsorption process and the subsequent filling of the core hole by emission of an Auger electron or a fluorescence photon. The Auger electron yield (and excited secondary electron yield) has been used for the NEXAFS spectroscopy of soot.

- **XPS** is another surface characterization technique that can analyze a sample to a depth of 2 to 5 nm. Electrons in specific bound states can be excited by irradiating a sample with x-rays of sufficient energy. A typical XPS experiment uses enough energy to induce the ejection of photoelectrons from the sample (Figure 9) has been used for the NEXAFS spectroscopy of soot. Ejected photoelectrons from core levels have slight energy shifts depending on the outer valence configuration of the material examined. In addition, the specific energy of an elemental core level transition occurs at a specific binding energy that can uniquely identify the element. In a typical XPS spectrum, some of the ejected photoelectrons inelastically scatter through the sample to the surface, while others undergo prompt emission and suffer no energy loss in the process. An electron analyzer measures the kinetic energy of the ejected photoelectrons, producing an energy spectrum of intensity (number of photoelectrons versus time) versus binding energy (the energy that the electrons had before they left the atom). Each energy peak in the spectrum corresponds to a specific element. In addition to identifying elements in the sample, the peak area is proportional to the number of atoms present in each element. The sample chemical composition is obtained by calculating the respective contribution of each peak area.

Chemical composition characterization

Energy-dispersive X-Ray spectroscopy (EDX), **Organic to Elemental Carbon ratio** (OC/EC) analysis, **Laser Two-Step Mass Spectrometry** (L2MS) and **Time-of-Flight Secondary Ion Mass Spectrometry** (ToF-SIMS) techniques were also used for a complete chemical characterization of the samples.

- EDX spectroscopy uses a beam of electrons or high-energy radiation to excite core electrons to high energy states, creating a low-energy vacancy in the atom electronic structures. This leads to a cascade of electrons from higher energy levels until the atom regains a minimum-energy state. Due to energy conservation, the electrons emit X-rays during their transition to lower energy states. It is these X-rays that are being measured in X-ray spectroscopy. Since each element has a different nuclear charge, the energies of the core shells and, more importantly, the spacing between them vary from one element to the next. While not every peak in the spectrum of an element is exclusive to that element, there are enough characteristic peaks to be able to determine the composition of the sample, given sufficient resolving power.

- The OC/EC ratio was analyzed using Thermal-Optical Analysis fully compliant with the IMPROVE protocol [7]. First, the sample is heated in a completely oxygen-free helium atmosphere in four increasing temperature steps to remove all organic carbon from the sample. The transition from the third temperature to the fourth (from 500°C - 700°C) quickly decomposes inorganic carbonates, producing a sharp, characteristic peak. It should be noted that only one filter was used for the sampling, thus organic vapors can be adsorbed on the filter, leading to an overestimation of OC/TC. Samples collected at 30% engine regime are more sensible to this bias, since the organic compound concentration in the exhaust is higher in this regime.

- L2MS and ToF-SIMS are two mass spectrometry techniques able to measure the surface chemical composition of aerosol particles. In L2MS [14] (Figure 10), the adsorbed phase is probed by nanosecond laser desorption and then the ejected molecules are ionized with a second nanosecond laser and further

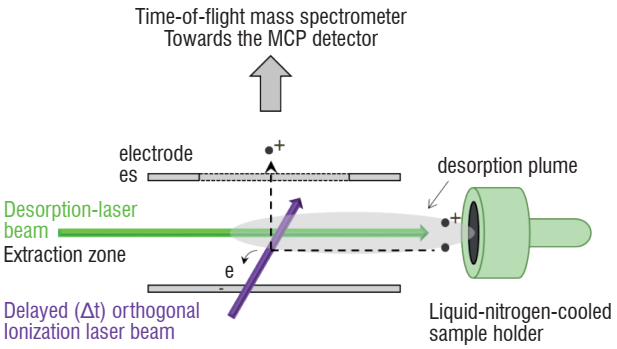

Figure 10 - L2MS technique schematic diagram

mass-separated by ToF-MS. For desorption, the collimated beam of a nano-second Nd:YAG laser is directed through a circular pinhole onto the sample. The laser irradiance can be carefully controlled to maximize the signal of the parent molecules and to avoid the direct fragmentation of the species during the desorption step. This configuration is particularly well suited for the detection of aromatic species like Polycyclic Aromatic Hydrocarbons (PAHs).

- ToF-SIMS is similar to L2MS. It uses a pulsed primary ion beam (Bi_3^+) to desorb and ionize species from a sample surface. The resulting secondary ions are accelerated into a mass spectrometer, where they are mass analyzed by measuring their time-of-flight from the sample surface to the detector (Figure 11). In addition to the mass spectra acquired from the molecular species on the sample surface, this instrument is able to provide an image of the sampled surface, enabling the distribution of individual species to be visualized on the surface of the sample. There are three different modes of analysis in TOF-SIMS:

The main advantage of the L2MS technique compared to ToF-SIMS is the low fragmentation of the analyzed compounds achieved through a careful tuning of desorption and ionization energies (Figure 12, left panel). On the one hand, the highest mass resolution achieved in L2MS is around 1000 while in ToF-SIMS, depending of the substrate morphology, it is possible to reach up to 10000. As can be seen in Figure 12, right panel, the L2MS mass resolution is not sufficient to distinguish different compounds with the same integer mass but different elemental composition, as opposed to ToF-SIMS.

Results

Particle number, mass, surface area and size distribution

The properties of non-volatile emitted particles vary with the engine thrust rate. The size distribution, the particle number density, the mass and the surface concentration can be affected.

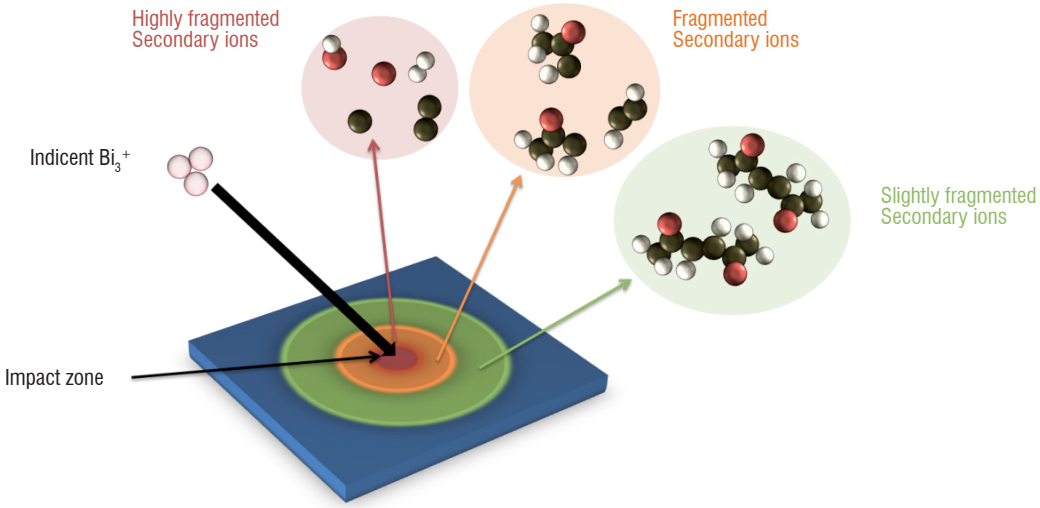

Figure 11 - Ion beam desorption/ionization performed in the ToF-SIMS instrument

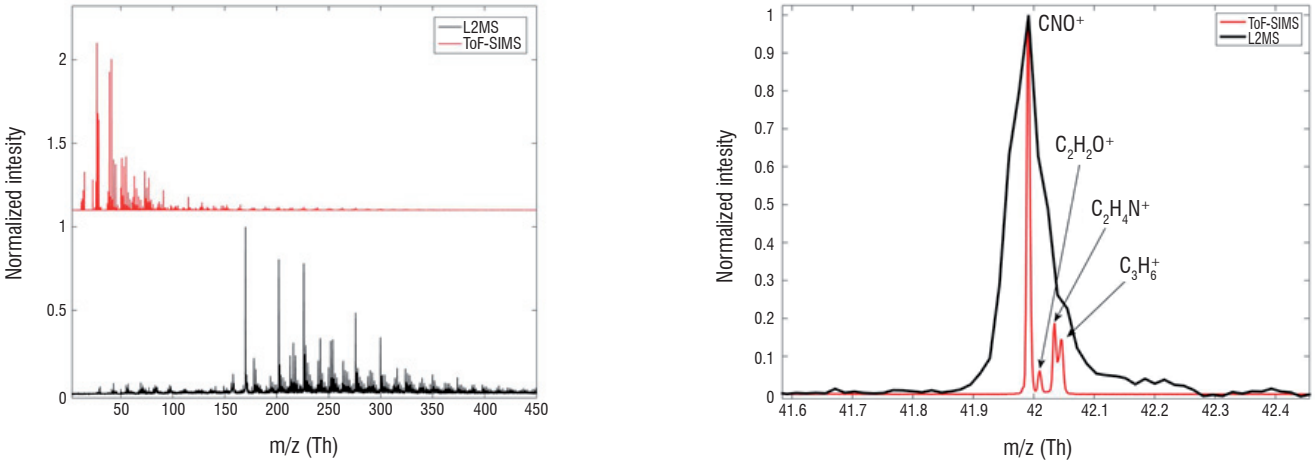

Figure 12 - L2MS and ToF SIMS spectra obtained from the same soot sample collected at 70% engine regime. Left panel, illustration of fragmentation produced in L2MS and ToF-SIMS techniques. Right panel, illustration of the different mass resolution obtained with L2MS and ToF-SIMS for the same sample.

For all of the investigated engine regimes, a monomodal log-normal type particle size distribution has been obtained (Figure 13). The modal diameter has also been found to grow with increasing regime up to 85% (Figure 14) and to remain constant beyond. The greatest change is produced between the 30% case regime, where the modal diameter is 24.1+/- 1.2 nm, and the 70% regime, where the modal diameter increases up to 47.2 +/- 2.6 nm. The studies by [5] on a C-130 Hercules and by [6] on various military turbofan, turboprop and turboshaft aircraft also showed a trend of increasing particle diameter with increasing engine power settings. On the other hand, the results reported from the APEX campaign showed that the particle diameter first decreases when the engine thrust increases from low to medium settings and then increases at higher thrust [19].

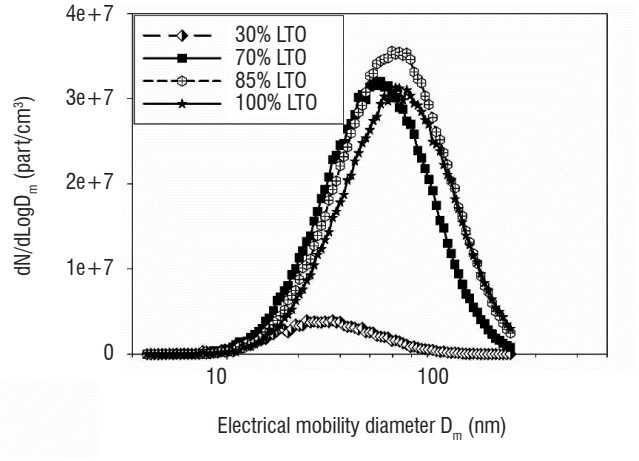

Figure 13 - Size distributions for number concentration obtained for various engine regimes (values not corrected for particle loss in the sampling line)

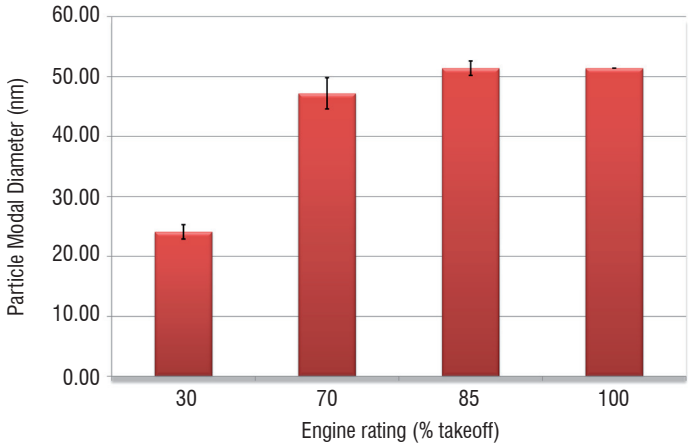

Figure 14 - Particle modal diameter for each engine regime

Number and mass concentrations present similar trends, both increase with the engine regime up to 85%, remaining almost constant between 85% and 100%. In general, CPC and PPS-M agreement on particle number is quite good, with the only exception of the 30% regime, where the particle number density measured by CPC is larger than that measured by PPS-M. The reason behind this discrepancy might be the different nature of the particles produced at 30%, which include a larger fraction of organic particles, probably volatile, that are measured by the CPC but not measured by the PPS-M. In addition, the cutoff diameter for both instruments was different; while CPC counted particles larger than 5 nm, the PPS-M cutoff was 20 nm. Since the size distribution for the 30% regime is shifted towards smaller sizes, this difference might be more evident in this regime. Again the largest shift is observed between the 30% and 70% regimes. These results

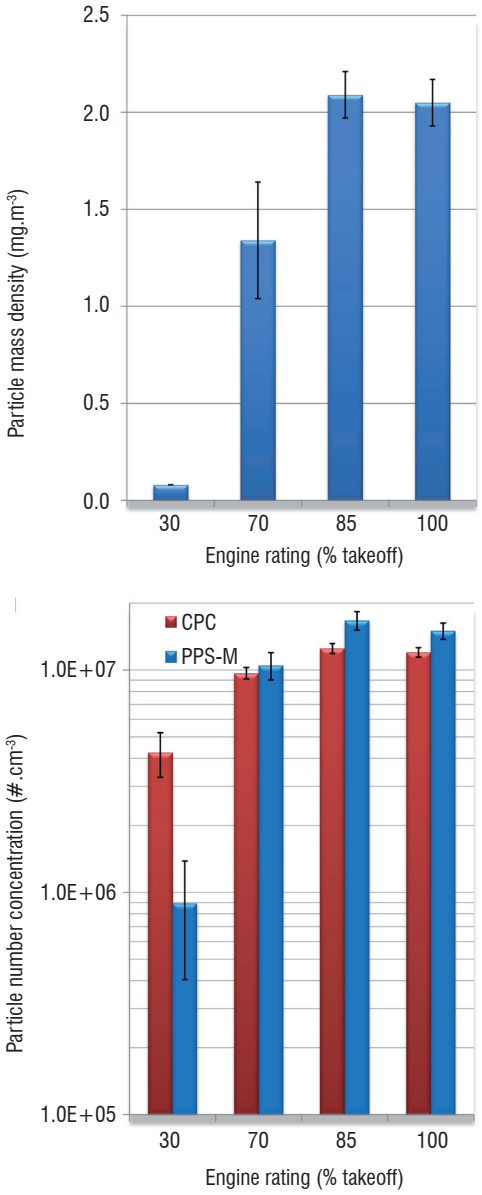

Figure 15 - Top: Particle mass measured for each engine regime
Bottom: Particle number measured for each engine regime

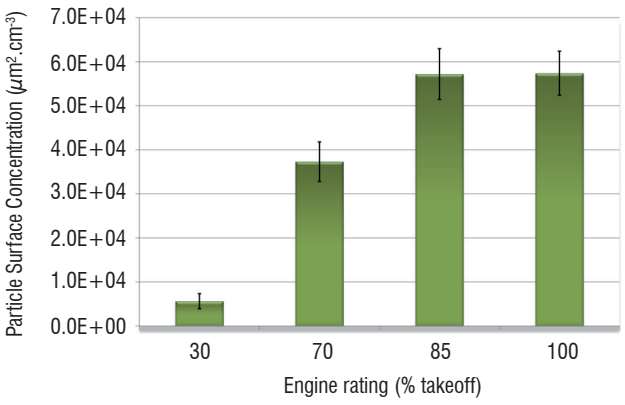

Figure 16 - Particle surface concentration for each engine regime

are in line with those presented by previous studies, where in most of the cases an increase in the engine regime results in an increase in the particle emission index ([28], [19], [6], [3]).

The surface concentration evolves in a similar way regarding the other investigated parameters. We found a large increase in surface concentration when the engine regime increased from 30% to 70% and an almost constant value between 85% and 100%. The values obtained range from roughly 6 x 10^3 to 6 x 10^4 $\mu m^2.cm^{-3}$. The studies reporting the surface concentration of airplane engine emitted particles are scarce. [29] measured the surface concentration of particles emitted from a GE-J85-5L in the NASA Lewis Research Center using an altitude-simulation facility at 95% and 100% engine regime, for various simulated altitudes. The authors reported a slight increase in the surface concentration between 95 and 100% at 36,000 ft. However, no difference could be observed at 41,000 and 45,000 ft. In addition, the authors highlighted a large impact of the simulated altitude on the particle surface concentration, increasing with decreasing altitude. Results ranged from 5.87 x 10^3 $\mu m^2.cm^{-3}$ at 45,000 ft to 1.28 x 10^4 $\mu m^2.cm^{-3}$ for measurements at 5,000 ft. [28] reports a 2 x 10^5 $\mu m^2.cm^{-3}$ surface concentration of particles emitted by ATTAS aircraft in flight (26,000 ft) with an engine regime of about 30%. Discrepancies can originate from different sampling or testing conditions (ground level, altitude test cell, in flight) but also from the different engine technologies used. The GE-J85-5L and the ATTAS engine (RR-SNECMA M-45H) are old generation engines from the 60s and 70s whereas the SaM146 has been certified very recently.

Morphology and structure characterization results

HR-TEM images illustrate the turbostratic structure of soot aggregates (Figure 17, top right panel) where a few graphene carbonaceous layers having a small lateral extension are stacked, with a random rotation angle between them, forming basic structural units concentrically oriented in space to form an onion-like structure [26].

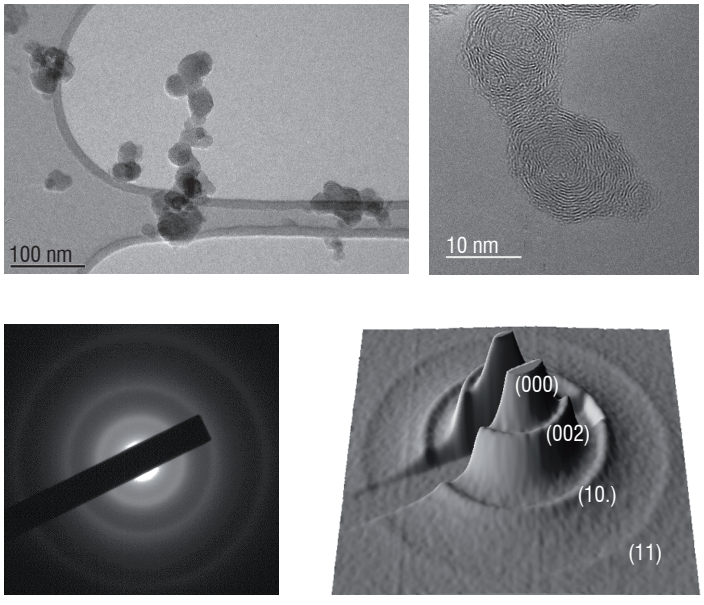

Figure 17 - Top left panel: HR-TEM image showing soot aggregates. Top right panel: Soot primary particles presenting a turbostratic structure. Bottom left panel: Diffractogram showing concentric rings. Bottom right panel: 3D representation of the diffractogram with diffraction ring indices

The morphology of the samples obtained at various engine regimes has been found to be very similar [25]. Carbon bonding lengths ranged from 0.138 to 0.141nm, which is slightly shorter than in graphite ($l_{C\text{-}C}$ = 0.142 nm) as usually determined for atmospheric soot [20]. The geometric length of carbonaceous layers ranged from 2.54 to 3.66 nm for engine thrust levels between 30%-100%. These values are of the same order of magnitude but higher than those reported by [34] for a CFM-56-2 engine (~0.7 nm).

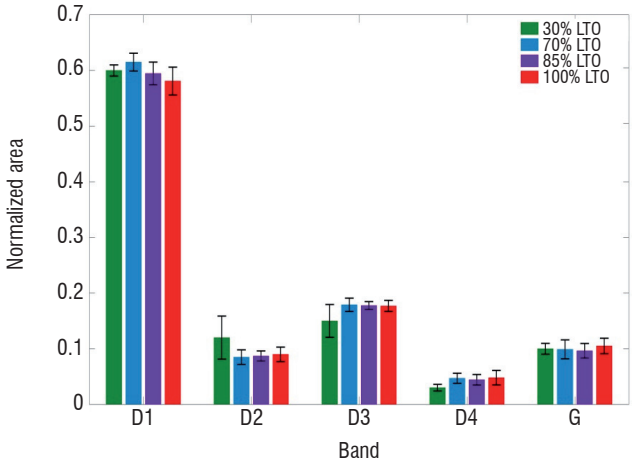

Figure 18 - Normalized area for D1, D2, D3, D4 and G bands for each sample analyzed

Analyzed samples presented very similar Raman spectra regardless of the engine regime [25] (Figure 18). The intensity of the fitted bands pointed to crystalline domains between 2.67 and 3.06 nm, in good agreement with the HR-TEM results. Also, the relative intensities of the D1 and D2 bands corresponded to a highly defective graphite structure. The presence of a D4 band indicated the presence of non-graphitic carbon, though it presented a rather low intensity.

As in the case of Raman and HR-TEM, the NEXAFS and XPS measurements did not show remarkable differences between the samples collected at different engine regimes [25]. With regard to the structure of the soot particles found in the samples, NEXAFS showed that their surface consists mainly of graphene layers of the same size as in the bulk, although more defective. The surface also presented a high concentration of unsaturated organic hydrocarbons that were not detected in the bulk. XPS spectra showed that the soot particles were poorly oxidized, with a slight enhancement of the oxidation rate at the very surface. Oxide functions were essentially ketones and carbonyls, with few hydroxyls and quinones.

Chemical composition characterization results

EDX analyses performed in the samples collected during the SAM146 campaign revealed that particles are free of metallic elements (within the detection limit of the technique) and are systematically made up of carbon, oxygen and traces of sulfur [25], due to its presence in the fuel. In addition, we found that the elemental bulk chemical composition did not evolve with engine thrust. Thus, on average, the elemental chemical composition of the samples can be considered as ~97% of carbon, ~3% of oxygen and atomic traces of sulfur (~0.1%).

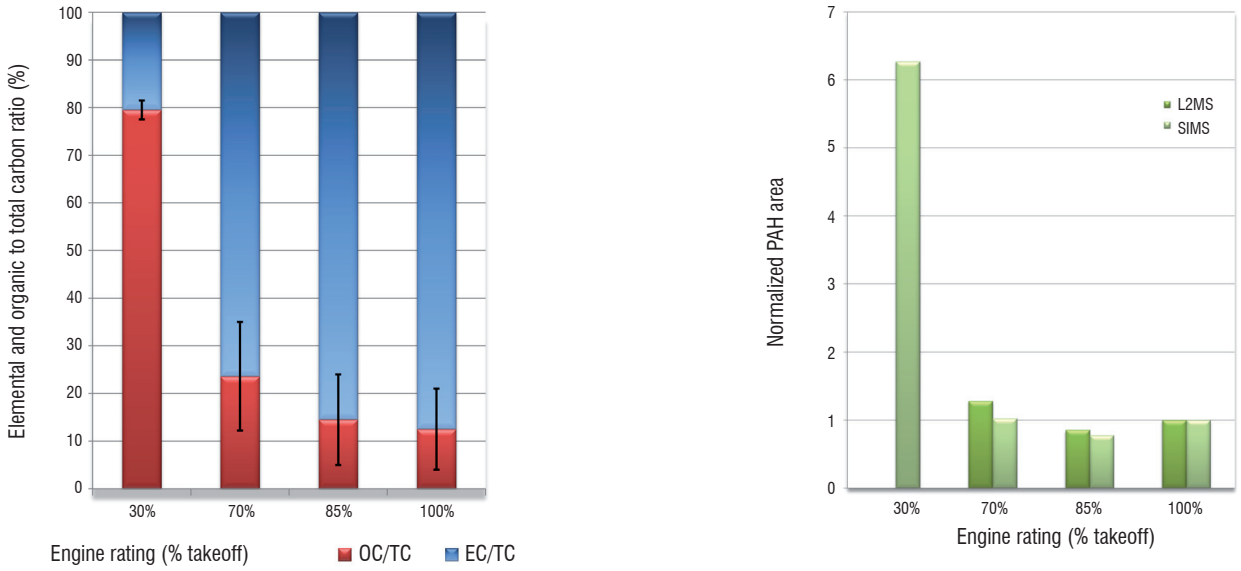

Figure 19 - Left panel: Organic carbon (red) and elemental carbon (blue) content of various samples analyzed
Right panel: Total PAHs content of various samples analyzed by the TOF-SIMS (light green) and L2MS (dark green) technique

Figure 19 (left panel) shows the OC/EC ratios measured for the samples collected during the SAM146 campaign at various engine regimes. We can see how the organic content decreases as the engine thrust increases, with a large decrease from ~79% for the 30% regime to ~24% for the 70% engine regime. In addition, L2MS and ToF-SIMS were used to determine the PAH content of various samples (Figure 19, right panel). As can be seen, both techniques present a good agreement with regard to the total PAH content. Unfortunately, we could not measure the total PAH content of the 30% sample with L2MS due to the low load of the sample. The total PAH content found by these two techniques is also in good agreement with the organic carbon content found in the OC/EC analysis. These results were in line with those reported in the literature, where the OC/EC ratio was found to decrease when the engine regime increased ([27]).Nevertheless, in the results reported by [27], the amount of organic carbon drops between the 7% and 30% engine regimes, with just a slight drop between the 30% and 80% regimes. In our case, the main drop in the organic content is observed between the 30% and 70% regimes. One possible reason for these differences might be the overestimation of the OC/TC ratio for the 30% regime due to the absorption of organic compounds present in the gas phase in the filters.

ToF-SIMS showed the presence on molybdenum oxides in some of the samples. These species were heterogeneously distributed over the sample surface. To obtain a better insight of the origin of these compounds, we performed an imaging study of the samples. Thanks to this, we were able to distinguish two different kinds of aerosol particles, containing sulfate and molybdenum oxides respectively, from the substrate (Silicon wafer) (Figure 20).

We found that the particles containing sulfate were smaller and were distributed over all of the substrate, while the signal corresponding to molybdenum oxides was associated with lubricant oil droplets collected on the substrate. Most probably, these compounds come

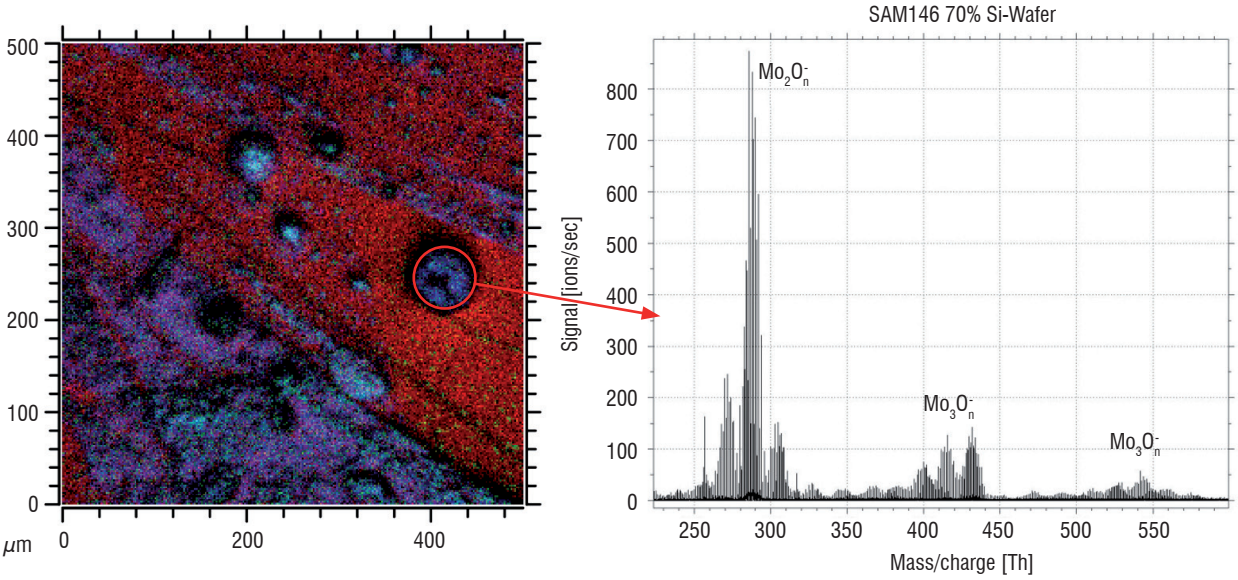

Figure 20 - Left panel: Mapping of an aerosol sample collected over a silicon wafer; the red areas indicate the presence of SiO_2^- ions, the blue areas indicate the presence of $Mo_2O_6^-$ ions and the green areas indicate the presence of HSO_4^- ions. Right panel: mass spectra of the selected particle showing Molybdenum oxide peaks.

from the motor gear, in which molybdenum doped stainless steel is used for some parts. The presence of oil droplets on the engine exhaust has also been reported in previous studies. A study from [35] identified lubricant oil droplets in the particulate matter emissions from various commercial aircraft at two airports.

Conclusions

In this work we presented a complete sampling and characterization methodology of nVPM. We applied it to the measurement of the nvPM emitted by a SaM146 engine. It was operated at various engine regimes corresponding to four LTO cycle certification regimes and a regime representative of a cruise fuel air ratio condition. We found that the size, number, mass and surface concentration of the emitted particles increase when the engine regime increases up to 85%, staying constant above this limit. The largest increase for all of these properties was found between the 30% and 70% engine regimes. These results are in line with those available in the literature. From the point of view of chemical characterization, the three different techniques used point to a larger content of organic carbon in the 30% sample. L2MS and ToF-SIMS show a high content in PAHs in this sample as well. In this case, though previous results show a similar trend, the organic content found in the 30% sample is greater than that reported in previous studies. Regarding the physical and chemical properties of the emitted soot primary particles, we did not find a significant change between the various engine regimes. These particles present an onion-like nanostructure, consisting of concentric graphitic layers with small lateral extensions ranging from 2.54 to 3.66 nm. They present a low degree of oxidation, with a slight enhancement at the surface. Our results show how some properties, like the morphology of soot particles, were not affected by the engine regime, while others like the chemical composition or particle size, number mass and surface concentration were largely affected. These results illustrate the importance of a complete characterization of nvPM emissions to fully evaluate the potential impact of emissions on climate ■

Acknowledgements

This work was supported by the CORAC MERMOSE project for the characterization of emissions by aircraft engines and funded by the DGAC (French Civil Aviation Authority).

References

[1] E. BAR-ZIV, A. ZAIDA, P. SALATINO, O. SENNECA - *Diagnostics of Carbon Gasification by Raman Microprobe Spectroscopy*. Proceedings of the Combustion Institute, 28, 2369–2374, 2000.

[2] S. BAU - *Étude des moyens de mesure de la surface des aérosols ultrafins pour l'évaluation de l'exposition individuelle*. Thèse de Doctorat de l'INPL, Nancy, 3 Décembre 2008.

[3] J. CAIN, M.J. DEWITT, D. BLUNCK, E. CORPORAN, R. STRIEBICH, D. ANNEKEN, C. KLINGSHIRN, W.M. ROQUEMORE,R. VANDER WAL - *Characterization of Gaseous and Particulate Emissions from a Turboshaft Engine Burning Conventional, Alternative, and Surrogate Fuels*. Energy and Fuels, 27, 2290-2302, 2013.

[4] T. CATELANI, G. PRATESI, M. ZOPPI - *Raman Characterization of Ambient Airborne Soot and Associated Mineral Phases*. Aerosol Science & Technology, 48, 13–21, 2014.

[5] M. D. CHENG, E. CORPORAN, M. J. DEWITT, C. W. SPICER, M. W. HOLDREN, K. A. COWEN, A. LASKIN, D. B. HARRIS, R. C. SHORES, R. KAGANN, R. HASHMONAY - *Probing Emissions of Military Cargo Aircraft: Description of a Joint Field Measurement Strategic Environmental Research and Development Program*. Journal of the Air and Waste Management Association, 58, 787-796, 2008.

[6] M. D. CHENG, E. CORPORAN - *A Study of Extractive and Remote-Sensing Sampling and Measurement of Emissions from Military Aircraft Engines*. Atmospheric Environment, 44, 4867-4878, 2010.

[7] J. C. CHOW, J. G. WATSON, L.-W. A. CHEN, M. C. O. CHANG, N. F. ROBINSON, D. TRIMBLE, S.KOHL - *The IMPROVE_A Temperature Protocol for Thermal/Optical Carbon Analysis: Maintaining Consistency with a Long-Term Database*. Journal of the Air & Waste Management Association, 57, 1014-1023, 2007.

[8] A. CUESTA, P. DHAMELINCOURT, J. LAUREYNS, A. MARTINEZ-ALONSO, J. M. D. TASCON - *Raman Microprobe Studies on Carbon Materials*. Carbon, 32, 1523–32, 1994.

[9] E. DI DONATO, T. TOMMASINI, G. FUSTELLA, L. BRAMBILLA, C. CASTIGLIONI, G. ZERBI, C. D. SIMPSON, K. MULLEN, F. NEGRI - *Wavelength-Dependent Raman Activity of D2h Symmetry Polycyclic Aromatic Hydrocarbons in the D-Band and Acoustic Phonon Regions*. Chemical Physics, 301, 81-93, 2004.

[10] B. DIPPEL, H. JANDER, J. HEINTZENBERG - *NIR FT Raman Spectroscopic Study of Flame Soot*. Physical Chemistry Chemical Physics, 1, 4707–4712, 1999

[11] B. DIPPEL, J. HEINTZENBERG - *Soot Characterization in Atmospheric Particles from Different Sources by NIR FT Raman Spectroscopy*. Journal of Aerosol Science, 30 (Suppl.1), 907–908, 1999.

[12] M. S. DRESSELHAUS, G. DRESSELHAUS, Topics in applied physics, vol. 51. Berlin: Springer-Verlag, p. 3-57, 1982.

[13] A. ECKMAN, A. FELTEN, A. MISCHENKO, L. BRITNELL, R. KRUPKE, K. S. NOVOSELOV, C. CASIRAGHI - *Probing the Nature of Defects in Graphene by Raman Spectroscopy*. Nano Letters, 12, 3925-3930, 2012.

[14] A. FACCINETTO, P. DESGROUX, M. ZISKIND, E. THERSSEN, C. FOCSA - *High-Sensitivity Detection of Polycyclic Aromatic Hydrocarbons Adsorbed onto Soot Particles Using Laser Desorption/Laser Ionization/Time-of-Flight Mass Spectrometry: An Approach to Studying the Soot Inception Process in Low-Pressure Flames*. Combustion and Flame, 158, 227-239, 2011.

[15] D. J. HOFMANN, J. M. ROSEN - *Balloon Observations of a Particle Layer Injected by Stratospheric Aircraft at 23 km*. Geophysical Research Letters, Vol. 5(6), 1978

[16] J.E.PENNER, D.H. LISTER, D.J. GRIGGS, D.J. DOKKEN, M. MCFARLAND (Eds.) – *Intergovernmental Panel on Climate Change (IPCC)*. Aviation and the Global Atmosphere Special Report, Cambridge University Press, UK., pp 373, 1999

[17] T. JAWHARI, A. ROID, J. CASADO - *Raman Spectroscopic Characterization of some Commercially Available Carbon Black Materials*. Carbon, 33, 1561–1565, 1995.

[18] G. KATAGIRI, H. ISHIDA, A. ISHITANI - *Raman Spectra of Graphite Edge Planes*. Carbon, 26, 565–571, 1998.

[19] J. S. KINSEY, Y. DONG, D. C. WILLIAMS, R. LOGAN - *Physical Characterization of the Fine Particle Emissions from Commercial Aircraft Engines During the Aircraft Particle Emissions eXperiment (APEX) 1-3*. Atmospheric Environment, 44, 2147-2156, 2010.

[20] V. KOVACS KIS, M. POSFAI, J. L. LABAR - *Nanostructure of Atmospheric Soot Particles*. Atmospheric Environment, 40, 5533−5542, 2006.

[21] D. S. LEE, G. PITARI, V. GREWE, K. GIERENS, J. E. PENNER, A. PETZOLD, M. J. PRATHER, U. SCHUMANN, A. BAIS, T. BERNTSEN, D. IACHETTI, L. L. LIM, R. SAUSEN - *Transport Impacts on Atmosphere and Climate: Aviation*. Atmospheric Environment, 44, 4678-4734, 2010.

[22] T. LIVNEH, E. BAR-ZIV, P. SALATINO, O. SENNECA - *Evolution of Reactivity of Highly Porous Chars from Raman Microscopy*. Combustion Science and Technology, 153, 65–82, 2000.

[23] D. LOTTIN, D. FERRY, J.-M. GAY AND D. DELHAYE - *Towards an Identification of Aircraft Soot among Urban Background: Focus on Nanoparticles Emitted by CFM56 Turbofan Engines*. European Aerosol Conference, Granada, Spain, 2 - 7 September 2012.

[24] F.-X. OUF, E. BRUGIÈRE, D. FERRY, S. PONTREAU AND J. YON - *Characterization of Aerosols Produced by a Commercial Combustion Aerosol Generator MiniCASTTM 5201: EC/TC, Size Distribution, Morphology and Optical Properties*. European Aerosol Conference, Granada, Spain, 2-7 September 2012.

[25] P. PARENT, C. LAFFON, I. MARHABA, D. FERRY, T.Z. REGIER, I.K. ORTEGA, B. CHAZALLON, Y. CARPENTIER, C. FOCSA - *Nanoscale Characterization of Aircraft Soot: A HRTEM, Raman, NEXAFS and XPS Study*. Carbon, under review, 2015.

[26] M. PAWLITA, J. N. ROUZAUD, S. DUBER - *Raman Microspectroscopy Characterization of Carbon Blacks: Spectral Analysis and Structural Information*. Carbon, 84, 479−490, 2015.

[27] A. PETZOLD, F.P. SCHRÖDER - *Jet Engine Exhaust Aerosol Characterization*. Aerosol Science and Technology, 28, 63-77, 1998.

[28] A. PETZOLD, J. STROM, F.P. SCHRODER, B. KARCHER, *Carbonaceous Aerosol in Jet Engine Exhaust: Emission Characteristics and Implications for Heterogeneous Chemical Reactions*. Atmospheric Environment, Vol. 33(17), 2689–2698, 1999.

[29] J. E. RICKEY - *The Effect of Altitude Conditions on the Particle Emissions of a J85-GE-5L Turbojet Engine*. NASA Technical Memorandum TM-106669, 52p, 1995.

[30] A. SADEZKY, H. MUCKENHUBER, H. GROTHE, R. NIESSNER, U.PÖSCHL - *Raman Microspectroscopy of Soot and Related Carbonaceous Materials: Spectral Analysis and Structural Information*. Carbon, 43, 1731-42, 2005.

[31] J. SCHMID, B. GROB, R. NEISSNER, P. IVLEVA - *Multi-Wavelength Raman Microscopy for Rapid Prediction of Soot Oxidation Reactivity*. Analytical Chemistry, 83, 1173-1179, 2010.

[32] J. STOHR, *NEXAFS Spectroscopy*. Springer, Berlin, 1992.

[33] J. P. R. SYMONDS, K. REAVELL - *Calibration of a Differential Mobility Spectrometer*. European Aerosol Conference, Salzburg, Austria, September 9-14, 2007.

[34] R. L.VANDER WAL, V. M. BRYG, C. H. HUANG - *Aircraft Engine Particulate Matter: Macro- Micro- and Nanostructure by HRTEM and Chemistry by XPS.* Combustion and Flame, 161, 602-611, 2014.

[35] Z. YU, S.C. HERNDON, L.D. ZIEMBA, M.T. TIMKO, D.S. LISCINSKY, B.E. ANDERSON, R.C. MIAKE-LYE - *Identification of Lubrication Oil in the Particulate Matter Emissions from Engine Exhaust of In-Service Commercial Aircraft*. Environmental Science and Technology, 46, 9630 -9637, 2012.

[36] V. ZAIDA, E. BAR-ZIV, L. R. ZADOVIC, Y.-J. LEE - *Further Development of Raman Microprobe Spectroscopy for Characterization of Char Reactivity*. Proceedings of the Combustion Institute, 31, 1873–1880, 2006.

List of acronyms

BC	(Black Carbon)
CAEP	(Committee for Aviation Environmental Protection)
CPC	(Condensation Particle Counter)
DMA	(Differential Mobility Analyzer)
DMS	(Differential Mobility Sizer)
EDX	(Energy-Dispersive X-Ray Spectroscopy)
HEPA	(High Efficiency Particulate Air Filter)
HR-TEM	(High Resolution Transmission Electron Microscopy)
ICAO	(International Civil Aviation Organization)
L2MS	(Laser Two-Step Mass Spectrometry)
MAAP	(Multi-Angle Absorption Photometer)
MERMOSE	(Mesure et Etude de la Réactivité des Emissions de Moteurs Aéronautiques)
NEXAFS	(Near-Edge X-Ray Absorption Fine Structure)
NSAM	(Nanoparticle Surface Area Monitor)
nvPM	(Non-Volatile Particulate Matter)
PAH	(Polycyclic Aromatic Hydrocarbons)
PPS-M	(Pegasor Particle Sizer M-Sensor)
SMPS	(Scanning Mobility Particle Sizer)
SN	(Smoke Number)
TEM	(Transmission Electron Microscopy)
ToF-SIMS	(Time-of-Flight Secondary Ion Mass Spectrometry)
XPS	(X-Ray Photoelectron Spectroscopy)

Ismael Ortega received his PhD degree in atmospheric Sciences in 2006 from the University of Jaén and the Spanish national council for research (CSIC). From 2007 to 2013 He has worked as post-doc researcher in the Atmospheric Science division of the University of Helsinki and in the Department of Environmental Science and Analytical Chemistry at the University of Stockholm. During this period, he focused his research in the field of atmospheric aerosol, more specifically in understanding the formation of aerosol particles in the atmosphere. In 2013 he joins the Laboratoire de Physique des Lasers, Atomes et Molécules PhLAM at University of Lille 1, where we focused his work in the characterization airplane engine emission. From November 2015 he is member of the department of Fundamental and applied Energetics (DEFA) at ONERA, where he keeps working on airplane engine emission characterization.

David Delhaye (PhD University of Marseille, 2007) has been working as an emission measurement specialist at ONERA since 2004. He received in 2007 the Jean Bricard award for his PhD dealing with the characterization of aircraft engine soot. He then joined the DLR in 2008 at the Institute of Atmospheric Physics (DLR Oberpfaffenhofen - Germany) in framework of European Network of Excellence ECATS scientific exchange for 15 months where he worked on various national or European research projects (BIOCLEAN, CONCERT, SAMPLE). He has been working since 2009 in the ONERA's Atmospheric Environment team with a special emphasis on soot particles characterization. He has been involved in EU projects like ECATS (NoE, 2005-2010), SAMPLE1&2&3 (EASA, 2009-2011) and also national funded projects like MERMOSE (2012-2015). He is a member of the SAE–E31 experts subcommittee on aircraft engine particulate matter emissions.

François-Xavier Ouf is a research scientist at IRSN (Institut de Radioprotection et de Sûreté Nucléaire). He joined in 2002 the Aerosol Physics and Metrology Laboratory and received the degree of Doctor of Physics from the University of Rouen in 2006. He received the same year the Jean Bricard award for his PhD dealing with the characterization of fire generated aerosols. Since 2006 he is in charge of researches and studies dealing with the physico-chemical characterization of combustion generated aerosol and their impact on the containment of nuclear installations (radioactive release, HEPA filters clogging). He is involved in many industrial and academic partnerships and since 2010 he is chairing the working group "combustion aerosols" of the EAA. He is the author or co-author of more than 25 publications in high-impact international journals.

Daniel Ferry is a research scientist at the Centre National de la Recherche Scientifique (CNRS) in Marseille, France. He received his PhD degree in Material Sciences in 1997 from the University Aix-Marseille. During 10 years he studied interactions of molecules with solid surfaces and the structure, dynamics and thermodynamics of molecular layers. Since 2006 his research aims at understanding physical and chemical properties of carbonaceous aerosols. He is currently working at determining the link between nanoscopic properties of solid aerosols and their reactivity with atmospheric gases by using electron microscopy as well as photonic spectroscopies.

Cristian Focsa (43) received his PhD in molecular spectroscopy in 1999 from the University of Lille 1. After a post-doc in University of Waterloo (Canada), he was appointed as Associate Professor (1999) and then Professor (2009) at University of Lille 1. Since 2002 he is the leader of the ANATRAC (Analysis of Traces) research group (currently 9 people) within the Laboratoire de Physique des Lasers, Atomes et Molécules (PhLAM, UMR CNRS 8523). Since 2010 he is the director of CERLA (Centre d'Etudes et de Recherches Lasers et Applications). His main current research interest is in the applications of laser ablation in environment, medicine, and materials sciences.

Cornelia Irimiea received the M.S. degree in Plasma Physics, Spectroscopy and Self-Organization from "Alexandru Ioan Cuza University", Iasi, Romania, in 2011. She is currently pursuing a Ph.D degree at Lille 1 University, Villeneuve d'Ascq, France. Her current research interests include the study of soot mechanisms formation in laboratory flames using laser based techniques coupled with mass spectrometry.

Yvain Carpentier received his PhD degree in 2009 from the University Paris XI. His PhD thesis was focused on the production and spectroscopic characterization of astrophysically-relevant carbonaceous molecules and nanograins. Since 2011, he is Associate Professor of Physics at the PhLAM Laboratory (University Lille 1). He works in particular on the L2MS technique to determine the surface chemical composition of aerosols, especially soot particles.

Bertrand Chazallon received his Ph.D. degree from University of Lyon1 in 1999 on the spectroscopy, neutron diffraction and molecular modeling of gas hydrates. He joined the PhLAM laboratory of University Lille 1 in 2001 as associate professor to work on multiphasic processes of environmental interests. Since 2012, Dr. Chazallon is Professor in Physics at the University of Lille1. His current research is focused on the ice nucleation activity of anthropogenic and biogenic aerosols. He develops original methods for CO_2 capture and mitigation of greenhouse gases by hydrate crystallization.

Philippe Parent is Directeur de Recherche at the Centre National de la Recherche Scientifique, France. He received the degree of Doctor in Physics (Material Sciences) in 1991 at the Université Pierre-et-Marie Curie, Paris, France. During 15 years of research at LURE, the first synchrotron radiation facility in France (Orsay), he contributed to the development of soft X-ray absorption spectroscopy applied to surface science and environmental physical chemistry. In 2005 he moved to Paris (Laboratoire de Chimie-Physique, Matière et Rayonnement) and then in 2013 to Marseille (Centre Interdisciplinaire de Nanoscience), where he presently works on the surface properties of nanoscale materials, with emphasis on environmental solids, using spectroscopic tools (laboratory and synchrotron) and nanoscience techniques.

Carine Laffon is a research scientist at the CNRS (Centre National de la Recherche Scientifique), France. She received the degree of Doctor of Physics from the Université de Paris Sud (Orsay) in 1990. Her research interest initially focused on the structure and electronic properties of solids, of adsorbates on metal surfaces, and of molecular solids using X-ray absorption spectroscopy. She is currently working at the Centre Interdisciplinaire de Nanoscience de Marseille (CINaM) on the nanostructure, reactivity and electronic properties of aerosols and environmental solids, using electronic spectroscopies with laboratory and synchrotron light sources (NEXAFS, photoemission).

Olivier Penanhoat became engineer from Ecole Centrale de Lyon in 1986, and received his PhD in theoretical mechanics from University Pierre et Marie Curie in 1990. He has been working at Snecma for more than 20 years, mainly in the field of combustion (technology, CFD, pollution, future fuels). He was involved in many European programs, in particular as coordinator of LOWNOX III and LOPOCOTEP technological projects. Currently he is coordinator of the European network FORUM-AE, dedicated to all environmental issues linked to aircrafts emissions and is Snecma representative to the emissions technical group of the ICAO Committee on Aviation Environmental Protection. He was also formerly responsible of SaM146 engine certification and was till 2016 professor of combustion in Mines de Nancy.

Nadine Harivel received her Ph.D. degree in 1981 from University of Poitiers. She joined Snecma in 1981 where she was involved in combustor studies. She is currently in charge of measurement of aircraft engine exhaust gas concentrations, smoke number and particulate matter. She is involved in the emission certification tests of civil engines.

Daniel Gaffié obtained his PhD from the University Paul Sabatier of Toulouse in 1982 in the field of modelling and numerical simulation of the rheology of multiphase dispersed flows. Second PhD on the numerical simulation of hyperbolic systems encountered in Mechanics Fluid applications. From 1997 to 2009, he leads research unit on “Multiphase Turbulent combustion modeling”. Since 2010, he helds at ONERA the position of Special Advisor on Aeronautical Propulsion systems providing expert technical assistance in R&D for the aeronautical applications. Alongside, Daniel Gaffié ensures since 1989, a teaching charge at the University Pierre et Marie Curie in the framework of the master "Energy and Environment" and assumes a charge of Professor at the Superior Engineer School for Aeronautic Techniques and Car Manufacturing.

Xavier Vancassel received a PhD degree in chemical physics from the University of Strasbourg, 2003. He joined ONERA in 2006, after a two years post-doctoral research position at the University of Oxford. He currently heads the Engine Emission and Environmental impact research unit, in the Fundamental and Applied Energetics Department. He has been working on aviation emissions related projects since 2000 and has been involved in many international and national programmes.

P. Gajan, F. Simon, M. Orain, V. Bodoc
(ONERA)

E-mail: Pierre.Gajan@onera.fr

DOI : 10.12762/2016.AL11-09

Investigation and Modeling of Combustion instabilities in Aero Engines

Combustion instability results from a coupling between acoustic and heat release fluctuations. From the analysis of published works by various research teams including ONERA, this paper describes the coupling lines involved, the model used to describe it and the methods developed to predict the thermo-acoustic risks. The application is focused on the liquid-fueled aero engine specificities. Recent results obtained at ONERA on the influence of the liquid flow behavior on these couplings are described and compared with LES results.

Introduction

Confined devices with an internal heat source are predisposed to thermo-acoustic instabilities, resulting from a coupling between the acoustic field, pressure and velocity fluctuations (respectively p' and u'), and the unsteady heat release (q'). This phenomenon was first observed by Higgins [1] and Rijke [2] and explained by Lord Rayleigh in 1878 [3]. During the second half of the 20th century, many studies were first focused on instabilities occurring in liquid propellant rockets [4] and later in other combustion devices such as industrial furnace, boilers or other propulsion systems like solid rockets, gas turbines or afterburners. For these different applications, the coupling line between the acoustic components and the unsteady heat release greatly depends on the combustion regime (premixed or not), the reactant characteristics and state (solid, liquid or gaseous) and the injection procedure. In the same way, the feedback loop between the unsteady heat release and the acoustic state depends on the device geometry, its boundary conditions and the Mach number distribution. As a result, each configuration induces specificities that must be taken into account.

Over the last few decades, many studies on combustion instabilities have concerned land-based turbine or aero engines. In these fields (energy production or civil air transport), manufacturers try to reduce the environmental impact by modifying their engine concept. In particular, over the past two decades, they have been developing shorter combustion chambers operating at higher OPR (Overall Pressure Ratio) in lean combustion regimes, in order to minimize pollutant formation (NOx, soot, etc.). In these new combustors, a higher air mass flow rate is required for the combustion; therefore, less air is available for cooling the combustor walls. Consequently, walls with multiple perforations are generally used for cooling, which modifies their acoustic impedance. Some of these geometric modifications may enhance the onset of combustion instabilities, which lead to large cyclic pressure or velocity fluctuations inside the chamber and consequently generate significant heat transfer at the combustor walls, or large amplitude vibrations of the structure. This can result in the damaging of the combustor, or even its destruction, which is incompatible with the safety and durability standards required in the aeronautical industry.

The aim of this paper is to present the recent developments, in particular at ONERA, on combustion instabilities encountered in aero engines. In the first section of this paper, the main mechanisms involved in the $p'\,q'$ coupling are described, with a specific focus on liquid-fueled devices. The different approaches used to model this coupling and to predict the instability onset are presented in the second and third sections respectively. Their application on the ONERA setup LOTAR (Liquid Fueled ONERA ThermoAcoustic Rig) is then discussed.

Description of the main mechanisms involved in the $p'q'$ coupling

The coupling can be described as a closed loop of interactions, back and forth, between acoustic components and heat release, as schematically represented in Figure 1. It was shown in the works of Putman and Dennis [5], or Nicoud and Poinsot [6] that the flame stability depends on an extended Rayleigh criterion, which compares the source term of acoustic energy from the flame with the acoustic fluxes at the boundary surfaces, as shown in Eq. (1). The source term depends on the phase relationship between pressure and heat release oscillations in the combustor, which is imposed by the different time delays appearing in the p'-q' coupling.

$$\frac{1}{T}\int_T \left\{ \frac{\gamma-1}{\gamma\,\overline{p}} \iiint_\Omega p'\,q'\,dV - \oiint_\Sigma p'\,u'\,dA \right\} dt > 0 \qquad (1)$$

In Eq. (1), γ is the heat capacity ratio; p', u', q' are respectively the pressure, velocity, and heat release rate fluctuations; T is the instability cycle period; $\overline{p}$ is the average pressure over the system control volume, Ω; Σ is the system control surface; and, finally, dV and dA are respectively the volume and surface integration variables.

This equation states that the acoustic energy increases only if the source term due to combustion is larger than the acoustic losses on the combustor inlet and outlet surface Σ. The experimental evaluation of acoustic fluxes on the boundaries of the burner is difficult and less attention has been paid in the literature to their influence. Nevertheless, experimental methods based on multiple-microphone measurements or *LDA* and microphone measurements are used to identify such losses in the case of liners enabling acoustic energy to be damped inside of aero engines [7].

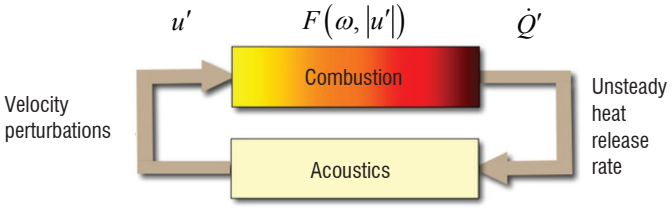

Figure 1 - Coupling loop at the origin of thermo-acoustic instabilities

Pressure fluctuation production from the flame

On the lower side of the coupling loop presented in Figure 1, unsteady heat release produces pressure (or velocity) fluctuations. The fundamental mechanism involved in the sound generation is the unsteady gas expansion induced by heat release fluctuations [8-10]. Similarly, it was shown by Marble and Candel [10], Polifke et al. [12], and Huet and Giauque [12] that pressure fluctuations could arise when entropy or vorticity waves, coming from the unsteady flame or upstream flow, interact with an abrupt modification of the flow cross-section. Note that, in most cases, the Mach number in the combustor being low, the convection of entropy or vorticity waves induces large time delays between the unsteady heat release, q', and the pressure fluctuations, p', in comparison with the time scale associated with the direct acoustic perturbation produced by the flame. It must be noticed that the relevance of such waves in the pressure production depends greatly on their dispersion rate between the reactive zone and the combustion chamber outlet. In particular, Sattelmeyer [14] showed that the related convection time limits this effect in many applications.

The acoustic pressure and velocity fluctuations propagate in the volume domain and interact with the boundary surface leading either to energy losses or reflection, depending on their own frequency and propagation mode and the local conditions (Mach number, surface characteristics, etc.). According to the flow characteristics (temperature, Mach number) and the boundary conditions, standing or spinning waves characterized by their wavelength, spatial distribution and amplitude take place in the volume domain. They correspond to particular eigenmodes, which can be deduced from an acoustic analysis based on the Helmholtz equation or linearized Euler equations [15-17].

Origins of heat release fluctuations

On the upper side of the loop, the production of heat release fluctuations from p' or u' is not so clear and depends upon the characteristics of the combustion system. In premixed flames, local modifications of the flame area induced by turbulent or vortical structures, or wall interaction, control the mixing between fresh and unburned gases and consequently the reaction rate in the flame [9]. In their configuration, Noiray et al. [17] observed that these flame surface variations are induced by upstream velocity oscillations. Gutmark [18] reviewed the main mechanisms linking the heat release fluctuations to vortical structures formed in shear layers. These structures capture fresh gases or fuel in their center, while the flame is located at their periphery. During interactions between two adjacent structures or with a wall, rapid mixing occurs, which leads to a spot of heat release. Many studies show that the eddy formation in shear layers may be driven by external acoustic excitations. Thus, when the acoustic level increases, a high coupling appears between the acoustic components and the unsteady heat release.

Another source of unsteady heat release originates from the interaction between inhomogeneous equivalence ratio regions and the flame [19]. For a premixed flame, pressure oscillations close to the injection interact with the fuel line and induce an oscillation in the fuel flow rate creating a local modification of the equivalence ratio, which propagates towards the combustion zone [20]. The same phenomena can be also observed with a constant fuel injection rate but oscillating air velocity. This convective transport induces a time delay linked to the fresh gas velocity and the distance between the injection and the flame locations.

Specificity of the liquid fuel flames

In the literature, many articles deal with gas-fueled combustors in premixed or diffusion regimes, in order to describe and model the phenomena considered and to determine the p' (or u') - q' relationship [8, 9]. When a liquid fuel is used, the coupling between the acoustic fluctuations and the unsteady heat release involves additional phenomena, such as spray atomization / transport / vaporization / combustion [21-24] and their interaction with turbulence, vorticity, chemistry, and acoustics. Eckstein et al. [21] analyzed the spray generated by an air-blast system subject to periodic air velocity fluctuations. The authors observed that the droplet size in the spray varied periodically at the same frequency as the velocity excitation. Moreover, they explained that, for a given liquid flow rate, high air velocities produce a large number of small droplets, whereas low air velocities produce a small amount of large droplets. In this way, when combustion instabilities occur, the periodic velocity fluctuations inside the atomizer create a time-varying droplet size distribution, which is transported further downstream to the flame as a droplet wave. During this convection phase, the small-droplet zones produce a larger amount of fuel vapor than the large-droplet zones. As a result, an equivalence ratio wave appears, which interacts with the flame to produce a periodic heat release oscillation.

In parallel, Giuliani et al. [22] and Gajan et al. [23] studied non-reactive spray behaviors downstream both from a simplified atomizer and from a Dextre-type industrial atomizer under non-reactive conditions. In the first case, droplets were formed from the disintegration of an axisymmetric liquid sheet sheared internally and externally by two co-swirling airflows. In the second case, a prefilming zone was formed before the atomization of the liquid fuel. In these experiments, velocity pulsations were created by a siren placed upstream or downstream from the atomizer. In both cases, droplet density waves convected downstream from the fuel injection location are observed (Figure II.2).

Giuliani [25] observed a great interaction between the droplet concentration fronts and the convection of annular vortices formed in the swirling air jet shear layer (Figure 2). A succession of vortex rings followed by a dense droplet front evolving on the surface of the spray envelope is created. The following ring vortex contains only sparse droplets. The measured convection velocity of the droplet density wave is approximately equal to half of the air velocity at the injector outlet.

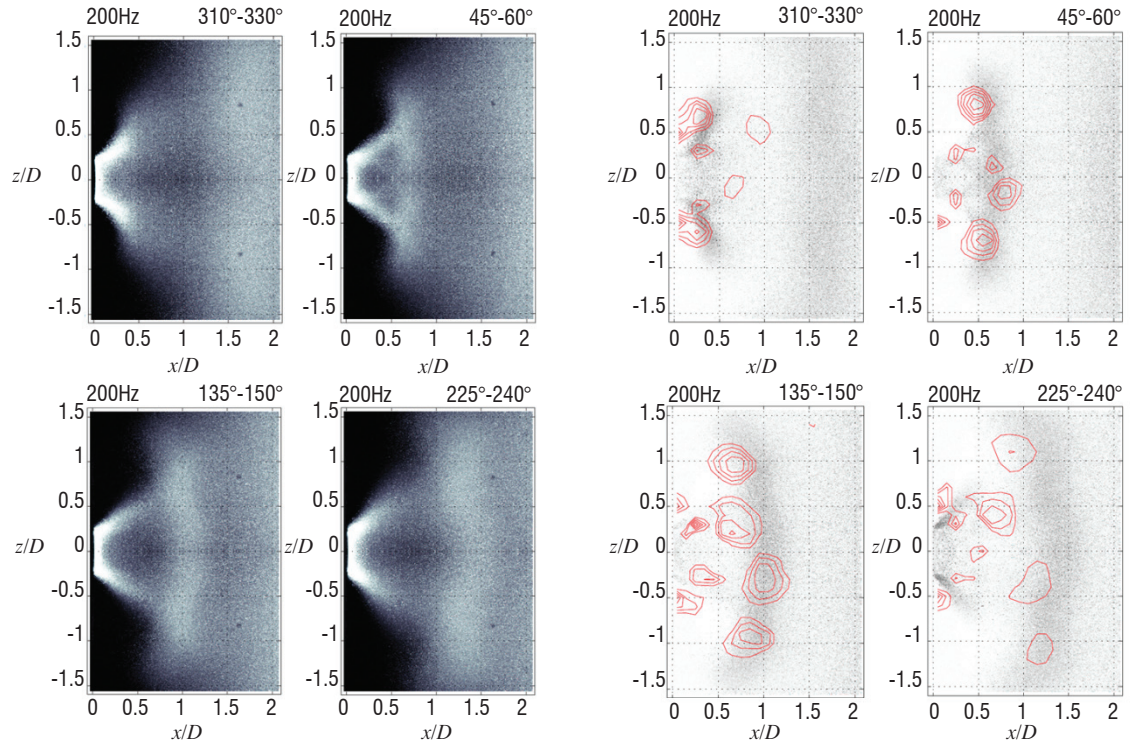

Figure 2 - Phase averaged images obtained of a spray subjected to upstream air pulsation:
Left: Maximum post-processing images, Right : Interaction between the spray and the vortex shedding [22,25](Video 1)

A phase-averaged post-processing method applied to Fraunhofer–Mie scattering or phase Doppler techniques allowed a deep analysis of the origin of these droplet density waves. A typical three-dimensional plotting of the results obtained at one measurement location is shown in Figure 3. The color scales correspond to the axial velocity of the droplets. This figure shows that the excitation imposes a significant modulation of the number of droplets during the cycle, mainly for small droplet sizes. Furthermore, the color scale reveals that the maximum velocity zone is reached between the minimum and the maximum of the droplet population. From these results, the propagation behavior of different droplet size classes was analyzed [23]. It reveals that the convection velocity of these waves depends on the droplet size (Figure 4) and that the wave amplitude increases during the convection phenomena. This last observation concerns mainly the small droplets.

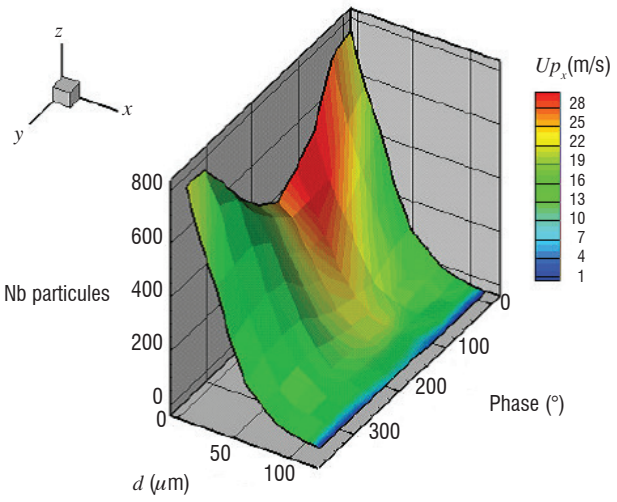

Figure 3 - Evolution of the droplet size histogram along the pulsation cycle [23]; Color levels correspond to the droplet velocity in the longitudinal direction; f =700 Hz, $x/d_{atomizer}$=0:45, $y/d_{atomizer}$=0:45, and $z/d_{atomizer}$=0.

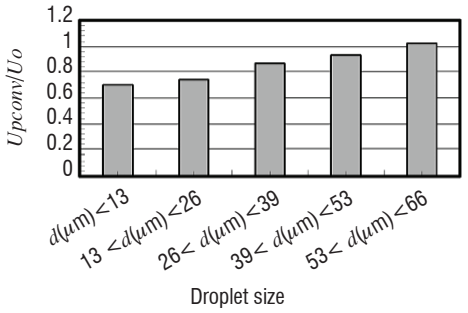

Figure 4 - Averaged convection velocity of the droplet density waves with respect to their size [23].

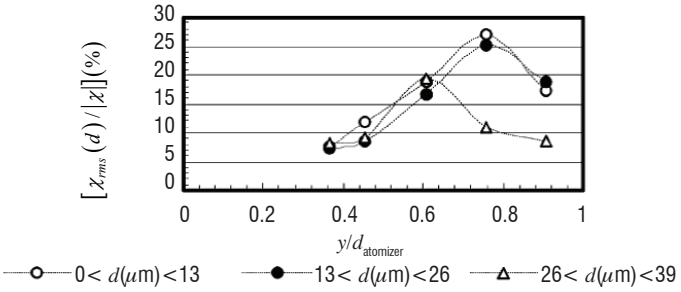

Figure 5 - Amplitude of the number-of-droplet wave at different locations with respect to the droplet size [23].

By using a one-dimensional model based on the Boussinesq-Basset-Oseen (BBO) transport equation, Giuliani et al. [22] and Gajan et al. [23] concluded that this phenomenon was due to the influence of the oscillating velocity field on the motion of the small droplets, which segregates them in space and therefore forms droplet concentration waves (Figure 6). Furthermore, Giuliani et al. [22] noted that the droplets involved had a Stokes number (calculated from the air pulsation period) smaller

than 0.2.The results obtained by this 1D analysis were compared to experimental results by Gajan et al. [23] The amplification phenomena observed experimentally was qualitatively obtained by the simulation (Figure 7).

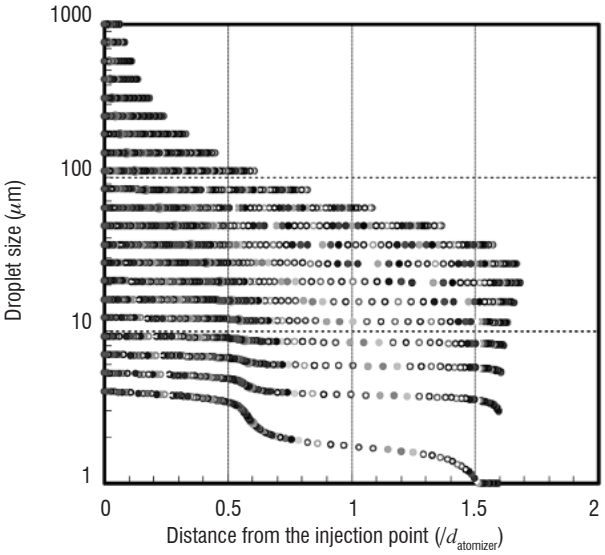

Figure 6 - Instantaneous droplet position and size obtained from the numerical simulation [23].

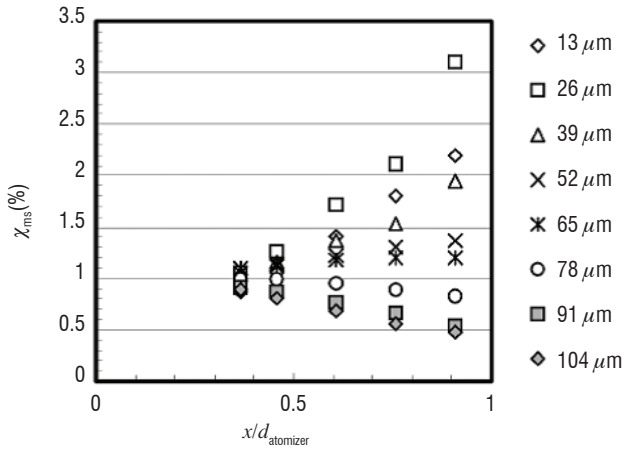

Figure 7 - Amplitude of the droplet concentration wave at different locations with respect to the droplet size [23].

More recently, Apeloig et al. [24] studied the unsteady interaction with the flame of a kerosene spray downstream from a multi-point injector (Figure 8).The injection system comprises two injection zones, a pilot zone composed of a pressure atomizer at the center and a multipoint zone at the periphery. In this zone, the liquid fuel is injected through a set of individual jets in crossflow. Axial and radial swirlers enable air flow rotation to be induced. The distribution of the fuel between the pilot and the multipoint zone is controlled though a Fuel Split Parameter (FSP) corresponding to the percentage of the overall kerosene mass flow rate through the pilot zone.

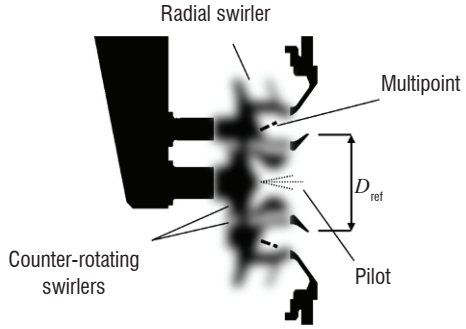

Figure 8 - Schematic diagram of a novel aero-engine injection system used in the experiments [24].

Phase-averaged processing of images obtained from planar laser-induced fluorescence (PLIF) on kerosene reveals that the spray pattern issuing from the multipoint zone fluctuates to a large extent, both spatially and in terms of fluorescence intensity, over the instability cycle (Figure 9). From the analysis of this sequence of images Apeloig et al. [24] defined three main characteristics of the spray dynamics and proposed that the spray behavior is linked to airflow fluctuations inside the injector, which modify the individual trajectories of the fuel jets. Such coupling between the air flow and the jet in the crossflow atomization process was shown by Anderson et al. [26] [Figure 10] and by Song and Lee [27]. When the momentum flux of the crossflow is greater than the momentum flux of the liquid jet ($J<1$), the atomization process results in the liquid jet and droplets hitting the inner wall of the radial swirler, producing a liquid film that is subsequently atomized at the edge of the diffuser. This phenomenon corresponds to a characteristic time, τ_1. When the momentum ratio J reaches a large enough value, the kerosene jet hits the outer wall of the radial swirler, forming a liquid film which is re-atomized further downstream,

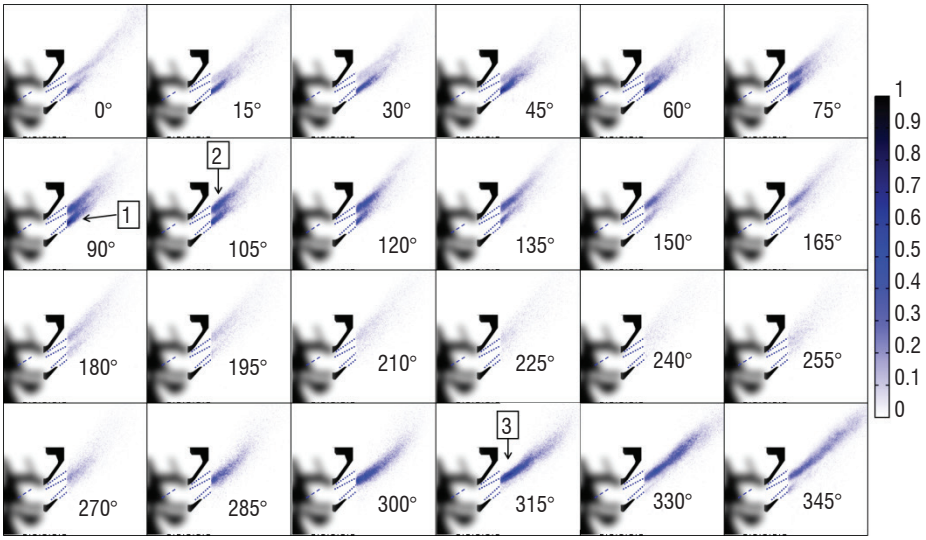

Figure 9 - Temporal sequence of the liquid kerosene spatial distribution during an instability cycle using phase-averaged analysis on PLIF images [24] (Video 2)

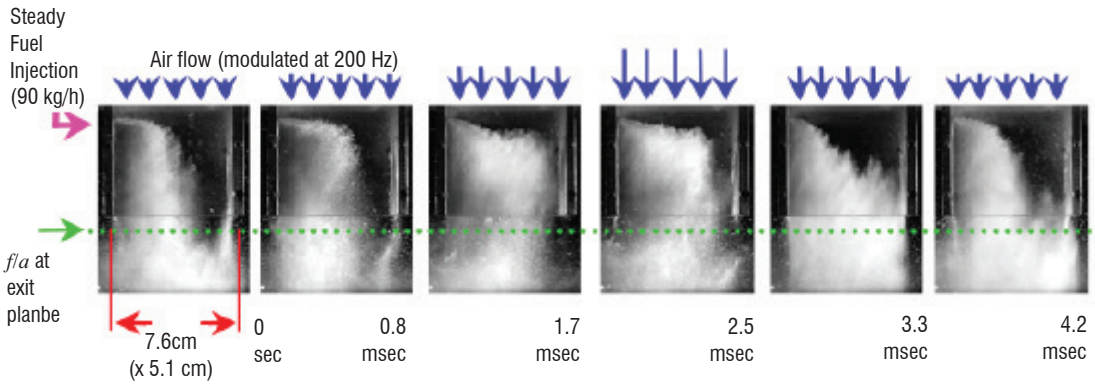

Figure 10 - Instantaneous frame sequence showing the effect of airflow modulation on a steady fuel jet in crossflow [26].

as well as generating droplet rebounds at the wall. This second step corresponds to a characteristic time, τ_2. The third spray pattern, with a characteristic time τ_3, requires further investigation: it may be that liquid fuel is directly transported to the combustor without hitting the walls of the multipoint circuit, and/or a combination of the two previous flux patterns. Different characteristic times thus appear due to the diverse convective mechanisms involved in the liquid atomization and transport from its injection point inside of the injector (wall filming or droplet transport) to the combustor.

The unsteady behavior of the spray influences the vapor concentration field further downstream, creating equivalence ratio fluctuations interacting with the flame. Such phenomena were visualized by Apeloig et al. [24] (Figure 11) indicating highest concentration levels around the liquid phase. In this figure, large fluctuations of the spatial distribution of kerosene vapor are also observed in terms of surface covered and trajectory. Spatial averaging of each phase-averaged field shows the temporal relationship between the different phenomena (Figure 12). In particular, it is evident that the OH emission fluctuations from the flame representative of heat release behavior are directly linked to the unsteady atomization process.

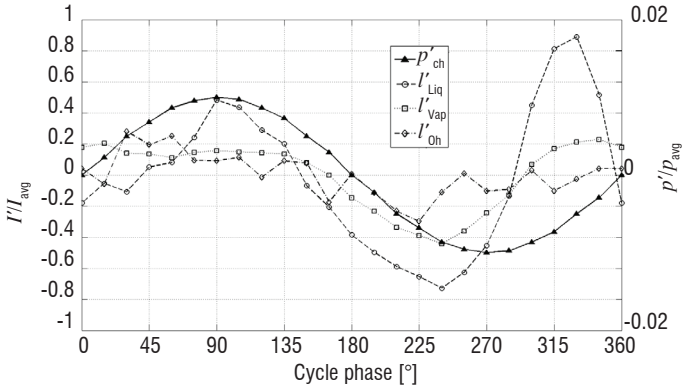

Figure 12 - Temporal sequence of the OH radical and kerosene fluorescence intensities during an instability cycle using phase-averaged analysis on PLIF images [24].

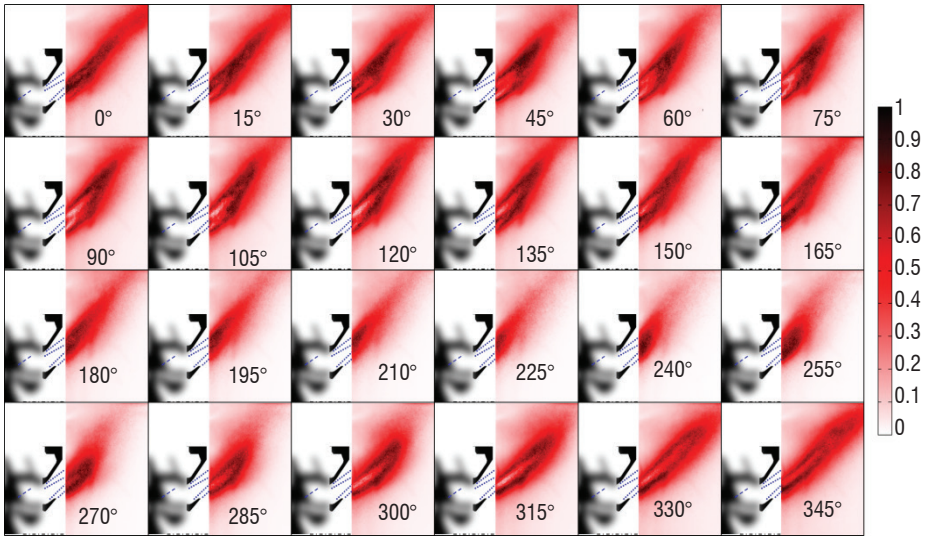

Figure 11 - Temporal sequence of the kerosene vapor spatial distribution during an instability cycle using phase-averaged analysis on PLIF images [24](Video 3).

Methods for defining the flame response to acoustic perturbations

The key point to predict combustion instabilities is the modeling of the flame response to acoustic perturbations. As shown in the previous section, various phenomena are involved in this response. Nevertheless, from a macroscopic point of view, this response was described through two parameters corresponding to the interaction degree and the time delay between the acoustic incident perturbation and the behavior of the flame. These two parameters were introduced by Crocco and Cheng [28] in their well-known n-τ model. In the frequency domain, these parameters correspond to the amplitude and the phase of the Flame Transfer Function (FTF), which depends on the frequency. These two approaches suppose that the flame response is linear, i.e., that it is proportional the excitation level. Although they can accurately describe the different instability modes, they cannot predict the limit cycle phenomena corresponding to a saturation effect when the amplitude of the excitation increases. In order to improve the prediction tool efficiency, many authors have proposed nonlinear models to describe the flame behavior [14, 15]. Illingworth and Juniper [29] analyzed this approach to represent the nonlinear behavior of the flame

Flame transfer function

The simplest flame transfer function corresponds to the n-τ model proposed by Crocco and Cheng [28]. It can be written in the frequency and temporal domain as follows [30]:

$$\frac{\gamma-1}{\rho_{up}c_{up}^2}\hat{Q}=S_{up}\cdot n\cdot\hat{u}\left(x_f\right)e^{-i\omega\tau_f}$$

$$\Leftrightarrow\frac{\gamma-1}{\rho_{up}c_{up}^2}Q(t)=S_{up}\cdot n\cdot u\left(x_f,t-\tau_f\right)$$

Where $Q(t)=\int_{x_{up}}^{x_d}S\cdot q'dx$ is the total unsteady heat release produced by the flame, n is the interaction index and τ_f is the flame time delay. The subscript "up" corresponds to conditions upstream from the flame and ($\hat{}$) to the Fourier transform. Bloxsidge et al. [31] added a second time scale, in order to take into account the damping phenomena that appear at high frequencies. A first order response can be written.

$$\frac{\gamma-1}{\rho_{up}c_{up}^2}\hat{Q}=\frac{S_{up}\cdot n\cdot\hat{u}\left(x_f\right)}{1+i\omega\tau_1}e^{-i\omega\tau}$$

$$\Leftrightarrow\frac{\gamma-1}{\rho_{up}c_{up}^2}\left(\tau_1\frac{d}{dt}+1\right)Q(t)=S_{up}\cdot n\cdot u\left(x_f,t-\tau\right)$$

Dowling [15] used a third time scale, in order to reproduce the behavior of the flame with a second order response law.

$$\frac{\gamma-1}{\rho_{up}c_{up}^2}\hat{Q}=\frac{S_{up}\cdot n\cdot\hat{u}\left(x_f\right)}{\left(1+i\omega\tau_1\right)\left(1+i\omega\tau_2\right)}e^{-i\omega\tau}$$

$$\Leftrightarrow\frac{\gamma-1}{\rho_{up}c_{up}^2}\left(\tau_1\frac{d}{dt}+1\right)\left(\tau_2\frac{d}{dt}+1\right)Q(t)=S_{up}\cdot n\cdot u\left(x_f,t-\tau\right)$$

The above approaches were mainly applied for premixed flames or assumed that equivalence ratio fluctuations can be neglected. As shown in the previous section, equivalence ratio fluctuations can be the main mechanism at the origin of the p' q' coupling. Lieuwen and Zinn [20] introduced the effect of these fluctuations in their flame response. They supposed that the equivalence ratio fluctuation produced near the fuel injection location is convected without diffusion toward the flame location. Therefore, in their model, a convective time τ_c proportional to the distance between these two locations and inversely proportional to the gas bulk velocity is used. Sattelmayer [14] takes into account the fuel diffusion through the following expression :

$$\frac{\varphi'_f}{\varphi'_{inj}}=\frac{1}{2\cdot\Delta\tau_c\cdot i\cdot\omega}\cdot e^{-i\omega\bar{\tau}_c}\left(e^{i\omega\Delta\tau_c}-e^{-i\omega\Delta\tau_c}\right)$$

In their application, the fuel line is choked, therefore the equivalence ratio fluctuation produced near the injection point is directly proportional to the local acoustic velocity. The response of the flame to these equivalence ratio fluctuations is given by Lieuwen [10] and is decomposed through two terms linked to the reaction heat and the flame speed perturbations respectively:

$$\frac{Q'}{\bar{Q}}=n_H\varphi'_f+n_S\frac{d\varphi'_{inj}}{dt}\quad\text{with}\quad n_H=\left.\frac{d\left(\Delta h'_R/\Delta\bar{h}_R\right)}{d\varphi}\right|_{\bar{\varphi}}$$

$$\text{and}\quad n_S=\frac{1}{3}\frac{L_F}{\bar{u}}\left.\frac{d\left(S'/\bar{S}\right)}{d\varphi}\right|_{\bar{\varphi}}$$

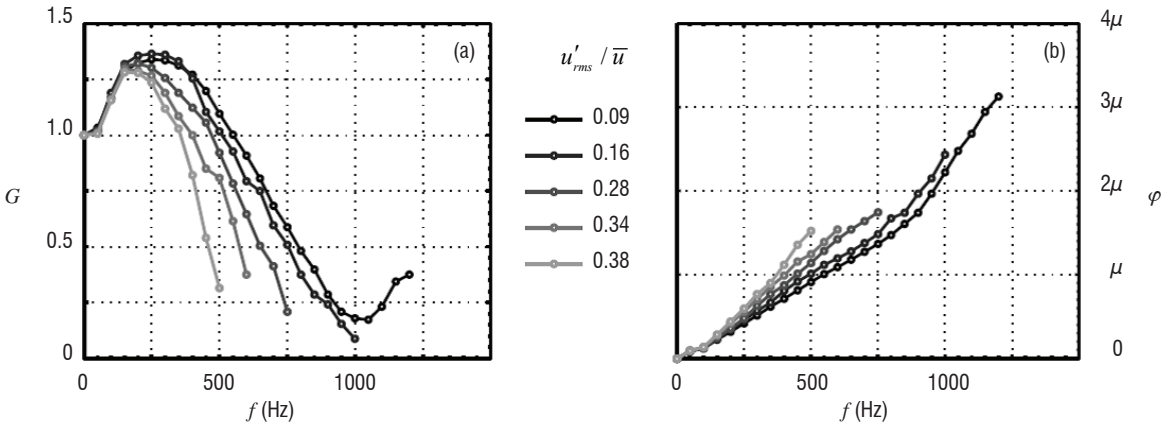

Figure 13 - Experimental flame transfer function for different normalized driving velocity amplitude rates. (a) Gain G. (b) Phase φ [17]

Flame describing function

In order to analyze, for a given system, the risks linked to thermoacoustic oscillations, it is important not only to define the linear frequencies and growth rates, but also to predict the amplitude and frequencies at the limit cycles. Various works were carried out first to explain and then to model the phenomena at the origin of these nonlinear behaviors. They used the describing function approach used in other application fields. The method treats the nonlinear element in a quasi-linear approach when sinusoidally forcing an induced nonlinear response. The response of the system depends both on the input frequency and amplitude. Dowling [16] represents the premixed flame response behind flame holder experiments by Langhorne et al. [32] through three upstream velocity conditions. For a negative upstream velocity, the flame vanishes ($q'=0$), the u' q' relationship is linear for velocities between 0 and two times the upstream bulk velocity, and finally q' saturates for higher velocities. Illingworth and Juniper [29], using the same approach, show that this nonlinear flame description generates harmonics.

A detailed analysis of the linear and nonlinear behavior of a burner formed by 420 elementary flames operating in the premixed regime is presented by Noray et al. [17]. The flame describing function obtained with this setup exhibits a clear dependence of the flame response on both the frequency and the amplitude of the velocity excitation.

Methods for predicting instability combustion risks

Low order methods

Various teams developed this method to predict the acoustic response of a given system. They are based on the linear acoustic approach. A multiport approach, which represents the system as a network of individual elements connected each other by jump conditions. A linear system of equations is constructed from the transfer matrices between two successive elements or between the inlet and the outlet of each element [30, 33]. The following relationship is obtained:

$$\begin{pmatrix} p'_{i+1} \\ u'_{i+1} \\ \phi'_{i+1} \\ ?. \end{pmatrix} = \begin{bmatrix} T_{pp}(\omega) & T_{pu}(\omega) & T_{p\phi}(\omega) & T_{p?}(\omega) \\ T_{up}(\omega) & T_{uu}(\omega) & T_{u\phi}(\omega) & T_{u?}(\omega) \\ T_{\phi p}(\omega) & T_{\phi u}(\omega) & T_{\phi\phi}(\omega) & T_{\phi?}(\omega) \\ T_{?p}(\omega) & T_{?u}(\omega) & T_{?\phi}(\omega) & T_{??}(\omega) \end{bmatrix} \begin{pmatrix} p'_i \\ u'_i \\ \phi'_i \\ ?. \end{pmatrix}$$

The flame response is introduced through the acoustic pressure and velocity jump across the flame zone. For this, the flame transfer function described before can be used. For compact flames, the acoustic jump across the combustion zone can be deduced from the integration of the linearized mass, momentum and energy balance equations [30]. This imposes that the acoustic pressure is continuous across the flame and the acoustic velocity jump is equal to:

$$S_{down}\hat{u}_{down} - S_{up}\hat{u}_{up} = \frac{\gamma - 1}{\rho_{up}c_{up}^2}\hat{Q}$$

Coupling all of the individual matrices, the overall system of linear equations is obtained [33]:

$$\overline{\overline{G}}(\omega).\vec{M} = \vec{0}$$

The dimension of the square matrix $\overline{\overline{G}}$ depends on the number of individual elements taken into account to represent the whole system and on the number of unknown variables of the problem. $\vec{M}$ is a vector containing all of the unknown variables. The complex eigenmodes of the system are obtained by solving the following equation:

$$\det(\overline{\overline{G}}(\omega)) = 0$$

The stability of the various eigenmodes $\omega = \omega_R + i \cdot \omega_I$ is obtained through the growth rate parameter GR [33]:

$$GR = e^{-2\pi\frac{\omega_I}{\omega_R}}$$

Where GR=1 represents the stability limit of a linear system or the limit cycle of a nonlinear system. In linear systems, GR<1 indicates stable modes, while GR>1 corresponds to unstable modes. From the use of the flame describing function concept, Noiray et al. [17] described the behavior of their setup for different overall lengths and velocity amplitudes. For some modes, a positive growth rate ω_i is obtained for small velocity amplitude levels, but vanishes for higher amplitudes, leading to a stable flame. For other modes, negative growth rates, obtained for small amplitudes corresponding to a linear stable mode, become positive above a certain amplitude threshold, reaching a maximum before decreasing and then vanishing for higher excitation values. The first behavior type induces a saturation effect corresponding to a limit cycle observed in many studies. Noiray et al. [17] have shown that the combination of these two behavior types is at the origin of the frequency jump observed experimentally for fixed setup lengths or the hysteresis phenomena obtained by increasing or decreasing this length.

CFD approach

Helmholtz solvers are used to calculate the eigenmode of linear vibrating systems. This approach is applied in acoustics for complex geometries, or to accurately take into account the temperature field and boundary conditions. For combustion instability purposes, the use of a source term from the flame enables the stable or unstable modes to be defined in the same way as was described for low order methods. These modes are the solution of the following equation [30]

$$\nabla \cdot \left(c_0^2 \nabla \hat{p}\right) + \omega^2 \hat{p} = i\omega(\gamma - 1)\hat{q}(x)$$

As shown before, the unsteady heat release is linked to the velocity fluctuation through the flame transfer or describing function.

Applications to the LOTAR experiment

A schematic diagram of this set-up is presented in Figure 14, where air flows from left to right. It is divided into three parts. The first part (on the left hand side) comprises a siren enabling the rig acoustics to be forced at different frequencies during the Flame Transfer Function (FTF) measurements. A 1 m-long straight pipe, equipped with four microphone taps and two intakes to mount a loudspeaker, is placed between the siren and the plenum of the combustor. The water-cooled combustion chamber is equipped with large windows allowing optical diagnostic applications right at the outlet of the injection system. The last part is a trombone-like section, composed of a fixed tube and a coaxial movable tube. This allows continuous modification of the Inner Exhaust Length (IEL), defined by the length between the exit plane of the injection system and the exit plane of the movable tube. This length change creates a variation of the natural resonant frequencies of the rig. Similarly to the first part upstream from the combustor, this last part is equipped with microphone taps and loudspeaker intakes.

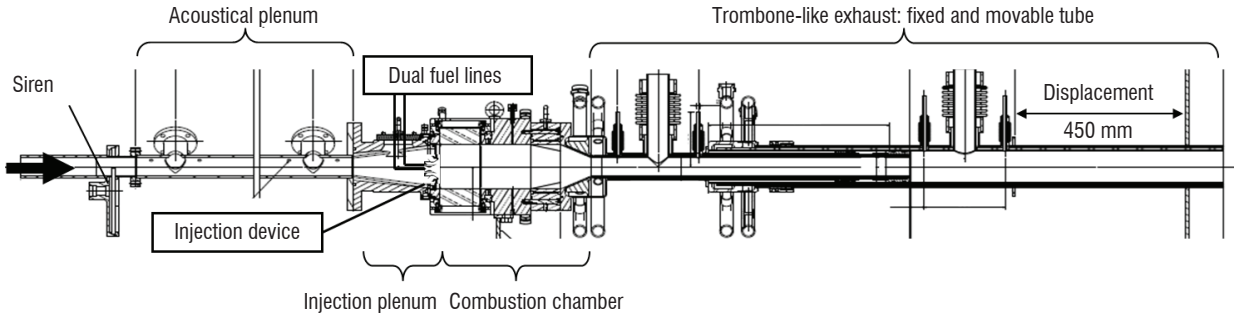

Figure 14 - Schematic diagram of the LOTAR experimental setup (Video 4).

The multipoint injection system used during the test was presented in § "Description of the main mechanisms involved in the p'q' coupling" (Figure 8). Various diagnostic methods, including phase Doppler anemometry, high-speed camera, PLIF and acoustic multiport techniques, were used to investigate the system behavior.

Flame response

Ghani et al. [34] have presented results of the ONERA LOTAR setup obtained from LES simulations with the AVBP code. In this case, the flame transfer function was performed by forcing the inlet velocity at fixed frequencies, with a modulation rate of 15%. The inlet and outlet boundary conditions are imposed through the non-reflecting Navier-Stokes Characteristic Boundary Condition (NSCBC) formulation, which enables acoustic reflection to be controlled. A local transfer function is deduced from the comparison between the local heat release fluctuations and the velocity signal obtained at a reference point located inside the injection system, yet upstream from the radial vane of the swirler (Figure 15). It is shown that the amplitude and time delays depend greatly on the downstream location. By averaging the heat release fluctuation over the volume domain, a global flame transfer function can be determined (Figure 16).

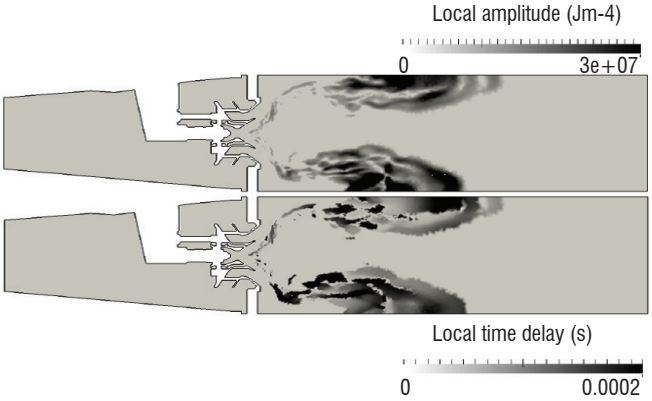

Figure 15 - Local fields of amplitude (top) and time delay (bottom) obtained from CFD (f=220 Hz) [34]

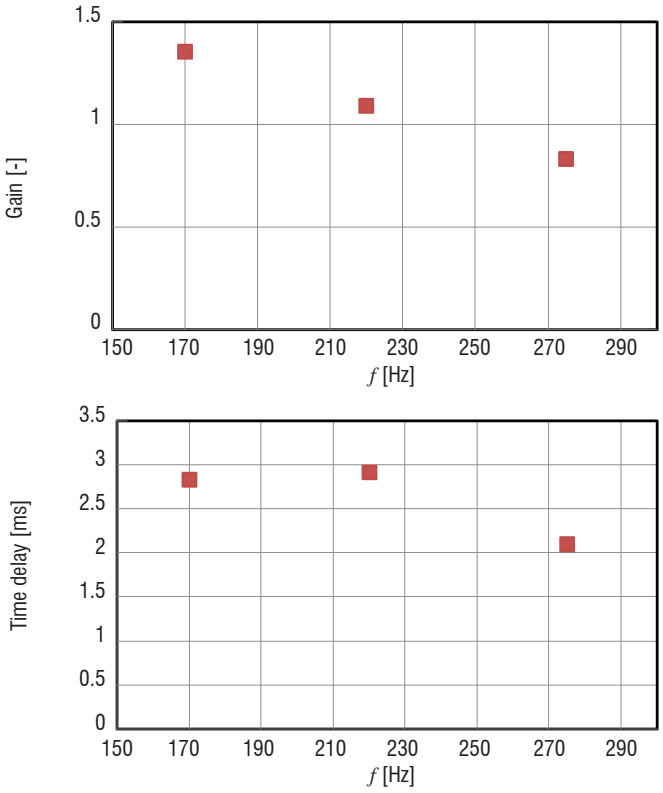

Figure 16 - Gain and Time delay obtained on the LOTAR setup [34].

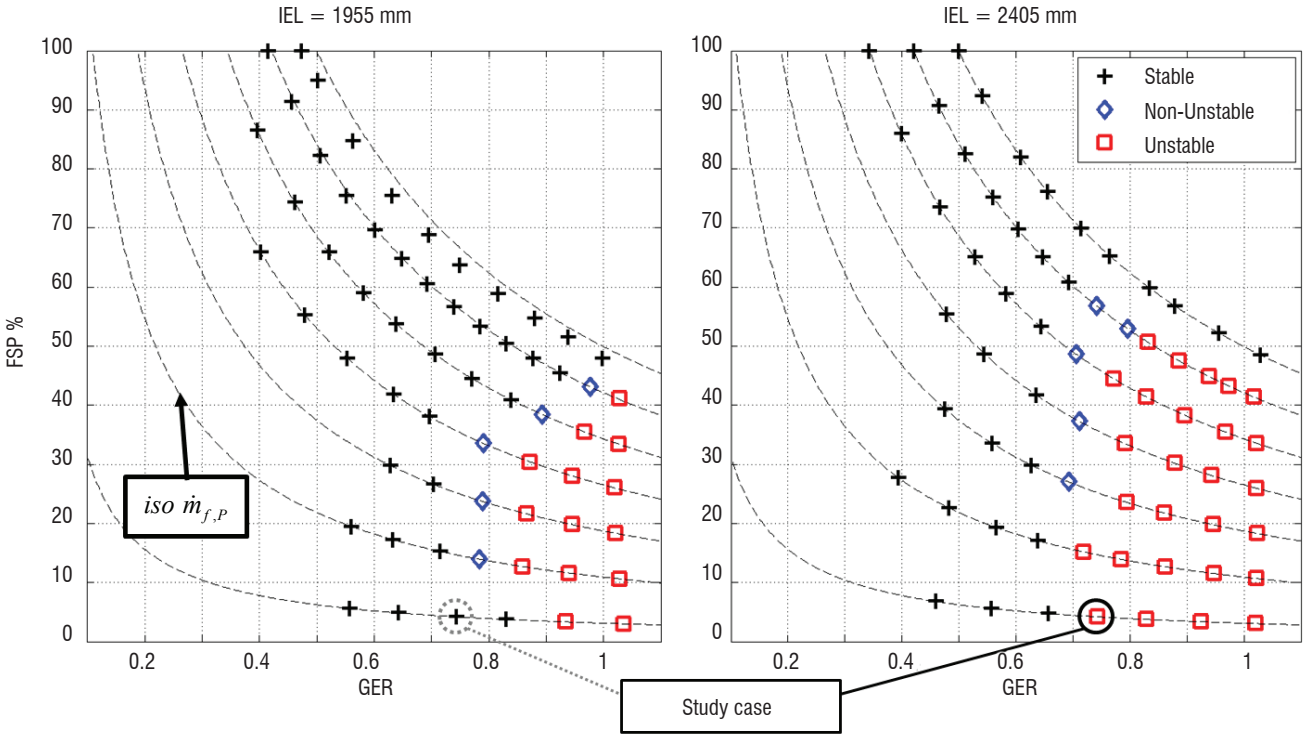

Figure 17 - LOTAR set-up stability map for IEL=1955 and 2405 mm, with $\dot{m}_{air}$ = 100 g/s, T_{air} = 473 K. [24]

Stability analysis

The influence of the Inner Exhaust Length (IEL) on the flame stability is illustrated in videos showing that, for a same flow condition, the flame changes from a stable condition for low IEL to unstable conditions for high IEL. A stability map of the setup with respect to the Global Equivalence Ratio (GER) and the fuel split ratio between the pilot and the multipoint zone was defined for two acoustic conditions corresponding to two IEL. The method used to define the stability criterion was inspired from the approach used by Samaniego et al. [35], which used the analysis of the pressure and flame radiation oscillations to identify the stability regime. From each signal, a stability map was drawn taking into account a threshold level for the fluctuation amplitude, delimiting the stable/unstable regions. As they conclude that a reasonably good overlapping of the unstable zones was deduced from each signal analysis, the definition of the combustion stability used on the LOTAR setup is based only on pressure fluctuation measurements. From a preliminary study, two criteria were used to define the flame stability: the sound pressure level of the resonant peak and the presence of at least one harmonic of the resonant frequency. The amplitude threshold was fixed at 145 dBSPL. Hence, three flame categories were defined. When both criteria are fulfilled, the flame is classified as "Unstable"; when no criterion is met, the flame is classified as "Stable"; and, finally, if only the amplitude criterion is met the flame is identified as "Non-Unstable".

The maps obtained for both IEL values are presented in Figure 17. The dash lines correspond to constant fuel mass flow rates through the pilot injector. It is noticeable that the uppermost line is always stable, which means that instabilities no longer appear if the fuel mass flow rate of the pilot injector is large enough. The unstable cases correspond to the region of higher global equivalence ratios, which is larger for IEL=2405 mm. As a result, as shown in the video, for some flow conditions, the flame changes from the stable to the unstable regime by modifying the IEL value.

The acoustic power $\vec{I}$ delivered by the setup can be used to quantify the coupling rate between the acoustics and the flame [36]. This acoustic power is defined by:

$$\vec{I} = \left\langle \left(1 + \frac{u_0^2}{c_0^2}\right) p\vec{u} + \vec{u}_0 \left(\rho_0 u^2 + \frac{p^2}{\rho_0 c_0^2}\right) \right\rangle$$

where $<>$ correspond to the temporal integration.

Munro and Ingard [37] developed a two-microphone technique enabling the acoustic power to be measured in ducts with a grazing air flow. This technique was applied on the LOTAR setup, by using the pressure signals measured on the two downstream taps located on the movable tube using a plane wave hypothesis. The influence of the IEL on the acoustic power delivered by the flame is plotted in Figure 18 for a fixed air and kerosene condition. It can be seen that the acoustic power increases greatly when the IEL increases. It reaches a maximum value for IEL around 2030 mm and then decreases.

The influence of the IEL on the growth rate was studied by Ghani [38] from a CFD approach, using the Helmholtz code AVSP (Figure 18). They observed a great increase in this parameter with the IEL The transition between the stable and the unstable configurations is obtained for IEL equal to 2350 mm. This comparison between the acoustic power and growth rate evolutions with respect to the IEL shows that the modification of this parameter changes the relationship between the pressure and the unsteady heat release in the chamber, leading to a great amplification of the acoustic energy delivered by the flame. It is noticeable that, for tube lengths below 2300 mm, even if the flame is still stable (growth rate negative), the acoustic power increases in

parallel to the growth rate. Furthermore, the higher acoustic power is reached close to the transition between the stable and unstable regimes

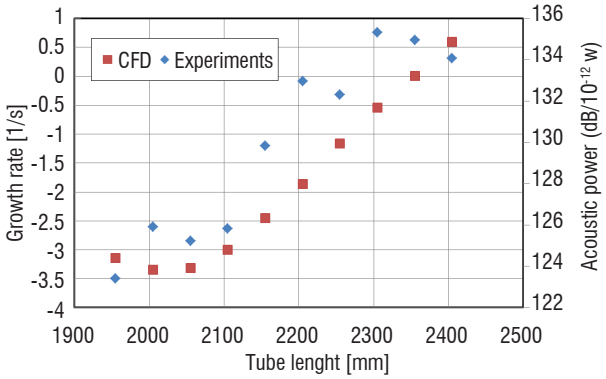

Figure 18 - Influence of the IEL on the acoustic power delivered by the combustion (Experiments) and the growth rate deduced from the CFD approach [38].

In order to complete this analysis on the interaction between the acoustic and the heat release from the flame, the local Rayleigh distribution, calculated from Eq. (2), is applied to the OH fluorescence results, similarly to the work of Samaniego et al. [34] and Lee et al. [39].

$$Ra(x,r) \propto \frac{1}{T}\int_{T} p'(x,r,t)q'(x,r,t)dt \qquad (2)$$

The computation of the local values is performed pixel by pixel, and yields the Rayleigh distribution displayed in Figure 19. For this representation, negative index values are represented in black, while positive ones are represented in red, and neutral ones are represented in white. Positive local Rayleigh index values mean that the local fluctuation of the unsteady heat release is in phase with the pressure fluctuation and therefore contributes to the combustion instability. On the other hand, the negative local Rayleigh index values indicate a stabilizing region, contributing to damp the instabilities due to unsteady heat release out of phase with the chamber pressure. A first conclusion that can be drawn from Figure 19 is that the IRZ (Inner Recirculation Zone), located in the flow region between the combustor longitudinal axis and the flame front (red area), sustains instabilities. Additionally, it reveals the position of the flame during the cycle. The flame angle is smaller during the first half of the pressure cycle, while this angle is wider during the second half of the pressure cycle, when the unsteady heat release is damping the instability phenomena (black area). Furthermore, the non-homogeneity of the Rayleigh index in the combustion chamber confirms the non-compact characteristic of the flame, as evidenced by LES simulations.

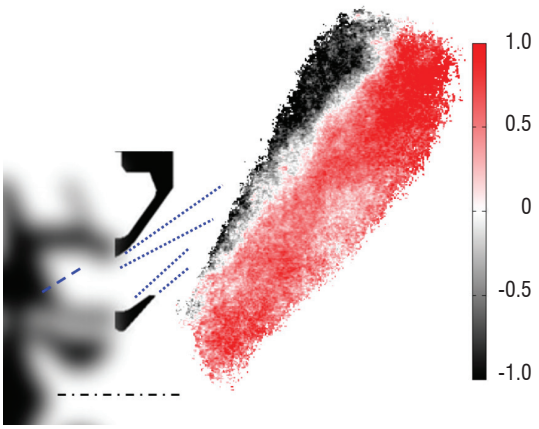

Figure 19 - Spatial distribution of the local Rayleigh index [24]

Conclusions and perspectives

Thermo-acoustic coupling is complex because many phenomena, such as combustion, chemistry, acoustic thermal transfer or one-phase or two-phase flow dynamics are involved. In many applications, this coupling may cause great pressure and heat release oscillations, which induce a risk for the safety of the systems involved. Many studies have been carried out over the years to understand and model the coupling lines and to develop numerical tools for predicting the appearance of instabilities and at last to try to prevent them. The key point of these models is certainly the measurement and, in parallel, the calculation of the time scales involved between the acoustic perturbations and the flame response. This analysis also shows that nonlinear phenomena in the flame response must be taken into account for an accurate description and, at last, prevention of the thermo-acoustic instabilities. Up to now, the flame response to acoustic excitations was determined from dedicated experiments performed on simplified configurations, mainly at low pressure. Their application to realistic conditions is not straightforward, because the pressure and the temperature may modify, even slightly, the flame position and structure which, finally, may have a drastic influence on the p'q' phase dependence. In order to improve this response identification, recent methods based on LES simulations have been proposed. Nevertheless, these simulations must accurately consider all of the individual phenomena involved in the $p'q'$ coupling, in order to obtain the right phase and amplitude response of the flame.

This paper is focused on applications dedicated to liquid-fueled aero engines. A description of the main approach found in the literature is proposed, with recent results obtained at ONERA where the liquid phase role in the $p'q'$ coupling is evidenced. It is shown that, depending on the injection method, various phenomena appearing between the fuel injection and its combustion can be taken into account in the models. The first concerned the response of the liquid phase to pressure or velocity oscillations close to the injection location. In this case, various flow patterns, such as liquid jet or liquid/wall interactions, must be considered. Other studies highlight that the heat release oscillations may be the result of the spray response to acoustic excitation. From these various works, it is evident that an accurate prediction of the combustion instability risks must take into account all of these phenomena. In particular, for liquid-fueled applications, the prediction of the flame response from the LES simulation can only be achieved if the unsteady behavior of the liquid phase is well modeled.

In order to achieve this objective, the ONERA project "Simulation des Instabilités de combustion Générées dans les Moteurs Aéronautiques et spatiaux (SIGMA)" was launched in 2015. In this project, the recent development of the multifluid approach in the ONERA CEDRE code (Refloch, 2011) will be used to calculate the response of the two-phase flow flames in aero engine and aerospace applications. In parallel, further experiments on the LOTAR setup will be performed to validate the simulations and to study in more details the non-linear response of the flame. The prediction of the combustion instability modes will be performed from both a low order approach and the Helmholtz code AVSP ■

References

[1] B. HIGGINS - *On the Sound Produced by a Current of Hydrogen Gas Passing Through a Tube*. Journal of Natural Philosophy, Chemistry and the Arts, 1, 129-131.

[2] P. RIJKE - *Notice of a New Method of Causing a Vibration of the Air Contained in a Tube Open at Both Ends*. Philosophical Magazine: Series 4, 17(116), 419-422.

[3] J. RAYLEIGH - *The Theory of Sound*. New York: Dover.

[4] D.J. HARRJE, F.H. READON - *Liquid Propellant Rocket Instability*. NASA SP 194.

[5] A.PUTNAM, W. DENNIS - *A Survey of Organ-Pipe Oscillations in Combustion Systems*. J. of Acoust. Soc. of America, 28(2), 246-259.

[6] F. NICOUD, T. POINSOT - *Thermoacoustic Instabilities: Should the Rayleigh Criterion be Extended to Include Entropy Changes?* Combustion and Flame, 142(1-2), 153-159.

[7] A. MINOTTI, F. SIMON, F. GANTIÉ - *Characterization of an Acoustic Liner by Means of Laser Doppler Velocimetry in a Subsonic Flow*. Aerospace Science and Technology, 12 , 398–407, doi:10.1016/j.ast.2007.09.007

[8] W. STRAHLE - *On Combustion Generated noise*. Journal of Fluid Mechanics, 49(2), 399-414.

[9] S. DUCRUIX, T. SCHULLER, D. DUROX, S. CANDEL - *Combustion Dynamics and Instabilities: Elementary Coupling and Driving Mechanisms.* Journal of Propulsion and Power, 19(5), 722-734.

[10] T. LIEUWEN - *Modeling Premixed Combustion-Acoustic Wave Interactions: A Review*. Journal of Propulsion and Power, 19(5), 765-781.

[11] F.E. MARBLE, S. CANDEL - *Acoustic Disturbance from Gas Non-Uniformity Convected through a Nozzle.* Journal of Sound and Vibration, 55(2), 225-243.

[12] W.POLIFKE, C.O. PASCHEREIT, K. DÖBBELING K - *Constructive and Destructive Interference of Acoustic and Entropy Waves in a Premixed Combustor with a Choked Exit.* International Journal of Acoustic and Vibration, 6(3), 135-146.

[13] M. HUET, A. GIAUQUE - *A non Linear Model for Indirect Combustion Noise Through a Compact Nozzle*. Journal of Fluid Mechanics, 733, 268-301.

[14] T. SATTELMAYER - *Influence of the Combustor Aerodynamics on Combustion Instabilities from Equivalence Ratio Fluctuations.* Journal of Engineering for Gas Turbines and Power 2003 125 (1), 2003, 11-19

[15] F. NICOUD, L. BENOIT, C. SENSIAU, T. POINSOT - *Acoustic Modes in Combustors with Complex Impedances and Multidimensional Active Flames*. AIAA Journal, 45, 426-441.

[16] A.P. DOWLING - *Nonlinear Self-Excited Oscillations of a Ducted Flame*. Journal of Fluid Mechanics, 346, 271-290.

[17] N. NOIRAY, D. DUROX, T. SCHULLER, S. CANDEL - *A Unified Framework for Nonlinear Combustion Instability Analysis Based on the Flame Describing Function*. Journal of Fluid Mechanics, 615, 139-167.

[18] E. GUTMARK - *Shear-Flow Role in Combustion Control*. A. I. Astronautics (Éd.), AIAA 97-2113. AIAA Fluid Dynamics Conference.

[19] S. HERMETH - *LES Evaluation of the Effects of Equivalence Ratio Fluctuations on the Dynamic Flame Response in a Real Gas Turbine Combustor Chamber.* Proceeding of the Combustion Institute, 3165-3173.

[20] T. LIEUWEN, B.T. ZINN - *Theoretical Investigation of Combustion Instability Mechanisms in Lean Premixed Gas Turbines*. AIAA-98-0641. American Society of Aeronautics and Astronautics.

[21] J. ECKSTEIN, E. FREITAG, C. HIRSCH, T. SATTELMAYER - *Experimental Study on the Role of Entropy waves in Low-Frequency Oscillations in a RQL Combustor.* Journal of Engineering for Gas Turbines and Power 128 (2), 2006, 264-270

[22] F. GIULIANI, P. GAJAN, O. DIERS, M. LEDOUX - *Influence of Pulsed Entries on a Spray Generated by an Airblast Injection Device : An Experimental Analysis on Combustion Instability Processes in Aeroengines.* Proceeding of the Combustion Institute, 29(1), 91-98.

[23] P. GAJAN, A. STRZELECKI, B. PLATET, R. LECOURT, F. GIULIANI - *Investigation of Spray Behavior Downstream of an Aeroengine Injector with Acoustic Excitation.* Journal of Propulsion and Power, 23(2), 390-397.

[24] J.M. APELOIG, H.X. D'HERBIGNY, F. SIMON, P. GAJAN, M. ORAIN, S. ROUX - *Liquid-Fuel Behavior in an Aeronautical Injector Submitted to Thermoacoustic Instabilities*. Journal of Propulsion and Power, 31(1), 309-319.

[25] F. GIULIANI - *Analysis on the Behaviour of an Aeroengine Air-Blast Injection*. Toulouse: PhD Thesis, ISAE.

[26] T.J. ANDERSON, W. PROSCIA, J.M. COHEN - *Modulation of a Liquid-Fuel Jet in an Unsteady Cross-Flow.* ASME Turbo expo 2001. New Orleans, Louisiana: ASME. Paper N° 2001-GT-0048.

[27] J. SONG, J.G. LEE - *Characterization of Spray Formed by Liquid Jet Injected Into Oscillating Air Crossflow*. ASME Turbo Expo. Montréal, Canada: ASME. Paper N° GT2015-43726.

[28] L. CROCCO, S. CHENG - *Theory of Combustion Instability in Liquid Properlant Motors.* (AGARDodograph, Éd.) London: Butterworths.

[29] S. ILLINGWORTH, M. JUNIPER - *When Will a Flame Describing Function Approach to Thermoacoustics Work Well?* International Conference on Sound and Vibration. Vilnius Lithuania.

[30] T. POINSOT, D. VEYNANTE - *Theoretical and Numerical Combustion*. 2nd Edition.Philadelphia, USA: R.T. Edwards.

[31] G.J. BLOXIDIDGE, A.P. DOWLING, P.J. LANGHORNE - *Reheat Buzz: an Acoustically Coupled Instability.* Part 2. Theory. Journal of Fluid Mechanics, 193, 445-473.

[32] P.J. LANGHORNE - *Reheat Buzz: an Acoustically Coupled Combustion Instability.* Part 1. Experiment. Journal of Fluid Mechanics, 193, 417-443.

[33] T. SATTELMAYER, W. POLIFKE - *Assessment of Methods for the Computation of the Linear Stability of Combustors.* Combustion Science and Technology, 175, 453-476.

[34] A. GHANI, L. GICQUEL, T. POINSOT - *Acoustic Analysis of a Liquid Fuel Swirl Combustor Using Dynamic Mode Decomposition*. ASME TURBO Expo 2015. Montréal: ASME. Paper N° GT2015-42769.

[35] J.M. SAMANIEGO, B. YIP, T. POINSOT, S. CANDEL - *Low-Frequency Combustion Instability Mechanisms in a Side-Dump Combustor.* Combustion and Flame, 94, 363-380.

[36] C.L. MORFEY - *Acoustic Energy in Non Uniform Flows*. Journal of Sound and Vibration, 14, 159-170.

[37] D.H. Munro, K.U. Ingard - *On Acoustic Intensity Measurements in the Presence of Mean Flow*. J. Acoust. Soc. Am., 65 (6), 1402-1406.

[38] A. GHANI - *LES of Self Excited Transverse Combustion Instabilities in Perfectly-Premixed and Swirling Spray Flames*. Ph D, Université de Toulouse. 'http://oatao.univ-toulouse.fr/15658/1/ghani.pdf '

[39] S.-Y.LEE, S. SEO, J.C. BRODA, S. PAL, R.J. SANTORO - *An Experimental Estimation of Mean Reaction Rate and Flame Structure During Combustion Instability in a Lean Premixed Gas Turbine Combustor.* Proceedings of the Combustion Institute, 28(2), 775-782.

[40] A.C. REFLOCH - *CEDRE Software.* (ONERA, Ed.) Aerospace Lab Journal(2), 1-10.

Nomenclature

Σ	=	surface of the control system boundary, m^2
Ω	=	volume of the control system, m^3
γ	=	heat capacity ratio
ρ	=	density, kg/m^3
τ	=	characteristic time, s
ω	=	pulsation angle, rad/s
ϕ	=	equivalence ratio
c	=	sound velocity, m/s
dA	=	surface integration variable, m^2
dt	=	time integration variable, s
dV	=	volume integration variable, m^3
D_{REF}	=	reference diameter
FDF	=	Flame Describing Function
FSP	=	Fuel Split Parameter
FTF	=	Flame Transfer Function
GER	=	Global Equivalence Ratio
I	=	light intensity over camera dynamics, # counts
IEL	=	Inner Exhaust Length, mm
J	=	momentum ratio
L	=	distance, m
$\dot{m}_{air}$	=	air mass flow rate, g/s
$\dot{m}_{f,P}$	=	fuel mass flow rate on the pilot system, g/s
$\dot{m}_{f,MP}$	=	fuel mass flow rate on the multipoint system, g/s
n	=	interaction index
p'	=	acoustic pressure, Pa
$\overline{P}$	=	averaged pressure, Pa
q'	=	unsteady heat release, W/m^3
Q	=	total heat release produced by the flame, W
Ra	=	local Rayleigh index
S	=	Surface, m^2
T	=	instability cycle period, s
T_{air}	=	air inlet temperature, K
u'	=	acoustic velocity, m/s

AUTHOR

Frank Simon graduated from ENSICA Toulouse with a degree in Aeronautical Engineering (1989), from Supaero Toulouse with a PhD in Mechanical Engineering (Acoustics) (1997) and from the University of Toulouse with Authorization to supervise PhD students (2007). He is a Research Master at Onera, specialized in the development of vibro-acoustic modeling and measurement techniques and has participated in various EC projects in the vibro-acoustic domains (RHINO, FACE, FRIENDCOPTER), as well as being in charge of internal noise in the Garteur group.

Mikael ORAIN received his Masters degree in fluid mechanics in 1996 and his PhD in Mechanical Engineering in 2001 from the Imperial College London (UK). He is a research scientist at ONERA/DMPH in charge of developing PLIF for the measurement of temperature and species concentrations in reacting and non-reacting two-phase flows.

Pierre GAJAN received the degree of Doctor of the University of Rouen in 1983 and that of Science Doctor in 1988. He has worked as a research engineer at ONERA since 1987 as an experimentalist and is in charge of the research unit on multiphase flows in the department of "Models for Aerodynamics and Energetics" since 2008. He has carried out many projects on flow dynamics in pipes, first under mono-phase conditions and then in two-phase flows for the gas industry. Since 2000, he has worked on combustion instabilities in order to analyze the role of the liquid phase on the thermoacoustic couplings.

Virginel BODOC graduated from the Military Technical Academy of Bucharest in 2003. In the following years, he worked as a Research Engineer at the Military Equipment and Technology Research Agency of Bucharest. After obtaining a Master Degree Diploma from the INP Toulouse in 2007, he joined ONERA as a Marie Curie doctoral fellow and defended his PhD in 2011. Since 2010, he has been involved in various research projects conducted at the LACOM combustion laboratory (Fauga-Mauzac center). Within the research team, his main field of activity is the development and application of optical measurement techniques (PIV, PDA/LDA, LIF, Rainbow Refractometry and Infrared Absorption) to characterize reacting and non-reacting gas/droplet flows. Since 2013 he has been in charge of the LACOM facility technical survey.

M. Huet, F. Vuillot, N. Bertier
(ONERA)

M. Mazur, N. Kings, W. Tao, P. Scouflaire, F. Richecoeur, S. Ducruix
(Laboratoire EM2C, CNRS, Centrale Supélec, Université Paris-Saclay)

C. Lapeyre, T. Poinsot
(Institut de Mécanique des Fluides de Toulouse)

E-mail : maxime.huet@onera.fr

DOI : 10.12762/2016.AL11-10

Recent Improvements in Combustion Noise Investigation: from the Combustion Chamber to Nozzle Flow

For a long time, engine noise has been dominated by fan and jet noise. With their reduction for modern turbojets, for instance, combustion noise is no longer negligible and efforts are concentrated on its understanding. The objective of the European project RECORD is to help to understand the fundamental mechanisms of core noise, in order to reduce it. In this paper, the recent advances achieved within the project for the noise generated through a nozzle are presented. This work includes the definition of a combustion test bench at the EM2C laboratory, equipped with various diagnostic techniques and an outlet nozzle to pressurize the chamber and generate entropy noise. Reactive simulations of this facility are performed by ONERA and CERFACS using LES. Finally, simulated flow fields are post-processed to determine direct (acoustic) and indirect (entropy) contributions to the global noise generated by the nozzle. This work is a first step before the modeling of a full engine, including the turbine stages.

Introduction

With increasingly severe environmental regulations, noise pollution is now a major concern for aircraft operators. Among all of the noise sources of an aircraft, engine noise is the major contributor and much attention remains focused on its reduction. For a turbojet engine, jet and fan noise are the dominant noise sources and, as such, have been the subject of great efforts for their reduction by the aeroacoustics community over the last decades. In modern engines, additional noise sources that were previously masked by those two main contributors can no longer be neglected, and may even become predominant for specific frequencies and operating points. As illustrated in Figure 1, this is the case for the combustion noise in the medium frequency range at the approach regime [1].

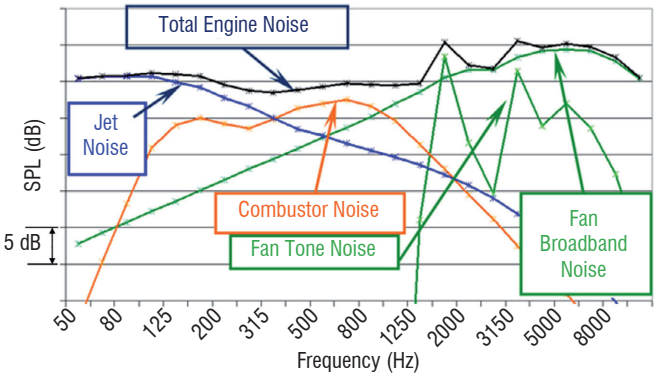

Figure 1 - Typical contribution of turbojet engine noise sources on approach, from SAFRAN Snecma [1]

The contribution of combustion noise was first evidenced in the 1970s with the engine noise being found to be higher than the sole contribution of the jet [2]. Being first referred to as excess noise [3], this additional noise was then associated with the combustion process and is now called core noise [4] or combustion noise [5]. First theoretical analyses where provided by Bragg [6] and Strahle [7] and this noise was shown to have two distinct origins. Pressure fluctuations can be generated by the unsteady heat release of the flame; it then corresponds to direct noise [6]-[13]. The unsteady turbulent flame also generates temperature (entropy) and velocity (vorticity) perturbations that create additional noise when accelerated by the mean flow through a nozzle or a turbine. The latter is called indirect noise [14]-[16]. Marble and Candel [17] were among the first to quantify the noise generated by small-amplitude entropy spots convected through a compact nozzle, where the wavelengths are assumed to be large compared to the considered geometry. Their approach was later extended to entropy and vorticity spots passing through turbine rows by Cumpsty and Marble [18].

Under normal operating conditions, the noise sources are incoherent and radiate a broadband of frequencies. For particular configurations, however, a coupling may appear between the fluctuations emitted by the flame and the boundaries of the combustion chamber and lead to combustion instabilities [19]-[22] with very high tonal noise that may even cause the destruction of the combustor. Recent studies showed the role of accelerated entropy spots on the onset or sustainability of these instabilities [23]-[28], highlighting the importance of understanding the basic mechanisms of combustion noise and its prediction. Combustion instabilities are however beyond the scope of this paper and will not be discussed. The reader can refer to the surveys

by Candel *et al* [29] and McManus *et al* [30] for a more detailed view of the state of knowledge in the field of combustion noise.

An illustration of the evaluation of combustion noise in modern aero-engines is proposed by Duran *et al* in an earlier issue of the journal [31]. In their paper, the authors focused on the direct and indirect combustion noise mechanisms. Reference experimental facilities (an entropy noise test bench [32] and an instrumented full-scale turbo-shaft engine [33], [34]) are also detailed and a numerical evaluation of combustion noise is illustrated for a model engine composed of a combustion chamber and turbine stages.

Recently, European research activities on the topic have been concentrated through the RECORD project, funded by the European Union [35]. The objective of the project is to aid in the understanding of the fundamental mechanisms of core noise generation and to propose ways to reduce it. To this end, experimental facilities, numerical simulations and analytical models are being set up to cover all of the stages of direct and indirect noise generation. The experimental activities consist, in detail, in the injection of acoustic and entropy waves through a nozzle for the evaluation of nozzle transfer functions [36], [37], in an instrumented pressurized combustion chamber with a one-stage swirl injector [38] and in a high-pressure turbine stage that can be fed with acoustic, entropy or vorticity waves [39].

This paper presents the recent advances achieved during the RECORD project with regard to the experimental evaluation and numerical prediction of combustion noise generated inside a combustion chamber equipped with a nozzle at its outlet. It combines experimental results on a dedicated combustor, unsteady reactive numerical simulations of the facility and analytical models to evaluate direct and indirect combustion noise. Measured, simulated and modeled results are cross-compared for validation and the contribution of acoustics and entropy perturbations to the noise generated in the combustor is evaluated. The paper is organized as follows. The experimental facility is described in a first step; the diagnostic techniques and operating points are particularly discussed. Numerical simulations reproducing the flame and its noise generation are presented in a second step. The acoustic post-processing of the simulations is then detailed. This section includes the methodology of wave extraction from the CFD fields and the evaluation of noise generation through the nozzle. The paper finally ends with conclusions and perspectives.

Experimental facility

The CESAM-HP Test bench for stabilizing a lean flame in a pressurized chamber

The CESAM-HP test bench was developed at the EM2C Laboratory with the aim of studying combustion noise and its contributors – direct and indirect combustion noise. Having been designed within the framework of the RECORD project, it features a one-stage swirl injector, a combustion chamber with large optical accesses and an exhaust nozzle used to pressurize the combustion chamber and generate indirect noise. Figure 2 shows a schematic drawing of the CESAM-HP test bench.

The test bench comprises the following elements:

- The Impedance Control System (ICS), consisting of a perforated plate with a bias air flow, which in connection with an adjustable cavity can be used to damp instabilities at a chosen frequency. The system has been developed as part of prior work at the EM2C Laboratory [40],[41]. The axial flow is also aimed at limiting the flame flash back. It can be balanced between a high-speed central jet and a lower speed flow going through the piston. This distribution of the air flow influences acoustic behavior on the test bench, as will be shown below.
- The injection system, consisting of one tangential stage where the air/propane premixture is injected. The tangential injection ensures a strong swirling motion, which results in a compact flame that can be operated in lean conditions.
- The square section chamber (70 mm × 70 mm × 140 mm), featuring top and bottom cooled walls, and a large optical access on one side. The last wall bears the ignition system and the pressure and temperature instrumentation. The test bench modularity enables the walls and glass window to be exchanged, depending on the diagnostic technique applied.
- The exhaust nozzle downstream of the combustion chamber, aimed at increasing the mean pressure and increasing the burnt gas velocity. At the operating points studied, the nozzle is choked and the chamber pressure rises to over 2 bars. The nozzle shape was acoustically optimized, in order to generate a maximal amount of entropy noise. This is done by describing the nozzle shape with several Bezier splines and by applying a genetic algorithm for optimization. [42]

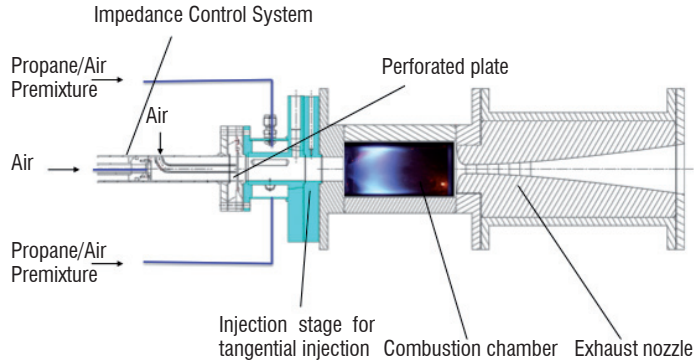

Figure 2 - Schematic drawing of the CESAM-HP test bench

Diagnostic techniques for measuring the dynamic properties of the flow

Various diagnostic techniques are used to quantify the flow properties and acoustics during operations. A schematic drawing of the combustion chamber in Figure 3 shows the various sensor positions.

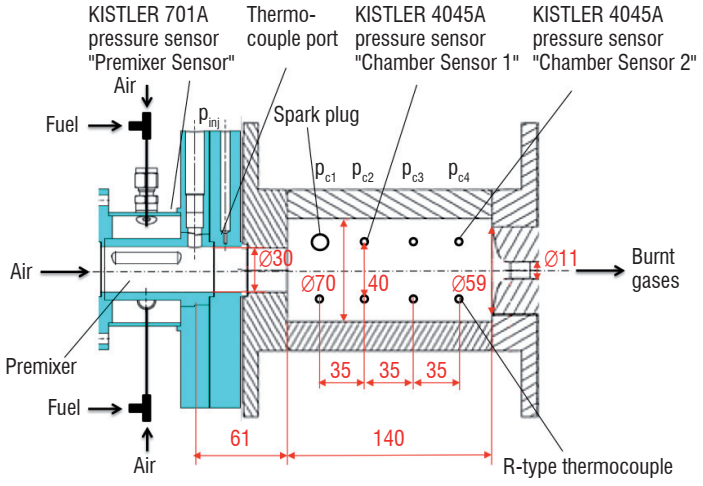

Figure 3 - Schematic drawing of the combustion chamber with its feeding lines and various sensor positions

Pressure measurements are performed on the test bench. Due to the pressurization of the test bench, piezo-resistive sensors (KISTLER 4045A) are installed directly in the chamber walls and can simultaneously measure the static pressure and dynamic pressure fluctuations. A reliable, stable and long-time operation is ensured by the integration into a combined system of thermal protection and water-cooling, made as part of previous work [43],[44],[45]. The dynamic pressure fluctuations in the injector are measured by dynamic-only sensors of the type KISTER 701A. The pressure evolution is recorded during operation for 4 s, with a sampling frequency equal to 25 kHz.

Thermocouple measurements are performed at several positions of the test bench for monitoring purposes, but also inside the combustor for global characterization. While slow in response, the R-type thermocouple installed in-chamber is able to measure temperatures up to 1600 °C and is therefore suitable for the measurement of the temperature of burnt gases.

Three operating points to test different injection strategies

For all of the operating points, most of the mass flow enters the chamber through the tangential injection, in order to guarantee an intense swirling motion. The axial mass flow comes either from the central orifice (at high-speed) or goes through the perforated back plate (at lower speed). The balance between the two axial injection systems has a significant influence on chamber acoustics. Among a large variety of possible operating points, three have been retained for their interest from an acoustic point of view. Their properties are summarized in Table 1.

Property	Values		
Name	op16-0-2-85	op16-2-0-85	op13-5-0-85
Fuel type	Propane	Propane	Propane
Fresh fuel and air temperature [°C]	20	20	20
Tangential air flow rate [g/s]	16	16	13
Tangential fuel flow rate [g/s]	0.968	0.968	0.968
Central jet air flow rate [g/s]	0	2	5
Piston air flow rate [g/s]	2	0	0
Global equivalence ratio	0.85	0.85	0.85
Power [kW]	44.9	44.9	44.9
Mean chamber pressure [bar]	2.02	2.02	2.01

Table 1 - Main properties of the studied operating points

For each operating point, we propose here to present the acoustic spectra that synthesize the dynamics at work in the chamber. Once the stable regime is reached, the dynamic pressure at the walls is recorded and power spectral densities are computed using Welch's periodogram method with segments of 2048 samples, Hamming windows and a 50% overlap. The resulting spectra are shown in Figure 4.

All of the spectra contain both a broadband acoustic power and some resonant peaks. This illustrates two phenomena at work: a large band noise and combustion instabilities. The proportion of each changes with the injection strategy.

The spectra of op16-0-2-85 and op16-2-0-85 are dominated by a low frequency peak around 120 Hz and its harmonics. Theoretical work determined that these are related to the feeding lines [38]. For point op16-0-2-85, the higher harmonics are slightly damped, but the change in the air injection location (through the back plate or through the central hole) does not strongly modify the power spectrum.

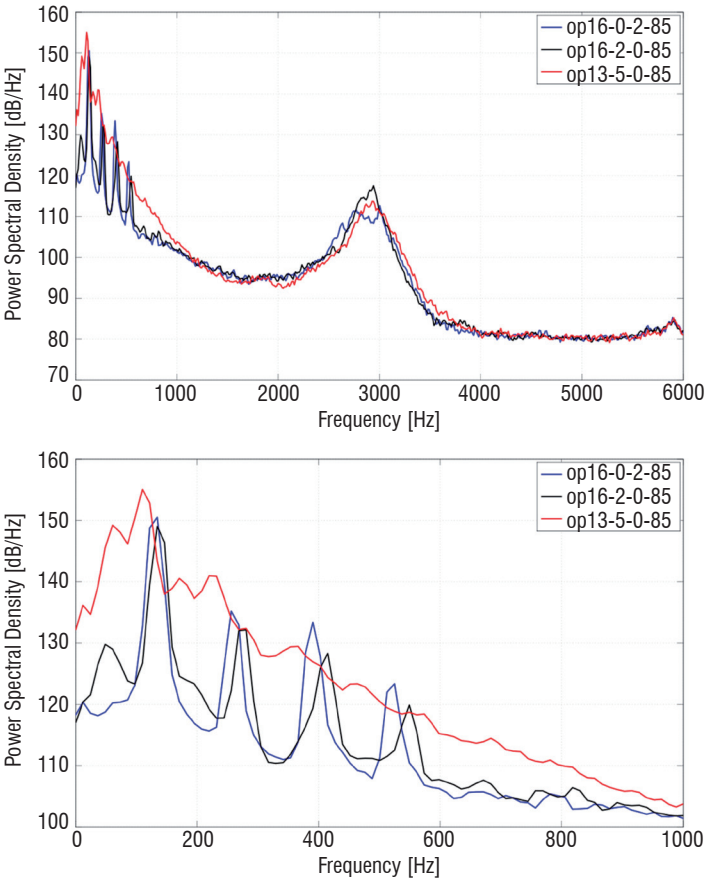

Figure 4 - Power Spectral Density of the three operating points, with a magnified view in the low frequency area at Sensor Position 2

For operating point op13-5-0-85, instabilities barely exist and a broadband low frequency peak is observed.

Most of the dynamics are concentrated under 1 kHz. At higher frequencies, all of the pressure spectra feature the same increase in amplitude around 3 kHz, potentially corresponding to a higher mode. However, contrary to what would be expected for an eigenmode, the peak is large and this might be associated with measurement noise. Further experimental results concerning the analysis of eigenmodes and eigenfrequencies are presented by Mazur *et al* [46] and Kings *et al* [47]. The purpose of this study is to describe additional diagnostic and processing tools that are necessary to point out the potential acoustic sources in the chamber.

Numerical simulations

In order to identify the sources of combustion noise, the decision was made for the RECORD project to support High Fidelity compressible Large Eddy Simulations (HFLES) of the experimental setup CESAM-HP from the EM2C (see above). These simulations were intended to provide detailed insight into the flow and combustion processes acting in the pressurized one-stage combustion chamber. Two HFLES compressible codes were used to conduct simulations of this setup: the AVBP code, which was used in collaboration by both CERFACS and EM2C; and CEDRE, which was used at ONERA. These codes present valuable differences in their numerical contents and

modeling approaches and have demonstrated their ability to represent such complex reacting flows involving strong interactions between unsteady fluid dynamics, acoustics and combustion. Moreover, compressible LES codes are very well suited for this study, since they enable the choked nozzle and sonic throat to be naturally included in the computations. This enables the unsteady behavior of the domain outlet to be fully reproduced, including acoustic impedance and full 3D effects. Finally, having two codes with different numerical approaches permitted very useful cross-calculations, which helped to finalize the experimental set-up definition and to choose appropriate operating points.

In the course of the RECORD project, several computations were performed by both teams on different configurations and helped to understand the strong unstable behavior of the initial set-up with a two-element injector. Once a proper operating point was established, both cold and reacting computations were performed and compared to the experiment for the reference one-element configuration. Only the reacting case results are presented here.

Code description

AVBP

The compressible Large Eddy Simulations of the CESAM-HP burner were conducted with the high-fidelity LES code AVBP [48]-[50] developed by CERFACS and IFP-EN. AVBP solves the 3D compressible Navier-Stokes equations using both DNS and LES approaches on unstructured and hybrid meshes. The numerical scheme in AVBP relies on the Cell Vertex (CV) Finite-Volume (FV) method [50]. The third-order in time and space Taylor-Galerkin Finite Element scheme TTGC [51] was used in the simulations for its accuracy on the propagation of vortices and acoustic waves. Turbulence on the subgrid scale was handled by the Sigma model [52]. Combustion kinetics were described by a global one-step reaction including five species (C_3H_8, O_2, N_2, CO_2, H_2O), while the turbulence-combustion interaction was described by the Dynamic Thickened Flame model [53] combined with the Charlette-Meneveau efficiency function [54]. The boundary conditions were implemented with the Navier-Stokes Characteristic Boundary Conditions (NSCBC) [55]. Specific heat resistances matching the cooling power applied on individual walls during the experiments were used to treat heat losses on these chamber walls. The flow through the perforations of the back plate was not resolved, due to its high computational cost. Instead, the perforated plate was replaced by a coupled boundary condition giving a uniform acoustic treatment based on the instantaneous pressure drop through the perforated holes. This approach, developed in [56], is aimed at recovering the frequency-domain acoustic impedance of the perforated plate in time-domain LES simulations.

CEDRE

The CEDRE code is being developed by ONERA for energetics and propulsion research and applications [57]-[61]. It is a fully parallel multi-physics code that relies on dedicated solvers for resolving various physical systems. In this work, only the gas phase solver CHARME has been used. It solves the compressible reactive multi-species Navier-Stokes equations on generalized unstructured meshes (polyhedra). It provides a zonal modeling approach based on user domain decomposition, where particular models can be activated. It is based on a finite volume cell-centered MUSCL approach, combined with explicit or implicit time integration. Space and time numerical schemes can be combined up to the fourth order in space and time [62]. Based on previous experience, these computations were carried out with a choice of second order space schemes, combined with a one-step implicit GMRES time integration. In order to capture the acoustic waves, CFL numbers were kept close to unity over most of the computational domain. The CHARME solver allows choosing among varied turbulence models, from RANS to LES, including hybrid approaches such as DDES or ZDES [60], [63]. All turbulence models can be completed by particular laws of the wall, which are activated when required by the grid resolution at the walls. Wall thermal conditions were imposed by approximated experimental conditions, as provided by the EM2CS team. These computations were run using the Smagorinsky LES model. Lean combustion enables the use of global combustion kinetics involving only five species (C3H8, O2, N2, CO2, H2O). For subgrid turbulence-combustion interaction, a Dynamic Thickened Flame model was used in conjunction with the Charlette efficiency function [54]. A controlled acoustic condition was used to represent the behavior of the ICS. It used a particular boundary condition available in the CEDRE code to represent in the time domain the complex acoustic impedance of the ICS, as measured by the EM2C team. This condition is based on previous work [64], [65].

Geometry and grids

The numerical test case for the modified CESAM-HP setup is described in Figure 5. It includes the entire swirled one-element tangential injection system, the pressurized chamber, and a part of the experimental nozzle truncated after the sonic throat. The rest of the diverging section of the nozzle is not included in the domain, since it is not needed to capture the sonic nozzle acoustic response for the reflected noise. However, it will be considered in some of the acoustic analysis (transmitted noise). The origin of the reference axes is set at the center of the plenum exit (dump plane), with the x-axis oriented in the direction of the flow (Figure 5).

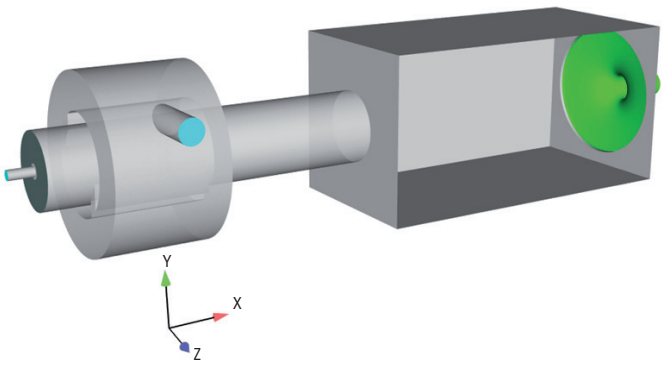

Figure 5 - Computational domain

One operating point was selected from the experimental data base and is summarized in Table 2. The inlet stagnation temperature is set at 290 K.

Operating point	Air MFR injection stage	Air MFR axial jet	Air MFR ICS	Overall equivalence ratio
OP13-5-0-85	13 g/s	5 g/s	0 g/s	0.85

Table 2 - Experimental operating conditions

The geometry and first grid used were built by CERFACS from the CAD file provided by EM2C team and are shown in Figure 5. The grids were generated with the Centaur mesh generator [66]. The nozzle divergent section is not fully meshed, since the nozzle will be choked for the reactive computations. A sufficient part of the divergent has been included, for the sonic line to always be in the computational domain.

Two similar meshes were used by ONERA and CERFACS for this geometry. Figure 6 shows the mesh used by ONERA, which ranges from the ICS to the nozzle divergent. Figure 7 shows the computational domain used by CERFACS, including the ICS. The CERFACS mesh is a fully tetrahedron unstructured mesh. The ONERA mesh was derived from the CERFACS mesh, to introduce three separate domains: Plenum/Injection, Chamber and Nozzle. It includes prisms along the nozzle walls and at the Plenum-Chamber interface. The main characteristics of these meshes are summarized in Table 3.

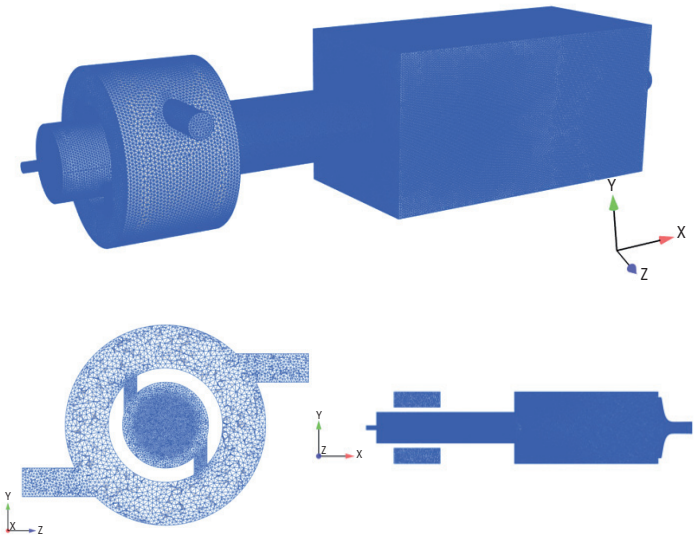

Figure 6 - Mesh used by CEDRE

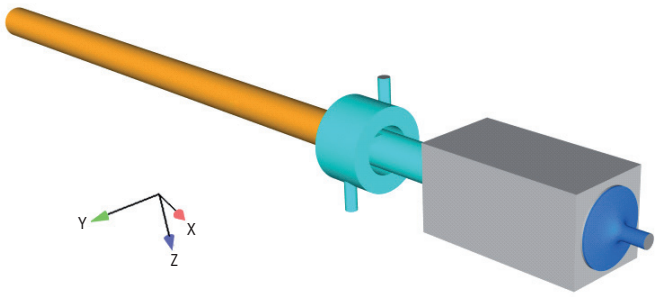

Figure 7 - Final mesh used by AVBP

A controlled acoustic condition was used to represent the behavior of the ICS, as mentioned previously. ONERA used a particular boundary condition available in the CEDRE code to represent in the time domain the complex acoustic impedance of the ICS, as measured by the EM2C team. A different approach was used by CERFACS, where the chamber upstream of the ICS was meshed and a coupled strategy was used to model the plate behavior. The capabilities of this approach in reproducing the actual impedance have been demonstrated before, with the AVBP code [56]. The proper treatment of the acoustic response of the ICS device appeared to be essential in the final results and both approaches provided satisfactory results.

Mesh	No. of cells	Element types	No. of domains
CERFACS	10.9 M	tetrahedra	1
ONERA	11.1 M	tetrahedra, prisms, pyramids	3

Table 3 - Main characteristics of the meshes

Finally, the main numerical parameters for the two codes are summarized in Table 4.

Code	Space discretization	Temporal integration	Time step
CEDRE	MUSCL (O2)	Implicit: backward Euler	1e-6 s
AVBP	TTGC (O3)	Explicit: RK2	1e-7 s

Table 4 - Numerical set-up

Results

The preliminary results from both teams had shown a strongly unstable behavior with marked flashback situations. Controlling this behavior involved several adjustments in the numerical set-ups. In particular, the proper handling of the ICS boundary condition appeared to be essential, as mentioned above. Additional adjustments were also performed and involved additional damping boundary conditions (AVBP) or modular treatments of the various zones of the computational domain (CEDRE). Concerning the CEDRE computations, a preliminary solution was obtained before the full ICS boundary condition was available, by simply de-activating the combustion in the Plenum/injection domain. This proved to be very efficient in suppressing flashback situations and provided interesting results. This computation will be referred to hereafter as the "-n" computation. However this simple solution lacked an important feature of the experiment, since the large low frequency motion was absent from this simulation. Once the ICS acoustic impedance was introduced into the computation, this simplified solution was completed by a fully reacting solution. This computation will be referred to hereafter as the "-b4n2" computation. Both solutions will be presented, since they provide interesting insight into the complex interactions between flow features, acoustics and combustion. The study of the flashback phenomenon in the CESAM-HP experiment is presented in reference [67]. Further details about the AVBP computations performed for this experiment can be found in the PhD theses of Lapeyre and Tao ([68], [69]).

Mean flow

The computed mean temperature fields are illustrated in Figure 8 for the three available computations. It can be noted that the AVBP and CEDRE "-n" computations provide similar mean temperature fields, where the plenum region is mostly unaffected by the flame, exhibiting low temperature levels. On the contrary, the CEDRE "-b4n2" computation shows that a relatively high temperature is observed in the plenum domain, due to marked low frequency motion of the flame across the dump plane. In Figure 8 d) numerical profiles are compared to measurements at the position X = -95 mm inside the plenum. This figure indicates that the results of the "-b4n2" computation are compatible with the measured temperature in the plenum, indicating that flame motion is indeed present in the experiment and leads to increased temperature levels in this region.

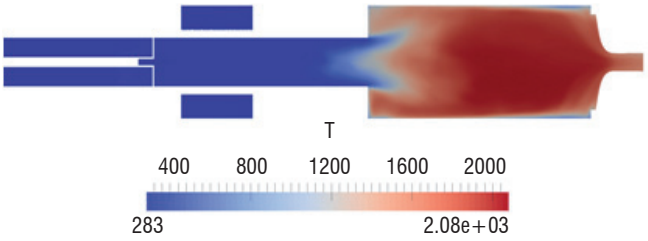

a)

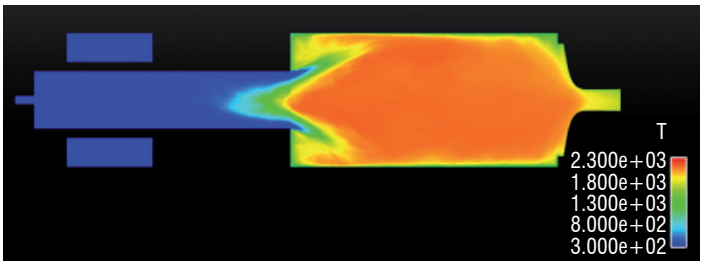

b)

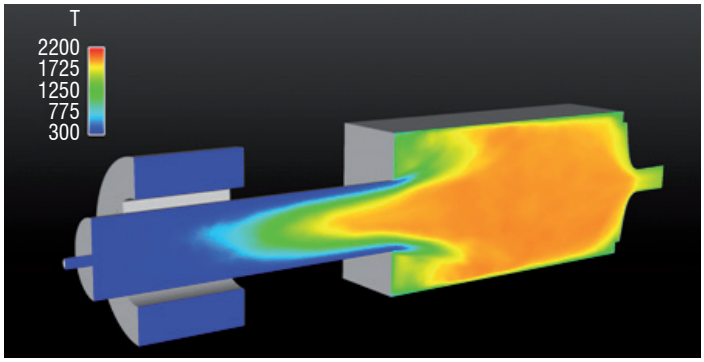

c)

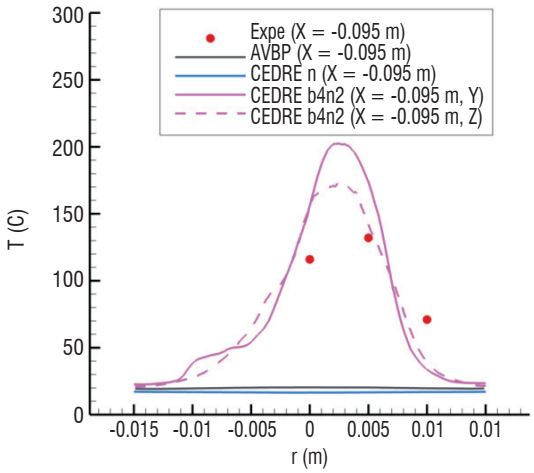

d)

Figure 8 - Mean temperature fields (K). From left to right and top to bottom, a) AVBP computation, b) CEDRE "-n" computation, c) CEDRE "-b4n2" computation, and d) comparison to measurements inside the plenum (x=-0.095 m)

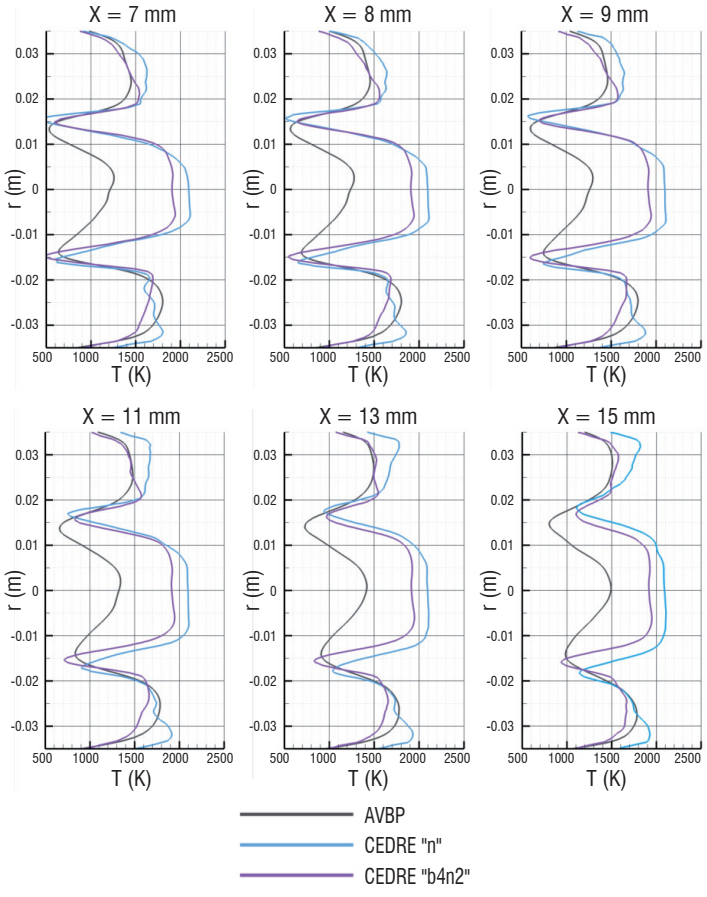

Figure 9 - Mean temperature profiles at the dump plane

Despite no other experimental mean temperature data being available, it is interesting to look at the computed mean temperature profiles in the combustion chamber. In the dump plane region (Figure 9), it appears that the AVBP computation shows a slower flame development, with a narrower angle, compared to both CEDRE computations. At the chamber exit (Figure 10), all computations recover, as expected, very similar levels of mean temperature approaching the equilibrium temperature (Teq = 2131.7 K). Please note that, since the grid used does not resolve the boundary layers, the mean temperature gradients that are visible in Figure 10 are not representative of the wall thermal boundary conditions, but rather of the complex flow structure that develops in the combustion chamber. Nevertheless, all of the computations were performed with suitable thermal boundary conditions reproducing the experimental heat losses at the various walls, which were water cooled except for the window wall, which was treated as an adiabatic wall. No marked influence of the wall thermal conditions on the unsteady flow was observed in the various computational results obtained during the RECORD project.

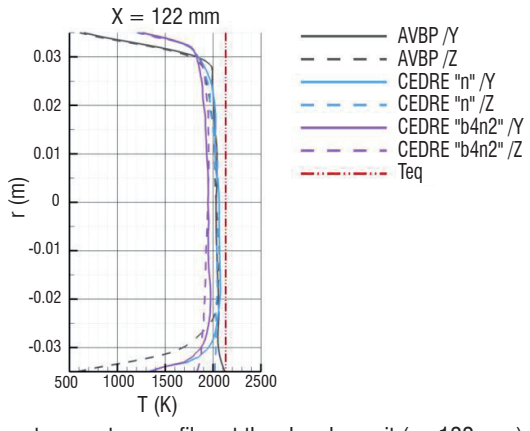

Figure 10 - Mean temperature profiles at the chamber exit (x=122 mm)

Figure 11 offers global comparisons of the mean and rms velocity fields between the "-b4n2" computation and the available PIV measurements performed on the test-bench, but these are not further presented here. This figure shows that an overall good comparison of the flow feature is recovered. However, it must be noted that the axial oscillations at the dump plane (rms plot) are stronger in the LES "-b4n2" computation than in the measurements.

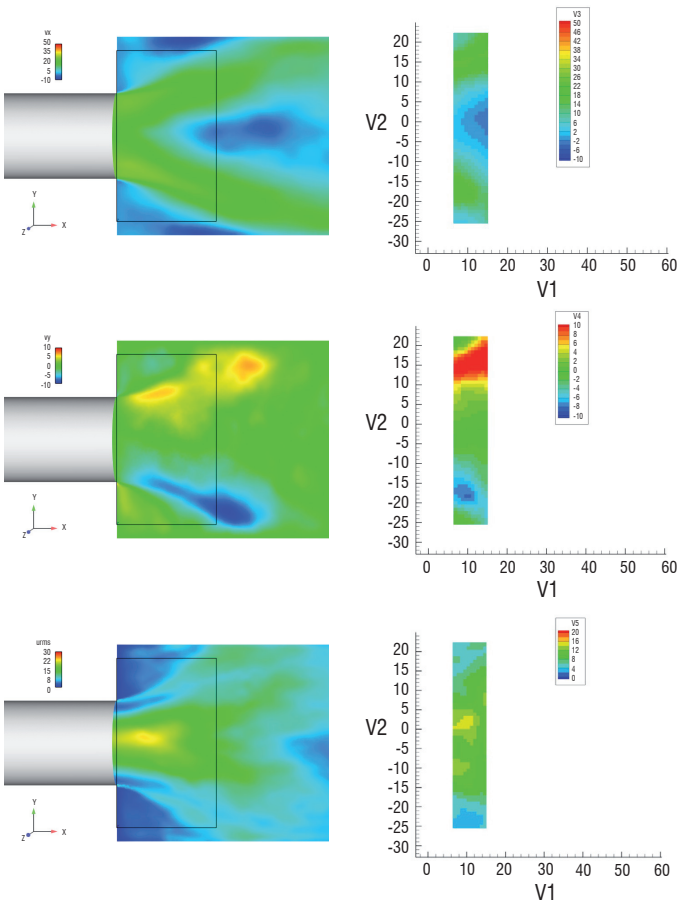

Figure 11 - Comparison of the mean and rms velocity fields. Computation "-b4n2" (left), experimental PIV (right). From top to bottom: Vx, Vy, Urms. The same color scale is used, except for the rms plot.

Detailed comparisons

Concerning cross calculations, a detailed comparison was performed using the profiles defined in Figure 12.

This section offers some comparisons of the LES computations to the available measurements for OP13-5-0-85. Figure 3 illustrates the experimental set-up and probe locations. Figure 12 illustrates the axial locations of the transverse profiles.

First, the time signal and its PSD at experimental Pressure Transducer 2 (see Figure 3) are presented in Figure 13. In this figure, the difference of the mean pressure level between computations and experiment is visible. This difference is due to nozzle erosion in the experimental set-up. Further, the absence of strong low frequency oscillations in the ONERA "-n" computation is also visible. Concerning the CERFACS/EM2C and the ONERA "-b4n2" computations, it is noted that both computations recover the low frequency oscillations, in good agreement with the experimental results. The PSD plot confirms this good agreement. It must be noted that the ONERA "-b4n2" computation slightly over-estimates this oscillation.

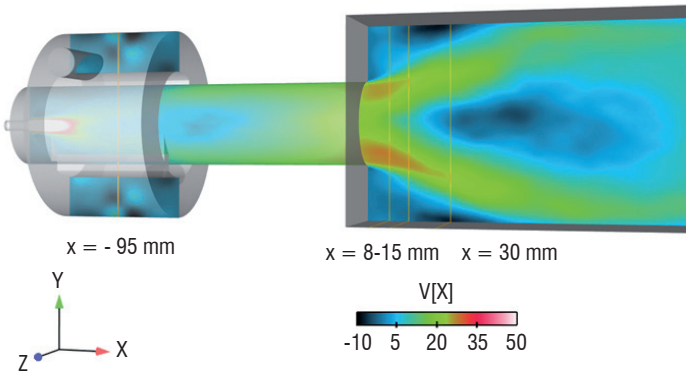

Figure 12 - Extraction planes for profile comparisons

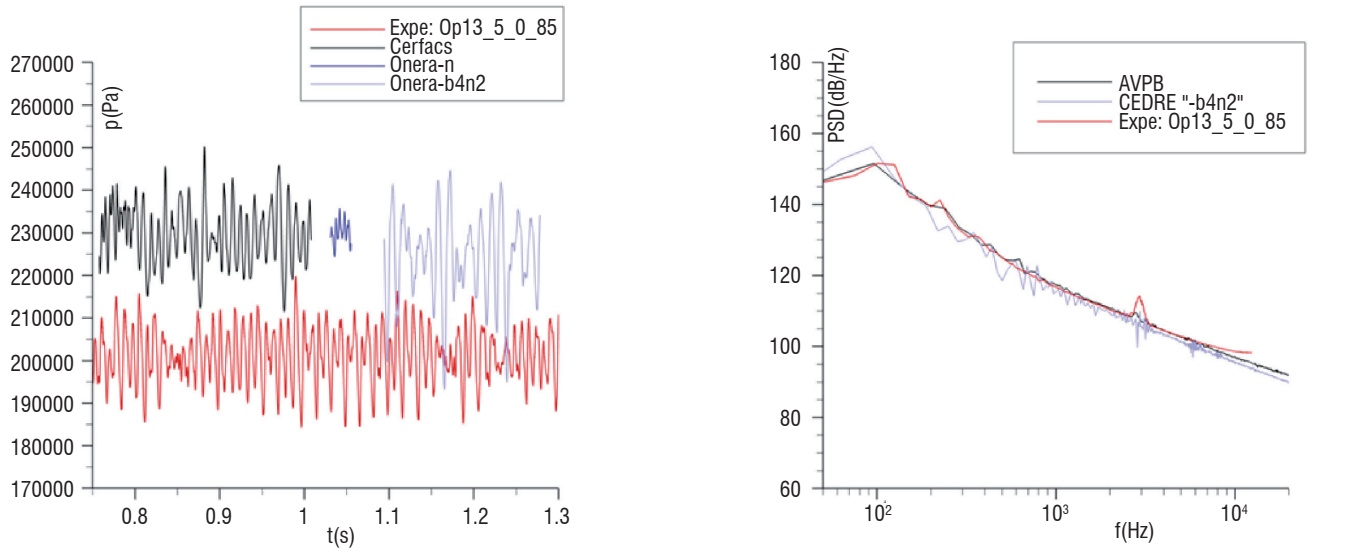

Figure 13 - Time signal (left, arbitrary time origin) and PSD (right) at Transducer 2

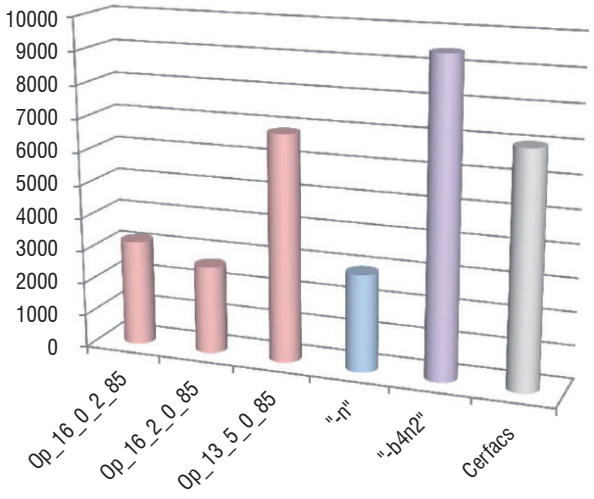

Figure 14 - RMS pressure at Transducer No. 2 (Pa)

The computed rms pressure at Transducer 2 is compared to available experimental data in Figure 14. This figure confirms the fact that the low-frequency high-amplitude oscillation is present in the Op_13_5_0_85 experiment and is recovered by the AVBP and CEDRE "-b4n2" computations, while the CEDRE "-n" computation produces much reduced levels comparable to the other experimental point. This enables the low-frequency oscillation to be linked to the flame motion across the dump plane, which implies burning inside the Plenum/injection domain.

Figure 15 (next page) presents the comparison of the computational results with available 2D PIV measurements at the dump plane region.

From Figure 15 it appears that the experimental profiles at the dump plane are difficult to perfectly recover from the computations. However, it can be noted that the ONERA "-n" computation shows very good mean velocity profile comparisons, while underestimating the rms levels. On the contrary, the "-b4n2" computation overestimates the rms levels and the mean profiles are not fully recovered. The CERFACS/EM2C computation, while achieving good agreement on the rms plots, shows marked discrepancies with the mean profiles, with a different flow cone angle. These results illustrate the difficulty in fully recovering the experiment in one computation, while overall agreement is deemed to be quite satisfactory from the pressure signals and frequency content.

Intermediate conclusion on HFLES results

The results show very favorable comparisons with experimental data. One noted difficulty was observed in the mean velocity profiles, just downstream from the dump plane (the first 15 mm), where the PIV measurements were available. In this limited region, the comparison work exhibited different results from the three analyzed computations, with difficulties in exactly recovering at the same time both the mean and rms profiles in one computation. However, the set of the three available computations well bracketed the measurements. Nevertheless the more global comparisons show that the computations correctly recovered the main flow features. Obviously, the difficulty lays in properly capturing the large-amplitude, low-frequency flame motion across the dump plane, moving in and out of the plenum domain. Under such conditions, the flashback phenomenon had to be controlled in the computations and the role of the ICS impedance turned out to be a key element in this process. Both codes could attain this result with different approaches. In such a complex situation, it is remarkable that both codes produced results in close agreement with the measurements, as illustrated by the time signal and PSD computed at Pressure Sensor 2 and by the temperature data in the plenum domain. This gives good confidence in the ability of the HFLES approach to describe complex combustion chamber phenomena.

Acoustic post-processing

Experiments or unsteady reactive numerical simulations provide the pressure and temperature fluctuations generated by the flame inside the combustion chamber. In the present case, the objective of the post-processing is, as a first step, to separate the waves (acoustic and entropy) present inside the chamber and, as a second step, to evaluate their relative contribution to the noise emitted by the nozzle and that goes back inside the chamber or enters the turbine stages that would be present in a real engine. A similar post-processing, with the propagation of noise and entropy waves through fixed and rotating blades of a compact turbine (low frequency limit) in order to compute the combustion noise generated at the outlet, has been performed by Duran *et al* [70]. In the following, an illustration of the post-processing is given using the CFD data presented in the previous section. With the current tools, it is assumed that the acoustic and entropy fluctuations, as well as the mean flow through the nozzle, are one-dimensional.

Wave extraction from CFD

The first step of the acoustic post-processing is the evaluation of the acoustic and entropy perturbations computed inside the combustion chamber. The determination of these waves is performed through a characteristic filtering [71], the principle of which is to separate the waves using their different propagation velocities. Instantaneous pressure, velocity and temperature fluctuations are stored on several planes downstream from the flame location, where the waves are supposed to propagate without source or damping terms, see Figure 16.

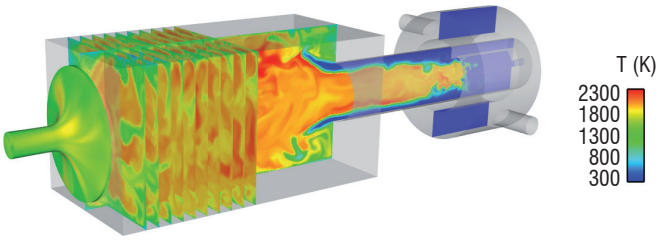

Figure 16 - Illustration of the storage planes used for the wave separation (the actual storage is performed on 20 planes)

Due to the three-dimensional, turbulent nature of the flow in the region downstream from the flame, the wave separation is achieved in three steps. First, a spatial averaging (area averaging) of the fluctuations is performed for each plane and at each time step, in order to construct 1D perturbations. By doing so, only the fluctuations corresponding to the planar waves are conserved, while the contributions of the higher

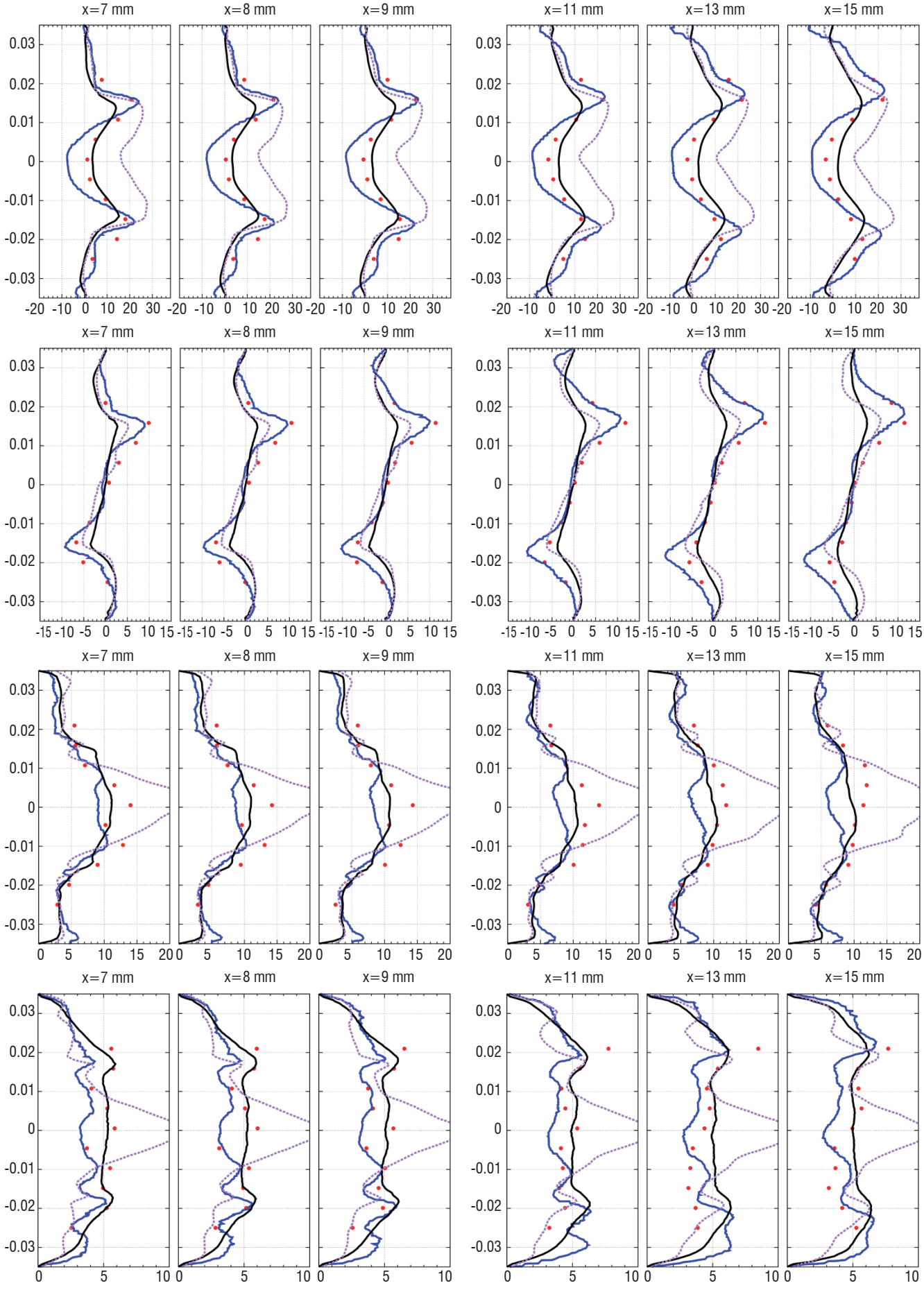

Figure 15 - Comparison of mean profiles. From top to bottom, axial, transverse mean velocities and axial, transverse rms velocities

— : AVBP, — : CEDRE "-n", ···: CEDRE "-b4n2", ●: experiment

modes are filtered. The linear acoustic (Riemann) and entropy invariants are constructed in a second step, using Eqs. (1)-(3):

$$P^{+} = \frac{1}{2}\left(\frac{p'}{\overline{\gamma p}} + \frac{u'}{\overline{c}}\right)$$

downstream propagating acoustic wave (velocity $\overline{u} + \overline{c}$) (1)

$$P^{-} = \frac{1}{2}\left(\frac{p'}{\overline{\gamma p}} - \frac{u'}{\overline{c}}\right)$$

upstream propagating acoustic wave (velocity $\overline{u} - \overline{c}$) (2)

$$\sigma = \frac{s'}{c_p}$$ entropy wave (velocity $\overline{u}$) (3)

These invariants still contain spurious contributions that come from the turbulence of the flow. In order to get rid of this turbulent contamination, a phase averaging of each invariant is finally performed by taking into account the different propagation velocities of the waves between the planes.

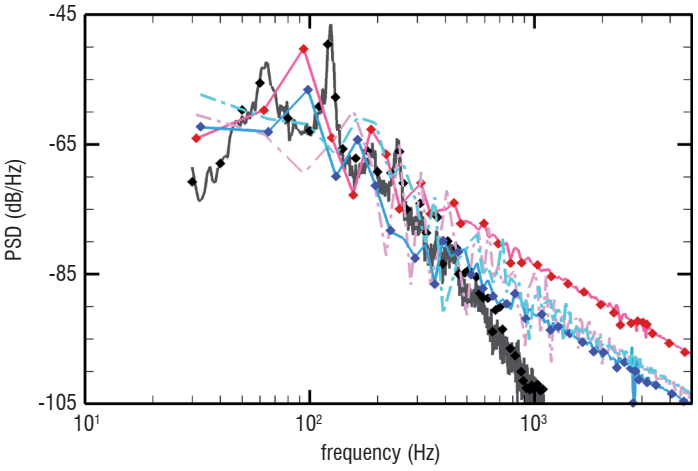

Figure 17 - Power spectral densities of the simulated invariants inside the combustion chamber (the reference amplitude is set to 1 for all invariants)

CEDRE: P_1^+ ; P_1^- ; σ_1

AVBP: P_1^+ ; P_1^- ; σ_1

Experiments: P_1^+ ; P_1^-

The wave extraction procedure is applied to the unsteady fields computed by CEDRE and AVBP. It must be mentioned here that P_1^+ corresponds to the wave propagating toward the nozzle and does not identify with the direct combustion noise generated by the flame, since it also includes reflections of P_1^- on the flame and on the combustor upstream boundary. The power spectral densities of the three invariants extracted from both simulations are reproduced in Figure 17, where the experimental acoustic invariants are also reproduced. The two computations exhibit a similar spectral content for the acoustic waves, with the most energetic fluctuations located in the low-frequency region. In particular, the levels of the two waves are identical, which indicates that the nozzle fully reflects the acoustic perturbations. In the experiments, the faster decrease of the levels above 300 Hz may arise from a limitation of the wave separation method due to the limited spatial resolution of the measurements.

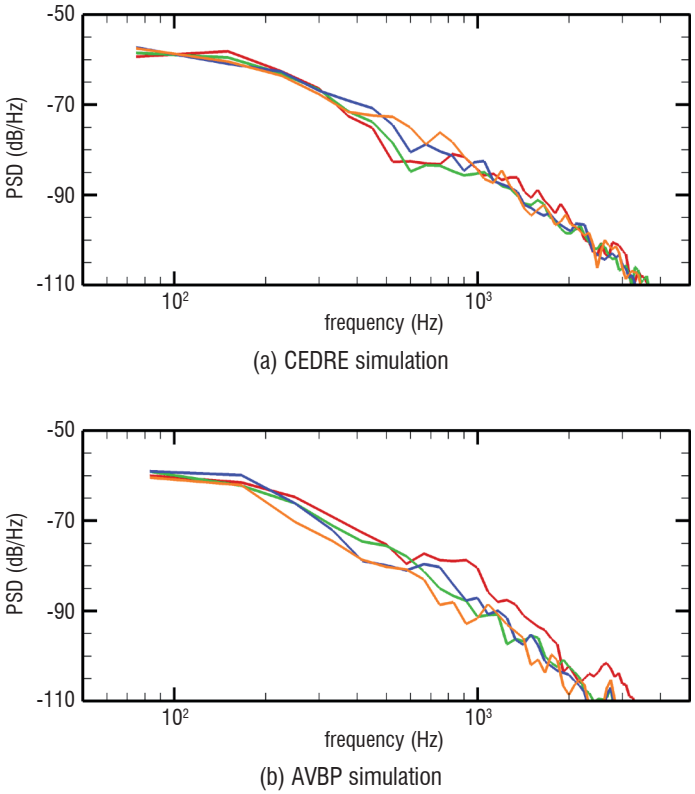

Figure 18 - Power spectral densities of the entropy invariant at various locations in the combustion chamber
x = 0.0875 m; x = 0.1015 m; x = 0.1155 m; x = 0.1295 m

Finally, the nondimensionalized entropy fluctuations generated by the flame are very similar to the acoustic ones, with the amplitude of the fluctuations decreasing with the increasing frequency.

The phase averaging performed to get rid of the turbulent contamination of the signals considers that the waves propagate without dissipation or diffusion. This hypothesis is well verified for the acoustic waves, however distortions may occur for the entropy waves, due for instance to the turbulent mixing. The power spectral densities of the entropy fluctuation on different storage planes, before the phase averaging, are illustrated in Figure 18. The energetic frequencies correspond to the large length scales ($\lambda \sim 10$ cm at 100 Hz), a length similar to that of the combustion chamber. Mixing and diffusion are therefore negligible at these low frequencies, as can be seen in the figure. The attenuation of the entropy fluctuations remains limited for all of the frequencies of interest, in particular for the CEDRE simulation. A slightly more important attenuation can be seen for AVBP, but still remains low. This figure also proves that the grids are sufficiently dense to convect the entropy wave without noticeable numerical dissipation.

Noise generation through the nozzle

At the end of the combustion chamber, the downstream acoustic wave and the entropy wave are accelerated through the nozzle. For the acoustic wave, this causes sound scattering with an attenuation of the acoustics transmitted through the nozzle, while some noise is reflected to the chamber; for the entropy wave, the flow acceleration generates indirect noise, both upstream and downstream from the nozzle. Marble & Candel were the first to provide an analytical model to account for both phenomena [17], by writing conservation

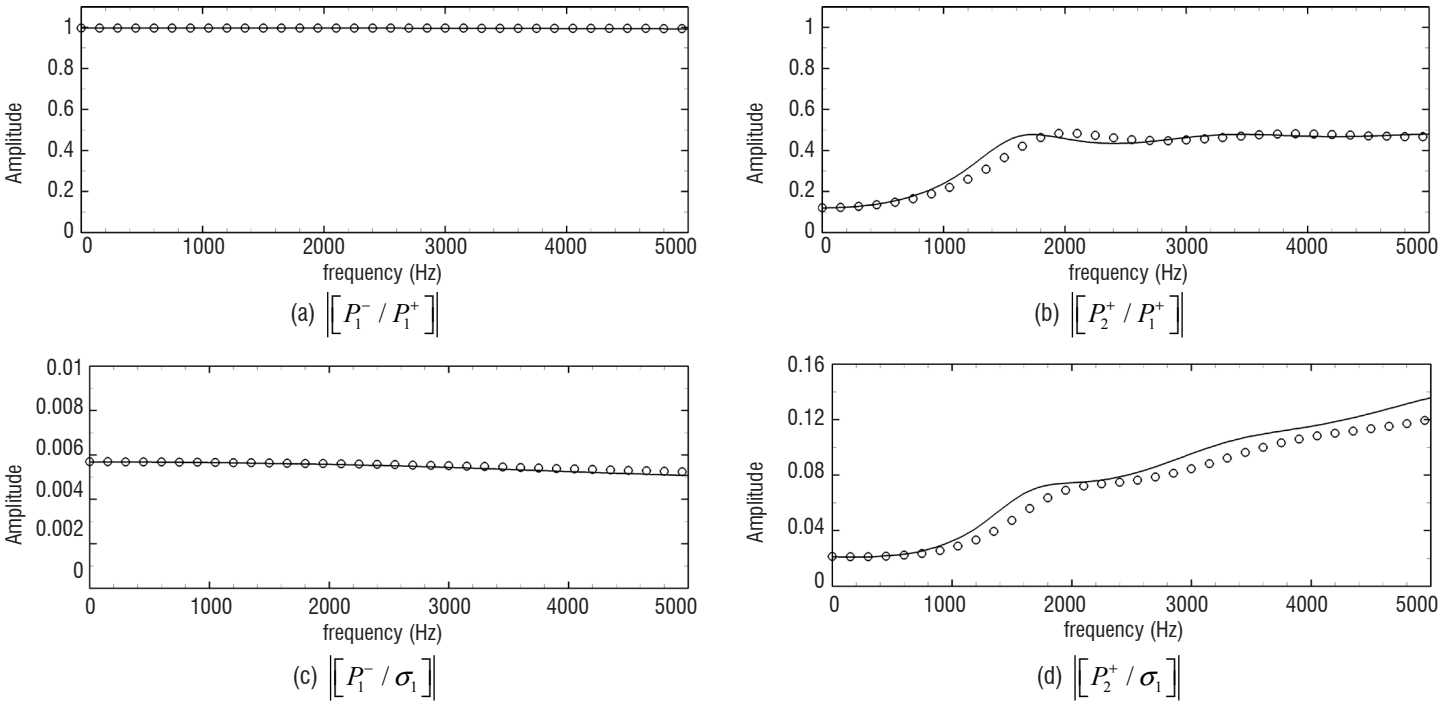

Figure 19 - Amplitude of the (a), (b) acoustic and (c), (d) thermoacoustic transfer functions of the nozzle – MarCan; ○ Anozzle

relations for the fluctuations of mass, stagnation temperature and entropy through the nozzle. This approach assumes that the nozzle is compact with respect to the considered harmonic perturbations, which limits its validity to low frequencies only. Even if combustion noise is assumed to lay in a rather low frequency range, the compact hypothesis seems too restrictive for real engines, and non-compact models are required for a correct estimation of the generated noise. A first linear model was proposed by Marble & Candel [17] for a supercritical nozzle with a linear velocity profile. They reduced the linearized Euler equations to a simple hypergeometric differential equation over the pressure, using a nondimensionalization based on the constant velocity gradient. Their approach was recently extended to piecewise-linear velocity profiles by Giauque *et al* [72] and to shocked nozzles by Moase *et al* [73], so that any nozzle geometry and flow condition can be modeled. This generalization relies on the resolution of a matrix system using the analytical expressions for the pressure, velocity and entropy perturbations in each element (as solutions of the hypergeometric differential equation) and continuity relations between two elements or through the shock. Following a different approach, Duran & Moreau [74] recast the linearized Euler Equations to write a differential system over the fluctuations of mass flow rate, stagnation temperature and entropy, which is solved using the Magnus expansion. Here again, the presence of a shock wave is addressed by using jump relations derived from Rankine and Hugoniot.

All of the above-mentioned models deal with a 1D mean flow and perturbations. However, as pointed out by Zheng *et al* [75], those models fail to reproduce the experimental results of Bake *et al* [32] for a subcritical nozzle, and a possible reason for their failure seems to be the experimental distortion of the entropy wave, which is not taken into account by the 1D models. Indeed, in practical cases, the velocity profile is not uniform over a section and the radial gradient of the axial velocity deforms the initially planar entropy front while being convected through the nozzle, thus modifying the indirect noise generation process. Zheng *et al* [75] extended the 1D models to 2 dimensional flows, in order to take into account this heterogeneous radial velocity profile, while Ullrich & Sattelmayer [76], [77] used linearized Navier-Stokes equations to evaluate the nozzle transfer functions numerically.

As an illustration, the analytical evaluation of the nozzle transfer functions obtained with the 1D models of ONERA (piecewise-linear velocity profile, MarCan code) and CERFACS (Magnus expansion, ANozzle code) are reproduced in Figure 19 for the nozzle located at the downstream end of the CESAM-HP combustion chamber (Subscripts 1 and 2 refer to values at the nozzle inlet and outlet). The nozzle is supercritical and a normal shock is located in the diffuser. The Mach numbers at the nozzle inlet and nozzle outlet are $\overline{M}_1 = 0.011$ and $\overline{M}_2 = 0.046$, respectively. The nozzle geometry and mean Mach number profile are reproduced in Figure 20. It has been verified with RANS and LES simulations, not presented here, that the flow remains attached in the diffuser, so the predictions of the 1D isentropic models are valid.

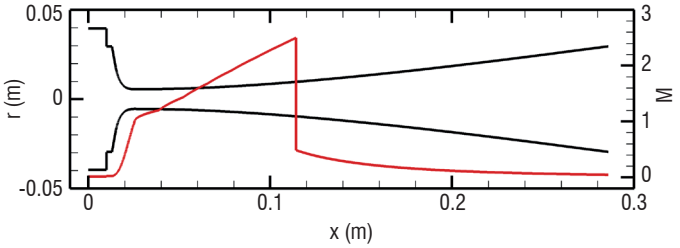

Figure 20 - Nozzle geometry and mean Mach number profile
nozzle walls (left axis); Mach profile (right axis)

Let us first discuss the noise reflections through the nozzle (waves P_1^- generated by acoustic and entropy forcings). Due to the choked nozzle configuration, only the converging part of the nozzle contributes to this noise. The converging nozzle being of small size, its response is essentially compact and does not vary for the considered frequencies. The converging nozzle is fully reflective for inlet acoustic disturbances, whereas the upstream-propagating noise generated by entropy perturbations is very low. The amplitude ratio of the transfer functions between the acoustic-generated and entropy-generated noise is over 150. Note that this ratio does not strictly correspond to the ratio between the scattered direct combustion noise and the entropy-generated noise (indirect combustion noise), since P_1^+ already includes entropy-generated noise through the reflection of P_1^- on the upstream boundary of the combustor.

Considering now the noise transmission through the nozzle (waves P_2^+), the length of the diverging part being largely higher than that of the converging one, the non-compactness of the nozzle on the generated noise is more visible for the downstream wave. For frequencies above 600 Hz, the nozzle is no longer compact and the amplitude of the nozzle response to the acoustic and entropy forcings increases. Once again, the amplitude of the acoustic-generated noise transfer function is larger than that of the entropy, but the ratio is limited to 5, a value much lower than for the upstream wave. The presence of a transmitted acoustic wave may seem unphysical at first sight, given that the nozzle is fully reflective for inlet acoustic disturbances. This paradox is solved by considering the energy of the waves. Indeed, the transfer functions deal with pressure fluctuations non-dimensionalised by the mean pressure, a quantity that is not conserved by the flow. In the present case, full reflection of the incident pressure fluctuations corresponds to a reflected acoustic energy below 1, because of the presence of the mean flow (see for instance [78]), leading to the transmission of some part of the acoustic energy.

Application to the combustion chamber

Once the characteristic waves inside the combustion chamber and the nozzle transfer functions are known, it is straightforward to analytically evaluate the noise scattered by (direct contribution) and produced inside (indirect contribution) the nozzle, and that returning inside the chamber or entering the turbine stages. This evaluation is performed in the spectral domain using Eqs. (4)-(5)

$$P_1^- = \left[\frac{P_1^-}{P_1^+}\right] P_1^+ + \left[\frac{P_1^-}{\sigma_1}\right] \sigma_1 \qquad (4)$$

$$P_2^+ = \left[\frac{P_2^+}{P_1^+}\right] P_1^+ + \left[\frac{P_2^+}{\sigma_1}\right] \sigma_1 \qquad (5)$$

where the terms in brackets correspond to the nozzle transfer functions and the perturbations incoming from the downstream part of the nozzle are assumed to be nil ($P_2^- = 0$).

The spectra of the waves P_1^- and P_2^+ evaluated numerically and analytically are reproduced in Figure 21. The results are very similar for the 2 simulations. The analytical spectrum of P_1^- collapses perfectly with the simulated one, which is a first validation of the approach applied here for the analytical reconstruction of the noise emitted by the nozzle. Given that the incoming acoustic and entropy fluctuations are of the same order and that the amplitude of the acoustic transfer function is 150 times larger than the thermo-acoustic one, the wave P_1^- comes exclusively from the scattering of P_1^+ through the nozzle. However, this result does not strictly demonstrate that direct noise dominates indirect noise, since P_1^+ does not identify with direct combustion noise because it includes reflections of P_1^- on the upstream boundary of the combustor.

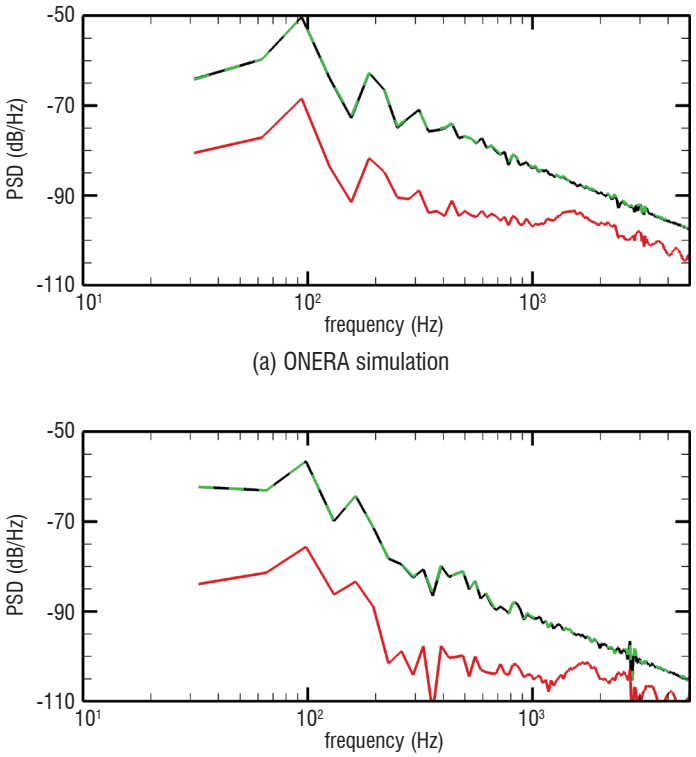

Figure 21 - Spectra of the acoustic invariants leaving the nozzle
— P_1^- from CFD; ··· P_1^- from analytical methods; — P_2^+ from analytical methods

In the present CFD simulations, the nozzle is choked and the region downstream from the throat is not represented in the numerical domain, which focuses on the flow inside the combustion chamber. It is therefore not possible to determine the amplitude of the downstream acoustic wave from the CFD, but this wave can be reconstructed using the analytical model. From the levels of the invariants inside the chamber and the amplitudes of the transfer functions, it is obvious that the downstream noise comes essentially from the transmission of the wave P_1^+ through the nozzle, with a very limited contribution of the entropy source. Given that the levels of the acoustic transfer function $\left[P_2^+ / P_1^+\right]$ are lower than that of $\left[P_1^- / P_1^+\right]$, the downstream acoustic wave exhibits levels below those of the upstream wave, from -18 dB in the low frequencies to -7 dB above 2 kHz. It may appear surprising that entropy-generated noise remains negligible compared to transmitted acoustics downstream from the nozzle, since incident acoustic and entropy waves exhibit similar levels and most of the incident acoustic energy is reflected to the combustion chamber. The thermo-acoustic transfer functions in Figure 19, however, indicate that energy conversion from entropy to acoustics is very limited in the present case. A detailed look at the compact response

(low-frequency limit) of nozzles to entropy forcing (see [73], [79]) indicates that this behavior is observed for almost all shocked nozzle regimes.

Conclusions and perspectives

With the important reduction of jet and fan noise achieved for recent turbojet engines, combustion noise now starts to emerge and attention must be focused on its understanding and reduction. The objective of the European project RECORD, run between 2013 and 2015, was to improve the global knowledge of the fundamental mechanisms of core noise generation, in order to provide tools for its evaluation and to propose ways for its reduction. To this end, the high-pressure combustor CESAM-HP has been built at EM2C laboratory, in order to experimentally investigate combustion noise and its contributors – direct (acoustic) and indirect (entropy) combustion noises. The facility features a one-staged swirl injector, a combustion chamber and an exhaust nozzle used to pressurize the combustion chamber and generate indirect noise. Special care has been taken to allow various diagnostic techniques to quantify the flow properties and acoustics, such as temperature and pressure measurements or large optical accesses inside the chamber. Numerical simulations of the reactive experiment have been conducted at ONERA and at CERFACS with different solvers. They have been shown to reproduce the experimental characteristics of the flame and the associated pressure fluctuations inside the chamber with a very good accuracy. In particular, it is remarkable that both codes produced results in close agreement with the measurements, as illustrated by the pressure time signal and PSD in the chamber and by the temperature data in the plenum domain. This gives good confidence in the ability of the HFLES approach to describe complex combustion chamber phenomena. Finally, an acoustic post-processing of the simulations has been performed to extract the waves present inside the combustion chamber (acoustic, entropy) and to propagate them through the nozzle, in order to model the direct and indirect contributions. The numerical method predicts the predominance of the direct contribution for the noise reflected by the nozzle, with the nozzle being fully reflective to the acoustic forcing. This behavior is confirmed by the comparison with the experiments. The numerical method also provides the noise transmitted by the nozzle and that is not measured experimentally. This information is of crucial importance for the modeling of a complete engine, where the fluctuations create additional noise when they are accelerated through the turbine stages.

Despite the differences with a real gas turbine combustor, the facility investigated in this paper exhibits some of its main characteristics and the demonstration that the numerical codes are able to capture combustion noise is an important step. Follow-up activities will require, for instance, liquid jet fuels and realistic combustion chambers to be considered. Noise modeling through a turbine is also a key issue for the correct prediction of combustion noise. In addition to the combustor test case, a full stator-rotor stage has been instrumented at the university *Politecnico di Milano* within the framework of RECORD, with various types of acoustic, entropic or vortical excitations. This facility is of prime interest for the experimental validation of turbine models. The coupling of the analytical models representing the various engine elements with the numerical simulation of the combustor will provide, in the end, the combustion noise radiated to the ground and will help to understand the relative contributions of the contributors, in order to finally design quieter aircraft ■

Acknowledgements

The numerical results were obtained during the RECORD project (Research on Core Noise Reduction). RECORD is a project funded by the European Union within the framework of the Seventh Framework Program (FP7/2007- 2013), under Grant Agreement No. 312444.

References

[1] A. P. DOWLING, Y. MAHMOUDI - *Combustion Noise*. Proceedings of the Combustion Institute, 35:65-100 (2015).

[2] W. C. STRAHLE - *A Review of Combustion Generated Noise*. 1st AIAA Aeroacoustics Conference, Paper AIAA 73-1023 (1973).

[3] D. G. CRIGHTON - *The Excess Noise Field of Subsonic Jets*. Journal of Fluid Mechanics, 56:683-694 (1972).

[4] N. A. CUMPSTY, F. E. MARBLE - *Core Noise from Gas Turbine Exhausts*. Journal of Sound and Vibration, 54:297–309 (1977).

[5] W. C. STRAHLE - *Combustion Noise*. Progress in Energy and Combustion Science, 4:157–176 (1978).

[6] S. BRAGG - *Combustion Noise*. Journal of the Institute of Fuel, 36:12–16 (1963).

[7] W. STRAHLE - *On Combustion Generated Noise*. Journal of Fluid Mechanics, 49:399–414 (1971).

[8] T. SMITH, J., KILHAM - *Noise Generated by Open Turbulent Flame*. Journal of the Acoustical Society of America, 35:715–724 (1963).

[9] A. THOMAS, G. WILLIAMS - *Flame Noise: Sound Emission From Spark-ignited Bubbles of Combustible Gas.* Proceedings of the Royal Society London A, 294:449–466 (1966).

[10] I. HURLE, R. PRICE, T. SUDGEN, A. THOMAS - *Sound Emission From Open Turbulent Flames*. Proceedings of the Royal Society London A, 303:409–427 (1968).

[11] W. STRAHLE - *Some Results in Combustion Generated Noise*. Journal of Sound and Vibration, 23:113–125 (1972).

[12] W. STRAHLE - *Refraction, Convection, and Diffusion Flame Effects in Combustion-Generated Noise*. Proceedings of the Combustion Institute, Pittsburgh, pp. 527–535 (1973).

[13] A. DOWLING, J. E. FFWOCS WILLIAMS - *Sound and Sources of Sound*. Ellis Horwood, Chichester, UK (1983).

[14] S. M. CANDEL - *Analytical Studies of Some Acoustic Problems of Jet Engines*. PhD thesis, California Institute of Technology, Pasadena (1972).

[15] F. E. MARBLE - *Acoustic Disturbance From Gas Non-Uniformities Convecting Through a Nozzle*. In Interagency Symposium on University Research in Transportation Noise, Stanford University, Stanford, CA, pp. 547–561 (1973).

[16] C. L. MORFEY - *Amplification of Aerodynamic Noise by Convected Flow Inhomogeneities*. Journal of Sound and Vibration, 31:391–397 (1973).

[17] F. E. MARBLE, S. M. CANDEL - *Acoustic Disturbance From Gas Non-Uniformities Convected Through a Nozzle*. Journal of Sound and Vibration 55:225-243 (1977).

[18] N. A. CUMPSTY, F. E. MARBLE - *The Interaction of Entropy Fluctuations With Turbine Blade Rows: a Mechanism of Turbojet Engine Noise*. Proceedings of the Royal Society of London A, 357:323–344 (1977).

[19] S. CANDEL - *Combustion Instabilities Coupled by Pressure Waves and Their Active Control*. Proceedings of the Combustion Institute, 24:1277–1296 (1992).

[20] F. CULICK, V. YANG - *Progress in Astronautics and Aeronautics: Liquid Rocket Engine Combustion Instability*. Vol. 169. AIAA, Ch. 1: Overview of combustion instabilities in liquid-propellant rocket engines, pp. 3–37 (1995).

[21] S. CANDEL - *Combustion Dynamics and Control: Progress and Challenges*. Proceedings of the Combustion Institute, 29:1–28 (2002).

[22] T. LIEUWEN, V. YANG (Eds.) - *Combustion Instabilities in Gas Turbine Engines: Operational Experience*. Fundamental Mechanisms, and Modeling, Progress in Astronautics and Aeronautics, Volume 210, AIAA, Washington (2005).

[23] A. GIAUQUE - *Fonctions de transfert de flamme et énergies de perturbation dans les écoulements réactifs*. PhD Thesis, *Institut National Polytechnique de Toulouse*, Toulouse, France (2007).

[24] M. J. BREAR, F. NICOUD, M. TALEI, A. GIAUQUE, E. R. HAWKES - *Disturbance Energy Transport and Sound Production in Gaseous Combustion*. Journal of Fluid Mechanics, 707:53-73 (2012).

[25] C. S. GOH, A. S. MORGANS - *The Influence of Entropy Waves on the Thermoacoustic Stability of a Model Combustor*. Combustion Science and Technology, 185:249-268 (2013).

[26] S. HOCHGREB, D. DENNIS, I. AYRANCI, W. BAINBRIDGE, S. CANT - *Forced and Self-excited Instabilities from Lean Premixed, Liquid-Fuelled Aeroengine Injectors at High Pressures and Temperatures*. In Proceedings of ASME Turbo Expo, Paper GT2013-95311 (2013).

[27] E. MOTHEAU, Y. MERY, F. NICOUD, T. POINSOT - *Analysis and Modeling of Entropy Modes in a Realistic Aeronautical Gas Turbine*. Journal of Engineering for Gas Turbines and Power, 135:092602 (2013).

[28] E. MOTHEAU, F. NICOUD, T. POINSOT - *Mixed Acoustic-Entropy Combustion Instabilities in Gas Turbines*. Journal of Fluid Mechanics 749:542-576 (2014).

[29] S. CANDEL, D. DUROX, S. DUCRUIX, A.-L. BIRBAUD, N. NOIRAY, T. SCHULLER - *Flame Dynamics and Combustion Noise: Progress and Challenges*. International Journal of Aeroacoustics, 8:1-56 (2009).

[30] K. R. MCMANUS, T. POINSOT, S. M. CANDEL - *A Review of Active Control of Combustion Instabilities*. Progress in Energy and Combustion Science, 19:1-29 (1993).

[31] I. DURAN, S. MOREAU, F. NICOUD, T. LIVEBARDON, E. BOUTY, T. POINSOT - *Combustion Noise in Modern Aero-Engines*. Aerospace Lab, 7 (2014).

[32] F. BAKE, C. RICHTER, B. MÜLHBAUER, N. KINGS, I. RÖHLE, F. THIELE, B. NOLL - *The Entropy Wave Generator (EWG): a Reference Case on Entropy Noise*. Journal of Sound and Vibration, 326:574-598 (2009).

[33] B. PARDOWITZ, U. TAPKEN, K. KNOBLOCH, F. BAKE, E. BOUTY, I. DAVIS, G. BENNETT - *Core Noise – Identification of Broadband Noise Sources of a Turbo-Shaft Engine*. 20th AIAA/CEAS Aeroacoustics Conference, Paper AIAA 2014-3321 (2014).

[34] D. BLACODON, S. LEWY - *Source Localization of Turboshaft Engine Broadband Noise Using a Three-Sensor Coherence Method*. Journal of Sound and Vibration, 338:250-262 (2015).

[35] F. BAKE, K. KNOBLOCH - *Research on Core Noise Reduction*. AeroDays 2015, London (2015)

[36] K. KNOBLOCH, T. WERNER, F. BAKE - *Noise Generation in hot Nozzle Flow*. Proceedings of ASME Turbo Expo, Paper GT2015-43702 (2015).

[37] K. KNOBLOCH, T. WERNER, F. BAKE - *Entropy Noise Generation and Reduction in a Heated Nozzle Flow*. 21st AIAA/CEAS Aeroacoustics Conference, Paper AIAA 2015-2818 (2015).

[38] M. MAZUR, W. TAO, P. SCOUFLAIRE, F. RICHECOEUR, S. DUCRUIX - *Experimental and Analytical Study of the Acoustic Properties of a Gas Turbine Model Combustor with a Choked Nozzle*. Proceedings of ASME Turbo Expo, Paper GT2015-43013 (2015).

[39] L. PINELLI, F. POLI, A. ARNONE, S. GUÉRIN, A. HOLEWA, J. R. F. APARICIO, R. PUENTE, D. TORZO, C. FAVRE, P. GAETANI, G. PERSICO - *On the Numerical Evaluation of Tone Noise Emissions Generated by a Turbine Stage: an In-Depth Comparison Among Different Computational Methods*. Proceedings of ASME Turbo Expo, Paper GT2015-42376 (2015).

[40] N. TRAN, S. DUCRUIX, T. SCHULLER - *Damping Combustion Instabilities with Perforates at the Premixer Inlet of a Swirled Burner*. Proceedings of the Combustion Institute 32:2917–2924 (2009).

[41] A. SCARPATO - *Linear and Nonlinear Analysis of the Acoustic Response of Perforated Plates Traversed by a Bias Flow*. PhD Thesis, *Ecole Centrale Paris* (2014).

[42] A. GIAUQUE, M. HUET, F. CLERO, S. DUCRUIX, F. RICHECOEUR - *Thermoacoustic Shape Optimisation of a Subsonic Nozzle*. Journal of Engineering for Gas Turbines and Power, 135:102601 (2013).

[43] J.-F. BROUCKAERT, M. MERSINLIGIL, M. PAU - *A Conceptual Design Study for a New High Temperature Fast Response Cooled Total Pressure Probe*. Proceedings of the ASME Turbo Expo 2008 Power for Land, Sea and Air, June 9-13, 2008, Berlin, Germany (2008).

[44] M. MERSINLIGIL, J.-F. BROUCKAERT, J. DESSET - *First Unsteady Pressure Measurements with a Fast Response Cooled Total Pressure Probe in High Temperature Gas Turbine Environments*. Proceedings of the ASME Turbo Expo 2010 Power for Land, Sea and Air, June 14-18, 2010, Glasgow, UK (2010).

[45] M. MERSINLIGIL, J. DESSET, J.-F. BROUCKAERT - *High Temperature High Frequency Turbine Exit Flow Field Measurements in a Military Engine with a Cooled Unsteady Total Pressure Probe*. Proceedings of the Institution of Mechanical Engineers, Part A: Journal of Power and Energy (2011).

[46] M. MAZUR, N. KINGS, P. SCOUFLAIRE, F. RICHECOEUR, S. DUCRUIX - *Combustion Noise Studies of a Swirled Combustion Chamber with a Choked Nozzle Using High-Speed Diagnostics*. X-NOISE Workshop 2015, La Rochelle, France (2015).

[47] N. KINGS, W. TAO, P. SCOUFLAIRE, F. RICHECOEUR, S. DUCRUIX - *Experimental and Numerical Investigation of direct and Indirect Combustion Noise Contributions in a Lean Premixed Laboratory Swirled Combustor*. Proceedings of ASME Turbo Expo, Paper GT2016-57848 (2016).

[48] T. SCHÖNFELD, M. RUDGYARD - *Steady and Unsteady Flow Simulations Using the Hybrid Flow Solver AVBP.* AIAA Journal, 37:1378-1385 (1999). doi:10.2514/2.636. http://arc.aiaa.org/doi/abs/10.2514/2.636.

[49] V. MOUREAU, G. LARTIGUE, Y. SOMMERER, C. ANGELBERGER, O. COLIN, T. POINSOT - *Numerical Methods for Unsteady Compressible Multi-Component Reacting Flows on Fixed and Moving Grids*. Journal of Computational Physics, 202:710-736 (2015).

[50] Cerfacs - *The AVBP HandBook (2008)*. http://www.cerfacs.fr/avbp7x//RESOURCES/HTML/main.html.

[51] O. COLIN, M. RUDGYARD - *Development of High-Order Taylor-Galerkin Schemes for LES*. Journal of Computational Physics, 162:338-371 (2000).

[52] F. NICOUD, H. B. TODA, O. CABRIT, S. BOSE, J. LEE - *Using Singular Values to Build a Subgrid-Scale Model for Large Eddy Simulations*. Physics of Fluids 23:085106 (2011).

[53] J. P. LEGIER, T. POINSOT, D. VEYNANTE - *Dynamically Thickened Flame LES Model for Premixed and Non-Premixed Turbulent Combustion*. Proceedings of the Summer Program: 157-168 (2011).

[54] F. CHARLETTE, C. MENEVEAU, D. VEYNANTE - *A Power-Law Flame Wrinkling Model for LES of Premixed Turbulent Combustion Part I: Non-Dynamic Formulation and Initial Tests*. Combustion and Flame 131:159–180 (2002).

[55] T. J. POINSOT, S. K. LELE - *Boundary Conditions for Direct Simulations of Compressible Viscous Flows*. Journal of Computational Physics 101:104–129 (1992).

[56] S. MENDEZ, J. D. ELDREDGE - *Acoustic Modeling of Perforated Plates with Bias Flow for Large-Eddy Simulations*. Journal of Computational Physics 228:4757–4772 (2009).

[57] A. REFLOCH, B. COURBET, A. MURRONE, P. VILLEDIEU, C. LAURENT, P. GILBANK, J. TROYES, L. TESSÉ, G. CHAINERAY, J.B. DARGAUD, E. QUÉMERAIS, F. VUILLOT - *CEDRE Software*. Aerospace Lab, 2 (2011).

[58] D. SCHERRER, F. CHEDEVERGNE, P. GRENARD, J. TROYES, A. MURRONE, E. MONTREUIL, F. VUILLOT, N. LUPOGLAZOFF, M. HUET, B. SAINTE-ROSE, P. THORIGNY, N. BERTIER, J.M. LAMET, T. LE PICHON, E. RADENAC, A. NICOLE, L. MATUSZEWSKI, M. ERRERA - Recent CEDRE applications. Aerospace Lab, 2 (2011).

[59] F. DUPOIRIEUX, N. BERTIER - *The Models of Turbulent Combustion in the CHARME Solver of CEDRE*. Aerospace Lab, 2 (2011).

[60] B. SAINTE-ROSE, N. BERTIER, S. DECK, F. DUPOIRIEUX - *A DES Method Applied to a Backward Facing Step Reactive Flow*. *Comptes Rendus Mécanique*, 337:340–351 (2009).

[61] M. LORTEAU, F. CLÉRO, F. VUILLOT - *Analysis of Noise Radiation Mechanisms in Hot Subsonic Jet from a Validated Large Eddy Simulation Solution*. Physics of Fluids 27:075108 (2015). doi: 10.1063/1.4926792

[62] F. HAIDER, J.-P. CROISILLE, B. COURBET - *Stability of the Cell Centered Finite-Volume MUSCL Method on Unstructured Grids*. *Numerische Mathematik*, 113:555-600 (2009).

[63] S. DECK - *Recent Improvements in the Zonal Detached Eddy Simulation (ZDES) Formulation*. Theoretical and Computational Fluid Dynamics, 26:523–550 (2012).

[64] F. VUILLOT, N. LUPOGLAZOFF - *Combustion and Turbulent Flow Effects in 2D Unsteady Navier-Stokes Simulations of Oscillatory Rocket Motors*. 34th AIAA Aerospace Sciences Meeting, paper 96-0884 (1996).

[65] N. LUPOGLAZOFF, F. VUILLOT - *Simulations of Solid Propellant Rocket Motors Instability Including Propellant Combustion Response*. 6th International Congress on Sound and Vibration (1999).

[66] Centaur grid generation software: https://www.centaursoft.com.

[67] C. J. LAPEYRE, M. MAZUR, P. SCOUFLAIRE, F. RICHECOEUR, S. DUCRUIX, T. POINSOT - *Acoustically Induced Vortex Core Flashback in a Staged Swirl-Stabilized Combustor*. Submitted to Flow, Turbulence and Combustion.

[68] C. LAPEYRE - *Étude numérique de la stabilité, la stabilisation et le bruit de flamme dans un brûleur tourbillonnaire en conditions amorcées*. PhD thesis, *Institut National Polytechnique de Toulouse*, Toulouse, France (2015).

[69] W. TAO - *Time Resolved Temperature and Pressure Based Methodology for Direct and Indirect Combustion Noise Separation*, PhD thesis, CentraleSupélec (2016).

[70] I. DURAN, M. LEYKO, S. MOREAU, F. NICOUD, T. POINSOT - *Computing Combustion Noise by Combining Large Eddy Simulations with Analytical Models for the Propagation of Waves Through Turbine Blades*. Compte Rendus Mecanique, 341:131-140 (2013).

[71] J. KOPITZ, E. BRÖCKER, W. POLIFKE - *Characteristics-Based Filter for Identification of Planar Acoustic Waves in Numerical Simulation of Turbulent Compressible Flow*. 12th International Congress on Sound and Vibration (2005).

[72] A. GIAUQUE, M. HUET, F. CLERO - *Analytical Analysis of Indirect Combustion Noise in Subcritical Nozzles*. Journal of Engineering for Gas Turbines and Power, 134:111202 (2012).

[73] W. H. MOASE, M. J. BREAR, C. MANZIE - *The Forced Response of Choked Nozzles and Supersonic Diffusers*. Journal of Fluid Mechanics, 585:281-304 (2007).

[74] I. DURAN, S. MOREAU - *Solution of the Quasi-One-Dimensional Linearized Euler Equations Using Flow Invariants and the Magnus Expansion*. Journal of Fluid Mechanics, 723:190-231 (2013).

[75] J. ZHENG, M. HUET, F. CLÉRO, A. GIAUQUE, S. DUCRUIX - *A 2D-Axisymmetric Analytical Model for the Estimation of Indirect Combustion Noise in Nozzle Flows*. 21st AIAA/CEAS Aeroacoustics Conference, Paper AIAA 2015-2974 (2015).

[76] W. C. ULLRICH, J. GIKADI, C. JÖRG, T. SATTELMAYER - *Acoustic-Entropy Coupling Behavior and Acoustic Scattering Properties of a Laval Nozzle*. 20th AIAA/CEAS Aeroacoustics Conference, Paper AIAA 2014-3193 (2014).

[77] W. C. ULLRICH, T. SATTELMAYER - *Transfer Functions of Acoustic, Entropy and Vorticity Waves in an Annular Model Combustor and Nozzle for the Prediction of the Ratio Between Indirect and Direct Combustion Noise*. 21st AIAA/CEAS Aeroacoustics Conference, Paper AIAA 2015-2972 (2015).

[78] K. KNOBLOCH, T. WERNER, F. BAKE - *Noise Generation in Hot Nozzle Flow*. Proceedings of ASME Turbo Expo 2015, Paper GT2015-43702 (2015).

[79] M. HUET - *Nonlinear Indirect Combustion Noise for Compact Supercritical Nozzle Flows*. Journal of Sound and Vibration, 374:211-227 (2016). http://dx.doi.org/10.1016/j.jsv.2016.03.028

Acronyms

CERFACS	(*Centre Européen de Recherche et de Formation Avancée en Calcul Scientifique)*
CESAM-HP	(*Combustion Etagée Swirlée Acoustiquement Maîtrisée - Haute Pression)*
DDES	(Delayed Detached Eddy Simulation)
DNS	(Direct Numerical Simulation)
EM2C	(*laboratoire d'Énergétique Moléculaire et Macroscopique, Combustion)*
HFLES	(High-Fidelity compressible Large Eddy Simulations)
ICS	(Impedance Control System)
IFP-EN	(*Institut Français du Pétrole - Energies nouvelles)*
LES	(Large Eddy Simulations)
ONERA	(*Office National d'Études et de Recherches Aérospatiales)*
PIV	(Particle Image Velocimetry)
PSD	(Power Spectral Density)
RANS	(Reynolds Averaged Navier Stokes)
RECORD	(REsearch on Core nOise ReDuction)
ZDES	(Zonal Detached Eddy Simulation)

AUTHOR

Maxime Huet graduated from Ecole Centrale Lyon in 2006 and received a Master degree in Acoustics from Lyon University the same year. He joined Onera in 2007 as a research scientist. His work is mainly dedicated to jet noise simulation and combustion noise modeling for their possible reduction.

Nicolas Bertier, graduated from ENS Cachan and PhD from Paris VI University, is senior researcher in the Energetics department of ONERA. He is project manager of CEDRE, which is the ONERA's code for energetics. His research activities focused on numerical simulations of reactive flows. He is also teaching combustion at Paris VI University and ISAE/Supaero (Toulouse).

François Vuillot graduated from Sup'Aero in 1981 and from U. of Washington in 1982. He is presently Scientific Advisor for complex simulations at the Fundamental and Applied Energetics Department of ONERA. He has been involved in unsteady numerical simulations for analyzing solid propellant rocket motor stability and jet noise for several years. He received the French "Académie des Sciences" Edmond Brun prize in 2008.

Marek Mazur graduated from RWTH Aachen University and Ecole Centrale Paris in 2013. He is a PhD student working on experimental studies of direct and indirect combustion noise in an aircraft type combustion chamber at EM2C Laboratory of CentraleSupélec and CNRS.

Nancy Kings has Ph.D. degree from TU Berlin. After her research assistant period at German Aerospace Center (DLR) she joined laboratoire EM2C of CNRS and CentraleSupélec as postdoctoral researcher focusing on combustion noise and on temperature measurement techniques.

Wenjie Tao graduated from Ecole Centrale de Pékin and Ecole Centrale Paris in 2011 and received her Ph.D. Degree on Combustion in 2016. Her Ph.D. thesis was on temperature and pressure measurements based methodology for direct and indirect combustion noise separation. She is now working as combustion and heat transfer engineer in ACAE.

Philippe Scouflaire is a CNRS Research Engineer in combustion, optical diagnostics, time resolved.

Franck Richecoeur has a PhD from Ecole Centrale Paris and a "Habilitation à Diriger des Recherches" from Université de Rouen. He is Lecturer at CentraleSupélec, where his activities are dedicated to experimental research on combustion instabilities, combustion noise, micro-combustion and processing of temporal data for the description of dynamical phenomena.

Sébastien Ducruix, laboratoire EM2C, CNRS, CentraleSupélec, Université Paris-Saclay. Engineering Degree, Master's Degree and PhD from Ecole Centrale Paris, "Habilité à Diriger des Recherches" (HDR) from Institut National Polytechnique de Toulouse. Sébastien Ducruix is Directeur de Recherche at the CNRS and presently Deputy Director of EM2C. His research activity mainly concerns the theoretical, experimental and numerical characterization of the dynamics of flames and fundamental mechanisms of combustion-acoustic interactions, in particular for gas turbines and rocket engines. Sébastien Ducruix is the scientific coordinator of the French-German collaborative program REST (Rocket Engine STability Initiative) set up by AIRBUS, CNES, DLR, ONERA and SAFRAN. He is Vanguard Chair for the Committee "Combustion, Fuel and Emission" of the international conference Turbine Technical Conference and Exposition -TurboExpo. He is Vice Chairman of the thematic area "Propulsion" for the ASTech cluster (Aeronautics and Space in Paris Region).

Corentin Lapeyre graduated from Ecole Centrale Lyon in 2011, and obtained a PhD in numerical combustion from INP Toulouse in 2015. His thesis work was performed at Cerfacs, and funded by the DISCERN ANR. It concerned compressible flame dynamics in pressurized systems, including flame noise and stability, as well as flashback. Since 2015 he is a Postdoctoral Fellow at IMFT, working on flame-vortex interactions for alternative fuels under the IDYLLE ANR grant.

Thierry Poinsot received his PhD thesis in heat transfer from Ecole Centrale Paris in 1983 and his Thèse d'Etat in combustion in 1987. He is a research director at CNRS, head of the CFD group at Cerfacs, senior research fellow at Stanford University and a consultant for various companies. After his thesis at Ecole Centrale Paris and after two years of post-doctoral work at Stanford, he started combustion activities at Cerfacs in 1992 and his group (60 persons in 2010) has produced a significant part of the recent research in the field of LES of turbulent combustion in gas turbines. He teaches numerical methods and combustion at many schools and universities (Ecole Centrale Paris, ENSEEIHT, Ensica, Supaero, UPS, Stanford, Von Karmann Institute, CEFRC Princeton and Beijing). He has authored more than 150 papers in refereed journals and 200 communications. He is the co-author of the textbook "Theoretical and numerical combustion" together with Dr D. Veynante and an associate editor of "Combustion and Flame". He received the first Cray prize in 1993, the BMW prize in 2002, the Grand Prix of the French Academy in 2003 and an ERC advanced grant in 2013.

G. K. Vedeshkin, E. D. Sverdlov, A. N. Dubovitsky

(Central Institute of Aviation Motors)

E-mail: gtu@ciam.ru

DOI : 10.12762/2016.AL11-11

Experimental Investigations of a Low-Emission Combustor Designed for Mid Power Gas Turbines

The paper describes the main mechanisms of NO_x formation (thermal, prompt NO_x and through N_2O). It is shown that, for combustion products when the gas temperature is less than 1650 K (T_{gas}<1650 K), the residence time has a weak influence on NO_x formation.

A concept for the simultaneous reduction of NO_x and CO in low-emission combustors with large residence time is suggested. Some methods to organize an operation process with low NO_x and CO formation are suggested as well. The low-emission combustor configuration is presented.

The paper describes both the experimental results of investigated model combustors and investigations of a low-emission combustor designed for mid power gas turbines, developed with the suggested operating process mechanism.

Introduction

Changing over to a mechanism of lean premixed burning of fuel-air mixtures resulted in a strong reduction of NOx and CO emissions in the combustors designed for industrial gas turbines, which operate on natural gas. Nowadays, the best low-emission gas turbine combustors, such as Siemens and General Electric, show no more than 10 μmol/mol in the main operating modes. Calculation investigations by some authors [1] reveal that, by means of enhancing the air-fuel mixing quality and mixture leaning, it is possible to achieve NO_x and CO emissions of about 1 μmol/mol.

However, in order to obtain such low amounts of adverse emissions with real low-emission combustors, it is necessary to solve a number of related complex scientific and technical problems, in particular, by intensifying the fuel and air mixing inside the burners. It is also necessary to increase the lean blow-off limits without any pilot support of the recirculation zone to stabilize combustion, and to carry out a purely convective cooling of the flame tube without any air supply to the lean mixture burning zone.

The main goal of the given work is the experimental verification of the performance of the low-emission combustor developed by the Central Institute of Aviation Motors (CIAM). The combustor, which operates on natural gas, had been developed for industrial gas turbines with $\pi_{compr.}$=20-23 [2]. The CIAM combustor is distinguished from other well-known combustors by its individual gas-dynamic flow and structural design. In order to stabilize the flame in the CIAM low-emission combustor, a conical stabilizer installed in the central tube at the burner outlet is used. To organize the recirculation zone for flame stabilization, intensive air swirling is not used, unlike with many well-known combustors. In addition to this, the flame tube walls in its first part are made as a conical diffuser. The combination of a conical flame stabilizer and a conical diffuser for the flame tube results in a significant increase in the recirculation zone dimensions, the residence time in the zone, and all of these significantly increase the lean blow-off limits, even without any pilot supply. The gas-dynamic pattern developed and the structural lay-out of the low-emission combustor make it possible to significantly reduce the combustible temperature during the steady burning of a lean mixture, as well as to reduce the emissions. In order to intensify the lean mixture burning and to reduce CO emissions, flame turbulators located on a conical surface of the flame stabilizer are used. In addition to this, it is important to mention that the configuration of the flame tube end for the low-emission combustor has dimension limitations specified with the casing design for the gas turbine.

Analysis of kinetic mechanisms for NOx and CO formation

The reduction of adverse emissions during combustion is achieved by means of mixture homogenization and its leaning. However, the

reduction of the flame temperature results in an increase in CO and unburnt hydrocarbon emissions. Investigations [3] have shown that, when methane is burning, the combustion efficiency reduction and the CO concentration increase in the mixture occur very abruptly if the temperature achieves the critical level, ~1500 K. It is possible to finalize the oxidation of CO to CO_2 by increasing the residence time within the admissible ranges for NO_x emission.

Let us analyze the kinetic aspects of NO_x formation with temperature variation. Several mechanisms are used in the models for nitrogen oxidizing with NO, NO_2 and N_2O formation:

1. A thermal mechanism according to the Zeldovich mechanism [4], which includes N_2 oxidizing and the interaction of N atoms with OH radicals (enlarged mechanism):

$$N_2 + O = NO + N$$
$$N + O_2 = NO + O$$
$$N + OH = NO + H$$

2. N_2O – the mechanism specified with the reaction group, where N_2O acts as an intermediate substance during NO formation:

$$N_2O + CO = NCO + NO$$
$$N_2O + H = NO + NH$$
$$N_2O + O = NO + NO$$

3. NO_2 – the mechanism resulting in NO formation by the way of the continuity of reactions below:

$$NO_2 + CO = NCO + NO$$
$$NO_2 + OH = HO_2 + NO$$
$$NO_2 + H = OH + NO$$
$$NO_2 + O = O_2 + NO$$
$$NO_2 + M = O + NO + M$$

4. A Fenimore mechanism (prompt NO mechanism) [5]. Prompt nitrogen oxides are formed at the stage when the fuel is burning in the flame front. The beginning of their formation involves N_2 interaction with CH and CH_2 radicals, which appear at fuel molecular decomposition:

$$N_2 + CH = HCN + N$$
$$N_2 + CH_2 = HCN + NH$$

The estimation of the input of Mechanisms 1, 3 and 4 into NO_x formation is described in [6]. It is shown that the temperature and the mixture composition define which N_2 oxidizing mechanism is the leading one. The time influences the type of leading N_2 oxidizing mechanism in stoichiometric mixtures. Mixture leaning reduces the role of the thermal and prompt NO mechanisms.

The analysis of Mechanisms 1– 4 shows that nitrogen oxidizing takes place with a large number of components in the reacting mixture. Taking this into account, nitrogen oxide formation at various temperatures has been calculated on the basis of the detailed kinetic scheme by Bowman-Miller [7], within the framework of a direct kinetic problem: $\rho dc_i/dt - W_i=0$, $dH/dt - q_r=0$ [6]. Here, c_i and W_i are concentrations and velocities for the formation of the mixture i-component; ρ and H are the density and enthalpy of the reacting mixture; q_r is the heat flux divergence; and t is time.

The scheme [7] comprises 235 convertible phases, with 52 participating components. It is widely approved in calculations for the burning of lean methane - air mixtures.

Using the model above in Reference [8], nitrogen oxide formation has been investigated in two stages for methane burning. The obtained results [8] show that, when combustion occurs within the interval of 3 to 10 ms, the temperature reduction in the second stage below 1700 K resulted in a significant reduction of NO_x formation, despite the reacting mixture composition. It proves that temperature variation has a determinant effect on NO_x emission. The obtained result is a universal one, because all of the mechanisms for NO_x formation (1-4) mentioned above were taken into account in calculations [8].

Let us evaluate a kinetically attributed reserve residence time increase in the combustor to reduce the decrease in the CO concentration during the temperature drop. This reserve is an additional time required to achieve the ultimately admissible (prescribed) NO level with the temperature decrease.

The combustible temperature in the calculations was varied by means of the change in the initial composition of lean methane-air mixtures.

The NO emission level is related to the burnt gas residence time in the combustor. The relationship between the formation of given amounts of NO (5 and 10 μmol/mol have been selected as the upper emission limits) and the temperature of burnt gas has been estimated using the global set of mechanisms presented above (Mechanisms 1 to 4) or using the Zeldovich mechanism alone. These calculations were performed for a mixture containing 15% of O_2 (i.e., burnt gas) and are presented in Figure 1.

As can be seen, the temperature reduction by 100 K over the entire examined range of temperature variations results in a time increase by practically an order of magnitude for NO formation. This effect occurs both for the whole process and for the thermal nitrogen oxidizing mechanism as well. Thus, nitrogen oxide formation at relatively low temperatures is not a factor for residence time, and it can be chosen from the calculated duration required for the CO oxidation into CO_2.

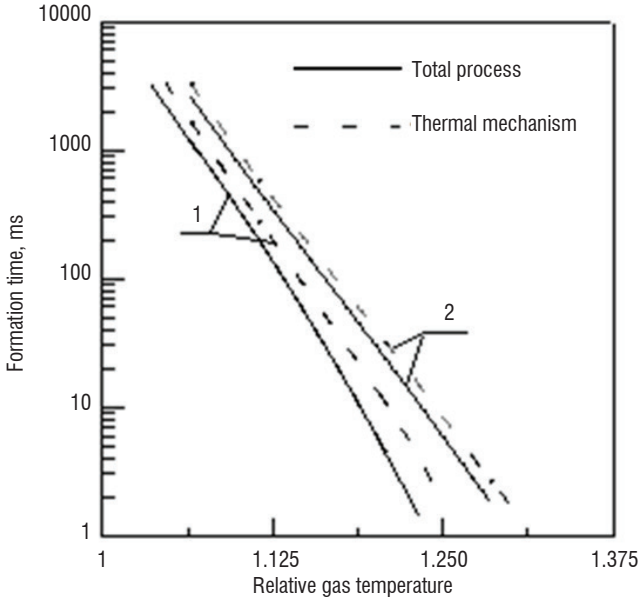

Figure 1 - Relationship between the relative burned gas temperature and the residence time of a given amount of NO. (at 15% of O_2): 1 – NO=5μmol/mol, 2 – NO = 10 μmol/mol. The combustion mode: P_c=0,1 MPa, T_a=720 K

The analysis performed is representative of a homogeneous mixture burning within the whole combustor volume.

Gas-dynamic methods to increase lean blow-off limits

In order to reduce NO_x emissions, first of all, the flame temperature must be reduced. To manage this, the lean blow-off flame limits must be increased in the low-emission combustor. The lean blow-off flame limits are described by Mikhelson's criterion for the combustion process in the recirculation zone:

$$K_m = \frac{W}{l_{REC}} \frac{a}{U_n^2} \geq 1$$

where W is the gas velocity in the combustor; l_{REC}. is the length of the recirculation zone; U_n is the laminar flame velocity; and a is the themal diffusivity coefficient. Taking this criterion into account, the lean blow-off flame limits can be extended by means of either gas-dynamic or kinetic methods.

In low-emission combustors, this problem is usually solved by means of kinetic methods, at the expense of mixture enrichment with fuel or additional pilot fuel supplied to the recirculation zone, resulting in an increase in U_n. Such a method to extend the lean blow-off limits results in a significant NOx increase, due to the temperature increase in the recirculation zone.

In order to extend the flame lean blow-off limits with gas-dynamic methods, it is necessary to increase the dimensions of the recirculation zone and to decrease the gas flow in the combustor. The gas velocity in the combustor (W) can be reduced by increasing the combustor cross-section. The possibilities to enlarge the dimensions of the combustor central recirculation zone grow with the initial conical extension of the channel cross-section area [9].

Both calculations and experimental investigations showed (Fig. 2) that, in the combustor with a conical diffuser, the length of the recirculation zone is proportional to the combustor diameter D_C, and at $L_C/D_C > 2.5$ can achieve $l_{REC} \sim 1.6\ D_C$. Compared with a combustor having an abrupt extension, it will be possible to increase the length of the recirculation zone by more than 2 times. Experimental investigations performed in the combustor with the conical diffuser at $T_a = 740\ K$, $P_a = 1$ MPa proved the possibility of extending the flame blow-off limits up to the air-fuel equivalence ratio $\alpha = 3.1$ ($T_g = 1420\ K$) without any additional fuel supply into recirculation zone. Extending the flame blow-off limits will make it possible to move the low-emission operation range to the area with lower flame temperatures.

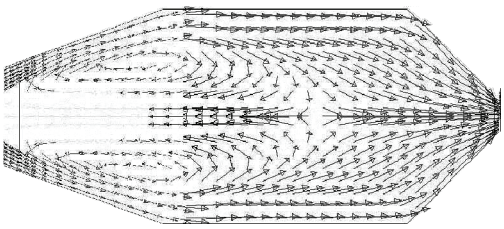

Figure 2 - Gas flow pattern in the low-emission combustor

Burner performance with low concentration field non-uniformity

Another very important condition for NO_x reduction in low-emission combustors is the maximal possible (admissible) reduction of the fuel concentration field non-uniformity at the combustor inlet. In one of the best Siemens burners, HR-3, the root-mean-square non-uniformity of the fuel concentration field at the burner outlet is 8% [1]. It is possible to improve the mixing quality at the expense of increasing the mixer length. However, other problems arise, such as flashback. Due to gas flow swirling, the flashback is especially strong near the central hub.

In this work, this problem is solved with a burner designed without any mixture swirling. Figure 3 shows a schematic diagram to measure concentration non-uniformity in the fuel-air mixture of the designed burner. Figure 4 shows the measurement results for the fuel concentrations in the fuel-air mixture. Investigations of the fuel concentration field in an annular slot at the burner outlet were performed with a 2-point gas-sampling probe and gas analyzer post-processing. The first sampling point was at 1/3 of the channel height, located between the stabilizer and the diffuser. The second one was at 2/3 of the channel height. Two measurements were performed. During each measurement, the sampling points in turn were switched into the gas analyzer. The sampling probe rotation speed was 1 degree per second. Figure 4 shows the measurement data. The measurements showed that the root-mean-square non-uniformity of the fuel concentration field at the outlet of the CIAM burner is ≈6 %.

This result, together with the leaning of the mean fuel-air mixture composition, is a basis for significant NO_x emissions reduction.

Influence of residence time on NO_x emission

The flame temperature, pressure in the combustion chamber and residence time influence the level of NO_x emissions when homogeneous mixtures are burned.

In real combustors, besides the mentioned parameters, fuel concentration oscillations and the quantity of pilot fuel supplied into the recirculation zone affect the NO_x level.

Investigations relating to model combustors with various calculated residence times ($\tau_{res.} \sim 25$ ms and $\tau_{res.} \sim 85$ ms) have been performed at the inlet temperature $T_a = 740$ K and combustor pressure $P_a \sim 0.5$-0.7 MPa.

In the low-emission combustors under consideration, the concentration field non-uniformity has been minimized; the diffusion pilot fuel has not been supplied into recirculation zones. Under such conditions (low non-uniformity and absence of pilot fuel), the residence time effect on NO_x should be similar to the effect of this parameter during ideal homogeneous fuel-air mixture burning.

Investigation results relating to the residence time effect on the NO_x formation are presented in Figure 5.

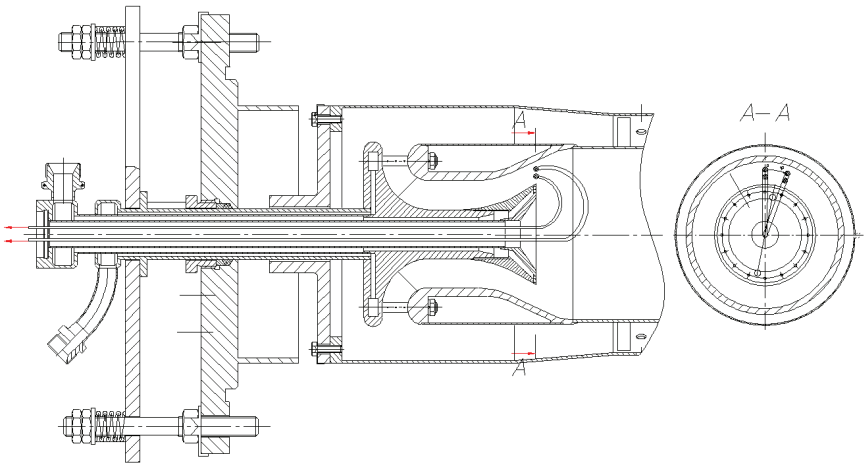

Figure 3 - Schematic diagram to measure fuel concentration non-uniformity in the fuel-air mixture

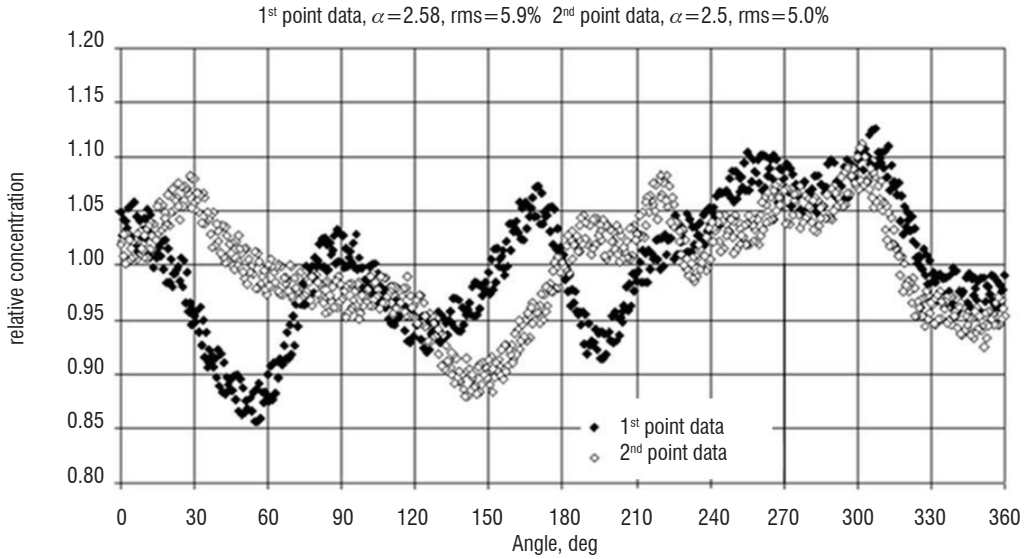

Figure 4 - Measurement results of fuel concentration non-uniformity at the burner outlet

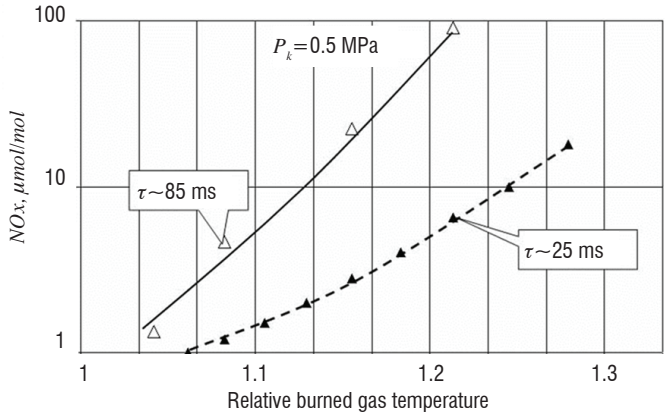

Figure 5 - Effect of the residence time on NO_x emissions

Investigations showed that, in the relatively high gas temperature area, the residence time effect is strong, and that a $\tau_{res.}$ increase results in a significant NO_x rise. By reducing the temperature of the combustion products and leaning the fuel-air mixture, the effect of the residence time decreases very quickly (i.e. the residence time for very lean mixtures practically does not have any effect on NO_x formation). When the relative gas temperature corresponds to $T_g < 1.1$ this effect is negligibly small and at $T_g < 1.07$ NO_x emissions is practically one and the same at $\tau_{res.} \sim 25$ ms and $\tau_{res.} \sim 85$ ms. The reduction of the residence time effect on NO_x emissions during the flame temperature decrease is a consequence of the thermal mechanism input on NO_x formation.

The results of experimental investigations prove the possibility of reducing NO_x formation during the combustion product temperature decrease in the combustors with high residence time.

Influence of residence time on CO emissions

Decreasing the combustion product temperature influences the increase in the CO emissions. An increase in the residence time may reduce CO emissions and extend the low-emission operating range of the combustor. Another parameter that affects CO emissions is the temperature of the flame tube walls, which causes additional gas cooling in the boundary layer at the combustor walls.

Investigations with different residence times ($\tau_{res.} \sim 25$ ms and $\tau_{res.} \sim 85$ ms) have been performed at the inlet temperature $T_a = 740$ K and combustor pressure $P_a \sim 0.5$-0.7 MPa. The results of experimental investigations relating to the residence time effect on CO formation in the low-emission combustor are presented in Figure 6.

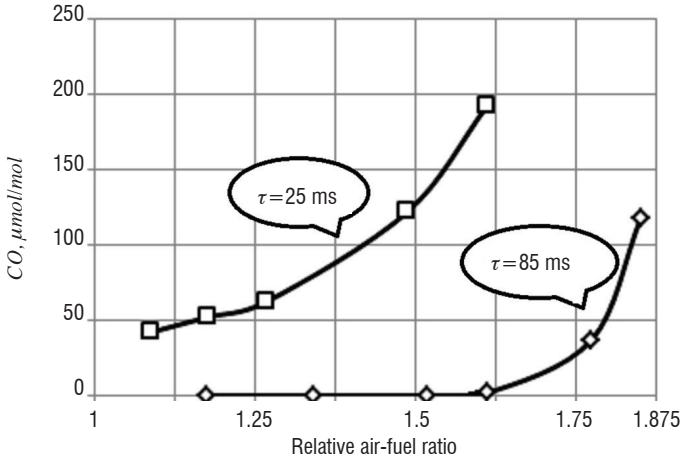

Figure 6 - Effect of the residence time on CO emissions

Investigations showed that by increasing the residence time $\tau_{res.} \sim 25$ ms up to $\tau_{res.} \sim 85$ ms, the low-emission operating range in terms of CO is extended significantly. A quick increase in CO emission is noticed for $\tau_{res.} \sim 25$ ms at the relative air-fuel ratio ≈ 1.38. Changing-over to $\tau_{res.} \approx 85$ ms made us possible to shift the quick rise of CO emission to the relative air-fuel ratio ≈ 1.75. The CO level in the low-emission operating range (at the relative air-fuel ratio ≈ 1.65) decreased to ~ 1 μmol/mol.

Thus, the experiments demonstrated the possibility of simultaneously decreasing CO and NO_x emissions by means of increasing the residence time.

Low-emission combustor performance for mid power industrial gas turbines

The configuration of the low-emission combustor developed with limited dimensions in the gas turbine casing differs from the model combustors presented in the first part of the paper. The differences are less combustor sectional areas, higher flow velocities and shorter residence time.

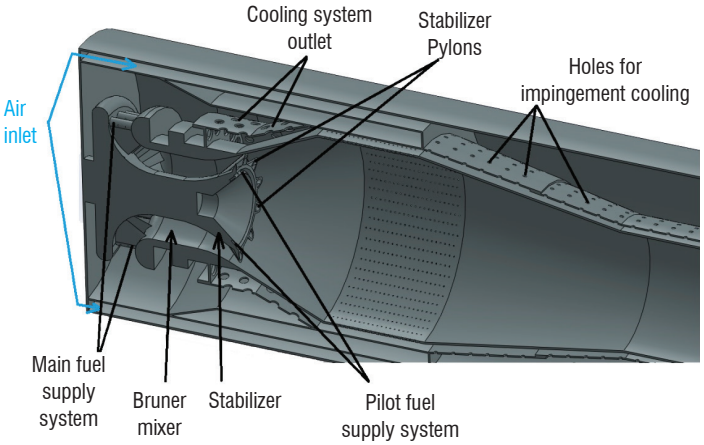

Figure 7 - Low-emission combustor

In addition to that, two new components have been added to the combustor configuration:

- acoustic holes to damp combustion instabilities;
- pylons located on the stabilizer to intensify combustion.

Low-emission combustor tests for the mid-power gas turbine have been performed in the axisymmetric single burner segment (Fig.7). NO_x and CO emission levels have been investigated in the range of 50 to 100 % load for industrial gas turbine operation.

Table 1 describes the main combustor operation modes and emission results.

N	P_a kPa	G_a kg/s	T_a K	PRF %	α	NO_x μmol/mol	CO μmol/mol
1	2013	3.15	7476	10.41	2.79	23	4
2	2005	3.14	746	10.2	2.60	39	4
3	2004	3.14	747	10.1	3.01	12	12
4	2302	4.00	781	10.0	3.00	12	3
5	2285	4.00	782	9.7	2.80	19	3
6	2283	4.01	783	12.3	2.62	53	4

Table 1 - Main results of combustor tests on low-emission operation modes, P_a, G_a, T_a are the pressure, air mass flow and temperature at the segment inlet, respectively. PFR is the pilot-fuel ratio; α is the air-fuel equivalence ratio.

Figure 8 shows the temperatures of the flame tube wall for the modes under study. The emission performances in the mode $P_a = 2$ MPa, $T_a = 746$ K, $\alpha = 2.79$, PFR = 10 % corresponded to $NO_x = 23$ μmol/mol, $CO = 4$ μmol/mol. The mode $P_a = 2.3$ MPa, $T_a = 781$ K, $\alpha = 3.0$, PFR = 10 % emission performances achieved $NO_x = 12$ μmol/mol, $CO = 3$ μmol/mol.

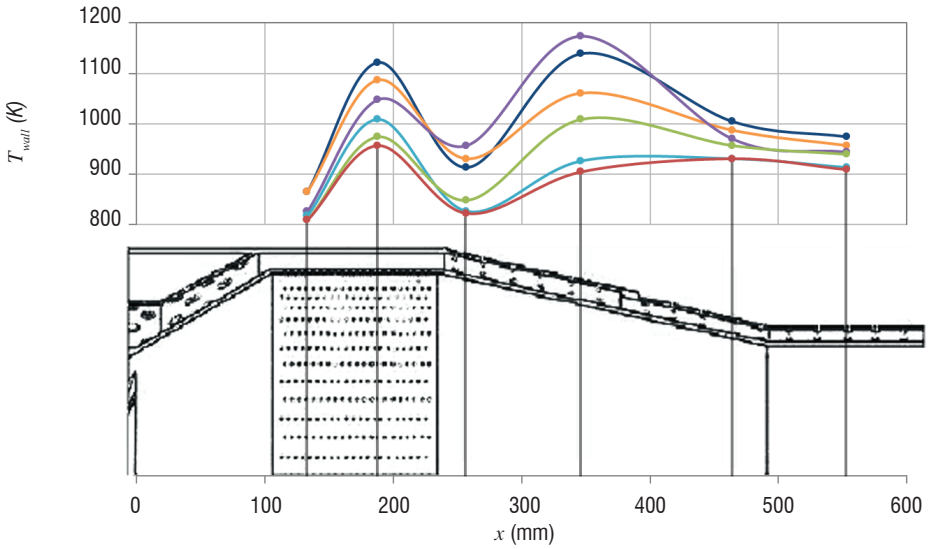

Figure 8 - Wall temperatures of the flame tube for various low-emission combustor operation modes

Conclusions

Based on the analysis of kinetic mechanisms for NO_x and CO formation, a concept to organize the operation process in the low-emission combustor has been made. The main feature of the concept is the combination of a rather long residence time and very lean mixtures at the burner outlet. This made it possible to achieve 5 μmol/mol of emission in the model combustors.

On the basis of investigated model combustors, CIAM specialists have developed and tested in the facilities a low-emission combustor designed for industrial gas turbines with natural gas as fuel. The described combustor differs from the majority of the well-known combustors, since it does not have any air swirling. It has a conical flame stabilizer at the burner outlet and a conical diffuser at the flame tube inlet. A lobe system has been incorporated at the flame stabilizer outlet in order to stimulate the burning of lean mixtures and to reduce CO. The tests on the combustor have been performed under conditions corresponding to those of a gas turbine with $\pi_{compr.}$=20 and 23. During the tests at P_a=2 MPa, T_a=746 K, α=2.79, PFR=10 %, the emission levels are: NO_x=23 μmol/mol, CO=4 μmol/mol. During the tests at P_a = 2.3 MPa, T_a=781 K, α=3.0, PFR=10 %, the emission levels are: NO_x= 12 μmol/mol, CO=3 μmol/mol ■

Acknowledgements

The emission performances achieved with the CIAM low-emission combustor meet the International Standards. Work supported by the Russian Ministry of Education and Science; the unique project ID is RFMEFI62815X0003

References

[1] H. STEB, B. PRADE, T. HAHNER, S. HOFFMAN - A*dvanced Burner Development for the VX 4.3A Gas Turbines*. Siemens AG, Power Generation Group KWU.

[2] G.K. VEDESHKIN, E.D. SVERDLOV, A.N. DOUBOVITSKY - *Influence of Flow Behavior in the Combustor on Combustion Instabilities Performance Operating on Homogeneous Fuel - Air Mixtures*. 20th ISABE Conference, September 12 – 16, 2011, Göteborg, Sweden.

[3] YU. YA. BURIKO, V. F. GOLTSEV - *Studies of Two-Stage Homogeneous Combustion of Methane-Air Mixture*. Combustion and Atmospheric Pollution: Environment Impact / Edited by G.D. Roy, S.M. Frolov, A.M. Starik. – Moscow: TORUS PRESS, 2004, pp. 69-78.

[4] YA.B. ZELDOVICH, P.YA. SADOVNIKOV, D.A. FRANK-KAMENETSKY - *Nitrogen Oxidizing During Combustion*. M.- L.: Academy of Science USSR, 1947, p 147.

[5] C.P. FENIMORE - *Formation of Nitric Oxide in Premixed Hydrocarbon Flames*. 13th Symp. (Int.) on Combust., The Combust. Inst., 1971, p.373.

[6] D.V. VOLKOV, S.A. ZAYTSEV, V.F. GOLTSEV - *Parametric Investigation of Nitrogen Oxides Formation During Homogeneous Methane – Air Mixture Combustion.* Physics of Combustion and Explosion, 1999, v.35 N° 2, pp.9-15.

[7] J.A. MILLER, C.T. BOWMAN - *Mechanism and Modeling of Nitrogen Chemistry in Combustion*. Progress in Energy and Combustion Science, 1989, v. 5, pp. 287-338.

[8] V.F. GOLTSEV - *Nitric Oxides Formation at Combustion of Homogeneous Methane-Air Mixtures Using Two-Stage Technology.* Non-equilibrium Processes, Vol. 1, Combustion and Detonation / Edited by G.D. Roy, S.M. Frolov, A.M. Starik. – Moscow: TORUS PRESS, 2005, pp. 148-157.

[9] A.K. GUPTA, D.G. LILLEY, N. SYRED - *Swirling Flows*. Abacus Press, 1984 r. c. 221-222

Nomenclature

a – temperature conductivity coefficient
D - diameter
G – gas flow rate
L, l - length
$L0$ – stoichiometric coefficient
P - pressure
PFR – pilot-fuel ratio
rms – root-mean square
T - temperature
T_g - relative burned gas temperature
U – flame velocity propagation
UH – unburnt hydrocarbons
W – gas velocity
τ - residence time, $\tau = L_c/U$
α – air-fuel ratio, $\alpha = G_a/G_f{*}L0$
$\pi_{compr.}$ – pressure ratio in the compressor, $\pi_{compr.} = P_{compr.}/P_0$

Indices

a - air
c - combustor
com – combustion products
f - fuel
fl - flame
m - main
n - normal
$res.$ - residence time
$rec.$ - recirculation
w - wall

AUTHORS

Georgy Vedeshkin joined the Central Institute of Aviation Motors in 1968 after receiving a degree in Aerospace Engineering at Samara Aerospace University.
Head of the CIAM Gas Turbine Division, program leader, he is a skilled specialist in investigations of operating processes in jet engines, gas turbines, testing and development of combustors.
Georgy Vedeshkin has been involved in, combustor testing and development, gas turbine testing. Dr. Vedeshkin has been the leader of several international contracts with GE, ALSTOM Power, Siemens, and AIRBUS. He is the author of more than 20 inventions and patents and more than 110 publications in Russian and foreign collected books

Evgeniy Sverdlov graduated from the All Union Engineering Institute. He joined the Central Institute of Aviation Motors in 1971. In 2010, he defended his thesis for a doctor's degree on Low-Emission Combustors designed for Industrial Gas Turbines. Head of Department in the Gas Turbine Division, program leader, he is a skilled specialist in, investigations of combustor operating processes, testing and development of burners and combustors.
Evgeniy Sverdlov is involved in, low-emission combustor testing and development and gas turbine testing.
He is the author of more than 10 inventions and patents, and more than 49 publications in Russian and foreign collected books

Alexey Dubovitsky joined the Central Institute of Aviation Motors in 1999 after receiving a degree as a Physics Engineer from the Moscow Institute of Physics and Technology. He is a skilled specialist in, investigations of operating processes in jet engines, gas turbines and testing and development of combustors.
Alexey Dubovitsky has been involved in, combustor testing and development and gas turbine testing. He is the author of 12 publications in Russian and foreign collected books.
Alexey Dubovitsky has been involved in international contracts with Alstom and Airbus

M. Bellenoue, B. Boust, P. Vidal, R. Zitoun
PPRIME (UPR3346 : CNRS-ENSMA-Université de Poitiers)

T. Gaillard, D. Davidenko
(ONERA)

M. Leyko
(SAFRAN Tech)

B. Le Naour
(MBDA France)

E-mail : marc.bellenoue@ensma.fr

DOI : 10.12762/2016.AL11-12

New Combustion Concepts to Enhance the Thermodynamic Efficiency of Propulsion Engines

The reduction of fuel consumption in future propulsive engines is an ambitious target that will be reached only with a technological breakthrough. Two of the possible solutions are being investigated experimentally and numerically by MBDA France, ONERA, PPRIME and SAFRAN Tech. Changing the actual thermodynamical cycle through the use of Constant-Volume Combustion or Rotative Detonation concepts could theoretically enable this target to be reached. Implementing such concepts requires a deep knowledge and control of several basic phenomena that will occur and interact in real engines, such as: mixing processes, ignition, flow effects, dilution by residual burnt gas, etc.
This article presents recent studies carried out on these elementary processes that must be considered in high-velocity flows and under non-stationary conditions, whatever the concept (CVC or RDE). The results provide a comprehensive insight into constant-volume combustion and detonation dynamics from simulation and experiments on a reduced scale or full scale prototype, which enables the physical phenomena to be understood and modeled, and the potential of such concepts for future propulsion to be highlighted.

Introduction

The Advisory Council for Aviation Research and Innovation in Europe (ACARE) set the goals to reduce CO_2 emissions by 75% and NOx emissions by 90% in 2050 relative to the aircraft emissions produced in 2000. After sixty years of constant research and development efforts, aircraft engines have now reached a high level of maturity. For example, the ability to use high operating pressure (OPR) and by-pass ratios (BPR) led to CO_2 emissions being reduced by 60%. However, there is also broad consensus among experts that these engine technologies have been stretched to their limits, leaving limited potential for further significant improvement in their performance. Thus, only technological breakthroughs will enable the aviation industry to reach the 2050 ACARE goals.

With regard to the combustion process, which is the one that generates most of the entropy for current engines, two alternatives to the usual Joule-Brayton cycle must be considered because they could lead to a remarkable reduction of around 20% [1] in the specific fuel consumption:

1) The constant-volume combustion process (CVC), which for jet engines is described by the Humphrey thermodynamic cycle. The potential of this cycle has been known for a long time and its analogue for piston engines has been successfully used.

2) The combustion detonation mode is described by a so-called "detonation cycle" proposed by Fickett and Jacobs (FJ).

The CVC-Humphrey and Detonation-FJ cycles applied to an airbreathing engine are very similar and lead to attractive improvements of the engine thermal efficiency. In addition, because a large part of the pressure increase is provided by the combustion process, the high pressure compressor could be eventually removed, opening the way to lighter and more compact engines.

Today, no turbine engine operates with the CVC mode, so there is no information available on kerosene CVC properties. Moreover, the thermodynamic conditions, flow characteristics, turbulence, dilution by residual burnt gases, and space and time scales for CVC turbine engines will be very different from those of piston engines, and prevent researchers from using most of the literature related to combustion in piston engines. Similarly, applications of detonation to propulsion have only been considered for a short time, although its fundamental processes have been studied for more than a century, essentially in the domains of defense and safety.

Thus, as regards airbreathing engines, estimates from ideal cycles indicate that the CVC and the Detonation modes would provide significantly higher efficiencies than constant-pressure combustion (CPC) because they both induce higher pressure and temperature in the burnt gas. In a detonation, this compression is obtained before the combustion zone, by means of the detonation leading shock that induces the chemical reaction process. In contrast, in a CVC engine, the pressure increase is achieved at the end of the heat release induced by the combustion itself. These two combustion modes, namely CVC and detonation, raise key scientific issues that require research efforts before they are applied for propulsion: some of them are currently being investigated within the framework of the Chair CAPA [2] dedicated to "Alternative Combustion Modes for Airbreathing Propulsion" and financially supported by ANR, SAFRAN Tech and MBDA.

The detonation cycle can also be used for liquid rocket propulsion, offering the possibility of improving engine performance, as well as some benefits for the propulsion system [26]. This can be an important breakthrough for space launcher technologies, because the performance of todays' liquid rocket engines is very close to the theoretical limit corresponding to the CPC cycle.

Constant-Volume Combustion mode for propulsion

The CVC mode is aimed at (i) benefiting from the better thermodynamic efficiency of isochoric combustion (Humphrey cycle), compared to isobaric combustion (Brayton cycle), and at (ii) reaching higher OPR, compared to conventional turbine engines. Depending on the engine configuration, the isochoric combustor could replace either the combustion chamber, or both the high-pressure compressor and the chamber. Preliminary estimates indicate that the expected benefit in fuel specific consumption could reach a few tens % [3]. This gain would be even higher for small engines, where size limitation does not allow the same compression ratio as in conventional turbine engines.

A few technological concepts have been considered, to allow for continuity in the quasi-steady flow between the turbine engine and the constant-volume combustor. For hypersonic flight up to Mach 4, DARPA (USA) is supporting research on CVC through the Vulcan Program (33 million US dollars), whose results will be also used for turbine-engines and ground-based engines (Vulcan II). Other concepts are currently being investigated, such as the "Wave Rotor" (USA, Glenn Research Center, NASA), "Shockless Explosion Combustion" (Germany, Berlin TU CRC 1029 [4]), the Rim-Rotor-Rotary Ramjet (Canada, Sherbrooke University, [5], [6]) and the "*Thermoréacteur*" (France, DGA, consortium COMAT/ Turbomeca/PPRIME, 2011-2014). The Wave Rotor features a rotating barrel of tube combustors, the inlets and outlets of which are enclosed by two walls with windows for fresh-gas intake and burned-gas exhaust. The barrel rotates at a given speed, depending on the intake, combustion and exhaust duration, but independently from the rotation of the low- or high-pressure shaft [7]-[8]. The *Thermoréacteur* concept (Patent FR2945316, 2009) features rotating valves inside a fixed combustor, allowing for intake and exhaust. The consistency of the CVC concept has been proved with successful experiments and simulation [3], and some scientific key issues have arisen.

Integration of a CVC chamber into an engine

The theoretical gains provided by CVC are extremely attractive. However, since the CVC system (including the compressor and turbine) will work in a completely different manner compared to conventional systems, complications arise in the integration of such technology into a turbo-engine. The side effects (cooling processes or compressor and turbine efficiency) may strongly affect the overall performance of the machine and completely cancel out the benefit of CVC. Indeed, the combustion system will periodically admit fresh air and periodically release burnt gases at high pressure and temperature. Therefore all of the surrounding components will undergo the unsteadiness generated by the combustion device. A CVC system will comprise multiple combustion chambers, which will be operated with a phase shift in order to smooth the average flow rate and minimize the overall pressure and temperature fluctuations. Nevertheless, temporal and spatial variations will remain significant, especially at the turbine entrance.

In conventional turbo engines, the compressor upstream delivers a steady flow with a quasi-uniform pressure distribution to the combustion system. The stability, efficiency and flow characteristics of steady flow compressors are well known. Designing a compressor operating under imposed rotating distortion and unsteady throttling without any loss of efficiency and stability is a real challenge that must be embraced in order to make CVC possible. The same analysis applies to the turbine, which will be fed with burnt gases at high pressure and temperature at the beginning of the exhaust phase and with the compressor pressure gases at almost the temperature of the fresh air (in the worst case) at the end of the scavenging phase. As a result, the flow velocity within the turbine stages will vary a lot during a cycle, whereas the velocity of the rotor blades will remain unchanged because of the significant mechanical inertia of the compressor-turbine spool. Therefore, the incidence on the blades will vary a lot, which can generate a dramatic loss of efficiency. A turbine operating under such conditions must be carefully studied and designed, in order to preserve the full advantage of the CVC.

In addition to this specific aerodynamic behavior encountered in turbomachinery working with a CVC system, many others aspects must be carefully studied as well. For instance, the vibrations induced by the pulsating overpressures must be mastered to provide a lifetime equivalent to conventional engines. The cooling and vent systems need to be completely rethought, since the maximum pressure point is in the hot gases and no longer in the fresh gases. Integration of such a technology is as challenging as the technology itself. Up to now, knowledge of the physical phenomena involved in combustion, compression and expansion processes does not allow the gain of such a real system to be quantified. As the center of the engine concept, combustion has to be studied first.

Laboratory scale CVC chamber experimentation

During the *Thermoréacteur* [3] project, experimental work has been carried out to address combustion and ignition issues related to the CVC concept. The facility set up in PPRIME is an original combustor designed by COMAT, operating the successive phases of a CVC cycle (intake, combustion, exhaust) using rotary valves. The 0.65 L combustion chamber is downstream from a carburation chamber, followed by an outlet duct to the atmosphere (see Figure 1). The firing operation is achieved with the injection of 240 mg of

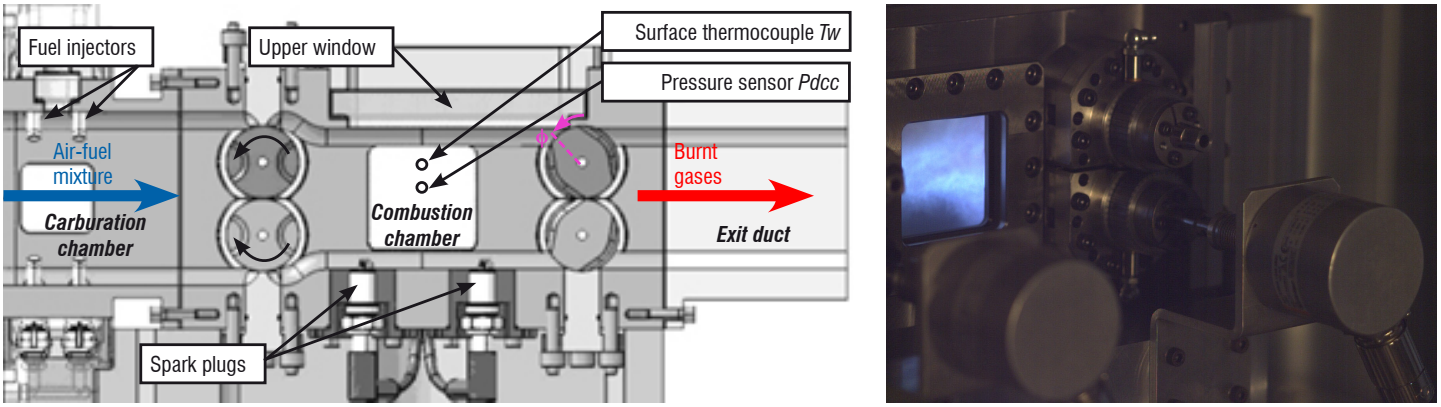

Figure 1 - Schematic diagram of the combustor and firing operation

isooctane into air at 0.3 MPa and 120°C, with a frequency of 40 Hz, $\Phi = 36°$ (phase difference between rotary valves), and ignition at intake valve closure ($\theta^* = 125°$). Flame propagation is resolved by high-speed imaging (Phantom v310, 3 kHz, 12 bit). Velocity measurements are performed using a PIV system (LaVision High-SpeedStar, 2.5 kHz).

After spark ignition, the flame propagates quickly with a stretched flame front, thus indicating a highly turbulent flow inside the chamber (see Figure 2). The flame is mainly blue, which is characteristic of a lean premixed combustion. Yellow zones appear, due to the combustion of remaining fuel droplets that have not yet completely vaporized. Overall, combustion propagates in a stratified field of velocity and composition, leading to the consumption of the charge mostly during the constant-volume phase.

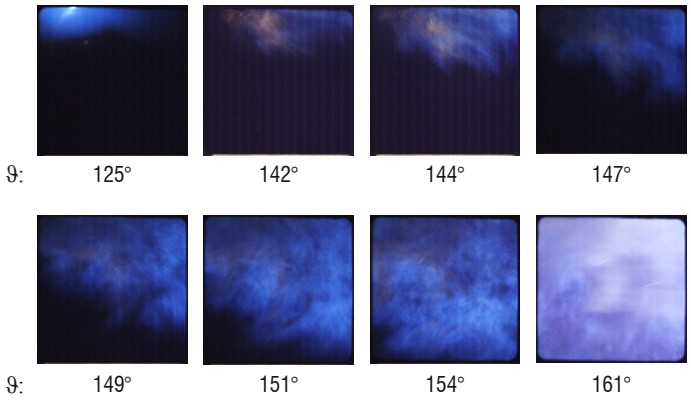

Figure 2 - Flame propagation – Ignition point C, 30 mJ, $\vartheta^* = 125°$

This operating point is also characterized by the combustion pressure (piezoelectric sensor Kistler 6125C) and wall heat flux Qw (surface E-thermocouple): see Figure 3. Average results confirm that the pressure increase due to combustion occurs mostly during the constant-volume phase, while the wall heat flux increases simultaneously due to flame-wall interaction and burnt gas convection.

The control of the air-fuel mixing is complex in this facility, because fuel injection is performed inside the carburation chamber, resulting in a "port-fuel injection" chamber. Unlike direct fuel injection, this strategy does not allow real control of the fresh charge composition before combustion. Indeed, the intake process begins with a scavenging phase, so most of the air-fuel charge is exhausted. The air-fuel mixture generated in the carburation chamber has an overall equivalence ratio of 1.18, which is measured through data processing. The fresh charge remaining inside the combustion chamber at the end of the intake is composed of air-fuel mixture, as well as residual burnt gas from the previous cycle. Therefore, the overall equivalence ratio inside the combustion chamber before ignition cannot be controlled precisely during operation, but the numerical simulation of this experiment reveals that the residual burnt gas represents up to 20% of the fresh charge [31] and varies from cycle-to-cycle. However, evaluating the local or global equivalence ratio remains a challenge due to flow unsteadiness and to the vaporization of fuel droplets, which can be incomplete, resulting in fuel deposit at the wall.

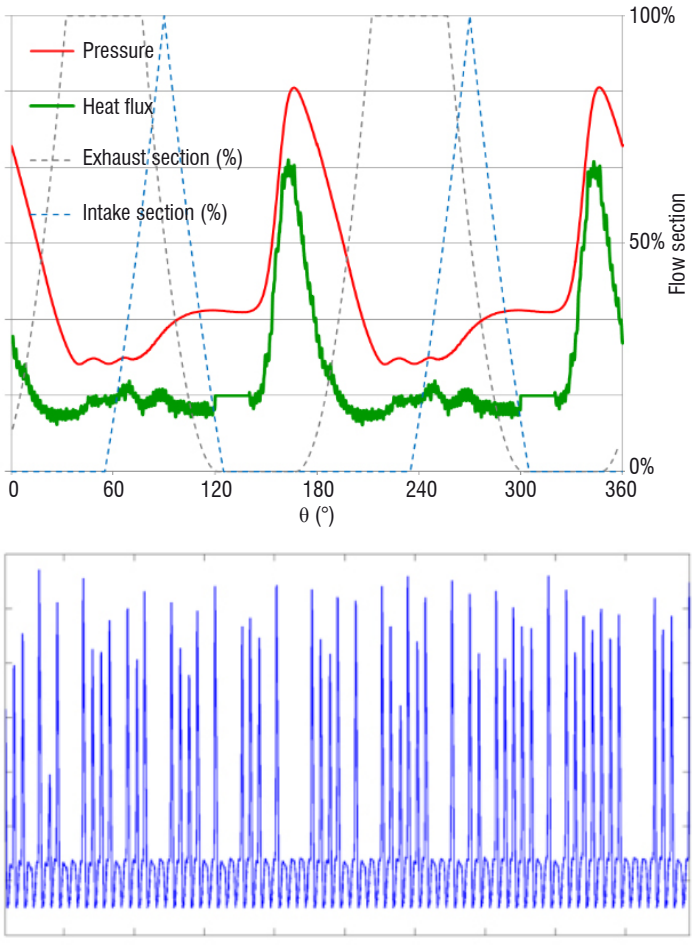

Figure 3 - Experimental signals in average (top) and successive pressure cycles (bottom) – Ignition point C, 30 mJ, $\vartheta^* = 125°$

Effect of experimental conditions on the successful operation of a CVC chamber

The efficiency of a CVC chamber requires the successful ignition of each cycle. However, experimental results demonstrate that misfires can occur, depending on ignition conditions (see Figure 3). Moreover, the pressure peaks obtained experimentally are lower than expected from ideal adiabatic isochoric combustion: this may be partially due to the wall heat loss (which is measured at a single point) but mostly due to the clearance between rotary valves, which allows the flow to exit as pressure increases during combustion. This point deserves further analysis in order to determine which phenomenon is prominent, using unsteady flow modeling for instance.

To reduce misfiring, the main solutions identified so far are to change the position of the ignition point, the ignition phasing, and the energy of the ignition discharge:

Ignition conditions	Ignition probability	Velocity V	Combustion time $t_{10\text{-}90}$ (a.u.)
$\theta^* = 125°$, point C, spark 30 mJ	65.4 %	14.7 ± 1.13 m/s	96 ±12%
$\theta^* = 135°$, point C, spark 30 mJ	100 %	11.8 ± 1.20 m/s	100 ±10%
$\theta^* = 125°$, Point F, spark 30 mJ	48.3 %	17.2 ± 1.44 m/s	85 ±18%
$\theta^* = 125°$, Point C, spark + arc 300 mJ	100 %	14.7 ± 1.13 m/s	94 ±14%

Table 1 - Effect of spark conditions on ignition success and combustion pressure

At first, ignition was located at point C, on inlet valve closure ($\theta^* = 125°$) or later ($\theta^* = 135°$), based on PIV measurements of the velocity field (see Figure 4). This additional delay allows the local flow velocity to reach a lower value, and thus suppress misfiring (see Table 1).

In order to confirm the effect of gas dynamics, the ignition point was moved from the upstream corner (point C) toward the center of the chamber (point F). Point C exhibits a higher ignition probability, thanks to a lower average flow velocity. However, when ignition succeeds at point F, the higher flow velocity leads to a substantial gain in combustion time (see Table 1). The influence of both ignition phasing and location indicates the effect of gas dynamics over the ignition and combustion processes. This shows the possible role of kernel blow-off or flame stretch due to high velocity magnitude.

Another solution to overcome misfires is to increase the spark discharge energy (30 mJ) by allowing an arc phase of higher energy (300 mJ). This result shows the effect of the discharge energy on ignition success: increasing energy prevents misfires, even at high velocity (see Table 1).

Far-seeing research imposed by CVC concept

Whatever the final concept retained to operate a Constant Volume Combustion engine (not necessarily the *Thermoreacteur*), the elementary phases encountered during the cycle (intake, mixture preparation, ignition, combustion and exhaust) recall those of the piston engine cycle, but the absence of piston motion leads to substantial differences. Therefore, the literature concerning internal flows, ignition and combustion in piston engines is very extensive, but not wholly consistent with the present cycle. The key issues indicated hereafter deserve specific investigation:

i) The intake phase involves mostly internal aerodynamics, creating a specific spectrum of flow structures from large-scale motion to turbulence.

ii) The preparation of a fresh mixture, diluted by residual burnt gases, depends on the fuel injection, the flow and temperature fields of the media influenced by molecular mixing, and the turbulent and bulk scale high-speed sheared flows that take place in such chambers.

iii) The ignition phase is a key point of pulsed combustion. Indeed, the use of fuel-lean mixtures that reduce fuel consumption and emissions, or the high flow velocity, increase the risk of misfire.

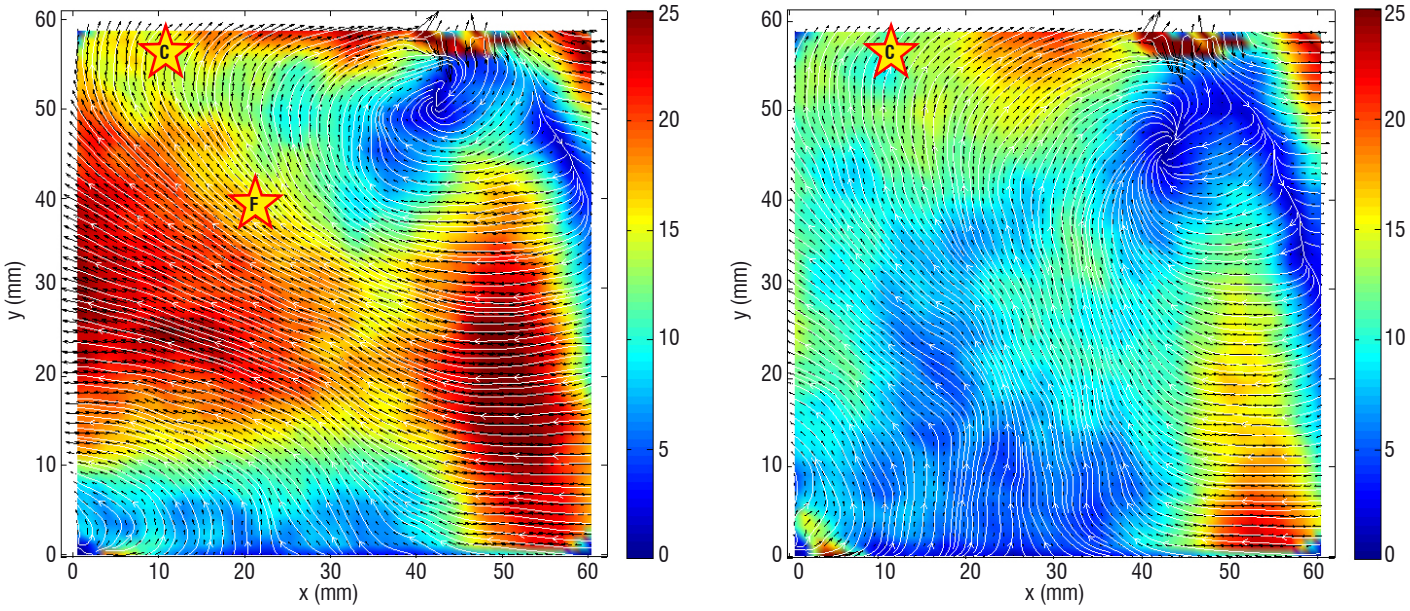

Figure 4 - Average velocity field at $\theta^* = 125°$ (left) and $\theta^* = 135°$ (right)

Thus, it is necessary to characterize the ignition conditions for jet fuels. Real thermal energy transfer to gas must be mastered and the minimum ignition energy and flammability limits of kerosene-air-diluent mixtures must be investigated. Since current aeronautic igniters are only used to start the engine, the technology used does not require a very large number of sparks to be performed like in a piston engine. Due to the pulsed combustion process implied by CVC mode, new ignition technologies should be developed to increase the lifetime of the igniter, to perform many more sparks.

iv) Finally the associated combustion regime cannot be estimated *a priori* (flamelet regime, wrinkled flamelets, thickened flames, auto-ignition, etc.) without strong control of all of the previous phenomena.

These scientific key issues, especially iii) and iv), are investigated within the framework of the CAPA Chair.

Detonation Combustion Mode for propulsion

Continuous wave detonation engine

Detonation is a combustion regime that provides an extremely rapid release of thermal energy. It is a supersonic combustion wave that generates great overpressures, about 15 to 40 times the initial pressure in gaseous reactive mixtures, and very high temperatures, up to 4000 K depending on the considered fuel and oxidizer. Thus, as regards its application to propulsion, implementing the detonation mode to replace the isobaric combustion mode in most propulsion engines represents a technological breakthrough for increasing the propulsive efficiency.

The main three detonation-based propulsive concepts that have been considered so far are the Oblique Detonation Wave Engine (ODWE), such as the RAMAC, the Pulsed Detonation Engine (PDE) and the Rotating Detonation Engine (RDE).

RDE has several important advantages over PDE: i) no complex valving or moving parts; ii) no need for repetitive detonation initiation; iii) a two-order of magnitude higher frequency (~10 kHz for RDE, ~100 Hz for PDE), hence much less noise and vibration; iv) much more uniform flow at the combustion chamber exit, without strong pressure and velocity fluctuations; v) easier integration into the propulsion system, due to the aforementioned factors and also thanks to the annular shape (unlike the tubular PDE).

The first studies on continuous detonation in an annular space date back to the 1960s. In particular, continuous detonation was the subject of many experimental and numerical studies (Zhdan *et al* 1990 [12]) conducted at the Lavrentyev Institute for Hydrodynamics (LIH, Novosibirsk). Various annular chamber geometries were considered to study the stabilization of a regime of rotating transverse detonation waves for several reactive mixtures with different sensitivity to detonation.

Recent studies on propulsion by detonation show an increasing interest in the RDE option in many countries, mainly France (Canteins 2006 [9]), Falempin *et al* 2006 [13], Falempin *et al* 2011 [14], Davidenko *et al* 2011 [15]), Japan (Hishida *et al* 2009 [16]), Uemura *et al* 2013 [17]), Poland (Kindracki *et al* 2011 [18]), China (Wang 2012 [19]), USA (Schwer and Kailasanath 2013 [20], Braun 2012 [21]), South Korea (Yi *et al* 2011 [22]), Russia (Frolov *et al* 2011 [23], Bykovskii *et al* 2009 [24]).

The operation of a RDE engine can be illustrated by considering the results of a 2D simulation with the CEDRE code (ONERA) shown in Figure 5 [30]. This simulation represents an idealized case with the following assumptions: the injection of H_2 and O_2 as gaseous propellants is fully premixed and uniformly distributed over the injection plane; the wall effects (annulus curvature, skin friction, and heat exchange), as well as the viscous effects in the flow are ignored. Nevertheless, it can be taken as a reference for more realistic simulations accounting for the aforementioned factors. This case has the following main characteristics: the domain dimensions are 50 mm by 20 mm; the injected mixture has a stoichiometric composition at a total temperature of 300 K; the mass flow rate per unit section is 100 kg/(s m^2).

The main flow features are visible in the temperature field in Figure 5a. The injection creates a layer of fresh mixture corresponding to the low-temperature zone, in which a detonation wave propagates from left to right. The injection is blocked right behind the detonation front

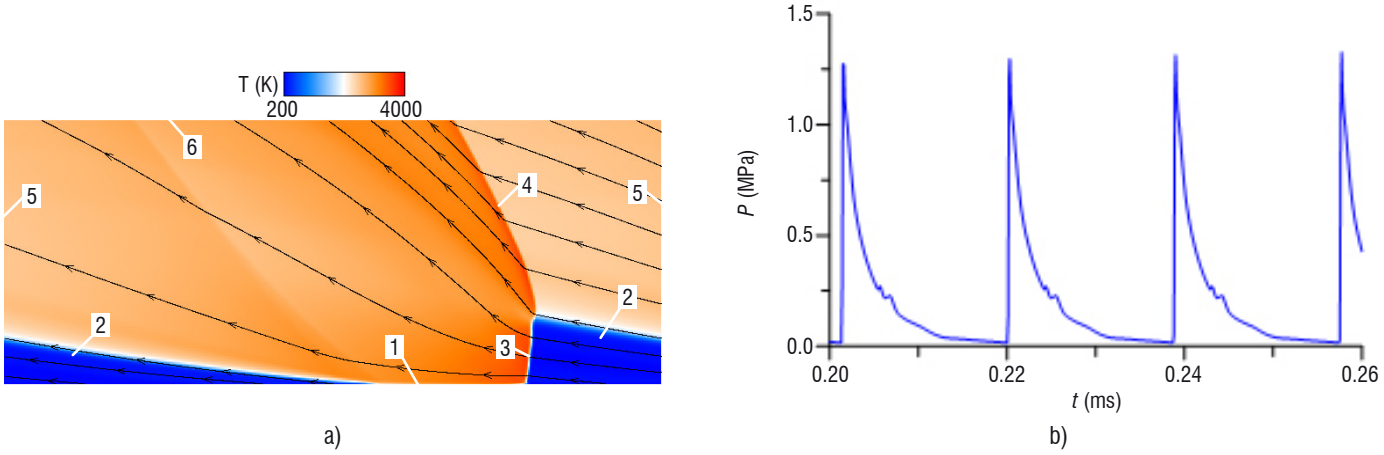

a) b)

Figure 5 - 2D simulation of a rotating detonation with distributed injection of a H_2-O_2 mixture.
a) Instantaneous temperature field with superimposed streamlines in the detonation reference frame:
1 – injection plane, 2 – fresh mixture layer, 3 – detonation front, 4 – shock front, 5 – periodic boundaries, 6 – outflow plane.
b) Pressure record at a fixed point on the injection plane; the spikes correspond to detonation passages.

by the compressed burnt gases, but the mixture is re-injected at some distance from the detonation during gas expansion. The burnt gas expansion is indicated by the streamline divergence past the detonation front, as well as by the pressure signal evolution in Figure 5b. This expansion also results in an oblique shock wave in the hot gases, which moves together with the detonation. The detonation wave propagates at a constant speed of 2670 m/s. The temporal period between detonation passages, defined by the geometric period, is less than 19 μs, which corresponds to a frequency of about 53 kHz.

Scientific key issues

The most difficult points to understand and to master are the basic physics of the propagation of the self-sustained rotating detonation in a narrow channel with the selection mechanism of the wave number and of the direction of the wave propagation. All of these dynamical features are directly related to the non-idealities present in the combustor, such as:

i) the curvature of the chamber and the width of the channel.

ii) the non-homogeneities of the initial mixture, induced by the mixing of fresh reactants in the chamber and by the mixing of fresh and burnt gases between successive detonation fronts.

These non-idealities combine in such a way that each wave front is very different from that described by the ideal Chapman-Jouguet model and that the initial mixture is strongly heterogeneous and unequally distributed in the annular chamber.

Non-ideality effects on detonation front propagation

Non-ideal propagation of detonation refers to dynamical phenomena that make detonation behaviors and properties different from those of the ideal detonation defined by the Chapman-Jouguet (CJ) model as a fully-reactive, planar and self-sustaining discontinuity wave. Detonation behaviors are often non-ideal, meaning that at least one of these three conditions is not met. The CJ detonation should thus be considered as the limiting process useful for defining reference thermodynamic states and indicating how far from ideality real detonations can be. Depending on whether the detonation regime is to be used or avoided, the fundamental problems are to determine sufficient conditions to obtain a quasi-CJ regime, and those that prevent detonation from propagating non-ideally.

In the context of using detonation as a combustion process for propulsive devices, the studies should thus address two objectives. The first is to determine the minimum size and the optimum shape of the combustion chamber, so detonation propagates as a quasi-CJ wave. The second is to develop robust low-energy ignition devices capable of generating detonation within characteristic times and lengths much shorter than those of the detonation propagation in the chamber. These objectives should be met for large ranges of mass flow rates and initial pressures.

Non-ideal detonation dynamical phenomena can be categorized into two groups. The first gathers global behaviors induced by initial and boundary or geometric conditions that lead to an incomplete combustion process in the detonation reaction zone. They result essentially from the adiabatic losses due to divergence of the reactive flow. Their most visible effect is a curved detonation leading shock, at the scale of the reaction zone thickness. The main consequence is the existence of critical sizes for detonation, such as minimum radii for diverging spherical detonations, minimum thicknesses for semi-confined detonations, etc. Indeed, adiabatic losses compete with heat production in the reaction zone, and too large losses lead to detonation quenching. The second group refers to local behaviors induced by the intrinsic instability of the reaction zone, which cause the reactive flow to have a specific three-dimensional cellular structure. This cellular instability results from the high sensitivity of the chemical reaction rates to very small state fluctuations, essentially that of temperature. The main consequence is that, close to the propagation limits, detonation has strongly unsteady and three-dimensional behaviors. Global and local dynamical behaviors often combine, and analyzing detonation dynamics can be a difficult task.

The simplest relevant picture of detonation is a shock followed by a high-pressure, high-temperature zone of chemical reactions triggered by this shock (Crussard, Zel'dovich, Von Neuman, Döring, ZND). Long enough after ignition, detonation reaches a self-sustaining propagation regime, such that the dependency domain of the leading shock is limited to all or part of the reaction zone. The whole flow behind the shock expands and two domains should be distinguished. The closest to the shock consists of most of the reaction zone and sustains this shock. The other is essentially made up of burnt products and does not sustain the shock. The separation boundary propagates with the local velocity of the acoustic perturbations (the "sonic surface").

Self-sustaining regimes result from a balance between the production of chemical energy, triggered by the leading shock, and the losses induced by the adiabatic expansion of the reactive flow behind the shock. Balance exists only if the sonic head of the release wave is far enough away from the shock for energy production to be high enough to counteract adiabatic cooling. For the planar self-sustaining detonation, the sonic head of the release wave is located at the end of the reaction zone (except for "pathological" reactive mixtures), because all of the chemical energy is produced between the shock and the release-wave head. This is the Chapman-Jouguet (CJ) detonation, which thus propagates with the maximum velocity D_{CJ}. For curved self-sustaining detonations, the sonic head of the expansion wave is located slightly before the end of the reaction zone. Such quasi-CJ detonations thus propagate with velocities smaller than D_{CJ}, since a small part of the available chemical energy is lost out of the shock dependency domain. Too large expansions cause too much energy to be lost, balance between energy production and adiabatic losses cannot be achieved, and too strongly curved detonations cannot be self-sustaining. This explains the global dynamical behaviors of detonation.

The CJ model gives the ideal detonation velocity D_{CJ} and the properties (p_{CJ}, T_{CJ}, etc.) at the reaction-zone end of the self-sustaining, planar detonation. The Taylor-Zel'dovich (TZ) model describes the expanding unsteady flow beyond this reaction zone. The ZND model complements the CJ model with a one-dimensional steady description of the flow in the reaction zone. These 3 models are the minimum necessary set of calculations for determining relevant detonation properties and characteristic chemical lengths and times. However, neither of the CJ, TZ and ZND models can provide information on conditions for detonation propagation or existence, which can only be assessed by considering non-idealities. Estimating detonation properties and efficiency by means of the CJ and TZ models is physically relevant only if the ZND characteristic lengths and times are much shorter than those of the non-idealities.

The CJ properties are obtained from thermochemical calculations, they only depend on the composition of the combustion products at chemical equilibrium (the "energetic content"), and on the initial pressure and temperature of the considered mixture. The ZND reaction profiles and evolutions are obtained by solving the one-dimensional steady balance laws coupled with a chemical kinetics scheme. The TZ flow beyond the reaction zone can also be simply obtained. In particular, the pressure that is applied on a rigid wall where a CJ detonation would have been ignited is about $p_{CJ}/3$.

However, chemical reaction rates in gases are very sensitive to small temperature fluctuations at the detonation leading shock, so the ZND reaction zone is unstable. Experiments show that gaseous detonation fronts have a complex three-dimensional unsteady structure made up of shock and combustion waves with transverse and longitudinal motions. A cut of the flow shows that the interaction points between longitudinal and transverse waves draw diamond-shaped patterns as detonation propagates. These patterns are called detonation cells and can be easily recorded experimentally by means of soot-covered steel foils inserted parallel to the main propagation direction of detonation, (the very large pressures at the interaction points erode the soot, e.g., Figures 6 and 7). Cells are more or less regular depending on the mixture, but an average width has been often considered for sake of analysis. Measured average widths λ have thus been observed to correlate with a ZND chemical characteristic length Lc and with the initial pressure p_0 of the mixture. Many experiments thus show that $\lambda = k\,Lc$ ($k \sim 15$-30) and that $\lambda = A\,p_0^{-n}$. Thus, the larger the detonation velocity or the higher the initial pressure, the smaller the characteristic chemical length and the smaller the detonation cell. Also, a large body of experimental results indicates that the capacity of a mixture to accept the detonation regime is defined by the average cell width λ compared to the transverse dimension of the detonation set-up. Robust experimental correlations bind the cell width λ to so-called dynamical parameters of detonation. These are the minimum energy for direct initiation of detonation, the minimum radius for the existence of self-sustaining diverging detonation, the minimum tube diameter for detonation transmission into a large volume and, to some extent, the deflagration-to-detonation transition length.

For example, a self-sustaining detonation in a channel can propagate close to the ideal CJ or ZND conditions only if the channel transverse dimension (e.g., the tube diameter) is at least about equal to 1/3 – 1/2 the average cell width for the considered initial pressure and temperature. If not, only so-called marginal modes of detonation propagation can be observed, or no detonation at all. Marginal detonations are very unstable, fully three-dimensional, with a limited number of transverse waves on the front surface. In contrast, a self-sustaining diverging spherical detonation propagates only if the local detonation radius is large enough compared to the detonation cell width, i.e., $Rc \sim 20$-40 λ. A CJ detonation propagating in a finite-diameter tube can be transmitted to a larger volume only if the tube-diameter is about at least 10 λ. For more complicated geometries, scaling laws relating the characteristic lengths of the system to the cell width can be obtained. Determining the cell width λ as a function of the initial pressure and temperature of the mixture is therefore the fundamental prerequisite for sizing a device meant for using or avoiding detonation. The CJ and ZND models must be viewed as describing the average properties of multi-front cellular detonations, i.e., detonations that propagate under geometry or confinement conditions compatible with a sufficiently large number of cells on the front.

To date, the capacity of a mixture to accept the detonation regime in a given system (geometry, size, etc.) can be assessed only by means of experiments. The key point is that detonation dynamics is self-similar with respect to the cell mean width. A typical methodology is thus to carry out experiments in small-scale systems, with initial pressure and temperature compatible with the identification of the dynamics and the limiting conditions for detonation. Then, after the coefficients of the scaling laws $\lambda = k.Lc$ and $\lambda = Ap_0^{-n}$ are obtained, extrapolation can be used to anticipate detonation behaviors for larger systems or other initial pressures and temperatures.

Figure 6 shows supercritical and critical detonation transmission through a curved channel from a straight one with the same square section, and detonation quenching when the channel is too curved. Supercritical transmission (Figure 6, left) is the case of a channel curvature that does not influence detonation propagation. The soot foil shows that the cell mean width is practically the same in the straight and curved parts of the channel. Critical transmission (Figure 6, center) is the situation for which channel curvature influences detonation propagation, but not sufficiently to prevent detonation transmission. The soot foil indicates that the cell mean width increases very rapidly from the point on the inner face of the channel where bending begins and detonation starts undergoing lateral expansion. Detonation then keeps curving and decelerating, mean cell width increases, and successive detonation quenchings and re-initiations induced by transverse shock reflections at the channel faces can be observed. However, detonation survives all along the curved channel length. The sub-critical case (Figure 6, right) is the situation for which channel curvature is too strong, and detonation eventually quenches despite a few attempts of re-initiation in the form of marginal detonations. This is an example of interplay between global curvature effects induced by the system boundaries, and local dynamical behaviors, from a multi-cellular front to marginal propagation and quenching.

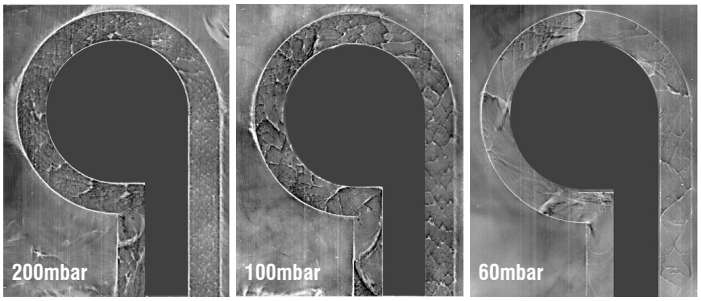

Figure 6 - Detonation dynamics in a curved channel.
Left: supercritical transmission. Center: critical transmission.
Right: quenching (Florian Gineste, 2015)

Figure 7 shows the dynamics of a detonation in a mixture with a non-uniform distribution of composition in a square-section channel. The gradient of initial composition is oriented in the propagation direction of detonation (from left to right). Before entering the variable initial-state part of the channel, the detonation has been travelling a large distance in a uniform stoichiometric composition, which smoothly becomes non-uniform and leaner from the left of the soot foil. The detonation dynamics then depend on how rapidly the initial composition changes. The case of an abrupt change is given in Figure 7, top. The leftmost part of the soot foil shows that detonation cells have a practically constant mean width much smaller than the channel width and about equal to that associated with the CJ detonation in the initial stoichiometric composition. After about one third of the channel length, cells increase very rapidly and disappear before half of the

length. In this strong-gradient situation, detonation quenches suddenly by means of a shock-flame decoupling mechanism. The case of a gradual composition change is given in Figure 7, bottom. The soot foil shows that the detonation cell mean width increases smoothly from its CJ value to values close to that of the channel width at about one third of the foil. A smooth transition from the multi-cell propagation mode to marginal propagation modes then takes place, with a very limited number of transverse waves. The transverse-wave number decreases as detonation propagates rightward in leaner compositions. In this weak-gradient situation, detonation quenches gradually by means of a smooth mechanism of transition from the quasi-1D, quasi-CJ multi-cell propagation mode to fully-3D unsteady marginal modes. This is an example of interplay between global effects from system boundaries and the local marginal propagation modes induced by changes in the initial composition.

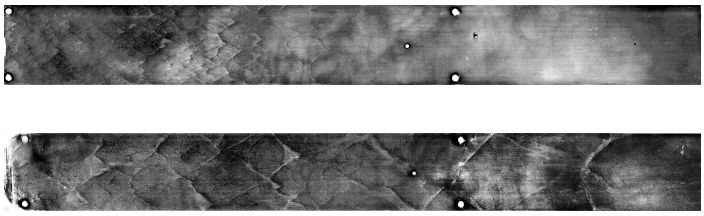

Figure 7 - Detonation quenching in a non-uniform composition contained in a square-section channel. Top: strong gradient. Bottom: weak gradient (Stephane Boulal, 2015)

Injector studies and RDE simulations with realistic injection conditions

Studies currently conducted at ONERA are aimed at applying rotating detonation to rocket propulsion, which is the most straightforward for the following reasons: i) the propellant mixture is concentrated and can easily detonate under the chamber conditions; ii) the engine mainly operates on a stable regime without strong variation of the global equivalence ratio and the chamber pressure; iii) integration of a detonation chamber in the engine architecture is not a critical point. In these studies, most attention is focused on the propellant injector because it is the key element of a detonation chamber.

Previous experimental and numerical studies have demonstrated RDE operation with various injector configurations, but the injector design was not a central point. Contrary to most known numerical simulations, in which fully premixed injection is mainly considered, propellants are always injected separately in the experiments for safety reasons.

At ONERA, we study various injector designs suitable for separate injection of gaseous propellants, trying to meet the following main requirements: i) fast and uniform propellant mixing; ii) limited pressure losses; iii) quick and efficient refilling of the chamber without excessive contact with burnt gases; iv) technological feasibility. The injector is assumed to be composed of a large number of identical injection elements regularly distributed over its face, as illustrated in Figure 8.

A special methodology has been devised enabling a single injection element to be analyzed, in order to model the operation of the entire injector. As the domain of interest is drastically reduced, large eddy simulations (LES) of the injected flow can be performed with fine resolution and at affordable cost. Thus, various geometrical configurations can be compared, in order to identify the optimum one.

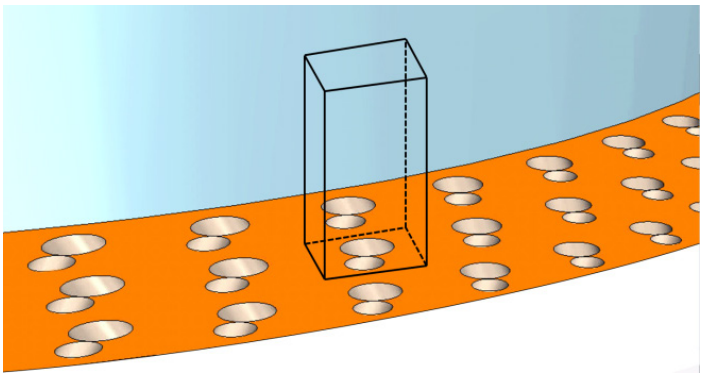

Figure 8 - Injection elements arranged in a regular pattern on the injector face. Black frame delimits a part of the chamber volume associated with a single injection element.

Using this methodology, a parametric study was first carried out by modeling the established injection of H_2 and O_2 in stoichiometric proportion [29]. By analyzing the simulated turbulent flow-fields, it was possible to identify the most efficient interaction between a pair of propellant jets, on the one hand, and the neighboring injection elements, on the other hand, providing the highest mixing efficiency.

As a second step, a transitory refill process after the detonation passage was simulated for a single injection element using a specific computational procedure [30], which enabled the mixture formation to be analyzed in detail and quantitatively characterized over time during the refill.

Since the latest publications [29]-[30], significant progress has been achieved in improving the injection element design. For the new injector design, a transitory refill process is illustrated in Figure 9, by LES results. The initial condition at $t = 0$ is obtained just after a detonation propagating in a uniform layer of fresh mixture. The development of a jet of fresh mixture during the gas expansion in the chamber is shown every 20 μs. Figure 9 shows the isothermal surface of 400 K surrounding the region filled with injected propellants, whereas its color indicates the mixture quality. Zero quality corresponds to fully unmixed propellants and unity corresponds to a stoichiometric composition not diluted by burnt gases. One can see that the propellants, being unmixed at the injector outlet, quickly mix in the chamber and occupy the volume attributed to the injection element at a short distance from the injector face. Zones of high mixture quality are observed from the very beginning of jet development, which means that the injection element operation is efficient during the whole refill process.

The final step in the injector design evaluation consists in rotating detonation simulation with many injection elements. In order to allow comparison with the idealized 2D simulation shown in Figure 9, the same main conditions are used in 3D simulations with 21 injection elements set in one row along the injection plane. Computational results from these simulations are presented in Figure 10, through the temperature fields in a mid-plane. Backflow is simulated in the admission lines but it cannot be shown for confidentiality reasons. The blocking time of the injection by the detonation products expansion represents up to 25% of the refill period. The first field shown in Figure 10a corresponds to the injection of a homogeneous premix of H_2 and O_2 in stoichiometric proportion. With respect to the 2D case, the mixture layer is no longer continuous, but rather composed of propellant jets surrounded by burnt gases. The jets have a slightly greater height than the 2D layer at the detonation front.

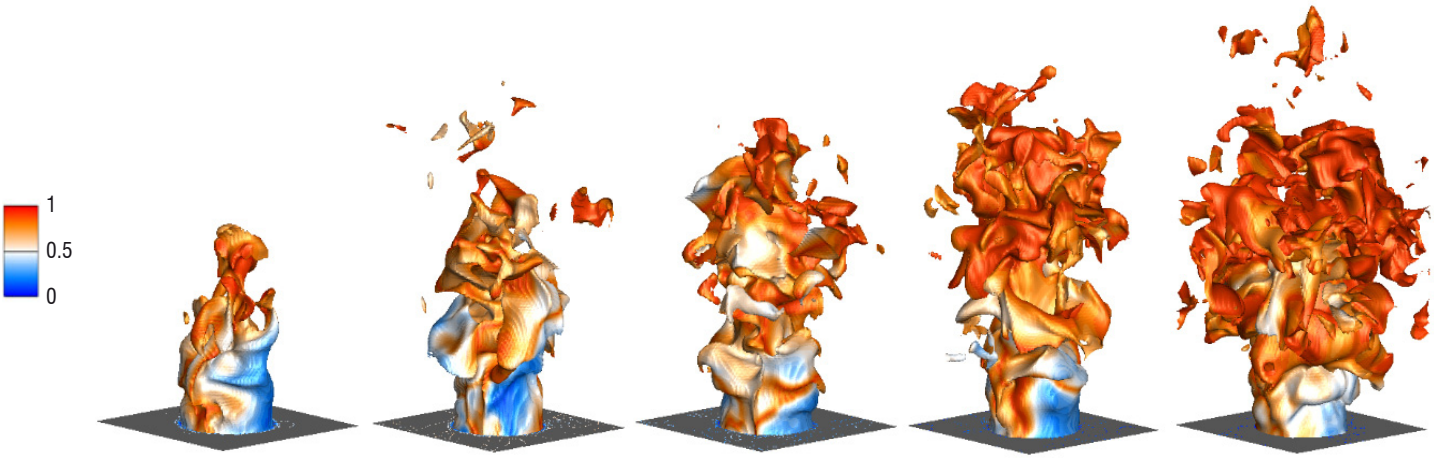

Figure 9 - Reinjection of the H_2-O_2 mixture after a detonation passage at different time instants: a) 20 μs ; b) 40 μs ; c) 60 μs ; d) 80 μs ; e) 100 μs. Isothermal surfaces of 400 K colored by mixture quality.

The detonation front is more perturbed as it propagates in a non-homogeneous layer and these perturbations produce a sequence of acoustic waves in the burnt gases, as can be seen in the field. This is not a realistic case because of the premixed injection, contrary to the second field shown in Figure 10b, which corresponds to the separate injection, keeping the global mass flow rates of H_2 and O_2 unchanged. Two main differences are observed between premixed and separate injection: the detonation front becomes more perturbed, as well as the whole flow-field; due to imperfect mixing in the jets, propellants are not completely burned by the detonation, but partially remain in small cold pockets that progressively dissipate and burn in the hot gases.

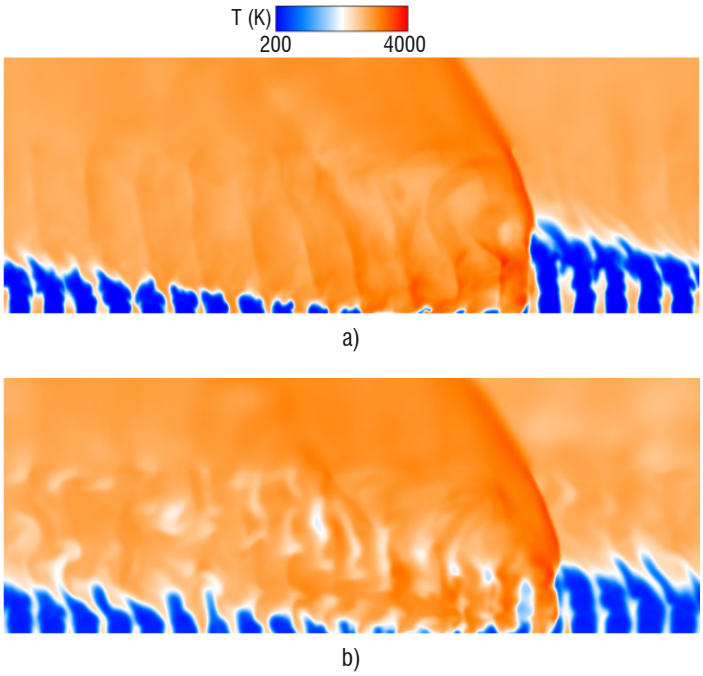

Figure 10 - Instantaneous temperature fields in a mid-plane from 3D simulations of a rotating detonation with 21 injection elements in a row: a) fully premixed injection, b) fully separate injection.

These are the very first results of 3D simulations with an improved injector design and realistic injection conditions. An important step towards an operational RDE design has been made compared to the simplified injection approach. Future studies include the evaluation of mixture heterogeneities to determine its effect on the detonation velocity and the chamber pressure, for instance.

Laboratory scale experimentation of rotating detonation

In the propulsion context, an experimental RDE device was designed and has been operated at PPRIME since 2003, within the framework of a feasibility project supported by CNES [9]. The experimental investigations led to the observations of the simultaneous stable rotation of 1 to 8 reactive fronts, depending on the injection conditions and the geometrical configurations. The global propulsive performance at sub-atmospheric and atmospheric pressures was evaluated on the basis of thrust and specific impulse measurements.

The RDE feasibility having been demonstrated, the current work is aimed at achieving a better understanding of the physics governing the complex flow field in an annular chamber and at providing the type and level of propulsive performance generated. Various RDE devices are currently under study.

In the first RDE device, the annular chamber currently being tested has an injection system enabling mass-flow rate operation up to 100 g/s. The inner diameter d_i of the chamber is 50 mm, with a channel width e of 10 mm. These new scales lead to a maximum specific mass flow rate, about 53 kg/(s m^2), which is close to the conditions used in several existing RDE chambers [10]. This experimental investigation is focused on the effect of the ratio (e/λ) on the detonation regime by varying the width λ of the detonation, since the width e of the annular chamber is maintained constant. The injection properties are

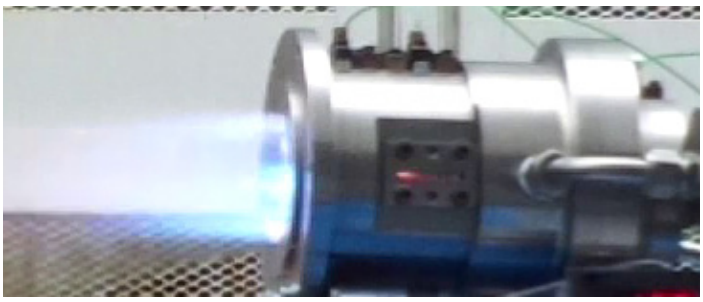

Figure 11 - Test in annular chamber

characterized by the mass-flow rate, equivalence ratio and pressure. The first results obtained with $C_2H_4/O_2/N_2$ stoichiometric mixtures with total mass flow rate of about 80 g/s show (Figure 11).

For a N_2 dilution corresponding to an oxidant composition with 30% of N_2, a deflagration is observed; the detonation cell size is about 10 mm. The ratio e/λ is lower than one.

For a N_2 dilution corresponding to an oxidant composition with 50% of N_2, a propagation of a reactive front is obtained with a main velocity of 1100 m/s. In this case, the width of the detonation cells is around 3 mm, the ratio e/λ is greater than one and $d_i < d_{min}$, where dmin is the minimum diameter given by dmin = 40λ and allowing steady detonation propagation [9].

The modular design of the second RDE device enables a large parametric study with a maximum mass-flow rate of 300 g/s to be carried out. These parameters concern the inner diameter d_i, the channel width e, various fuels and oxidizers, and the geometry of the injectors and nozzles.

Operational applications of RDE

For more than 12 years, MBDA has been actively developing technologies related to PDE and has led several R&T efforts in cooperation with French, Russian and Singaporean research institutions [13]. These efforts have been focusing on both rocket and airbreathing modes. Within the framework of this work, some specific studies have been performed to numerically simulate the DDT (deflagration to detonation) process in a pre-detonation tube; experimental work has been performed in cooperation with DSO (Singapore) and numerical results have been confirmed. This background has been used to design an operational ignition device for a RDE and has led to the development and demonstration of an efficient device (Figure 12).

From 2002 to 2012, the objectives were to better understand RDE operation and address some key issues for an actual use as part of

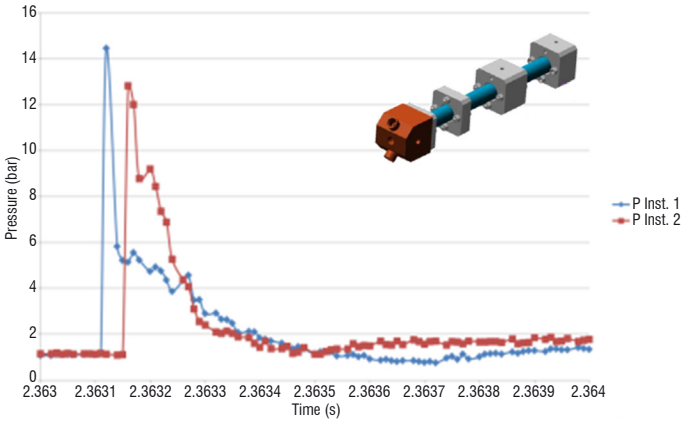

Figure 12 - Time evolution of the pressure at two points of the ignition device of an actual RDE

a propulsion system (Figure 13). This effort was mainly focused on the rocket mode, but some dedicated actions were taken with regard to airbreathing systems, including preliminary assessment of NOx production. A preliminary feasibility study of thermostructural composite fuel-cooled structure has been performed and some experiments in an actual detonation chamber have led to concluding results [26]. One specific characteristic of the RDE was also demonstrated during this program: the self-adaptation of the detonation to the fresh mixture local mass flow made it possible to achieve thrust vectoring by locally changing the injected mass flow rate (Figure 14).

Based on these studies and considering the growing interest shown around the world for the concept of RDE, a subscale demonstration engine was designed and manufactured in 2011 with the support of the Airbus Group Nursery [27]. This small demo was aimed, as a first step, at replicating experimental works performed at LIH. However, as a second step, it allowed enabled the test duration to be extended and the testing of the detonability of the H_2/CH_4 mixture. The

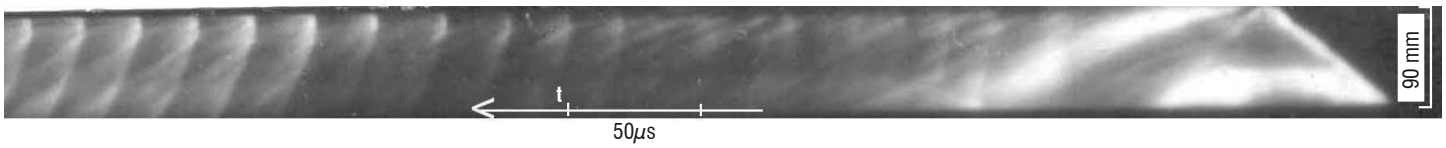

Figure 13 - Typical example of a high speed image acquisition done by LIH during RDE testing

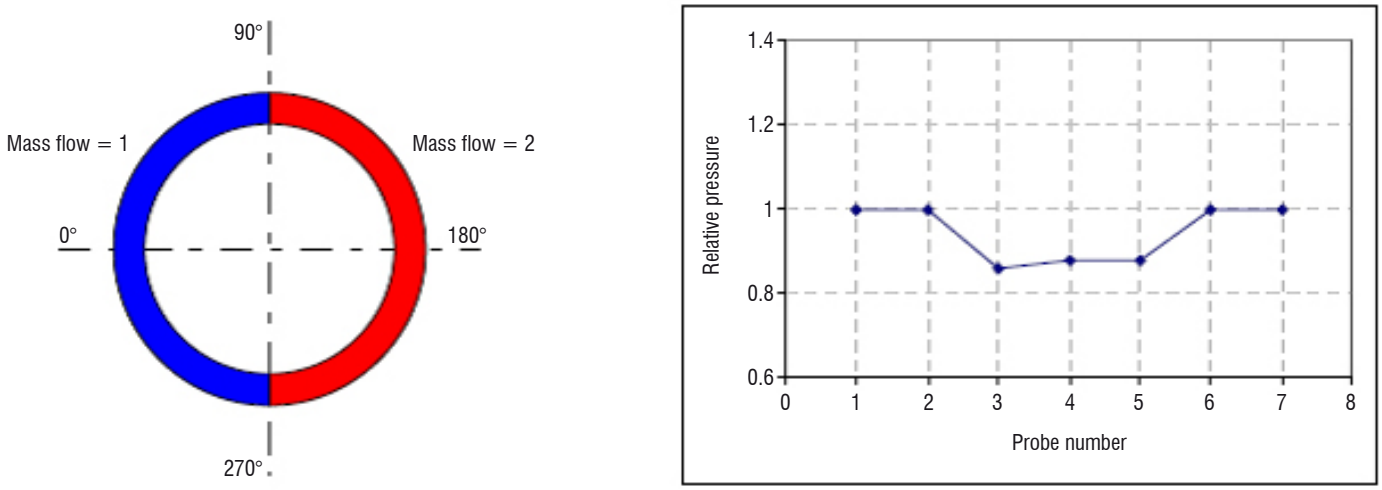

Figure 14 - Pressure evolution along the RDE circumference when varying the injected mass flow on each half of the chamber [24]

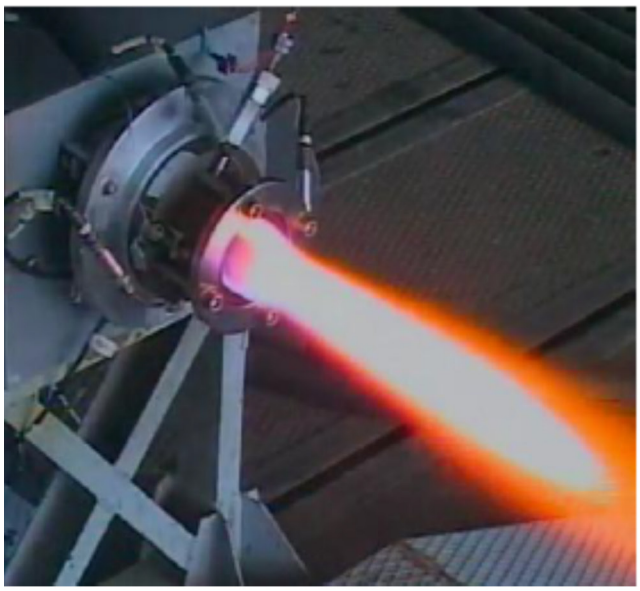

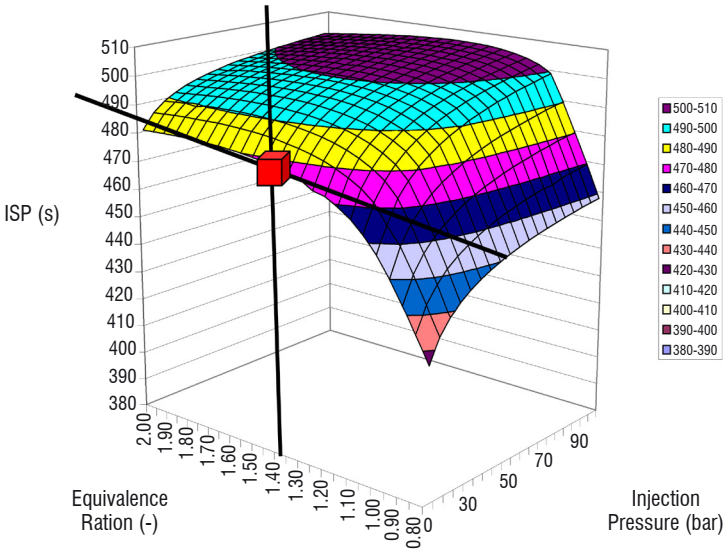

Figure 15 - RDE testing at MBDA and comparison of the test result (red cube) with the numerical prediction

annular chamber of the engine has inner and outer diameters of 80 mm and 100 mm. The test bench was equipped with force transducers enabling the thrust produced by the chamber when the detonation regime is established (Figure 15) to be measured.

The results were in line with theoretical estimations and helped to validate its in-house numerical models for the operation of a RDE. These models (0D, 1D and 2D) are daily used by MBDA to estimate performances and to design some future operational systems based on this new promising way of propulsion.

Today, based on several own patents related to RDE and with support from European FEDER funds and from Airbus Group Nursery, MBDA is developing a large scale test bench at Bourges-Subdray, dedicated to RDE.

Conclusion and perspectives

A huge reduction in the fuel consumption of future propulsive engines is an ambitious target set by the ACARE for 2050. Such a gain could be achieved only with a technological breakthrough. Two of the possibilities have been considered and are being investigated experimentally and numerically by MBDA France, ONERA, PPRIME and SAFRAN. Changing the actual thermodynamical cycle through Constant Volume Combustion or rotative detonation concepts could theoretically enable the target to be achieved.

To date, knowledge of the basic physical phenomena involved during combustion does not allow the potential profit of real propulsion engine using CVC or RDE combustion chamber to be quantified with good accuracy. Based on the first studies performed on specific prototypes by partners, for both CVC and RDE, the need for fundamental and basic research developments has been identified. Indeed, implementing such a concept requires the understanding and control of several basic phenomena that will jointly exist in a real engine, such as: the mixing process, ignition, dilution by residual burnt gas, and nonidealities. All of these phenomena must be considered under high-flow velocity and non-stationary conditions, whatever the concept (CVC or RDE). The combination of studies on elementary processes like the curvature effect on detonation dynamics, and on a reduced-scale or full-scale prototype, enables us to understand and model physical phenomena and highlight the potentialities of such concepts. The work carried out within the framework of the Chair CAPA, which started in 2015 for a period of 4 years, fulfills these main objectives.

Finally, in order to evaluate the final benefit of such concepts, integration tests should be performed considering a full engine composed of a compressor, a combustion chamber and a turbine when an air-breathing engine is considered, or a combination of a combustion chamber and a nozzle when a rocket application is targeted ■

Acknowledgements

The authors wish to thank all partners, and acknowledge the financial support of agencies during the programs:

- Chair CAPA: research program on Alternative Combustion Modes for airbreathing Propulsion supported by SAFRAN Tech, MBDA France and ANR (National Research Agency)
- RAPID *Thermoréacteur*: research program on Constant-Volume Combustion supported by the DGA in collaboration with COMAT and Turbomeca

References

[1] E. Wintenberger, J.E. Shepherd - *Thermodynamic Cycle Analysis of Propagating Detonations*. Journal of Propulsion and Power, Vol. 22: 694-698, 2006.

[2] Industrial Chair CAPA, www.agence-nationale-recherche.fr/?Projet=ANR-14-CHIN-0003, 2014.

[3] M. Bellenoue, B. Boust, L. Herrero, G. Taliercio - *Rapport final Thermoréacteur*. DGA RAPID project, 2014.

[4] B. Bobusch, P. Berndt, C.O. Paschereit, R. Klein - *Shockless Explosion Combustion: an Innovative Way of Efficient Constant Volume Combustion in Gas Turbines*. Combustion Science and Technology, Vol. 186: 1680-1689, 2014.

[5] D. Rancourt, M. Picard, M. Denninger, J. Chen, A. Yousefpour, J.-S. Plante - *A High Power Density Rim-Rotor-Rotary Ramjet Engine Part 1: Structural Design Proof of Concept*. Journal of Propulsion & Power, vol.28, pp.1293-1303, 2012.

[6] M. Picard, D. Rancourt, J.-S. Plante, M. Brouillette - *A High Power Density Rim-Rotor-Rotary Ramjet Engine Part 2: One-Dimensional Aerothermodynamic Flow Design*. Journal of Propulsion & Power, vol.28, pp.1304-1314, 2012.

[7] J. Wilson, G.E. Welch, D.E. Paxson - *Experimental Results of Performance Tests on a Four-Port Wave Rotor*. NASA/TM 2007-214488, 2007.

[8] P. Akbari, R. Nalim, N. Mueller - *A Review of Wave Rotor Technology and its Applications*. Journal of Engineering for Gas Turbines and Power Vol. 128: 717–735, 2006.

[9] G. Canteins - *Étude de la détonation continue rotative. Application à la propulsion*. PhD thesis, Université de Poitiers, 2006.

[10] F.A. Bykovskii, S.A. Zhdan, E.F. Vedernikov - *Continuous Spin Detonation of Hydrogen-Oxygen Mixtures. 1. Annular Cylindrical Combustors*. Combustion, Explosion, and Shock Waves, Vol. 44: 150-162, 2008.

[11] F.A. Bykovskii, S.A. Zhdan, E.F. Vedernikov - *Continuous Spin Detonations*. Journal of Propulsion and Power, Vol. 22: 1204-1216, November 2006.

[12] S.A. Zhdan, A.M. Mardashev, W. Mitrofanov - *Calculation of the Flow of Spin Detonation in an Annular Chamber*. Combustion, Explosion and Shock Waves, vol. 26(2), pp. 210–214, 1990.

[13] F. Falempin, E. Daniau, E. Getin, F. Bykovskii, S. Zhdan - *Toward a Continuous Detonation Wave Rocket Engine Demonstrator*. AIAA Paper, 2006.

[14] F. Falempin, B. Le Naour, F. Miquel - *Recent Experimental Results Obtained on Continuous Detonation Wave Engine*. AIAA Paper, 2011, 2235

[15] D. Davidenko, Y. Eude, I. Gokalp, F. Falempin - *Theoretical and Numerical Studies on Continuous Detonation Wave Engines*. AIAA Paper, 2011.

[16] M. Hishida, T. Fujiwara, P. Wolanski - *Fundamentals of Rotating Detonation*. Shock Waves, 2009, volume 19.

[17] Y. Uemura, A. Koichi, A.K. Hayashi, M. Asahara - *Transverse Wave Generation Mechanism in Rotating Detonation*. Proceedings of the Combustion Institute, 2013, Volume 34, Issue 2, pp 1981–1989.

[18] J. Kindracki, P. Wolanski, Z. Gut - *Experimental Research on the Rotating Detonation in Gaseous Fuels-Oxygen Mixtures*. Shock Waves , 2011, Volume 21, Issue 2, pp 75-84.

[19] J.P. Wang - *Numerical and Experimental Study on Continuously Rotating Detonation Engine at Peking University*. DWP 2012.

[20] D. Schwer, K. Kailasanath - *Fluid Dynamics of Rotating Detonation Engines with Hydrogen and Hydrocarbon Fuels*. Proc. the Combustion Institute, 2013, Volume 34, Issue 2, pp 1991–1998.

[21] E.M. Braun - *New Concept for Propulsion and Power Generation*. 2012, PHD, Univ. of Texas at Arlington.

[22] H. Yi, J. Lou, C. Turangan, J.Y. Choi, P. Wolanski - *Propulsive Performance of a Continuously Rotating Detonation Engine*. Journal of Propulsion and Power, (2011) vol. 27, no. 1, pp. 171-181.

[23] S.M. Frolov, V.S. Ivanov, A.V. Dubrovskii - *Transient 3D Simulation of Hydrogen – Air Rotating Detonation Engine with the Emphasis to Fuel Injection and Heat Transfer Phenomena*. DWP 2011.

[24] B.A. Bykovskii, S.A. Zhdan, E.F. Vedernikov - *Realization and Modeling of Continuous Spin Detonation of a Hydrogen–Oxygen Mixture in Flow-Type Combustors. 2. Combustors with Expansion of the Annular Channel*. Combustion, Explosion, and Shock Waves, Vol. 45, No. 6, pp. 716–728, 2009.

[25] F. Falempin, B. Le Naour - *R&T Effort on Pulsed and Continuous Detonation Wave Engines*. AIAA 2009-7284 - 16th International Space Planes and Hypersonic Systems and Technologies Conference, 2009.

[26] E. Daniau, F. Falempin, S. Zhdan - *Pulsed and Rotating Detonation Propulsion Systems : First Step Toward Operational Engines*. AIAA 2005-3233 – 13th International Space Planes and Hypersonic Systems and Technologies Conference, 2005.

[27] B. Le Naour, F. Falempin, F. Miquel - *Recent Experimental Results Obtained on Continuous Detonation Wave Engine*. AIAA 2011-2235 – 17th AIAA International Space Planes and Hypersonic Systems and Technologies Conference, 2011.

[28] D. Davidenko, Y. Eude, I. Gökalp, and F. Falempin - *Theoretical and Numerical Studies on Continuous Detonation Wave Engines*. AIAA Paper 2011-2334 – 17th AIAA International Space Planes and Hypersonic Systems and Technologies Conference, 2011.

[29] T. Gaillard, D. Davidenko, F. Dupoirieux - *Numerical Study of Injection and Mixing Suitable for Rocket Operation in the Continuous Detonation Mode*. Acta Astronautica, Vol. 111: 334-344, 2015.

[30] T. Gaillard, D. Davidenko, F. Dupoirieux - *Numerical Investigation of an Unsteady Injection Adapted to the Continuous Detonation Wave Rocket Engine Operation*. 6th EUCASS, 2015.

[31] L. Labarrère, T. Poinsot, A. Dauptain, M. Bellenoue, B. Boust - *Experimental and Numerical Study of Cyclic Variations in a Constant Volume Combustion Chamber*. Submitted to Combust. Flame, 2015.

List of acronyms

CJ	(*Chapman-Jouguet)*
CPC	(*Constant-Pressure Combustion*)
CVC	(*Constant-Volume Combustion)*
CWDE	(*Continuous Wave Detonation Engine)*
PDE	(*Pulsed Detonation Engine)*
RDE	(*Rotating Detonation Engine)*

AUTHORS

Marc Bellenoue graduated from the *École Nationale Supérieure de Mécanique et d'Aérotechnique* (ISAE-ENSMA - French engineering school specialized in space and aeronautics) in 1992 and received his PhD in Fluid Mechanics and Combustion from the University of Poitiers in 1997. Professor at ISAE-ENSMA since 2005 (Combustion and Propulsion). Head of the CAPA Chair dedicated to the Alternative Combustion mode for Airbreathing Propulsion and funded by ANR, SAFRAN Tech and MBDA France. His research interests include experimental investigations on the advanced combustion mode for propulsion (mixing process, ignition, extinction, flame-wall interaction, combustion propagation).

Bastien Boust graduated from the *École Nationale Supérieure de Mécanique et d'Aérotechnique* (ISAE-ENSMA - French engineering school specialized in space and aeronautics) in 2003 and received his PhD in Fluid Mechanics and Combustion from the University of Poitiers in 2006. Research Engineer in PPRIME combustion department since 2006. His research interests include experimental investigations on combustion applied to propulsion (constant-volume combustion, spray combustion, flame-wall interaction).

Pierre Vidal graduated from the *École Nationale Supérieure de Mécanique et d'Aérotechnique* (ISAE-ENSMA - French engineering school specialized in space and aeronautics) in 1986 and received his PhD in Fluid Mechanics and Combustion from the University of Poitiers in 1990. Researcher at Centre National de la Recherche Scientifique (CNRS) since 1990. His research interests include experimental and theoretical investigations on detonation dynamics in gaseous or condensed homogeneous explosives, and high pressure and temperature constitutive relations.

Ratiba ZITOUN received her PhD in Fluid Mechanics and Combustion from the University of Poitiers in 1995. Assistant-Professor at Poitiers University since 2000 (Combustion, Thermodynamics and Heat Transfer). Her research interests include experimental investigations on detonation for propulsion (Dynamics of detonation in RDE and PDE, Detonation initiation, Deflagration Detonation Transition).

Thomas Gaillard graduated from the ISAE-ENSMA engineering school in Poitiers in 2013. He specialized in combustion and propulsion studies. Thomas started his PhD Thesis in 2013 at ONERA. His PhD work is currently dedicated to the numerical study of a rotating detonation engine with an application to spatial propulsion.

Dmitry Davidenko is currently senior research engineer specialized in the rocket propulsion area. He obtained a PhD in Mechanics and Energetics from the University of Orléans. He has been working at ONERA since 2011. Dmitry's principal activities are in the field of detailed modeling of composite solid propellant combustion. He also participates in projects on the simulation of complex reacting flows in solid rocket motors. Another activity concerns numerical studies on the use of rotating detonation for rocket propulsion.

Matthieu Leyko graduated from the National Institute of Applied Sciences (INSA) of Rouen in Energy and Propulsion in 2006. He received his PhD in Fluid Dynamics in 2010 for the investigation of the combustion noise in aero-engines at CERFACS for the SNECMA (SAFRAN group) acoustic department. Until 2014, he was responsible for powerplant aerodynamic integration and design at SNECMA. He later joined the Research and Technology division of SAFRAN (called SAFRAN TECH) where he is in charge of the development of innovative combustion systems in the Energy and Propulsion team. He has authored more than 30 patents applications related to aeronautic propulsion and he is a specialist in propulsive performance.

Bruno Le Naour graduated in 2004 from the National Institute of Applied Sciences (INSA) of Rouen, France as a Propulsion engineer. Since 2008 he works as an Engineer in the APL department of MBDA France, in charge of high speed propulsion studies (scramjet) and advanced propulsion systems (detonation based propulsion) in Bourges, France. Special attention to chemical fuel modelling and test conduction at the Bourges-Subdray High-Speed Propulsion Test Facility. Internal and external teacher of propulsion and energetics.

Y. Fabignon, J. Anthoine, D. Davidenko, R. Devillers, J. Dupays, D. Gueyffier, J. Hijlkema, N. Lupoglazoff, J. M Lamet, L. Tessé, A. Guy, C. Erades
(ONERA)

E-mail : yves.fabignon@onera.fr

Recent Advances in Research on Solid Rocket Propulsion

DOI : 10.12762/2016.AL11-13

This paper is devoted to a review of some recent studies conducted at ONERA within the framework of solid rocket propulsion for missiles, as well as space launchers. The viewpoint adopted is to present the physical phenomena studied using modeling, simulations and experimentations. Three major scientific topics will be investigated in this article: combustion of solid propellants; motor interior ballistics with a focus on two-phase flows, turbulence and radiative effects; rocket exhaust plumes, including phenomena in the vicinity of the aft body.

Introduction

Solid Rocket Motors (SRM) serve as the propulsion back-bone for strategic and tactical missiles, as well as space launchers. Since most missions do not require the sophistication of multiple restart and throttling operations, solid propulsion becomes an interesting choice because of its inherent safety, reliability, simplicity, high density impulse, minimum maintenance, and low cost. The configuration of a rocket motor has to be designed to meet requirements or operational conditions, depending on the mission. The combustion of solid propellant controls the operational conditions of a SRM through the burn rate versus the chamber pressure and temperature sensitivity. The understanding of the combustion mechanisms of solid propellants is therefore an important field of interest for the solid grain designer. A section dedicated to this topic is presented in this article, with a focus on numerical approaches to study the combustion of solid propellants.

The addition of aluminum powder in the propellant improves SRM thrust performance, but leads to the formation of liquid aluminum oxide droplets and therefore produces a two-phase flow in the chamber. This two-phase flow can impact pressure oscillations and may lead to some issues, such as slag accumulation, nozzle erosion, two-phase losses, and so on. The main physical phenomena at the origin of the two-phase flow in the rocket chamber are presented in a second section of this article. Experimental and numerical approaches are also discussed.

Turbulence can play a significant role in the motor chamber and its prediction remains a difficult task, due to the flow induced by mass injection from the propellant surface. Extensive experimental works on cold flows with surface transpiration were carried out in the past, in order to represent the flow in the motor chamber. Results showed the transition to turbulence and the coupling with acoustics. Numerical simulations have been performed to study the flow field in a motor chamber using RANS approaches and, more recently, LES of nonreacting flows. Still today, it turns out that modeling the transition to turbulence inside an actual SRM is a challenging task. A section of this article is devoted to this difficult problem, using recent advances in High Performance Computing (HPC).

Metalized solid propellants have higher final flame temperatures and therefore higher radiant intensities than non-metalized propellants. The importance of radiative heat feedback on the propellant surface, in case of the combustion of metalized propellants, is often ignored by researchers and can lead to discrepancies in the measured and predicted gas temperatures. A short review on radiative effects in the rocket chamber is presented in a section of this article, with some applications using numerical simulations.

The last topic discussed in this article concerns phenomena in the vicinity of the aft body of solid rocket motors and their exhaust plumes. In the first part of this section, we describe an experimental setup, in order to validate numerical simulations in the base region of a solid rocket motor with an external flow field. The second part is devoted to the simulation of exhaust plumes motivated by the need of predicting infrared and radar signatures.

Within the framework of space launchers, large SRMs are used and are subject to pressure and thrust oscillations whose origin relies on the coupling between hydrodynamic instabilities and the first longitudinal acoustic modes of the combustion chamber. ONERA, in collaboration with SAFRAN/HERAKLES and CNES, has investigated this physical phenomenon thoroughly over the last two decades [1, 2].

In particular, small scale firing tests, numerical simulations and application of the linear stability theory were performed to better understand the mechanism of pressure oscillations and to propose practical solutions, in order to remove them, or at least reduce them [3-6]. This section will not be further described in the paper, but the reader can refer to the listed references for more details.

Combustion of solid propellants

Ammonium Perchlorate (AP) and a binder, such as polybutadiene, are the main ingredients in propellants used in major operational SRMs. The combustion of AP results in a premixed flame at about 1 μm from the surface, at roughly 1200 K or higher. Combustion modeling of this energetic ingredient has been the subject of numerous investigations over last decades, but only some researchers have described the flame structure accurately. The methodology used at ONERA to calculate the AP flame structure is to consider a one-dimensional model, taking into account a detailed gas-phase chemistry with 36 species and 216 reactions [7]. The corresponding nonlinear system of differential equations is numerically solved by using adaptive continuation techniques [8]. One of the new results from the model is the structure of the temperature profile (Figure 1). For usual operating pressure, there are two maxima: the first one (≈1300 K) is due to the AP premixed flame while the second maximum (≈1400 K) corresponds to the equilibrium temperature. The multi-scale character of the combustion is due to the slow kinetics of nitrogen-based components modifying the flame structure.

Steady-state sensitivity parameters, namely pressure and initial temperature sensitivities of the burning rate and surface temperature, are also numerically obtained [9]. For an intrinsically stable combustion, the Zel'dovich-Novozhilov or (ZN) [10] response function can be calculated, using steady-state sensitivity parameters. For solid propellants, the response function R_p is defined as follows:

$$R_p = \frac{m'/\bar{m}}{p'/\bar{p}}$$

Where $\bar{m}$ and $\bar{p}$ are respectively the steady-state mass flow rate and pressure at the propellant surface, and m' and p' are the corresponding unsteady fluctuations. The response function is a linear representation of the coupling between acoustics and combustion. It is an important parameter in the analysis of SRM instabilities [11]. For AP, the real part of the ZN response function (Figure 2) has been compared with the data of Finlinson *et al* [12]. Beyond the linear approach, the model developed has been used to study acoustic/elastic wave propagation. It has been shown [13] that the interface between the gas and solid phases can reflect back a wave of the same frequency as the incident wave. In the particular case used, the classical linear response function can be affected [14].

As mentioned above, composite propellants in major operational SRMs consist of oxidizer particles (AP) embedded in a polybutadiene; therefore, they are heterogeneous at the scale of the oxidizer particles. Consecutively, the burning rate is influenced by the propellant morphology and the size distribution of the oxidizer particles. In the previous decade, we tried to calculate the burning rate of the heterogeneous propellant by using a method based on the averaging of the component burning rates. It turned out that this method was not accurate and required much experimental data for validation. Any serious attempt to simulate the propellant burning rate numerically must incorporate an adequate representation of its microstructure by random packing. This realistic approach was developed and used in many modeling studies [15-17]. At ONERA, the modeling approach based on random packing representation of composite propellants has been also investigated. Here, some results are presented to demonstrate the application of the main modeling tools. The reader can find more details in the recent publication [18].

Generation of random particle packs must satisfy the necessary requirements for a high packing density, a wide particle size distribution, and a large number of particles. At present, two packing methods for multidisperse spherical particles have been realized in efficient numerical tools. One of these methods, based on Lubachevsky's algorithm, processes a system of randomly moving particles whose size grows in time. Being computationally expensive, this method can produce very dense random packs close to the jamming limit when the particles have no room to move. Another method is based on the Random Sequential Adsorption (RSA) algorithm, which is much less expensive but results in packs of relatively low density. For the first time, we used the RSA method to generate propellant packs with realistic granulometry and demonstrated that it is capable of producing model packs with the desired density. As an illustration, a 3D

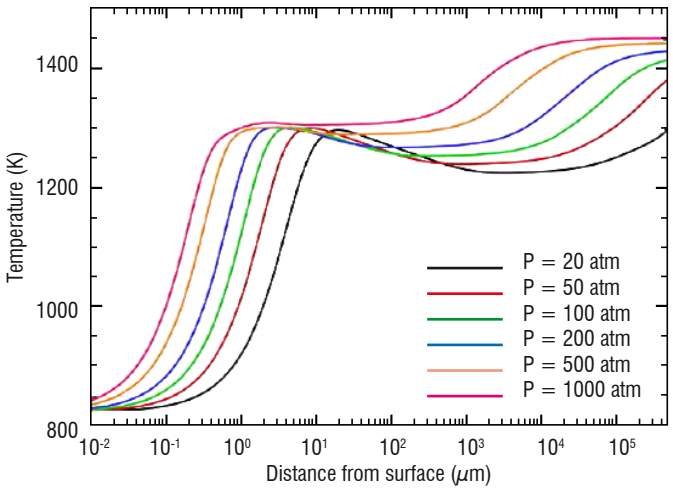

Figure 1 - AP flame structure at different pressures

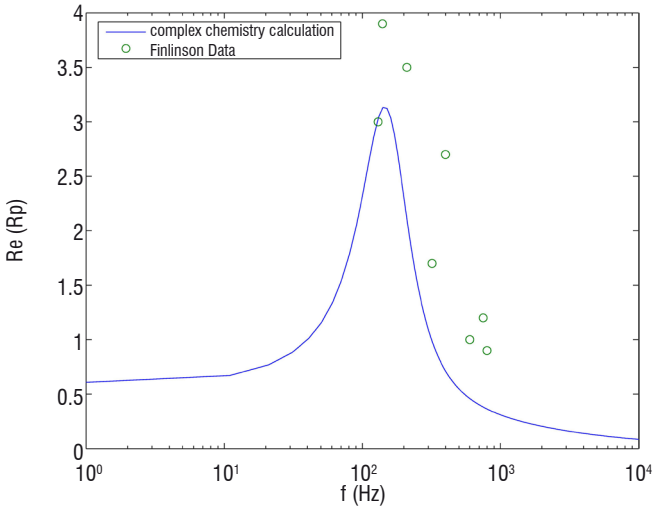

Figure 2 - Real part of ZN response function and comparison with the data of Finlinson *et al* [12]

random pack of 10^5 AP particles, generated with the RSA method, is shown in Figure 3. It is composed of 38 particle classes with a real size distribution. The packing density is 77%, which corresponds to a real propellant.

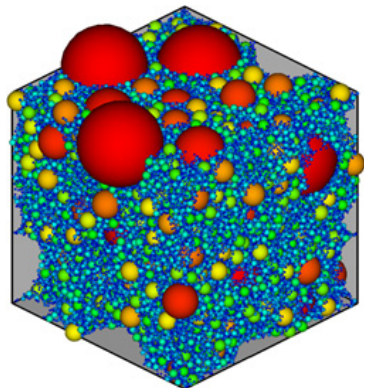

Figure 3 - Random pack of 10^5 AP particles in a cubic periodic domain. Colors correspond to different particle classes

Heat transfer modeling in composite propellants requires specific care, because of very different thermophysical properties of the propellant components and a wide range of geometrical scales. A specific approach, based on the finite-volume method, has been developed for propellants composed of AP and aluminum particles in a HTPB binder. We have focused on minimizing the numerical error due to the material structure discretization on a Cartesian mesh. Computational results obtained for an AP-HTPB sample under steady-state heat transfer are presented in Figure 4, which shows 2D and 3D maps of relative non-uniformity of the temperature field in a mid-section of the sample.

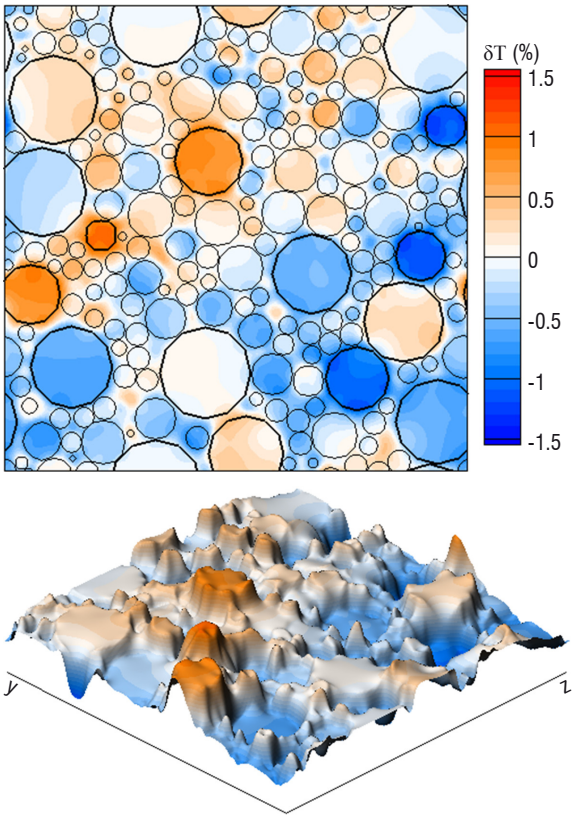

Figure 4 - Temperature non-uniformity in an AP-HTPB sample under steady-state heat transfer. 2D map on the top and 3D on the bottom

Correct prediction of the temperature field in the solid propellant is very important for combustion modeling that requires a coupled treatment of physico-chemical processes in the solid propellant and the hot gas of combustion products. In order to simulate the gas flow, a Navier-Stokes solver for a multispecies reacting gas has been developed according to the low-Mach formulation. The numerical solution for the solid and gas phases is sought on a common Cartesian mesh and coupled by some interface conditions on the regression surface. The propellant surface regression is governed by pyrolysis laws for each ingredient and strongly depends on the local temperature, thus the regression surface features a rather complex geometry and motion. It is treated by the level set method suitable for any arbitrary shape and topology of the regression surface. A level set simulation of the regression of a 3D sample is illustrated in Figure 5. The regression speed is specified as a function of the material composition. Being initially planar, the regression surface evolves to an irregular shape, due to the sample random structure. Another illustration is shown in Figure 6 for the combustion of a 2D AP-HTPB sample. The propellant composition is visualized in the solid zone and the field of combustion product fractions in the fluid zone. Oxygen-rich product P1 is generated in flame fronts near the AP particles (blue zones), then it reacts with fuel-rich gases from HTPB pyrolysis to produce a final product P2 in diffusion flames (red zones). These results demonstrate that the propellant flame has a multifront structure that constantly evolves over time.

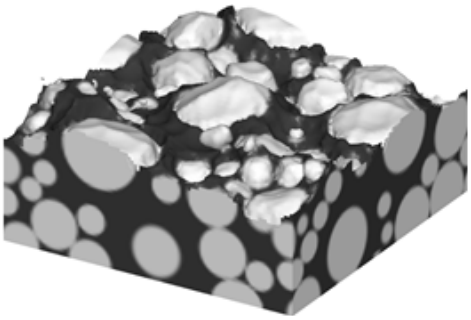

Figure 5 - Simulation of regression surface motion in a 3D sample by the level set method. Regression surface on the top

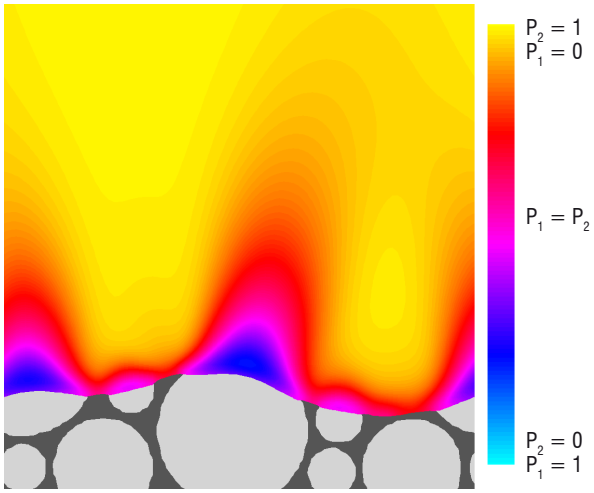

Figure 6 - Combustion simulation with a 2D AP-HTPB sample. Propellant structure and field of combustion product fractions of AP (P_1) and HTPB (P_2)

Two-phase flows due to aluminum particles

Aluminum powder is generally introduced into the propellant in a significant proportion to increase the flame temperature and thus the motor performance. However, the expected gain is lowered by the presence of a massive amount, often exceeding 30% by weight, of aluminum oxide residues and smoke in the combustion products.

This condensed phase increases the rocket exhaust plume emission and tends to reduce the ejection gas velocity through the drag effect in the expanding nozzle. The resulting so-called "two-phase losses" are generally the main contribution of the total performance loss that affects nozzle efficiency [19], [20]. Inside the motor, these droplets are the source of slag material that may remain in the motor during firing and thereby cause additional performance loss and excessive heating, leading to subsequent insulation erosion where they collect [21]. In addition, aluminum combustion, distributed above the propellant surface, and aluminum oxide behavior in the whole chamber, can also affect combustion instabilities by acting as driving or damping mechanisms through very complex interactions with acoustic waves and various transient or unsteady processes occurring in the confined volume of the chamber [21-24]. Detailed knowledge of condensed phase characteristics and behavior in the motor and the plume are essential to improve motor performance and stability predictions, and also the plume emission estimate.

Experimental and numerical approaches are combined to evaluate the impact of the condensed phase in solid propulsion. Experiments give input data for numerical models or some convenient validation cases, to test both the models and the numerical strategy. They are often conducted with a small to moderate sample of propellant and operated with various measuring, collecting, analyzing and visualization devices. Initial aluminum droplet and residue size distributions, droplet burning time, droplet initial motion characteristics and particle-size distribution in the plume are some examples of useful input or validation data collected from dedicated experiments. For instance, a nephelometer is used for determining the size distribution in the plume from angular static light-scattering measurements [25]. Characteristics of particles in a motor environment are obtained by using two dedicated setups described in the following sections.

The analysis of particles above the surface of burning propellant samples is conducted by using a focusing shadowgraphy setup [26] that enables particle visualization at a high repetition rate (Figure 7). Small propellant samples are tested under a nitrogen atmosphere up to 4 MPa. At higher pressure, smoke is too dense to determine the contours of particles. Propellant ignition is obtained via a high-power laser beam, so that the imaged area remains undisturbed by other ignition species. The hot combustion gases, close to the burning surface, are imaged at repetition rates of up to

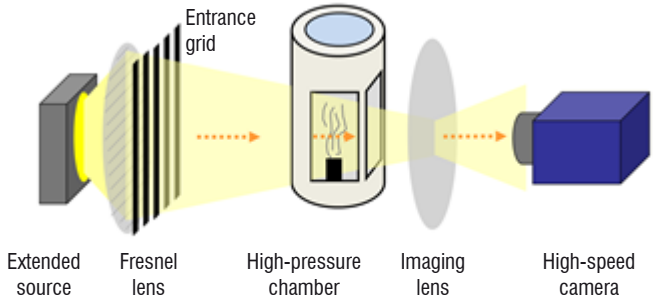

Figure 7 - Experimental shadowgraphy setup used to visualize particles above the propellant surface

10 kHz, with spatial resolutions making it possible to detect particles as small as 10 μm. Hence, common aluminum particles in the range of 20 to 200 μm are well resolved and followed in their vertical movement away from the surface, as seen in the experimental image samples (Figure 8).

Figure 8 - Shadowgraphy images of aluminum particles leaving the surface of burning propellants

The experimental images are analyzed with automatic image processing tools, to detect and characterize the particles. Automatic scripts are necessary, since 10^3 to 10^4 images can be acquired during a typical combustion test, each of them showing several dozens of aluminum particles. The main parameters of interest are particle size distributions and velocity distributions, both of which are crucial input parameters for two-phase flow simulations from solid propellant combustion. The analysis process is first validated with research propellants seeded with inert particles [27], because the size of inert particles is well characterized. Other aspects are also being investigated, such as the detailed morphological characterization of burning aluminum droplets, like the ones shown also in Figure 8. Morphological characterization is a way to validate various physical assumptions underlying the aluminum-combustion models used in the numerical codes.

The size distribution of aluminum oxide residues and smoke present in the combustion products is obtained with the so-called KeRC setup (Figure 9), developed by the Russian Keldysh Research Center. It allows for the iso-kinetic sampling, controlled cooling and capture of liquid aluminum oxide droplets inside a solid propellant motor. Details of the conception, validation and error assessment of the operating method can be found in [28].

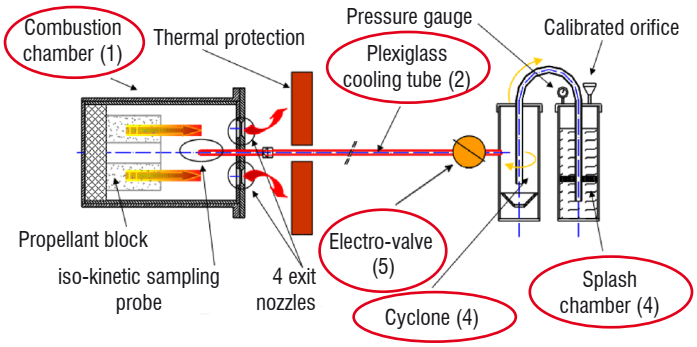

Figure 9 - KeRC experimental setup

The first validation runs of the KeRC setup with a propellant seeded with calibrated, inert particles yielded a systematic bias in favor of the bigger particles. CFD has shown that large vortices at the edge of the cylindrical block deflect smaller particles away from the axis. Replacing the cylindrical grain with a grain without particles and adding a small sample in the center of the block confirmed this hypothesis and improved the measured size distribution. However, the small number of particles in the flow increased the influence of pollutants generated as a by-product of the combustion process. The simulations of the inert experiments have confirmed the potential of the ONERA simulation code CEDRE [29] to correctly reconstruct the internal flow of the KeRC setup. In order to overcome the experimental bias, an "inverse" CFD approach with liquid particles including coalescence and break-up modeling has been developed. By modifying the size distribution of the particles injected at the surface of the grain, based on the comparison of the size distribution of the particles entering the sample probe with the experimental results, we can hope to find a realistic representation of the particles as they leave the surface of the burning propellant grain. Figure 10 shows an illustration of simulation results on a two-phase flow in a typical sampling experiment and a comparison of the experimental and simulated particle size distributions [28]. We numerically inject a bi-modal distribution of particles with mean diameters of 1μm and 15μm and we find a distribution very close to the experimental results inside the sampling probe.

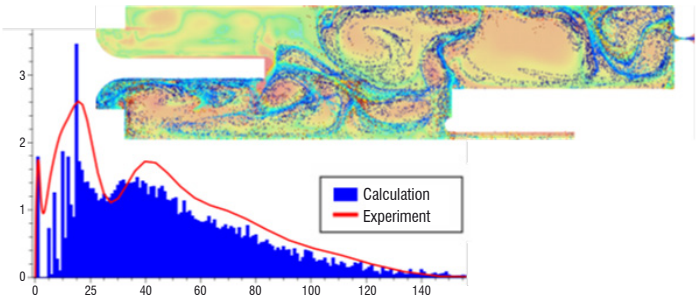

Figure 10 - CEDRE simulations of a typical KeRC experiment

and break-up models, in addition to classical gas-droplet interaction models [30]. Figure 11 shows an example of a simulation performed with the Eulerian sectional approach on an unsteady segmented motor configuration subject to parietal vortex shedding [31]. This approach is based on a piecewise continuous modeling of the particle size distribution defined in a fixed interval (or section) [31, 32]. Such an approach offers in particular a rigorous formalism to manage coalescence and break-up models. Three sections are defined for the simulation, shown in Figure 11, and particles are supposed to be inert so that the size variation is due only to particle-particle interactions.

Turbulence in the chamber

Flow evolution in a porous duct with surface mass injection resembles the flowfield ensuing from the burning of solid propellant in a rocket motor. The analysis of the transition to turbulence with appreciable fluid injection through a permeable duct has been studied in the past [33], as well as more recently [34]. Results showed that the transition of the mean axial velocity profiles occurs farther downstream in the fully developed turbulent flowfield.

Modeling the transition to turbulence inside an actual SRM is a challenging task, because complex geometries and more physical flows must be taken into account. Any serious attempt to simulate the transition to turbulence in a motor chamber must use an unsteady compressible Navier-Stokes approach, in order to study the effect of Mach number on the turbulence and interactions of acoustic waves with turbulent eddies at a fundamental level.

The CEDRE code [29], developed at ONERA for various applications in the field of energetics, has been used for this task. Its generality and its multiphysics capabilities are greatly appreciated for LES or MILES simulations of SRM internal flows. The experimental setup "c1xb" used (Figure 12) is a small SRM chamber that was designed to develop a vortex shedding phenomenon locked on the first axial mode,

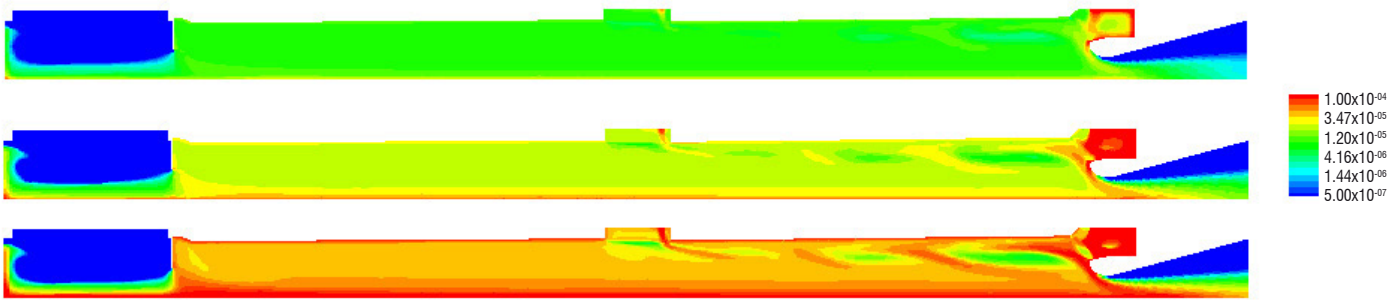

Figure 11 - Particle volume fraction per section (top to bottom: from smaller to larger particles) in the chamber of a segmented motor subject to parietal vortex shedding.

Reliable predictions of the impact of the condensed phase by numerical means need a correct assessment of the complex interactions occurring between the gas and the particles, and between the particles themselves. Together with the particle mass loading, the particle size is a key parameter to correctly reproduce these interactions. The modeling must be able to describe the initial polydisperse particle size distribution and its subsequent evolutions throughout the chamber and the nozzle resulting from interactions with the flow and from particle-particle interactions. Both Lagrangian and Eulerian approaches, available in the CEDRE code, are used with dedicated coalescence

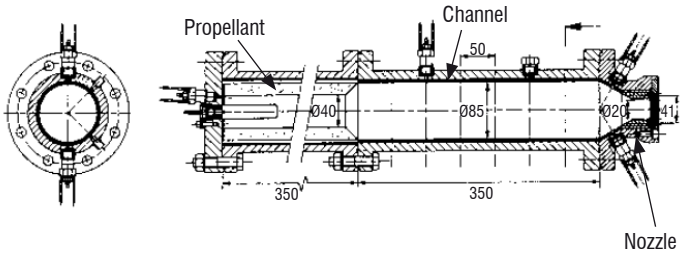

Figure 12 - Schematic diagram of the experimental setup "c1xb" (dim in mm)

as observed in some large SRMs. In the setup, the vortex roll comes from the destabilization of the shear layer generated from a chamfered edge of the propellant. This geometrical singularity is located in the middle of the chamber, to focus the coupling between the vortex roll and the acoustics of the chamber on the first axial mode [35].

All tests experienced pressure oscillations with some bursts corresponding to a sustained self-excitation phenomenon [36]. 2D computations were performed in the past corresponding to several burn times. They have given different vortex shedding frequencies, which were found to correspond to the experimental results [37, 38]. It was noticed that the agreement was good after half-combustion. However, the absence of pressure oscillations during the first half of the combustion could not be explained by 2D computations. The transition to turbulence was suspected to interact with the acoustics.

Recently, with the advent of HPC, a large simulation of the transition to turbulence has been launched within the framework of a GENCI project. The feasibility of a computation in the experimental setup "c1xb", using a mesh of over a billion cells, has been carried out. The initial grain (corresponding to 0 mm burnt) geometry has been chosen for computations, because the flow field should be in transition to turbulence. Gases are injected from both the cylindrical and chamfered parts of the grain, as in the experiments. Four levels of mesh refinements have been considered (Table 1). The CEDRE code was installed on CINES' Occigen, a new massively parallel machine using Haswell processors. A million hours were allocated for computations. Results are shown in Figure 13 for grids 2GG, GM and GF in terms of the so-called Q criterion. One can see that the position of the transition to turbulence is clearly modified between the fine mesh GF and the coarse mesh 2GG. Small turbulent structures are described with the fine mesh GF. The turbulent structures are larger in the case of the mesh 2GG.

Mesh	Number of cells	Number of processors
GG	276 480	64
2GG	6 259 959	256
GM	97 130 691	1008
GF	1 046 185 757	2016 to 4080

Table 1 - Meshes used in the "c1xb" setup and number of processors on the CINES-Occigen supercomputer

An estimation of the Kolmogorov scale η has been performed for the 2GG, GM and GF meshes. Figure 14 shows the ratio of the local grid size Δ divided by the Kolmogorov scale η.

A billion cells (GF mesh) enable convergence to nearly a DNS, because the grid size is approximately five times larger than the Kolmogorov scale. In this SRM, we have estimated that a mesh with 100 billion cells would be necessary for a DNS calculation. Such an approach offers new insights for the study of complex flows in SRMs.

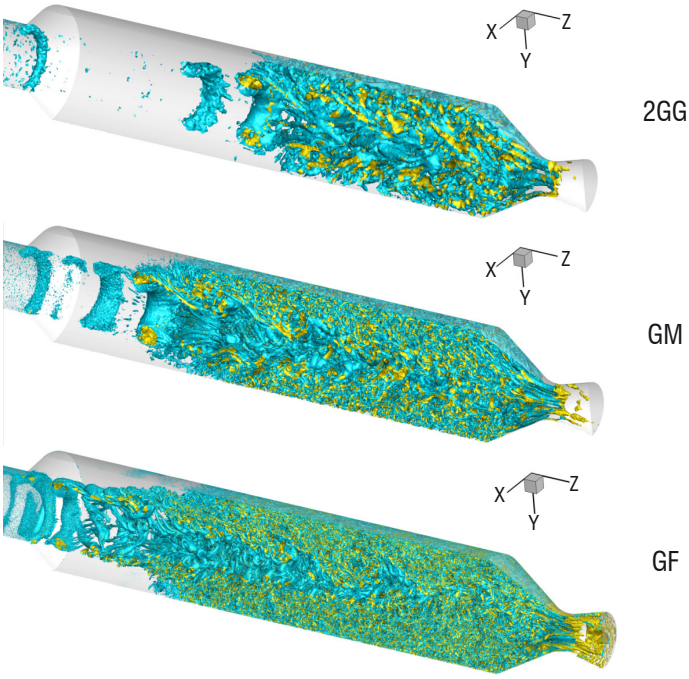

Figure 13 - Snapshots of Q criterion isosurfaces for three different meshes (GF, GM, 2GG)

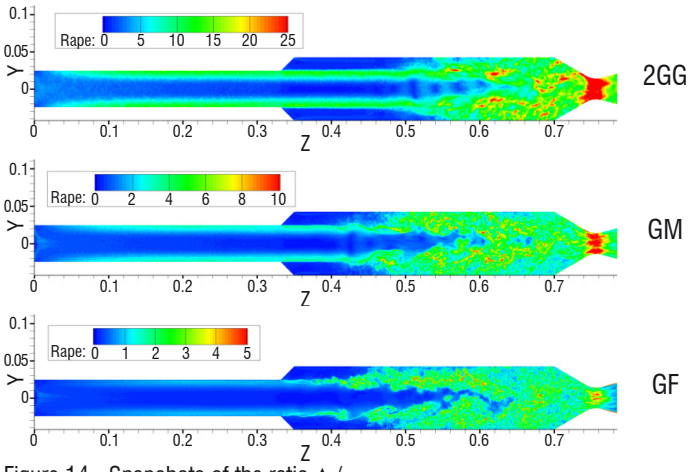

Figure 14 - Snapshots of the ratio Δ / η

Radiative effects in the chamber

Hot gas and a particle mixture generated by the combustion of an aluminized AP-HTPB propellant is a semi-transparent medium that emits, absorbs and scatters radiation. Usually, four gaseous species are taken into account to compute radiative transfer in a SRM: H_2O, CO_2, CO and HCl [39, 40]. Moreover, in an aluminized solid propellant, the contribution of alumina droplets is generally higher than in a gas propellant. Temperatures of up to 3600 K and a pressure of between 3 to 15 MPa are reached in the combustion chamber, leading to an optically thick medium. A typical extinction length value is about 1 mm [39]. Due to this small value of typical extinction length, wall radiative fluxes strongly depend on the temperature, volume fraction and particle size profiles in the boundary layer.

Numerical methods and computation codes

Two numerical methods have been developed at ONERA: the Discrete Ordinates Method (DOM) in the REA solver [40, 41] and the Monte Carlo Method (MCM) in the ASTRE code [41-46]. The first method offers a good compromise between accuracy and CPU time, but it solves only the differential form of the Radiative Transfer Equation (RTE), with a gas radiative property model necessarily formulated in terms of the absorption coefficient. Moreover, its use requires some assumptions about physical phenomenon modeling (for example, it is impossible to take the turbulence-radiation interaction or spectral correlations rigorously into account when reflecting walls or scattering particles are present). The MCM is a statistical approach that can be used to solve any kind of problem, since it solves the integral form of the RTE, enabling the use of both types of gas radiative property models formulated in terms of the absorption coefficient and transmissivity. Given that the MCM is statistical, exact results can be approximated if enough events are simulated. That is why results obtained with MCM are often considered as reference solutions. Another advantage of MCM is that even the most complicated problem can be solved with minimum assumptions. However, this statistical method is known to converge slowly.

The DOM is based on a discrete representation of the directional variation of the radiative intensity. Thus, the differential form of the RTE is replaced by a system of partial differential equations (one equation for each ordinate direction) and integrals over a range of solid angles are approximated by weighted sums over the ordinate directions within that range. Gaussian quadratures, called level symmetric or S_N quadratures, are often used. That is why DOM is also called the S_N method. N is an even number that indicates the order of the solution. In a three-dimensional problem, N(N+2) discrete ordinate directions are considered. The REA parallelization is carried out by mesh splitting: each core deals with a piece of the whole computational domain.

MCM consists in following a large number of energy bundles (discrete amounts of energy, which can be pictured as a group of photons bound together) throughout their transport histories, from emission to absorption. Bundle characteristics, namely wave number, initial direction and emission point, and physical events (scattering, reflection of walls, etc., except absorption) along bundle trajectories are chosen according to probability distributions, by drawing random numbers. The absorption phenomenon is treated with the pathlength method, also called energy partitioning, which consists in computing the exponential absorption along the path. Therefore, a bundle contributes to every cell that it traverses. It is traced until it either leaves the computational domain, or until its energy is depleted below a given cut-off level. Since all of the bundles are statistically independent, the parallelization is achieved by distributing them over the processor cores.

As well as the conventional Forward Method (FM), various reciprocal methods, based on the exchange formulation of radiative transfer, are implemented in ASTRE [42-44]: the Emission, Absorption and Optimized Reciprocity Methods, ERM, ARM and ORM, respectively. Reciprocal methods converge faster than FM in optically thick media, like a solid propellant rocket motor [42-44]. Moreover, ERM is very useful to compute only radiative fluxes on selected walls [43, 44].

Gas radiative property modeling

Due to high pressure in the combustion chamber, radiative transfer can be calculated without taking into account gas spectral correlations. Indeed, at a high pressure, due to the collision broadening effect, the gas absorption spectra display smoother spectral dynamics than those at atmospheric pressure [41]. In this case, the spectral correlation effect is weak and the box model can be used to model the gas radiative properties. Such an approach has been used by Duval [39, 47] or Joumani [40].

In the REA solver, to compute the absorption coefficients of the gaseous mixture, the parameters generated by Duval *et al* [47] are used. These parameters have been tabulated for 43 spectral bands in the infrared spectral range (1 μm – 73 μm) and for 14 temperatures between 300 K and 2900 K. For upper temperatures, parameters at 2900 K are used.

In the ASTRE code, the same model parameters can be used. Moreover, the updated Statistical Narrow Band (SNB) model parameters, generated by Rivière and Soufiani [48], are also available. In ASTRE, this SNB model can be used in its complete form (formulated in terms of transmissivity [46]) or combined with the weak absorption approximation. This second approach is equivalent to the box model [39, 41]. Indeed, the weak absorption approximation is, for example, valid when pressure is high.

Particle radiative property modeling

Concerning the particles, only alumina droplets are considered in our simulations. They are assumed to be spherical, homogeneous and isothermal. In a first approximation, aluminum particles are not taken into account in radiative transfer calculations. Then, the Mie theory is applied to compute radiative properties [41]: absorption and scattering coefficients and phase function. The alumina complex refraction index m is modeled as a function of wavelength λ and temperature T, in accordance with the expression given by Dombrovsky [49]. Alumina droplets can be in thermal non-equilibrium with the gases, if particle temperatures are calculated by a solver for the dispersed phase.

Moreover, to compute particle radiative properties, a particle size distribution is needed [41]. Two approaches are possible. The particle size distribution can be either calculated by a solver for the dispersed phase, based on a sectional approach, or approximated by several particle classes. From one to five classes are typically considered. For each class, a Gaussian function, centered around a chosen mean diameter with a relative standard deviation of 10 %, is used to model the size distribution.

Examples of radiative effects

Radiation plays a significant role in SRMs with aluminized propellant. In order to protect the structural parts of the motor, several types of thermal protecting materials are used. The prediction of convective and radiative fluxes on these materials is important, since the flux levels directly affect performance (ablation in the nozzle throat, impulse to weight ratio) and the safety of the motor. The flux levels may be of the order of several $MW.m^{-2}$ and radiative contributions range from practically 100% (internal parts) to about 10% (divergent part of the nozzle). Moreover, it has been shown that radiative fluxes have a strong effect on the ignition of a SRM, due to the radiative heat feedback on the propellant surface, which is a significant fraction of the total heat feedback.

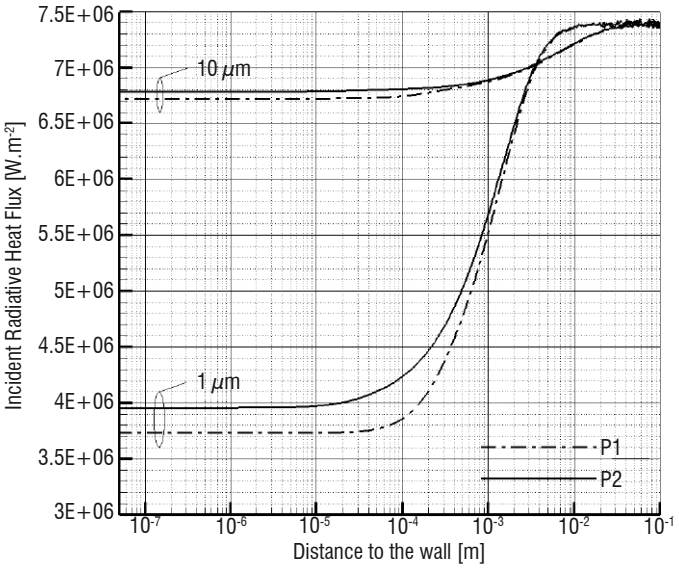

Figure 15 - Incident radiative heat flux as a function of distance to the burning surface [50]

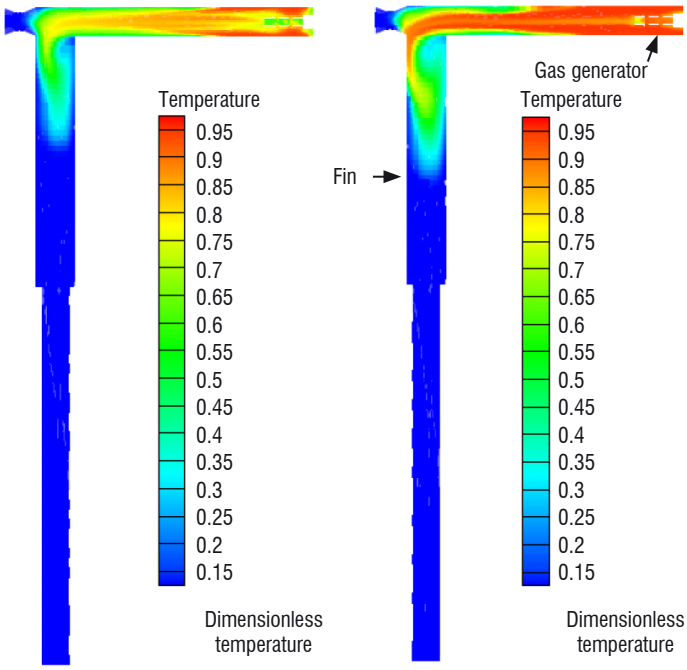

Figure 16 - Dimensionless temperatures, at a given time, obtained by simulations without (on the left) and with (on the right) taking into account radiative flux on the propellant surface.

For example, a recent study [50] shows that, for AP/HTPB composite propellants with 17% of aluminum, the radiative flux contribution to the total heat flux on the propellant surface varies from 10% to 25%. Incident radiative heat flux to the burning surface as a function of distance to the propellant surface is illustrated in Figure 15, for two AP/HTPB composite propellants (P1 and P2) and two alumina droplet diameters (1 μm and 10 μm). The propellant P1 contains micro-sized aluminum particles with a mass mean diameter of 6 μm and the propellant P2 contains 20% of micro-sized aluminum particles (mass mean diameter of 6 μm) and 80% of nano-sized aluminum particles (mass mean diameter of 100 nm). The additional heat flux, due to radiation, influences burning rates and, consequently, the propellant ignition. Unsteady simulations of propellant ignition, with or without radiation, show in particular a significant role of radiative fluxes, as is shown in Figure 16. Dimensionless gas temperatures, obtained by simulations at the same physical time in an experimental setup studied at ONERA, are represented in this figure. This experimental facility consists of an igniter in a cylindrical gas generator and a perpendicular parallelepiped fin containing a test propellant to study the flame-spreading. As expected, Figure 16 shows that the propellant ignition is faster in the gas generator in which radiative flux is accounted for. The flame spread time in the fin is then modified.

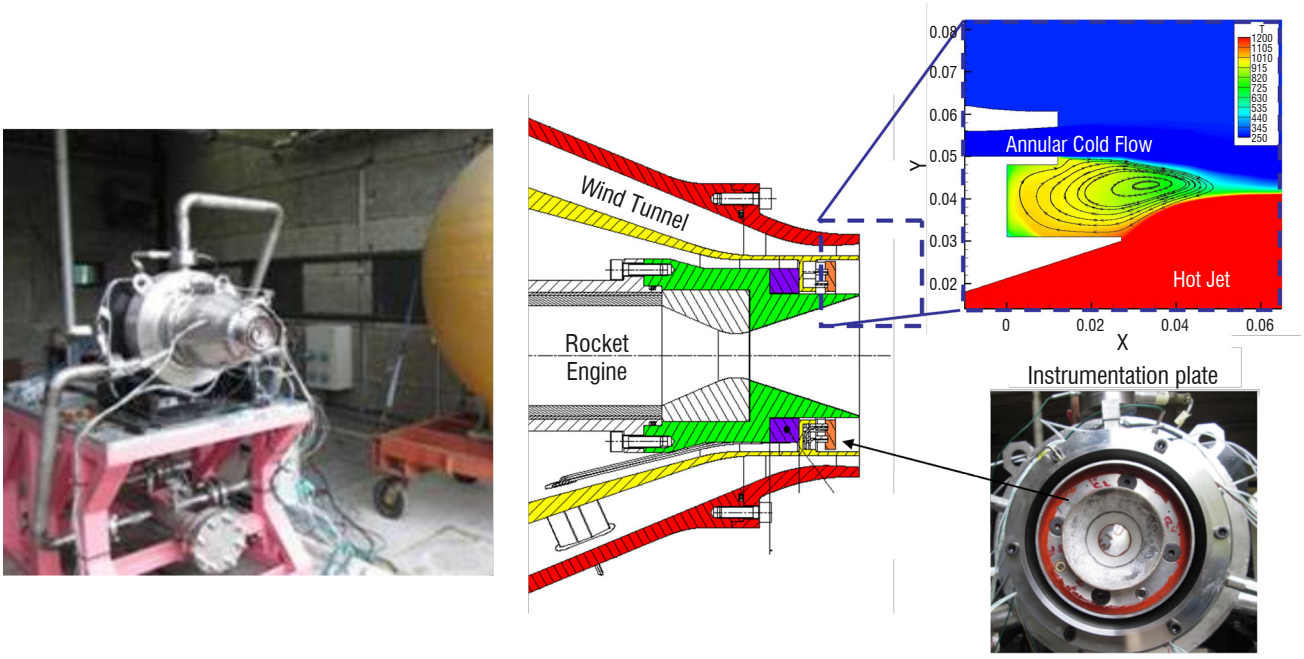

Figure 17 - The LP13 firing test facility consisting of a rocket motor jet surrounded by an annular cold air flow

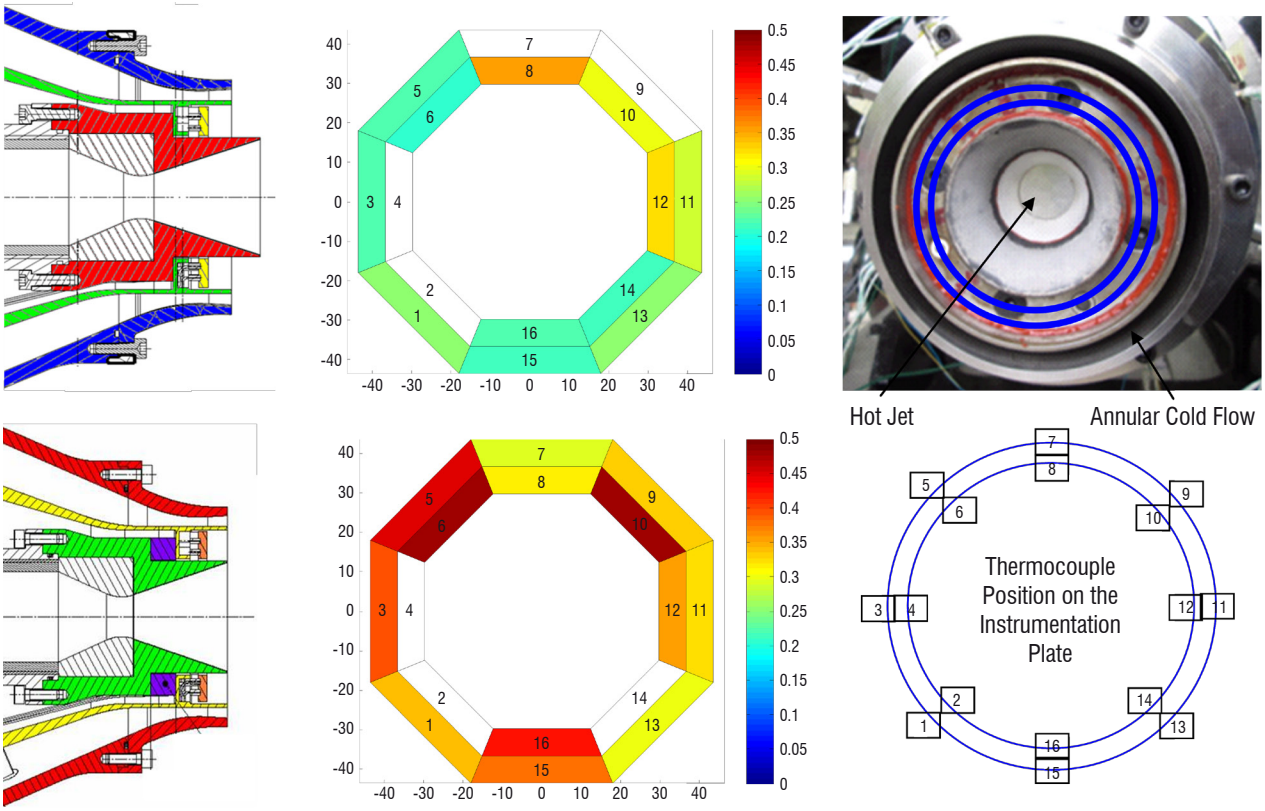

Figure 18 - Color representation of the heat flux level measured at different azimuthal positions in the base region between the hot jet and the annular cold air flow for two relative positions of the SRM with respect to the cold air flow nozzle

Phenomena in the vicinity of the aft body

Flow separation is encountered in the vicinity of the aft body of a space launcher or a missile. Separated flows are highly unsteady and can introduce significant unsteady loads and loss of efficiency for a vehicle. The flow separation occurs because of a discontinuous variation in the aft body geometry and features strong oscillation of the propulsive system at transonic regime (buffeting). These phenomena are valid for both liquid rocket and solid rocket motors. In the latter case, a possible post-combustion of the propellant combustion gases with the ambient air may also occur in the exhaust jet. This post-combustion can be promoted by the presence of alumina particles in the recirculation zone induced by the separated flows around the nozzle. This induces very high heat fluxes in the vicinity of the aft body of the SRM, which needs to be taken into account in the design of the vehicle.

The flow conditions in the near wake of a vehicle propelled by a SRM are usually determined numerically. In order to validate these numerical tools, it is necessary to experimentally reproduce an external flow around the nozzle of a SRM, which required the development of a dedicated test bench. To be representative of the air flow environment in the aft body region of the motor, firing tests have to be performed inside a wind tunnel. The risks due to the pyrotechnic means, as well as the pollution of the wind tunnel due to the emission of the combustion gases and particles, make this solution difficult to achieve. An alternative consists in designing a custom wind tunnel around a SRM.

The developed test bench, called the LP13 [51] firing test facility (Figure 17), consists of two parts, the motor and the wind tunnel. The motor is a downscaled SRM with a simplified geometry. The wind tunnel, being constructed around the motor, produces an annular cold flow around the hot jet of the SRM. The air flow capability ranges from subsonic to supersonic regimes. The test bench is highly instrumented throughout the air supply system, in the combustion chamber and in the aft body of the motor. Pressure, temperature and heat flux are measured at multiple points, especially in the base region.

Several firing tests have been performed by changing different parameters, such as the mass flow rate of the annular air flow and the relative position of the nozzle exit with respect to the cold flow nozzle exit. For instance, as indicated in Figure 18, the fact to back the position of the motor increases the heat flux in the aft body. The experimental database is used successfully to validate simulation results with the CEDRE code. The pressure and heat flux in the base region are well recovered by the simulation, which can predict the effect of the relative position of the two exits and the effect of the mass flow rate level.

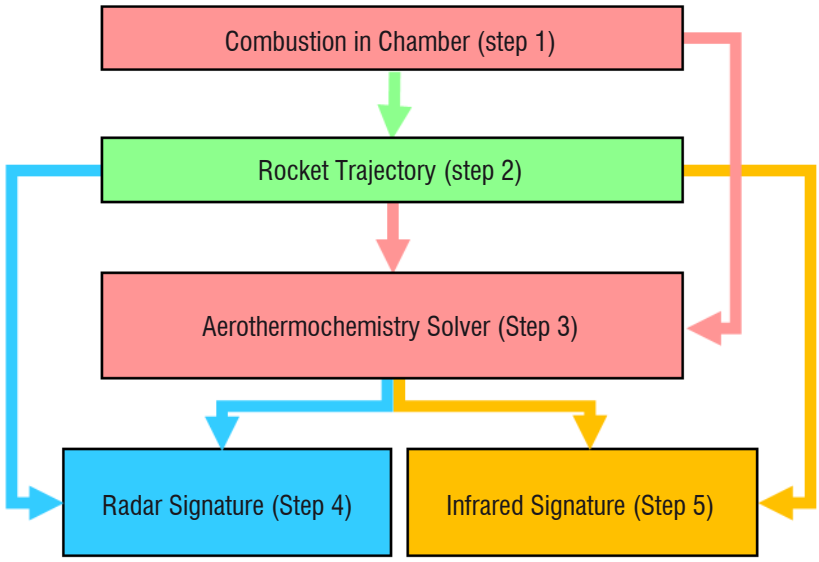

Figure 19 - The computation of plume signatures involves sequentially coupled multi-physics codes

Solid rocket exhaust plumes

The study of rocket exhaust plumes is an exciting challenge for both numerical and experimental research. An exhaust plume is a supersonic afterburning flame, which appears in the mixing layer between combustion gases accelerated in the rocket nozzle and the atmosphere gases. With solid rocket motors with aluminized propellants, the flame is often visible to the naked eye, mainly because high-temperature alumina particles contained in the flow radiate in the visible part of the spectrum. Research on rocket plumes at ONERA most often finds its application in the prediction of infrared [52, 53] and radar signatures [54] of launchers or ballistic and tactical missiles. Other applications include the prediction of radiative and thermal transfers in the nozzle and aft regions of the rocket [55] or the study of pollutant diffusion in the atmosphere [56, 57]. In this section, we summarize recent developments in the research on signatures of rocket exhaust-plumes. We study these signatures with a dual approach, using both numerical simulations and comparison to measurements on small SRMs.

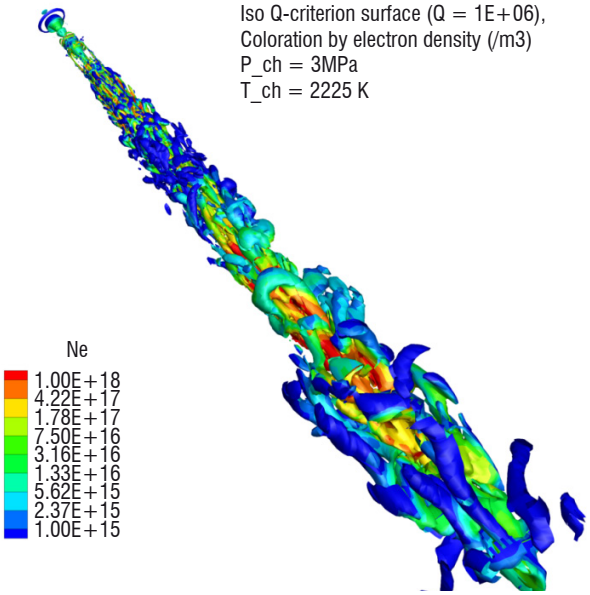

Figure 20 - Large eddy simulation of an ionized plume of a SRM. The isosurface of Q criterion is colored with the electron number density.

Simulation platform

Our calculations of infrared and radar signatures of rocket plumes involve sequentially coupled multi-physics solvers, see Figure 19.

We calculate the composition of the burnt gas mixture (Step 1) in the rocket chamber using a chemical equilibrium code like STANJAN [58], or a rocket performance code like COPPELIA [59].

The rocket trajectory is then computed (Step 2) and the flight conditions are obtained at a given altitude. This information provides us with the necessary quantities to enforce the conditions on the boundaries of the computational domain for the plume flow simulation.

ONERA's CEDRE Platform [29] is used to simulate (Step 3) the supersonic gas flow in the plume. This solver performs calculations on unstructured meshes with cells of arbitrary geometry. We make use of a robust nonlinear Riemann solver for the treatment of shocks and rarefaction waves in the flow. The CEDRE solver also tracks alumina particles using Eulerian or Lagrangian approaches [30], with coupled interactions between particle dynamics and fluid flow. Turbulence creation and transport can be evaluated using a RANS model and a 2D-axisymmetric steady state solution is then obtained. Unsteady turbulent structures can also be computed using a 3D MILES approach, see Figure 20. A set of chemical reactions has been developed to describe the afterburning flame. This system involves 12 species (O, O_2, H, H_2, CO, CO_2, OH, H_2O, HCl, Cl, Cl_2, N_2), ionized species (K^+, Na^+, Cl^-, e^-) and 17 combustion reactions and additional ionization reactions whose rates are computed using a chemical kinetic mechanism developed at ONERA.

Computation of signatures

In order to compute the static and dynamic radar signatures (Step 4) of the rocket plume, an ionization model has been developed [54] and integrated into the CEDRE code. In this model, we assume ambipolar diffusion for the ion and electron mixture in the plume. Electron number density and electron-neutral collision frequencies are used to compute the electric permittivity of the ionized plume. The radar signature of this non-homogeneous plasma is then computed by inverting the macroscopic Maxwell equations in the harmonic time domain.

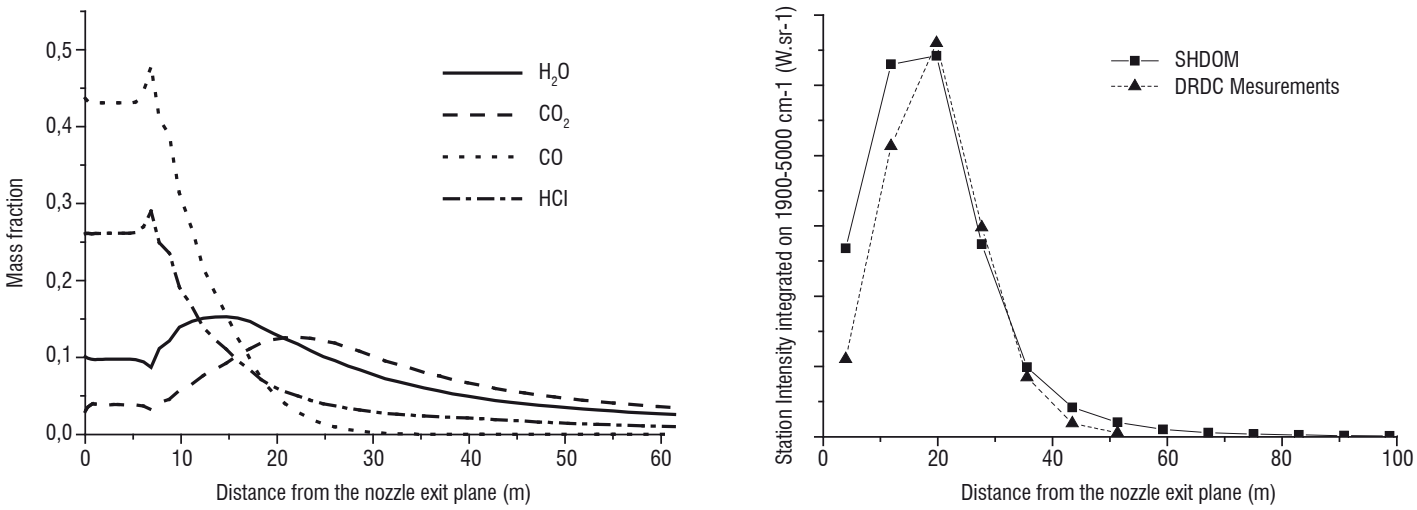

Figure 21 - Left: mass fraction of the radiating species computed by CEDRE along the center line of a Black Brant rocket at an altitude of 7.9 km
Right: comparison between the computed and measured station radiation– spectral band 1900-5000 cm^{-1}

The calculation of the plume infrared signature (Step 5) uses as input the plume temperature and pressure, the concentrations of the H_2O, CO_2, CO and HCl species and of the alumina particles computed with CEDRE, see Figure 21 (left). Radiative transfer computation is performed in a non-scattering medium, with either a line-by-line model or a statistical narrow-band model called RGM3000. The scattering media are dealt with by using the SHDOM solver [60]. We obtain good agreement between flight measurements and computations of the infrared signature of a Black Brant rocket [53], as shown in Figure 21 (right).

Ground firing of a solid rocket motor

In this paragraph, we shortly describe the experimental setup currently in use at ONERA to study the plume static and dynamic radar signatures. A small scale 2.5 kN thrust SRM is attached to the ground and fired during about 3 seconds. The ionization level in the chamber is controlled by adding 10 to 300 ppmw of potassium and sodium in the propellant, which itself originally contains traces (usually of the order of 10 ppmw) of such alkali metals. We make use of AP-HTPB propellant, with or without aluminum, the former leading to higher ionization levels in the plume. The backscattering of electromagnetic waves is studied using an UHF Doppler radar system, whose emitter and receiver are shown in the background in Figure 22. The ionization level is strong enough for the radar system to record an energy spectrum with a Doppler shift between -4 kHz and 4 kHz. Further analysis of the Doppler signal is underway.

Conclusions and future work

We have developed numerical and experimental platforms to study solid rocket motor exhaust plumes. Our numerical platform makes use of a complex aerothermochemical solver and of a novel ionization model, which are sequentially coupled with infrared and electromagnetic codes to compute rocket plume signatures. We have been able to obtain a good comparison between the measured and simulated infrared signatures for rockets under real flight conditions. We have also recently begun to experimentally measure static and dynamic radar signatures underground conditions, and comparison with large eddy simulation results is underway. Future prospects include the modeling of exhaust plumes in a rarefied atmosphere to account for the high altitude of the rocket, with coupling between our Navier-Stokes solver and a DSMC (Dynamic Simulation Monte Carlo) code.

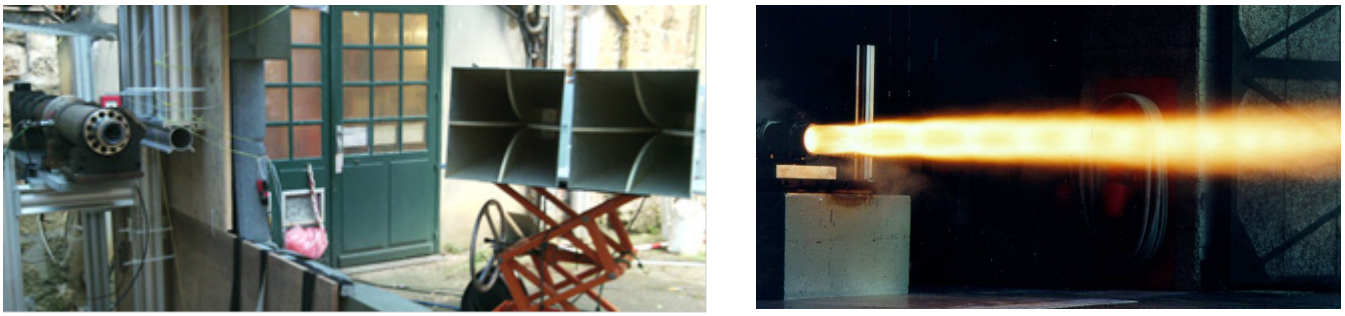

Figure 22 – Left: rocket nozzle to the left of the picture, radar emitter and receiver antennas in the background
Right: exhaust plume during rocket firing.

Conclusions and perspectives

The physical phenomena observed in a SRM chamber and in an exhaust plume are complex and involve interactions between chemistry, acoustics, turbulence, two-phase flows and radiative effects. Despite considerable experience accumulated by the industry in designing solid rocket motors for missiles, as well as space launchers, new developments require the physical phenomena to be more precisely understood, in order to guide the designer quickly towards less expensive and more reliable technical solutions. For this reason, research is being carried out in order to predict the behavior of solid rocket motors and their interaction with the atmosphere. This article has allowed some physical phenomena currently studied at ONERA to be briefly described within the framework of several programs. CFD has become increasingly important and clearly brings new insights into solid rocket propulsion. However, well-instrumented experiments will always be necessary to validate numerical simulations or dedicated models.

In the near future, new projects will give us the opportunity to further investigate multi-physics and multi-scale phenomena in solid rocket propulsion, using parallel computing in order to analyze systems of ever increasing complexity ■

Acknowledgements

This work has been done within the framework of several research programs supported by the DGA, the French Ministry of Defense, the CNES (*Centre National d'Études Spatiales*) and ONERA. The massively parallel simulations required for the turbulence study in a SRM have been performed on GENCI machines. The authors would like to thank the CINES. They also want to acknowledge valuable discussions with research engineers from SAFRAN/HERAKLES.

References

[1] Y. FABIGNON, J. DUPAYS, G. AVALON, F. VUILLOT, N. LUPOGLAZOFF, G. CASALIS, M. PRÉVOST - *Instabilities and Pressure Oscillations in Solid Rocket Motors*. Aerospace Science and Technology, Vol. 7, No. 3, 2003, pp. 191–200.

[2] J. ANTHOINE - *Solid Propellant Pressure Oscillations*. VKI / STO-AVT-206 Lecture Series on Fluid Dynamics Associated to Launcher Developers, von Kármán Inst., Rhode-Saint-Genèse, Belgium, April 2013.

[3] J. HIJLKEMA, M. PRÉVOST, G. CASALIS - *On the Importance of Reduced Scale Ariane 5 P230 Solid Rocket Motor Models in the Comprehension and Prevention of Thrust Oscillations*. CEAS Space Journal, Vol. 1, No. 4, 2011, pp. 99–107.

[4] J. ANTHOINE, P. JÉZÉQUEL, P. PRÉVOT, M. PRÉVOST, G. CASALIS - *Variable Fuel Grains Burn Velocities to Reduce Solid-Rocket-Motor Pressure Oscillations*. Journal of Propulsion and Power, Vol. 31, No. 1, January-February 2015, pp. 342-351.

[5] F. CHEDEVERGNE, G. CASALIS, T. FÉRAILLE - *Biglobal Linear Stability of the Flow Induced by Wall Injection*. Physics of Fluids, Vol. 18, January 2006.

[6] G. BOYER, G. CASALIS, J-L. ESTIVALÈZES - *Stability and Sensitivity Analysis in a Simplified Solid Rocket Motor Flow*. Journal of Fluid Mechanics, vol. 722, pp. 618-644, 2013.

[7] N. MEYNET - *Simulation numérique de la combustion d'un propergol solide*. Ph.D. Thesis, Université Paris VI, Paris 2005.

[8] V. GIOVANGIGLI, N. MEYNET, M. SMOOKE - *Application of Continuation Techniques to Ammonium Perchlorate Plane Flames*. Combustion Theory and Modeling, Vol. 10, No. 5, 2006, pp. 771-798.

[9] S. RAHMAN, V. GIOVANGIGLI, V. BORIE - *Pressure and Initial Temperature Sensitivity Coefficient Calculations in Ammonium Perchlorate Flames*. Journal of Propulsion and power, Vol. 27, No. 5, 2011, pp. 1054-1063.

[10] B. NOVOZHILOV - *Theory of Nonsteady Burning and Combustion Stability of Solid Propellants by the Zel'dovich-Novozhilov Method*. Progress in Astronautics and Aeronautics, Vol. 143, chap. 15, 1992, pp. 601-641.

[11] F.E.C. CULICK - *Unsteady Motions in Combustion Chambers for Propulsion Systems*. AGARDograph AG-AVT-309, RTO/NATO, Neuilly sur Seine, France, 2006.

[12] J. FINLINSON, F. STALNAKER, F. BLOMSHIELD - *Ultra Pure Ammonium Perchlorate T-Burner Pressure Coupled Response at 500, 100 and 1800 psi.* 34th AIAA Joint Propulsion Conference, AIAA Paper 98-3554, July 1998.

[13] V. GIOVANGIGLI, S. RAHMAN - *Numerical Simulation of Unsteady Planar Ammonium Perchlorate Flames Including Detailed Gas Phase Chemistry and Fluid-Structure Interaction*. Compte Rendu Académie des Sciences. Paris, C.R. Mécanique, 341, 152-160, 2013.

[14] S. RAHMAN - *Modélisation et simulation numérique de flammes planes instationnaires de perchlorate d'ammonium*. Ph.D. Thesis, Université Paris VI, Paris 2012.

[15] T.L. JACKSON - *Modeling of Heterogeneous Propellant Combustion: A Survey.* AIAA Journal, Vol. 50, No. 5, 2012, pp. 993-1006.

[16] M. PLAUD, S. GALLIER, M. MOREL - *Simulations of Heterogeneous Propellant Combustion: Effect of Particle Orientation and Shape*. Proceedings of the Combustion Institute, Vol. 35, 2015, pp. 2447-2454.

[17] M.L. GROSS, T.D. HEDMAN, S.F. SON, T.L. JACKSON, M.W. BECKSTEAD - *Coupling Micro and Meso-Scale Combustion Models of AP/HTPB Propellants*. Combustion and Flame, Vol. 160, 2013, pp. 982–992.

[18] D. DAVIDENKO, Y. FABIGNON - *Some Aspects of Detailed Modeling of Solid Rocket Composite Propellants*. 6th EUCASS, Krakow, Poland, 29 June - 3 July 2015.

[19] R.F. HOGLUND - *Recent Advances in Gas-Particle Nozzle Flows*. ARS Journal 32 (5), 1962, pp. 662-671.

[20] R.W. HERMSEN - *Aluminum Oxide Particle Size for Solid Rocket Motor Performance Prediction*. AIAA paper 81-0035, AIAA 19th Aerospace Sciences Meeting, Jan. 12-15, 1981, St Louis, MO.

[21] J. DUPAYS, Y. FABIGNON, P. VILLEDIEU, G. LAVERGNE, J.L. ESTIVALEZES - *Some Aspects of Two-Phase Flows in Solid-Propellant Rocket Motors*. Solid Propellant Chemistry, Combustion, and Motor Interior Ballistics, edited by V. Yang, T. B. Brill, and W.-Z. Ren, Vol. 185, Progress in Astronautics and Aeronautics, AIAA, Reston, 2000, pp. 859-883.

[22] J. DUPAYS, F. GODFROY, O. ORLANDI, P. PRÉVOT, M. PRÉVOST, S. GALLIER, S. BALLEREAU, Y. FABIGNON - *Inert Condensed Phase Driving Effect of Combustion Instabilities in Solid Rocket Motor*. Space Propulsion 2008, May 5-9, 2008, Heraklion, Greece.

[23] M.W. BECKSTEAD - *Evidences for Distributed Combustion*. Proceedings of the 24th JANNAF Combustion Meeting, CPIA Pub. 476, Vol. I, 1987, pp. 1-12.

[24] S. GALLIER, F. GODFROY - *Aluminum Combustion Driven Instabilities in Solid Rocket Motors*. Journal of Propulsion and Power 25 (2) 509-521, 2009.

[25] L. HESPEL, A. DELFOUR, B. GUILLAME - *Mie Light-Scattering Granulometer With an Adaptative Numerical Filtering Method*. II. Experiments. Applied Optics 40 (6) 974-985, 2001.

[26] F. CAUTY, C. ERADES - *Tracking of Aluminum Particles Burning in Solid Propellant Combustion Gases by Focusing Schlieren Technique*. 15th International Symposium on Flow Visualization, Minsk, Belarus, June 25-28, 2012.

[27] R. DEVILLERS, C. ERADES, D. LAMBERT, J. BELLESSA - *Mesure et suivi de particules, agglomérats et gouttes en combustion au-dessus de la surface d'un propergol en combustion*. 14ème Congrès Francophone de Techniques Laser, CFTL 2014, Marseille, 15-19 septembre 2014.

[28] J. HIJLKEMA, P. PRÉVOT - *Numerically-Assisted Particle Size Distribution Measurements in Reduce-Scale Solid Rocket Motors*. Journal of Propulsion and Power 31 (2) 714-724, 2015.

[29] A. REFLOCH, B. COURBET, A. MURRONE, P. VILLEDIEU, C. LAURENT, P. GILBANK, J. TROYES, L. TESSÉ, G. CHAINERAY, J.B. DARGAUD, E. QUÉMERAIS, F. VUILLOT - *CEDRE Software*. Aerospace Lab, vol. 2, 2011.

[30] A. MURRONE, P. VILLEDIEU - *Numerical Modeling of Dispersed Two-Phase Flows*. Aerospace Lab Journal AL02-04, pp. 1-13, 2011, http://www.aerospacelab-journal.org/al2.

[31] F. DOISNEAU - *Eulerian Modeling and Simulation of Polydisperse Moderately Dense Coalescing Spray Flows with Nanometric-to-Inertial Droplets: Application to Solid Rocket Motors*. Ecole Centrale Paris thesis, 2013.

[32] F. DOISNEAU, F. LAURENT, A. MURRONE, J. DUPAYS, M. MASSOT - *Eulerian Multi-Fluid Models for the Simulation of Dynamics and Coalescence of Particles in Solid Propellant Combustion*. Journal of Computational Physics 234, pp. 230-262, 2013.

[33] R.A. BEDDINI - *Injection-Induced Flows in Porous-Walled Ducts*. AIAA Journal, Vol. 24, No. 11, 1986, pp. 1766-1773.

[34] B. GAZANION, F. CHEDEVERGNE, G. CASALIS - *On the Laminar-Turbulent Transition in Injection-Driven Porous Chambers*. Experiments in Fluids, 55:1643, 2014.

[35] F. VUILLOT - *Vortex Shedding Phenomena in Solid Rocket Motors*. Journal of propulsion and power 11 (4), 627-639, 1995.

[36] J. DUPAYS - *Contribution à l'étude du rôle de la phase condensée dans la stabilité d'un propulseur solide pour lanceur spatial*. Ph.D. Thesis, INPT, 1996.

[37] F. VUILLOT, N. LUPOGLAZOFF - *Comparison Between Firing Tests and Numerical Simulation of Vortex Shedding in a 2D Test Solid Motor*. AIAA paper 93-3066, AIAA 24th Fluid Dynamics Conference, Orlando, Florida, USA, July 1993.

[38] F. VUILLOT, N. LUPOGLAZOFF - *Combustion and Turbulent Flow Effects in 2D Unsteady Navier-Stokes Simulations of Oscillatory Rocket Motors*. AIAA paper 96-0884, AIAA 34th Aerospace Sciences Meeting, Reno, Nevada, USA, Jan. 1996.

[39] R. DUVAL - *Transferts radiatifs dans les moteurs à propergol solide*. Ph.D. Thesis, École Centrale Paris, 2002.

[40] Y. JOUMANI - *Transferts radiatifs dans les moteurs à propergol solide*. Ph.D. Thesis, Université de Valenciennes et du Hainaut Cambresis, 2001.

[41] L. TESSÉ, J.-M. LAMET - *Radiative Transfer Modeling Developed at Onera for Numerical Simulations of Reactive Flows*. AerospaceLab Journal, Issue 2, March 2011, http://www.aerospacelab-journal.org/al2.

[42] F. DUPOIRIEUX, L. TESSÉ, A. AVILA J. TAINE - *An Optimized Reciprocity Monte Carlo Method for the Calculation of Radiative Transfer in Media of Various Optical Thicknesses*. International Journal of Heat and Mass Transfer, Vol. 49, pp. 1310-1319, 2006.

[43] L. TESSÉ - *Modélisation des transferts radiatifs dans les flammes turbulentes par une méthode de Monte Carlo*. Ph.D. Thesis n°2001-34, École Centrale de Paris, 2001.

[44] L. TESSÉ, F. DUPOIRIEUX, B. ZAMUNER, J. TAINE - *Radiative Transfer in Real Gases Using Reciprocal and Forward Monte Carlo Methods and a Correlated-k Approach*. International Journal of Heat and Mass Transfer, Vol. 45, pp. 2797-2814, 2002.

[45] L. TESSÉ, F. DUPOIRIEUX, J. TAINE - *Monte Carlo Modeling of Radiative Transfer in a Turbulent Sooty Flame*. International Journal of Heat and Mass Transfer, Vol. 47, pp. 555-572, 2004.

[46] O. ROUZAUD, L. TESSÉ, T. SOUBRIÉ, A. SOUFIANI, PH. RIVIÈRE, D. ZEITOUN - *Influence of Radiative Heating on a Martian Orbiter*. Journal of Thermophysics and Heat Transfer, Vol. 22, No. 1, pp. 10-19, January-March 2008.

[47] R. DUVAL, A. SOUFIANI, J. TAINE - *Coupled Radiation and Turbulent Multiphase Flow in an Aluminized Solid Propellant Rocket Engine*. Journal of Quantitative Spectroscopy and Radiative Transfer, Vol. 84, pp. 513-526, 2004.

[48] PH. RIVIÈRE, A. SOUFIANI - *Updated Band Model Parameters for H_2O, CO_2, CH_4 and CO Radiation at High Temperature*. International Journal of Heat and Mass Transfer, Vol. 55, pp. 3349-3358, 2012.

[49] L. A. DOMBROVSKY - *Possibility of Determining the Disperse Composition of a Two-Phase Flow from the Small-Angle Light Scattering*. High Temperature, Vol. 20, pp.472-479, 1982.

[50] J.M. LAMET, Y. FABIGNON, L. TESSÉ, J. DUPAYS, E. RADENAC - *Modeling of Propellant Combustion with Nano-Sized Aluminum Particles*. Proceedings of the 5th European Conference for AeroSpace Sciences (EUCASS 2013), Munich, Allemagne, 1-5 juillet 2013.

[51] L. PASCAL, P. PRÉVOT, P. REULET, J. DUPAYS, J. ANTHOINE - *Development of a Test Facility for Investigating the Solid Rocket Motor Base Region in Representative External Flow Conditions*. To be presented at Space Propulsion 2016, Roma, Italy, 2-6 May 2016.

[52] A. BOISCHOT, A. ROBLIN, L. HESPEL, I. DUBOIS, P. PREVOT, T. SMITHSON - *Evaluation of Computation Codes for Rocket Plume's Infrared Signature by Using Measurements on a Small Scale Aluminized Composite Propellant Motor*. Proceedings of SPIE - The International Society for Optical Engineering, 17-18 April, 2006, Kissimmee, Florida, USA.

[53] V. RIALLAND, A. GUY, D. GUEYFFIER, P. PEREZ, A. ROBLIN, T. SMITHSON - *Infrared Signature Modeling of a Rocket Jet Plume - Comparison with Flight Measurements*. Journal of Physics: Conference Series, in press.

[54] D. GUEYFFIER, B. FROMENTIN-DENOZIERE, J. SIMON, A. MERLEN, V. GIOVANGIGLI - *Numerical Simulation of Ionized Rocket Plumes*. Journal of Thermophysics and Heat Transfer, 2014, Vol. 28:2, pp. 218-225.

[55] J.B. DARGAUD, J. TROYES, J.M. LAMET, L. TESSÉ, F. VUILLOT, C. BAILLY - *Numerical Study of Solid-Rocket Motor Ignition Overpressure Wave Including Infrared Radiation*. Journal of Propulsion and Power, 30(1), pp. 164-174, 2013.

[56] A.D. KOCH, C. BAUER, E. DUMONT, F. MINUTOLO, M. SIPPEL, P. GRENARD, G. ORDONNEAU, H. WINKLER, L. GUÉNOT, C. LINCK, C. R. WOOD, J. VIRA, M. SOFIEV, V. TARVAINEN - *Multidisciplinary Approach for Assessing the Atmospheric Impact of Launchers*. 4th CEAS Air & Space Conference, 2013.

[57] A. POUBEAU - *Simulation des émissions d'un moteur à propergol solide: vers une modélisation multi-échelle de l'impact atmosphérique des lanceurs*. Ph.D. Thesis, Université de Toulouse, Université Toulouse III-Paul Sabatier, 2015.

[58] W. C. REYNOLDS - *The Element Potential Method for Chemical Equilibrium Analysis: Implementation in the Interactive Program STANJAN*. Department of Mechanical Engineering, Stanford University, 1986.

[59] B. BOURASSEAU - *Code COPPELIA: version 3.0. Calcul de la composition de produits de combustion contenant de nombreuses phases condensées*. ONERA Report, RT 40/4386 DEFA/N.

[60] J.B. PAUTRIZEL, A. ROBLIN, P. PEREZ, V. RIALLAND - *Absorption-Scattering Coupling for the Infrared Signature of an Aluminized Solid Rocket Motor*. Proceedings of the 6th International Symposium on Radiative Transfer, Antalya, Turkey, 13-19 June 2010.

List of acronyms

AP	(Ammonium Perchlorate)
ARM	(Absorption Reciprocity (Monte Carlo) Method)
CEDRE	(*Calcul d'Ecoulements Diphasiques Réactifs pour l'Energétique*)
CFD	(Computational Fluid Dynamics)
CINES	(*Centre Informatique National de l'Enseignement Supérieur*)
CPU	(Central Processing Unit)
DNS	(Direct Numerical Simulation)
DOM	(Discrete Ordinates Method)
ERM	(Emission Reciprocity (Monte Carlo) Method)
FM	(Forward (Monte Carlo) Method)
GENCI	(*Grand Equipement National de Calcul Intensif*)
HPC	(High Performance Computing)
HTPB	(Hydroxyl-Terminated PolyButadiene)
KeRc	(Keldysh Research center)
LES	(Large Eddy Simulation)
MCM	(Monte Carlo Method)
MILES	(Monotonically Integrated Large Eddy Simulation)
ORM	(Optimized Reciprocity (Monte Carlo) Method)
RANS	(Reynolds-Averaged Navier Stokes (equations))
RSA	(Random Sequential Adsorption)
RTE	(Radiative Transfer Equation)
SNB	(Statistical Narrow-Band)
SRM	(Solid Rocket Motor)
ZN	(Zel'dovich-Novozhilov (response function))

Yves Fabignon is currently the Head of the Solid Propulsion Unit of the Fundamental and Applied Energetics Department (DEFA) at ONERA. He obtained a Ph.D. in Energetics from the University of Poitiers, ENSMA in 1984. He worked previously for 8 years at the SNPE (now SAFRAN/HERAKLES) before joining ONERA.

Jérôme Anthoine is currently the Head of the Propulsion Laboratory Unit of the Aerodynamics and Energetics Modeling Department (DMAE) at ONERA. He received the Mechanical Engineering Degree from the *Faculté Polytechnique de Mons* (Belgium) in 1995 and the von Karman Institute Diploma in 1996. Then, he obtained a Ph.D. in Space Propulsion from the *Université Libre de Bruxelles* (Belgium) in 2000. At that time, he joined the Faculty of the von Karman Institute as Assistant Professor and then Associate Professor, to develop the aeroacoustics and space propulsion activities. Since 2009, he joined ONERA as senior scientist in Space Propulsion and is currently managing research activities on pressure oscillations in solid rocket motors and on hybrid chemical propulsion.

Dmitry Davidenko is currently a senior research engineer specialized in the rocket propulsion area. He obtained a PhD in Mechanics and Energetics from the University of Orléans. He has been working at ONERA since 2011. Dmitry's principal activities are in the field of detailed modeling of composite solid propellant combustion. He also participates in projects on simulation of complex reacting flows in solid rocket motors. Another activity concerns numerical studies on the use of rotating detonation for rocket propulsion.

Robin Devillers has been a research engineer at ONERA since 2013. He is in charge of experimental measurements associated with solid propellant studies, ranging from material characterization to combustion imaging. He worked previously for 4 years at the National Research Center of Canada in Ottawa on optical diagnostics for soot emission characterization in gas flares, with measurement campaigns performed in oil refineries in Mexico. He obtained his PhD from *École Centrale Paris* for his work on laser techniques for temperature measurements in engines at IFP. He has a MSc and an engineering degree from *École Centrale Paris*.

Joël Dupays is currently a senior scientist and project manager at ONERA. Specialized in the solid propulsion area, his research activity combines fluid dynamics and energetics with a special focus on droplet combustion and unsteady polydisperse two-phase flow modeling and simulation. He received a PhD in Fluid Mechanics from the National Polytechnic Institute of Toulouse in 1996.

Denis Gueyffier is currently a senior scientist at ONERA. He performs research on numerical simulation of solid rocket propulsion and manages projects with government agencies and industrial customers. He was previously a researcher at NASA Goddard Institute of Space Studies in NYC, in the climate modeling team. As a Research Scientist at the Courant Institute in NYC, he contributed to the design of fast algorithms accelerating by orders of magnitude molecular electrostatics and fluid dynamics computations. He was also an Instructor of Applied Mathematics at MIT, where he did research on numerical simulation of multiphase flows. He obtained a PhD from the University of Paris VI in the field of Fluid Mechanics with a fellowship from the French Space Agency.

Jouke Hijlkema is a senior scientist at ONERA. He performs research in the domain of rocket propulsion and manages projects with government agencies and industrial customers. He received a masters degree in aeronautical engineering from *Hogeschool Haarlem* and a masters degree in mathematics from the university of Nijmegen, both in the Netherlands. He obtained a PhD from ISAE in Toulouse, in the field of applied mathematics.

Nicolas Lupoglazoff is a senior scientist, graduated from the "*École Nationale Supérieure de l'Aeronautique et de l'Espace*" in 1987. He joined ONERA's Energetics Department in 1988, and is now in the Fundamental and Applied Energetics Department. He is working in the field of CFD and is specialized in aerodynamics and acoustics in engine nozzles and jets. He is also working on the numerical simulation of the instabilities and turbulence inside solid rocket motors.

Lionel Tessé received his Ph.D. degree, in energetics and the physics of transfer, from the *École Centrale Paris* in 2001. For his Ph.D., he worked on the modeling, using the Monte Carlo method, of radiative transfer in a turbulent sooty flame, focusing on the interaction between turbulence and radiation. He has been a research scientist at ONERA, in the Applied and Fundamental Energetics Department, since 2001. His research topics include the modeling and simulation of radiative transfer in aeroengine combustors, solid propellant rocket motors and hypersonic flows occurring during atmospheric (re-)entries. He is in charge of the development of the ASTRE code (Monte Carlo) and is involved in the development of the REA code (DOM), both codes dedicated to radiative transfer computations.

Jean-Michel Lamet graduated from the *École Nationale Supérieure d'Ingénieurs* de Poitiers in 2005 and received his Ph.D. degree from École Centrale Paris in 2009. For his Ph.D., he worked on the radiative transfer in atmospheric re-entry hypersonic flows. He now holds a position of research scientist in the ONERA Applied and Fundamental Energetics Department. His activity includes the modeling and simulation of radiative transfer in combustion chambers and hypersonic flows. He is involved in the development of the ASTRE and REA codes dedicated to radiative transfer.

Aurélien Guy has been a junior research engineer at ONERA since 2014. His activities are focused on exhaust plume modeling and numerical simulation for application, including optical and electromagnetic signature prediction. He obtained a PhD from the Em2c laboratory at the École Centrale Paris in 2013 in the field of energetics, working on the thermochemical modeling and simulation of shock waves for atmospheric reentry using collisional-radiative models.

Charles Erades, Aerospace engineer, has been working at ONERA in the Fundamental and Applied Energetics Department for the past 30 years. He has developed experimental setups for the characterization of solid propellants and internal thermal protections for rocket motors. He is specialized in non-intrusive ultrasonic methods for the evaluation of pyrolysis and burning rates. He has also worked on characterizing aluminum-droplet burning time with the optical diagnostics that he developed. Furthermore, he implemented experimental motor-jet studies and investigated burning instabilities, as well as studying propellant-ignition delays.

J-Y. Lestrade, J. Messineo, J. Hijlkema, P. Prévot, G. Casalis, J. Anthoine
(ONERA)

E-mail: Jean-Yves.Lestrade@onera.fr

DOI : 10.12762/2016.AL11-14

Hybrid Chemical Engines: Recent Advances from Sounding Rocket Propulsion and Vision for Spacecraft Propulsion

Hybrid propulsion generally combines a liquid oxidizer with a solid fuel. Compared to solid or bi-liquid engines, this type of propulsion offers advantages in terms of cost and flexibility. For several years, ONERA has been providing expertise in this area, both in experimental and numerical simulations. Various hybrid rocket motors have been designed and tested on ground, including under low ambient pressure conditions and in flight. The Propulsion Laboratory unit of the DMAE uses fully instrumented engine breadboards in order to optimize the oxidizer/fuel pair, as well as the injection system and the combustion efficiency. In addition, 0D and 1D codes for engine design are actively being developed. More recently, studies have been undertaken as part of the LEOP future satellite platforms, with the development of an innovative new combustion chamber.

Hybrid propulsion concept and principle

The development efforts carried out for many years on solid and liquid chemical engines made their use almost exclusively for launcher applications (missiles, commercial launchers, sounding rockets, etc.). However, these two concepts have budgetary, performance and environmental disadvantages (cost, complexity, safety, reliability, environmental impact, etc.). They also hinder the development of new applications, such as space tourism, nano-launchers, micro-gravity experiments or landers. Thanks to its benefits in terms of safety, cost, reliability, environmental impact and performances, hybrid propulsion is a promising candidate to overcome these constraints and hence facilitate the development of these new applications [3,25].

The most common configuration of a hybrid engine (Figure 1) comprises an oxidizer (stored as a liquid and vaporized in the forward dome of the motor or gasified by flowing through a catalyst bed), which flows through long fuel channels and burns with the pyrolysis gases resulting from the solid fuel regression to form a turbulent boundary layer. In this case, the solid fuel is cast in the combustion chamber as for the solid rocket motor technology, whereas the oxidizer is stored in a proper tank as in the liquid propulsion technology. The convective and radiative heat fluxes stemming from the diffusion flame provide the energy needed for the solid grain pyrolysis to sustain heterogeneous combustion [29]. Such a cycle produces, from hybrid combustion, a self-sustained phenomenon that occurs as a macroscopic diffusion flame. This implies a dependency of the fuel regression rate on the heat and mass transfer processes. This stabilized combustion continues for as long as the oxidizer is being injected and the solid fuel grain is regressing. The extinction of the engine can be achieved by closing the oxidizer valve.

A hybrid engine is an innovative propulsion system that has a well-known safety level thanks to its simple structure and the wide range of inert propellants that it can use. It can be throttled, restarted or turned off in case of an abort procedure. It has appreciably high specific impulse associated with reduced costs and a reduced environmental impact, since fuels mainly burn into steam and carbon dioxide [2,23]. These advantages are detailed in Box 1.

For the common configuration and as opposed to solid and liquid chemical engines, the amount of ablated fuel, and thus the combustion chamber oxidizer-to-fuel mixture (O/F) ratio, is directly linked to the heat received by the fuel grain from the reacting flow and thus varies along the length of the motor. Since the flame between the oxidizer and the pyrolysis gases is essentially conditioned by their diffusion towards each other, the regression rate is also mostly dependent upon the mass flow rate within the fuel channel. Thus, the fuel regression rate varies with the mass flux and along the length of the combustion chamber following the relatively simple expression [1,2,33]:

$$\dot{r} = aG^n x^m \quad (1)$$

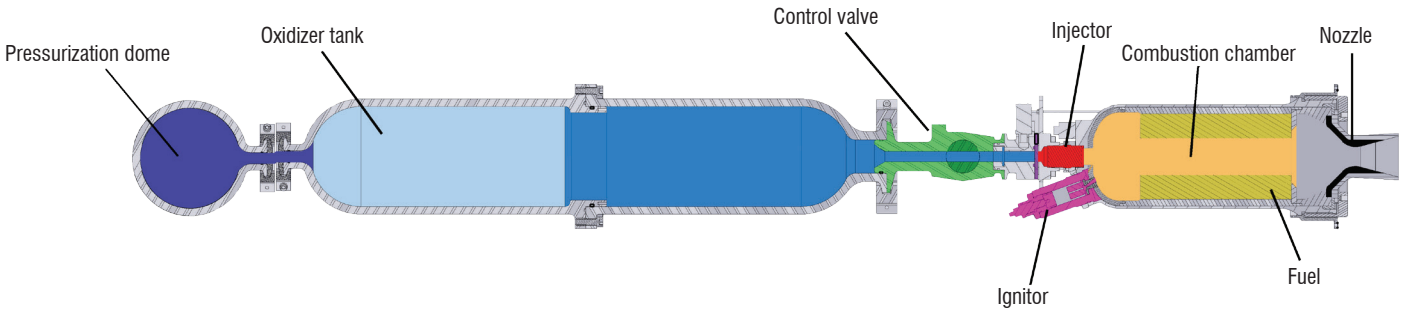

Figure 1 – Hybrid chemical engine concept

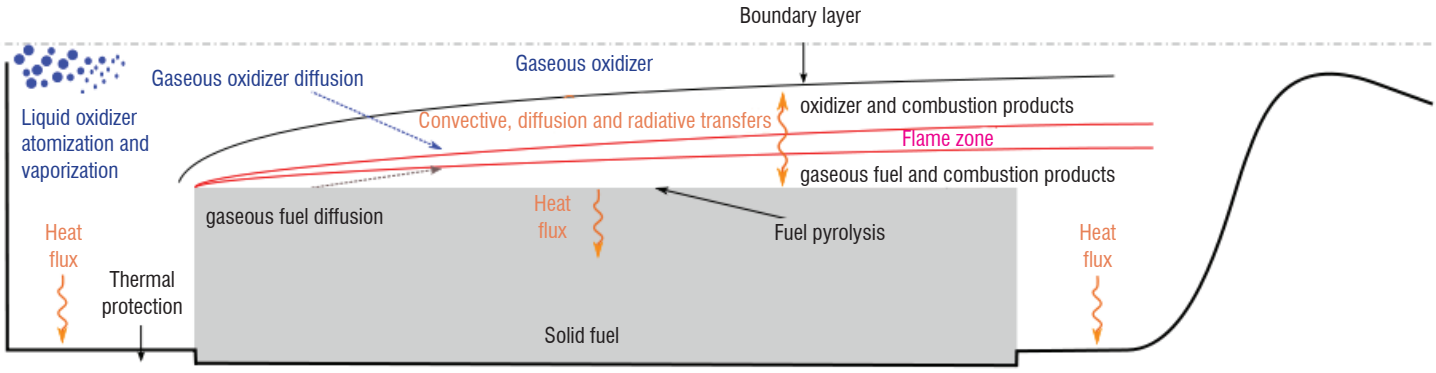

Figure 2 - Hybrid propulsion physics

Box 1 - Advantages of hybrid propulsion

Safety

Inert manufacturing / transportation / assembly / storage
Safe launch-pad operations
Reduced risk of catastrophic failure
Abort by engine shutdown

Reliability / Operating flexibility / Simplicity

Engine verification prior to lift-off
Tolerant to grain defects
Thrust modulation for aerodynamic load relief
or mission optimization
Start-stop capability
One liquid, simplified injector set-up

Costs

Reduced development costs
Reduced recurring costs
Safe materials

Environmental impact

On pad and in flight, very reduced

where $\dot{r}$ is the fuel regression rate, G is the total propellant mass flux, x is the distance down the combustion chamber and a, n and m are the regression rate constants, which are characteristic of the propellants and of the combustion chamber geometry. Since G includes the mass flow from both the injected oxidizer and the fuel that has vaporized from the surface of the fuel, it increases continuously down the combustion chamber. The solid fuel regression rate is one of the most important values in the hybrid conceptual design process used to determine the propulsive performance.

The combustion phenomenon is similar to that of a turbulent diffusion flame for which the flame zone is established within the boundary layer [32] (Figure 2) and results from the coupling of the:

- Kinetics of the condensed phase pyrolysis;
- Homogenous combustion mechanism in the gaseous phase;
- Convective and radiative heat transfers in the gaseous phase;
- Mass transfer of the chemical species.

This process can be treated by an idealized model that considers the flame zone as a point of discontinuity in the temperature gradient and composition. Actually, the flame zone is thicker and both the oxidizer and the pyrolysis gases from the fuel enter the flame zone by diffusing towards each other through the boundary layer. The combustion zone is established at the point where an approximate stoichiometric mixture ratio has been achieved.

Hybrid chemical propulsion physics includes many complex phenomena: fluid dynamics coupled with combustion, turbulence, spray atomization and vaporization processes, soot formation and radiation, fuel surface pyrolysis and fuel liquid film (for liquefying fuels, see later). The knowledge of the complex interactions between these wide-ranging physical phenomena is fundamental for hybrid motor design and performance prediction.

Modeling physical phenomena in the combustion chamber

The design of a hybrid engine generally requires lab-scale firing tests to characterize the regression rate as a function of the engine operating

conditions, the propulsive performances, etc. In order to limit these costly experimental campaigns, reliable numerical simulations are required. These simulations range from one-dimensional representations of the gaseous flow to three-dimensional and time resolved simulations of the internal geometry of the combustion chamber, with the degree of modeling complexity depending on the desired application. Thus, one-dimensional codes are preferred during the preliminary design phases, in order to be able to carry out many calculations in a relatively short time. The full Navier-Stokes simulations, providing much more details but being very costly in computation time, are, in turn, generally used for optimization steps and for the detailed understanding of physical phenomena. These two approaches need to be combined with experimental tests in order to validate the models and/or provide input conditions for the numerical calculations.

Description of a typical lab-scale facility

In order to validate the models and the numerical simulations, experiments are still required on instrumented lab-scale engines such as the HYCOM facility (Figure 3, left). Like most lab-scale hybrid rocket motors, the HYCOM facility is composed of five parts (Figure 3, right): a forward end-plate including the injector, a pre-chamber including the igniter, a combustion chamber, a post-chamber and a nozzle. This facility was designed by making the different parts modular, to easily change the lengths of the pre- and post-chambers, the geometry and the type of fuel grain, etc. Some tests were performed with a catalytic injector, combining a catalyst bed and a gaseous swirl injector, instead of the classical atomizer [26]. The engine, which can operate at up to 7.5 MPa, is instrumented with a Coriolis mass flow meter for the oxidizer and four pressure probes (two in the pre-chamber and two in the post-chamber), and is connected to a thrust sensor to achieve the propulsive performances. In order to measure the fuel regression rate, the engine is also instrumented with ultrasound sensors (one located at the head-end of the fuel grain and two at the rear-end). This technique was initially developed for solid rocket applications and adapted for lab-scale hybrid engines [7,9,42]. It has the advantage of being non-intrusive and easily implemented, unlike visualization and X-rays measurement techniques.

Several firing tests have been performed and a large database is available for various configurations: oxidizer/fuel pair, fuel length and initial port diameter, oxidizer mass flux, nozzle throat diameter, etc. A typical result is presented in Figure 4. In this configuration, a catalyst injector was used [26].

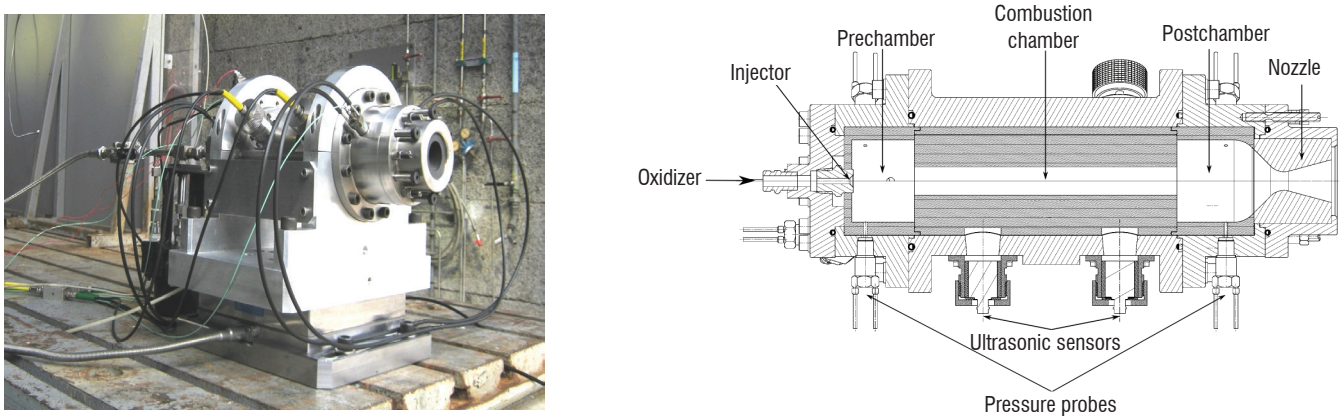

Figure 3 - HYCOM lab-scale engine (left) and schematic view of this facility (right)

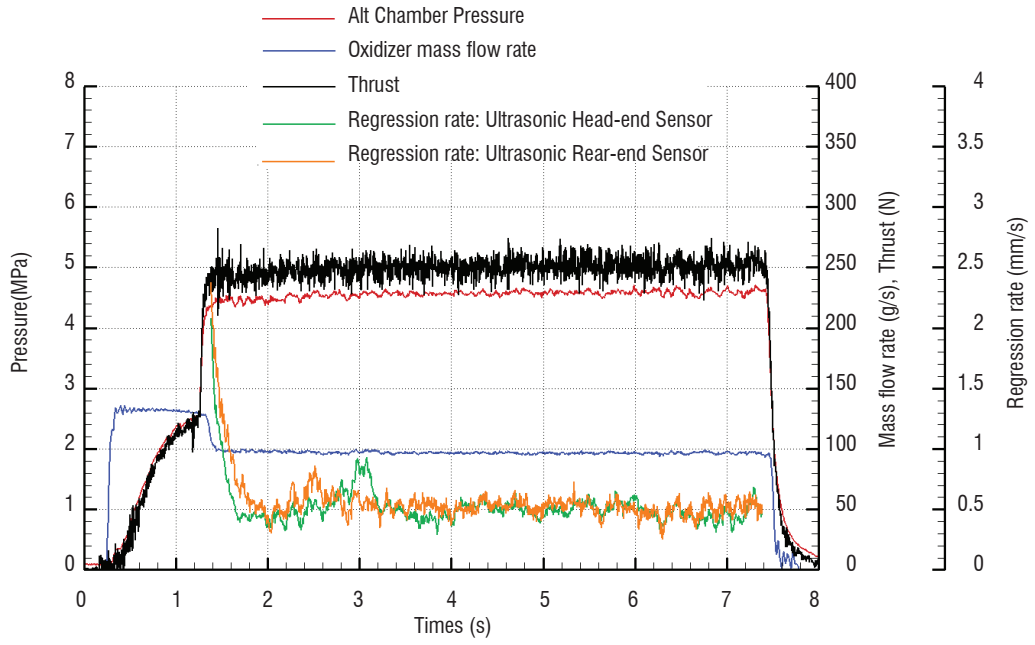

Figure 4 - Typical result obtained with the HYCOM facility

1D modeling

The objective of mono-dimensional codes is to provide a quick estimation of the propulsive performance of a hybrid engine as a function of the operating conditions, such as the oxidizer/fuel pair, the oxidizer mass flow rate, the dimensions and geometry of the fuel grain and the nozzle characteristics. Such codes also give an estimation of the average properties of the gaseous flow and of the fuel regression rate.

The main part of these numerical codes concerns the treatment of the flow inside the fuel channel. Since velocity gradients pilot heat and mass transfers, an aerothermochemical model based on an integral description of the flow in the combustion chamber seems more appropriate to describe the gaseous phase. The boundary layer integral method consists in integrating all of the transport equations along the normal direction of the fuel grain [27,33]. However, two configurations must be distinguished, according to the boundary layer development in a channel. For the first one, the boundary layer does not fully extend into the channel and an inviscid zone must be treated apart from the boundary layer zone while, for the second one, the boundary layer is fully developed and the confined fluid obeys a Poiseuille flow. It must be noted that this second configuration is only encountered for a high L/D ratio. With closure relations, the modeling of the gaseous flow provides the physical data (mass and thermal fluxes, etc.) at the gaseous/fuel interface to determine the fuel regression rate. This part has to be treated with two different approaches, according to the nature of the fuel grain.

For classical polymeric fuels, such as HTPB or polyethylene, the regression rate is modeled by an Arrhenius law (Equation (2)). This equation has to be combined with the energy balance at the solid/gas interface, which involves a balance between the convective, diffusive and radiative fluxes on the gas side and the diffusive and heat of pyrolysis fluxes on the solid fuel side. Finally, these two relations are closed, as described by Sankaran [43], due to the one-dimensional thermal conduction in the solid fuel, since its derivative form expresses the conduction heat loss in the fuel grain required in the energy balance at the solid/gas interface.

$$\dot{r} = A.\exp\left(\frac{-E_a}{RT_s}\right) \tag{2}$$

where A is the pre-exponential factor, E_a is the activation energy, R is the universal gas constant and T_s is the fuel surface temperature. The constants A and E_a only depend on the thermochemical properties of the fuel and are determined from fundamental experiments without reactive flow.

Although classical fuels have been largely studied, they suffer from a low regression rate (around 1 mm/s), which is detrimental for applications requiring high thrust values such as sounding rockets. Several studies were conducted in order to increase this regression rate value (addition of metallic particles, improvement of convective transfers between the gaseous flow and the solid fuel, etc.), without success [6,13,24,35,41]. A significant improvement was obtained when liquefying fuels, such as paraffin-wax, were experimentally tested by Karabeyoglu [17], providing regression rates two to four times higher than the values encountered with conventional fuels. Contrary to classical polymeric fuels, liquefying fuels pass into gaseous phase by forming a thin and hydro-dynamically unstable liquid layer, which is convected, vaporized and atomized, leading also to an increase in the fuel regression rate (Figure 5). The physics inside the combustion chamber thus differs from that encountered with classic fuels and, consequently, a new model had to be developed for the liquefying fuel regression rates.

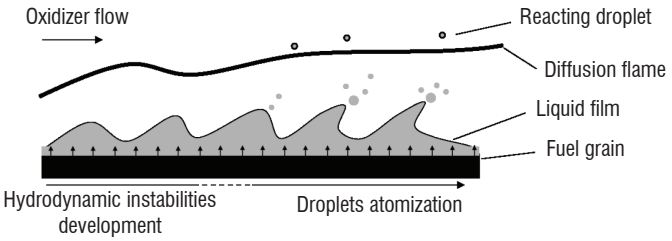

Figure 5 - Karabeyoglu's schematic diagram of the entrainment process for liquefying fuels [17]

As presented by Lestrade [27], such a model is based on a single equation model of the liquid film (Equation (3)). Combined with the momentum and energy equations in this layer and with the one-dimensional thermal conduction in the solid fuel (Equation (4)), this model provides the liquid film thickness, which determines the heat and mass transfers between the solid, liquid and gaseous phases. The mass transfer from the solid phase corresponds to the fuel regression rate.

$$\frac{d\rho_l \overline{u_l} h_l}{dx} = Q_{melt}\left(1-\frac{\rho_l}{\rho_s}\right) - Q_{vap} - Q_{atom} \tag{3}$$

where h_l is the liquid film thickness, $\overline{u_l}$ is the cross average liquid film velocity, ρ_s and ρ_l are the solid and liquid densities and Q_{melt}, Q_{vap} and Q_{atom} are the molten, vaporized and atomized mass fluxes.

$$T_s(y) = T_{amb} + (T_{melt} - T_{amb})\exp\left(\frac{Q_{melt} c_{p,s}}{\lambda_s} y\right) \tag{4}$$

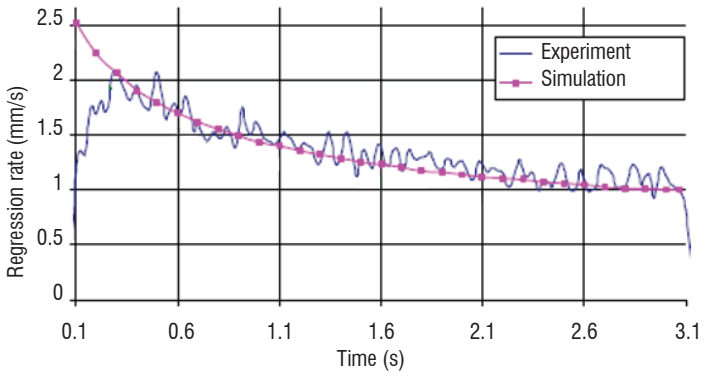

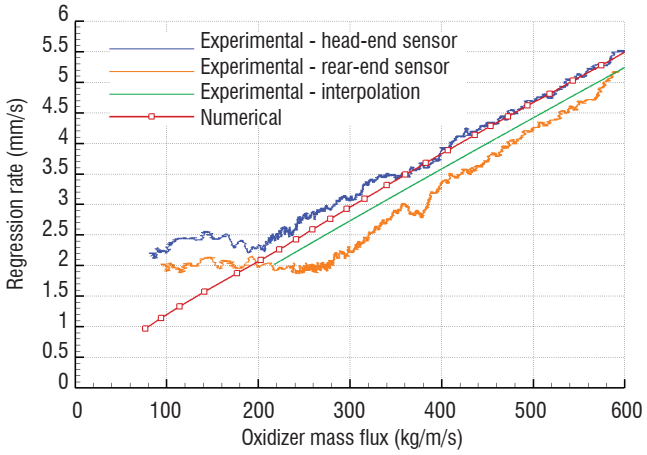

Figure 6 - Comparison between experimental and numerical regression rates for classical fuel (left) [3] and liquefying fuel (right) [27]

where T is the solid grain temperature, T_{amb} and T_{melt} are the ambient and the melting temperatures, $c_{p,s}$ is the solid heat capacity and λ_s is the solid heat conductivity.

As presented in Figure 6, the model developed to determine the regression rate for both classical and liquefying fuels is in agreement with experimental values obtained using HYCOM-like facilities. These two one-dimensional codes can thus be used to provide a good estimation of hybrid engine propulsive performances as function of their size and operating conditions. Nevertheless, the use of these numeral codes is limited to the quick dimensioning of hybrid engines and does not help to understand the internal physical phenomena occurring in the combustion chamber. 2D and/or 3D CFD simulations are required.

Computational Fluid Dynamics for hybrid engines

Numerical simulations are used to improve the comprehension of the internal flow and predict the behavior of the engines. Cheng et al [10] developed a 3D RANS model including, respectively, a Lagrangian approach for liquid droplet transport and an Eulerian approach for the gaseous stream. Surface pyrolysis based on an Arrhenius law has been used by Sankaran and Merkel [44] and by Serin and Gogus [45]. Sankaran [43] made an important contribution to hybrid flowfield calculations. His model is based on the time-dependent Navier-Stokes equations, including turbulence, gas-phase radiation, a finite-velocity model for the combustion, and a coupling between the gaseous and solid-fuel phases based on Relation (2).

Numerical simulations have recently been performed at ONERA [31] using the CFD finite volume code CEDRE [36] to numerically analyze an experimental firing test performed with decomposed hydrogen peroxide as oxidizer and high density polyethylene as fuel. These simulations are based on the Unsteady-Reynolds-Averaged Navier-Stokes equations with an additional transport equation for the species. The k-ωSST model [30] is used for turbulence, combining the k-ω model close to the walls and the k-ω model in the external flow. The gaseous phase reactions are defined by a two-step mechanism (Equation (5)). As done by the authors mentioned above, the chemical reaction rates are modeled by an Arrhenius law whose coefficients are given by Westbrook and Dryer [46]. Reactive phase flows are generally modeled by simplified mechanisms. Thermal radiation is not taken into account.

$$\begin{aligned} C_2H_4 + 2O_2 &\rightarrow 2CO + 2H_2O \\ CO + 0.5O_2 &\leftrightarrow CO_2 \end{aligned} \qquad (5)$$

The computation geometry, considered to be 2D axisymmetric, is fixed at the initial instant. The flow is completely single-phase and the walls are assumed to be adiabatic. The fuel boundary condition is treated as an injecting wall (no slip condition). The fuel mass flow rate is constant and defined based on the measurements from the baseline firing test [31], since the regression rate model (Equation (2)) is under development in CEDRE. When such a law becomes available, the model will provide a local and temporal estimation of the fuel mass flow rate, including its possible fluctuations. The oxidizer injection mass flow rate and temperature are imposed from the baseline test measurements.

The comparison between numerical and experimental results is based on the internal pressure. Numerical sensors have been placed at the same locations as the pressure probes in the experimental facility, which enables the experimental pressure to be compared to the simulated pressure and their Fast Fourier Transform. The 2D U-RANS computation gives a mean pressure of 4.32 MPa compared to the experimental pressure of 4.15 MPa. This difference may be explained by various factors: firstly, the real injection geometry is approximated (holes were replaced by axisymmetric rings). Secondly, the boundary condition for the fuel mass flow rate is uniform along the grain and the thermal losses are not taken into account in the simulation.

According to the ratio between the turbulent and the classical viscosities, which changes from 20 to about 500, and to the Reynolds number based on the fuel port diameter, which is around 150 000, the flow can be considered as fully turbulent. The diffusion flame is consequently located within the turbulent boundary layer (Figure 7). The oxidizer is concentrated along the engine axis and the gaseous flow is accelerated due to the total mass flow rate increase along the fuel grain.

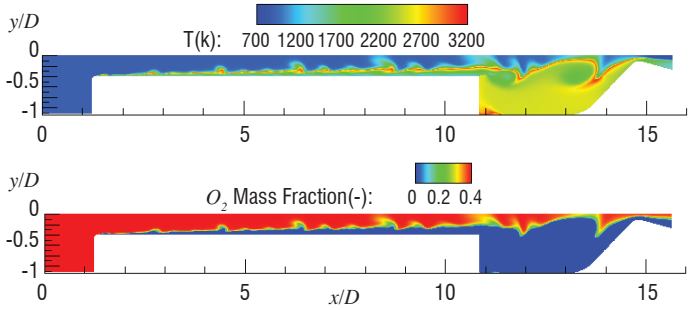

Figure 7 - Temperature and oxidizer mass fraction fields

The correspondence between the fuel mass fraction and vorticity fields shows that large-scale vortices containing unburnt fuel are formed at the end of the fuel grain (Figure 8). These coherent structures seem to play a major role in the mixing in the post-chamber, since they transport unburnt fuel from the end of the grain to the nozzle.

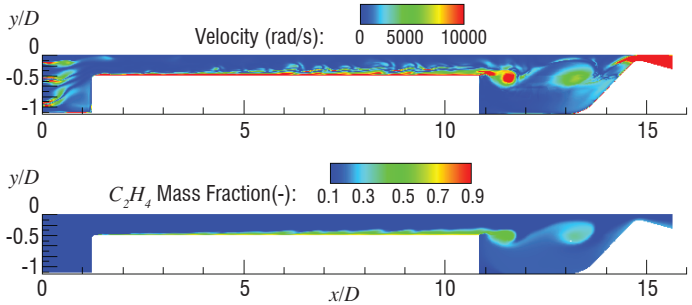

Figure 8 - Vorticity and fuel mass fraction fields

Crossing the nozzle throat, these structures lead to pressure fluctuations in the combustion chamber, which can be visualized by calculating the FFT on the pressure signals (Figure 9). A large peak at 470 Hz is observed for the firing test and at 530 Hz for the simulation. The numerical amplitude of the pressure instability is close to 2.5% of the mean pressure in comparison to the 1.9% during the experimental firing test. The results are close, even though the computation presents pressure instabilities with slightly higher frequencies and magnitudes than the firing test. A more detailed analysis of this instability is presented in the next part.

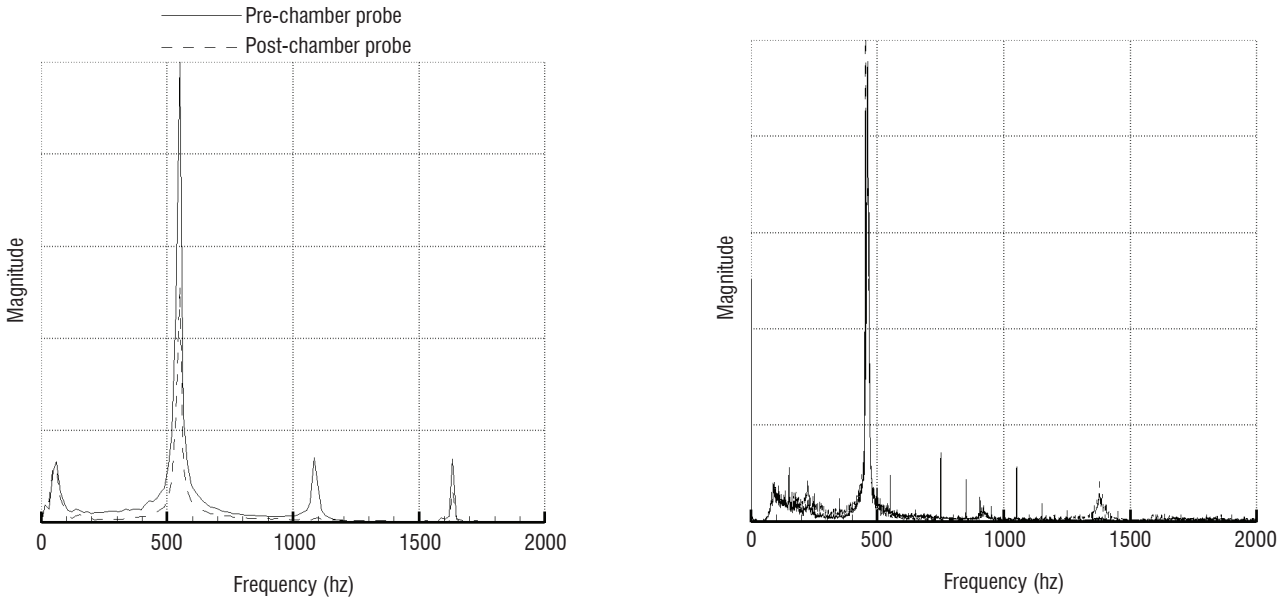

Figure 9 – Numerical (left) and experimental (right) FFT on the pressure signal

Instabilities

Several kinds of instabilities are possible in hybrid engines and may be provoked by acoustics, hydrodynamics or combustion. Low frequency instabilities have been studied by Karabeyoglu et al [16,18] and combine thermal lag in the solid grain, combustion and gas dynamics. Carmicino [8] studied the interaction between different instabilities and revealed the importance of vortex shedding for hybrid rocket motors. Recent studies showed the formation of small-scale vortices in the near wall region leading to small variations in the pressure amplitude [19,20]. Acoustic instabilities are generally related to classical longitudinal modes or to the Helmholtz modes [11].

In this study (Figure 9), the main instability is hydrodynamic and provoked by vortex shedding at the end of the fuel grain, as described by Carmicino [8]:

$$f = \eta c_{th}^{*} \psi^{2} S_{D} \frac{D_t^2}{D^3} \qquad (6)$$

where η is the combustion efficiency, c_{th}^{*} is the theoretical characteristic velocity, ψ is a function of the isentropic coefficient, S_p is the Strouhal number based on the end-port diameter D, and D_t is the nozzle throat diameter. The Strouhal number varies in the range of 0.25 to 0.5 for free and ducted non-reacting jets, which could lead to the frequency range of 440-880 Hz. The relation provides a good order of magnitude, but the estimated frequency is strongly dependent on the Strouhal number, a priori unknown.

Another approach, based on the Rossiter vortex shedding theory in a cavity [40], is used to provide an approximation of the main frequency peak. The vortex impingement on a surface generates an acoustic pulse traveling back upstream and generating a new vortex at the shear layer initiation point. For small Mach numbers, it can be expressed as [37]:

$$f = \frac{U}{L}\left(\frac{m-\alpha}{M+1/k}\right) \qquad (7)$$

where L and m are respectively the distance and the number of vortices between the shear-layer initiation and the impingement point, U and M are the freestream velocity and Mach number, k is the ratio of the vortex transport velocity to the freestream velocity and α is a dimensionless empirical constant. The empirical model leads to the range of 380-510 Hz for the vortex shedding frequency, which is in agreement with the observed peak at 470 Hz.

Finally, a low frequency shift ranging from 470 Hz to 455 Hz was observed during the firing test. This shift was explained based on the Rossiter's approach considering the variations of the end-port diameter as inducing a variation in the main stream velocity [31].

Application to sounding rocket propulsion

Hybrid rocket engines are not competitive for the first stages of large launchers. However, they could become competitive for the third stages of such launchers, or for new space missions, such as sounding rockets for Cubesat launches, mars landers, space debris deorbiting systems, spacecraft propulsion, missile systems, etc. [28]. The application to sounding rockets is discussed in this section, while a vision for spacecraft propulsion is presented in the last section.

LEX sounding rocket

The earliest work on hybrid rockets was conducted in 1933 by Tikhonravov and Korolev. With the GIRD-9 sounding rocket based on LOx and jellified gasoline, they reached an altitude of 1.5 km. In the late 1930s, both Germany and the USA started also developing hybrid engines and a rocket was taken to an altitude of about 9 km [14] in June 1951.

Intensive research on hybrid propulsion started at ONERA as from 1956, at the initiative of Barrère and Moutet [4,5,12]. The program, called LEX for Lithergol Experimental, was aimed at developing an autonomous rocket with reduced technological developments and a low-cost production. Six years later, ONERA investigated all aspects of hybrid propulsion and developed the MT.27 hybrid engine using a hypergolic propellant based on nitric acid and an amine fuel. The combustion time of the engine was between 30 and 35 s for an operating

pressure of 75 bar and a thrust of 10 kN, providing a total impulse of 100 kN.s. The MT.27 hybrid engine was integrated into the LEX sounding rocket. The first flight (LEX.01) took place in April 1964 and was the first flight of a hybrid rocket in Europe. It was limited to 12 s of operation by reducing the oxidizer mass, in order to avoid reaching a populated area. The launch was aimed at comparing flight data to ground firing tests and the performances were found to be identical. This first test was followed by three successful flights in 1965 and four other flights in 1967, both with the LEX.02. Figure 10 shows the drawing and main features of the LEX02 rocket and a launch from the Isle of Levant. The last flight exceeded an altitude of 100 km, with a rocket weighing 80.5 kg and a meteorological payload of 9.5 kg, which was a record for that time. An instrumented parachute, dropped at the apogee, allowed wind measurements during the 31 min of the descent. The flight tests of 1967, which concluded the LEX program, proved that a hybrid engine with modulated thrust could be cheap and that the performance of this hybrid engine combined with its simplicity make it the best candidate for sounding rockets.

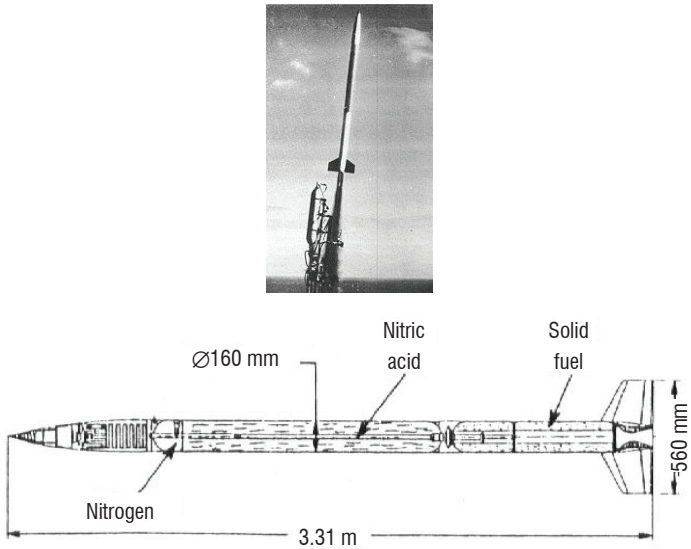

Figure 10 - LEX02 sounding rocket section (bottom) and flight test (top)

PERSEUS project

The PERSEUS project (Projet Etudiant de Recherche Spatiale Européen Universitaire et Scientifique / University and scientific European space research student project) is an initiative of the Launch Directorate of the CNES, the French Space Agency, to promote the emergence of innovative technical solutions for space projects, accomplished by students [34]. The main objective of the project is to make a set of ground and flight demonstrators as a precursor to a nano-satellite (from 10 to 50 kg) launch system.

ONERA's propulsion laboratory has been actively participating in this adventure from the beginning, particularly through the development of a small hybrid engine meant to propel experimental rockets developed by students and flown during the annual C'Space meeting [35]. This FUSEX engine in its original form consists of:

- a 3.5 liter reservoir;
- a pyrotechnical guillotine valve;
- a titanium combustion chamber;
- a graphite convergent and nozzle.

The self-pressurization capacities of N_2O allow an extremely simple concept without pumps or supplementary pressurization systems.

Thrust modulation

For its fifth flight on a rocket named Amidala and developed by S^3 (the student rocketry club involved), the FUSEX engine has been equipped with a two-stage valve upstream from the guillotine valve. This allowed for an in-flight variation of the oxidizer mass flow and hence for a thrust modulation during flight [15]. During the take-off phase, the valve is completely open and the oxidizer mass flow is unobstructed. At a pre-defined instant, a linear motor retracts and releases a notch. The spring loaded valve flips and partially obstructs the flow. Both the instant of modulation and the reduction level are variable, but defined before flight. A possible, future, modification would be to replace the spring and notch mechanism with a stepper motor, to allow for continuous modulation during the entire flight. Several cold ground tests have validated the concept.

Encouraged by a successful first test run with half of the oxidizer charge (1.4 kg of N_2O), we repeated the run, this time with a full oxidizer tank (2498 g) and we delayed the valve timing to 2.5 s with a reduction of 92% of the passage surface in order to obtain a thrust reduction of around 50%. Figure 11 (left) gives the results of this run and has confirmed that the design was working and resulted in a 59% thrust reduction, a total impulse of 7545 N.s and a specific impulse of 227 s. We decided to keep the same configuration for the certification firing (needed to obtain flight authorization from the organization of the C'Space event). Figure 11 (right) yields the results of this final test run and once again confirms the flawless and reproducible functioning of our Thrust Modulation Module (TMM). This last run resulted in a 57% thrust reduction, a total impulse of 7609 N.s and a specific impulse of 220 s. The variation in impulse and thrust values is due to the sensibility of our self-pressurized oxidizer

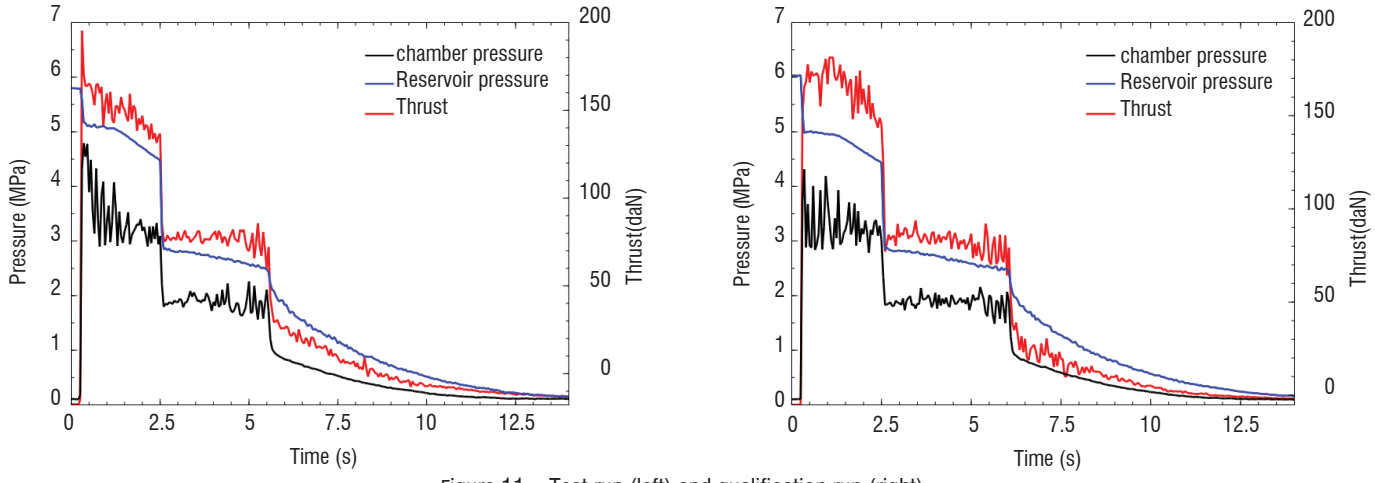

Figure 11 – Test run (left) and qualification run (right)

system to the external temperature. This is a drawback that proved to be rather severe during the launch.

On August 21st, 2011, students, rocket and engine were taken to the C'Space site near Biscarosse. There, the final assembly and tests were completed before the launch date, set for August 24th. One of the C'Space regulations states that the recovery system timing has to be fixed to a certain period of time after the rupture of the umbilical. The period is to be determined with a performance simulation, using a spreadsheet simulation provided by Planètes Sciences called Trajecto. This works reasonably well for solid propulsion, where engine performances are more or less reproducible. However, for our self-pressurized hybrid engine this is a problem, since the engine performance depends significantly on the external conditions, especially the ambient temperature at the time of the launch. This played a major role in the events that followed.

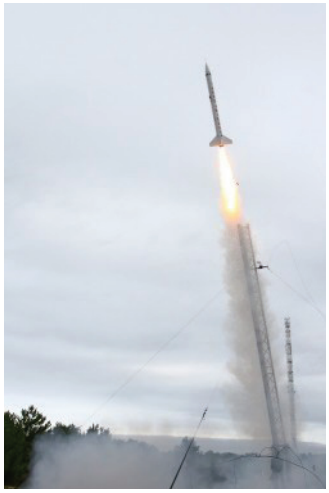

Figure 12 - Lift off (courtesy of Julian Franc (Planètes Sciences))

On the 24th , we were ready to go but already at dawn we noticed that the weather god was not on our side; it rained and instead of the heat that we had suffered from during the preparation phase we measured a meager 17°C. So much for our predictions! We only managed around 50 bars of reservoir pressure, which is at least 10 bars less than for the qualification test (Figure 11). The water also hindered the packing of the parachute, adding insult to injury. Despite the weather, we managed to get Amidala ready on the launch pad at 10:15. Several seconds later, with a roar that is typical for hybrid engines, Amidala freed itself from the launchpad and hurled into the overcast skies. About 2.5 seconds after lift-off a sudden change in pitch indicated that the TMM had kicked in. About 20 seconds later, Amidala pierced the clouds and disappeared from sight. We all waited for the distinct thud of the parachute opening but instead we only heard an increasing whining followed by a bang as Amidala hit the ground. It was clear that the recovery system had failed and that our rocket had gone ballistic. Due to the lower tank pressure, performances were diminished and the rocked reached apogee too soon. Therefore, when the deployment timer triggered the release mechanism, the air speed was too high and the ejection mechanism not strong enough to overcome the dynamic pressure; the destruction was quasi complete. Apart from the on-board camera, which miraculously survived the crash, all of the payload was wrecked leaving us with only the down-linked data (limited to reservoir pressure and temperature) and the Pitot pressures stored in the nosecone but valid only up until separation.

Given the limited data, the reconstruction of the flight was difficult and approximate at best. Coupling data from the high-speed camera at lift-off, the telemetry and the Pitot measurements resulted in the reconstructed thrust curves given in Figure 13. We see that there is a rather large difference in the maximum thrust found through the various methods. This is certainly due to the big differences between the conditions of the flight and those of the ground-based experiments that served to convert the flight data. However, it is very clear that the objective, that is, an in-flight modulation of the thrust, was met. This makes Amidala's flight a European first.

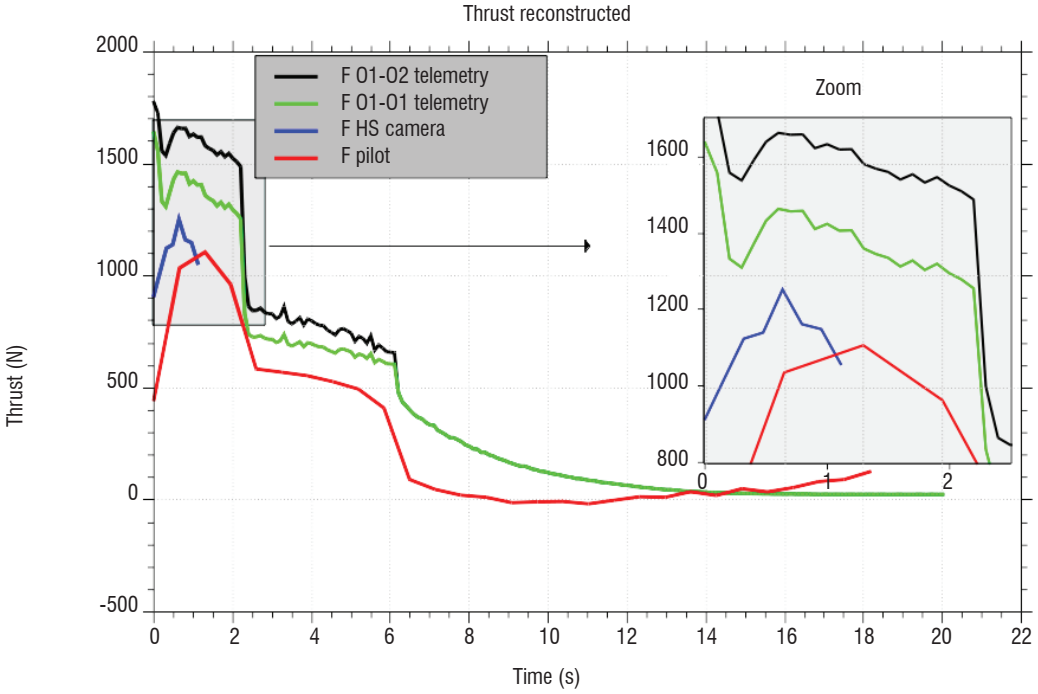

Figure 13 - Reconstruction of the thrust evolution

Vision for spacecraft propulsion

Although some hybrid rockets were tested in flight [15,22,34,35,38,39], thrust levels achieved with new fuels (liquefying and additive-doped classical fuels) still fall short of those provided by solid propellants and, consequently, hybrid propulsion cannot currently be competitive compared to solid propulsion. Nevertheless, thanks to its low regression rates and due to theoretical propulsive performances comparable to those of liquid engines, hybrid propulsion could be competitive with regard to liquid technology for missions requiring long firing duration, moderate thrust levels, flexibility (thrust modulation) and good propulsive performances (specific impulse and characteristic velocity).

Within the framework of the NEOSAT program, a new European platform for telecommunication satellites is under development, based on full electrical propulsion. Combining a chemical engine with the electric propulsion could be a very efficient alternative or complement (as an intermediate carrier) by reducing the GTO to GEO transfer duration from several months (full electrical) to few days (electrical / chemical). Compared to the current bi-liquid engine based on monomethylhydrazine (MMH) and nitrogen tetroxide (N_2O_4), hybrid propulsion offers positive expected impact at system level in terms of dry mass, performance and recurring cost. Indeed, with a theoretical specific impulse of the order of 300 s in a vacuum [28], hybrid propulsion is slightly less efficient than the current bi-liquid engines (320 s specific impulse in a vacuum and a few daN thrust). However, its design is simpler, and thus expected to be cheaper and lighter, and the density specific impulse is higher (fuels in solid phase generally have higher densities than those in liquid phase) reducing the overall system volume. Last but not least, hybrid propulsion is REACh (Registration, Evaluation and Authorization of Chemicals) compatible, thereby facilitating its implementation, and has throttling and restart capabilities to perform the satellite orbital injection.

However, the aforementioned theoretical specific impulse of 300 s was never experimentally proven from vacuum firing tests, mainly because of low combustion efficiency of this technology. Secondly, a sustained long duration burn (of the order of hours) with medium thrust is far from the specifications of a rocket propulsive phase and would require a dedicated design. These new mission requirements have a direct impact on the solid fuel regression rate in order to limit the size of the solid fuel combustion chamber. Regression rates of less than 0.1 mm/s would be needed, but these values are one order of magnitude below the regression rates obtained with polymeric fuels. The risk of combustion instabilities at such small regression rates is not negligible and neither is the risk of self-extinction of the engine. Another disadvantage of the conventional hybrid engine configuration (Figure 1) is the variation of the oxidizer-to-fuel ratio (O/F) during operation, since the fuel burn area steadily increases as the burn progresses, resulting in variations in the specific impulse. This is especially limits the application of hybrid propulsion for the satellite apogee engine when considering the conventional engine configuration. This is not the case for solid rocket engines, in which the stoichiometric ratio is obtained by the correct mixing of the oxidizer and fuel directly cast in a solid powder. For bi-liquid engines, the stoichiometric ratio is guaranteed by using controlled injection valves and turbo-pumps.

In order to demonstrate the vacuum specific impulse, ONERA developed and qualified a new research facility for high-altitude testing. Due to time and budget constraints (only four months to design and put into service the vacuum test facility), an existing low-density wind tunnel was recycled into an 18 m^3 "vacuum" test facility (Figure 14, top) and adaptations were made to make it compatible with hybrid propulsion testing. A vacuum pump was used to provide an initial pressure of 1 mbar in the vacuum chamber. However, since the vacuum pump did not run during firing tests, the pressure inside the vacuum facility constantly increased during a test due to the exhaust gas, restricting the test duration. Wall passages through flanges of the vacuum chamber were set up to enable the cabling of the instrumentation connected to the engine, in order to operate the engine and to feed the engine with the oxidizer. The HYCOM hybrid engine (Figure 3) was modified with a new nozzle adapted to low ambient pressure. Two pressure taps were added on either side of the nozzle exit section, one inside the nozzle and one outside (Figure 14, low). Since the ambient pressure constantly increased during firing tests, these two measurements enabled us to know when the nozzle was adapted during the test.

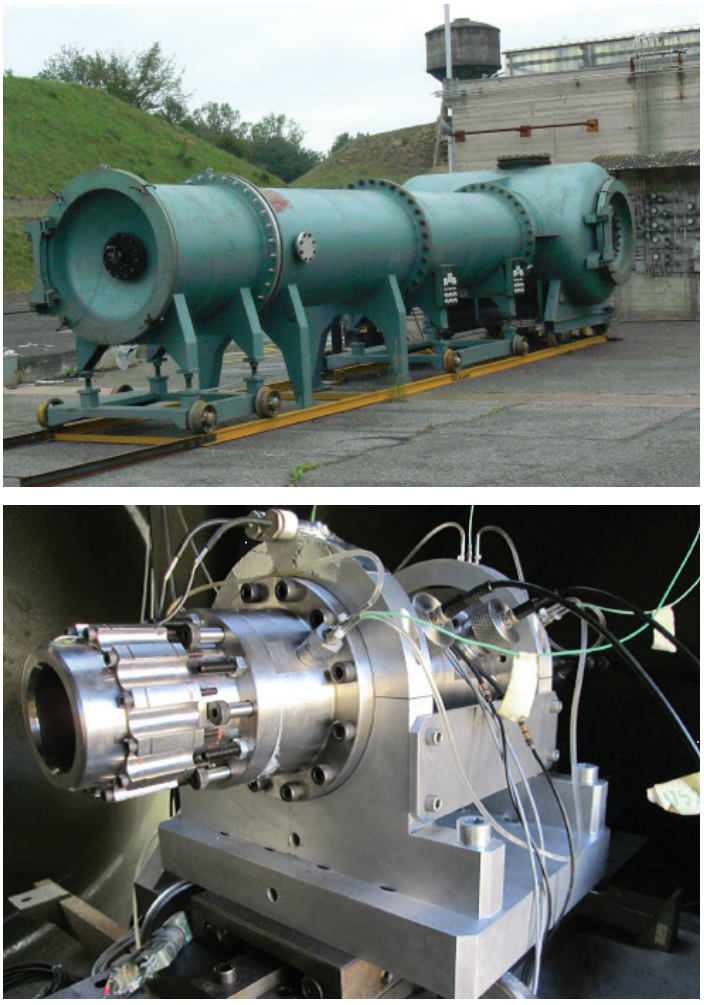

Figure 14 - Research facility for high-altitude testing

The expected performance of hybrid propulsion under satellite environmental conditions was assessed experimentally. The parameters of the hybrid engine have been selected to operate close to the stoichiometric oxidizer-to-fuel ratio. The first test campaign in the new test facility, based on a nozzle expansion ratio of 50, resulted in a combustion efficiency of the order of 85% and a specific impulse of around 230 s. The deficit in the specific impulse performance is mainly due to the low value of the combustion efficiency. According

to the state-of-the-art in hybrid propulsion, how the oxidizer is injected strongly influences the engine performance, which can be explained by the role of the injector in the swirling and turbulence properties of the injected flow and in the atomization of the oxidizer.

The type of injector is the main parameter to increase the combustion efficiency. The first campaign involved a swirl injector providing coarse droplets. When using a swirl injector generating very fine droplets, the combustion efficiency was enhanced by 6%. Another way to increase the combustion efficiency is the catalytic injection of the oxidizer. Indeed, the injection of a hot gaseous oxidizer is expected to improve the mixture with the pyrolysis gas coming from the fuel grain and avoid using a part of the generated heat flux to vaporize and warm the liquid oxidizer. The catalytic decomposition of H_2O_2 also enables the combustion to be initiated without a pyrotechnic igniter.

Within the framework of a collaborative project between ONERA, Nammo and Saab, supported by the NEOSAT program, ONERA has recently plugged the Saab catalyzer and the Nammo swirl injector into the ONERA hybrid engine, whose instrumentation enables the instantaneous evolutions of the propulsive performances to be deduced [26]. Three firing tests for an oxidizer-to-fuel ratio close to the optimum one were performed: the two first tests at atmospheric pressure and the third one under low pressure conditions in the high-altitude test facility. The three firing tests have provided a mono-propellant phase of 1 s followed by a hybrid mode of more than 6 s (Figure 15). Thanks to the pressurization system of the oxidizer tank, the oxidizer mass flow rate was quite constant and very close to 100 g/s during the hybrid mode, which provided a chamber pressure of 4.5 MPa. The thrust for the tests at atmospheric pressure was equal to 250 N, while it achieved 300 N for the test under low ambient pressure conditions.

The experimental results from the three firing tests were analyzed following two methods. The first one, based on averaged quantities, showed a very good repeatability of the three firing tests in terms of chamber pressure, oxidizer mass flow rate, mixing ratio and combustion efficiency, which achieved 98%. The averaged specific impulses were in agreement, for the two tests at atmospheric pressure, with a value close to 230 s. This value was increased for the test under low pressure conditions and reached 272 s with a nozzle expansion ratio of 50, which is consistent with the extrapolation made from the results of the atmospheric pressure tests. Compared to the first test campaign, the combustion efficiency has been improved by over 15% and a gain of over 40 s was measured in the specific impulse. The second analysis method considered the instantaneous data based on the ultrasonic measurement technique, which enabled the evolution of the fuel regression rate during the firing tests to be deduced. It is then possible to plot the instantaneous evolution of the experimental specific impulse as a function of the oxidizer-to-fuel ratio, which presents an evolution similar to the theoretical one (Figure 16). The dispersion of the experimental data around the averaged value is due to both the combustion instabilities inherent to all types of chemical engines and the uncertainty in the ultrasonic sensor measurements.

Based on the experimental results of the test performed under low pressure conditions, an extrapolation to the satellite conditions can be achieved by assuming the same efficiencies (98% and 91.4% for the combustion and engine efficiencies), the same chamber pressure and the same oxidizer-to-fuel ratio. According to the isentropic laws, the extrapolated performances with a nozzle expansion ratio of 400 should be 302 s in a vacuum for hydrogen peroxide concentrated at 87.5%. Moreover, according to the hydrogen peroxide supplier, it would be possible to consider H_2O_2 at 98% for a commercial engine. In this case and assuming a catalyzer adapted to this hydrogen peroxide concentration, the vacuum specific impulse should be 320 s for a nozzle expansion ratio of 400. It should be noted that the two previous extrapolated values are computed based on a nozzle efficiency of 93%, which can still be improved. Using a standard nozzle efficiency of 98%, the expected specific impulse for a hybrid engine operating with a nozzle expansion ratio of 400 and with hydrogen peroxide concentration of 98% would be 337 s. This value is competitive if compared to the current bi-liquid MMH/N_2O_4 engine.

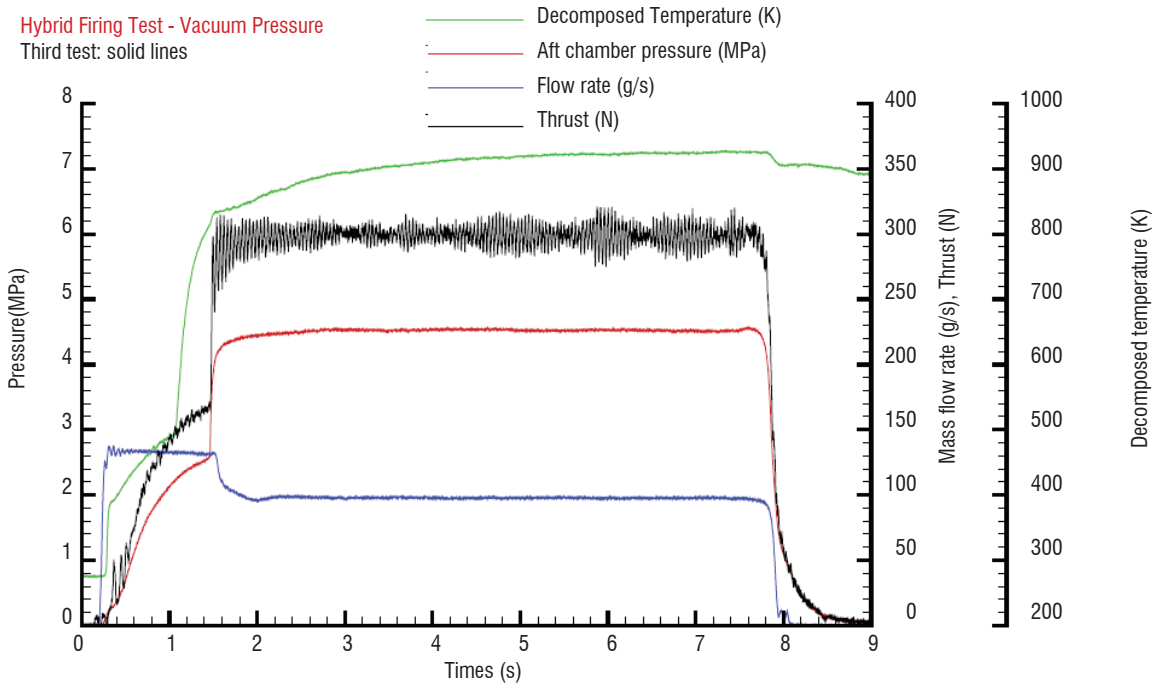

Figure 15 - Experimental results of the firing test performed under low pressure conditions

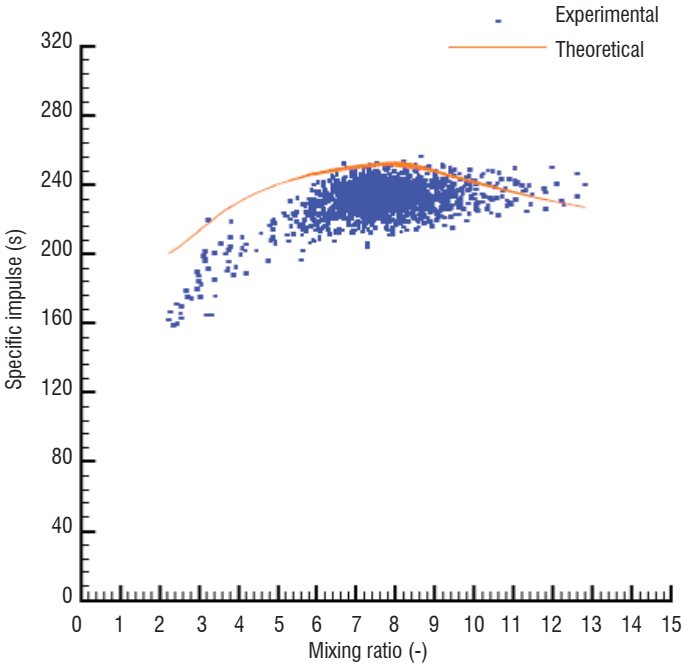

Figure 16 - Evolution of the specific impulse as a function of the mixing ratio for the first atmospheric firing test

The next step consists in developing a hybrid engine compatible with the satellite mission requirements, i.e., a long duration burn with medium and constant thrust. Long duration meaning more than one hour, this represents a technology breakthrough compared to the rocket engine applications. The main impact concerns the combustion chamber configuration and the nozzle erosion. These challenges are being investigated within the framework of the H2020 European project HYPROGEO, coordinated by Airbus DS. The project is aimed at improving the technological maturity of key components of the hybrid chemical propulsion technology, in order to allow independent access to new space transportation missions and to obtain significant cost reductions. The targeted application is a kick-stage module that can be plugged into a full electrical satellite platform in order to reduce the transfer duration from the GTO to the GEO orbits. This module also combines hybrid chemical engines and electrical thrusters to optimize its efficiency in term of propulsive performances, mass, cost, etc. In this context, the objective of WP2, led by ONERA, is to develop a new innovative combustion chamber architecture compatible with the mission needs. Indeed, due to the radial regression of the fuel, the classical configuration of a hybrid engine (Figure 1) is not reconcilable with these specifications, since the propulsive performances evolve over time and the diameter of the fuel grain would not be consistent with the accommodation constraints. At the beginning of the HYPROGEO project, highly innovative combustion chamber designs were created, but only one should remain at the end of the project. Consequently, the first task in the WP2 was to perform a trade-off between these concepts to select the most promising architecture of the combustion chamber, which will be further investigated, manufactured and tested later in the project. The selected architecture is based on the piston concept, in which the fuel grain burns like a cigarette and its regression is balanced with the displacement of the fuel grain thanks to a system to be defined (i.e., pressurized gas at the top of fuel associated with a stop in the combustion chamber, etc.). The gaseous oxidizer, coming from the catalyzer, is injected from the wall to the center of the combustion chamber. Further R&D activities

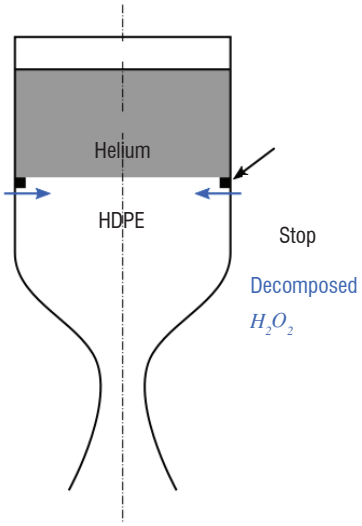

Figure 17 - Principle scheme of the combustion chamber for the satellite apogee engine

are now planned, including CFD analysis to help the design of the hybrid engine demonstrator. The firing tests are planned for the beginning of 2017.

Concluding remarks

New transportation vehicles for space exploration missions or microgravity experiments would require simplified, low-cost and thrust-modulated operations combined with a high level of performance, reliability and availability. These capabilities could be achieved through hybrid propulsion, which combines a solid fuel with a liquid oxidizer. However, the hybrid propulsion concept has never been the subject of thorough studies, mainly because heavy investments were made in liquid and solid space propulsion making them today nearly unavoidable for large space launchers and sounding rockets. The demand for a new small launch system could justify maturing this technology today. However, the scaling of hybrid rocket technology would first need to be demonstrated, in order to develop this technology for these kinds of applications.

ONERA has developed a know-how of more than 40 years in the hybrid propulsion concept, based on theoretical, experimental and numerical approaches. The first European hybrid rocket (LEX) was launched by ONERA in 1964, followed by 7 other successful flights in 1965 and 1967. Twenty years ago, ONERA again started research activities on hybrid propulsion based on polymeric fuels and more recently on liquefying fuels, which provide higher regression rates compatible with launcher applications. A large database of static firing tests is available for various operating conditions and fuel compositions. Some successful flight tests also took place within the PERSEUS program. Appropriate numerical models are also available for predicting the fuel regression rate and CFD is now widely used to better understand the physical mechanisms and instabilities inside the combustion chamber. Finally, firing tests were performed to demonstrate the validity of the extrapolation of the propulsive performances from atmospheric pressure to vacuum pressure conditions.

Future activities are based on the development of an innovative combustion chamber architecture compatible with satellite mission requirements, within the framework of the HYPROGEO project. Moreover,

this development does not require a scale factor study, since the geometry of such a combustion chamber and its dimensions are comparable with current lab-scale facilities. From 2016 to 2020, ONERA will also support and finance its own project on hybrid propulsion, called HYSAC. It will be aimed at strengthening ONERA skills in terms of numerical modeling of the combustion chamber, oxidizer injection, fuel formulation, definition of thermal protection materials and optimization of propulsive performance of the hybrid propulsion technology, with the goal of designing an innovative engine for a launcher upper-stage ■

Acknowledgements

The authors would like to thank the French Space Agency (CNES), the French Armament Procurement Directorate (DGA), the H2020 program of the European Union, the Midi-Pyrénées Region, Airbus DS and Thales Alenia Space for funding research studies and equipment that contributed to this research work. The authors would also like to thank Michel Prévost, Yves Maisonneuve, Gérard Lavergne and Nicolas Pelletier.

References

[1] D. ALTMAN, A. HOLZMAN - *Overview and History of Hybrid Rocket Propulsion.* Fundamentals of Hybrid Rocket Combustion and Propulsion, edited by M. J. Chiaverini and K. K. Kuo, Progress in Astronautics and Aeronautics, Vol. 218, Academic Press, New York, 2007, pp. 1-36.

[2] D. ALTMAN, R. HUMBLE - *Hybrid Rocket Propulsion Systems.* Space propulsion analysis and design, edited by R. Humble, G. Henry and W. Larson, McGraw-Hill, New York, 1995, pp. 365-441.

[3] J. ANTHOINE, Y. MAISONNEUVE, M. PREVOST - *The Hybrid Propulsion to Serve Space Exploration and Micro-Gravity Experiments*. 61st International Astronautical Congress, Prague, Czech Republic, 2010, IAC-10-C4.6.9.

[4] M. BARRÈRE, A. MOUTET - *La propulsion par fusées hybrides*. 14th International Astronautical Congress, Paris, France, September 25 - October 1, 1963.

[5] M. BARRÈRE, A. MOUTET - *Liquid-Solid Rockets*. International Science and Technology, August 1967, pp. 64-74.

[6] M. CALABRO, L.T. DE LUCA, L. GALFETTI, H. RAINA, C. PERUT - *Advanced Hybrid Solid Fuels.* International Astronautical Congress, Hyderabad, Inde, 2007, IAC-07-C4.2.09.

[7] C. CARMICINO, A. RUSSO-SORGE - *Performance Comparison Between Two Different Injector Configurations in a Hybrid Rocket*. Aerospace Science and Technology, Vol.11, 2007, pp. 61-67.

[8] C. CARMICINO - *Acoustics, Vortex Shedding, and Low-Frequency Dynamics Interaction in an Unstable Hybrid Rocket*. Journal of Propulsion and Power. Vol. 25, No. 6, 2009, pp. 1322-1334.

[9] F. CAUTY - *Non-Intrusive Measurement Techniques Applied to the Hybrid Motor Solid Fuel Degradation.* 2rd International Conference on Green Propellants for Space Application, Chia Laguna, Italy, 2004.

[10] G. CHENG, R. FARMER, H. JONES, J. MCFARLANE - *Numerical Simulation of the Internal Ballistics of a Hybrid Rocket Motor.* 32nd Aerospace Sciences Meeting and Exhibit, 1994, AIAA Paper 1994-554.

[11] S. DE ZILWA, G. ZILLIAC, M. REINATH, M. A. KARABEYOGLU - *Time-Resolved Fuel-Grain Port Diameter Measurement in Hybrid Rockets.* Journal of Propulsion and Power. Vol. 20, No. 4, 2004, pp. 684-689.

[12] P. DUBAN - *La fusée sonde LEX*. Aéronautique et Astronautique, Vol. 2, 1968.

[13] B. EVANS, N.A. FAVORITO, E. BOYER, G.A. RISHA, R.B. WEHRMAN, K.K. KUO - *Characterization of Nano-Sized Energetic Particle Enhancement of Solid-Fuel Burning Rates in an X-ray Transparent Hybrid Rocket Engine*. 40th Joint Propulsion Conference, July 2004, AIAA Paper 2004-3821.

[14] E.G. EWING - Journal of the Pacific Rocket Society, Vol. 2, 1947.

[15] J. HIJLKEMA, G. CASALIS, F. LAURENDEAU - *On the Development and Successful Application of a Thrust Modulation Module for the FUSEX Hybrid Rocket Motor.* Space Propulsion 2012, Bordeaux, France, 2012.

[16] M. A. KARABEYOGLU, D. ALTMAN - *Dynamic Modeling of Hybrid Rocket Combustion*. Journal of Propulsion and Power. Vol. 15, No. 4, 1999, pp. 562-571.

[17] A. KARABEYOGLU, G. ZILLIAC, B.J. CANTWELL, S. DE ZILWA, P. CASTELLUCI - *Scale-Up Tests of High Regression Rate Liquefying Hybrid Rocket Fuels*. 41st AIAA Aerospace Sciences Meeting & Exhibit, 2003, AIAA Paper 2003-6475.

[18] M. A. KARABEYOGLU, S. DE ZILWA, B. CANTWELL, G. ZILLIAC - *Modeling of Hybrid Rocket Low Frequency Instabilities*. Journal of Propulsion and Power. Vol. 21, No. 6, 2005, pp. 1107-1116.

[19] B. KIM, Y. NA, K.-H. SHIN, C. LEE - *Nonlinear Combustion and Fluid Mechanics in a Hybrid Rocket*. Journal of Propulsion and Power. Vol. 28, No. 6, 2012, pp. 1351-1358.

[20] B. KIM, Y. NA, C. LEE - *Non-linear Combustion and LES Study for the Fluid Mechanics in Hybrid Rocket*. 4th European Conference for Aerospace Sciences (EUCASS). Saint Petersburg, Russia, 2011.

[21] W. KNUTH, D. GRAMER, M. CHIAVERINI, J. SAUER - *Solid-Fuel Regression Rate Behavior of Vortex Hybrid Rocket Engines*. Journal of Propulsion and Power, Vol. 18, No. 3, 2002, pp. 600-609.

[22] P. KUENTZMANN, H.J. STERNFELD - *What Future for Hybrid Rocket Propulsion?* "Symposium on Launcher Propulsion Towards the Year 2010," Bordeaux, France, 1991, pp. 159–168.

[23] K. K. KUO, M. CHIAVERINI - *Challenges of the Hybrid Rocket Propulsion in the 21st Century.* Fundamentals of Hybrid Rocket Combustion and Propulsion, edited by M. J. Chiaverini and K. K. Kuo, Progress in Astronautics and Aeronautics, Vol. 218, Academic Press, New York, 2007, pp. 593-638.

[24] C. LEE, Y. NA, J.W. LEE & Y.H. BYUN - *Effect of Induced Swirl Flow on Regression Rate of Hybrid Rocket Fuel by Helical Grain Configuration*. Aerospace Science and Technology, Vol. 11, No. 1, 2007, pp. 68-76.

[25] G. LENGELLE, Y. MAISONNEUVE - *Hybrid Propulsion: Past, Present and Future Perspectives*. 6th International Symposium on Propulsion for Space Transportation of the 21st Century, Versailles, France, 2002.

[26] J.-Y. LESTRADE, J. ANTHOINE, O. VERBERNE, A. J. BOIRON, G. KHIMECHE, C. FIGUS - *Experimental Demonstration of the Vacuum Specific Impulse of a Hybrid Rocket Engine*. 50th AIAA/ASME/SAE/ASEE Joint Propulsion Conference, 2014, AIAA Paper 2014-3951.

[27] J-Y. LESTRADE, J. ANTHOINE, G. LAVERGNE - *Liquefying Fuel Regression Rate Modeling in Hybrid Propulsion*. Aerospace Science and Technology, Vol.42, 2015, pp. 80-87.

[28] F. MARTIN, A. CHAPELLE, O. ORLANDI, P. YVART - *Hybrid Propulsion Systems for Future Space Applications*. "46th AIAA Joint Propulsion Conference," 2010. AIAA Paper 2010-6633.

[29] G. MARXMAN, M. GILBERT - *Turbulent Boundary Layer Combustion in the Hybrid Rocket*. 9th International Symposium on Combustion, Academic Press, 1963, pp. 371-372.

[30] F. R. MENTER - *Zonal Two-Equation k-omega Turbulence Models for Aerodynamic Flows*. 24th AIAA Fluid Dynamics Conference, 1993, AIAA Paper 1993-2906.

[31] J. MESSINEO, J.-Y. LESTRADE, J. ANTHOINE - *Numerical Simulation of a H_2O_2/PE Hybrid Rocket Motor*. 6th European Conference for Aerospace Sciences (EUCASS). Krakow, Poland, 2015.

[32] R.J. MUZZY - *Schlieren and Shadowgraph Studies of Hybrid Boundary Layer Combustion*. AIAA Journal, Vol. 1, 1963, p. 2159.

[33] N. PELLETIER, Y. MAISONNEUVE - *A Numerical Code for Hybrid Space Propulsion Design & Test*. 3rd International Conference on Green Propellants for Space Propulsion, Poitiers, France, 2006.

[34] M. PRÉVOST, Y. MAISONNEUVE, C. DUPONT, M. BULLOCK, R. BEC, N. PILLET, R. BARENES - *The PERSEUS Student Launcher Project and Associated Hybrid Propulsion Activities*. "42nd AIAA Joint Propulsion Conference," 2006. AIAA Paper 2006-4317.

[35] M. PRÉVOST, P. PRÉVOT, E. ROBERT - *Realisation of the FUSEX Hybrid Engine: Development, Tests: the First Success in Flight*. 2nd International Symposium on Propulsion for Space Transportation, Heraklion, Greece, 2008.

[36] A. REFLOCH, B. COURBET, A. MURRONE, P. VILLEDIEU, C. LAURENT, P. GILBANK, J. TROYES, L. TESSÉ, G. CHAINERAY, J. B. DARGAUD, E. QUÉMERAIS, F. VUILLOT - *CEDRE Software*. Journal AerospaceLab, 2011, Issue AL02-11.

[37] D. ROCKWELL - *Oscillations of Impinging Shear Layers*. Journal of the American Institute of Aeronautics and Astronautics.Vol. 21, No. 5, 1983, pp. 645-664

[38] J.E. RONNINGEN - *Post-Flight Analysis of a Hybrid Test Rocket Flight*. "59th International Astronautical Congress," Glasgow, United Kingdom, 2008. IAC-08-C4.2.7.

[39] J.E. RONNINGEN, N. KUBBERUD - *Hybrid Rocket Motor Testing at Nammo Raufoss A/S*. "17th ESA Symposium on European Rocket and Balloon Programmes and Related Research," Sandefjord, Norway, 2005. ESA SP-590.

[40] J. E. ROSSITER - *Wind Tunnel Experiments on the Flow Over Rectangular Cavities at Subsonic and Transonic Speeds*. Aeronautical Research Council Reports and Memoranda. No. 3438, 1964.

[41] A. RUSSO SORGE, C. CARMICINO - *Performance Comparison Between Two Different Injector Configurations in a Hybrid Rocket*. Aerospace Science and Technology, Vol. 11, No. 1, 2007, pp. 61-67.

[42] A. RUSSO SORGE, A. ESPOSITO, G. QUARANTA, G. TORELLA - *Regression Rate Measurements in a Hybrid Rocket*. 36th AIAA/ASME/SAE/ASEE Joint Propulsion Conference, 2000, AIAA Paper 2000-3438.

[43] V. SANKARAN - *Computational Fluid Dynamics Modelling of Hybrid Rocket Flowfields*. Fundamentals of Hybrid Rocket Combustion and Propulsion, M. J. Chiaverini, K. K. Kuo editors. Progress in Astronautics and Aeronautics Series. Vol. 218, Chap. 8, 2007, pp. 323-349.

[44] V. SANKARAN, C. MERKLE - *Size Scale-Up in Hybrid Rocket Motors*. 34th Aerospace Science Meeting and Exhibit, 1996, AIAA Paper 96-0647.

[45] N. SERIN, Y. GOGUS - *Navier-Stokes Investigation on Reacting Flow Field of HTPB/O2 Hybrid Motor and Regression Rate Evaluation*. 39th AIAA/ASME/SAE/ASEE Joint Propulsion Conference and Exhibit, 2003, AIAA Paper 2003-4462.

[46] C. K. WESTBROOK, F. L. DRYER - *Simplified Reaction Mechanisms for the Oxidation of Hydrocarbon Fuels in Flames.* Combustion Science and Technology. Vol. 27, 1981, pp. 31-43.

AUTHOR

Jean-Yves Lestrade is a research scientist at ONERA. He received his Engineering diploma from ENSIETA in 2009, a Master of Sciences Degree from ISAE-ENSMA in 2009 and a PhD in Energetic and Transfers from ISAE in 2012. His research activities are mainly related to hybrid propulsion. He is also the WP2 leader of the H2020 HYPROGEO project and is the coordinator of the HYSAC project

Jérôme Messineo has been a PhD student at ONERA's Propulsion Laboratory since October 2013. His research field is mainly focused on numerical simulations and instabilities of hybrid rocket engines. He received his Engineering Diploma from ISAE-ENSMA and a Master of Sciences Degree from UPS at ISAE-SUPAERO in 2013.

Jouke Hijlkema is a senior scientist at ONERA. He performs research in the domain of rocket propulsion and manages projects with government agencies and industrial customers. He received a masters degree in aeronautical engineering from Hogeschool Haarlem and a masters degree in mathematics from the university of Nijmegen, both in the Netherlands. He obtained a PhD from ISAE in Toulouse in the field of applied mathematics.

Pierre Prévot, is a senior scientist at ONERA. He has worked for many years in studies and tests in the fields of solid, liquid and hybrid propulsion at the Propulsion Laboratory. He received his engineering diploma from ESSTIN in Nancy in the field of fluid mechanics and energetics.

Grégoire Casalis is the scientific deputy director of DMAE. His scientific topics are related to flow stability from generic configurations (laminar boundary layer) to complex ones (internal solid rocket motor flow).

Jérôme Anthoine is the Head of the Propulsion Laboratory Unit of the ONERA Aerodynamics and Energetics Modeling Department (DMAE). He received a Mechanical Engineering Degree from the Faculté Polytechnique de Mons (Belgium) in 1995, the von Karman Institute Diploma in 1996 and a Ph.D. in Space Propulsion from the Université Libre de Bruxelles in 2000. Then, he joined the Faculty of the Von Karman Institute to develop the aeroacoustics and space propulsion activities. Since 2009, he has been a senior scientist in Space Propulsion at ONERA and is currently managing research activities on pressure oscillations in solid rocket motors and on hybrid chemical propulsion.

L. Vingert, G. Ordonneau, N. Fdida, P. Grenard
(ONERA)

E-mail: lucien.vingert@onera.fr

DOI : 10.12762/2016.AL11-15

A Rocket Engine under a Magnifying Glass

Even though the technology of cryogenic rocket engines is well mastered today, and has been applied successfully in many launchers all over the world, research activities on the various elementary or coupled processes involved in these complex systems are still relevant and useful for future developments, cost reduction, and knowledge improvement.
The Mascotte test facility was designed and built with this in mind twenty years ago. Since then, numerous configurations have been tested, enabling almost all of the phenomena involved in the operation of a rocket engine to be investigated, in a research lab environment, but nevertheless under representative conditions.
Research items addressed on the Mascotte test rig include: injector concepts; liquid oxygen jet atomization and combustion, new propellant combinations (methane instead of hydrogen), ignition, heat transfer at the chamber walls, high frequency instabilities, flow-separation in an over-expanded nozzle, plume and infrared signature.

Introduction

Chemical propulsion relies on the principle that energy is stored in the chemical reactants and supplied to the system through exothermic reactions. Despite the fact that reactants have a fixed amount of energy per unit mass, which limits the achievable exhaust velocity or specific impulse, and because the propellants are their own energy source, the rate at which energy can be supplied for propulsion is independent from the propellant mass. Thus, very high powers and thrust levels can be achieved. Among the numerous available propellants, the hydrogen/oxygen combination is the most efficient in terms of specific impulse. Even though the development of a device often precedes detailed understanding of the phenomena prevailing there, for instance liquid oxygen/hydrogen (LOX/H2) was envisaged for J2 and RL10 engines at the end of the fifties and used in the Apollo program, the best use and optimization of an engine performance are possible only if the basic physical phenomena and their coupling are well understood and described. These various items require well instrumented testing, modeling and research activities. It is the reason why many teams all over the world have worked on this subject for decades, and still do.

It is indisputable that the technology of cryogenic rocket engines is well known today, and that it has been applied successfully in many launchers (Saturn V, Ariane 1 to 5, Space Shuttle, H-II, etc.), but the low cost development of such complex systems, which have to be increasingly performing and reliable, is still a big challenge for the manufacturers, even more so with reusability, which appears as the main driver for future applications [1]. In addition, in recent years, the propellant combination liquid oxygen/methane (LOX/CH4) has attracted considerable attention in the USA, Europe and Japan for attitude control, upper stage or booster engines. Methane has two advantages over hydrogen, which compensates for the slight loss in specific impulse: its higher specific mass and the proximity of its thermal characteristic to those of oxygen, especially its liquefaction temperature. Both permit cost reduction through simplification of the stage: smaller tank volume and easier to handle cryogenic technology, thanks to the higher temperature, around 100 K instead of 20.

Up to now, the standard practice in the design of space propulsion systems has mostly relied on accumulated know-how and trial and error methodologies, even though computational tools have been progressively introduced in the design process, taking advantage of the increase in computational power. Nevertheless, numerical codes need to be validated on detailed experimental results, gained under well controlled, but as representative as possible, operating conditions. With this objective in mind, ONERA designed the Mascotte test bench to examine a broad range of processes controlling the combustion of cryogenic propellants, such as atomization, droplet vaporization, combustion at high pressure under subcritical and transcritical conditions, etc. Other topics of major importance in liquid rocket engines, like ignition, combustion instabilities, heat transfer and nozzle flow separation, are investigated too. It was initially decided to work on single injector configurations fed with cryogenic propellants under

representative pressure and temperature conditions, but the more recent studies of ignition and high frequency instabilities were carried out on multiple injector configurations comprising up to five units arranged in a row or as a pack. The first years of Mascotte were devoted to the progress, in three directions in parallel. The first one was to increase the operation domain by progressively exploring high pressure conditions and reaching supercritical conditions of the type prevailing in cryogenic engines. The second point was the development of advanced and non-intrusive optical diagnostics adapted to these extreme conditions. These included high resolution spectroscopy, backlighting, OH* emission imaging, Planar Laser Induced Fluorescence (PLIF) of OH radicals, Raman scattering of oxygen and Coherent Anti-Stokes Raman Spectroscopy (CARS) of H2 and H2O molecules. The third work package was the building of an experimental database through intensive testing.

A number of research projects were carried out in the basic configuration of a coaxial injector fed with liquid oxygen and gaseous hydrogen. It was first important to examine the flame structure, stabilization process, operating parameter effects, pressure effects, processes controlling transcritical combustion and geometrical effects associated with the recess of the liquid oxygen channel. At the start of this experimental program, it was not known whether the flame was stabilized aerodynamically at a distance from the injection unit or whether the flame was attached to the injector unit or close to that unit. There were no data, at least in the open literature, that provided this information. While most experts believed that the flame was formed at a distance from the injector unit because of the very large velocities characterizing the hydrogen stream, the data gathered in the first experiments at low pressure (1, 5 and 10 bar) clearly indicated that the anchor point was very close to the oxygen channel lip. This contradicted initial beliefs and gave a lot of insight for engineering design. This essential finding was supported by direct emission imaging of the flame and by combined imaging using, for the first time in the case of cryogenic flames, Planar Laser Induced Fluorescence of OH and tomographic imaging of laser light scattering. Another important milestone was the application of Abel transform methods to emission imaging data. This tomographic technique allowed a slice of the mean flame to be extracted from imaging data gathered by line of sight techniques. It was the first demonstration of this method and its application to cryogenic flames. Again, these flame structures clearly indicated that emission from OH* radicals began in the near vicinity of the injector unit. The Abel transform method has since been applied in most studies where the mean flame structure is axisymmetric. Another issue of considerable engineering consequence was to understand the effect of a recess of the LOX channel. The recess that is typically adopted in rocket injectors is of the order of one diameter. Emission imaging combined with Abel transform techniques provided the fundamental information required to characterize the change of flame expansion rate due to the recess. Many of the studies performed at that time within the framework of the Coordinated Research Network “Combustion in liquid rocket engines” were summarized in previous review papers [4], [15], [42]. The effects of operating parameters were also extensively documented. It was in particular shown that the momentum flux ratio determined to a large extent the flame structure by directly influencing the quality of atomization. The momentum flux ratio was used in most studies dealing with the atomization and combustion processes at subcritical pressures, as in [8], [10], [11], [23] and [30]. The effect of pressure and in particular the structure of cryogenic flames under transcritical conditions was investigated during the later years of the 1990th and reported in [17]. This article describes the structure of cryogenic flames formed by injection of liquid oxygen and gaseous hydrogen at pressures exceeding the oxygen critical pressure of 5.04 MPa. The data was supplemented a few years later with images obtained from PLIF of OH at a pressure of 6.3 MPa. This dataset is perhaps the only one today that corresponds to laser induced fluorescence imaging at very high pressure [39].

The extension of the Mascotte test bench, which took place in a second stage [43] allowed new studies of flames formed by liquid oxygen and methane [46]. This has led to some unique findings [37], with in particular the first detailed analysis of flames formed by liquid oxygen and gaseous or liquid methane. The peculiar structure of liquid oxygen/liquid methane flames will be described later in this article. Much of the effort carried out up to the year 2005 was summarized in [5] and in [14]. Further work on liquid oxygen /methane flames was carried out with laser induced fluorescence imaging and emission imaging techniques. These allowed a detailed analysis of the flame structure up to a pressure of 2 MPa [38], [40]. In parallel, the CARS technique was adapted to use the methane as probe molecule [2] and later, a unique coupling between two CARS systems sampling simultaneously H2 and H2O [13] was operated within the framework of the European “In Space Propulsion” program[28]. The problem of flame stabilization was also revisited, by comparing the near field structures of liquid oxygen/gaseous hydrogen and liquid oxygen/methane flames [41]. This was used to verify a stability criterion derived in [18]. On a more practical level, a number of injector design issues have been considered. This is the subject of references [6] and [9] and will be used later on as an example of application of the test bench.

Much of the recent work on the Mascotte facility was carried out within the framework of the French-German REST (Rocket Engine Stability) program dealing with high frequency instabilities in rocket engines. Studies have been focused on the interaction between transverse acoustic waves and multiple flames established in a rectangular chamber equipped with large visualization windows and comprising an external actuator. A remarkable coupling observed in this configuration was reported in References [31] and [32]. Further experimental data were obtained using a novel actuator concept: the Very High Amplitude Modulator (VHAM). This was specifically intended to obtain very high amplitude levels of modulation in the transverse direction. It was thus possible to obtain acoustic pressure fluctuations in excess of 20% of the mean chamber pressure and to observe the interaction between multiple flames and transverse acoustic oscillations induced by the VHAM. An initial demonstration of the VHAM is proposed in [21]. Some experimental results obtained with the VHAM are reported in [22]. The VHAM was also used successfully in the very high pressure range (above the critical pressure of oxygen) and results obtained were used to validate a full Large Eddy Simulation of the Multiple Injector Combustor mounted on the Mascotte test bench [16]. Much of the data gathered on the Mascotte test bench has served to validate the new Large Eddy Simulation derived in recent years to calculate transcritical flows with combustion. This is exemplified in [36] where the case of a liquid oxygen /gaseous methane flame is considered. It is shown that the calculation retrieves most of the flame structure features and provides a good prediction of the flame length.

Another topic of considerable practical consequence is that of heat transfer to the chamber walls. This has been considered in a series of studies [7], [27], [29], [45] and some results will be used to illustrate this point. An aspect that also deserves attention is that of ignition.

Of course, it is difficult to represent conditions prevailing in the real engine at the start, but it is nevertheless interesting to examine ignition and subsequent flame spreading in a well-controlled set-up. The data could then be used for code validation. This is illustrated in [24], [35] and [44] and used as an example later in this article. The Mascotte facility has also been used to look at problems that do not concern the thrust chamber, but are closely related, such as the plume and infrared signature [3], [33], or the dynamics of the flow in the divergent part of the nozzle. Detailed measurements using state of the art laser diagnostics have been used to examine the possible combustion of the rich gases exhausted by the chamber with air entrained from the ambient atmosphere in the region of flow-separation in an over-expanded nozzle [25], [26] and [34]. This will be described in further detail in a later section of this article.

The previous review gives a synthetic view of the broad collection of results obtained using the Mascotte facility and underlines some of the highlights of research carried out with this test bench. Much more is available in the original references and no attempt will be made to bring these together. In what follows, after a brief presentation of the Mascotte test rig, we examine a set of four illustrative cases. § "Ignition" is concerned with ignition. Atomization is discussed in § "Atomization". The problem of flow separation in the nozzle is briefly considered in § "Flow separation in an over-expanded nozzle". Studies on heat transfer to the chamber walls are briefly described in § "Heat transfer" and a few other topics are mentioned in § "Other topics.

The Mascotte test facility

A brief history

The Mascotte test rig was developed at the beginning of the 90s to experimentally investigate the basic phenomena that occur in the combustion chamber of a cryogenic rocket engine, especially in the vicinity of a coaxial injector fed with liquid oxygen (LOX) and gaseous hydrogen (GH2). The research conducted there is linked to the need to continuously increase the performance and the reliability of the launchers, while simultaneously reducing costs and development times [15]. The objectives are to improve the knowledge of cryogenic propellants combustion, including dynamic aspects, to create an extended experimental data base, which will be later used to validate numerical codes, and to facilitate the selection of innovative technological concepts.

Successive versions were developed over the years to increase the operating domain and to extend the possibilities to new subjects. Versions 1 to 3, operated from 1994 to 2001, were dedicated to the LOX/H2 combustion studies, from atmospheric pressure, up to 70 bar [42]. The latter lies in the supercritical domain of oxygen, were most of the actual rocket engines operate (the critical pressure of oxygen is 50.4 bar) [5]. Various combustion chambers may be used, all equipped with optical access, like the one shown in Figure 1, which is a single-element combustor. In 2002, the facility was improved to offer the possibility to burn methane, in gaseous or liquid state, as well as hydrogen. This extension is referred to as version 4 [43]. During the period 2002-2005, new research topics were addressed, including dynamic aspects of the combustion like ignition, flame propagation with multi-element injection plates and instabilities at low and high frequency. Flow separation in over-expanded nozzles and also more technological considerations, for instance new injector's concepts, were investigated too. The present version 5, in operation since 2006, allows the use of gaseous oxygen at room temperature, while only liquid oxygen was available before. But the main change between versions 4 and 5 is related to the combustion chamber rather than to the test stand itself: a water-cooled chamber was designed and built that can be operated at a mixture ratio as high as 7.5 (oxygen/hydrogen), which is representative of thrust-chamber conditions, while the previous combustors, all based on the heat-sink technology, were limited to a mixture ratio of 3, and were therefore more suited for gas-generator studies. With this increase to more severe experimental conditions, a significant effort was also put on the improvement of safety and quality.

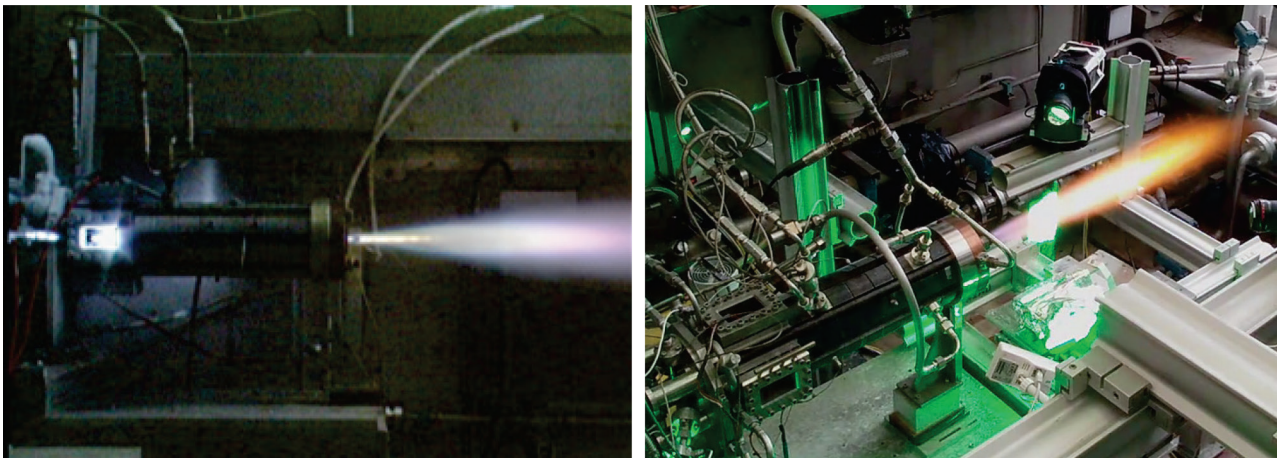

Figure 1 - Mascotte LOX/methane hot fire tests. Both cases: chamber pressure ≈ 10 bar, mixture ration ≈ 1.5
Left: liquid/gas injection Right: gas/gas injection with PIV in the plume.

Main characteristics - operating domain

With its main characteristics, recalled in Figure 2, Mascotte lies in an intermediate range, between laboratory scale setups and full scale industrial test rigs, with a dual purpose of investigating cryogenic propellants combustion and at the same time develop and apply advanced diagnostics [14] like Coherent Anti-Stokes Raman Spectroscopy [2], [13], Planar Laser Induced Fluorescence [25], [40], Phase Doppler Particle Sizing [11], Particle Image Velocimetry [9], [26]... Complementarity with the DLR means, P8 and M3, of the Space Propulsion Institute in Lampoldshausen may also be mentioned [15].

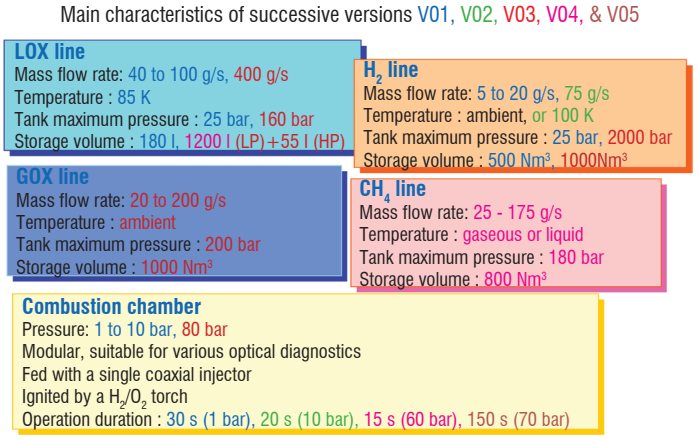

Figure 2 – Main characteristics of Mascotte

Ignition

Ignition of cryogenic rocket engines is still a challenging issue. It became critical in Europe in the mid-eighties when hard starts were responsible for flight failures. At that time, manufacturers and space agencies had to deal with the emergency of flight recovery, and the problem was fixed by purely empirical means. Today, the specifications of the European engine VINCI, which is an expander cycle engine, include the ability of successive re-ignitions during the flight. The problem is therefore again of major importance, a framework in which CNES and ONERA, together with DLR, decided to follow a more scientific approach to the topic [24]. With this objective, specific test series were run on Mascotte [44] and on the DLR Lampoldshausen M3 facility [35]. The main difference lies in the ignition procedure: an H2/O2 torch as in an actual engine on Mascotte, and laser ignition on M3. The latter certainly yields more detailed information on the basic physics of the primary ignition phase and on the flame front velocity, but it has to be completed with more representative conditions, which is in fact the objective of on-going activities at the DLR P8 facility. Using laser ignition is indeed an option for future launcher evolutions. The main objective of the Mascotte test series was to characterize the influence of fuel injection on the ignition process. The parameters that were varied are the nature of the fuel (hydrogen or methane) and its injection velocity (i.e., mass flow rate), while all other parameters: geometry, test sequence and liquid oxygen flow, were maintained constant. A combustor equipped with large windows (Figure 4), fed by three coaxial injectors and ignited by a hydrogen/oxygen torch placed on the top of the chamber, was used for this purpose. Figure 3 shows the successive ignitions of the three injectors recorded at 25 frames per second.

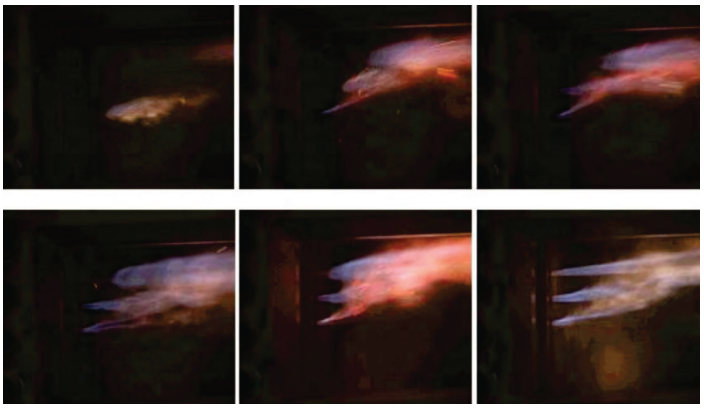

Figure 3 – Successive ignitions of the three jets(40 ms between 2 images)

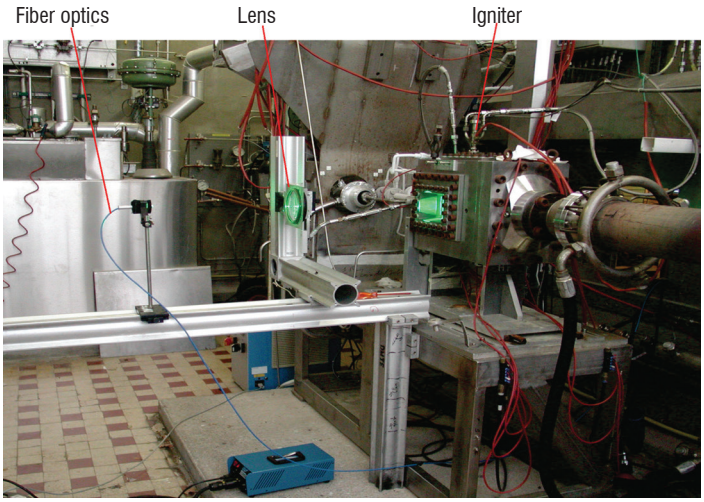

Figure 4 – Experimental setup: shadowgraphy with a laserstrobe as light source

The ignition process was recorded by means of two high speed digital video cameras. The first one (Phantom V4), operated by ONERA, was devoted to the visualization of the phenomena in the visible light range and the second one (Photron APX), operated by DLR, recorded the flame emission in the ultraviolet spectral band (i.e., the emission of the OH* radical at a wavelength of 306 - 320 nm). Both cameras were synchronized to the test stand monitoring and measurement acquisition systems. Besides the main parameters of the feed lines upstream of the injectors, three dynamic pressure transducers were recorded at a data rate of 40 kHz. The injection valve opening and torch ignition signals were also recorded at the same acquisition rate, in order to ensure that all devices were reproducible enough to state that any variation observed in the ignition delay was actually due to the physics, i.e., to a change in one of the investigated injector flow parameters, and not to any dispersion in the test sequence. Experiments corresponding to the various operating conditions were repeated four times: once with hydrogen and once with methane, and for two locations of the igniter. The operating points with the two fuels are very similar, in terms of dimensionless numbers (momentum flux ratio J and Weber number We). Figure 5 shows the reproducibility of the automatic sequence for the 58 acceptable tests. It appears that only the LOX valve response time is a little dispersed, but this has no incidence on the rest of the process, because we used a LOX-lead sequence. The opening of the LOX valve is the first event and, due to its size, its internal cross section becomes bigger than that of the cavitating venturi, which is used to regulate the LOX flow as soon as it is open a few per cent. This is confirmed by the LOX injection

pressures recorded for the same 58 tests (Figure 6): only run 56 is completely out of the family.

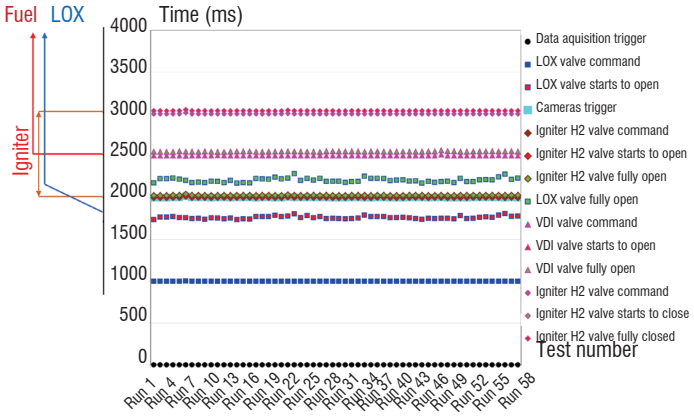

Figure 5 – Test sequence reproducibility (valves response and opening times in ms)

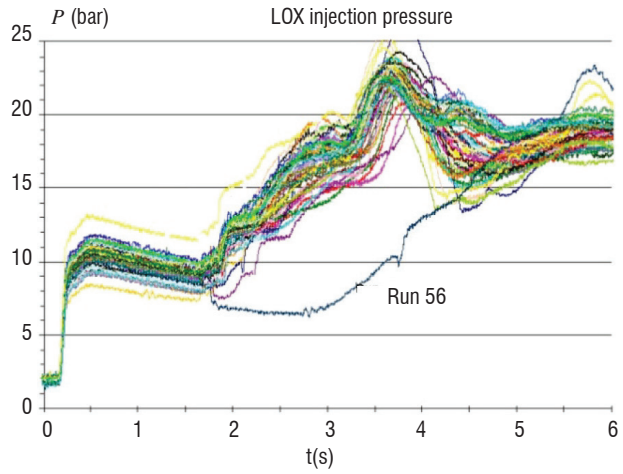

Figure 6 – LOX flow reproducibility (LOX injection pressure)

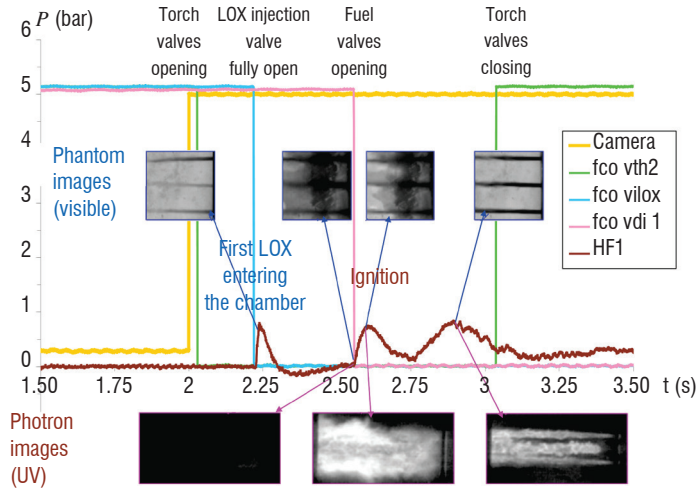

Figure 7 – Typical test: automatic sequence, dynamic pressure and images

The chamber dynamic pressure measured by means of a Kistler transducer located at the bottom of the combustor, in front of the igniter upstream position, has a similar time evolution for all validated tests (shown in Figure 7), with a first peak due to the chemical reaction between the first oxygen entering the chamber and the hot gases produced by the fuel rich igniter. The actual ignition of the jets, however, occurs only at the opening of the fuel valve and this corresponds to the second peak. This is confirmed by the images of the Photron camera (bottom images): no OH* radical emission is detected near the injectors before the second pressure peak. The third maximum is not well identified by the images: it happens during the stabilization phase of the flames on the lips of the LOX posts.

Figure 8 shows that the time delay between the opening of the fuel valve and the occurrence of the pressure overshoot decreased with the fuel mass flow rate (the fuel upstream pressure). A correlation equation can be found, with a correlation coefficient R^2=88% for the hydrogen tests. The methane tests are a little more scattered (R^2=60%), but the trend is clearly the same. It appears also that the ignition of the jets is delayed by around 50 ms when methane is used instead of hydrogen.

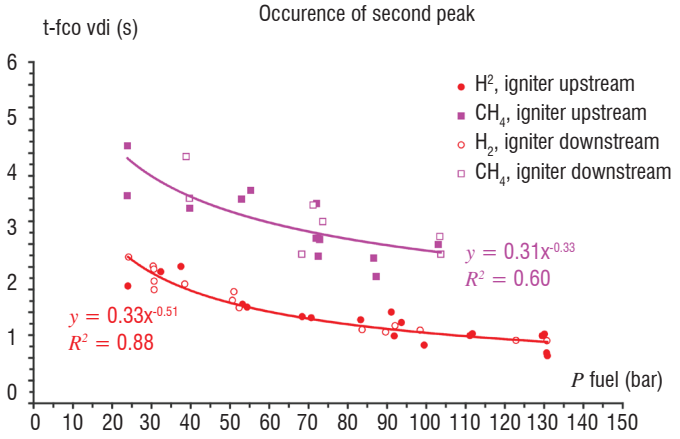

Figure 8 – Time delay between the fuel valve opening and pressure peak at ignition

Atomization

Injectors of cryogenic liquid rocket engines produce large polydisperse and dense sprays (Figure 9) due to the pressure and mass flow conditions. Atomization is the dominating process that drives the flame behavior in cryogenic jet flames, when the propellants are injected in subcritical conditions. The characterization of a liquid oxygen spray in gaseous hydrogen, under reacting conditions, was carried out on the Mascotte test bench [10] to complete the existing database [11] on a reference operating point, used as a test case for numerical simulation [23], [30]. In the breakup region, where liquid fragments detach from the LOX jet to disintegrate into smaller elements, liquid particles are not spherical. Since laser based drop size techniques make the assumption of spherical particles, they suffer from a low validation rate and thus imaging techniques can be better suited to characterize the spray. High speed shadowgraphs were used to provide the spray characteristics, such as sizes and velocities of the LOX dispersed phase atomized by a GH2 co-flow injected by a shear coaxial injector in a 10 bar combustion chamber.

The reacting case was compared qualitatively to a cold flow test, with helium instead of hydrogen, for which LOX spray shadowgraphs were also recorded. The morphology of the LOX jet at the injector exit was illustrated with small sized images, recorded at high frequency, for cold and reacting conditions, similar in terms of Reynolds and Weber numbers. The cold LOX jet was constituted by an envelope of small droplets

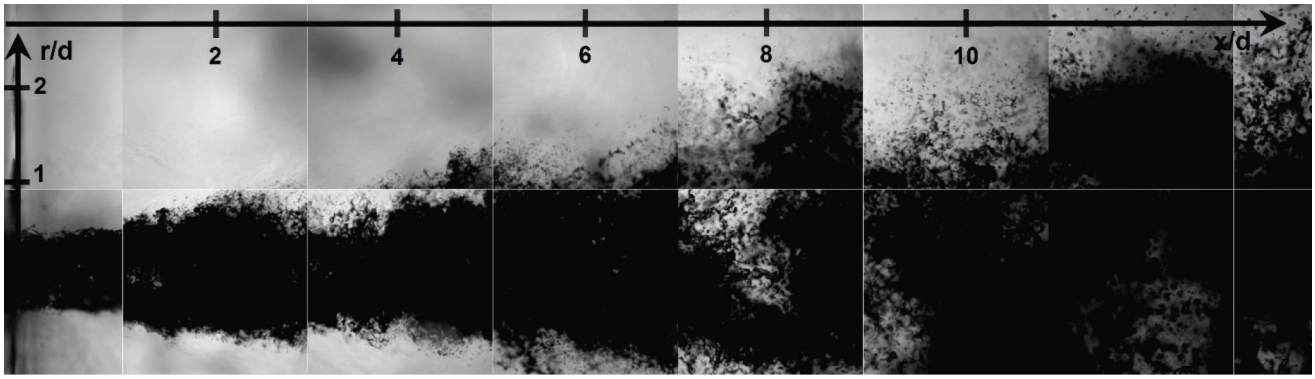

Figure 9 – Liquid oxygen jet structure at 10 bar (1 MPa)

around the LOX core, whereas in the reacting case, those small droplets were not present and larger liquid structures were revealed. The flame filters the smallest structures by vaporizing them from the beginning of the jet at the LOX post exit. The droplet sizes of the spray were obtained in the first and secondary atomization zone. The Sauter mean diameter evolution with axial distance showed a slight decrease towards the smallest diameters from $x/d=$ 6 to 12, at a radial distance of $r/d=2$, where d is the LOX post diameter. Far from the injector ($x/d=18$), the Sauter mean diameter was found to be similar to that measured in Ref. [11], with a Phase Doppler Particle Analyzer (PDPA). However, close to the injector, at $x/d=6$, where droplets are not spherical, size measurements were not in agreement and difficult to compare because the PDPA validation rate was very low in this area. The probability density functions pdf, illustrated in Figure 10, showed some features of such a burning spray: a large shape that seemed to be translated towards larger diameters, as the axial distance from the injector increased, which is probably due to droplet vaporization.

The velocity of the dispersed phase under reacting conditions was obtained with two different imaging methods, which were applied to the same shadowgraphs: a PTV (Particle Tracking Velocimetry) algorithm and PIV (Particle Image Velocimetry) software, FOLKI-SPIV, developed at ONERA. Velocity measurements obtained with both algorithms showed that droplet velocities decreased by a factor of 3 from $x/d=6$ to $x/d=12$. The droplet size was combined with PTV to obtain the droplet size/velocity correlations, presented in Figure 11, which are essential to understand the dynamics of the dispersed phase. The smallest droplets were decelerated more rapidly than the larger ones because, having less inertia, they are more sensitive to the aerodynamic forces in the turbulent flame. Close to the injector exit, at $x/d=6$, all droplets, whatever their size, were ejected with the same velocity. This particular area of the spray could indicate the first atomization zone where the droplet velocity comes from the liquid jet.

The velocity of the dispersed phase was also obtained with FOLKI-SPIV applied directly to shadow images. This method can be useful to obtain information on such a LOX spray, which is not compatible with most seeding particles. PIV and PTV algorithms agreed well in terms of U, V mean velocity and radial profiles in the investigated areas. FOLKI-SPIV gave better results in terms of the cross-correlation score and agreement when using a large interrogation window 99 pixels wide. In areas where the droplet density was not high enough, both methods diverged and we could not conclude in areas where the gas phase is in majority. Thus we chose to mask those areas where the algorithm was less reliable than PTV in terms of score.

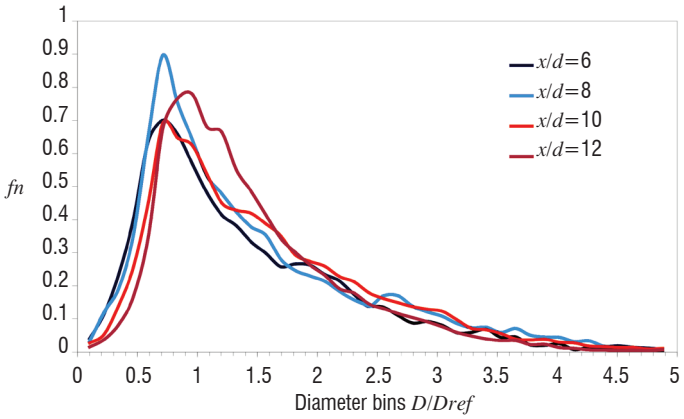

Figure 10 – Drop size distribution (pdf) evolution towards the injection axis from $x/d=$ 6 to 12, at a radial distance of $r/d=2$.

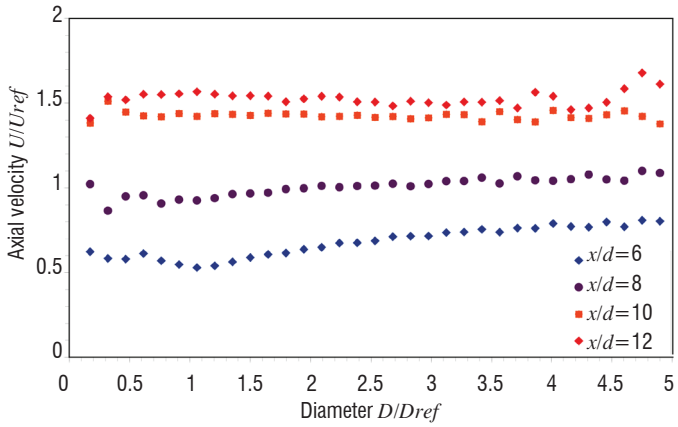

Figure 11 – Mean droplet axial velocity measured by PTV as a function of diameter class, evolution towards the injection axis from $x/d=$ 6 to 12, at a radial distance of $r/d=2$ (reacting case).

Flow separation in an over-expanded nozzle

The thrust delivered by a rocket engine depends on the combustion pressure, but also on the performance of the nozzle, which is characterized by its aspect ratio ε equal to the exit area divided by the throat area. The thrust increases with respect to the aspect ratio, while the pressure at the nozzle exit decreases in the same proportion. Knowing that the nozzles of the first stage of a launcher have to operate in a large range of ambient pressures, from sea-level atmospheric conditions (10^5 Pa) to very low pressure conditions

at high altitude (10^{-5} Pa), it appears that, at the very beginning of the flight, the wall pressure level required for an adapted attached flow can be much lower than the ambient pressure. This leads to a flow separation in the nozzle extension. In addition, due to the high level of stagnation enthalpy in liquid-rocket nozzles, the wall of the nozzle extension is exposed to high heat fluxes. These can be overcome by using a cooling film. The problem is that the film has to remain efficient all along the wall, even if an over-expansion shock interacts with it.

Within the joint CNES-ONERA research program on nozzle and after-body aerodynamics (ATAC), a general test plan for the establishment of a database for the validation of aerothermochemical codes has been drawn. The experimental set-up consists of a 2D nozzle operating with hot gases resulting from oxygen/hydrogen combustion. The first test series, aimed at investigating the re-ignition process and obtaining a correlation between pressures and temperatures at the walls, which are the only measurements available on a full-scale nozzle [25]. In addition, optical measurements, such as Planar Laser-Induced Fluorescence (PLIF), Particle Image Velocimetry (PIV) and Coherent Anti-Stokes Raman Scattering (CARS), previously successfully applied in a study on reactive rocket engine plume [33], are required to characterize the aerothermomechanical flowfield in the separation zone for various separation configurations (i.e., without separation, incipient separation and effective separation) corresponding to stagnation pressures from 20 to 60 bar.

For this purpose, it was necessary to design a planar geometry for the sub-scale nozzle, in order to fit it with appropriate windows, and to meet several criteria linked to the operating conditions of the set-up and to the aerodynamic pattern of the flow field. These were chosen to ensure similarities with nozzles planned for future launch vehicles. Moreover, the geometry had to be optimized, in order to obtain a sufficiently large recirculation zone where optical measurements can be performed. The main geometrical characteristics of the nozzle profiles are presented in Figure 12a. The nozzle width is 26 mm. One of the most critical parts of the nozzle is the 1 mm lip, where the film is injected, which is subject to high thermal stress.

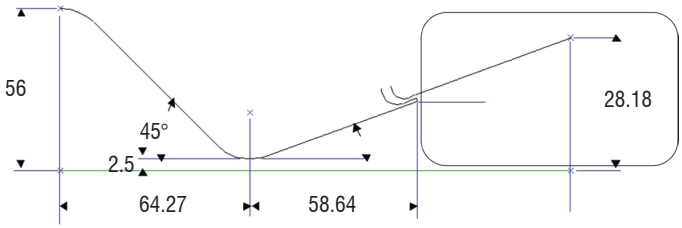

a) Geometrical characteristics of the nozzle with window

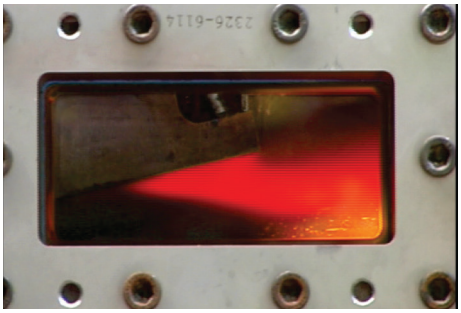

b) flame in the separated zone

Figure 12 – The two-dimensional nozzle of the ATAC program

Currently, PLIF on the OH* radical [26] was used to analyze the combustion region in the nozzle (Figure 13). The laser pulse was emitted by a Nd:YAG pumped dye laser (Quantel YG780 and TDL70) and a doubling crystal. The pumping laser wavelength was tuned to the appropriate transition Q1(3). Among the operating points tested during the adaptation campaign, only those at 25 bar (effective separation) and 40 bar (incipient separation) were retained to perform PLIF measurements.

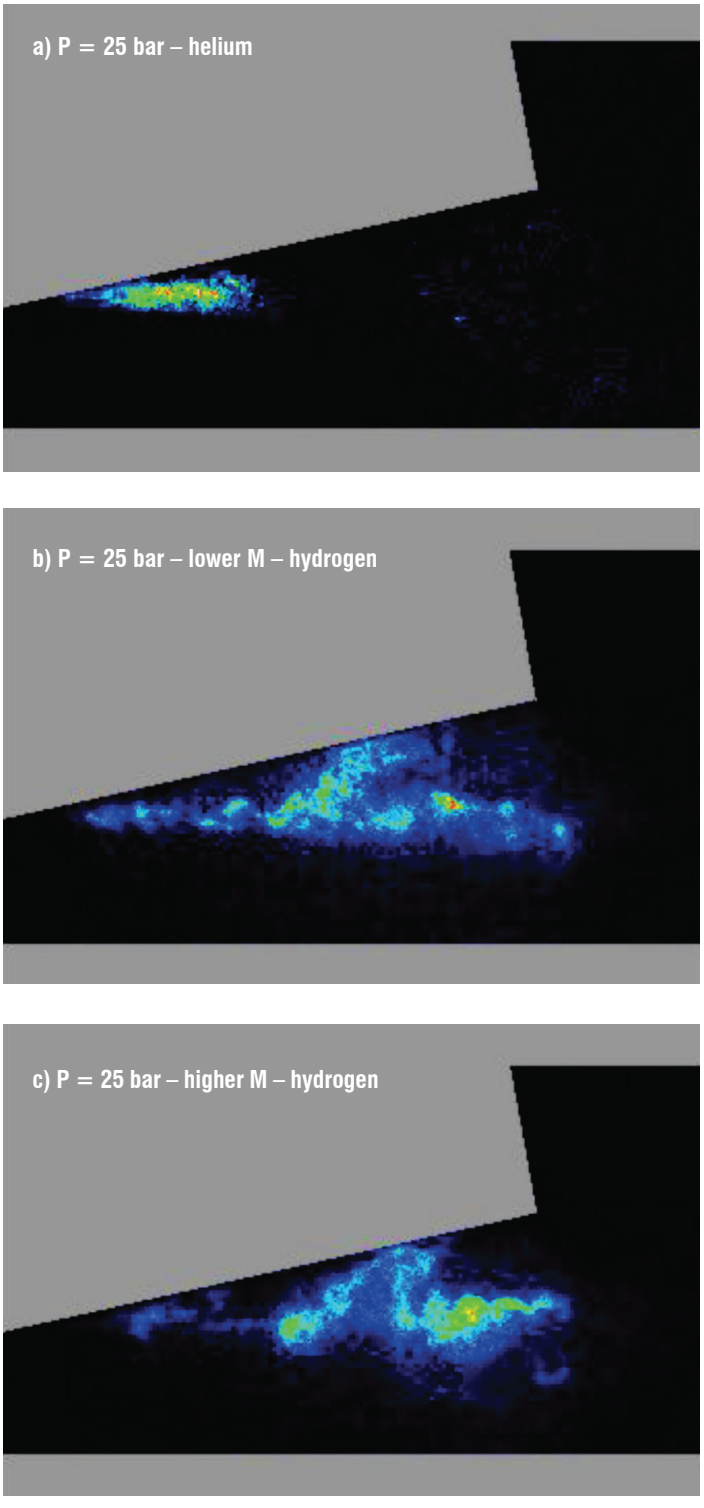

Figure 13 – Instantaneous PLIF images of OH radical concentration

For a 25 bar chamber pressure condition, instantaneous PLIF-OH images show a reactive zone near the upper wall of the nozzle, which indicates that the hydrogen rich jet can burn with fresh air (Figure 13b).

Figure 14 – Flow structures (Experimental (left) – Numerical (right))

If the cooling film is fed with helium instead of hydrogen, this zone has a limited spatial extent and is close to the wall. The fluorescence intensity distribution is quite homogeneous in the reactive zone, whatever the instantaneous image but it shows large fluctuations due to unsteadiness linked to turbulence in the recirculation zone, as shown by the Delayed Detached Eddy Simulation (DDES) in [34]. Moreover, spontaneous OH* imaging at 8 kHz revealed the dynamics of the flow, consistent with pressure measurements. More recently, PIV coupled with Schlieren imaging has been tested in cold flow conditions. Similar experiments are planned with combustion, to map the velocity flowfield in the hot gas flow.

Heat transfer

Heat transfer at the combustion chamber wall is a key issue, directly linked to the lifetime of the combustion chamber for a reusable liquid rocket engine and to the overall performance of an expander cycle motor. It is therefore a challenging field, where the precise evaluation and prediction by numerical tools remains difficult and, due to the high temperature (more than 3000 K in the combustion chamber), only few “global” measurements are available.

In order to better understand and measure heat fluxes at the wall, which is mandatory to improve numerical tools and models able to give an accurate description of those phenomena, a high pressure - high mixture ratio subscale combustion chamber was developed within the framework of the ONERA-CNES CONFORTH project (Figure 15). It is water-cooled, fed with five coaxial injectors arranged in a cross pattern and able to reproduce representative liquid rocket engine conditions (70 bar, O/F=7). The choice was made to overcome the limitations of “global” measurements, such as calorimeter sections, by implementing hundreds of thermocouples on the injector plate, as well as on both the hot gas and cooling fluid sides of the cylindrical segment walls of the combustion chamber.

A first test series was successfully conducted in 2010 [27], from 20 to 65 bar and a mixture ratio from 2 to 7, demonstrating the test domain possibilities of the combustion chamber. Further test campaigns were performed in the time period 2012-2015 [7], [29] in liquid-gas and gas-gas injection conditions, in both the “thermal” configuration, to measure temperature and heat fluxes at the walls and the “visualization” configuration, in order to see the flame shape and atomization process [8]. The obtained running conditions for the thermal campaigns, in a (Pressure, Mixture Ratio) plane is shown in Figure 16. A similar gas-gas and liquid gas point (black circle) can be used for comparison between these two types of flows.

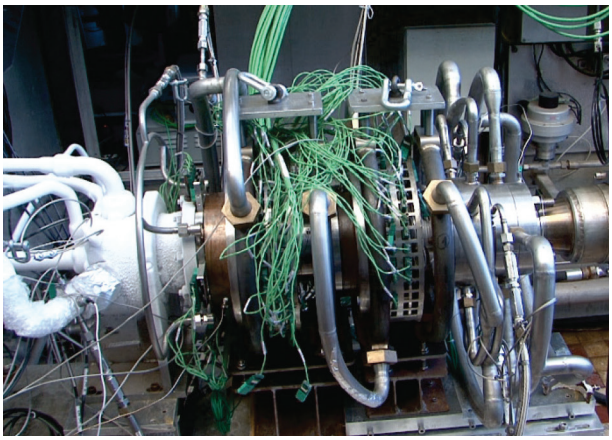

Figure 15 – The High Pressure High Mixture Ratio Combustor of the CONFORTH project

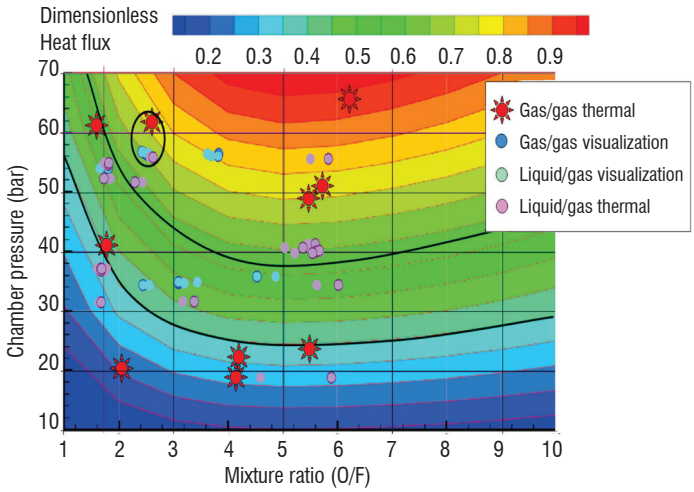

Figure 16 – Heat transfer measurement points obtained experimentally

An example of thermal acquisition of the “hot gas side”, versus time, is shown in Figure 17 for this condition. It shows that the overall temperature levels are very similar in both cases, but with greater discrepancy for the liquid-gas condition. Also, the temperature is locally higher in the first segment for liquid-gas conditions, whereas it is higher in the second segment for gas-gas conditions, which tends to indicate that the flame is probably shorter for the liquid-gas condition.

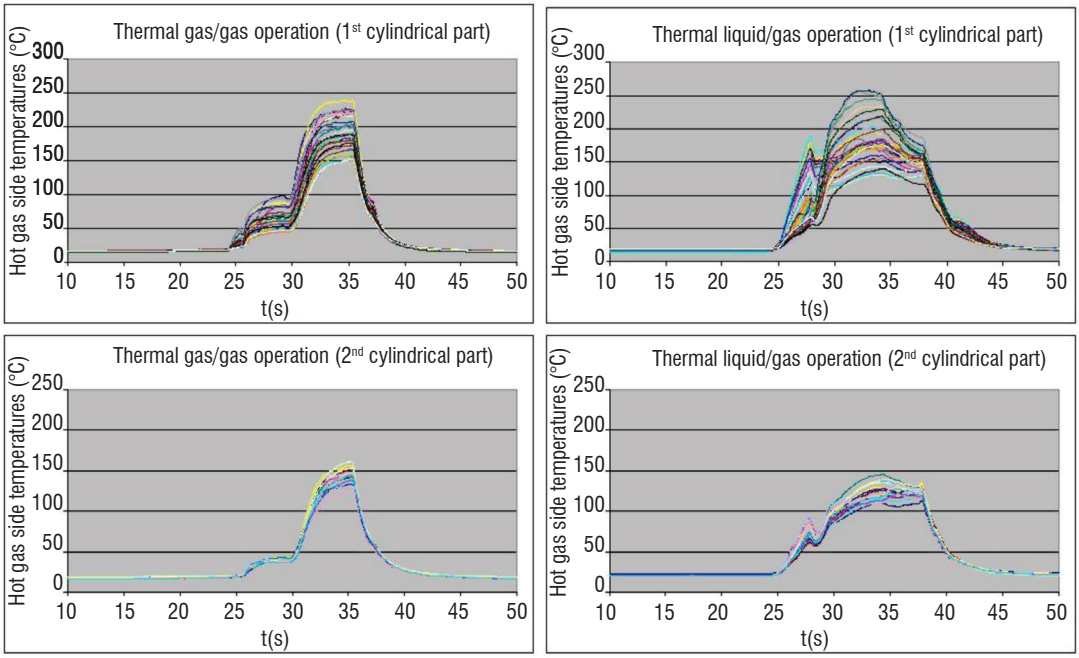

Figure 17 – Experimental measurements for a similar (P,M) condition. Liquid-gas and gas-gas comparison

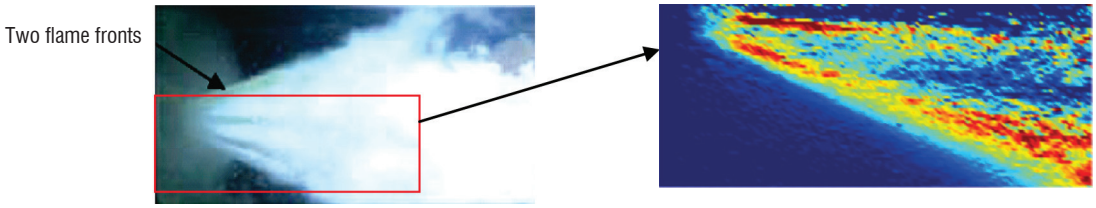

Figure 18 – LOX/LCH4 operation. Left: high speed visualization. Right: OH* chemiluminescence

Other topics

Most of the experiments performed on Mascotte with methane as a fuel were linked to other topics, ignition, high frequency instabilities, etc., mainly to compare how the system, injector or combustion chamber, behaves when it is fed with methane rather than hydrogen. Nevertheless, one point may be mentioned: the heat exchanger installed on the Mascotte fuel line, to cool the hydrogen from ambient to 100 K, is powerful enough to liquefy the methane, enabling liquid/liquid operation. This enabled, for example, the observation of two flame fronts appearing in a coaxial injector flame [37], [40]. This unexpected pattern was emphasized by OH* radical imaging, as well as by high speed visualization in the visible range (Figure 18).

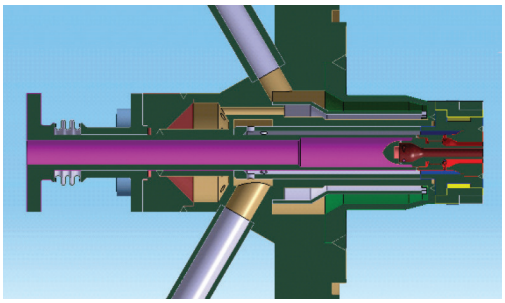

Figure 19 – Sketch of a double-swirl injector

Besides this completely unusual pattern, it has also been stated that the shear coaxial element leads to rather poor performance when operated in liquid/liquid, which is one of the reasons why various injectors concepts like double-swirl (Figure 19 and Figure 21) [9] or confined elements (Figure 20 and Figure 22) [1] were tested.

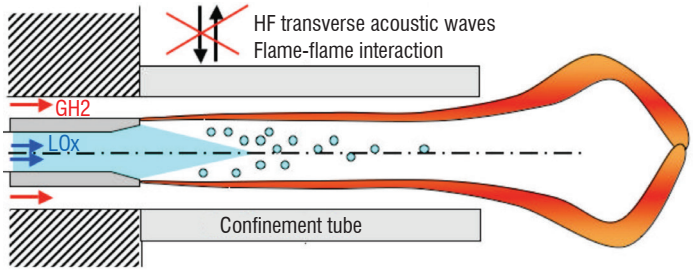

Figure 20 – Illustration of the confined coaxial injector concept

Figure 21 – Hollow cone spray produced by a swirl injector (without combustion, LOX side alone)

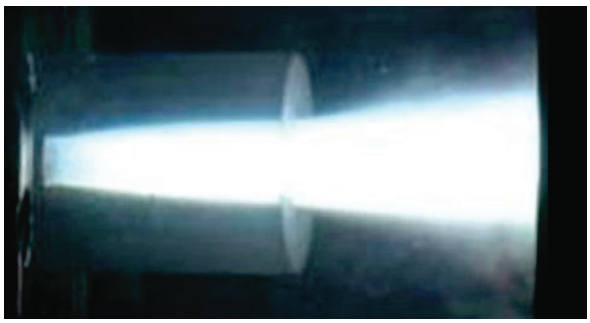

Figure 22 – Operation of a confined coaxial injector

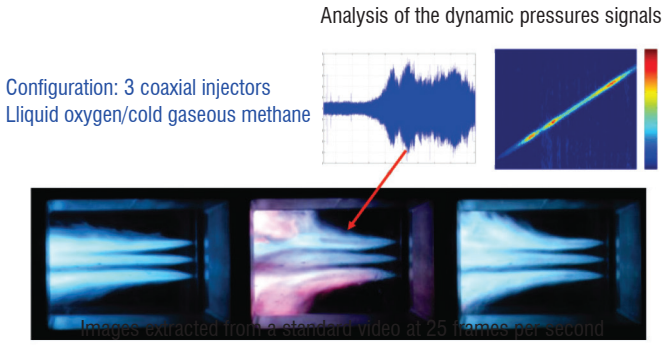

Figure 23 – HF burst observed in LOX/CH4 operation
(flow from right to left on the images of the video)

Several Mascotte test campaigns were dedicated to the study of high-frequency combustion instabilities (HF), firstly with LOX/hydrogen and more recently with LOX/methane [20], [22], [31]. Figure 23 shows an example of HF burst observed in the combustion chamber of Figure 24. In this case, the three coaxial injectors were fed with liquid oxygen and cold gaseous methane. The chamber acoustic modes were excited by means of a toothed wheel, which was accelerated in order to cross all of the modes between 1 and 3 kHz.

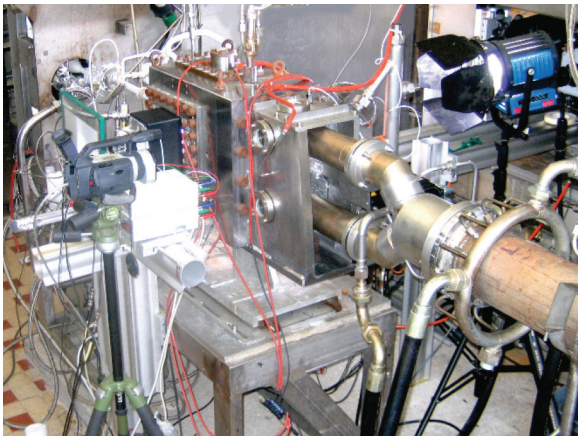

Figure 24 – Experimental setup for HF studies with forced oscillations
(Very High Amplitude Modulator)

Conclusion

Twenty years ago, the Mascotte test bench was designed and built to operate under various conditions, from atmospheric to supercritical conditions, with the aim of building a database of combustion around a coaxial jet. During the last decade, numerous new configurations were tested, enabling almost all of the phenomena involved in the operation of a rocket engine to be studied in a lab research environment, but under the conditions encountered in an actual rocket engine. Mascotte remains an essential tool in the understanding of physical phenomena and the development of measuring methods. Moreover, thanks to its flexibility, it allows the testing of new hardware before implementation on larger bench combustors or even actual engines ■

References

[1] L. BOCCALETTO - *A comparison Between Two Possible Thermodynamic Schemes for Reusable LOX/LCH$_4$ Engines*. AIAA Paper 2004- 3356, 2004

[2] E. BERTSEVA, F. GRISCH, M. HABIBALLAH, H. BERGER, F. CHAUSSARD, T. GABARD, E. JOURDANNEAU, R. SAINT-LOUP - *CARS Spectroscopy of CH$_4$ for Temperature Measurements in a Cryogenic Combustion Chamber*. 1st EUCASS, Moscow, Russia, 2005

[3] A. BRESSON, P. BOUCHARDY, F. GRISCH - *Experimental Investigation of a Supersonic Rocket Engine Plume Using OH*-Emission, OH-PLIF and CARS Thermometry*. 11th International symposium on applications of laser techniques to fluid mechanics, paper 16-4, Lisbon 2002

[4] S. CANDEL, G. HERDING, R. SNYDER, P. SCOUFLAIRE, C. ROLON, L. VINGERT, M. HABIBALLAH, F. GRISCH, M. PÉALAT, P. BOUCHARDY, D. STEPOWSKI, A. CESSOU, P. COLIN - *Experimental Investigation of Shear Coaxial Cryogenic Jet-Flame.* Journal of Propulsion and Power. 14, pp. 826-834, 1998

[5] S. CANDEL, M. JUNIPER, G. SINGLA, P. SCOUFLAIRE, C. ROLON - *Structure and Dynamics of Cryogenic Flames at Supercritical Pressure*. Combustion Science and Technology, 178 pp. 161-192, 2006

[6] C. CRUZ, L. VINGERT, M. THÉRON, S. PETITOT, C. VERPLANCKE - *Characterization of Confined Shear Coaxial Injection: LOX/GH$_2$*. 2nd Space Propulsion Conference, San Sebastian, Spain, 2010

[7] L.H. DOREY, P. GRENARD, L. MATUSZEWSKI, L. SELLE - *Experimental and Numerical Study of a Cooled Rocket Combustion Chamber.* 15th International Heat Transfer Conference IHTC15-9238, 2014

[8] N. FDIDA, L. VINGERT, G. ORDONNEAU, S. PETITOT - *Coupling High-Speed Imaging Diagnostics to Study a LOX/GH$_2$ Flame in a High-Pressure Rocket Combustor.* 5th EUCASS, Munich, Germany, 2013

[9] N.FDIDA, L. VINGERT, G. ORDONNEAU, A. RISTORI, C. BROSSARD, R. STÜTZER, J. SENDER - *Characterization of a Double Swirl Injector in a LOX/LCH$_4$ Fueled Combustor on Mascotte Test Bench*. 5th EUCASS, Munich, Germany, 2013

[10] N. FDIDA, L. VINGERT, A. RISTORI, Y. LE SANT - *Droplet Size and Velocity Measurements in a Cryogenic Jet Flame of a Rocket-Type Combustor Using High Speed Imaging*. Atomization and Sprays, under publication, DOI: 10.1615/ AtomizSpr.2015011814, 2016

[11] P. GICQUEL, L. VINGERT - *Flow Investigations of Cryogenic Sprays in Combustion at Sub and Supercritical Conditions*. 16th Annual Conference in Liquid Atomization and Spray Systems, Darmstadt, Germany, 2000

[12] P. GRENARD, L. VINGERT - *CFD Simulation of the GCH4/GO2 Mascotte Test Bench*. 3rd Space Propulsion Conference, Bordeaux, France, 2012

[13] F. GRISCH, L. VINGERT, P. GRENARD, V. FABELINSKY, K. VERSHAGIN - *CARS Measurements at High Pressure in a CH$_4$/O$_2$ Jet Flame*. 4th EUCASS, St Petersburg, Russia, 2011

[14] M. HABIBALLAH, M. ORAIN, F. GRISCH, L. VINGERT, P. GICQUEL - *Experimental Studies of High-Pressure Cryogenic Flames on the Mascotte Test Facility.* Combustion Science and Technology 178, pp. 101-128, 2006

[15] O.J. HAIDN, M. HABIBALLAH - *Research on High Pressure Cryogenic Combustion*. ONERA-DLR Aerospace Symposium, 2000

[16] L. HAKIM, A. RUIZ, T. SCHMITT, M. BOLLEAU, G. STAFFELBACH, S. DUCRUIX, B. CUENOT, S. CANDEL - *Large Eddy Simulations of Multiple Transcritical Coaxial Flames Submitted to High-Frequency Transverse Acoustic Modulations*. Proceedings of the Combustion Institute 35 pp. 1461-1468, 2015

[17] M. JUNIPER, A. TRIPATHI, P. SCOUFLAIRE, J.C. ROLON, S. CANDEL - *Structure of Cryogenic Flames at Elevated Pressures.* Proceedings of the Combustion Institute, 28, pp. 1103-1109, 2000

[18] M. JUNIPER, S. CANDEL - *Edge Diffusion Flame Stabilization Behind a Step Over a Liquid Reactant*. Journal of Propulsion and Power 19 pp. 332-342, 2003

[19] J. LUX, D. SUSLOV, M. BECHLE, M. OSCHWALD, O. HAIDN - *Investigation of Sub- and Supercritical LOX/Methane Injection Using Optical Diagnostics*. 42nd JPC, Sacramento, 2006

[20] Y. MERY, S. DUCRUIX, P. SCOUFLAIRE, L. VINGERT, C. CRUZ, M. THÉRON, S. CANDEL - *Subcritical and Transcritical Injection under High Amplitude Transverse Acoustic Oscillations*. 3rd EUCASS, Versailles, France, 2009

[21] Y. MERY, S. DUCRUIX, P. SCOUFLAIRE, S. CANDEL - *Injection Coupling with High Amplitude Transverse Modes: Experimentation and Simulation.* Comptes Rendus Mecanique 337 pp. 426-437, 2009

[22] Y. MERY, L. HAKIM, P. SCOUFLAIRE, L. VINGERT, S. DUCRUIX, S. CANDEL - *Experimental Investigation of Cryogenic Flame Dynamics under Transverse Acoustic Modulations*. Comptes Rendus Mecanique 341 pp. 100-109, 2013

[23] A. MURRONE, N. FDIDA, C. LE TOUZE, L. VINGERT - *Atomization of Cryogenic Rocket Engines Coaxial Injectors; Modeling Aspects and Experimental Investigations.* 4th Space Propulsion Conference, Cologne, Germany, 2014

[24] G. ORDONNEAU, H. DOUCHET - *Numerical Simulation of the Vinci Thrust Chamber Ignition.* 4th Int. Conf. on Launcher Technology, Liège, Belgium, 2002

[25] G. ORDONNEAU, P. HERVAT, F. GRISCH, L. VINGERT - *PLIF Investigation of Reactive Flows in the Separation Region of an Over-Expanded Two-Dimensional Nozzle*. 42nd JPC, Sacramento, 2006

[26] G. ORDONNEAU, F. GRISCH, P. HERVAT, P. REIJASSE, L. VINGERT - *Experimental Characterization of Reactive Flows in the Separation Region of an Over-Expanded Two-Dimensional Nozzle*. 6th Int. Conf. on Launcher Technology, Munich; Germany, 2006

[27] G. ORDONNEAU, P. HERVAT, L. VINGERT, S. PETITOT, B. POUFFARY - *First Results of Heat Transfer Measurements in a New Water-Cooled Combustor on the Mascotte Facility*. 4th EUCASS, St Petersburg, Russia, 2011

[28] G. ORDONNEAU, L. VINGERT, N. SLAVINSKAYA, J. SENDER, D. SUSLOV, S. SOLLER, M. ONOFRI, C. BRUNO, D. LENTINI, F. NASUTI, M. VALORANI - *Oxygen-Methane Combustion Studies in In Space Propulsion Program.* 4th EUCASS, St Petersburg, Russia, 2011

[29] S. PETITOT, L. VINGERT, N. FDIDA, P. GRENARD, M. THERON, S. PALERM - *Heat Transfer and GOX&LOX/GH$_2$ Flame Imaging in a High-Pressure and High-Mixture Ratio Rocket Combustor.* 4th Space Propulsion Conference, Cologne, Germany, 2014

[30] M. POUROUCHOTTAMANE, F. DUPOIRIEUX, L. VINGERT, M. HABIBALLAH - *Numerical Analysis of the 10 Bar Mascotte Flow Field.* 2nd International Workshop on Rocket Combustion Modeling, Lampoldshausen, Germany, 2001

[31] F. RICHECOEUR, P. SCOUFLAIRE, S. DUCRUIX, S. CANDEL - *Interactions Between Propellant Jets and Acoustic Modes in Liquid Rocket Engines: Experiments and Simulations*. 42nd JPC, Sacramento, 2006

[32] F. RICHECOEUR, S. DUCRUIX, P. SCOUFLAIRE, S. CANDEL - *High Frequency Ransverse Acoustic Coupling in a Multiple Injector Cryogenic Combustor.* Journal of Propulsion and Power 22 pp. 790-799, 2006

[33] A. ROBLIN, I. DUBOIS, F. GRISCH, A. BOISCHOT, L. VINGERT - *Comparison Between Computations and Measurements of a H_2/LOX Rocket Motor Plume*. 8th Joint Thermophysics and Heat Transfer Conference, St. Louis, Missouri, 2002

[34] B. SAINTE-ROSE, N. BERTIER, S. DECK, F. DUPOIRIEUX - *Numerical Simulations and Physical Analysis of an Over-Expanded Reactive Gas Flow in a Planar Nozzle*. Combustion and Flame, 2012

[35] V. SCHMIDT, D. KLIMENKO, O. HAIDN, M. OSCHWALD, A. NICOLE, G. ORDONNEAU, M. HABIBALLAH - *Experimental Investigation and Modeling of the Ignition Transient of a Coaxial H_2/O_2-Injector.* 5th Int. Conf. on Liquid Rocket, Chattanooga, 2003

[36] T. SCHMITT, Y. MÉRY, M. BOILEAU, S. CANDEL - *Large Eddy Simulation of Oxygen/Methane Flames Under Transcritical Conditions*. Proceedings of the Combustion Institute 33 pp. 1383-1390, 2011

[37] G. SINGLA, P. SCOUFLAIRE, J.C. ROLON, C. CANDEL - *Transcritical Oxygen / Transcritical or Supercritical Methane Combustion*. Proceedings of the Combustion Institute 30 pp. 2921-2928, 2005

[38] G. SINGLA, P. SCOUFLAIRE, C. ROLON, S. CANDEL, S. ZURBACH, J.L. THOMAS - *Experiments and Simulations of LOX/CH_4 Combustion at High Pressures.* 1st EUCASS, Moscow, Russia, 2005

[39] G. SINGLA, P. SCOUFLAIRE, C. ROLON, S. CANDEL - *Planar Laser induced Fluorescence of OH in High Pressure Cryogenic LOX/GH_2 Jet Flames*. Combustion and Flame 144 pp. 151-169, 2006

[40] G. SINGLA, P. SCOUFLAIRE, J.C. ROLON, S. CANDEL, L. VINGERT - *OH PLIF and Emission Imaging in High Pressure Cryogenic LOX/Methane Flames.* Journal of Propulsion and Power 23, pp. 593-602, 2007

[41] G. SINGLA, P. SCOUFLAIRE, C. ROLON, S. CANDEL - *Flame Stabilization in High Pressure LOX/GH_2 and GCH_4 Combustion.* Proceedings of the Combustion Institute, 31 pp. 2215-2222, 2007

[42] L. VINGERT, M. HABIBALLAH, P. VUILLERMOZ, S. ZURBACH - *Mascotte, a Test Facility for Cryogenic Combustion Research at High Pressure*. 51st International Astronautical Congress, Rio de Janeiro. IAF-00-S.3.06, 2000

[43] L. VINGERT, M. HABIBALLAH, P. VUILLERMOZ - *Upgrading of the Mascotte Cryogenic Test Bench to the LOX/Methane Combustion Studies.* 4th Int. Conf. on Launcher Technology, Liège, Belgium, 2002

[44] L. VINGERT, P. GICQUEL, M. BARAT, J. SENDER - *Characterization of Cryogenic Propellants Ignition on the Mascotte Test Rig*. Preliminary Results. 1st EUCASS, Moscow, Russia, 2005

[45] L. VINGERT, P. GRENARD, G. ORDONNEAU, S. PETITOT, S. PALERM - *Improvement of Knowledge and Modelling of Heat Transfer in Cryogenic Combustion Chambers*. 6th EUCASS, Krakow, Poland, 2015

[46] S. ZURBACH, J.L. THOMAS, M. SION, T. KACHLER, L. VINGERT, M. HABIBALLAH - *Recent Advances on LOX/Methane Combustion for Liquid Rocket Engine Injector.* 38th JPC, Indianapolis, 2002

AUTHORS

Lucien Vingert graduated from ISAE/Sup'Aéro in Toulouse in 1983. He joined the Energetics Department of ONERA in 1986. He was first involved in atomization studies, mainly related to the coaxial injection elements of the Vulcain engine. From 1990 to 1993, he was also involved in numerical analysis of combustion instabilities, in close contact with the European industry in charge of Ariane's liquid rocket engines.
Since 1993, he has been working on the cryogenic test facility Mascotte, in charge of the successive improvements of the facility and of all the test campaigns, whatever their objectives: combustion efficiency, stability, heat transfer, atomization ...

Gérard Ordonneau is currently the Head of Liquid Propulsion Unit at ONERA, in the Fundamental and Applied Energetics Department. He graduated in Aerospace Engineering (1982) from ISAE/Sup'Aéro in Toulouse. His main interests are the research on combustion instabilities (low and high frequency), ignition and system studies in connection with Ariane's engines development.

Nicolas Fdida graduated from "Ecole Nationale Supérieure de Mécanique et Microtechniques" in Besançon and received his PhD in energetics from the University of Rouen in 2008. He works at ONERA as a research scientist in the Fundamental and Applied Energetics Department, applying various optical diagnostics (Phase Doppler, Laser Induced Fluorescence, high-speed imaging...) to track physical processes of reacting flows. His current research addresses the atomization of two phase flows and the investigation of combustion instabilities.

Philippe Grenard graduated from the French engineer school École Polytechnique and Supaéro. Philippe Grenard is a research engineer working at Onera in the Fundamental and Applied Energetics Departement (DEFA). He is in charge of computational activities regarding the in-house CEDRE platform (modeling, development and computations) in the Liquid Propulsion Unit. His activities focus on combustion and thermal loads in the combustion chamber and nozzle of liquid propellant engines.

P. Gaillard, C. Le Touze, L. Matuszewski, A. Murrone
(ONERA)

E-mail: lionel.matuszewski@onera.fr

DOI : 10.12762/2016.AL11.16

Numerical Simulation of Cryogenic Injection in Rocket Engine Combustion Chambers

The numerical simulation of cryogenic combustion is crucial for a better understanding of the complex physics involved in reactive flows of rocket engines and to help to reduce the development cost of these engines. The focus of this study is set on the oxidizer injection and its dispersion through jet dense core destabilization and atomization or supercritical mixing. Specific models have been implemented in the CFD code CEDRE created by ONERA to address these physical phenomena.

Introduction

In the field of chemical rocket propulsion, oxygen and hydrogen are favored over other types of fuel due to the high specific impulse (Isp) that they produce. This Isp represents the ratio between the thrust (in mass equivalent units) and the fuel consumption, so that the higher the Isp, the heavier the payload can be. Oxygen and hydrogen can be easily obtained through air distillation and hydrocarbon cracking, but these components are gaseous at ordinary temperature. In order to minimize the rocket fuel tank structure, oxygen and hydrogen are liquefied at a very low temperature, hence leading to cryogenic combustion.

Such extreme conditions require specifically designed test benches, such as the MASCOTTE test bench [1], in order to provide an insight into the characteristic phenomena involved in cryogenic combustion.

To complement this experimental approach, numerical simulations with the CEDRE [2] code are conducted on test-case configurations, in order to develop numerical tools and models with the ultimate aim being predictable numerical simulation, which would make the designing of industrial scale rocket engines easier.

This paper focuses on oxidizer dispersion through dense core destabilization, which leads to small scale structures eventually breaking into droplets or dense clusters, depending on the chamber pressure. This dispersion of oxygen greatly influences the flame shape and thus the overall combustion process, but is still difficult to represent numerically since it involves very different large scales.

Subcritical regime and atomization

Two-phase flows resulting from the atomization of liquid jets play a significant role in the proper functioning of cryogenic liquid-propellant rocket engines under subcritical operating conditions [3]. As depicted in figure 1, the great velocity difference between the two phases (liquid Ox and Gaseous H_2) at the exit of a coaxial cryogenic injector generates fluctuating accelerations. Due to these fluctuations, Rayleigh-Taylor instabilities destabilize the liquid to create ligaments. These instabilities then grow and eventually cause the peeling of the main LOx jet, which is referred to as "primary atomization". Large random-shaped liquid structures are thereby ejected towards the gas flow, subsequently undergoing "secondary break-up" when inertia forces exceed the liquid surface tension. This results in a spray of small LOx droplets, mainly spherical, which are dispersed by the turbulent gas flow and finally vaporized to feed the combustion with hydrogen. Such a configuration therefore exhibits a two-phase flow where the liquid phase is only composed of LOx, whereas the gas phase is made up of hydrogen H_2, vaporized oxygen O_2 and combustion products. Eventually, the resulting high-enthalpy combustion products exhaust through a nozzle at supersonic speed, thereby providing the required thrust.

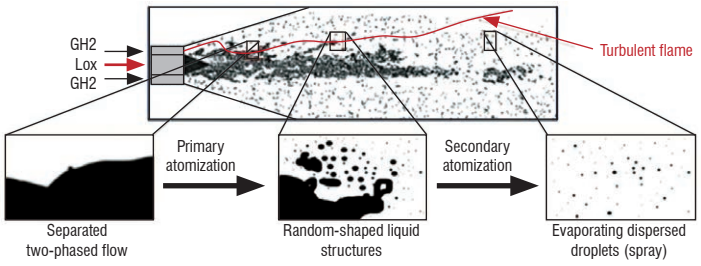

Figure 1 – Configuration of a combustion chamber within liquid-propellant rocket engines under subcritical operating conditions

Since the experimental investigation of such propulsion devices is complex and expensive, developing numerical tools able to accurately simulate their functioning, including all of the physical phenomena and their interactions, is a crucial but nonetheless ambitious objective. Indeed, the harsh conditions within cryogenic rocket engines, where great temperature, velocity and density gradients are encountered, severely challenge the robustness of numerical methods. Another major difficulty is due to the multiscale nature of the problem.

A large amount of models is available in the literature for the numerical simulation of multiphase flows. These range from interface tracking methods (Level Set, Volume of Fluid) to diffuse interface methods with potentially different levels of physical modeling (from the 7-equation model to the 4-equation model), and to kinetic (statistical) models for dispersed phases. The problem is that if the simulation of a whole combustion chamber is sought, even in a simplified single-injector configuration such as the MASCOTTE bench, any mesh that would be refined enough to capture the smallest droplets with any of the interface tracking methods is still absolutely unattainable. With diffuse interface methods, it is possible to describe the liquid phase in a continuous way, from injection to primary and secondary atomization and vaporization. For instance, primary atomization can be described as a source term based on a transport equation for the surface area density [4]. However, sprays are best described by dedicated statistical models based upon either a Lagrangian or Eulerian formalism, in which local polydispersity can be taken into account. Unfortunately, there is no straightforward coupling between diffuse interface models (or interface tracking models) and statistical models, which would be interesting for predictive simulations of reactive flows including primary atomization.

Based on this observation, the work presented here is aimed at setting up a coupling strategy between different models, each one being suitable for a specific two-phase flow topology. The approach adopted specifically consists, within the scope of the multiphysics CEDRE software developed at ONERA, in coupling:

- a model suitable for the "separated" and "mixed" areas of the two-phase flow (see figure 1), based on a diffuse interface approach and a locally homogeneous flow assumption ("4-equation" model), in a LES context and resolved by the CHARME solver of CEDRE,
- and a Eulerian kinetic model for the dispersed phase, based on a sectional method to describe the droplet size distribution and resolved by the SPIREE solver of CEDRE.

Note that similar strategies have been developed in the literature. However, most of them are based on a RANS formulation and a Lagrangian formalism when coupling with the dispersed phase (see [5] and related works), whereas this work is aimed at Large Eddy Simulation and uses a fully Eulerian formalism.

In order to achieve this goal, we have developed a coupling model between the CHARME and SPIREE solvers of CEDRE, intended to account for primary atomization. In the following we first further explain our strategy for the simulation of primary atomization applied to subcritical cryogenic combustion: what has been done so far and what remains to be done in future works. Then, we briefly present the details of the equations resolved by each solver, give a few details on source term expression and numerical methods (further details on these topics can be found in [3] and [8]), and introduce the primary atomization model. We finally present some first numerical results of a Large Eddy Simulation using the proposed strategy. This simulation has been performed on the MASCOTTE test bench configuration, specifically on the 10-bar operating point corresponding to cryogenic rocket engines under subcritical operating conditions. Eventually, it should be stressed that this is still a work in progress and more advanced simulation results on the MASCOTTE configuration are to be presented in future communications.

Description of the coupling strategy

Figure 2 illustrates the coupling strategy between the CHARME and SPIREE solvers. In this figure, the subscripts "CH" and "SP" respectively stand for CHARME and SPIREE, the color red indicates the gas phase and the color blue represents the liquid phase. The green dashed lines illustrate the coupling between CHARME and SPIREE. This is obviously a schematic representation: in reality the phenomena are not fully decoupled and sequential. On the contrary, there exists a large area where atomization, secondary break-up, evaporation and even combustion in gaseous phase occur almost simultaneously. Besides, it is important to specify that both solvers share exactly the same computation domain (and the same mesh as well). Thus, the SPIREE solver deals with the entire geometry and is not restricted to a pre-defined area, even though there are obviously large zones of the geometry where the dispersed phase is never encountered. Note that in these no-droplet areas the computational cost of SPIREE is reduced to almost zero. Hence, the sub-domain decomposition of the computation domain must be performed carefully so as to reach an optimal overall load balancing.

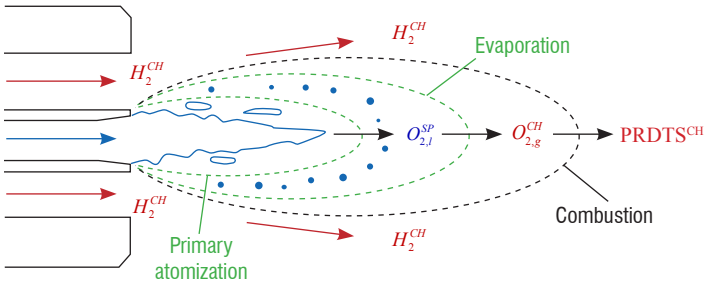

Figure 2 – Coupling strategy between the CHARME and SPIREE solvers

Going into more details, the strategy as illustrated in figure 2 is as follows:

- The CHARME solver performs the Large Eddy Simulation of the two-phase fluid, which gathers a turbulent reactive gaseous phase made up of multiple chemical species (including oxygen, hydrogen and combustion products) and a liquid phase made up of only one species: the LOx. The description of the liquid phase with CHARME is restricted to the "separated" and "mixed" areas of the two-phase-flow, which are precisely the dense liquid core and the mixture zone downstream the injector exit, where the liquid jet is sheared by the co-axial high velocity gaseous flow. The mesh is designed so as to be refined enough to describe the instabilities at the surface of the liquid core and even the formation of some ligaments.
- It is impossible to pursue this strategy up to the description of the droplets, given that any mesh that would be refined enough for that would be absolutely unattainable for practical applications. In other words, the droplet generation is inevitably a phenomenon that must be addressed at the sub-grid scale level. This is the reason why we operate a transfer from CHARME to SPIREE, so that the droplets can be described with a dedicated model. Under the effect of a source term based on some local criteria (see the following sections), the LOx mass (as well as the associated momentum and energy) is withdrawn from the CHARME solver, in the "mixed" two-phase flow area, and transferred to the SPIREE solver. When in SPIREE, the LOx mass is assumed to be in the form of purely spherical dispersed droplets.

• Then, the droplets are transported within the SPIREE solver, in which they break-up and vaporize. The latter is a reverse transfer towards the CHARME solver: the mass of liquid oxygen droplets is transferred to the gaseous oxygen species in the CHARME solver. Note that vaporization is only taken into account in this way, namely when LOx is in the form of droplets. It could be also possible to include a vaporization term within the CHARME solver, so as to describe the LOx vaporization prior to droplet formation. This would therefore be an "intern" source term in the CHARME solver, describing a transfer between both liquid and gaseous oxygen species. This point has not been considered for now.

• Finally, the chemical reaction between the gaseous oxygen coming from the droplet vaporization and hydrogen (turbulent diffusion flame) is described within the CHARME solver through dedicated source terms.

Note that the strategy still needs to be enhanced for a better description of the "mixed" zone. For instance, the use of a transport equation for the surface density area (adapted to the LES context) should improve the description of the sub-grid dispersion of the liquid phase, thereby enabling a more continuous and accurate description of the transition from the "mixed" topology (ligaments, non-spherical large "droplets", etc.) to the spray generation. Note however that this point is obviously of lesser importance here, in a LES context, than it would be within a RANS framework. Besides, let us add the following comments:

• The coupling between CHARME and SPIREE is only through source terms (the volume fraction of the dispersed phase is assumed to be negligible and therefore not taken into account in CHARME) and is fully conservative in mass, momentum and energy. Coupling source terms describe mass, momentum and energy transfers respectively, because of primary atomization (transfer from the liquid phase of the fluid towards the dispersed phase) and vaporization (transfer from the dispersed phase towards the gaseous phase of the fluid), drag force and heat flux. Each solver has also "intern" source terms, to describe combustion in the case of CHARME and to describe secondary fragmentation in the case of SPIREE.

• Using the Eulerian formalism rather than the Lagrangian one for the dispersed phase seems more natural, convenient and effective when setting up the kind of coupling strategy presented here. Indeed this facilitates a conservative and robust coupling (see [8] for further discussion on this issue).

In the following two sections, the equations of the models used for both "separated" (CHARME solver) and "dispersed" (SPIREE) two-phase-flow are presented.

Diffuse interface model for the "separated" two-phase flow (CHARME)

The system resolved by the CHARME solver is a so-called "4 equation" diffuse interface model, based on a locally homogeneous flow assumption. This is nothing other than the multi-species compressible Navier-Stokes system, where we consider a fluid mixture composed by one gaseous phase of ng species and one liquid phase made up of only one species, which is the dense LOx. The classical Navier-Stokes system in vectorial form is written as:

$$\frac{\partial \mathbf{Q}(\mathbf{U})}{\partial t} + \nabla \bullet \left[F_c(\mathbf{U}) - F(\mathbf{U}, \nabla \mathbf{U}) \right] = S(\mathbf{U})$$

In this system, conservative and primitive sets of variables respectively are written as:

$$\mathbf{Q}(\mathbf{U}) = \left(\rho Y_1 \quad \dots \quad \rho Y_{n_g} \quad \rho Y_l \quad \rho \mathbf{v} \quad \rho e_{tot} \right)^t$$

$$\mathbf{U}(\mathbf{Q}) = \left(P \quad T \quad \mathbf{v} \quad Y_1 \quad \dots \quad Y_{n_g} \quad Y_l \right)^t$$

where $Y_i \quad i = 1, \dots, n_g$ stand for the mass fractions of gaseous species while Y_l stands for the mass fraction of the dense LOx. Thus, ρ is the mixture density, e_{tot} is the total energy and P, $\mathbf{v}$, T respectively stand for the local unique pressure, velocity vector and temperature of the whole fluid. The convective and diffusive fluxes can be written in the form:

$$F_c(\mathbf{U}) = \mathbf{Q} \otimes \mathbf{v} + P \left(0 \quad \dots \quad 0 \quad \mathbf{I}_3 \quad \mathbf{v} \right)^t$$

$$F(\mathbf{U}, \nabla \mathbf{U}) = \left(F_{\rho Y_1} \quad \dots \quad F_{\rho Y_{n_g}} \quad F_{\rho Y_l} \quad F_v \quad F_e \right)^t$$

Let us give the following important detail: in this work we do not include any subgrid-scale turbulence modeling and therefore only consider an implicit approach for LES. Accurate modeling of subgrid-scale dissipation in a compressible two-phase flow context and on general heterogeneous unstructured meshes is a complex issue, which will be addressed in future works. Therefore, the diffusive fluxes only gather here the classical laminar diffusion terms: the molecular species diffusion in the gas phase described by Fick's law, the viscous stress tensor and Fourier's law for heat conduction. Finally, the source term vector $S(\mathbf{U})$ includes combustion modeling and coupling source terms between the CHARME and SPIREE solvers (see details in the following sections).

Eulerian kinetic-based model for the dispersed phase (SPIREE)

At the highest level of precision, the modeling of dispersed two-phase flows is based on a mesoscopic description provided by the Williams-Boltzmann kinetic equation. Particles are assumed to be spherical and fully characterized by a small set of variables: position $\mathbf{x}$, radius r, velocity $\mathbf{v}$ and temperature θ. The following Boltzmann-like equation expresses the conservation of the number density function (n.d.f) $f(t, \mathbf{x}, r, \mathbf{v}, \theta)$ in the phase space:

$$\frac{\partial f}{\partial t} + \nabla_{\mathbf{x}} . (\mathbf{v} f) + \nabla_{\mathbf{v}} . (\mathbf{F} f) + \frac{\partial}{\partial r}(R f) + \frac{\partial}{\partial \theta}(H f) = \Gamma + Q$$

In this balance equation, the left-hand-side stands for the "transport" of the particles in the phase space ($\mathbf{F}$, R and H respectively correspond to the force acting on a particle, the evaporation rate and the heat exchange rate), while Γ, Q on the right-hand-side respectively stand for the effect of fragmentation and collision phenomena. Note that $\mathbf{F}$, R and H depend on the local gas composition, velocity and temperature.

All fluid models for gas-particle flows are based on conservation equations for some particular moments of the number density function. These models can be formally derived from the kinetic equation by particular closure assumptions. The details of this derivation are not reproduced here (see for instance [6], [7], [8]). Only note that the choice of the discretization strategy for the size variable is of utmost importance, since we want to precisely describe the polydispersity of the spray. This is why we opt for the sectional approach, which is illustrated in figure 3. Information regarding the droplet size distribution

is kept at the macroscopic level thanks to a finite volume discretization with respect to the size variable. A set of equations is derived for each section and, in this type of model, sections are coupled thanks to mass, momentum and heat fluxes. More complex phenomena such as coalescence and fragmentation can also be easily included. Here we only consider the fragmentation term Γ.

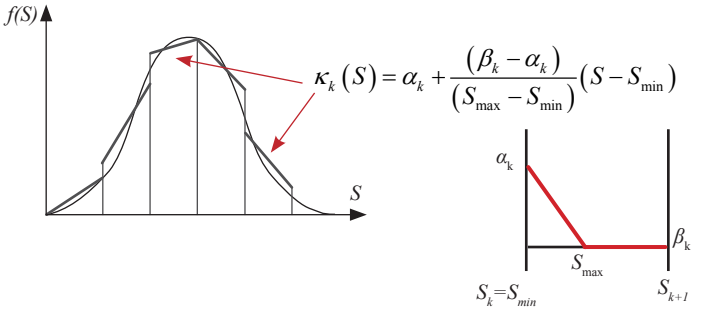

Figure 3 – Sectional approach with piecewise linear function reconstruction

Compared to other reconstructions, the main advantages of the linear function reconstruction are the positivity conservation when computing the inversion between the moments (mass and number density) and the reconstruction coefficients (α_k, β_k, s_{min}, s_{max}), and the computational cost reduction [7]. When using this reconstruction, we also maintain the possibility of performing the exact computation of the integrated source terms. Finally, the system of equations resolved by the SPIREE solver for each section of the dispersed phase is written as:

$$\frac{\partial \mathbf{q}(\mathbf{u})}{\partial t} + \nabla \bullet \left[f_c(\mathbf{u}) \right] s(\mathbf{u}) + \Gamma \text{ where } f_c(\mathbf{u}) = \mathbf{q} \otimes \mathbf{v}_d$$

The conservative and primitive variables are:

$$\mathbf{q}(\mathbf{u}) = \left(\rho_d \quad \rho_d \mathbf{v}_d \quad \rho_d h_d \quad N_d \right)$$
$$\mathbf{u} = \left(D \quad \mathbf{v}_d \quad T_d \quad \alpha \right)$$

In this system, $\rho_d = \alpha \rho_0$ stands for the bulk density of particles (ρ_0 is the density of pure liquid), N_d for the average number of particles per unit of volume and h_d for the total energy. The primitive variables D, $\mathbf{v}_d$, T_d, α are respectively the mean particle diameter, the velocity vector, the temperature and the volume fraction. The source terms vector $s(\mathbf{u})$ gathers the classical source terms between the gas phase in the CHARME solver and the dispersed phase (drag force, heat and mass transfer), as well as the new source term specifically designed to describe the coupling between the liquid phase in the CHARME solver and the dispersed phase (primary atomization). The secondary break-up vector Γ comprises source terms between the size sections: the break-up of large droplets into smaller droplets results in a mass, momentum and energy transfer between the various sections.

Source term expression and numerical methods

Let us now describe the components of the source term vectors $s(\mathbf{u})$ and $S(\mathbf{u})$, concerning respectively each section of particles in the SPIREE solver and the CHARME solver. The first component in s(u) represents, for a given section, the increase in the droplet mass due to primary atomization and its decrease by vaporization. In the second component (momentum), we find the effect of the drag force. The third component (total energy) includes the power of the drag force and the heat flux. Finally, the last component for the number density comprises a term corresponding to the new droplets that are created by primary atomization. If we now look at the source term $S(\mathbf{u})$ assigned to the carrier phase CHARME, the first n_g components (gas species) include combustion terms (the reaction rates are obviously zero for inert species). If we assume that the first species is the gaseous oxygen, then the first term also includes the evaporation of liquid oxygen droplets. The component number n_g+1 is for the liquid species and therefore includes the primary atomization source term. It transfers the dense LOx of CHARME into "dispersed" LOx in the appropriate sections of SPIREE.

$$s(\mathbf{u}) = \begin{pmatrix} s_{\rho_d} \\ s_{\rho_d \mathbf{v}_d} \\ s_{\rho_d h_d} \\ s_{N_d} \end{pmatrix} = \begin{pmatrix} \dot{M}_{ato} - N_d \dot{m}_{vap} \\ s_{\rho_d} \mathbf{v}_d + N_d \mathbf{F}_D \\ s_{\rho_d} h_d + N_d \left(\mathbf{F}_D . \mathbf{v}_d + \varphi_c \right) \\ \dot{N}_{ato} \end{pmatrix} \quad S(\mathbf{U}) = \begin{pmatrix} \dot{w}_{O_2} + N_d \dot{m}_{vap} \\ \dot{w}_i \\ \vdots \\ \dot{w}_{n_g} \\ -\dot{M}_{ato} \\ -s_{\rho_d \mathbf{v}_d} \\ -s_{\rho_d h_d} \end{pmatrix}$$

Classical coupling source terms between the gas phase and the dispersed phase

The evaporation and heat transfer modeling ($\dot{m}_{vap}$ and ϕ_c) is based on the classical Abramzon-Sirignano model [9] and the drag force $\mathbf{F}_D$ is modeled using the Schiller-Naumann correlation. Details on these models can be found in [8].

Fragmentation source terms

The expression of the fragmentation source terms vector Γ is based on:

- a model for the break-up of an isolated droplet, whose expression can be found in the literature (see [10] for instance),
- a numerical integration procedure in order to turn this model at the droplet scale into a mean fragmentation operator Γ (see [11]).

More details on these points can be found in [8] and in the above-mentioned references.

Turbulent Combustion

The H_2-O_2 combustion is modeled using an infinitely fast chemistry assumption (high Damkohler number). This means that kinetic effects are not taken into account. The species production rates are related to the gap between the local and equilibrium concentrations, respectively Y_i and $Y_{i,eq}$. In other words, the reacting species are relaxed towards chemical equilibrium with a finite relaxation time driven by a turbulent time scale ν_{turb}^{-1}. In the LES framework, such a time scale can be assumed from the resolved strain tensor. This approach is similar to the well-known “Eddy Break-Up” model, since in both approaches infinitely fast chemistry is assumed. Fortunately however, taking into account a local equilibrium involving radical species renders a much more accurate flame temperature. The reaction rate is then written as:

$$\dot{w}_i = ctev_{turb} \left(Y_{i,eq} - Y_i \right)$$

Numerical methods

The numerical methods used in this work are based on a Finite Volume approach for general unstructured meshes, for both the CHARME and

SPIREE solvers. Given that the coupling between these two solvers includes a large variety of phenomena, we use a time splitting technique whose details can be found in [3]. Concerning spatial approximation, we have developed a new second-order multislope MUSCL technique for general unstructured meshes [12], in order to ensure the robustness of the simulation. We also use upwind schemes, such as the classical HLLC scheme for the CHARME solver and a Godunov-like scheme for SPIREE adapted to the weak hyperbolicity of the system of particles (equivalent to the system of pressureless gas dynamics).

Primary atomization modeling

The model developed to describe the mass transfer between solvers accounting for primary atomization is written as:

$$\dot{M}_{ato} = \rho Y_l \nu_{ato} \lambda_{ato}(Y_l)$$

where ρY_l is the liquid mass in a given control volume, ν_{ato} is the characteristic frequency of the primary atomization process and $\lambda_{ato}(Y_l)$ is an efficiency function. We assume the atomization frequency to be directly connected to the strength of the velocity gradient, which is the only information locally available in the 4-equation framework (no velocity difference is known). This could be estimated using several approaches, amongst which are the Q criterion, the vorticity or the resolved strain tensor, all of these being based on the velocity gradient. In this study we have chosen to use the latter approach:

$$\nu_{turb} = \sqrt{2D^2} \quad ; \quad D^2 = \sum_{ij} D_{ij} D_{ij} \quad ; \quad D_{ij} = \frac{1}{2}\left(\frac{\partial \bar{u}_i}{\partial x_j} + \frac{\partial \bar{u}_j}{\partial x_i} \right)$$

The efficiency function is written as:

$$\lambda_{ato}(Y_l) = 1 - \tanh(a_\lambda Y_l^{b_\lambda}) \quad a_\lambda = 4, \quad b_\lambda = 2$$

It is designed to ensure that when some LOx mass is transferred from the fluid towards the spray in a given control volume, the corresponding vanishing volume in the fluid is actually negligible. Otherwise, the gas would experience some unphysical expansion in the control volume, which obviously has to be avoided, and the dispersed phase hypothesis made for the spray would not be respected. In other words, we use the numerical diffusion, which spreads the interface over several mesh elements, in order to carry out the mass transfer in a smooth way.

At this point with this model, the properties of the created droplets resulting from the primary atomization have to be assumed. They cannot be computed locally from resolved quantities, since the 4-equation formalism provides too little information. Actually, these properties are estimated based on the instability analysis from the reference [13]. In the latter work, the drop size and velocity distributions of the spray are estimated as a function of the injected propellant properties (density ratio, inlet velocities, vorticity thickness, etc.). Consequently, the knowledge of the steady operating conditions of the MASCOTTE configuration enables an overall mean droplet diameter subsequent to the primary atomization process to be derived and a corresponding mean droplet velocity:

$$d_{ato} = 260\mu m, \quad \|v_{ato}\| = 16 m s^{-1}$$

The direction given to the droplet velocity in each mesh cell has been set to that of the fluid, which may be actually a rough approximation. Note that even if the created droplet diameter is assumed, the use of a secondary break-up model is expected to rapidly modify and somehow correct the local droplet diameter. In fact, the zone of secondary atomization is expected to be correctly computed. Concerning the zone of primary atomization, the computation is limited by the 4-equation model, in which only one velocity is available. Finally, the temperature of the created droplet is just set to the constant value that was used to describe the liquid phase in the fluid, namely 85 K, corresponding to the LOx injection temperature.

It should also be stressed that the primary atomization model, which describes only the transfer from the separated phase CHARME solver to the dispersed phase solver SPIREE, can be combined with another model describing the inverse liquid-liquid transfer, namely from the SPIREE solver to the CHARME solver. This term is intended to describe, for instance, the case of droplets impacting the main liquid jet. Details on this term are not provided here, but can be found in [8].

Finally, let us specify that, even if the created droplets all have the same size, the use of the sectional approach is completely relevant. Indeed, it allows us to describe the local size polydispersity, which is subsequent to primary atomization as droplets undergo secondary break-up and evaporation. Consequently, this improves the evaluation of the gas-particle source terms, since they all depend on the droplet size: vaporization, drag force and heat exchange. Also, the improvement of the primary atomization model is planned for future works, for instance by using a transport equation for the surface density area and/or by switching to a diffuse interface model giving more local information than the 4-equation model: a two-temperature (5-equation) model, or even a two-temperature two-velocity (7-equation) model. Therefore, this should enable us to predict distributions (size, velocity, etc.) for the droplets subsequent to primary atomization, rather than just assumed mean values, which will we be much easier in a sectional framework.

Numerical results

In this section, we present some numerical results obtained with the coupling strategy applied to the MASCOTTE bench configuration. The 3D geometry is depicted in figure 4. The overall device is approximately 50 cm long, with a 50 mm wide section. The LOx post has a 5 mm diameter, whereas the total diameter of the injector (axial LOx + coaxial H_2) is 12 mm. We use a tetrahedral unstructured mesh made up of approximately 9.8M elements. The mesh has been built so that the finest refinement is located near the injector exit, where atomization takes place. The smallest cell size is of the order of 100 μm (in the blue zone), whereas the maximum cell size is of the order of 3mm at the end of the chamber. Figure 4 also represents the mesh with a zoom near the injector. For the sake of simulation, the computational geometry has been split into 1920 sub-domains and then dispatched into 480 processors to allow parallel computing. The physical time step of the computation is about 2.10-8s. The total physical time computed is 17ms, which corresponds to a total CPU time of about one million hours. Numerical results are presented in the rest of the section. Comparisons with experimental results are only qualitative because the results are not yet converged, as illustrated in figure 5.

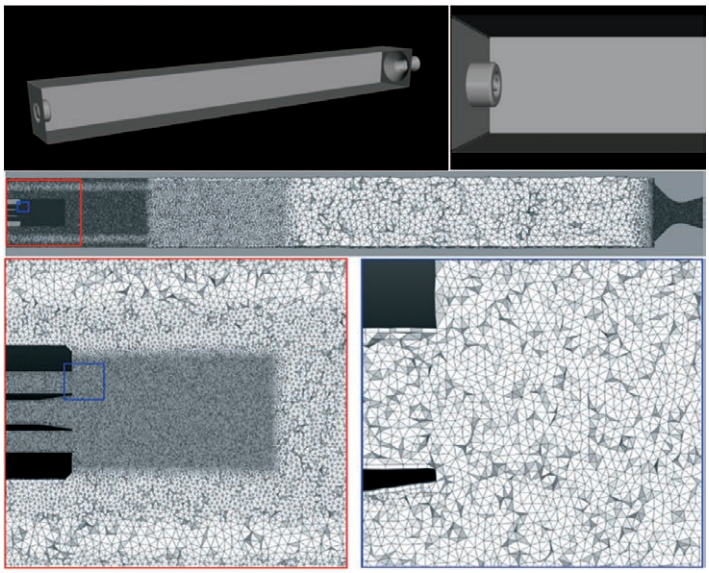

Figure 4 – Representation of the geometry and associated mesh for the MASCOTTE cryogenic test bench

Figure 5 shows the evolution of pressure and temperature obtained by the resolution of the CHARME solver, as well as the spray volume fractions obtained by the SPIREE solver (the volume fraction of each section is shown and the total one as well). Also shown is the evolution of the length of the liquid core over time. Results appear clearly not converged at this point of the computation because they include the end of the transient regime. The mean pressure decreases in the interval [0ms, 4ms] and reaches a minimum value equal to 7 bar. Then, the first droplets appear and feed the combustion, which induces an increase in the pressure. Between the times of 4 and 13 ms, the pressure increases to a maximum value equal to 10.7 bars and then decreases to reach 10.1 bars. In the experiments, the nominal pressure is equal to 11 bars. The maximum temperature can be related to the formation of the stable flame. A maximum value between 3500K and 3600K is obtained at 4 ms. Figure 5 also represents the evolution of the volume fraction for the three sections of the spray that are not empty. The volume fraction of the three sections globally increases with a total volume fraction that tends towards 0.02. Likewise, we can observe that the transient regime is not finished and that the LES "averaged" results have not converged. We have also plotted the length of the liquid core, which is evaluated in the simulation with the position of the isoline of the liquid volume fraction equal to 0.99. This length increases during the simulation as expected and seems to stabilize around a value between 11 and 13 mm. This length is approximately stable at 8 ms.

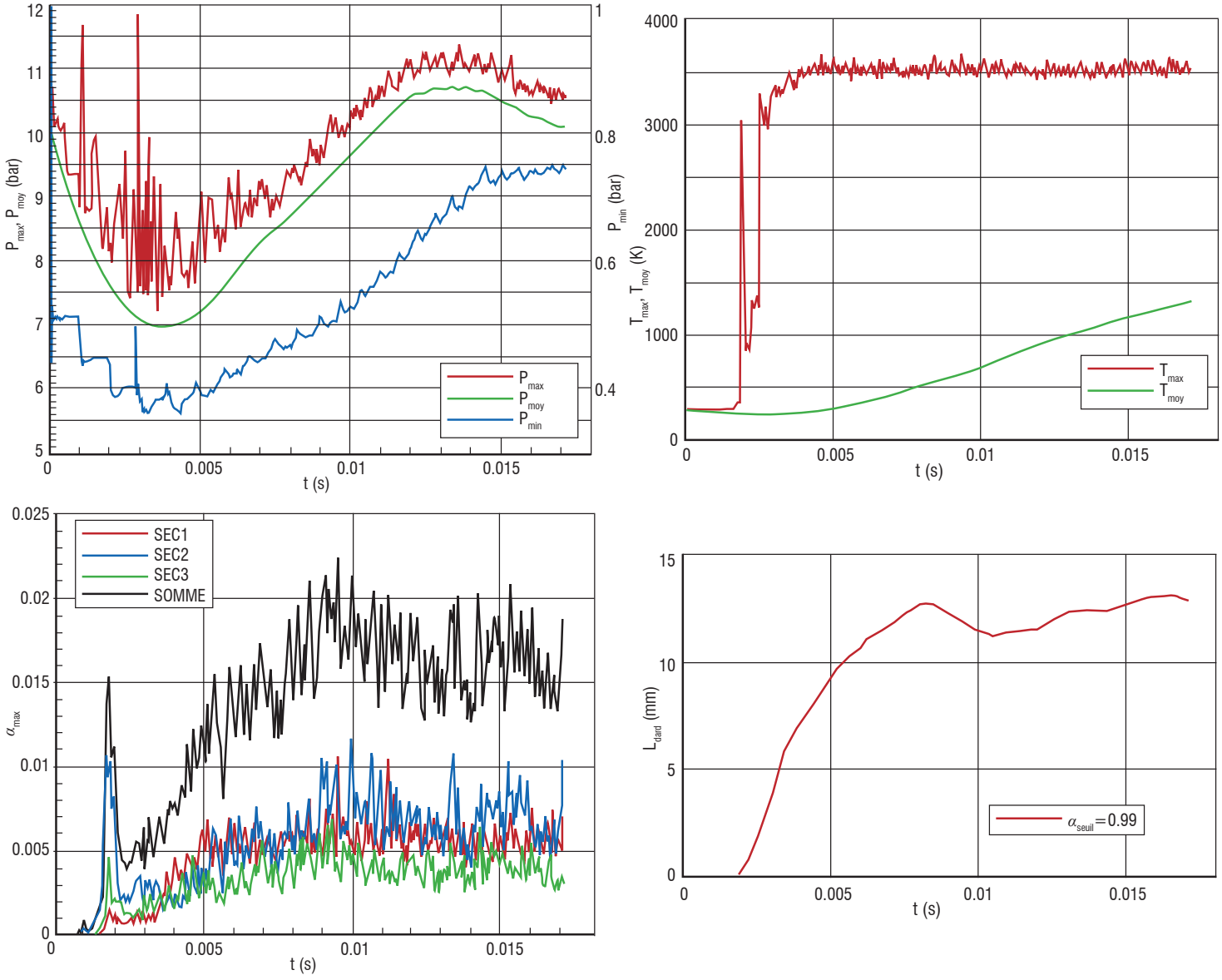

Figure 5 – Time evolution of pressure, temperature, volume fractions and penetration depth

The comparison with the theoretical value of 8 mm or experimental values between 8 and 41 mm is quite good, but must be confirmed with a higher level of convergence. In addition, the interpretation of the penetration depth must be made carefully because of numerical diffusion.

We then present different mean fields for the fluid solver in figure 6 to figure 10. The averaged field is computed between times 13 ms and 17 ms. Each variable is represented in the (XZ) plane and we have plotted the temperature and velocity isovalues, as well as the liquid and gaseous oxygen mass fraction and the H_2 gas and the H_2O product of combustion. The velocity norm is represented with logarithmic scaling. We can observe the recirculation of the coaxial H_2 with high velocity around the liquid oxygen, which has a low velocity and is atomized. In the lateral position, we can also observe the helium film, which is used in the experiment to cool the walls. A recirculation of H_2 is also observed. The mean value of the mass fraction clearly illustrates the transition region between separated and dispersed two-phase flow.

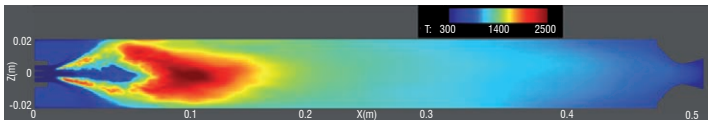

Figure 6 – Temperature mean field

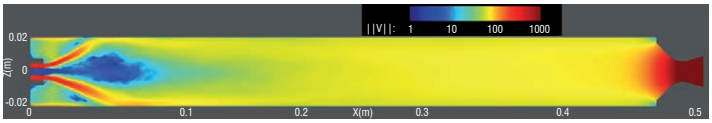

Figure 7 – Velocity norm mean field

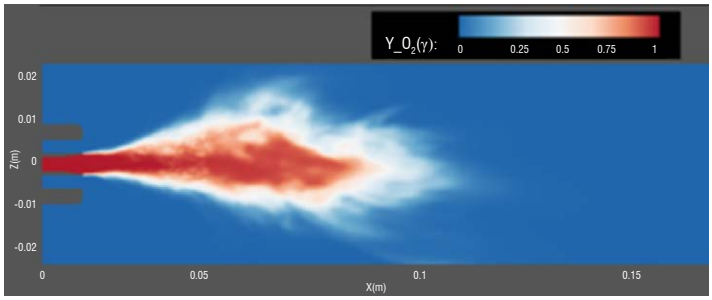

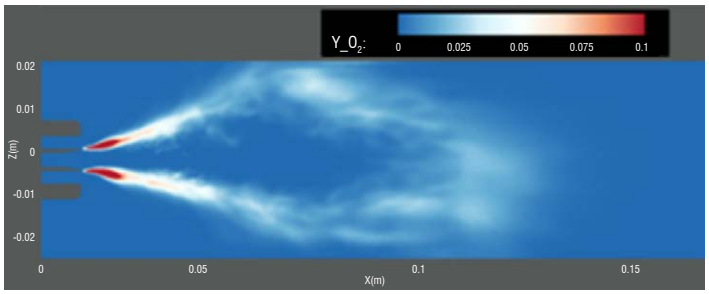

Figure 8 – Liquid oxygen (top) and gaseous oxygen (bottom) mass fraction mean field

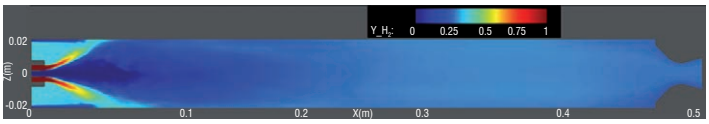

Figure 9 – Gaseous H_2 mass fraction mean field

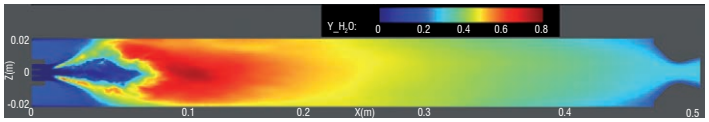

Figure 10 – Gaseous H_2O combustion product mean field

We also present on figure 11 instantaneous fields in the plane (XY) of both the total spray volume fraction (including all size sections), and the net liquid-liquid mass source term (labeled as ΔS_L in the key). The latter is the difference between the inverse liquid-liquid mass source term (re-impingement) and the primary atomization source term. Therefore negative values indicate zones where atomization takes place (mass is transferred from the continuous "separated phases" description to the "dispersed phase" description), whereas positive values indicate zones where the inverse transfer occurs.

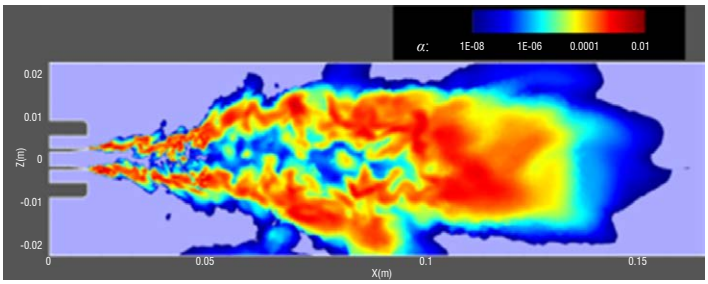

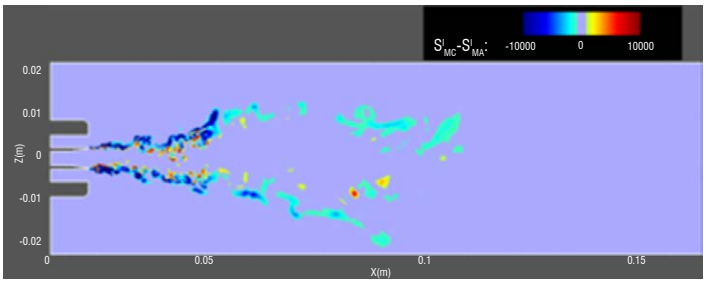

Figure 11 – Top: instantaneous field of the total spray volume fraction (all size sections). Bottom: instantaneous field of the net liquid-liquid mass source term

Finally, we give in figure 12 a qualitative comparison between experiments and numerical results for the instantaneous field. Figure 12a is an experimental visualization on the Mascotte test bench and figure 12b is an iso-surface (Y_l=0.95) of the LOx mass fraction in the CHARME solver.

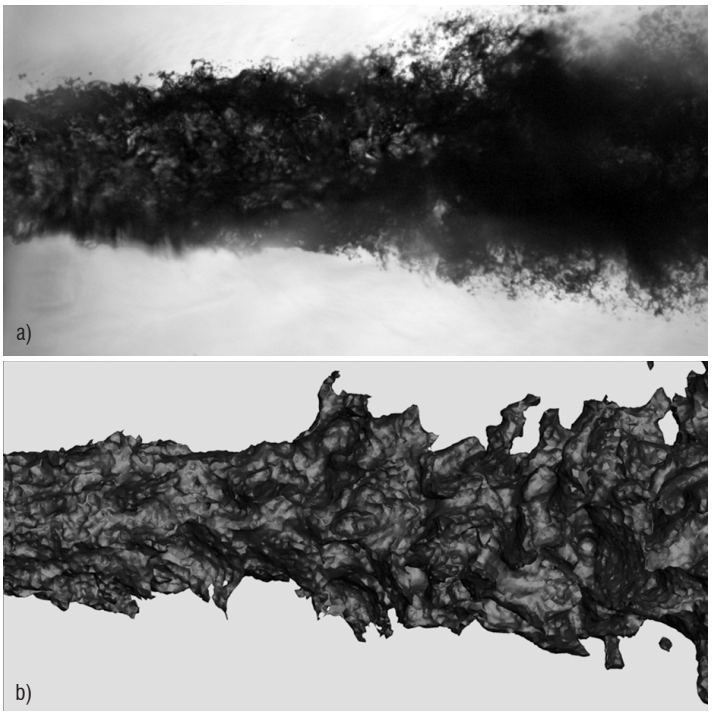

Figure 12 – Comparison between experiments and numerical results

Supercritical regime

For cryogenic engines running at high pressure, typically above 5 MPa, there is no phasic behavior between the cold injected oxygen and the warmer fluid where combustion phenomena occur. In this so-called supercritical regime, the lack of surface tension greatly modifies the mixing process, which does not involve droplet scattering as was the case in the subcritical regime. Oxygen dense core atomization is somewhat replaced by a peeling process, which strips off some oxygen dense clusters. These clusters are then rapidly stretched and heated, their surface to volume ratio not being minimized by interfacial energy consideration. The dense oxygen then undergoes a pseudo-boiling process, which is a continuous heating process from liquid-like dense states to gas-like thermodynamic states.

Fluid modeling

From a modeling point a view, supercritical regime thus appears at first sight as simpler than the subcritical regime, for neither scattered phase nor multiphasic bulk flow seem to be required. Some pressure laws, such as cubic equations of state (see BOX1), allow an analytic and continuous representation of supercritical fluids and one may think that a direct implementation of real gas thermodynamics in a standard CFD code would lead directly to a real gas capable code. This may be the case for DNS approaches [15], but more roughly discretized approaches such as LES or RANS need further development.

The reason for this lies in the fact that the width of the pseudo-boiling front results from a competition between heat conductivity and flow heterogeneities, such as stretch and turbulence. In rocket engine applications, the huge difference between the fuel injection speed leads to intense turbulence and thus to a pseudo-boiling front with a width of a few micrometers. Even with coarse front discretization, the number of points required to mesh one cubic centimeter of interest would be tremendous. Furthermore, with finite volume compressible approaches, the non-linearity of real gas thermodynamics in the pseudo-boiling region does not allow laxness in the front discretization, otherwise pressure oscillations are prone to appear.

Supercritical regime problems thus coincide with those encountered in the subcritical regime, that is to say, sharp interfacial or pseudo-interfacial phenomena that need to be discretized on coarse meshes. It is only natural that the way to handle it would also be similar.

A first approach is to spread the pseudo-boiling front over a sufficient number of discretization points using artificial diffusion [16]. This diffusion is triggered by a sensor allowing it to be active only in the pseudo-interfacial area and care must be taken to ensure that these extra terms in conservation equations do not themselves induce pressure oscillations. This could be achieved by adding compensatory energy source terms to nullify pressure variations.

Another approach consists in getting rid of thermodynamic non-linearity by means of a multi-fluid formulation. The pseudo-boiling interface is then no longer discretized, but rather distributed over the mesh cells where both fluids are present. This approach allows a sharper transition zone than the previous one for a given mesh, but requires additional conservation equations to be solved. The multi-fluid formulation is fundamentally a thermodynamic closure proposition for an averaged conservation equation in the way that it models subgrid structure complexity. Classical assumptions have indeed been shown [17] to fail, even with an LES filter size four time greater than the DNS grid size, and the proposed correction, based on pressure expansion in a Taylor series, is bound to fail for a greater LES filter size. The *a priori* distinction between the fluids can be interpreted as a Dirac delta based pdf in the thermodynamic space.

The simulations conducted at ONERA use a weakened multi-fluid approach, here dubbed a multi-phasic approach, enabling an easier implementation in the CFD code CEDRE created by ONERA. Indeed, if mass conservation equations are solved for each phase, only one total energy conservation equation is solved, the temperature of each "phase" being deduced from a mean temperature by means of *a priori* relations. These relations are designed in such a way that for the cold phase, the phase temperature corresponds to the mean temperature for low temperatures and smoothly reaches a maximal temperature T^c chosen below the pseudo-boiling temperature T^b for which the thermodynamical non-linearity is the greatest. Similarly, the hot phase temperature corresponds to the mean temperature for high temperatures and smoothly reaches a minimal temperature $T^h > T^b$ as the mean temperature decreases. This modification of the phase temperature can also be interpreted as a smooth prolongation of both phase thermodynamics before the non-linear zone is encountered, and thus as a smooth thermodynamic closure for the previously mentioned pdf. For the multi-phasic approach, only one global momentum equation is resolved, inducing equality of the phase velocities.

Mass exchange between the various phases is modeled as a volumic source term designed to relax in a given number of numerical time-steps the weight of the Dirac delta to a prescribed value depending on the mean temperature, so as to model pseudo-vaporization phenomena. This rather crude description of pseudo-interfacial phenomena, which only play a role in the one or two cell depth transition area where both phases are present, allows most of the thermodynamics non-linearity to be overcome in an energy-conservative way.

The small kinetic time scale for hydrogen combustion enables the use of a simplified combustion model based on relaxation toward a chemical equilibrium state in the hot phase. The time scale of this relaxation is linked to the turbulent time scale, in order to represent the limitation of combustion by the mixing phenomena.

Numerical simulation

Some LES have been performed on MASCOTTE test-bench configurations and yield satisfactory results concerning simulation stability. However, the fine representation of oxygen dense core breakup leads to the introduction and the coupling of time scales of rather different magnitude. Through developing Kelvin-Helmholtz instabilities, the oxygen dense core indeed breaks up into large dense clusters, which are slowly convected and pseudo-vaporized. The heterogeneity of dense core topology, especially its terminating clusters, greatly influences the flame, which rapidly adapts to it. A few dense core residence time must be waited in order to obtain the convergence of the mean dense core structure. The disparity of the time scales between the dense core and the hydrogen co-flow leads to the better representation of dense core breakup greatly increasing the cost of the simulation. This situation is worsened if one wishes to compute the entire MASCOTTE chamber. The rather slow motion of the burnt gases increases again to two fold the convergence time. As a consequence, the simulation presented here is not yet converged and only preliminary results are discussed.

Figure 13 shows a comparison between an experimental backlighting image [18] and an isodensity surface snapshot of the LES. As previously stated, the transition surface between cold dense oxygen and lighter hot gases is wrinkled by the co-flow, even if no small scale dense clusters are to be seen around the dense core. The numerical picture is taken just before a final breakup event as can be inferred from the shape of the isosurface, which displays a constricted shape near its end where separation will occur.

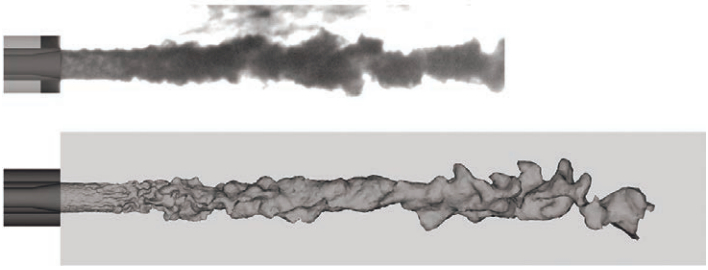

Figure 13 – Comparison between an experimental backlighting image of the A60 case [18] and a 200 kg/m^3 isodensity surface LES snapshot

The shape of the flame is shown in figure 14, in which a 1500 K isotemperature surface is drawn. This trumpet-like shape is the consequence of the flame being constrained by the backward-facing step toroidal recirculation vortex. Where the mean flow reattaches itself to the chamber boundary, the flame follows, leaving behind it a low velocity area, as already noted in similar configurations [19][20].

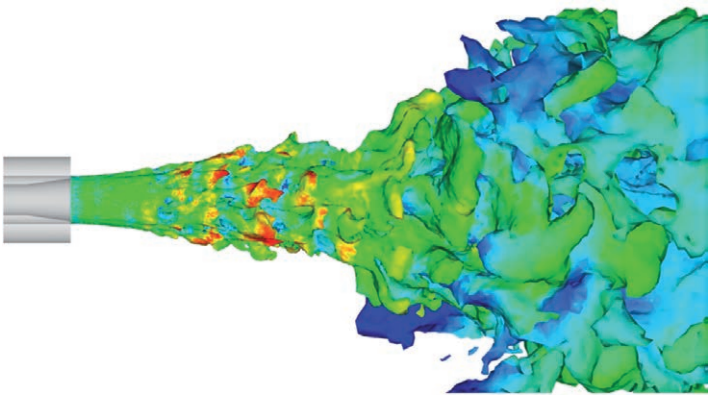

Figure 14 – 1500 K isotemperature surface LES snapshot

The comparison of the numerical results with the Abel transform of the OH* emission, which gives the position of the flame away, is performed in figure 15. The Abel transform from [21] is displayed at the bottom of this figure for reference. In the top picture, the far-from-being-converged mean OH production field is shown in pink over the reference picture and reasonable agreement is found between the experimental flame location and the numerical field.

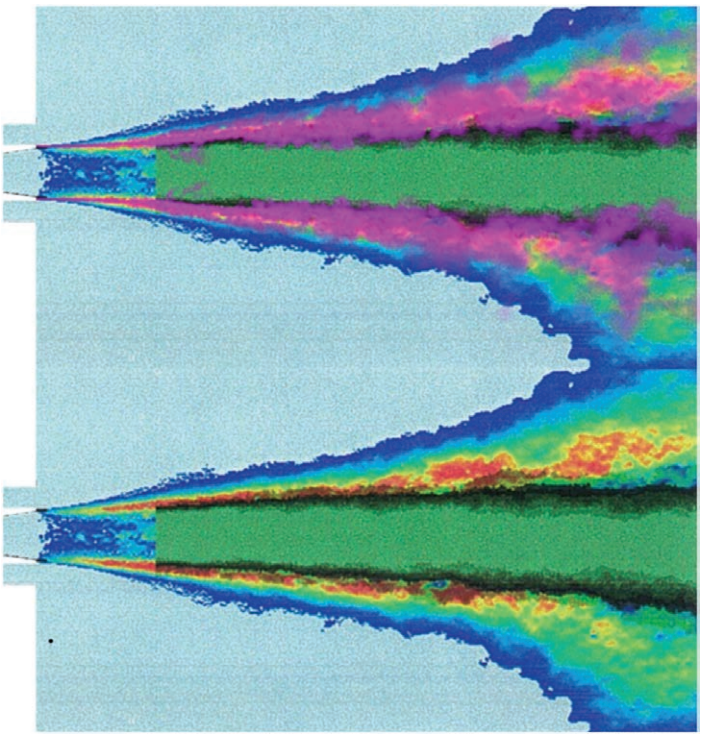

Figure 15 – Visualization of the comparison between experimental OH* [21] (up with computed mean OH production in pink)

Conclusion

Progress has been made in the modeling and simulation of physical phenomena at work in the field of cryogenic combustion.

A Large Eddy Simulation of the primary atomization in cryogenic combustion chamber has been performed by means of a fully Eulerian coupling strategy between a diffuse interface 4-equation (1-velocity) model and a kinetic based model, using specific numerical methods to ensure accuracy and robustness of the computation. The first results seem to be very promising, but need to be converged. For this reason, the comparisons with experiments are only qualitative at this moment. In the future, we intend to use a 7-equation (2-velocity) model, in order to improve the physical modeling of the primary atomization.

Supercritical oxygen dense core destabilization has been simulated with a specific dense to diluted transition model based on a weakened multi-fluid approach. As for the subcritical primary atomization case, the coupling between the different time scales and the need for a refined mesh to capture the pseudo interface topology lead to rather expensive simulation. In order to reduce the computational cost, pseudo interface modeling approaches are to be investigated ■

Box 1 - Cubic equation of state

Cubic equations of state have been obtained from the van der Waals equation of state [14] and can be written in the common form:

$$P = \left(\sum_{i=1}^{n_e} \frac{Y_i}{M_i} \right) \frac{RT}{v-b} - \frac{a(T)}{v^2 + uv + w}$$

where b stands for the covolume and $a(T)$ is an attraction parameter, which represents the effect of the London dispersion forces for molecules without permanent multipole moments. Further developments of the van der Waals equation of state led to various mixing rules used for the computation of the mixture covolume and attraction parameters from pure-species parameters, to various temperature dependencies of the attraction parameter $a(T)$ and to the introduction of the long range shape parameters u and w.

Pure species parameters are usually deduced from critical properties, in such a way that the cubic equation of state yields an exact pure-species critical point. Figure B1-1 shows the isothermal behavior of the cubic equation of state in a one-species case, the green square being the critical point of the represented species. For temperatures lower than the critical temperature, the phase equilibrium can be computed between a liquid phase and a gaseous phase, whereas above the critical temperature only a single-phase flow can occur. Despite their overall simplicity, which allows the analytic inversion of the pressure law thanks to Cardan's formulas, cubic equations of state reproduce reasonably well the fluid thermodynamic behavior and, as a consequence, they are often used in the field of CFD.

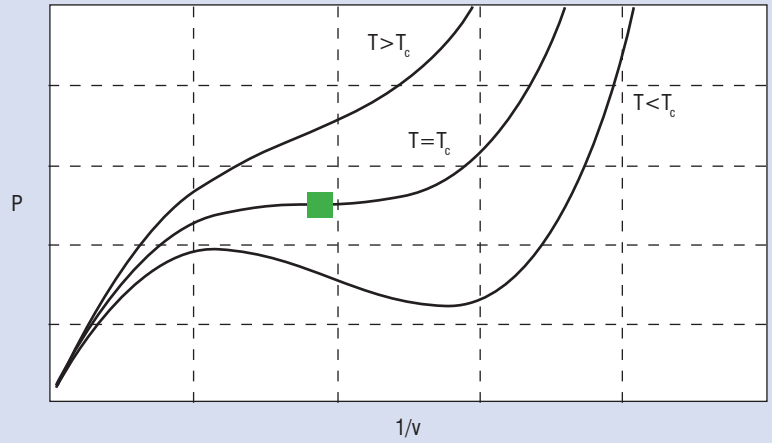

Figure B1-1 – Isothermal behavior of the cubic equation of state

References

[1] L. VINGERT, G. ORDONNEAU and P. GRENARD – *A Rocket Engine under a Magnifying Glass*. AerospaceLab Journal, Vol. 11, 2015.
[2] A. REFLOCH, B. COURBET, A. MURRONE, P. VILLEDIEU, C. LAURENT, P. GILBANK, J. TROYES, L. TESSE, G. CHAINERAY, J.B. DARGAUD, E. QUEMERAIS and F. VUILLOT – *CEDRE Software*. Aerospace Lab Journal, Issue 2, 2011.
[3] A. MURRONE and C. LE TOUZE – *Eulerian Coupling of Two-Phase Flow Models for the Large Eddy Simulation of the Atomization in Cryogenic Combustion Chamber*. 6th European Conference for Aeronautics and Space Sciences (EUCASS), Krakow, 2015.
[4] A. VALLET, A. BURLUKA and R. BORGHI – *Development of a Eulerian Model for the Atomization of a Liquid Jet*. Atomization and Sprays. 11:619–642, 2001.
[5] R. LEBAS, T. MENARD, P. A. BEAU, A. BERLEMONT and F.X. DEMOULIN – *Numerical Simulation of Primary Break-Up and Atomization : DNS and Modelling Study*. International Journal of Multiphase flow. 35:247–260, 2009.
[6] A. MURRONE and P. VILLEDIEU – *Numerical Modeling of Dispersed Two-Phase Flows*. AerospaceLab Journal, Issue 2, 2011.
[7] A. SIBRA – *Modélisation et étude de l'évaporation et de la combustion de gouttes dans les moteurs à propergol solide par une approche eulérienne Multi-Fluide*. PhD thesis, 2015.
[8] C. LE TOUZE – *Couplage entre modèles diphasiques à « phases séparées » et à « phase dispersée » pour la simulation de l'atomisation primaire en combustioncryotechnique*. PhD thesis, 2015.
[9] B. ABRAMZON and W.A. SIRIGNANO – *Droplet Vaporization Model for Spray Combustion Calculations*. International Journal of Heat and Mass Transfer, 32:160-16, 1989.
[10] K. POUGATCH, M. SALCUDEAN, E. CHAN and B. KNAPPER – *A Two-Fluid Model of Gas-Assisted Atomization Including Flow Through the Nozzle, Phase Inversion, and Spray Dispersion*. International Journal of Multiphase Flow, 35:7, 661–675, 2009.
[11] G. DUFOUR – *Modélisation multi-fluide eulérienne pour les écoulements diphasiques à inclusions dispersées*. PhD thesis, 2005.
[12] C. LE TOUZE, A. MURRONE and H. GUILLARD – *Multislope Muscl Method for General Unstructured Meshes*. Journal of Computational Physics, Vol. 284 , 2015, 389–418
[13] P. MARMOTTANT and E. VILLERMAUX – *On Spray Formation*. Journal of Fluid Mechanics, 498:73-112, 2004.
[14] J. D. VAN DER WAALS – *Over de Continuiteit van den Gas - en Vloeistoftoestand*. P.H.D thesis, Leiden, 1873.
[15] J. C. OEFELEIN – *Mixing and Combustion of Cryogenic Oxygen-Hydrogen Shear-Coaxial Jet Flames at Supercritical Pressure*. Combustion Science and Technology, Vol. 178, 2006.
[16] T. SCHMITT, L. SELLE, A. RUIZ and B. CUENOT – *Large-Eddy Simulation of Supercritical-Pressure Round Jets*. AIAA Journal, Vol. 48, 2010.
[17] L. C. SELLE, N. A. OKONG'O, J. BELLAN and K. G HARSTAD – *Modelling of Subgrid-Scale Phenomena in Supercritical Transitional Mixing Layers : an a priori Study*. Journal of Fluid Mechanics, Vol. 593, 2007.
[18] P. GICQUEL, M. BARAT and L. VINGERT – *Campagne de visualisation LOx sur le boîtier MASCOTTE à 6 MPa*. RT 1/06254 DEFA/DMTE, Nov. 2001.
[19] T. SCHMITT, Y. MERY, M. BOILEAU and S. CANDEL – *Large-Eddy Simulation of Oxygene/Methane Flames under Transcritical Conditions*. Proceedings of the Combustion Institute, Vol. 33, 2011.
[20] A. RUIZ – *Unsteady Numerical Simulations of Transcritical Turbulent Combustion in Liquid Rocket Engines*. P.H.D thesis, INP Toulouse 2012.
[21] S. CANDEL, M. JUNIPER, G. SINGLA, P. SCOUFLAIRE and C. ROLON – *Structure and Dynamics of Cryogenic Flames at Supercritical Pressure*. Combustion Science and Technology, Vol. 178, 2006.

AUTHORS

Pierre Gaillard is an engineer at MBDA, now working on ramjet and scramjet applications. He graduated from the Ecole Polytechnique and ISAE engineer schools in 2012 and received his PhD degree in mechanics from Université Paris 6 in 2015. His PhD work focused on supercritical flow and combustion.

Lionel Matuszewski is a research engineer at ONERA, working in the Liquid Propulsion Unit of the Fundamental and Applied Energetics Department (DEFA). He graduated from the Ecole Polytechnique and ISAE engineer schools in 2007. His research field is mainly focused on dense fluid modeling with application to supercritical combustion.

Clément Le Touze graduated from INSA de Rouen in 2011 with an engineering degree in propulsion and energetics, and received his PhD degree in applied mathematics from Université Nice Sophia Antipolis in 2015. He is now a research engineer in the Energetics department at ONERA. His main activities focus on the modeling and simulation of two-phase flows in the field of propulsion. He is also involved in the development of the CEDRE code, especially within the Eulerian SPIREE solver dedicated to dispersed two-phase flows.

Angelo Murrone graduated as an engineer from "Ecole Polytechnique Universitaire de Marseille" in 2000 and received a Ph.D. degree in Mechanics and Energetics from the University of Aix-Marseille I, France, in 2003. He has been working at ONERA since 2005 and his research concerns numerical modelling of multiphase flows and multi-physics simulations for Energetics and propulsion. He's currently head of the unit research in charge of the in-house multi-physics CEDRE code development.